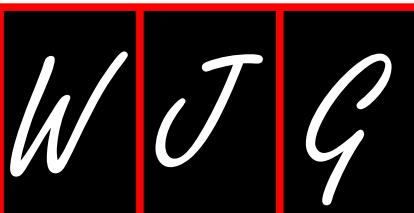


World Journal of *Gastroenterology*

World J Gastroenterol 2011 January 7; 17(1): 1-136





Editorial Board

2010-2013

The *World Journal of Gastroenterology* Editorial Board consists of 1144 members, representing a team of worldwide experts in gastroenterology and hepatology. They are from 60 countries, including Albania (1), Argentina (8), Australia (29), Austria (14), Belgium (12), Brazil (10), Brunei Darussalam (1), Bulgaria (2), Canada (20), Chile (3), China (69), Colombia (1), Croatia (2), Cuba (1), Czech (4), Denmark (8), Ecuador (1), Egypt (2), Estonia (2), Finland (8), France (24), Germany (75), Greece (14), Hungary (10), India (26), Iran (6), Ireland (7), Israel (12), Italy (101), Japan (112), Jordan (1), Kuwait (1), Lebanon (3), Lithuania (2), Malaysia (1), Mexico (10), Moldova (1), Netherlands (29), New Zealand (2), Norway (11), Pakistan (2), Poland (11), Portugal (4), Romania (3), Russia (1), Saudi Arabia (3), Serbia (3), Singapore (10), South Africa (2), South Korea (32), Spain (38), Sweden (18), Switzerland (11), Thailand (1), Trinidad and Tobago (1), Turkey (24), United Arab Emirates (2), United Kingdom (82), United States (249), and Uruguay (1).

HONORARY EDITORS-IN-CHIEF

James L Boyer, *New Haven*
Ke-Ji Chen, *Beijing*
Martin H Floch, *New Haven*
Emmet B Keeffe, *Palo Alto*
Geng-Tao Liu, *Beijing*
Lein-Ray Mo, *Tainan*
Eamonn M Quigley, *Cork*
Rafiq A Sheikh, *Sacramento*
Nicholas J Talley, *Rochester*
Ming-Lung Yu, *Kaohsiung*

PRESIDENT AND EDITOR-IN-CHIEF

Lian-Sheng Ma, *Beijing*

ACADEMIC EDITOR-IN-CHIEF

Tauseef Ali, *Oklahoma City*
Mauro Bortolotti, *Bologna*
Tarkan Karakan, *Ankara*
Weekitt Kittisupamongkol, *Bangkok*
Anastasios Koulaouzidis, *Edinburgh*
Bo-Rong Pan, *Xi'an*
Sylvia LF Pender, *Southampton*
Max S Petrov, *Auckland*
George Y Wu, *Farmington*

STRATEGY ASSOCIATE EDITORS-IN-CHIEF

Peter Draganov, *Florida*
Hugh J Freeman, *Vancouver*
Maria C Gutiérrez-Ruiz, *Mexico*
Kazuhiro Hanazaki, *Kochi*
Akio Inui, *Kagoshima*
Kalpesh Jani, *Baroda*
Javier S Martin, *Punta del Este*

Natalia A Osna, *Omaha*
Wei Tang, *Tokyo*
Alan BR Thomson, *Edmonton*
Harry HX Xia, *Hanover*
Jesus K Yamamoto-Furusho, *Mexico*
Yoshio Yamaoka, *Houston*

ASSOCIATE EDITORS-IN-CHIEF

You-Yong Lu, *Beijing*
John M Luk, *Singapore*
Hiroshi Shimada, *Yokohama*

GUEST EDITORIAL BOARD MEMBERS

Chien-Jen Chen, *Taipei*
Yang-Yuan Chen, *Changhua*
Jen-Hwey Chiu, *Taipei*
Seng-Kee Chuah, *Kaohsiung*
Wan-Long Chuang, *Kaohsiung*
Ming-Chih Hou, *Taipei*
Kevin Cheng-Wen Hsiao, *Taipei*
Po-Shiuan Hsieh, *Taipei*
Tsung-Hui Hu, *Kaohsiung*
Wen-Hsin Huang, *Taichung*
Chao-Hung Hung, *Kaohsiung*
I-Rue Lai, *Taipei*
Teng-Yu Lee, *Taichung*
Ching Chung Lin, *Taipei*
Hui-Kang Liu, *Taipei*
Hon-Yi Shi, *Kaohsiung*
Chih-Chi Wang, *Kaohsiung*
Jin-Town Wang, *Taipei*
Cheng-Shyong Wu, *Chia-Yi*
Jaw-Ching Wu, *Taipei*
Jiunn-Jong Wu, *Tainan*
Ming-Shiang Wu, *Taipei*

Ta-Sen Yeh, *Taoyuan*
Hsu-Heng Yen, *Changhua*
Ming-Whei Yu, *Taipei*

MEMBERS OF THE EDITORIAL BOARD



Albania

Bashkim Resuli, *Tirana*



Argentina

Julio H Carri, *Córdoba*
Eduardo de Santibañes, *Buenos Aires*
Bernardo Frider, *Buenos Aires*
Carlos J Pirola, *Buenos Aires*
Bernabe Matias Quesada, *Buenos Aires*
Silvia Sookoian, *Buenos Aires*
Adriana M Torres, *Rosario*
Maria Ines Vaccaro, *Buenos Aires*



Australia

Leon Anton Adams, *Nedlands*
Richard Anderson, *Victoria*
Minoti V Apte, *New South Wales*
Andrew V Biankin, *Sydney*
Filip Braet, *Sydney*
Christopher Christophi, *Melbourne*
Philip G Dinning, *Koagarah*
Guy D Eslick, *Sydney*
Michael A Fink, *Melbourne*

Robert JL Fraser, *Daw Park*
 Jacob George, *Westmead*
 Mark D Gorrell, *Sydney*
 Alexander G Heriot, *Melbourne*
 Michael Horowitz, *Adelaide*
 John E Kellow, *Sydney*
 William Kemp, *Melbourne*
 Finlay A Macrae, *Victoria*
 Daniel Markovich, *Brisbane*
 Vance Matthews, *Melbourne*
 Phillip S Oates, *Perth*
 Shan Rajendra, *Tasmania*
 Rajvinder Singh, *Elizabeth Vale*
 Ross C Smith, *Sydney*
 Kevin J Spring, *Brisbane*
 Nathan Subramaniam, *Brisbane*
 Phil Sutton, *Melbourne*
 Cuong D Tran, *North Adelaide*
 Debbie Trinder, *Fremantle*
 David Ian Watson, *Bedford Park*



Austria

Herwig R Cerwenka, *Graz*
 Ashraf Dahaba, *Graz*
 Peter Ferenci, *Vienna*
 Valentin Fuhrmann, *Vienna*
 Alfred Gangl, *Vienna*
 Alexander M Hirschl, *Wien*
 Kurt Lenz, *Linz*
 Dietmar Öfner, *Salzburg*
 Markus Peck-Radosavljevic, *Vienna*
 Markus Raderer, *Vienna*
 Stefan Riss, *Vienna*
 Georg Roth, *Vienna*
 Michael Trauner, *Graz*
 Thomas Wild, *Kapellerfeld*



Belgium

Rudi Beyaert, *Gent*
 Benedicte Y De Winter, *Antwerp*
 Inge I Depoortere, *Leuven*
 Olivier Detry, *Liège*
 Philip Meuleman, *Ghent*
 Marc Peeters, *De Pintelaan*
 Freddy Penninckx, *Leuven*
 Jean-Yves L Reginster, *Liège*
 Mark De Ridder, *Brussels*
 Etienne M Sokal, *Brussels*
 Kristin Verbeke, *Leuven*
 Eddie Wisse, *Keerbergen*



Brazil

José LF Caboclo, *São José do Rio Preto*
 Roberto J Carvalho-Filho, *São Paulo*
 Jaime Natan Eisig, *São Paulo*
 Andre Castro Lyra, *Salvador*
 Marcelo Lima Ribeiro, *Braganca Paulista*
 Joao Batista Teixeira Rocha, *Santa Maria*
 Heitor Rosa, *Goiania*
 Damiao C Moraes Santos, *Rio de Janeiro*
 Ana Cristina Simões e Silva, *Belo Horizonte*
 Eduardo Garcia Vilela, *Belo Horizonte*



Brunei Darussalam

Vui Heng Chong, *Bandar Seri Begawan*



Bulgaria

Zahariy Krastev, *Sofia*
 Mihaela Petrova, *Sofia*



Canada

Alain Bitton, *Montreal*
 Michael F Byrne, *Vancouver*
 Kris Chadee, *Calgary*
 Wangxue Chen, *Ottawa*
 Ram Prakash Galwa, *Ottawa*
 Philip H Gordon, *Montreal*
 Waliul Khan, *Ontario*
 Qiang Liu, *Saskatoon*
 John K Marshall, *Ontario*
 Andrew L Mason, *Alberta*
 Kostas Pantopoulos, *Quebec*
 Nathalie Perreault, *Sherbrooke*
 Baljinder Singh Salh, *Vancouver*
 Eldon Shaffer, *Calgary*
 Martin Storr, *Calgary*
 Pingchang Yang, *Hamilton*
 Eric M Yoshida, *Vancouver*
 Claudia Zwingmann, *Montreal*



Chile

Marcelo A Beltran, *La Serena*
 Xabier De Aretxabala, *Santiago*
 Silvana Zanlungo, *Santiago*



China

Hui-Jie Bian, *Xi'an*
 San-Jun Cai, *Shanghai*
 Guang-Wen Cao, *Shanghai*
 Xiao-Ping Chen, *Wuhan*
 Chi-Hin Cho, *Hong Kong*
 Zong-Jie Cui, *Beijing*
 Jing-Yuan Fang, *Shanghai*
 De-Liang Fu, *Shanghai*
 Ze-Guang Han, *Shanghai*
 Chun-Yi Hao, *Beijing*
 Ming-Liang He, *Hong Kong*
 Ching-Lung Lai, *Hong Kong*
 Simon Law, *Hong Kong*
 Yuk-Tong Lee, *Hong Kong*
 En-Min Li, *Shantou*
 Fei Li, *Beijing*
 Yu-Yuan Li, *Guangzhou*
 Zhao-Shen Li, *Shanghai*
 Xing-Hua Lu, *Beijing*
 Yi-Min Mao, *Shanghai*
 Qin Su, *Beijing*
 Paul Kwong-Hang Tam, *Hong Kong*
 Yuk Him Tam, *Hong Kong*
 Ren-Xiang Tan, *Nanjing*
 Wei-Dong Tong, *Chongqing*
 Eric WC Tse, *Hong Kong*

Fu-Sheng Wang, *Beijing*
 Xiang-Dong Wang, *Shanghai*
 Nathalie Wong, *Hong Kong*
 Justin CY Wu, *Hong Kong*
 Wen-Rong Xu, *Zhenjiang*
 An-Gang Yang, *Xi'an*
 Wei-Cheng You, *Beijing*
 Chun-Qing Zhang, *Jinan*
 Jian-Zhong Zhang, *Beijing*
 Xiao-Peng Zhang, *Beijing*
 Xuan Zhang, *Beijing*



Colombia

Germán Campuzano-Maya, *Medellín*



Croatia

Tamara Cacev, *Zagreb*
 Marko Duvnjak, *Zagreb*



Cuba

Damian C Rodriguez, *Havana*



Czech

Jan Bures, *Hradec Kralove*
 Milan Jirsa, *Praha*
 Marcela Kopacova, *Hradec Kralove*
 Pavel Trunečka, *Prague*



Denmark

Leif Percival Andersen, *Copenhagen*
 Asbjørn M Drewes, *Aalborg*
 Morten Frisch, *Copenhagen*
 Jan Mollenhauer, *Odense*
 Morten Hylander Møller, *Holte*
 Søren Rafaelsen, *Vejle*
 Jorgen Rask-Madsen, *Skodsborg*
 Peer Wille-Jørgensen, *Copenhagen*



Ecuador

Fernando E Sempértogui, *Quito*



Egypt

Zeinab Nabil Ahmed, *Cairo*
 Hussein M Atta, *El-Minia*



Estonia

Riina Salupere, *Tartu*
 Tamara Vorobjova, *Tartu*



Finland

Saila Kauhanen, *Turku*

Thomas Kietzmann, *Oulu*
 Kaija-Leena Kolho, *Helsinki*
 Jukka-Pekka Mecklin, *Jyväskylä*
 Minna Nyström, *Helsinki*
 Pauli Antero Puolakkainen, *Turku*
 Juhani Sand, *Tampere*
 Lea Veijola, *Helsinki*



France

Claire Bonithon-Kopp, *Dijon*
 Lionel Bueno, *Toulouse*
 Sabine Colnot, *Paris*
 Catherine Daniel, *Lille Cedex*
 Alexis Desmoulière, *Limoges*
 Thabut Dominique, *Paris*
 Francoise L Fabiani, *Angers*
 Jean-Luc Faucheron, *Grenoble*
 Jean Paul Galmiche, *Nantes cedex*
 Boris Guiu, *Dijon*
 Paul Hofman, *Nice*
 Laurent Huwart, *Paris*
 Juan Iovanna, *Marseille*
 Abdel-Majid Khatib, *Paris*
 Philippe Lehours, *Bordeaux*
 Flavio Maina, *Marseille*
 Patrick Marcellin, *Paris*
 Rene Gerolami Santandera, *Marseille*
 Annie Schmid-Alliana, *Nice cedex*
 Alain L Servin, *Châtenay-Malabry*
 Stephane Supiot, *Nantes*
 Baumert F Thomas, *Strasbourg*
 Jean-Jacques Tuech, *Rouen*
 Frank Zerbib, *Bordeaux Cedex*



Germany

Erwin Biecker, *Siegburg*
 Hubert Blum, *Freiburg*
 Thomas Bock, *Tuebingen*
 Dean Bogoevski, *Hamburg*
 Elfriede Bollschweiler, *Köln*
 Jürgen Borlak, *Hannover*
 Christa Buechler, *Regensburg*
 Jürgen Büning, *Lübeck*
 Elke Cario, *Essen*
 Bruno Christ, *Halle/Saale*
 Christoph F Dietrich, *Bad Mergentheim*
 Ulrich R Fölsch, *Kiel*
 Nikolaus Gassler, *Aachen*
 Markus Gerhard, *Munich*
 Dieter Glebe, *Giessen*
 Ralph Graeser, *Freiburg*
 Axel M Gressner, *Aachen*
 Nils Habbe, *Marburg*
 Thilo Hackert, *Heidelberg*
 Wolfgang Hagmann, *Heidelberg*
 Dirk Haller, *Freising*
 Philip D Hard, *Giessen*
 Claus Hellerbrand, *Regensburg*
 Klaus R Herrlinger, *Stuttgart*
 Eberhard Hildt, *Berlin*
 Andrea Hille, *Goettingen*
 Joerg C Hoffmann, *Berlin*
 Philippe N Khalil, *Munich*
 Andrej Khandoga, *Munich*
 Jorg Kleeff, *Munich*
 Ingmar Königsrainer, *Tübingen*
 Peter Konturek, *Erlangen*

Stefan Kubicka, *Hannover*
 Joachim Labenz, *Siegen*
 Michael Linnebacher, *Rostock*
 Jutta Elisabeth Lüttges, *Riegelsberg*
 Peter Malfertheiner, *Magdeburg*
 Oliver Mann, *Hamburg*
 Peter N Meier, *Hannover*
 Sabine Mihm, *Göttingen*
 Klaus Mönkemüller, *Bottrop*
 Jonas Mudter, *Erlangen*
 Sebastian Mueller, *Heidelberg*
 Robert Obermaier, *Freiburg*
 Matthias Ocker, *Erlangen*
 Stephan Johannes Ott, *Kiel*
 Gustav Paumgartner, *Munich*
 Christoph Reichel, *Bad Brückenau*
 Markus Reiser, *Bochum*
 Steffen Rickes, *Magdeburg*
 Elke Roeb, *Giessen*
 Christian Rust, *Munich*
 Hans Scherubl, *Berlin*
 Martin K Schilling, *Homburg*
 Joerg F Schlaak, *Essen*
 Rene Schmidt, *Freiburg*
 Andreas G Schreyer, *Regensburg*
 Karsten Schulmann, *Bochum*
 Henning Schulze-Bergkamen, *Mainz*
 Manfred V Singer, *Mannheim*
 Jens Standop, *Bonn*
 Jurgen M Stein, *Frankfurt*
 Ulrike S Stein, *Berlin*
 Wolfgang R Stremmel, *Heidelberg*
 Harald F Teutsch, *Ulm*
 Hans L Tillmann, *Leipzig*
 Christian Trautwein, *Aachen*
 Joerg Trojan, *Frankfurt*
 Arndt Vogel, *Hannover*
 Siegfried Wagner, *Deggendorf*
 Frank Ulrich Weiss, *Greifswald*
 Fritz von Weizsäcker, *Berlin*
 Thomas Wex, *Magdeburg*
 Stefan Wirth, *Wuppertal*
 Marty Zdichavsky, *Tübingen*



Greece

Helen Christopoulou-Aletra, *Thessaloniki*
 T Choli-Papadopoulos, *Thessaloniki*
 Tsianos Epameinondas, *Ioannina*
 Ioannis Kanellos, *Thessaloniki*
 Elias A Kouroumalis, *Heraklion*
 Ioannis E Koutroubakis, *Heraklion*
 Michael Koutsilieris, *Athens*
 Andreas Larentzakis, *Athens*
 Emanuel K Manesis, *Athens*
 Spilios Manolakopoulos, *Athens*
 Konstantinos Mimidis, *Alexandroupolis*
 George Papatheodoridis, *Athens*
 Spiros Sgouros, *Athens*
 Evangelos Tsiambas, *Ag Paraskevi Attiki*



Hungary

György M Buzás, *Budapest*
 László Czákó, *Szeged*
 Gyula Farkas, *Szeged*
 Peter Hegyi, *Szeged*
 Peter L Lakatos, *Budapest*

Yvette Mándi, *Szeged*
 Zoltan Rakonczay, *Szeged*
 Ferenc Sipos, *Budapest*
 Zsuzsa Szondy, *Debrecen*
 Gabor Veres, *Budapest*



India

Philip Abraham, *Mumbai*
 Vineet Ahuja, *New Delhi*
 Giriraj Ratan Chandak, *Hyderabad*
 Devinder Kumar Dhawan, *Chandigarh*
 Radha K Dhiman, *Chandigarh*
 Pankaj Garg, *Panchkula*
 Pramod Kumar Garg, *New Delhi*
 Debidas Ghosh, *Midnapore*
 Uday C Ghoshal, *Lucknow*
 Bhupendra Kumar Jain, *Delhi*
 Ashok Kumar, *Lucknow*
 Bikash Medhi, *Chandigarh*
 Sri P Misra, *Allahabad*
 Gopal Nath, *Varanasi*
 Samiran Nundy, *New Delhi*
 Jagannath Palepu, *Mumbai*
 Vandana Panda, *Mumbai*
 Benjamin Perakath, *Tamil Nadu*
 Ramesh Roop Rai, *Jaipur*
 Nageshwar D Reddy, *Hyderabad*
 Barjesh Chander Sharma, *New Delhi*
 Virendra Singh, *Chandigarh*
 Rupjyoti Talukdar, *Guwahati*
 Rakesh Kumar Tandon, *New Delhi*
 Jai Dev Wig, *Chandigarh*



Iran

Mohammad Abdollahi, *Tehran*
 Peyman Adibi, *Isfahan*
 Seyed-Moayed Alavian, *Tehran*
 Seyed Mohsen Dehghani, *Shiraz*
 Reza Malekzadeh, *Tehran*
 Alireza Mani, *Tehran*



Ireland

Billy Bourke, *Dublin*
 Ted Dinan, *Cork*
 Catherine Greene, *Dublin*
 Ross McManus, *Dublin*
 Anthony P Moran, *Galway*
 Marion Rowland, *Dublin*



Israel

Simon Bar-Meir, *Hashomer*
 Alexander Becker, *Afula*
 Abraham R Eliakim, *Haifa*
 Sigal Fishman, *Tel Aviv*
 Boris Kirshtein, *Beer Sheva*
 Eli Magen, *Ashdod*
 Menachem Moshkowitz, *Tel-Aviv*
 Assy Nimer, *Safed*
 Shmuel Odes, *Beer Sheva*
 Mark Pines, *Bet Dagan*
 Ron Shaoul, *Haifa*
 Ami D Sperber, *Beer-Sheva*



Italy

Donato F Altomare, *Bari*
 Piero Amodio, *Padova*
 Angelo Andriulli, *San Giovanni Rotondo*
 Paolo Angeli, *Padova*
 Bruno Annibale, *Rome*
 Paolo Aurello, *Rome*
 Salvatore Auricchio, *Naples*
 Antonio Basoli, *Rome*
 Claudio Bassi, *Verona*
 Gabrio Bassotti, *Perugia*
 Mauro Bernardi, *Bologna*
 Alberto Biondi, *Rome*
 Luigi Bonavina, *Milano*
 Guglielmo Borgia, *Naples*
 Roberto Berni Canani, *Naples*
 Maria Gabriella Caruso, *Bari*
 Fausto Catena, *Bologna*
 Giuseppe Chiarioni, *Vareggio*
 Michele Cicala, *Rome*
 Dario Conte, *Milano*
 Francesco Costa, *Pisa*
 Antonio Craxi, *Palermo*
 Salvatore Cucchiara, *Rome*
 Giuseppe Currò, *Messina*
 Mario M D'Elios, *Florence*
 Mirko D'Onofrio, *Verona*
 Silvio Danese, *Milano*
 Roberto de Franchis, *Milano*
 Paola De Nardi, *Milan*
 Giovanni D De Palma, *Naples*
 Giuliana Decorti, *Trieste*
 Gianlorenzo Dionigi, *Varese*
 Massimo Falconi, *Verona*
 Silvia Fargion, *Milan*
 Giammarco Fava, *Ancona*
 Francesco Feo, *Sassari*
 Alessandra Ferlini, *Ferrara*
 Alessandro Ferrero, *Torino*
 Mirella Fraquelli, *Milan*
 Luca Frulloni, *Verona*
 Giovanni B Gaeta, *Napoli*
 Antonio Gasbarrini, *Rome*
 Edoardo G Giannini, *Genoa*
 Alessandro Granito, *Bologna*
 Fabio Grizzi, *Milan*
 Salvatore Gruttadauria, *Palermo*
 Pietro Invernizzi, *Milan*
 Achille Iolascon, *Naples*
 Angelo A Izzo, *Naples*
 Ezio Laconi, *Cagliari*
 Giovanni Latella, *L'Aquila*
 Massimo Leverro, *Rome*
 Francesco Luzzza, *Catanzaro*
 Lucia Malaguarnera, *Catania*
 Francesco Manguso, *Napoli*
 Pier Mannuccio Mannucci, *Milan*
 Giancarlo Mansueto, *Verona*
 Giulio Marchesini, *Bologna*
 Mara Massimi, *Coppito*
 Giovanni Milito, *Rome*
 Giuseppe Montalto, *Palermo*
 Giovanni Monteleone, *Rome*
 Luca Morelli, *Trento*
 Giovanni Musso, *Torino*
 Mario Nano, *Torino*
 Gerardo Nardone, *Napoli*
 Riccardo Nascimbeni, *Brescia*
 Valerio Nobili, *Rome*
 Fabio Pace, *Milan*
 Nadia Peparini, *Rome*

Marcello Persico, *Naples*
 Mario Pescatori, *Rome*
 Raffaele Pezzilli, *Bologna*
 Alberto Piperno, *Monza*
 Anna C Piscaglia, *Rome*
 Piero Portincasa, *Bari*
 Michele Reni, *Milan*
 Vittorio Ricci, *Pavia*
 Oliviero Riggio, *Rome*
 Mario Rizzetto, *Torino*
 Ballarin Roberto, *Modena*
 Gerardo Rosati, *Potenza*
 Franco Roviello, *Siena*
 Cesare Ruffolo, *Treviso*
 Massimo Rugge, *Padova*
 Marco Scarpa, *Padova*
 Carmelo Scarpignato, *Parma*
 Giuseppe Sica, *Rome*
 Marco Silano, *Rome*
 Pierpaolo Sileri, *Rome*
 Vincenzo Stanghellini, *Bologna*
 Fiorucci Stefano, *Perugia*
 Giovanni Tarantino, *Naples*
 Alberto Tommasini, *Trieste*
 Guido Torzilli, *Rozzano Milan*
 Cesare Tosetti, *Porretta Terme*
 Antonello Trecca, *Rome*
 Vincenzo Villanacci, *Brescia*
 Lucia Ricci Vitiani, *Rome*
 Marco Vivarelli, *Bologna*



Japan

Kyoichi Adachi, *Izumo*
 Yasushi Adachi, *Sapporo*
 Takafumi Ando, *Nagoya*
 Akira Andoh, *Otsu*
 Masahiro Arai, *Tokyo*
 Hitoshi Asakura, *Tokyo*
 Kazuo Chijiwa, *Miyazaki*
 Yuichiro Eguchi, *Saga*
 Itaru Endo, *Yokohama*
 Munechika Enjoji, *Fukuoka*
 Yasuhiro Fujino, *Akashi*
 Mitsuhiro Fujishiro, *Tokyo*
 Kouhei Fukushima, *Sendai*
 Masanori Hatakeyama, *Tokyo*
 Keiji Hirata, *Kitakyushu*
 Toru Hiyama, *Higashihiroshima*
 Masahiro Iizuka, *Akita*
 Susumu Ikehara, *Osaka*
 Kenichi Ikejima, *Bunkyo-ku*
 Yutaka Inagaki, *Kanagawa*
 Hiromi Ishibashi, *Nagasaki*
 Shunji Ishihara, *Izumo*
 Toru Ishikawa, *Niigata*
 Toshiyuki Ishiwata, *Tokyo*
 Hajime Isomoto, *Nagasaki*
 Yoshiaki Iwasaki, *Okayama*
 Satoru Kakizaki, *Gunma*
 Terumi Kamisawa, *Tokyo*
 Mototsugu Kato, *Sapporo*
 Naoya Kato, *Tokyo*
 Takumi Kawaguchi, *Kurume*
 Yohei Kida, *Kainan*
 Shogo Kikuchi, *Aichi*
 Tsuneo Kitamura, *Chiba*
 Takashi Kobayashi, *Tokyo*
 Yasuhiro Koga, *Isehara*
 Takashi Kojima, *Sapporo*
 Norihiro Kokudo, *Tokyo*
 Masatoshi Kudo, *Osaka*
 Shin Maeda, *Tokyo*
 Satoshi Mamori, *Hyogo*
 Atsushi Masamune, *Sendai*
 Yasushi Matsuzaki, *Tsukuba*
 Kenji Miki, *Tokyo*
 Toshihiro Mitaka, *Sapporo*
 Hiroto Miwa, *Hyogo*
 Kotaro Miyake, *Tokushima*
 Manabu Morimoto, *Yokohama*
 Yoshiharu Motoo, *Kanazawa*
 Yoshiaki Murakami, *Hiroshima*
 Yoshiki Murakami, *Kyoto*
 Kunihiko Murase, *Tsushima*
 Akihito Nagahara, *Tokyo*
 Yuji Naito, *Kyoto*
 Atsushi Nakajima, *Yokohama*
 Hisato Nakajima, *Tokyo*
 Hiroki Nakamura, *Yamaguchi*
 Shotaro Nakamura, *Fukuoka*
 Akimasa Nakao, *Nagoya*
 Shuhei Nishiguchi, *Hyogo*
 Mikio Nishioka, *Niihama*
 Keiji Ogura, *Tokyo*
 Susumu Ohmada, *Maebashi*
 Hirohide Ohnishi, *Akita*
 Kenji Okajima, *Nagoya*
 Kazuichi Okazaki, *Osaka*
 Morikazu Onji, *Ehime*
 Satoshi Osawa, *Hamamatsu*
 Hidetsugu Saito, *Tokyo*
 Yutaka Saito, *Tokyo*
 Naoaki Sakata, *Sendai*
 Yasushi Sano, *Chiba*
 Tokihiko Sawada, *Tochigi*
 Tomohiko Shimatan, *Hiroshima*
 Yukihiko Shimizu, *Kyoto*
 Shinji Shimoda, *Fukuoka*
 Yoshio Shirai, *Niigata*
 Masayuki Sho, *Nara*
 Shoichiro Sumi, *Kyoto*
 Hidekazu Suzuki, *Tokyo*
 Masahiro Tajika, *Nagoya*
 Yoshihisa Takahashi, *Tokyo*
 Toshinari Takamura, *Kanazawa*
 Hiroaki Takeuchi, *Kochi*
 Yoshitaka Takuma, *Okayama*
 Akihiro Tamori, *Osaka*
 Atsushi Tanaka, *Tokyo*
 Shinji Tanaka, *Hiroshima*
 Satoshi Tanno, *Hokkaido*
 Shinji Togo, *Yokohama*
 Hitoshi Tsuda, *Tokyo*
 Hiroyuki Uehara, *Osaka*
 Masahito Uemura, *Kashihara*
 Yoshiyuki Ueno, *Sendai*
 Mitsuyoshi Urashima, *Tokyo*
 Takuya Watanabe, *Niigata*
 Satoshi Yamagiwa, *Niigata*
 Taketo Yamaguchi, *Chiba*
 Mitsunori Yamakawa, *Yamagata*
 Takayuki Yamamoto, *Yokkaichi*
 Yutaka Yata, *Maebashi*
 Hiroshi Yoshida, *Tokyo*
 Norimasa Yoshida, *Kyoto*
 Yuichi Yoshida, *Osaka*
 Kentaro Yoshika, *Toyoake*
 Hitoshi Yoshiji, *Nara*
 Katsutoshi Yoshizato, *Higashihiroshima*
 Tomoharu Yoshizumi, *Fukuoka*



Jordan

Ismail Matalka, *Irbid*

**Kuwait**

Islam Khan, *Safat*

**Lebanon**

Bassam N Abboud, *Beirut*
Ala I Sharara, *Beirut*
Rita Slim, *Beirut*

**Lithuania**

Giedrius Barauskas, *Kaunas*
Limas Kupcinskas, *Kaunas*

**Malaysia**

Andrew Seng Boon Chua, *Ipoh*

**Mexico**

Richard A Awad, *Mexico*
Aldo Torre Delgadillo, *Mexico*
Diego Garcia-Compean, *Monterrey*
Paulino M Hernández Magro, *Celaya*
Miguel Angel Mercado, *Distrito Federal*
Arturo Panduro, *Jalisco*
Omar Vergara-Fernandez, *Tlalpan*
Saúl Villa-Trevio, *Mexico*

**Moldova**

Igor Mishin, *Kishinev*

**Netherlands**

Ulrich Beuers, *Amsterdam*
Lee Bouwman, *Leiden*
Albert J Bredenoord, *Nieuwegein*
Lodewijk AA Brosens, *Utrecht*
J Bart A Crusius, *Amsterdam*
Wouter de Herder, *Rotterdam*
Pieter JF de Jonge, *Rotterdam*
Robert J de Knecht, *Rotterdam*
Wendy W Johanna de Leng, *Utrecht*
Annemarie de Vries, *Rotterdam*
James CH Hardwick, *Leiden*
Frank Hoentjen, *Haarlem*
Misha Luyer, *Sittard*
Jeroen Maljaars, *Maastricht*
Gerrit A Meijer, *Amsterdam*
Servaas Morré, *Amsterdam*
Chris JJ Mulder, *Amsterdam*
John Plukker, *Groningen*
Albert Frederik Pull ter Gunne, *Tilburg*
Paul E Sijens, *Groningen*
BW Marcel Spanier, *Arnhem*
Shiri Sverdlov, *Maastricht*
Maarten Tushuizen, *Amsterdam*
Jantine van Baal, *Heidelberglaan*
Astrid van der Velde, *The Hague*
Karel van Erpecum, *Utrecht*
Loes van Keimpema, *Nijmegen*

Robert Christiaan Verdonk, *Groningen*
Erwin G Zoetendal, *Wageningen*

**New Zealand**

Andrew S Day, *Christchurch*

**Norway**

Olav Dalgard, *Oslo*
Trond Peder Flaten, *Trondheim*
Reidar Fossmark, *Trondheim*
Rasmus Goll, *Tromsø*
Ole Høie, *Arendal*
Asle W Medhus, *Oslo*
Espen Melum, *Oslo*
Trine Olsen, *Tromsø*
Eyvind J Paulssen, *Tromsø*
Jon Arne Søreide, *Stavanger*
Kjetil Søreide, *Stavanger*

**Pakistan**

Shahab Abid, *Karachi*
Syed MW Jafri, *Karachi*

**Poland**

Marek Bebenek, *Wroclaw*
Tomasz Brzozowski, *Cracow*
Halina Cichoż-Lach, *Lublin*
Andrzej Dabrowski, *Bialystok*
Hanna Gregorek, *Warsaw*
Marek Hartleb, *Katowice*
Beata Jolanta Jabłońska, *Katowice*
Stanislaw J Konturek, *Krakow*
Jan Kulig, *Krakow*
Dariusz M Lebensztejn, *Bialystok*
Julian Swierczynski, *Gdansk*

**Portugal**

Raquel Almeida, *Porto*
Ana Isabel Lopes, *Lisboa Codex*
Ricardo Marcos, *Porto*
Guida Portela-Gomes, *Estoril*

**Romania**

Dan L Dumitrascu, *Cluj*
Adrian Saftoiu, *Craiova*
Andrada Seicean, *Cluj-Napoca*

**Russia**

Vasiliy I Reshetnyak, *Moscow*

**Saudi Arabia**

Ibrahim A Al Mofleh, *Riyadh*
Abdul-Wahed Meshikhes, *Qatif*
Faisal Sanai, *Riyadh*

**Serbia**

Tamara M Alempijevic, *Belgrade*
Dusan M Jovanovic, *Sremska Kamenica*
Zoran Krivokapic, *Belgrade*

**Singapore**

Madhav Bhatia, *Singapore*
Kong Weng Eu, *Singapore*
Brian Kim Poh Goh, *Singapore*
Khek-Yu Ho, *Singapore*
Kok Sun Ho, *Singapore*
Fock Kwong Ming, *Singapore*
London Lucien Ooi, *Singapore*
Nagarajan Perumal, *Singapore*
Francis Seow-Choen, *Singapore*

**South Africa**

Rosemary Joyce Burnett, *Pretoria*
Michael Kew, *Cape Town*

**South Korea**

Sang Hoon Ahn, *Seoul*
Sung-Gil Chi, *Seoul*
Myung-Gyu Choi, *Seoul*
Hoon Jai Chun, *Seoul*
Yeun-Jun Chung, *Seoul*
Young-Hwa Chung, *Seoul*
Kim Donghee, *Seoul*
Ki-Baik Hahm, *Incheon*
Sun Pyo Hong, *Geonggi-do*
Seong Gyu Hwang, *Seongnam*
Hong Joo Kim, *Seoul*
Jae J Kim, *Seoul*
Jin-Hong Kim, *Suwon*
Nayoung Kim, *Seongnam-si*
Sang Geon Kim, *Seoul*
Seon Hahn Kim, *Seoul*
Sung Kim, *Seoul*
Won Ho Kim, *Seoul*
Jeong Min Lee, *Seoul*
Kyu Taek Lee, *Seoul*
Sang Kil Lee, *Seoul*
Sang Yeoup Lee, *Gyeongsangnam-do*
Yong Chan Lee, *Seoul*
Eun-Yi Moon, *Seoul*
Hyoung-Chul Oh, *Seoul*
Seung Woon Paik, *Seoul*
Joong-Won Park, *Goyang*
Ji Kon Ryu, *Seoul*
Si Young Song, *Seoul*
Marie Yeo, *Suwon*
Byung Chul Yoo, *Seoul*
Dae-Yeul Yu, *Daejeon*

**Spain**

Maria-Angeles Aller, *Madrid*
Raul J Andrade, *Málaga*
Luis Aparisi, *Valencia*
Gloria González Aseguinolaza, *Navarra*
Matias A Avila, *Pamplona*

Fernando Azpiroz, *Barcelona*
 Ramon Bataller, *Barcelona*
 Belén Beltrán, *Valencia*
 Adolfo Benages, *Valencia*
 Josep M Bordas, *Barcelona*
 Lisardo Boscá, *Madrid*
 Luis Bujanda, *San Sebastián*
 Juli Busquets, *Barcelona*
 Matilde Bustos, *Pamplona*
 José Julián calvo Andrés, *Salamanca*
 Andres Cardenas, *Barcelona*
 Antoni Castells, *Barcelona*
 Fernando J Corrales, *Pamplona*
 JEDomínguez-Muñoz, *Santiago de Compostela*
 Juan Carlos Laguna Egea, *Barcelona*
 Isabel Fabregat, *Barcelona*
 Antoni Farré, *Barcelona*
 Vicente Felipo, *Valencia*
 Laureano Fernández-Cruz, *Barcelona*
 Luis Grande, *Barcelona*
 Angel Lanas, *Zaragoza*
 Juan-Ramón Larrubia, *Guadalajara*
 María IT López, *Jaén*
 Juan Macías, *Seville*
 Javier Martin, *Granada*
 José Manuel Martin-Villa, *Madrid*
 Julio Mayol, *Madrid*
 Mireia Miquel, *Sabadell*
 Albert Parés, *Barcelona*
 Jesús M Prieto, *Pamplona*
 Pedro L Majano Rodriguez, *Madrid*
 Joan Roselló-Catafau, *Barcelona*
 Eva Vaquero, *Barcelona*



Sweden

Lars Erik Agréus, *Stockholm*
 Mats Andersson, *Stockholm*
 Roland Andersson, *Lund*
 Mauro D'Amato, *Huddinge*
 Evangelos Kalaitzakis, *Gothenburg*
 Greger Lindberg, *Stockholm*
 Annika Lindblom, *Stockholm*
 Sara Lindén, *Göteborg*
 Hanns-Ulrich Marschall, *Stockholm*
 Pär Erik Myreliid, *Linköping*
 Åke Nilsson, *Lund*
 Helena Nordenstedt, *Stockholm*
 Kjell Öberg, *Uppsala*
 Lars A Pahlman, *Uppsala*
 Stefan G Pierzynowski, *Lund*
 Sara Regnér, *Malmö*
 Bobby Tingstedt, *Lund*
 Zongli Zheng, *Stockholm*



Switzerland

Pascal Bucher, *Geneva*
 Michelangelo Foti, *Geneva*
 Jean L Frossard, *Geneva*
 Andreas Geier, *Zürich*
 Pascal Gervaz, *Geneva*
 Gerd A Kullak-Ublick, *Zürich*
 Fabrizio Montecucco, *Geneva*
 Paul M Schneider, *Zürich*
 Felix Stickel, *Berne*
 Bruno Stieger, *Zürich*
 Inti Zlobec, *Basel*



Trinidad and Tobago

Shivananda Nayak, *Mount Hope*



Turkey

Sinan Akay, *Tekirdag*
 Metin Basaranoglu, *Istanbul*
 Yusuf Bayraktar, *Ankara*
 A Mithat Bozdayi, *Ankara*
 Hayrullah Deric, *Balıkesir*
 Eren Ersoy, *Ankara*
 Mukaddes Esrefoglu, *Malatya*
 Can Goen, *Kutahya*
 Selin Kapan, *Istanbul*
 Aydin Karabacakoglu, *Konya*
 Cuneyt Kayaalp, *Malatya*
 Kemal Kismet, *Ankara*
 Seyfettin Köklü, *Ankara*
 Mehmet Refik Mas, *Etilik-Ankara*
 Osman C Ozdogan, *Istanbul*
 Bülent Salman, *Ankara*
 Orhan Sezgin, *Mersin*
 Ilker Tasci, *Ankara*
 Müge Tecder-Ünal, *Ankara*
 Ahmet Tekin, *Mersin*
 Mesut Tez, *Ankara*
 Ekmel Tezel, *Ankara*
 Özlem Yilmaz, *Izmir*



United Arab Emirates

Fikri M Abu-Zidan, *Al-Ain*
 Sherif M Karam, *Al-Ain*



United Kingdom

Simon Afford, *Birmingham*
 Navneet K Ahluwalia, *Stockport*
 Mohamed H Ahmed, *Southampton*
 Basil Ammori, *Salford*
 Lesley A Anderson, *Belfast*
 Chin Wee Ang, *Liverpool*
 Yeng S Ang, *Wigan*
 Anthony TR Axon, *Leeds*
 Kathleen B Bamford, *London*
 Jim D Bell, *London*
 John Beynon, *Swansea*
 Chris Briggs, *Sheffield*
 Geoffrey Burnstock, *London*
 Alastair D Burt, *Newcastle*
 Jeff Butterworth, *Shrewsbury*
 Jeremy FL Cobbold, *London*
 Jean E Crabtree, *Leeds*
 Tatjana Crnogorac-Jurcevic, *London*
 William Dickey, *Londonderry*
 Sunil Dolwani, *Cardiff*
 Emad M El-Omar, *Aberdeen*
 A M El-Tawil, *Birmingham*
 Charles B Ferguson, *Belfast*
 Andrew Fowell, *Southampton*
 Piers Gatenby, *London*
 Daniel R Gaya, *Edinburgh*
 Anil George, *London*
 Rob Glynne-Jones, *Northwood*
 Jason CB Goh, *Birmingham*
 Gianpiero Gravante, *Leicester*

Brian Green, *Belfast*
 William Greenhalf, *Liverpool*
 Indra N Guha, *Nottingham*
 Stefan G Hübscher, *Birmingham*
 Robin Hughes, *London*
 Pali Hungin, *Stockton*
 Nawfal Hussein, *Nottingham*
 Clement W Imrie, *Glasgow*
 Janusz AZ Jankowski, *Oxford*
 Sharad Karandikar, *Birmingham*
 Peter Karayiannis, *London*
 Shahid A Khan, *London*
 Patricia F Lalor, *Birmingham*
 John S Leeds, *Sheffield*
 Ian Lindsey, *Oxford*
 Hong-Xiang Liu, *Cambridge*
 Dileep N Lobo, *Nottingham*
 Graham MacKay, *Glasgow*
 Mark Edward McAlindon, *Sheffield*
 Anne McCune, *Bristol*
 Donald Campbell McMillan, *Glasgow*
 Giorgina Mieli-Vergani, *London*
 Jamie Murphy, *London*
 Guy Fairbairn Nash, *Poole*
 James Neuberger, *Birmingham*
 Patrick O'Dwyer, *Glasgow*
 Christos Paraskeva, *Bristol*
 Richard Parker, *North Staffordshire*
 Thamara Perera, *Birmingham*
 Kondragunta Rajendra Prasad, *Leeds*
 D Mark Pritchard, *Liverpool*
 Alberto Quaglia, *London*
 Akhilesh B Reddy, *Cambridge*
 Kevin Robertson, *Glasgow*
 Sanchoy Sarkar, *Liverpool*
 John B Schofield, *Kent*
 Marco Senzolo, *Padova*
 Venkatesh Shanmugam, *Derby*
 Paul Sharp, *London*
 Chew Thean Soon, *Manchester*
 Aravind Suppiah, *East Yorkshire*
 Noriko Suzuki, *Middlesex*
 Simon D Taylor-Robinson, *London*
 Frank I Tovey, *London*
 A McCulloch Veitch, *Wolverhampton*
 Vamsi R Velchuru, *Lowestoft*
 Sumita Verma, *Brighton*
 Catherine Walter, *Cheltenham*
 Julian RF Walters, *London*
 Roger Williams, *London*



United States

Kareem M Abu-Elmagd, *Pittsburgh*
 Sami R Achem, *Florida*
 Golo Ahlenstiel, *Bethesda*
 Bhupinder S Anand, *Houston*
 M Ananthanarayanan, *New York*
 Balamurugan N Appakalal, *Minneapolis*
 Dimitrios V Avgerinos, *New York*
 Shashi Bala, *Worcester*
 Anthony J Bauer, *Pittsburgh*
 Kevin E Behrns, *Gainesville*
 Roberto Bergamaschi, *New York*
 Henry J Binder, *New Haven*
 Edmund J Bini, *New York*
 Wojciech Blonski, *Philadelphia*
 Mark Bloomston, *Columbus*
 Edward L Bradley III, *Sarasota*
 Carla W Brady, *Durham*

David A Brenner, *San Diego*
 Adeel A Butt, *Pittsburgh*
 Shi-Ying Cai, *New Haven*
 Justin MM Cates, *Nashville*
 Eugene P Ceppa, *Durham*
 Jianyuan Chai, *Long Beach*
 Ronald S Chamberlain, *Livingston*
 Fei Chen, *Morgantown*
 Xian-Ming Chen, *Omaha*
 Ramsey Chi-man Cheung, *Palo Alto*
 Denesh Chitkara, *East Brunswick*
 Clifford S Cho, *Madison*
 Parimal Chowdhury, *Arkansas*
 John David Christein, *Birmingham*
 Thomas Clancy, *Boston*
 Ana J Coito, *Los Angeles*
 Ricardo Alberto Cruciani, *New York*
 Joseph J Cullen, *Iowa City*
 Mark J Czaja, *New York*
 Mariana D Dabeva, *Bronx*
 Jessica A Davila, *Houston*
 Conor P Delaney, *Cleveland*
 Laurie DeLeve, *Los Angeles*
 Anthony J Demetris, *Pittsburgh*
 Sharon DeMorrow, *Temple*
 Bijan Eghtesad, *Cleveland*
 Yoram Elitsur, *Huntington*
 Mohamad A Eloubeidi, *Alabama*
 Wael El-Rifai, *Nashville*
 Sukru H Emre, *New Haven*
 Giamila Fantuzzi, *Chicago*
 Ashkan Farhadi, *Irvine*
 Ronnie Fass, *Tucson*
 Martín E Fernández-Zapico, *Rochester*
 Alessandro Fichera, *Chicago*
 Josef E Fischer, *Boston*
 Piero Marco Fisichella, *Maywood*
 Fritz Francois, *New York*
 Glenn T Furuta, *Aurora*
 T Clark Gamblin, *Pittsburgh*
 Henning Gerke, *Iowa City*
 Jean-Francois Geschwind, *Baltimore*
 R Mark Ghobrial, *Texas*
 John F Gibbs, *Buffalo*
 Shannon S Glaser, *Temple*
 Ajay Goel, *Dallas*
 Jon C Gould, *Madison*
 Eileen F Grady, *San Francisco*
 James H Grendell, *New York*
 John R Grider, *Richmond*
 Anna S Gukovskaya, *Los Angeles*
 Chakshu Gupta, *St. Joseph*
 Grigoriy E Gurvits, *New York*
 Hai-Yong Han, *Phoenix*
 Yuan-Ping Han, *Los Angeles*
 Imran Hassan, *Springfield*
 Charles P Heise, *Madison*
 Lisa J Herrinton, *Oakland*
 Oscar Joe Hines, *Los Angeles*
 Samuel B Ho, *San Diego*
 Steven Hochwald, *Gainesville*
 Richard Hu, *Los Angeles*
 Eric S Hungness, *Chicago*
 Jamal A Ibdah, *Columbia*
 Atif Iqbal, *Omaha*
 Hartmut Jaeschke, *Tucson*
 Donald M Jensen, *Chicago*
 Robert Jensen, *Bethesda*
 Leonard R Johnson, *Memphis*
 Andreas M Kaiser, *Los Angeles*
 JingXuan Kang, *Charlestown*
 John Y Kao, *Michigan*
 Randeep Singh Kashyap, *New York*
 Rashmi Kaul, *Tulsa*

Jonathan D Kaunitz, *Los Angeles*
 Stephen M Kavic, *Baltimore*
 Ali Keshavarzian, *Chicago*
 Amir Maqbul Khan, *Marshall*
 Kusum K Kharbanda, *Omaha*
 Chang Kim, *West Lafayette*
 Dean Y Kim, *Detroit*
 Miran Kim, *Providence*
 Burton I Korelitz, *New York*
 Josh Korzenik, *Boston*
 Richard A Kozarek, *Seattle*
 Alyssa M Krasinskas, *Pittsburgh*
 Shiu-Ming Kuo, *Buffalo*
 Michelle Lai, *Boston*
 Michael Leitman, *New York*
 Dong-Hui Li, *Houston*
 Ming Li, *New Orleans*
 Zhiping Li, *Baltimore*
 Gary R Lichtenstein, *Philadelphia*
 Chen Liu, *Gainesville*
 Zhang-Xu Liu, *Los Angeles*
 Craig D Logsdon, *Houston*
 Kaye M Reid Lombardo, *Rochester*
 Michael R Lucey, *Madison*
 Kirk Ludwig, *Wisconsin*
 James D Luketich, *Pittsburgh*
 Patrick M Lynch, *Houston*
 John S Macdonald, *New York*
 Willis C Maddrey, *Dallas*
 Mercedes Susan Mandell, *Aurora*
 Christopher Mantyh, *Durham*
 Wendy M Mars, *Pittsburgh*
 John Marshall, *Columbia*
 Robert CG Martin, *Louisville*
 Laura E Matarese, *Pittsburgh*
 Craig J McClain, *Louisville*
 Lynne V McFarland, *Washington*
 David J McGee, *Shreveport*
 Valentina Medici, *Sacramento*
 Stephan Menne, *New York*
 Didier Merlin, *Atlanta*
 George Michalopoulos, *Pittsburgh*
 James M Millis, *Chicago*
 Pramod K Mistry, *New Haven*
 Emiko Mizoguchi, *Boston*
 Huanbiao Mo, *Denton*
 Robert C Moesinger, *Ogden*
 Smruti R Mohanty, *Chicago*
 John Morton, *Stanford*
 Peter L Moses, *Burlington*
 Sandeep Mukherjee, *Omaha*
 Million Mulugeta, *Los Angeles*
 Michel M Murr, *Tampa*
 Pete Muscarella, *Columbus*
 Ece A Mutlu, *Chicago*
 Masaki Nagaya, *Boston*
 Laura E Nagy, *Cleveland*
 Aejaz Nasir, *Tampa*
 Udayakumar Navaneethan, *Cincinnati*
 Stephen JD O'Keefe, *Pittsburgh*
 Robert D Odze, *Boston*
 Giuseppe Orlando, *Winston Salem*
 Pal Pacher, *Rockville*
 Georgios Papachristou, *Pittsburgh*
 Jong Park, *Tampa*
 William R Parker, *Durham*
 Mansour A Parsi, *Cleveland*
 Marco Giuseppe Patti, *Chicago*
 Zhiheng Pei, *New York*
 CS Pitchumoni, *New Brunswick*
 Parviz M Pour, *Omaha*
 Xiaofa Qin, *Newark*
 Florencia Georgina Que, *Rochester*
 Massimo Raimondo, *Jacksonville*

Raymund R Razonable, *Minnesota*
 Kevin Michael Reavis, *Orange*
 Robert V Rege, *Dallas*
 Douglas K Rex, *Indianapolis*
 Victor E Reyes, *Galveston*
 Basil Rigas, *New York*
 Richard A Rippe, *Chapel Hill*
 Alexander S Rosemurgy, *Tampa*
 Philip Rosenthal, *San Francisco*
 Raul J Rosenthal, *Weston*
 Joel H Rubenstein, *Ann Arbor*
 Shawn D Safford, *Norfolk*
 Rabih M Salloum, *Rochester*
 Bruce E Sands, *Boston*
 Tor C Savidge, *Galveston*
 Michael L Schilsky, *New Haven*
 Beat Schnüriger, *California*
 Robert E Schoen, *Pittsburgh*
 Matthew James Schuchert, *Pittsburgh*
 Ekihiro Seki, *La Jolla*
 Le Shen, *Chicago*
 Perry Shen, *Winston-Salem*
 Stuart Sherman, *Indianapolis*
 Mitchell L Shiffman, *Richmond*
 Shivendra Shukla, *Columbia*
 Bronislaw L Slomiany, *Newark*
 Scott Steele, *Fort Lewis*
 Branko Stefanovic, *Tallahassee*
 Lygia Stewart, *San Francisco*
 Luca Stocchi, *Cleveland*
 Daniel S Straus, *Riverside*
 Robert Todd Striker, *Madison*
 Jonathan Strosberg, *Tampa*
 Christina Surawicz, *Seattle*
 Patricia Sylla, *Boston*
 Wing-Kin Syn, *Durham*
 Yvette Taché, *Los Angeles*
 Kazuaki Takabe, *Richmond*
 Kam-Meng Tchou-Wong, *New York*
 Klaus Thaler, *Columbia*
 Charles Thomas, *Oregon*
 Natalie J Torok, *Sacramento*
 George Triadafilopoulos, *Stanford*
 Chung-Jyi Tsai, *Lexington*
 Thérèse Tuohy, *Salt Lake City*
 Andrew Ukleja, *Florida*
 Santhi Swaroop Vege, *Rochester*
 Aaron Vinik, *Norfolk*
 Dinesh Vyas, *Washington*
 Arnold Wald, *Wisconsin*
 Scott A Waldman, *Philadelphia*
 Jack R Wands, *Providence*
 Jiping Wang, *Boston*
 Irving Waxman, *Chicago*
 Wilfred M Weinstein, *Los Angeles*
 Steven D Wexner, *Weston*
 John W Wiley, *Ann Arbor*
 Jackie Wood, *Ohio*
 Jian Wu, *Sacramento*
 Wen Xie, *Pittsburgh*
 Guang-Yin Xu, *Galveston*
 Fang Yan, *Nashville*
 Radha Krishna Yellapu, *New York*
 Anthony T Yeung, *Philadelphia*
 Zobair M Younossi, *Virginia*
 Liqing Yu, *Winston-Salem*
 Run Yu, *Los Angeles*
 Ruben Zamora, *Pittsburgh*
 Michael E Zenilman, *New York*
 Mark A Zern, *Sacramento*
 Lin Zhang, *Pittsburgh*
 Martin D Zielinski, *Rochester*
 Michael A Zimmerman, *Colorado*



Contents

Weekly Volume 17 Number 1 January 7, 2011

EDITORIAL

- 1 Peroral cholangioscopy in the new millennium
Parsi MA
- 7 Imaging techniques used for the real-time assessment of angiogenesis in digestive cancers
Săftoiu A, Vilmann P

TOPIC HIGHLIGHT

- 9 Autofluorescence imaging and magnification endoscopy
Filip M, Iordache S, Săftoiu A, Ciurea T
- 15 Optical coherence tomography and Doppler optical coherence tomography in the gastrointestinal tract
Osiac E, Săftoiu A, Gheonea DI, Mandrila I, Angelescu R
- 21 Confocal laser endomicroscopy and immunoendoscopy for real-time assessment of vascularization in gastrointestinal malignancies
Gheonea DI, Cârțână T, Ciurea T, Popescu C, Bădăraș A, Săftoiu A
- 28 Contrast-enhanced and targeted ultrasound
Postema M, Gilja OH
- 42 Contrast-enhanced endoscopic ultrasonography
Reddy NK, Ioncică AM, Săftoiu A, Vilmann P, Bhutani MS
- 49 Hybrid ultrasound imaging techniques (fusion imaging)
Sandulescu DL, Dumitrescu D, Rogoveanu I, Săftoiu A
- 53 Optical molecular imaging for detection of Barrett's-associated neoplasia
Thekkekk N, Anandasabapathy S, Richards-Kortum R

REVIEW

- 63 New endoscopic approaches in IBD
Neumann H, Neurath MF, Mudter J

ORIGINAL ARTICLE	69	<p>S100A4 over-expression underlies lymph node metastasis and poor prognosis in colorectal cancer</p> <p><i>Huang LY, Xu Y, Cai GX, Guan ZQ, Sheng WQ, Lu HF, Xie LQ, Lu HJ, Cai SJ</i></p>
	79	<p>MiRNA profile in esophageal squamous cell carcinoma: Downregulation of miR-143 and miR-145</p> <p><i>Wu BL, Xu LY, Du ZP, Liao LD, Zhang HF, Huang Q, Fang GQ, Li EM</i></p>
BRIEF ARTICLE	89	<p>Impact of diet on long-term decline in gastric cancer incidence in Poland</p> <p><i>Jarosz M, Sekula W, Rychlik E, Figurska K</i></p>
	98	<p>Endoscopic management of occluded biliary uncovered metal stents: A multicenter experience</p> <p><i>Katsinelos P, Beltsis A, Chatzimavroudis G, Paikos D, Paroutoglou G, Kapetanios D, Terzoudis S, Lazaraki G, Pilpilidis I, Fasoulas K, Atmatzidis S, Zavos C, Kountouras J</i></p>
	105	<p>Effect of ginger on gastric motility and symptoms of functional dyspepsia</p> <p><i>Hu ML, Rayner CK, Wu KL, Chuah SK, Tai WC, Chou YP, Chiu YC, Chiu KW, Hu TH</i></p>
	111	<p>Protection of the liver against CCl₄-induced injury by intramuscular electrotransfer of a kallistatin-encoding plasmid</p> <p><i>Diao Y, Zhao XF, Lin JS, Wang QZ, Xu RA</i></p>
	118	<p>Risk factors and gene polymorphisms of inflammatory bowel disease in population of Zhejiang, China</p> <p><i>Wang ZW, Ji F, Teng WJ, Yuan XG, Ye XM</i></p>
	123	<p>Surgical vs percutaneous radiofrequency ablation for hepatocellular carcinoma in dangerous locations</p> <p><i>Huang JW, Hernandez-Alejandro R, Croome KP, Yan LN, Wu H, Chen ZY, Prasoon P, Zeng Y</i></p>
CASE REPORT	130	<p>Foregut duplication cysts: A report of two cases with emphasis on embryogenesis</p> <p><i>Khoury T, Rivera L</i></p>
LETTERS TO THE EDITOR	135	<p>Duplicated appendix complicated by appendiceal cancer</p> <p><i>Freeman HJ</i></p>

Contents

World Journal of Gastroenterology
Volume 17 Number 1 January 7, 2011

ACKNOWLEDGMENTS I Acknowledgments to reviewers of *World Journal of Gastroenterology*

APPENDIX I Meetings
I-VI Instructions to authors

ABOUT COVER Neumann H, Neurath MF, Mudter J. New endoscopic approaches in IBD.
World J Gastroenterol 2011; 17(1): 63-68
<http://www.wjgnet.com/1007-9327/full/v17/i1/63.htm>

AIM AND SCOPE *World Journal of Gastroenterology* (*World J Gastroenterol*, *WJG*, print ISSN 1007-9327, DOI: 10.3748) is a weekly, open-access, peer-reviewed journal supported by an editorial board of 1144 experts in gastroenterology and hepatology from 60 countries.
The major task of *WJG* is to report rapidly the most recent results in basic and clinical research on esophageal, gastrointestinal, liver, pancreas and biliary tract diseases, *Helicobacter pylori*, endoscopy and gastrointestinal surgery, including: gastroesophageal reflux disease, gastrointestinal bleeding, infection and tumors; gastric and duodenal disorders; intestinal inflammation, microflora and immunity; celiac disease, dyspepsia and nutrition; viral hepatitis, portal hypertension, liver fibrosis, liver cirrhosis, liver transplantation, and metabolic liver disease; molecular and cell biology; geriatric and pediatric gastroenterology; diagnosis and screening, imaging and advanced technology.

FLYLEAF I-VII Editorial Board

EDITORS FOR THIS ISSUE

Responsible Assistant Editor: *Xiao-Fang Liu*
Responsible Electronic Editor: *Wen-Hua Ma*
Proofing Editor-in-Chief: *Lian-Sheng Ma*

Responsible Science Editor: *Li Xu*
Proofing Editorial Office Director: *Jian-Xia Cheng*

NAME OF JOURNAL

World Journal of Gastroenterology

LAUNCH DATE

October 1, 1995

RESPONSIBLE INSTITUTION

Department of Science and Technology of Shanxi Province

SPONSOR

Taiyuan Research and Treatment Center for Digestive Diseases, 77 Shuangta Xijie, Taiyuan 030001, Shanxi Province, China

EDITING

Editorial Board of *World Journal of Gastroenterology*, Room 903, Building D, Ocean International Center, No. 62 Dongsihuan Zhonglu, Chaoyang District, Beijing 100025, China
Telephone: +86-10-5908-0039
Fax: +86-10-8538-1893
E-mail: wjg@wjgnet.com
<http://www.wjgnet.com>

PUBLISHING

Baishideng Publishing Group Co., Limited, Room 1701, 17/F, Henan Building, No.90 Jaffe Road, Wanchai, Hong Kong, China
Fax: +852-3115-8812
Telephone: +852-5804-2046
E-mail: baishideng@wjgnet.com
<http://www.wjgnet.com>

SUBSCRIPTION

Beijing Baishideng BioMed Scientific Co., Ltd., Room 903, Building D, Ocean International Center, No. 62 Dongsihuan Zhonglu, Chaoyang District, Beijing 100025, China
Telephone: +86-10-8538-1892
Fax: +86-10-8538-1893
E-mail: baishideng@wjgnet.com
<http://www.wjgnet.com>

PRINT SUBSCRIPTION

RMB 245 Yuan for each issue, RMB 11760 Yuan for one year.

ONLINE SUBSCRIPTION

One-Year Price 864.00 USD

PUBLICATION DATE

January 7, 2011

CSSN

ISSN 1007-9327 (print)
ISSN 2219-2840 (online)

HONORARY EDITORS-IN-CHIEF

James L. Boyer, *New Haven*
Ke-Ji Chen, *Beijing*
Martin H Floch, *New Haven*
Geng-Tao Liu, *Beijing*
Emmet B Keefe, *Palo Alto*
Lein-Ray Mo, *Tainan*
Eamonn M Quigley, *Cork*
Rafiq A Sheikh, *Sacramento*
Nicholas J Talley, *Rochester*
Ming-Lung Yu, *Kaohsiung*

PRESIDENT AND EDITOR-IN-CHIEF

Lian-Sheng Ma, *Beijing*

ACADEMIC EDITOR-IN-CHIEF

Tauseef Ali, *Oklahoma*
Mauro Bortolotti, *Bologna*
Tarkan Karakan, *Ankara*
Weekitt Kittisupamongkol, *Bangkok*
Anastasios Koulaouzidis, *Edinburgh*
Gerd A Kullak-Ublick, *Zürich*
Bo-Rong Pan, *Xi'an*
Sylvia LF Pender, *Southampton*
Max S Petrov, *Auckland*
George Y Wu, *Farmington*

STRATEGY ASSOCIATE EDITORS-IN-CHIEF

Peter Draganov, *Florida*
Hugh J Freeman, *Vancouver*
Maria Concepción Gutiérrez-Ruiz, *México*
Kazuhiro Hanazaki, *Kochi*

Akio Inui, *Kagoshima*
Kalpesh Jani, *Baroda*
Javier S Martin, *Punta del Este*
Natalia A Osna, *Omaha*
Wei Tang, *Tokyo*
Alan BR Thomson, *Edmonton*
Harry HX Xia, *Hanover*

ASSOCIATE EDITORS-IN-CHIEF

You-Yong Lu, *Beijing*
John M Luk, *Pokfulam*
Hiroshi Shimada, *Yokohama*

EDITORIAL OFFICE

Jian-Xia Cheng, Director
World Journal of Gastroenterology
Room 903, Building D, Ocean International Center, No. 62 Dongsihuan Zhonglu, Chaoyang District, Beijing 100025, China
Telephone: +86-10-5908-0039
Fax: +86-10-8538-1893
E-mail: wjg@wjgnet.com
<http://www.wjgnet.com>

COPYRIGHT

© 2011 Baishideng. All rights reserved; no part of this publication may be reproduced, stored in a retrieval system, or transmitted in any form or by any means, electronic, mechanical, photocopying, recording, or otherwise without the prior permission of Baishideng. Authors are required to grant *World Journal of Gastroenterology* an exclusive license to publish.

SPECIAL STATEMENT

All articles published in this journal represent the viewpoints of the authors except where indicated otherwise.

INSTRUCTIONS TO AUTHORS

Full instructions are available online at http://www.wjgnet.com/1007-9327/g_info_20100315215714.htm. If you do not have web access please contact the editorial office.

ONLINE SUBMISSION

<http://www.wjgnet.com/1007-9327/office>



Peroral cholangioscopy in the new millennium

Mansour A Parsi

Mansour A Parsi, Center for Endoscopy and Pancreatobiliary Disorders, Department of Gastroenterology and Hepatology, Digestive Disease Institute, Cleveland Clinic, Cleveland, OH 44195, United States

Author contributions: Parsi MA contributed entirely to this manuscript.

Correspondence to: Mansour A Parsi, MD, Center for Endoscopy and Pancreatobiliary Disorders, Department of Gastroenterology and Hepatology, Digestive Disease Institute, Cleveland Clinic, 9500 Euclid Avenue, Desk A31, Cleveland, OH 44195, United States. parsim@ccf.org

Telephone: +1-216-4454880 **Fax:** +1-216-4446284

Received: July 15, 2010 **Revised:** August 27, 2010

Accepted: September 4, 2010

Published online: January 7, 2011

Abstract

Peroral cholangioscopy was first described in 1970s and has recently gained popularity. Peroral cholangioscopy is appealing to therapeutic endoscopists because a direct intraluminal view of the biliary duct system offers possibilities for diagnosis and interventions beyond that which other imaging or endoscopic modalities can provide. As the image quality of cholangioscopies improves, so too does their diagnostic capability, and as their durability and maneuverability increases, so too does their potential use for therapeutic applications. This editorial is intended to provide a brief review of recent developments in peroral cholangioscopy and current indications for its use.

© 2011 Baishideng. All rights reserved.

Key words: Endoscopic retrograde cholangiopancreatography; Cholangioscopy; Peroral cholangioscopy; Cholangiocarcinoma; Biliary stricture; Pancreatic cancer; Biopsy; Brush cytology

Peer reviewer: Richard A Kozarek, MD, Executive Director, Digestive Disease Institute, Virginia Mason Medical Center 1100 Ninth Avenue, PO Box 900, Seattle, WA 98111-0900, United States

Parsi MA. Peroral cholangioscopy in the new millennium. *World J Gastroenterol* 2011; 17(1): 1-6 Available from: URL: <http://www.wjgnet.com/1007-9327/full/v17/i1/1.htm> DOI: <http://dx.doi.org/10.3748/wjg.v17.i1.1>

INTRODUCTION

Diseases of the biliary system are frequently encountered in clinical practice^[1]. An examination of the bile ducts is often required for the appropriate diagnosis and management of patients with biliary diseases. The dramatic technical advances of flexible endoscopy during the last four decades have resulted in endoscopic retrograde cholangiopancreatography (ERCP) being used as a primary method of diagnosing and treating many biliary diseases^[1]. In the United States alone, approximately half a million ERCP procedures are performed annually. ERCP can demonstrate the anatomy of the biliary tract and reveal anatomical abnormalities, strictures and intraductal filling defects. However, this technique does not always differentiate the biological nature of bile duct lesions and can fail to determine their intraluminal extension. Furthermore, it is unable to provide information about biliary mucosal lesions that do not project into the biliary lumen. Peroral cholangioscopy as an adjunct to ERCP is a promising procedure that provides direct visualization of the biliary tree. It has been shown to have value in treating difficult-to-remove biliary stones^[2], assessing indeterminate biliary strictures^[3], and distinguishing between different intraductal lesions of the biliary tree^[4]. In recent years, cholangioscopy has gained popularity in the United States and is being performed in increasing numbers not only in academic institutions and large tertiary care referral centers, but also in smaller hospitals and private practices. In this paper, clinical applications of peroral cholangioscopy and its role in diagnosis and management of biliary disorders are reviewed.

HISTORICAL PERSPECTIVES

The first peroral cholangioscopy was performed in 1975

Table 1 Comparison of currently available single and dual operator cholangioscopies

	Endoscopists needed	Image quality	Tip deflection	Simultaneous irrigation and instrumentation	Fragility
Single operator (SpyGlass)	One	Moderate - good	4 way (up/down, left/right)	Yes	No ¹
Dual operator					
Fiberoptic cholangioscopies	Two	Moderate - good	2 way (up/down)	No	Yes
Video cholangioscopies	Two	Excellent	2 way (up/down)	No	Yes

¹All components of the spyglass system are single-use with the exception of the spyprobe (the light and image conveyor of the system) which is multi-use. The spyprobe is fragile and has to be handled with care.



Figure 1 Cholangioscopic view of normal intrahepatic biliary mucosa (image by a prototype video cholangioscope, CHF type Y0002, Olympus Corporation, Tokyo, Japan).

using a prototype cholangioscope that was thin enough to pass through the accessory channel of a duodenoscope^[5]. The concept of passing a thinner endoscope through a larger one later became known as the “mother-baby” or “mother-daughter” concept. Even today, almost all cholangioscopy systems are based on this concept. The initial prototype cholangioscope had poor image quality, no instrumentation or irrigation capability, and no tip deflection. Despite all its shortcomings, it proved that peroral cholangioscopy is feasible. In the mid-1980s second generation cholangioscopes were introduced^[5]. These cholangioscopies had added tip deflection and an accessory channel that could be used either for irrigation or instrumentation. In the late 1990s and early in the new millennium, advances in imaging technology led to the introduction of video cholangioscopies with improved image quality that enabled satisfactory views of the biliary mucosa (Figure 1). Addition of narrow band imaging (NBI) capability led to further improvements in detection of abnormal vascularization of biliary mucosa, which is of importance for diagnosis of certain biliary malignancies^[6]. The first semi-disposable single-operator cholangioscopy system was developed in 2005 and made it possible for a single endoscopist to operate both the baby and mother endoscopes.

SINGLE AND DUAL OPERATOR CHOLANGIOSCOPY SYSTEMS

In cholangioscopy, the terms “single operator” and “dual

operator” refer to the number of endoscopists required to perform the procedure. As a general rule, dual operator cholangioscopy systems require two endoscopists, while single operator cholangioscopy systems require only one endoscopist for performance. There are, however, reports of use of dual operator cholangioscopy systems by a single operator with the help of appropriate accessory equipment^[7].

Currently, most cholangioscopy systems are dual operator. Dual operator cholangioscopies of varying length, diameter and image quality are available. Most dual operator cholangioscopies have fiberoptic image quality. There is limited commercial availability of video cholangioscopies with enhanced image quality. At present, all video cholangioscopies with NBI capability are prototypes and not commercially available.

The only single operator cholangioscopy system currently available is the SpyGlass direct visualization system (Boston Scientific, Natick, MA, USA). This system is fiberoptic-based and has single and multi-use components.

Some of the advantages and disadvantages of the currently available single and dual operator cholangioscopies are summarized in Table 1.

CLINICAL APPLICATIONS

Several clinical applications for peroral cholangioscopy have been described. With expanded use, additional indications are expected to be reported. Clinical applications of cholangioscopy can be divided into common, uncommon and rare applications. Common applications include stone therapy and diagnosis of indeterminate biliary strictures. Uncommon applications include guidewire placement during ERCP, assessment of post-liver-transplantation biliary strictures, and evaluation of indeterminate intraductal filling defects or irregularities of the bile duct wall seen on imaging studies such as computed tomography (CT), magnetic resonance imaging (MRI), endoscopic ultrasound (EUS) or ERCP. Rare applications include staging and ablation of biliary neoplasms, investigation of recurrent pancreatitis, and evaluation of hemobilia.

Common applications

Currently, most peroral cholangioscopy procedures are performed for two indications: biliary stones and indeterminate biliary strictures.

Table 2 Common factors associated with failed biliary stone removal during endoscopic retrograde cholangiopancreatography

Patient factors
Abnormal anatomy
Prior surgery
Extremely J-shaped stomach
Large hernias
Malrotations
Unstable or difficult endoscope position
Short duodenal bulb
Abnormal anatomy
Long duodenoscope position
Bile duct abnormalities
Presence of ductal strictures
Severely dilated ducts
Stone factors
Size
Large size
Location
Intrahepatic
Cystic duct
Proximal to strictures
Impacted stones

Biliary stones

Difficult to remove stones: Gallstone disease or cholelithiasis continues to be a major health problem throughout the world, and affects 10%-20% of the Caucasian population^[8-13]. It has been estimated that 15%-20% of patients with gallstone disease also have stones in their bile ducts (choledocholithiasis)^[13]. Stones in the bile ducts have to be removed because of their potential to cause jaundice, cholangitis, and pancreatitis^[14-16]. This is accomplished in close to 95% of the cases during ERCP by conventional methods such as sphincterotomy with or without sphincter dilatation, use of extraction balloons or retrieval baskets, mechanical lithotripsy, or a combination of these methods^[17]. At times, however, stone extraction by standard methods is not possible. There are a number of reasons as to why some stones cannot be removed by conventional means; some of the most common of which are presented in Table 2.

A variety of methods have been devised for endoscopic extraction of stones that are not removable by conventional means during ERCP. As a general rule, these methods involve using shock waves to crush or fragment the stones inside the bile duct, with subsequent removal of the fragments (Figure 2). The shock waves for fragmentation of biliary stones are usually generated using electric spark (electrohydraulic lithotripsy) or laser light (laser lithotripsy). Probes that pass through the accessory channels of cholangioscopes for laser or electrohydraulic lithotripsy are commercially available. Although use of these probes through an extraction balloon under fluoroscopic guidance has been reported^[18,19], in our institution, we use them under direct visualization by utilizing a cholangioscope. These probes have to be precisely positioned on the stone to increase effectiveness and reduce complications. Direct visualization ensures that the shock waves

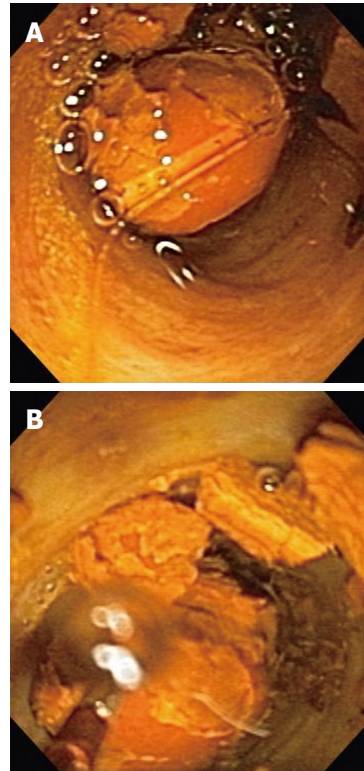


Figure 2 Cholangioscopic views of a bile duct stone prior to (A) and after (B) electrohydraulic lithotripsy. The lithotripsy probe is visible in the left lower corner of (B).

are aimed at the stone and not the bile duct wall, because shock waves delivered to the bile duct wall can cause bleeding and perforation. Direct visualization by cholangioscopy also allows distinction between stone fragments, air bubbles or blood clots, which can be indistinguishable on contrast cholangiography^[20].

Laser or electrohydraulic lithotripsy has been used for fragmentation and subsequent extraction of difficult to remove stones for many years, and both techniques have been shown to be safe and effective^[21,22]. In a recent multicenter study, cholangioscopy-guided laser or electrohydraulic lithotripsy were effective in > 90% of the cases^[2].

There are currently no randomized studies that have compared the effectiveness of laser and electrohydraulic lithotripsy for fragmentation and subsequent extraction of difficult-to-remove biliary stones.

Missed stones: Cholangioscopy allows detection of stones that might have been missed during cholangiography. Small stones can be “drowned” in contrast and be missed, and larger stones can block a duct, thus preventing passage of contrast, and evade detection during ERCP (Figure 3). In a study of patients with primary sclerosing cholangitis, stones were not detectable on cholangiography in seven of 23 patients (30%)^[23]. In a more recent multicenter study, stones were missed in 29% of patients who presented for ERCP for different indications. In that study, ERCP was immediately followed by peroral cholangioscopy, which led to detection of the stones^[24].

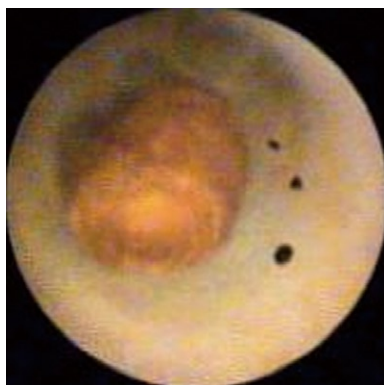


Figure 3 Cholangioscopic view of a small stone surrounded by contrast in an intrahepatic duct. The stone was missed during endoscopic retrograde cholangiopancreatography (image by Spyglass Direct Visualization System, Boston Scientific, Natick, USA).

Indeterminate biliary strictures

Biliary strictures can be benign or malignant. Accurate diagnosis of biliary strictures is essential for treatment planning and the correct choice of treatment, such as surgical resection or endoscopic stenting. However, differentiation of malignant from benign ductal lesions remains a challenge^[25]. Brush cytology during ERCP or fine needle aspiration by EUS has become the preferred initial method of pursuing a diagnosis in many patients with pancreatobiliary malignancies^[25,27]. These techniques allow easy and convenient sampling and have a low complication rate^[25,27,28]. The diagnostic specificity of biliary brush cytology or fine needle aspiration is very high and few false-positive diagnoses have been reported^[25,29]. The major limitation of these techniques has been the relatively modest diagnostic sensitivity, ranging from 10% to 50% in most series^[25,29].

There have been attempts to improve the sensitivity of brush cytology obtained during ERCP. Physical changes to the brushing device itself, such as use of longer and stiffer brushes, have not been shown to improve sensitivity^[30]. Balloon dilatation of strictures, to expose underlying tissue, prior to obtaining brush samples has been tried but not shown to be of any benefit^[31]. Mutation analysis of the cells obtained by brushing does not seem to improve diagnostic accuracy^[32], and DNA methylation analysis of ERCP brush specimens has shown only small benefit^[25].

It has been suggested that peroral cholangioscopy can improve diagnosis of indeterminate biliary strictures by visualization of the mucosa at the site of the stricture, and by targeted biopsy.

Visualization of the mucosa at the site of the stricture: It is well known that the presence of irregularly dilated and tortuous blood vessels (so-called tumor vessels) due to neovascularization at the site of pancreatic or biliary strictures is indicative of malignancy^[33]. Tumor vessels can be detected by direct visualization using a cholangioscope. Intraductal nodules or masses can also be indicative of malignancy and be easily detected by cholangioscopy. However, tumor vessels and intraductal masses can be ap-

preciated only in a fraction of malignant strictures; probably those with more advanced disease. Certain types of cholangiocarcinoma involve submucosal layers of the bile duct wall and cannot be detected by cholangioscopy, which visualizes the superficial layers. Biliary strictures caused by extraluminal compression, such as those associated with pancreatic cancer, cannot be detected by cholangioscopy, unless at later stages when the tumor has infiltrated and penetrated the bile duct wall.

Studies to assess the value of stricture visualization by cholangioscopy have reported high sensitivity for detection of malignant lesions^[4,34]. The reported sensitivity in some of these studies has approached 100%^[4]. In these studies, however, the criteria used for labeling a stricture as malignant have been somewhat lax. As an example, irregular biliary mucosa has been used to label a stricture as malignant. It is well known that irregular biliary mucosa on cholangioscopy can also be seen in benign lesions such as primary sclerosing cholangitis, or chronic inflammation associated with choledocholithiasis or recurrent cholangitis^[35]. Therefore, the high sensitivity in such studies is often achieved at the cost of lower specificity. This is alarming, because false-positive results can have a devastating impact on the affected patients' lives.

Although, undoubtedly, direct visualization of indeterminate biliary strictures can aid in their diagnosis, the true value of peroral cholangioscopy for this purpose has not been vigorously studied.

Targeted biopsy: Targeted biopsy is defined as biopsy of the sites that are clearly affected by disease under direct visualization. Theoretically, targeted biopsy should improve cancer detection rate in malignant biliary strictures by allowing sampling of the sites that appear suspicious. In a recent multicenter study that assessed the role of cholangioscopy-guided targeted biopsy for diagnosis of indeterminate biliary strictures, initial observations suggested a large improvement in sensitivity^[3]. However, later observations at conclusion of the study have indicated a somewhat more modest benefit^[24]. Well-designed studies are needed to assess better the value of cholangioscopy-guided targeted biopsy for evaluation of indeterminate biliary strictures.

Uncommon applications: In our institution, 10%-20% of peroral cholangioscopy procedures are performed for indications other than stone disease and stricture diagnosis. Some of these indications are discussed below.

Characterization of indeterminate intraductal lesions or filling defects

Increased use of imaging studies such as CT, MRI and EUS has led to an increase in incidental findings such as intraductal biliary lesions or filling defects. Although, most often these findings are real, they can also be due to artifacts.

Direct visualization of the intraluminal biliary tree is the most appropriate way to investigate further the nature of these findings. Cholangioscopy has been shown to be effective for this purpose^[4,36].

Assessing post-liver-transplantation anastomotic strictures

Various refinements in surgical techniques and postoperative and immunosuppressive management have reduced the incidence of complications after liver transplantation. Biliary complications, however, continue to be a significant cause of morbidity after liver transplantation^[37,38].

In selected cases, cholangioscopy can prove beneficial in diagnosis and treatment of biliary complications after liver transplantation. In a study of 20 liver transplant patients, cholangioscopy helped diagnose ischemia, ulcerations, scar tissue, intraductal clots, and retained suture material, which otherwise might have been missed by ERCP alone^[39]. The role of cholangioscopy in assessment of anastomotic strictures after liver transplantation is evolving.

Assistance in guidewire placement

ERCP has attained a primary role in the treatment of biliary strictures and biliary stones. Success of ERCP in these cases, however, depends on the ability to traverse the stricture or the stone with a guidewire that is then used to direct instruments such as dilating balloons or lithotripsy baskets^[40]. In the vast majority of cases, this is accomplished easily. With severe strictures or impacted stones, however, it can represent a time-consuming challenge, and in some studies, a failure rate of up to 20% has been reported^[41]. In such cases, cholangioscopy can facilitate guidewire placement and prevent more invasive procedures such as transhepatic access or surgery. Several studies have highlighted the value of cholangioscopy in such instances^[40,42].

Rare applications: We define rare applications as those responsible for $\leq 1\%$ of our peroral cholangioscopy volume. For obvious reasons, these indications have been reported only in one or two case reports and no studies have assessed the true value of peroral cholangioscopy in these settings.

Evaluation of recurrent pancreatitis

Peroral cholangioscopy was used in a 62-year-old post-cholecystectomy patient with recurrent acute pancreatitis of undetermined etiology. It revealed a T-tube remnant in the cystic duct stump, which served as a nidus for biliary sludge and stone formation. The T-tube remnant had evaded detection by ERCP, CT and magnetic resonance cholangiopancreatography. Removal of the T-tube remnant prevented further episodes of pancreatitis^[43].

Determination of source of bleeding in hemobilia

A 54-year-old man was reported to have bleeding from arteriovenous malformations of the bile duct, which was detected by peroral cholangioscopy, with subsequent successful treatment by endovascular intervention^[44]. In another study, the cause of hemobilia in a 57-year-old man could not be identified by ERCP, CT or angiography. Peroral cholangioscopy revealed multiple biliary ulcers. Biopsies were consistent with cytomegalovirus cholangiopathy that responded to antiviral therapy, with subsequent cessation of bleeding^[45].

Staging and ablation of biliary neoplasms

Peroral cholangioscopy was used in a 78-year-old man to determine the extent of a biliary neoplasm. Use of a video cholangioscope with NBI capability allowed precise determination of the margins of the lesion. Successful ablation of the neoplasm with brachytherapy was confirmed by repeat peroral cholangioscopy at 1 mo follow-up^[46].

CONCLUSION

Recent advances such as introduction of a single operator cholangioscopy system or video cholangioscopies with high image quality have led to renewed interest in cholangioscopy, with subsequent expanded use. Currently, the most common indications for cholangioscopy are stone therapy and evaluation of indeterminate biliary strictures. Several other clinical applications have been described. As this technology is gaining more popularity and use, other indications are certain to be described.

REFERENCES

- 1 **Cohen S**, Bacon BR, Berlin JA, Fleischer D, Hecht GA, Loehrer PJ Sr, McNair AE Jr, Mulholland M, Norton NJ, Rabeneck L, Ransohoff DF, Sonnenberg A, Vannier MW. National Institutes of Health State-of-the-Science Conference Statement: ERCP for diagnosis and therapy, January 14-16, 2002. *Gastrointest Endosc* 2002; **56**: 803-809
- 2 **Parsi MA**, Neuhaus H, Pleskow D, Binmoeller KF, Hawes RH, Petersen BT, Sherman S, Stevens PD, Deviere J, Haluszka O, Costamagna G, Meisner S, Ponchon T, Slivka A, Chen YK. Peroral cholangioscopy guided stone therapy - report of an international multicenter registry. *Gastrointest Endosc* 2008; **67**: AB102
- 3 **Pleskow D**, Parsi MA, Chen YK, Neuhaus H, Slivka A, Haluszka O, Petersen BT, Deviere J, Sherman S, Meisner S, Hawes RH, Stevens PD, Ponchon T, Costamagna G, Binmoeller KF. Biopsy of indeterminate biliary strictures - does direct visualization help? - A multicenter experience. *Gastrointest Endosc* 2008; **67**: AB103
- 4 **Fukuda Y**, Tsuyuguchi T, Sakai Y, Tsuchiya S, Saisyo H. Diagnostic utility of peroral cholangioscopy for various bile-duct lesions. *Gastrointest Endosc* 2005; **62**: 374-382
- 5 **Nakajima M**, Mukai H, Kawai K. Peroral cholangioscopy and pancreatoscopy. In: Sivak MV, editor. *Gastrointestinal Endoscopy*. 2nd ed. Philadelphia: WB Saunders, 2000: 1055-1068
- 6 **Itoi T**, Neuhaus H, Chen YK. Diagnostic value of image-enhanced video cholangiopancreatography. *Gastrointest Endosc Clin N Am* 2009; **19**: 557-566
- 7 **Farrell JJ**, Bounds BC, Al-Shalabi S, Jacobson BC, Brugge WR, Schapiro RH, Kelsey PB. Single-operator duodenoscopy-assisted cholangioscopy is an effective alternative in the management of choledocholithiasis not removed by conventional methods, including mechanical lithotripsy. *Endoscopy* 2005; **37**: 542-547
- 8 **Steiner CA**, Bass EB, Talamini MA, Pitt HA, Steinberg EP. Surgical rates and operative mortality for open and laparoscopic cholecystectomy in Maryland. *N Engl J Med* 1994; **330**: 403-408
- 9 **Everhart JE**, Khare M, Hill M, Maurer KR. Prevalence and ethnic differences in gallbladder disease in the United States. *Gastroenterology* 1999; **117**: 632-639
- 10 **Everhart JE**, Yeh F, Lee ET, Hill MC, Fabsitz R, Howard BV, Welty TK. Prevalence of gallbladder disease in American Indian populations: findings from the Strong Heart Study. *Hepatology* 2002; **35**: 1507-1512

- 11 **Aerts R**, Penninckx F. The burden of gallstone disease in Europe. *Aliment Pharmacol Ther* 2003; **18** Suppl 3: 49-53
- 12 **Festi D**, Dormi A, Capodicasa S, Staniscia T, Attili AF, Loria P, Pazzi P, Mazzella G, Sama C, Roda E, Colecchia A. Incidence of gallstone disease in Italy: results from a multicenter, population-based Italian study (the MICOL project). *World J Gastroenterol* 2008; **14**: 5282-5289
- 13 **Tazuma S**. Gallstone disease: Epidemiology, pathogenesis, and classification of biliary stones (common bile duct and intrahepatic). *Best Pract Res Clin Gastroenterol* 2006; **20**: 1075-1083
- 14 **Caddy GR**, Tham TC. Gallstone disease: Symptoms, diagnosis and endoscopic management of common bile duct stones. *Best Pract Res Clin Gastroenterol* 2006; **20**: 1085-1101
- 15 **Forsmark CE**, Baillie J. AGA Institute technical review on acute pancreatitis. *Gastroenterology* 2007; **132**: 2022-2044
- 16 **Moreau JA**, Zinsmeister AR, Melton LJ 3rd, DiMaggio EP. Gallstone pancreatitis and the effect of cholecystectomy: a population-based cohort study. *Mayo Clin Proc* 1988; **63**: 466-473
- 17 **Van Dam J**, Sivak MV Jr. Mechanical lithotripsy of large common bile duct stones. *Cleve Clin J Med* 1993; **60**: 38-42
- 18 **Cho YD**, Cheon YK, Moon JH, Jeong SW, Jang JY, Lee JS, Shim CS. Clinical role of frequency-doubled double-pulsed yttrium aluminum garnet laser technology for removing difficult bile duct stones (with videos). *Gastrointest Endosc* 2009; **70**: 684-689
- 19 **Moon JH**, Cha SW, Ryu CB, Kim YS, Hong SJ, Cheon YK, Cho YD, Kim YS, Lee JS, Lee MS, Shim CS, Kim BS. Endoscopic treatment of retained bile-duct stones by using a balloon catheter for electrohydraulic lithotripsy without cholangioscopy. *Gastrointest Endosc* 2004; **60**: 562-566
- 20 **Darcy M**, Picus D. Cholangioscopy. *Tech Vasc Interv Radiol* 2008; **11**: 133-142
- 21 **Bratcher J**, Kasmin F. Choledochoscopy-assisted intraductal shock wave lithotripsy. *Gastrointest Endosc Clin N Am* 2009; **19**: 587-595
- 22 **Piraka C**, Shah RJ, Awadallah NS, Langer DA, Chen YK. Transpapillary cholangioscopy-directed lithotripsy in patients with difficult bile duct stones. *Clin Gastroenterol Hepatol* 2007; **5**: 1333-1338
- 23 **Awadallah NS**, Chen YK, Piraka C, Antillon MR, Shah RJ. Is there a role for cholangioscopy in patients with primary sclerosing cholangitis? *Am J Gastroenterol* 2006; **101**: 284-291
- 24 **Chen YK**, Parsi MA, Binmoeller KF, Hawes RH, Pleskow D, Slivka A, Haluszka O, Petersen BT, Sherman S, Deviere J, Meisner S, Stevens PD, Costamagna G, Ponchon T, Neuhaus H. Peroral cholangioscopy (POC) using a disposable steerable single operator catheter for biliary stone therapy and assessment of indeterminate strictures - A multicenter experience using Spyglass. *Gastrointest Endosc* 2009; **69**: AB264-AB265
- 25 **Parsi MA**, Li A, Li CP, Goggins M. DNA methylation alterations in endoscopic retrograde cholangiopancreatography brush samples of patients with suspected pancreaticobiliary disease. *Clin Gastroenterol Hepatol* 2008; **6**: 1270-1278
- 26 **Mansfield JC**, Griffin SM, Wadehra V, Matthewson K. A prospective evaluation of cytology from biliary strictures. *Gut* 1997; **40**: 671-677
- 27 **Selvaggi SM**. Biliary brushing cytology. *Cytopathology* 2004; **15**: 74-79
- 28 **Govil H**, Reddy V, Kluskens L, Treaba D, Massarani-Wafai R, Selvaggi S, Gattuso P. Brush cytology of the biliary tract: retrospective study of 278 cases with histopathologic correlation. *Diagn Cytopathol* 2002; **26**: 273-277
- 29 **Moreno Luna LE**, Kipp B, Halling KC, Sebo TJ, Kremers WK, Roberts LR, Barr Fritcher EG, Levy MJ, Gores GJ. Advanced cytologic techniques for the detection of malignant pancreaticobiliary strictures. *Gastroenterology* 2006; **131**: 1064-1072
- 30 **Fogel EL**, deBellis M, McHenry L, Watkins JL, Chappo J, Cramer H, Schmidt S, Lazzell-Pannell L, Sherman S, Lehman GA. Effectiveness of a new long cytology brush in the evaluation of malignant biliary obstruction: a prospective study. *Gastrointest Endosc* 2006; **63**: 71-77
- 31 **Ornellas LC**, Santos Gda C, Nakao FS, Ferrari AP. Comparison between endoscopic brush cytology performed before and after biliary stricture dilation for cancer detection. *Arq Gastroenterol* 2006; **43**: 20-23
- 32 **Stewart CJ**, Burke GM. Value of p53 immunostaining in pancreatico-biliary brush cytology specimens. *Diagn Cytopathol* 2000; **23**: 308-313
- 33 **Kim HJ**, Kim MH, Lee SK, Yoo KS, Seo DW, Min YI. Tumor vessel: a valuable cholangioscopic clue of malignant biliary stricture. *Gastrointest Endosc* 2000; **52**: 635-638
- 34 **Itoi T**, Sofuni A, Itokawa F, Tsuchiya T, Kurihara T, Ishii K, Tsuji S, Moriyasu F, Gotoda T. Peroral cholangioscopic diagnosis of biliary-tract diseases by using narrow-band imaging (with videos). *Gastrointest Endosc* 2007; **66**: 730-736
- 35 **Seo DW**, Lee SK, Kim MH, Min YI. Benign lesions of bile ducts and gallbladder. In: Seo DW, Lee SK, Kim MH, Min YI, eds. Cholangioscopy. Seoul: Koonja Publishing, 2002: 57-83
- 36 **Abdel Aziz AM**, Sherman S, Binmoeller KF, Deviere J, Hawes RH, Haluszka O, Neuhaus H, Pleskow D, Rajman I. SpyGlass cholangioscopy - Impact on patients with bile duct filling defect(s) of uncertain etiology. *Gastrointestinal endoscopy* 2008; **67**: AB325
- 37 **Shah SA**, Grant DR, McGilvray ID, Greig PD, Selzner M, Lilly LB, Girgrah N, Levy GA, Cattral MS. Biliary strictures in 130 consecutive right lobe living donor liver transplant recipients: results of a Western center. *Am J Transplant* 2007; **7**: 161-167
- 38 **Tashiro H**, Itamoto T, Sasaki T, Ohdan H, Fudaba Y, Amano H, Fukuda S, Nakahara H, Ishiyama K, Ohshita A, Kohashi T, Mitsuta H, Chayama K, Asahara T. Biliary complications after duct-to-duct biliary reconstruction in living-donor liver transplantation: causes and treatment. *World J Surg* 2007; **31**: 2222-2229
- 39 **Siddique I**, Galati J, Ankoma-Sey V, Wood RP, Ozaki C, Monsour H, Rajman I. The role of choledochoscopy in the diagnosis and management of biliary tract diseases. *Gastrointest Endosc* 1999; **50**: 67-73
- 40 **Parsi MA**, Guardino J, Vargo JJ. Peroral cholangioscopy-guided stricture therapy in living donor liver transplantation. *Liver Transpl* 2009; **15**: 263-265
- 41 **Hisatsune H**, Yazumi S, Egawa H, Asada M, Hasegawa K, Kodama Y, Okazaki K, Itoh K, Takakuwa H, Tanaka K, Chiba T. Endoscopic management of biliary strictures after duct-to-duct biliary reconstruction in right-lobe living-donor liver transplantation. *Transplantation* 2003; **76**: 810-815
- 42 **Parsi MA**. Peroral cholangioscopy-assisted guidewire placement for removal of impacted stones in the cystic duct remnant. *World J Gastrointest Surg* 2009; **1**: 59-61
- 43 **Parsi MA**, Sanaka MR, Dumot JA. Iatrogenic recurrent pancreatitis. *Pancreatol* 2007; **7**: 539
- 44 **Hayashi S**, Baba Y, Ueno K, Nakajo M. Small arteriovenous malformation of the common bile duct causing hemobilia in a patient with hereditary hemorrhagic telangiectasia. *Cardiovasc Intervent Radiol* 2008; **31** Suppl 2: S131-S134
- 45 **Prasad GA**, Abraham SC, Baron TH, Topazian MD. Hemobilia caused by cytomegalovirus cholangiopathy. *Am J Gastroenterol* 2005; **100**: 2592-2595
- 46 **Lu XL**, Itoi T, Kubota K. Cholangioscopy by using narrow-band imaging and transpapillary radiotherapy for mucin-producing bile duct tumor. *Clin Gastroenterol Hepatol* 2009; **7**: e34-e35

S- Editor Sun H L- Editor Kerr C E- Editor Lin YP

Imaging techniques used for the real-time assessment of angiogenesis in digestive cancers

Adrian Săftoiu, Peter Vilmann

Adrian Săftoiu, Research Center of Gastroenterology and Hepatology, Gastroenterology Department, University of Medicine and Pharmacy Craiova, Craiova, Dolj, 200349, Romania
 Peter Vilmann, Department of Surgical Gastroenterology, Copenhagen University Hospital Herlev, Endoscopic Unit at Gentofte Hospital, 2900 Hellerup, Denmark

Author contributions: Săftoiu A and Vilmann P contributed equally to this paper.

Correspondence to: Adrian Săftoiu, Professor, MD, PhD, MSc, Research Center of Gastroenterology and Hepatology, Gastroenterology Department, University of Medicine and Pharmacy Craiova, 2-4 Petru Rares, Craiova, Dolj, 200349, Romania. adrian.saftoiu@webmail.umfcv.ro

Telephone: +40-744-823355 Fax: +40-251-310287

Received: July 2, 2010 Revised: August 29, 2010

Accepted: October 6, 2010

Published online: January 7, 2011

Peer reviewer: Tsuneo Kitamura, Associate Professor, Department of Gastroenterology, Juntendo University Urayasu Hospital, Juntendo University School of Medicine, 2-1-1 Tomioka, Urayasu-shi, Chiba 279-0021, Japan

Săftoiu A, Vilmann P. Imaging techniques used for the real-time assessment of angiogenesis in digestive cancers. *World J Gastroenterol* 2011; 17(1): 7-8 Available from: URL: <http://www.wjgnet.com/1007-9327/full/v17/i1/7.htm> DOI: <http://dx.doi.org/10.3748/wjg.v17.i1.7>

FROM THE EDITOR

Angiogenesis plays a critical role in tumor growth and metastasis. Most of the digestive cancers depend strictly on the development of an adequate blood supply in the form of neovascularization, which has a pivotal role in primary tumor growth and the development of metastasis. Thus, new blood vessels formed inside the tumor are usually highly permeable and provide a route for cancer cells to enter blood circulation^[1]. Tumor vascularization has been attracting a lot of attention in recent years due to possible implications in semi-quantitative diagnosis, as well as in prognosis stratification and targeted treatment^[2]. There are several ways traditionally proposed for investigation of tumor vascularization, but all these methods have several methodological flaws, including artifacts induced by air or fat [contrast-enhanced transabdominal ultrasound (US)], reduced resolution [contrast-enhanced computer tomography (CT)] or invasiveness (angiography or surgery)^[3].

Categorizing the patients through mini-invasive procedures, before chemotherapy or surgery, is of crucial importance. This has implications for the appropriate design of clinical trials, but also for the improvement of the decision making process, by selecting the tumors that are most likely to respond to treatment. Recently developed angiogenesis inhibitors represent a highly attractive target for tumor therapy, since they theoretically offer the hope of long-term control of tumor progression^[4]. Several anti-angiogenic inhibitors were recently developed

Abstract

Angiogenesis has a critical role in primary tumor growth and the development of metastases. Several angiogenesis inhibitors were recently developed, being a very attractive target for digestive tumor therapy. However, individualized therapy should not only be based on the pre-treatment imaging evaluation, but also on sensitive monitoring of microvascular changes during treatment. State-of-the-art imaging techniques have the potential to visualize and characterize angiogenesis, although the technology and methodologies employed are recent and need further validation. The aim of this series of reviews was to analyze and enhance current knowledge and future perspectives about the real-time assessment of angiogenesis in digestive cancers, used for the longitudinal monitoring of the effects of chemo-radiotherapy (including anti-angiogenic therapies), as well as for the precise targeting of drugs through molecular-based drug-delivery systems.

© 2011 Baishideng. All rights reserved.

Key words: Angiogenesis; Digestive cancers; Chemo-radiotherapy

and have already been proven to be effective in clinical trials: bevacizumab (recombinant humanized anti-VEGF monoclonal antibody), cetuximab (anti-EGFR monoclonal antibody), erlotinib (tyrosine-kinase inhibitor), *etc*^[5]. Even though anti-angiogenic treatments are an established anti-cancer therapy, several mechanisms of tumor evasion and refractoriness have been described after inhibition of a single pro-angiogenic pathway, due to compensatory upregulation of different angiogenic pathways^[6]. Tailoring the anti-angiogenesis therapy as a function of the pre-operative imaging evaluation would be the next step, with a consequent decrease of toxicity, as well as an increase of median progression-free survival. Furthermore, these procedures would possibly allow a sensitive monitoring of microvascular changes caused by chemoradiotherapy or other ablative treatments. The ultimate goal would be to achieve an early diagnosis where the “angiogenic switch” could be delayed and tumor evasion mechanisms could be prevented, in order to induce a dormant state, while transforming cancer into a chronic disease^[7].

The main objectives of our series of reviews include the discussion of several advanced imaging techniques, complementary used for the real-time assessment of angiogenesis in digestive cancers. The advanced imaging techniques discussed will include several “red-flag” endoscopic techniques used for the depiction of minute changes in the vessel pattern of preneoplastic and neoplastic lesions (tri-modal imaging including autofluorescence imaging, zoom endoscopy and narrow band imaging)^[8]. Utility of Doppler-optical coherence tomography (D-OCT) for the depiction and quantification of low-velocity, low-volume blood flow will also be reviewed^[9]. These techniques will be supplemented by the presentation of confocal laser endomicroscopy and the potential applications of this breakthrough technique for the in-vivo assessment of vascularization based on the use of specific vascular contrast agents^[10]. Targeted contrast-enhanced ultrasound and its role in the depiction of angiogenesis, as well as ultrasound-directed drug delivery and the physics behind sonoporation will also be discussed^[11]. A comprehensive discussion will focus also on the use of contrast-enhanced endoscopic ultrasound (including specific harmonic imaging)^[12]. Current and future hybrid imaging techniques like real-time virtual sonography (a combination of US/EUS with CT/magnetic resonance imaging) will also be briefly described^[13]. Lastly, molecular imaging perspectives and new developments of targeted

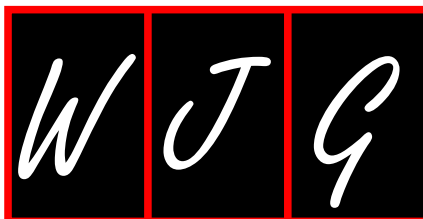
contrast agents will be critically analyzed^[14].

The aim of this series of reviews will be to analyze and enhance the current knowledge and future perspectives of the *in-vivo*, real-time assessment of angiogenesis in digestive cancers, used for the longitudinal monitoring of the effects of chemo-radiotherapy (including anti-angiogenic therapies), as well as for the precise targeting of drugs through molecular based drug-delivery systems.

REFERENCES

- 1 **Folkman J.** Fundamental concepts of the angiogenic process. *Curr Mol Med* 2003; **3**: 643-651
- 2 **Ellis LM, Walker RA, Gasparini G.** Is determination of angiogenic activity in human tumours clinically useful? *Eur J Cancer* 1998; **34**: 609-618
- 3 **Kitano M, Kudo M, Maekawa K, Suetomi Y, Sakamoto H, Fukuta N, Nakaoka R, Kawasaki T.** Dynamic imaging of pancreatic diseases by contrast enhanced coded phase inversion harmonic ultrasonography. *Gut* 2004; **53**: 854-859
- 4 **Saif MW.** Anti-angiogenesis therapy in pancreatic carcinoma. *JOP* 2006; **7**: 163-173
- 5 **Liu CC, Shen Z, Kung HF, Lin MC.** Cancer gene therapy targeting angiogenesis: an updated review. *World J Gastroenterol* 2006; **12**: 6941-6948
- 6 **Abdollahi A, Folkman J.** Evading tumor evasion: current concepts and perspectives of anti-angiogenic cancer therapy. *Drug Resist Updat* 2010; **13**: 16-28
- 7 **Naumov GN, Folkman J, Straume O, Akslen LA.** Tumor-vascular interactions and tumor dormancy. *APMIS* 2008; **116**: 569-585
- 8 **Filip M, Iordache S, Săftoiu A, Ciurea T.** Autofluorescence imaging and magnification endoscopy. *World J Gastroenterol* 2011; **17**: 9-14
- 9 **Osiac E, Săftoiu A, Gheonea DI, Mandrila I, Angelescu R.** Optical coherence tomography and Doppler optical coherence tomography in the gastrointestinal tract. *World J Gastroenterol* 2011; **17**: 15-20
- 10 **Gheonea DI, Cârțână T, Ciurea T, Popescu C, Bădărău A, Săftoiu A.** Confocal laser endomicroscopy and immunofluorescence for real-time assessment of vascularization in gastrointestinal malignancies. *World J Gastroenterol* 2011; **17**: 21-27
- 11 **Postema M, Gilja OH.** Contrast-enhanced and targeted ultrasound. *World J Gastroenterol* 2011; **17**: 28-41
- 12 **Reddy NK, Ioncică AM, Săftoiu A, Vilmann P, Bhutani MS.** Contrast-enhanced endoscopic ultrasonography. *World J Gastroenterol* 2011; **17**: 42-48
- 13 **Sandulescu DL, Dumitrescu D, Rogoveanu I, Săftoiu A.** Hybrid ultrasound imaging techniques (fusion imaging). *World J Gastroenterol* 2011; **17**: 49-52
- 14 **Thekkekk N, Anandasabapathy S, Richards-Kortum R.** Optical molecular imaging for detection of Barrett's-associated neoplasia. *World J Gastroenterol* 2011; **17**: 53-62

S- Editor Sun H L- Editor Rutherford A E- Editor Ma WH



Adrian Săftoiu, MD, PhD, Professor, and Peter Vilmann, MD, PhD, Professor, Series Editors

Autofluorescence imaging and magnification endoscopy

Monalisa Filip, Sevastița Iordache, Adrian Săftoiu, Tudorel Ciurea

Monalisa Filip, Sevastița Iordache, Adrian Săftoiu, Tudorel Ciurea, Research Center of Gastroenterology and Hepatology, University of Medicine and Pharmacy, Craiova, Dolj, 200349, Romania

Author contributions: Filip M, Iordache S, Săftoiu A and Ciurea T performed the research; Filip M, Iordache S, Săftoiu A and Ciurea T analyzed the data; Filip M and Săftoiu A wrote the paper.

Correspondence to: Monalisa Filip, MD, Gastroenterology Department, University of Medicine and Pharmacy, 2-4 Petru Rares Street, Craiova, Dolj, 200349, Romania. monalisafilip@yahoo.com

Telephone: +40-72-7972250 Fax: +40-25-1310287

Received: July 2, 2010 Revised: August 26, 2010

Accepted: September 2, 2010

Published online: January 7, 2011

Abstract

It is well known that angiogenesis is critical in the transition from premalignant to malignant lesions. Consequently, early detection and diagnosis based on morphological changes to the microvessels are crucial. In the last few years, new imaging techniques which utilize the properties of light-tissue interaction have been developed to increase early diagnosis of gastrointestinal (GI) tract neoplasia. We analyzed several "red-flag" endoscopic techniques used to enhance visualization of the vascular pattern of preneoplastic and neoplastic lesions (e.g. trimodal imaging including autofluorescence imaging, magnifying endoscopy and narrow band imaging). These new endoscopic techniques provide better visualization of mucosal microsurface structure and microvascular architecture and may enhance the diagnosis and characterization of mucosal lesions in the GI tract. In the near future, it is expected that trimodal imaging endoscopy will be practiced as a standard endoscopy technique as it is quick, safe and accurate for making a precise diagnosis of gastrointestinal pathology, with an emphasis on the diagnosis of early GI tract cancers. Further large-scale randomized controlled trials comparing these modalities in different patient subpopulations

are warranted before their endorsement in the routine practice of GI endoscopy.

© 2011 Baishideng. All rights reserved.

Key words: Angiogenesis; Autofluorescence imaging; Multiband imaging; Narrow band imaging; Zoom endoscopy

Peer reviewer: Naoaki Sakata, MD, PhD, Division of Hepato-Biliary Pancreatic Surgery, Tohoku University Graduate School of Medicine, 1-1 Seiryō-machi, Aoba-ku, Sendai, Miyagi 980-8574, Japan

Filip M, Iordache S, Săftoiu A, Ciurea T. Autofluorescence imaging and magnification endoscopy. *World J Gastroenterol* 2011; 17(1): 9-14 Available from: URL: <http://www.wjgnet.com/1007-9327/full/v17/i1/9.htm> DOI: <http://dx.doi.org/10.3748/wjg.v17.i1.9>

INTRODUCTION

It is well known that angiogenesis is critical in the transition from premalignant to malignant lesions. Consequently, early detection and diagnosis based on morphologic changes to the microvessels are crucial. Conventional endoscopic diagnosis using white light is based on subtle morphological changes such as superficially elevated, flat, or depressed lesions and minimal changes in color. However, these findings are difficult to recognize, especially for inexperienced endoscopists. As a result, the diagnosis may be inaccurate or a superficial cancer in the gastrointestinal (GI) tract may be overlooked.

New imaging techniques which utilize the properties of light-tissue interaction have recently been developed to enhance early diagnosis of GI tract neoplasia. Endoscopic autofluorescence imaging (AFI) produces real-time pseudocolor images based on the detection of natural tissue fluorescence generated from endogenous fluorophores (collagen, nicotinamide, adenine dinucleotide, flavin and

porphyrins) through emission induced by excitation light. The system can visualize lesions, including malignancies, by differences in tissue fluorescence properties and can reveal early stage cancers not detectable by conventional white light endoscopy (WLE)^[1,2]. Magnifying endoscopy with narrow band imaging (ME-NBI) represents a real-time endoscopic imaging technique which enhances visualization of the surface texture and the vascular network of the mucosa with the aim of improving tissue characterization and differentiation^[3].

AUTOFLUORESCENCE IMAGING

The principle of autofluorescence diagnosis is based on the interaction between light with a specific wavelength and tissue fluorophores. When tissues are exposed to short wavelength light, endogenous fluorophores (collagen, nicotinamide, adenine dinucleotide, flavin and porphyrins) are excited, leading to the emission of fluorescent light of a longer wavelength (i.e. autofluorescence)^[4]. Normal, inflamed and neoplastic tissue have different autofluorescence characteristics that may thus enable their differentiation. Thus, normal tissue is pseudocolored as green, blood vessels as dark green, while hypertrophic fundic mucosa of the stomach and dysplastic/neoplastic areas appear as magenta. During AFI, a suspected neoplasia (AFI-positive lesion) is defined as any area that is different in color from the surrounding mucosa, and which has a defined circumferential margin^[5].

Autofluorescence is abnormal in neoplastic tissues due to several mechanisms: (1) increase in the nuclear-cytoplasmic ratio, which consequently determines decreased autofluorescence as nuclei show no autofluorescence as compared with cytoplasm; (2) loss of collagen, submucosal collagen is the strongest fluorophore which disappears due to thickening of the mucosa; and (3) neovascularization, inducing increased hemoglobin concentration which absorbs autofluorescence light^[6].

Several published studies showed an increased sensitivity for the detection of high-grade dysplasia and early cancer in the GI tract when autofluorescence techniques were used^[1,2,5-9]. Kara *et al.*^[7] showed the effectiveness of AFI in identifying high-grade dysplasia and early cancer in patients with Barrett's esophagus. Compared with WLE and random 4-quadrant biopsies, AFI increased the detection of high-grade dysplasia and esophageal adenocarcinoma by an additional 6 out of 60 patients, representing an increase of 10%, from 23% to 33%. False-positive lesions were determined by the presence of acute inflammation. On the other hand, Kara *et al.*^[8] showed that fluorescence imaging with light-induced fluorescence endoscopy (LIFE) using a fiber-optic endoscope was no better than standard WLE for the detection of high-grade dysplasia and early cancer in a randomized crossover study of patients with Barrett's esophagus. Another study tested the diagnostic performance of AFI for early gastric neoplasms, thus Ohkawa *et al.*^[9] concluded that LIFE is highly sensitive (sensitivity 96.4%) but not very specific (specificity 49.1%), since 50.9% of benign lesions were also identified

as having abnormal fluorescence images. Using the latest technology incorporated in AFI systems, Kato *et al.*^[5] obtained similar results, with approximately 25% of superficial elevated neoplasia diagnosed only by AFI and missed by WLE. In principle, a superficial elevated neoplasm of a similar hue to the surrounding mucosa might be overlooked during WLE, but it can be revealed by AFI if the elevated neoplasm appears as magenta within a normal looking green mucosa (Figures 1-4).

While all these studies demonstrate the vast potential of AFI to target premalignant lesions (high grade dysplasia) and early cancers, they also reveal important limitations of this technique and set-up directions for future improvement. The large number of false-positive results with a consequent low positive predictive value implies a potential benefit from adjunct methods such as ME-NBI, optical-coherence tomography (OCT) or confocal laser endomicroscopy (CLE)^[10] which would provide greater detection specificity. The use of trimodal imaging endoscopy that includes WLE, AFI and ME-NBI incorporated in one endoscopy system might improve diagnostic accuracy for high-grade dysplasia and early cancer^[11-13]. ME-NBI is currently considered the technique of choice for improvement of diagnostic accuracy because it reduces the high rate of false-positive results associated with WLE and AFI. Autofluorescence consists primarily of visible light, resulting in images limited essentially to the mucosal surface. Consequently, the development of infrared techniques may provide greater tissue penetration, obtaining images with greater contrast between lesions and their surrounding regions, and allowing the visualization of vascularization in deeper lesions, including the submucosa. Some studies reported that infrared endoscopy is capable of detecting abnormal submucosal vascularization in tumor lesions, with retention of indocyanine green being correlated with the size of the submucosal vascular bed^[14-18]. There is also a direct correlation between the presence of infrared fluorescence and the number of submucosal vessels. With the development of tumor invasion, there is a tendency for more abnormal blood vessels to be formed, further accompanied by an increase in fluorescence^[18].

NARROW BAND IMAGING

Narrow band imaging (NBI) is an optical image technology that enhances structural mucosal patterns (pit-pattern), as well as mucosal/submucosal vessels, by employing the characteristics of the light spectrum. The technology consists of placing narrow bandpass filters in front of a conventional white-light source to obtain tissue illumination at selected narrow wavelength bands. Currently available NBI systems use 2 narrow band filters that provide tissue illumination in the blue (415 nm) and green (540 nm) spectrum of light. The superficial penetrating wavelength of 415 nm corresponds to the main peak on the absorption spectrum of hemoglobin, while the deeper penetrating wavelength of 540 nm corresponds to a secondary hemoglobin absorption peak. Capillaries in the superficial mucosal layer are emphasized by the 415 nm light and are

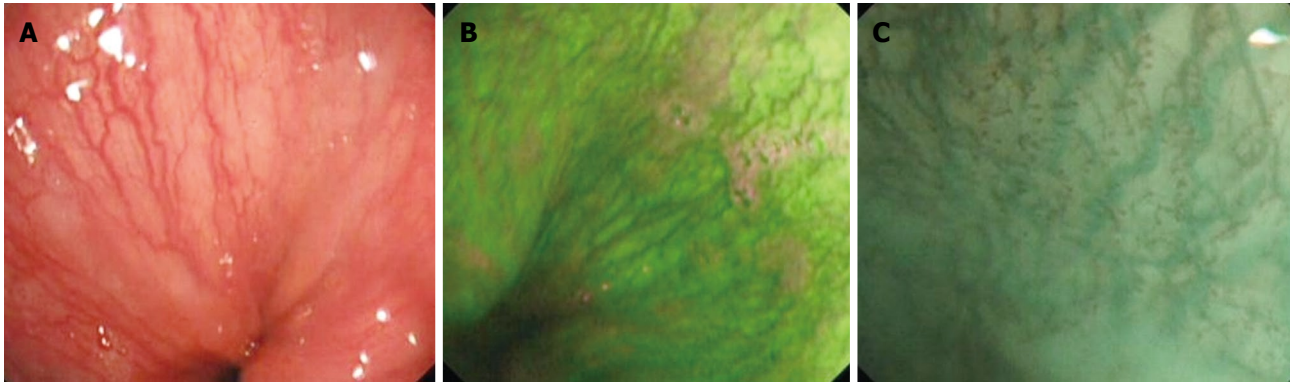


Figure 1 Normal esophageal mucosa. A: Normal vascular pattern above the gastroesophageal (GE) junction visualized in white light endoscopy; B: Autofluorescence imaging of the normal mucosa and vascular pattern above the GE junction; C: Magnifying endoscopy with narrow band imaging depicting the submucosal vessels in cyan and intrapapillary capillary loops in brown.

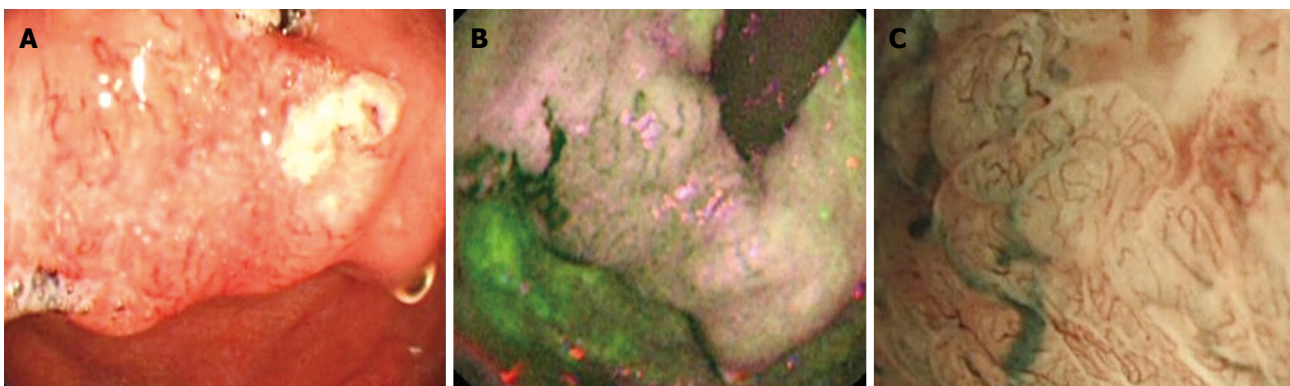


Figure 2 Esophageal squamous cell carcinoma invading the gastroesophageal junction. A: Elevated irregular mucosa with abnormal vascular pattern, difficult to see in white light endoscopy in retroflexion, immediately below the gastroesophageal junction; B: Autofluorescence imaging showing the lesion extension in magenta, with surrounding green normal mucosa; C: Magnifying endoscopy with narrow band imaging showing irregular, thick and distorted mucosal vessels characteristic for tumor angiogenesis.

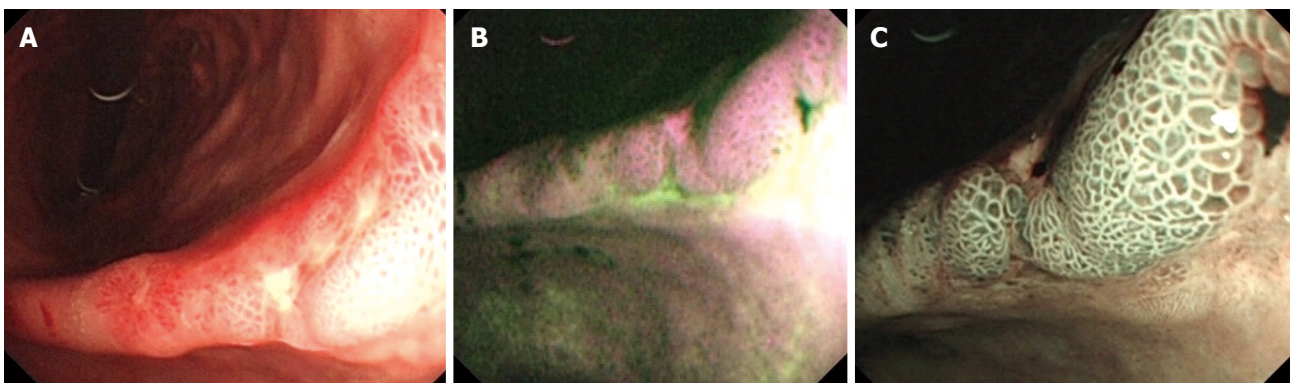


Figure 3 Early gastric adenocarcinoma at the level of the gastric angle. A: Irregular ulcer visualized in white light endoscopy (WLE); B: Autofluorescence imaging showing in magenta the neoplastic margins and a larger lesion extension, as compared with WLE; C: Magnifying endoscopy with narrow band imaging showing a modified pit pattern, with irregular and distorted vascular pattern in the center suggesting high-grade dysplasia/early cancer, and with villous pits and light blue crest sign in the margins suggesting intestinal metaplasia.

displayed in brown, whereas deeper mucosal and submucosal vessels are made visible by the 540 nm light and are displayed in cyan (Figures 1-4). NBI performance is certainly maximized when it is combined with magnification (ME-NBI)^[3,19]. This technique improves the morphological analysis of epithelial crests of the mucosa and enables

a more precise analysis of the abnormal surface architecture (pit-pattern) of neoplastic lesions. However, the most important contribution is represented by the clear visualization of the vascular network in the mucosa, being especially useful in evaluation of the abnormal neoangiogenesis process in high-grade dysplasia/early cancer^[20].



Figure 4 Gastric polyp with moderate dysplasia. A: White light endoscopy showing a 10 mm gastric polyp; B: Autofluorescence imaging with magenta areas on the surface of the polyp, surrounded by green normal mucosa; C: Magnifying endoscopy with narrow band imaging showing a modified pit pattern of the mucosa with an increased number of capillaries.

It was previously recognized that the morphological changes of an intrapapillary capillary loop (IPCL) might represent a new option for early diagnosis of squamous cell carcinoma in the esophagus^[21,22]. However, evaluation of IPCLs under white light observation requires high levels of proficiency and is usually not possible during the usual clinical workup. By using the magnifying scope, the normal appearance of the IPCL is identified as red dots. NBI enables a more vivid observation of the IPCLs, increasing diagnostic accuracy, especially for inexperienced endoscopists (Figure 1C)^[23]. Branching vessels which are located relatively deeper in the wall layers are observed in cyan, while IPCLs which are located in a more superficial layer, are observed as brown loops (brown dots).

Changes in the IPCL pattern include dilatation, tortuosity and/or caliber change of individual IPCL or multiple IPCLs of various shapes. According to the degree of change, these are classified into five types^[23,24]: type I is associated with normal epithelium and IPCLs are observed as smooth running small-diameter capillary vessels; type II involves minimal dilatation and elongation of IPCLs, and is often equivalent to regenerative tissue or inflammation; type III assumes minimal changes in IPCLs and corresponds to borderline lesions which potentially include esophagitis and low-grade intraepithelial neoplasia; in type IV, 3 of the 4 abnormal IPCLs patterns are present and correspond to high-grade intraepithelial neoplasia; finally, type V includes all 4 abnormal IPCLs characteristics and signifies the presence of cancer. Type V is subdivided in four types, type V-1, V-2, V-3 to V_N which reflect cancer infiltration depth. In type V-1, IPCLs demonstrate characteristic changes, dilatation, meandering, irregular caliber and variable form, and corresponds to m1 lesions (carcinoma *in situ*). As it advances to m2 and m3, destruction of IPCL advances gradually and these changes are further extended into the submucosa. Thus, in type V_N, which is characteristic of sm deep invasive carcinoma, new tumor vessels appear, around 10 times larger than the irregular vessels which appear in IPCLs type V-3 (Figure 2C)^[23,24].

ME-NBI is very useful for identifying superficial squamous cell carcinoma in the head and neck region. Muto *et al*^[25,26] reported that visualization of abnormal

microvessel architecture in cancerous lesions is significantly improved by NBI as compared with WLE. This finding is clinically significant because no cases of superficial cancer in the oropharynx or hypopharynx were previously reported before the advent of NBI.

Most of the studies using NBI were designed to evaluate the mucosal pattern and capillary network of patients with Barrett's esophagus, knowing that during WLE it is difficult to identify dysplastic and early neoplastic changes. In all these studies, the accuracy of the diagnosis was higher for NBI as compared with WLE^[27-34]. NBI with magnifying endoscopy thus enables visualization of the details of the mucosal surface and capillary networks without using dyes. Regular villous/gyrus-forming mucosal patterns, as well as flat mucosa with long branching blood vessels are highly predictive for specialized intestinal metaplasia without dysplasia. Irregular/disrupted mucosal pattern, an irregular vascular pattern and abnormal blood vessels are associated with high-grade intraepithelial neoplasia or early cancer. Abnormal vascularity was defined as dilated, corkscrew vessels with increased vascularity and an abnormal, nonuniform branching pattern (Figure 2C)^[27,28]. All high-grade intraepithelial neoplasia have at least one abnormality, and 85% have two or more abnormalities^[27]. Goda *et al*^[29] reported that the addition of capillary pattern to fine mucosal patterns improved the diagnostic value of ME-NBI for detecting specialized intestinal metaplasia and superficial adenocarcinoma.

In a recent study, Singh *et al*^[30] validated a simplified classification of the various morphologic patterns visualized in Barrett's esophagus in four easily distinguishable types: A, round pits with regular microvasculature (columnar mucosa without intestinal mucosa); B, villous/ridge pits with regular microvasculature (intestinal metaplasia); C, absent pits with regular microvasculature (intestinal metaplasia); D, distorted pits with irregular microvasculature (high-grade intraepithelial neoplasia). This classification showed reproducibility and repeatability, both by experienced endoscopists and for those unfamiliar with NBI, suggesting a rapid learning curve. Therefore, ME-NBI allows all endoscopists to perform targeted biopsies for specialized intestinal metaplasia and high-grade intraepi-

thelial neoplasia with a high rate of success^[30-34].

There is no evidence to prove the clinical usefulness of NBI during non-magnifying endoscopic observation for detecting abnormal pathology within the stomach and the duodenum. From a technical point of view, the mucosal image by non-magnification observation with NBI is too dark and noisy for meaningful investigation, because the lumen of the stomach is large^[35]. Feasibility studies showed the potential of NBI with magnification to identify gastric intestinal metaplasia^[36], predict the histologic subtypes of early gastric cancer^[37], and improve margin delineation of gastric cancer for endoscopic mucosal resection^[38]. Uedo *et al.*^[36] reported that a distinctive finding called light blue crests is a good indicator of histological intestinal metaplasia, which is a well-known risk factor for the development of differentiated-type gastric cancer. NBI observation of a light blue crest, defined as a fine blue-white line on the crests of the epithelial surface or gyri, correlated with the histologic diagnosis of intestinal metaplasia with 89% sensitivity and 93% specificity. The light blue crest was frequently observed in the mucosa surrounding differentiated-type early gastric cancers, and it demarcated the extent of the tumors (Figure 3C).

In a study involving 165 patients with depressed-type early gastric cancers, Nakayoshi *et al.*^[37] reported that ME-NBI is not sufficient to replace conventional histology, but is capable of predicting the histological characteristics of gastric cancer. They classified the abnormal microvascular pattern into two types. In the case of differentiated-type depressed early gastric cancer, a relatively regular fine network pattern was more likely to be observed, while for the undifferentiated-type, a irregular, twisting, or corkscrew pattern was more likely to be observed, representing a relatively low density of microvessels. However, ME-NBI may not be sufficient to replace conventional histology, but it may allow improved differentiation between benign and malignant minute lesions and may be useful for diagnosing the extent of cancerous infiltration.

MULTIBAND IMAGING

Multiband imaging (MBI) represents a digital image processing technique that enhances the appearance of mucosal surface structures by using selected wavelengths of light in reconstructed virtual images. MBI technology uses a software-driven image-processing algorithm that is based on spectral estimation methods. A standard image captured by a color charge-coupled device video endoscope is sent to a spectral estimation matrix processing circuit contained in the video processor. Here, reflectance spectra of corresponding pixels that make up the conventional image are mathematically estimated. From these spectra, it is feasible to reconstruct a virtual image of a single wavelength. Three such single-wavelength images can be selected and assigned to the red, green and blue monitor inputs, respectively, to display a composite color-enhanced MBI image in real-time^[9]. There are very few published data thus far on the efficacy of MBI for detection or differentiation of GI tract lesions, although the technique

seems to be superior to WLE, noninvasive and may more easily detect lesions without dye, during both routine and detailed examinations^[39,40].

In conclusion, these new endoscopic techniques provide better visualization of mucosal surface microstructure and microvascular architecture and may enhance the diagnosis and characterization of mucosal lesions in the GI tract. In the near future, trimodal imaging endoscopy, which combines WLE, AFI and ME-NBI, is expected to be practiced as a standard endoscopy technique as it is quick, safe and accurate for making a precise diagnosis of GI pathology. Although there is compelling evidence that these new techniques are superior to conventional endoscopy, current clinical guidelines are still limited. Further large-scale randomized controlled trials comparing these modalities in different patient subpopulations are, of course, warranted before their endorsement in the routine practice of GI endoscopy.

REFERENCES

- 1 Haringsma J, Tytgat GN, Yano H, Iishi H, Tatsuta M, Ogihara T, Watanabe H, Sato N, Marcon N, Wilson BC, Cline RW. Autofluorescence endoscopy: feasibility of detection of GI neoplasms unapparent to white light endoscopy with an evolving technology. *Gastrointest Endosc* 2001; **53**: 642-650
- 2 Uedo N, Iishi H, Tatsuta M, Yamada T, Ogiyama H, Imanaka K, Sugimoto N, Higashino K, Ishihara R, Narahara H, Ishiguro S. A novel videoendoscopy system by using autofluorescence and reflectance imaging for diagnosis of esophagogastric cancers. *Gastrointest Endosc* 2005; **62**: 521-528
- 3 Song LM, Adler DG, Conway JD, Diehl DL, Farraye FA, Kantsevov SV, Kwon R, Mamula P, Rodriguez B, Shah RJ, Tierney WM. Narrow band imaging and multiband imaging. *Gastrointest Endosc* 2008; **67**: 581-589
- 4 Haringsma J, Tytgat GN. Fluorescence and autofluorescence. *Baillieres Best Pract Res Clin Gastroenterol* 1999; **13**: 1-10
- 5 Kato M, Kaise M, Yonezawa J, Yoshida Y, Tajiri H. Autofluorescence endoscopy versus conventional white light endoscopy for the detection of superficial gastric neoplasia: a prospective comparative study. *Endoscopy* 2007; **39**: 937-941
- 6 Ragunath K. Autofluorescence endoscopy--not much gain after all? *Endoscopy* 2007; **39**: 1021-1022
- 7 Kara MA, Peters FP, Ten Kate FJ, Van Deventer SJ, Fockens P, Bergman JJ. Endoscopic video autofluorescence imaging may improve the detection of early neoplasia in patients with Barrett's esophagus. *Gastrointest Endosc* 2005; **61**: 679-685
- 8 Kara MA, Smits ME, Rosmolen WD, Bultje AC, Ten Kate FJ, Fockens P, Tytgat GN, Bergman JJ. A randomized crossover study comparing light-induced fluorescence endoscopy with standard videoendoscopy for the detection of early neoplasia in Barrett's esophagus. *Gastrointest Endosc* 2005; **61**: 671-678
- 9 Ohkawa A, Miwa H, Namihisa A, Kobayashi O, Nakaniwa N, Ohkusa T, Ogihara T, Sato N. Diagnostic performance of light-induced fluorescence endoscopy for gastric neoplasms. *Endoscopy* 2004; **36**: 515-521
- 10 Wang TD, Triadafilopoulos G. Autofluorescence imaging: have we finally seen the light? *Gastrointest Endosc* 2005; **61**: 686-688
- 11 Curvers WL, Singh R, Song LM, Wolfsen HC, Ragunath K, Wang K, Wallace MB, Fockens P, Bergman JJ. Endoscopic trimodal imaging for detection of early neoplasia in Barrett's esophagus: a multi-centre feasibility study using high-resolution endoscopy, autofluorescence imaging and narrow band imaging incorporated in one endoscopy system. *Gut* 2008; **57**: 167-172

- 12 **Kara MA**, Bergman JJ. Autofluorescence imaging and narrow-band imaging for the detection of early neoplasia in patients with Barrett's esophagus. *Endoscopy* 2006; **38**: 627-631
- 13 **Kato M**, Kaise M, Yonezawa J, Goda K, Toyozumi H, Yoshimura N, Yoshida Y, Kawamura M, Tajiri H. Trimodal imaging endoscopy may improve diagnostic accuracy of early gastric neoplasia: a feasibility study. *Gastrointest Endosc* 2009; **70**: 899-906
- 14 **Gostout CJ**, Jacques SL. Infrared video imaging of subsurface vessels: a feasibility study for the endoscopic management of gastrointestinal bleeding. *Gastrointest Endosc* 1995; **41**: 218-224
- 15 **Iseki K**, Tatsuta M, Iishi H, Sakai N, Yano H, Ishiguro S. Effectiveness of the near-infrared electronic endoscope for diagnosis of the depth of involvement of gastric cancers. *Gastrointest Endosc* 2000; **52**: 755-762
- 16 **Mataki N**, Nagao S, Kawaguchi A, Matsuzaki K, Miyazaki J, Kitagawa Y, Nakajima H, Tsuzuki Y, Itoh K, Niwa H, Miura S. Clinical usefulness of a new infrared videoendoscope system for diagnosis of early stage gastric cancer. *Gastrointest Endosc* 2003; **57**: 336-342
- 17 **Ito S**, Muguruma N, Kimura T, Yano H, Imoto Y, Okamoto K, Kaji M, Sano S, Nagao Y. Principle and clinical usefulness of the infrared fluorescence endoscopy. *J Med Invest* 2006; **53**: 1-8
- 18 **Kimura T**, Muguruma N, Ito S, Okamura S, Imoto Y, Miyamoto H, Kaji M, Kudo E. Infrared fluorescence endoscopy for the diagnosis of superficial gastric tumors. *Gastrointest Endosc* 2007; **66**: 37-43
- 19 **Muto M**, Horimatsu T, Ezoe Y, Hori K, Yukawa Y, Morita S, Miyamoto S, Chiba T. Narrow-band imaging of the gastrointestinal tract. *J Gastroenterol* 2009; **44**: 13-25
- 20 **Kuznetsov K**, Lambert R, Rey JF. Narrow-band imaging: potential and limitations. *Endoscopy* 2006; **38**: 76-81
- 21 **Inoue H**, Honda T, Nagai K, Kawano T, Yoshino K, Takeshita K, Endo M. Ultra-high magnification endoscopic observation of carcinoma in situ of the oesophagus. *Dig Endosc* 1997; **9**: 16-18
- 22 **Kumagai Y**, Inoue H, Nagai K, Kawano T, Iwai T. Magnifying endoscopy, stereoscopic microscopy, and the microvascular architecture of superficial esophageal carcinoma. *Endoscopy* 2002; **34**: 369-375
- 23 **Yoshida T**, Inoue H, Usui S, Satodate H, Fukami N, Kudo SE. Narrow-band imaging system with magnifying endoscopy for superficial esophageal lesions. *Gastrointest Endosc* 2004; **59**: 288-295
- 24 **Inoue H**, Kaga M, Sato Y, Sugaya S, Kudo S. Magnifying endoscopic diagnosis of tissue atypia and cancer invasion depth in the area of pharyngo-esophageal squamous epithelium by NBI enhanced magnification image: IPCL pattern classification. In: Cohen J, editor. Comprehensive atlas of high resolution endoscopy and narrow band imaging. Oxford, UK: Blackwell Publishing Ltd, 2007: 49-66
- 25 **Muto M**, Katada C, Sano Y, Yoshida S. Narrow band imaging: a new diagnostic approach to visualize angiogenesis in superficial neoplasia. *Clin Gastroenterol Hepatol* 2005; **3**: S16-S20
- 26 **Muto M**, Nakane M, Katada C, Sano Y, Ohtsu A, Esumi H, Ebihara S, Yoshida S. Squamous cell carcinoma in situ at oropharyngeal and hypopharyngeal mucosal sites. *Cancer* 2004; **101**: 1375-1381
- 27 **Kara MA**, Ennahachi M, Fockens P, ten Kate FJ, Bergman JJ. Detection and classification of the mucosal and vascular patterns (mucosal morphology) in Barrett's esophagus by using narrow band imaging. *Gastrointest Endosc* 2006; **64**: 155-166
- 28 **Sharma P**, Bansal A, Mathur S, Wani S, Cherian R, McGregor D, Higbee A, Hall S, Weston A. The utility of a novel narrow band imaging endoscopy system in patients with Barrett's esophagus. *Gastrointest Endosc* 2006; **64**: 167-175
- 29 **Goda K**, Tajiri H, Ikegami M, Urashima M, Nakayoshi T, Kaise M. Usefulness of magnifying endoscopy with narrow band imaging for the detection of specialized intestinal metaplasia in columnar-lined esophagus and Barrett's adenocarcinoma. *Gastrointest Endosc* 2007; **65**: 36-46
- 30 **Singh R**, Anagnostopoulos GK, Yao K, Karageorgiou H, Fortun PJ, Shonde A, Garsed K, Kaye PV, Hawkey CJ, Ragunath K. Narrow-band imaging with magnification in Barrett's esophagus: validation of a simplified grading system of mucosal morphology patterns against histology. *Endoscopy* 2008; **40**: 457-463
- 31 **Singh R**, Karageorgiou H, Owen V, Garsed K, Fortun PJ, Fogden E, Subramaniam V, Shonde A, Kaye P, Hawkey CJ, Ragunath K. Comparison of high-resolution magnification narrow-band imaging and white-light endoscopy in the prediction of histology in Barrett's oesophagus. *Scand J Gastroenterol* 2009; **44**: 85-92
- 32 **Herrero LA**, Curvers WL, Bansal A, Wani S, Kara M, Schenk E, Schoon EJ, Lynch CR, Rastogi A, Pondugula K, Weusten B, Sharma P, Bergman JJ. Zooming in on Barrett oesophagus using narrow-band imaging: an international observer agreement study. *Eur J Gastroenterol Hepatol* 2009; **21**: 1068-1075
- 33 **Curvers WL**, Bohmer CJ, Mallant-Hent RC, Naber AH, Ponssioen CI, Ragunath K, Singh R, Wallace MB, Wolfsen HC, Song LM, Lindeboom R, Fockens P, Bergman JJ. Mucosal morphology in Barrett's esophagus: interobserver agreement and role of narrow band imaging. *Endoscopy* 2008; **40**: 799-805
- 34 **Kara MA**, Peters FP, Rosmolen WD, Krishnadath KK, ten Kate FJ, Fockens P, Bergman JJ. High-resolution endoscopy plus chromoendoscopy or narrow-band imaging in Barrett's esophagus: a prospective randomized crossover study. *Endoscopy* 2005; **37**: 929-936
- 35 **Yao K**, Nagahama T, Hirai F, Sou S, Matsui T, Tanabe H, Iwashita A, Kaye P, Ragunath K. Clinical application of magnification endoscopy with NBI in the stomach and the duodenum. In: Cohen J, editor. Comprehensive atlas of high resolution endoscopy and narrow band imaging. Oxford, UK: Blackwell Publishing Ltd, 2007: 83-103
- 36 **Uedo N**, Ishihara R, Iishi H, Yamamoto S, Yamamoto S, Yamada T, Imanaka K, Takeuchi Y, Higashino K, Ishiguro S, Tatsuta M. A new method of diagnosing gastric intestinal metaplasia: narrow-band imaging with magnifying endoscopy. *Endoscopy* 2006; **38**: 819-824
- 37 **Nakayoshi T**, Tajiri H, Matsuda K, Kaise M, Ikegami M, Sasaki H. Magnifying endoscopy combined with narrow band imaging system for early gastric cancer: correlation of vascular pattern with histopathology (including video). *Endoscopy* 2004; **36**: 1080-1084
- 38 **Sumiyama K**, Kaise M, Nakayoshi T, Kato M, Mashiko T, Uchiyama Y, Goda K, Hino S, Nakamura Y, Matsuda K, Mochizuki K, Kawamura M, Tajiri H. Combined use of a magnifying endoscope with a narrow band imaging system and a multibending endoscope for en bloc EMR of early stage gastric cancer. *Gastrointest Endosc* 2004; **60**: 79-84
- 39 **Mouri R**, Yoshida S, Tanaka S, Oka S, Yoshihara M, Chayama K. Evaluation and validation of computed virtual chromoendoscopy in early gastric cancer. *Gastrointest Endosc* 2009; **69**: 1052-1058
- 40 **Parra-Blanco A**, Jiménez A, Rembacken B, González N, Nicolás-Pérez D, Gimeno-García AZ, Carrillo-Palau M, Matsuda T, Quintero E. Validation of Fujinon intelligent chromoendoscopy with high definition endoscopes in colonoscopy. *World J Gastroenterol* 2009; **15**: 5266-5273

S- Editor Sun H L- Editor Webster JR E- Editor Ma WH



Adrian Săftoiu, MD, PhD, Professor, and Peter Vilmann, MD, PhD, Professor, Series Editors

Optical coherence tomography and Doppler optical coherence tomography in the gastrointestinal tract

Eugen Osiac, Adrian Săftoiu, Dan Ionut Gheonea, Ion Mandrila, Radu Angelescu

Eugen Osiac, Adrian Săftoiu, Dan Ionut Gheonea, Ion Mandrila, Radu Angelescu, Centre for Research in Gastroenterology and Hepatology, University of Medicine and Pharmacy, 200349 Craiova, Romania

Author contributions: Osiac E and Gheonea DI wrote this paper; Osiac E, Săftoiu A and Gheonea DI designed research, collected tissue biopsies and performed the imaging procedures; Mandrila I and Angelescu R produced experimental models; Săftoiu A assisted the scientific writing of the paper.

Supported by Project number 99CP/I/2007 ANCS and Project number 12-106/2008 CNMP, Romania

Correspondence to: Dr. Eugen Osiac, Centre for Research in Gastroenterology and Hepatology, University of Medicine and Pharmacy, Petru Rares Street, Number 2, 200349 Craiova, Romania. e_osiac@yahoo.com

Telephone: +40-351-405683 Fax: +40-351-405683

Received: July 2, 2010 Revised: July 28, 2010

Accepted: August 4, 2010

Published online: January 7, 2011

Peer reviewer: Xiao-Peng Zhang, Professor, Department of Radiology, Peking University School of Oncology, Beijing Cancer Hospital and Institute, No. 52 Haidian District, Beijing 100142, China

Osiac E, Săftoiu A, Gheonea DI, Mandrila I, Angelescu R. Optical coherence tomography and Doppler optical coherence tomography in the gastrointestinal tract. *World J Gastroenterol* 2011; 17(1): 15-20 Available from: URL: <http://www.wjgnet.com/1007-9327/full/v17/i1/15.htm> DOI: <http://dx.doi.org/10.3748/wjg.v17.i1.15>

INTRODUCTION

Optical coherence tomography (OCT) is a relatively new method in medical imaging, with first attempts being recorded at the beginning of the last decade^[1]. Based on the analyses of light interference properties generated by a low-coherence source (low-coherence interference), OCT is a noninvasive, high-resolution method. With a resolution in the range of 10-15 μm for standard OCT and up to 1-5 μm if special sources are used^[2,3], this method offers cross-section imaging of the sample with a penetration depth of 2-3 mm. Depending on the OCT configuration, Doppler capabilities are also available in order to provide both structural and functional analyses. With the first application in the field of ophthalmology^[4], promising OCT systems have recently been developed for other fields of medicine including cardiology^[5-7], dermatology^[8] and gastroenterology^[9].

Angiogenesis describes the formation of new vessels from preexisting vasculature under physiological and pathological conditions. Tumor neo-angiogenesis is a fundamental step for solid tumor growth and for metastasis, because it results in spread and development of the network of capillaries from existing blood vessels that are capable of providing the necessary oxygen and nutrients. The process is mediated by various stimulatory and inhibi-

Abstract

Optical coherence tomography (OCT) is a noninvasive, high-resolution, high-potential imaging method that has recently been introduced into medical investigations. A growing number of studies have used this technique in the field of gastroenterology in order to assist classical analyses. Lately, 3D-imaging and Doppler capabilities have been developed in different configurations, which make this type of investigation more attractive. This paper reviews the principles and characteristics of OCT and Doppler-OCT in connection with analyses of the detection of normal and pathological structures, and with the possibility to investigate angiogenesis in the gastrointestinal tract.

© 2011 Baishideng. All rights reserved.

Key words: Optical coherence tomography; Doppler; Gastrointestinal tract; Gastrointestinal cancer; Angiogenesis

tory factors^[10], including cytokines (hormone-like peptides and low-molecular-weight albumins) and growth factors. These factors activate different enzymes (proteases, collagenases, gelatinases and heparinases) that degrade the extracellular matrix and proteins of the basal membrane, thus generating the proliferation and migration of endothelial cells. One of the main triggers of neo-angiogenesis is the secretion of the vascular endothelial growth factor (VEGF)/vascular permeability family of factors^[11,12]. VEGFs are cytokines that have many effects on vascular endothelium, and these multifunctional effects can contribute to angiogenic responses^[11].

The influence of these angiogenic factors is included in different mathematical models, using different living tissue or artificial tissue models such as chick embryo chorioallantoic membrane (CAM) or porous biomaterials^[13-15], in order to describe both the vascular network growth and flow modeling. The purpose of these studies was either to develop understanding of the angiogenesis mechanism or to describe the possibility of direct drug delivery and monitoring of the effects at the level of tumor blood vessels.

Evaluation of angiogenesis thus represents an important step for tumor assessment, especially because of the advent of angiogenesis inhibitors that are already established as anticancer agents. Consequently, to study such a complex process requires multiple correlated investigations that can assess and quantify low-velocity, low-volume blood flow. High-resolution functional imaging methods like 3D-OCT and/or Doppler-OCT could prove to be of considerable importance, especially for the real-time assessment of tumor microvascular flow.

OCT

For the sake of clarity and to associate the physics of the method with its medical applications, a short description of the OCT and Doppler-OCT principles, together with specific characteristics of the experimental system, are provided. Detailed description of the physical principles and mathematical equations that govern the method have been provided by several other papers^[16-20].

Basically, an OCT device provides an analysis similar to B-mode ultrasound investigation^[18]. The main difference is that, instead of using an ultrasound beam, OCT uses low-coherence light, which is provided by a source with emission in the infrared range, typically between 700 and 1500 nm, depending on the optical properties of the target^[21]. In the case of OCT measurements, direct analyses of the reflected intensity is not possible, because of using light, contrary to the case of ultrasound investigation, for which the image obtained is a direct mapping process of the reflected intensity from the target. This is due to the large difference between the velocity of the ultrasound beam and that of the light. Instead, in a standard OCT experiment (Figure 1), the infrared radiation is directed towards an interferometric set-up, where it is split into two beams: one used as reference and directed to a moving mirror, and the other is sent towards the

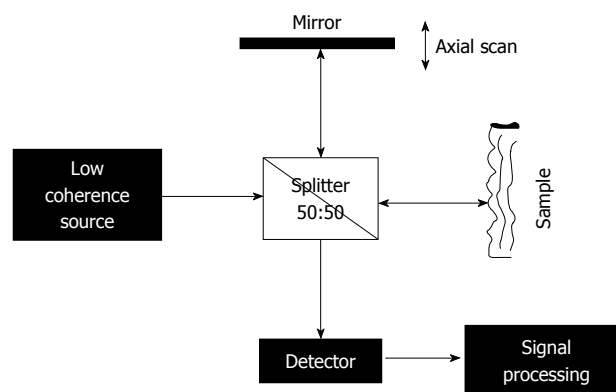


Figure 1 Scheme of a standard optical coherence tomography set-up based on a Michelson interferometer.

sample. After reflection, the sample and reference beams are mixed together, which produces the physical process of interference. Interference occurs only as long as they remain coherent, and the properties of the interference pattern are used as input signal for the imaging process. It should be emphasized that the characteristics of the OCT method are directly related to the properties of the light source used, with the optical characteristics of the sample and with the set-up type.

Based on the above-mentioned factors, advantages and disadvantages of OCT analysis in comparison with ultrasound investigation can be summarized as follows. (1) The main advantage of OCT analysis is higher resolution; 3-15 μm is possible^[2,3]. This is explained by the conditions for the interference process; to produce interference, two beams should be coherent. The light source is partially coherent, which means that coherence of the source is finite, and consequently, the two waves emitted by the source are coherent as long as they are not apart by more than a coherence length of the source. This means that the (optical) length of the reference and sample arm should not differ by more than the coherence length of the source; otherwise the two waves travelling back and forth along these arms do not interfere with each other. It also means that, by controlling the moving mirror in the reference arm (i.e. controlling the length of the reference arm), one has the possibility to control the depth in the sample, from where the reflected signal is received and analyzed (axial resolution); (2) Special mention should be made about the fact that, in an OCT experiment, no connection between the lateral and axial resolution of the measurements exists (in lateral resolution, both control and shape of the beam are playing a major role)^[18,20]. Axial resolution can be estimated using the formula^[16,18]: $\delta z = [(2 \ln 2) / \pi] [\lambda_0^2 / \Delta \lambda]$ (eq. 1), where λ_0 is the central wavelength and $\Delta \lambda$ is the bandwidth, with the assumption that the incoming beam has a Gaussian shape and it travels through the air; nevertheless, in many practical set-ups, the radiation is travelling through optical fibers; (3) Infrared radiation (low-energy photons) is used and the source also has low power (mW range), therefore, this method is completely noninvasive; and (4) A major disadvantage compared to ultrasound as-

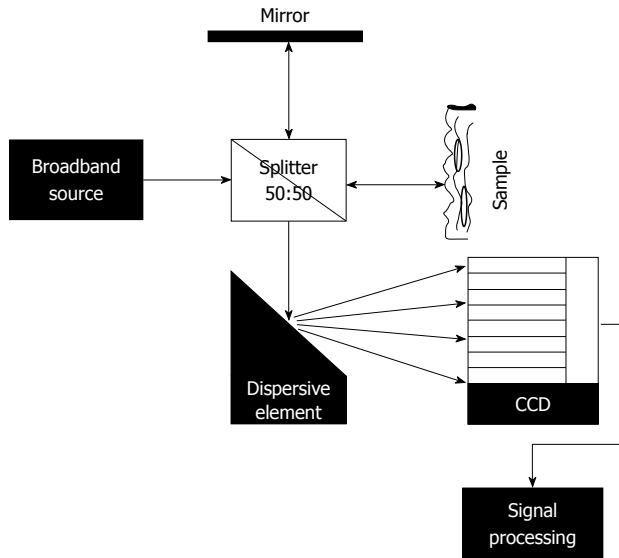


Figure 2 Scheme of Fourier domain-optical coherence tomography set-up.

assessment is the low penetration depth (2-3 mm, depending on the wavelength and optical properties of the analyzed sample^[21,22]), due to the high dispersion and absorption coefficient for the visible-infrared light in biological tissues. Nevertheless, in order to perform analyses that require only millimeter-range penetration depth (different types of mucosa investigation, surface blood microvessels), OCT investigations provide a valuable tool.

As mentioned above, a few parameters (properties of the light source, optical characteristics of the sample, and set-up type) determine the OCT experiments. There are several different set-up configurations for an OCT device used for medical investigations^[16-20]. These include time domain OCT (TD-OCT), Fourier domain OCT (FD-OCT), and swept source OCT (SS-OCT). FD-OCT and SS-OCT are usually grouped together under the name of spectral domain OCT.

TD-OCT was one of the first methods used and it involves a set-up similar to the well-known Michelson interferometer (Figure 1), which has the moving mirror in one arm and the sample in the other. It uses a broad-band light source^[23] and it works similar to the above description. The produced interferogram is measured by a single detector as a function of time delay between the light travelling back and forth along the two arms^[17]. The axial resolution depends on the coherence length of the source^[16,17], and can be given by the equation above (eq. 1). The main disadvantage of this OCT set-up is that it involves mechanical moving parts (moving mirror) that make it difficult to achieve the high scanning rate necessary for *in vivo* 2D and 3D investigations.

FD-OCT uses a charge coupled device or an array photodetector for registering the signal from the interfering light, instead of using a moving mirror and a single detector^[17,18]. A dispersive element (grating or spectrometer) is introduced in the set-up (Figure 2), which projects on to the detector a distribution of the intensity as a function of wavelength. A Fourier transform of the registered

signal provides the back-scattering signal from the sample as a function of time (practically as a function of penetration depth^[16-18]). The main disadvantage in this case is the presence of motion artefacts^[16,19,24].

SS-OCT is similar to FD-OCT but, instead of using a dispersive element to select different wavelengths and an array detector for analyses of the signal, it has a swept source (tunable laser) and a single detector^[17,18,25].

Both FD-OCT and SS-OCT allow direct access to the whole spectrum within one measurement, which offers high sensitivity and imaging resolution, together with high scan rates, which make possible 2D and 3D investigations or fast Doppler measurements^[18,22].

Of these three basic schemes, polarization sensitive detection or phase-sensitive detection can be added in order to improve the imaging process^[16,17].

Doppler-OCT basically estimates the shift in frequency of the laser beam (laser Doppler velocimetry) when the process of the scattering takes place on a moving element^[18,26,27]. As a result of the fact that OCT does not measure directly the reflected intensity, but an interference signal, special mathematical methods are required in order to analyze the received signal; methods which depend on the OCT set-up type^[18]. An important detail is represented by the fact that, if laminar flow is assumed^[20,28], then transversal measurements (in the range of $\pm 15^\circ$) are possible in order to visualize the blood vessels under the sample surface.

The system we have used in our measurements is an SS-OCT from THORLABS (OCS1300SS; Munich, Germany) (Figure 3). The source is a swept laser (55 kHz) with a central wavelength of 1325 nm and an average power of 12 mW. The system is capable of 2D and 3D scans (with an A-scan rate of 55 KHz), with an axial resolution of 12 μm and a lateral resolution of 15 μm . Optical power on the sample is 5 mW. A Doppler module is also available. The system has an image acquisition rate of 50 frames/s.

CLINICAL APPLICATIONS

The possibility offered by the OCT system to deliver near histopathological resolution images makes this method a valuable tool for assessing the gastrointestinal tract. The possibility to investigate tumor structures with high resolution, without performing a classical biopsy, has become very attractive, especially in situations when harvesting biopsy is difficult to realize, or is very hazardous^[9]. Several authors have investigated gastrointestinal cancers by OCT but, due to the late development of Doppler capabilities, few have performed investigations of the angiogenesis process. Generally, to date, most of the studies have evaluated the structural (architectural) changes in the digestive mucosa under pathological conditions, and have identified the correct OCT layer structure inside normal/pathological tissue.

Early studies using OCT techniques have focused on the structure and characteristics of the gastrointestinal tract layers, in order to distinguish between different conditions^[29-32] and patterns, in an attempt to develop computer-assisted diagnostic methods. Also, a lot of interest

has been directed towards the development of the OCT systems (e.g. new sources, fast acquisition rates, different types of catheters, and modeling of the involved physical processes) for the purpose of management during *in vivo* investigations^[29,31,33]. For example, it has been shown that the structure of the esophageal wall (i.e. squamous epithelium, lamina propria, muscularis mucosa, submucosa, and muscularis propria), as well as the stomach layers (i.e. glandular epithelium, muscularis mucosa, submucosa, and muscularis propria) can be assessed by OCT in order to diagnose pathological aspects^[32].

to illustrate the differences in pathology. A pilot study on six volunteers was performed, which made possible the observation of clear differences between normal glandular epithelium, normal squamous epithelium and chronic inflammation from ulcerative colitis.

From the point of view of gastrointestinal tract mapping, most of the studies have involved the upper tract (esophagus, with emphasis on Barrett's esophagus), where studies and imaging analysis are the most advanced^[9,20,43,44] and can assist classic endoscopy. A more challenging task is the stomach, where low resolution and penetration depths are observed^[9,20]. In contrast, the colon is a region where images with good investigative potential have been recorded^[9,18,31].

The Doppler-OCT technique was developed later than standard OCT, and only a few studies have been published^[27,45-48]. Most of the expectations for this method were initially to detect and analyze mucosal and submucosal microvascularization. Position (e.g. lamina propria and submucosa.) and size (small vessel $\leq 100\text{ }\mu\text{m}$, medium vessels $\leq 400\text{ }\mu\text{m}$, and large vessels $\geq 400\text{ }\mu\text{m}$) of the blood vessels could be detected^[48] in different parts of the gastrointestinal tract. Nevertheless, for the clinical translation of Doppler-OCT into a standard medical investigation, patterns and different characteristics of the microvascularization should be identified and used to produce computer-aided diagnostic procedures. There are not many sources that provide values for physical parameters of biological tissues, e.g. (refractive index, dispersion coefficient); values which are necessary for physical and mathematical modelling, and research should be directed towards such measurements.

We have conducted our early experiments on biopsies (Figure 4A and B) and in a chick embryo CAM model (Figures 5 and 6), where human biopsy implants (xenografts) were placed. The images clearly showed the pos-

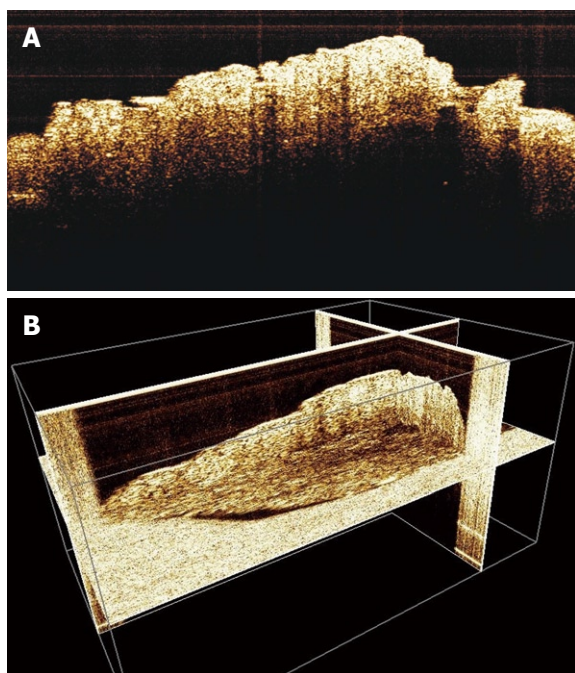


Figure 4 2-D (A) and 3-D (B) optical coherence tomography images of gastric tissue biopsy with visualization of normal components of the parietal layers.

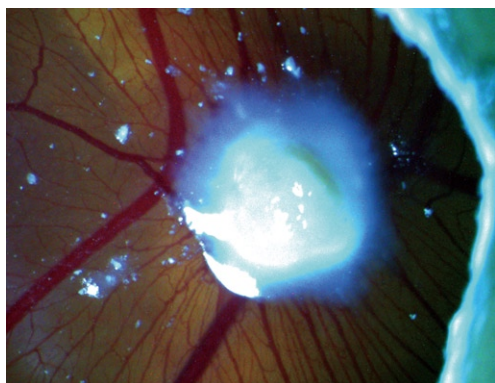


Figure 5 Macroscopic view of a chick embryo chorioallantoic membrane with human gastric tumor implant.

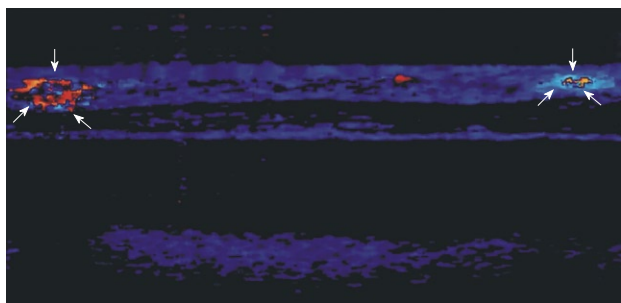


Figure 6 Doppler-optical coherence tomography imaging of a chick embryo chorioallantoic membrane (2 mm x 2 mm) showing capillary activity (arrows) near a human gastric tumor implant.

sibility to identify the microvascularization around the implant zone and the detection of blood flow. It seems that

parameters that characterize the capillary network, such as density, flux and diameter, are accessible to the imaging process, and in addition with other characteristics provided by OCT (i.e. architectural distortion, presence of submucosal glands, and alteration of the layer structure^[9,20]), they can be useful to describe the angiogenesis process.

CONCLUSION

Even though, at present, OCT investigations in gastroenterology are not able alone to provide adequate results (most of the published studies report accuracy and positive predictive values lower than endoscopy), it is worth developing combination of classical endoscopy and OCT techniques to harness the advantages of both. Also, given the large number of medical studies that use these types of devices, as well as recent technical improvements to the systems, it is clear that OCT methods are very promising. At the same time, acquisition of Doppler 3-D images could prove very valuable for the quantitative description of the angiogenesis process, due to the high resolution of this method and the fact that the results can be correlated with structural and functional properties of the samples.

REFERENCES

- 1 Huang D, Swanson EA, Lin CP, Schuman JS, Stinson WG, Chang W, Hee MR, Flotte T, Gregory K, Puliafito CA. Optical coherence tomography. *Science* 1991; **254**: 1178-1181
- 2 Herz P, Chen Y, Aguirre A, Fujimoto J, Mashimo H, Schmitt J, Koski A, Goodnow J, Petersen C. Ultrahigh resolution optical biopsy with endoscopic optical coherence tomography. *Opt Express* 2004; **12**: 3532-3542
- 3 Drexler W, Morgner U, Kärtner FX, Pitris C, Boppart SA, Li XD, Ippen EP, Fujimoto JG. In vivo ultrahigh-resolution optical coherence tomography. *Opt Lett* 1999; **24**: 1221-1223
- 4 Swanson EA, Izatt JA, Hee MR, Huang D, Lin CP, Schuman JS, Puliafito CA, Fujimoto JG. In vivo retinal imaging by optical coherence tomography. *Opt Lett* 1993; **18**: 1864-1866
- 5 Brezinski ME, Tearney GJ, Bouma BE, Izatt JA, Hee MR, Swanson EA, Southern JF, Fujimoto JG. Optical coherence tomography for optical biopsy. Properties and demonstration of vascular pathology. *Circulation* 1996; **93**: 1206-1213
- 6 Bouma BE, Tearney GJ. Clinical imaging with optical coherence tomography. *Acad Radiol* 2002; **9**: 942-953
- 7 Fujimoto JG. Optical coherence tomography for ultrahigh resolution in vivo imaging. *Nat Biotechnol* 2003; **21**: 1361-1367
- 8 Gambichler T, Moussa G, Sand M, Sand D, Altmeyer P, Hoffmann K. Applications of optical coherence tomography in dermatology. *J Dermatol Sci* 2005; **40**: 85-94
- 9 Zhang J, Chen Z, Isenberg G. Gastrointestinal optical coherence tomography: clinical applications, limitations, and research priorities. *Gastrointest Endosc Clin N Am* 2009; **19**: 243-259
- 10 Folkman J. Angiogenesis in cancer, vascular, rheumatoid and other disease. *Nat Med* 1995; **1**: 27-31
- 11 Goetz M, Ziebart A, Foersch S, Vieth M, Waldner MJ, Delaney P, Galle PR, Neurath MF, Kiesslich R. In vivo molecular imaging of colorectal cancer with confocal endomicroscopy by targeting epidermal growth factor receptor. *Gastroenterology* 2010; **138**: 435-446
- 12 Roy H, Bhardwaj S, Ylä-Herttuala S. Biology of vascular endothelial growth factors. *FEBS Lett* 2006; **580**: 2879-2887
- 13 Lemon G, Howard D, Tomlinson MJ, Buttery LD, Rose FR, Waters SL, King JR. Mathematical modelling of tissue-engineered angiogenesis. *Math Biosci* 2009; **221**: 101-120

- 14 **Stéphanou A**, McDougall SR, Anderson ARA, Chaplain MAJ. Mathematical modelling of the influence of blood rheological properties upon adaptative tumour-induced angiogenesis. *Math Comput Model* 2006; **44**: 96-123
- 15 **Ribatti D**, Vacca A, Roncali L, Dammacco F. The chick embryo chorioallantoic membrane as a model for in vivo research on anti-angiogenesis. *Curr Pharm Biotechnol* 2000; **1**: 73-82
- 16 **Schmitt JM**. Optical coherence tomography (OCT): a review. *IEEE J Sel Top Quantum Electron* 1999; **5**: 1205-1215
- 17 **Fercher AF**, Drexler W, Hitzinger CK, Lasser T. Optical coherence tomography - principles and applications. *Rep Prog Phys* 2003; **66**: 239-303
- 18 **Brezinski ME**. Optical coherence tomography: principles and applications. Boston: Academic Press, 2006
- 19 **Tomlins PH**, Wang RK. Theory, developments and applications of optical coherence tomography. *J Phys D Appl Phys* 2005; **38**: 2519-2535
- 20 **Fercher AF**. Optical coherence tomography - development, principles, applications. *Z Med Phys* 2010; **20**: 251-276
- 21 **Wang Y**, Nelson J, Chen Z, Reiser B, Chuck R, Windeler R. Optimal wavelength for ultrahigh-resolution optical coherence tomography. *Opt Express* 2003; **11**: 1411-1417
- 22 **Brezinski ME**, Fujimoto JG. Optical coherence tomography: high-resolution imaging in nontransparent tissue. *IEEE J Sel Top Quantum Electron* 1999; **5**: 1185-1192
- 23 **Unterhuber A**, Povazay B, Bizheva K, Hermann B, Sattmann H, Stingl A, Le T, Seefeld M, Menzel R, Preusser M, Budka H, Schubert Ch, Reitsamer H, Ahnelt PK, Morgan JE, Cowey A, Drexler W. Advances in broad bandwidth light sources for ultrahigh resolution optical coherence tomography. *Phys Med Biol* 2004; **49**: 1235-1246
- 24 **Yun SH**, Tearney G, de Boer J, Bouma B. Motion artifacts in optical coherence tomography with frequency-domain ranging. *Opt Express* 2004; **12**: 2977-2998
- 25 **Huber R**, Wojtkowski M, Fujimoto JG, Jiang JY, Cable AE. Three-dimensional and C-mode OCT imaging with a compact, frequency swept laser source at 1300 nm. *Opt Express* 2005; **13**: 10523-10538
- 26 **Chen Z**, Milner TE, Dave D, Nelson JS. Optical Doppler tomographic imaging of fluid flow velocity in highly scattering media. *Opt Lett* 1997; **22**: 64-66
- 27 **Yang V**, Gordon M, Qi B, Pekar J, Lo S, Seng-Yue E, Mok A, Wilson B, Vitkin I. High speed, wide velocity dynamic range Doppler optical coherence tomography (Part I): System design, signal processing, and performance. *Opt Express* 2003; **11**: 794-809
- 28 **Ren H**, Brecke KM, Ding Z, Zhao Y, Nelson JS, Chen Z. Imaging and quantifying transverse flow velocity with the Doppler bandwidth in a phase-resolved functional optical coherence tomography. *Opt Lett* 2002; **27**: 409-411
- 29 **Sergeev A**, Gelikonov V, Gelikonov G, Feldchtein F, Kuranov R, Gladkova N, Shakhova N, Snopova L, Shakhov A, Kuznetsova I, Denisenko A, Pochinko V, Chumakov Y, Streltsova O. In vivo endoscopic OCT imaging of precancer and cancer states of human mucosa. *Opt Express* 1997; **1**: 432-440
- 30 **Feldchtein F**, Gelikonov G, Gelikonov V, Kuranov R, Sergeev A, Gladkova N, Shakhov A, Shakhova N, Snopova L, Terent'eva A, Zagaynova E, Chumakov Y, Kuznetsova I. Endoscopic applications of optical coherence tomography. *Opt Express* 1998; **3**: 257-270
- 31 **Isenberg G**, Sivak MV Jr. Gastrointestinal optical coherence tomography. *Tech Gastrointest Endosc* 2003; **5**: 94-101
- 32 **Zuccaro G**, Gladkova N, Vargo J, Feldchtein F, Zagaynova E, Conwell D, Falk G, Goldblum J, Dumot J, Ponsky J, Gelikonov G, Davros B, Donchenko E, Richter J. Optical coherence tomography of the esophagus and proximal stomach in health and disease. *Am J Gastroenterol* 2001; **96**: 2633-2639
- 33 **Choma M**, Sarunic M, Yang C, Izatt J. Sensitivity advantage of swept source and Fourier domain optical coherence tomography. *Opt Express* 2003; **11**: 2183-2189
- 34 **Chen Y**, Aguirre AD, Hsiung PL, Huang SW, Mashimo H, Schmitt JM, Fujimoto JG. Effects of axial resolution improvement on optical coherence tomography (OCT) imaging of gastrointestinal tissues. *Opt Express* 2008; **16**: 2469-2485
- 35 **Evans JA**, Poneros JM, Bouma BE, Bressner J, Halpern EF, Shishkov M, Lauwers GY, Mino-Kenudson M, Nishioka NS, Tearney GJ. Optical coherence tomography to identify intramucosal carcinoma and high-grade dysplasia in Barrett's esophagus. *Clin Gastroenterol Hepatol* 2006; **4**: 38-43
- 36 **Evans JA**, Bouma BE, Bressner J, Shishkov M, Lauwers GY, Mino-Kenudson M, Nishioka NS, Tearney GJ. Identifying intestinal metaplasia at the squamocolumnar junction by using optical coherence tomography. *Gastrointest Endosc* 2007; **65**: 50-56
- 37 **Shen B**, Zuccaro G Jr. Optical coherence tomography in the gastrointestinal tract. *Gastrointest Endosc Clin N Am* 2004; **14**: 555-571, x
- 38 **Testoni PA**, Mangiavillano B, Albarello L, Mariani A, Arcidiacono PG, Masci E, Doglioni C. Optical coherence tomography compared with histology of the main pancreatic duct structure in normal and pathological conditions: an 'ex vivo study'. *Dig Liver Dis* 2006; **38**: 688-695
- 39 **Testoni PA**, Mangiavillano B. Optical coherence tomography for bile and pancreatic duct imaging. *Gastrointest Endosc Clin N Am* 2009; **19**: 637-653
- 40 **Westphal V**, Rollins AM, Willis J, Sivak MV, Izatt JA. Correlation of endoscopic optical coherence tomography with histology in the lower-GI tract. *Gastrointest Endosc* 2005; **61**: 537-546
- 41 **Hariri LP**, Tumlinson AR, Besselsen DG, Utzinger U, Gerner EW, Barton JK. Endoscopic optical coherence tomography and laser-induced fluorescence spectroscopy in a murine colon cancer model. *Lasers Surg Med* 2006; **38**: 305-313
- 42 **Adler DC**, Zhou C, Tsai TH, Schmitt J, Huang Q, Mashimo H, Fujimoto JG. Three-dimensional endomicroscopy of the human colon using optical coherence tomography. *Opt Express* 2009; **17**: 784-796
- 43 **Faruqi SA**, Arantes V, Bhutani MS. Barrett's esophagus: current and future role of endosonography and optical coherence tomography. *Dis Esophagus* 2004; **17**: 118-123
- 44 **Isenberg G**, Sivak MV Jr, Chak A, Wong RC, Willis JE, Wolf B, Rowland DY, Das A, Rollins A. Accuracy of endoscopic optical coherence tomography in the detection of dysplasia in Barrett's esophagus: a prospective, double-blinded study. *Gastrointest Endosc* 2005; **62**: 825-831
- 45 **Wong RC**, Yazdanfar S, Izatt JA, Kulkarni MD, Barton JK, Welch AJ, Willis J, Sivak MV Jr. Visualization of subsurface blood vessels by color Doppler optical coherence tomography in rats: before and after hemostatic therapy. *Gastrointest Endosc* 2002; **55**: 88-95
- 46 **Yang VX**, Gordon M, Tang SJ, Marcon N, Gardiner G, Qi B, Bisland S, Seng-Yue E, Lo S, Pekar J, Wilson B, Vitkin I. High speed, wide velocity dynamic range Doppler optical coherence tomography (Part III): in vivo endoscopic imaging of blood flow in the rat and human gastrointestinal tracts. *Opt Express* 2003; **11**: 2416-2424
- 47 **Ahn YC**, Jung W, Zhang J, Chen Z. Investigation of laminar dispersion with optical coherence tomography and optical Doppler tomography. *Opt Express* 2005; **13**: 8164-8171
- 48 **Yang VX**, Tang SJ, Gordon ML, Qi B, Gardiner G, Cirocco M, Kortan P, Haber GB, Kandel G, Vitkin IA, Wilson BC, Marcon NE. Endoscopic Doppler optical coherence tomography in the human GI tract: initial experience. *Gastrointest Endosc* 2005; **61**: 879-890

S- Editor Wang JL L- Editor Kerr C E- Editor Zheng XM

Adrian Săftoiu, MD, PhD, Professor, and Peter Vilmann, MD, PhD, Professor, Series Editors

Confocal laser endomicroscopy and immunoendoscopy for real-time assessment of vascularization in gastrointestinal malignancies

Dan Ionuț Gheonea, Tatiana Cârțână, Tudorel Ciurea, Carmen Popescu, Anca Bădărașu, Adrian Săftoiu

Dan Ionuț Gheonea, Tatiana Cârțână, Tudorel Ciurea, Adrian Săftoiu, Research Center of Gastroenterology and Hepatology, University of Medicine and Pharmacy Craiova, Craiova 200349, Romania

Dan Ionuț Gheonea, Physiology Department, University of Medicine and Pharmacy Carol Davila Bucharest, Bucharest 050474, Romania

Carmen Popescu, Cytology Laboratory, Emergency Hospital Craiova, Craiova 200642, Romania

Anca Bădărașu, Physiology Department, University of Medicine and Pharmacy Carol Davila Bucharest, Bucharest 050474, Romania

Author contributions: Gheonea DI and Cârțână T wrote this paper; Ciurea T, Săftoiu A and Gheonea DI designed the research and performed the imaging procedures; Popescu C interpreted the histology images; Bădărașu A assisted in the scientific writing of the paper.

Supported by Research Grant, No. 239/2007, entitled OCTEUS, financed by the CNCSIS Romania and by the Sectoral Operational Programme Human Resources Development (SOP HRD), financed from the European Social Fund and by the Romanian Government under the contract number POSDRU/89/1.5/S/64109

Correspondence to: Dan Ionuț Gheonea, MD, PhD, MSc, Research Center of Gastroenterology and Hepatology, University of Medicine and Pharmacy Craiova, 1 Mai, 66, Craiova, 200639, Romania. digheonea@gmail.com

Telephone: +40-751-268731 Fax: +40-251-310287

Received: September 12, 2010 Revised: October 19, 2010

Accepted: October 26, 2010

Published online: January 7, 2011

voted capillary network. Confocal laser endomicroscopy is a new technology which allows *in vivo* microscopic analysis of the gastrointestinal mucosa and its microvascularization during ongoing endoscopy by using topically or systemically administered contrast agents. Targeting markers of angiogenesis in association with confocal laser endomicroscopic examination (immunoendoscopy), as a future challenge, will add functional analysis to the morphological aspect of the neoplastic process. This review describes previous experience in endomicroscopic examination of the upper and lower digestive tract with emphasis on vascularization, resulting in a broad spectrum of potential clinical applications, and also preclinical research that could be translated to human studies.

© 2011 Baishideng. All rights reserved.

Key words: Confocal laser endomicroscopy; Immunoendoscopy; Fluoresceine; Acriflavine; Cancer

Peer reviewer: Yuji Naito, Professor, Kyoto Prefectural University of Medicine, Kamigyo-ku, Kyoto 602-8566, Japan

Gheonea DI, Cârțână T, Ciurea T, Popescu C, Bădărașu A, Săftoiu A. Confocal laser endomicroscopy and immunoendoscopy for real-time assessment of vascularization in gastrointestinal malignancies. *World J Gastroenterol* 2011; 17(1): 21-27 Available from: URL: <http://www.wjgnet.com/1007-9327/full/v17/i1/21.htm> DOI: <http://dx.doi.org/10.3748/wjg.v17.i1.21>

Abstract

Gastrointestinal cancers represent a major cause of morbidity and mortality, with incomplete response to chemotherapy in the advanced stages and poor prognosis. Angiogenesis plays a crucial part in tumor growth and metastasis, with most gastrointestinal cancers depending strictly on the development of a new and de-

INTRODUCTION

Confocal laser endomicroscopy (CLE) is an emerging technology which allows *in vivo* imaging of cellular and subcellular details of the gut mucosa and vessels during ongoing endoscopy. With real-time microscopic analysis of the mucosal layer at high resolution, an immediate di-

agnosis is possible for different diseases and types of tissues. A magnification of about $1000\times$ enables evaluation of the epithelial cells, connective tissue and changes in vascular patterns. By using intravenously administered fluorescein sodium, images of vessel architecture are readily available, and early recognition of vascular changes in the gastrointestinal (GI) neoplasia is possible^[1]. Furthermore, if real-time diagnosis cannot be obtained, the same technique allows targeted sampling of relevant areas ("smart biopsies") with fewer specimens sent to the pathologist but with significantly higher diagnostic yield compared to random biopsies^[2].

The potential role of CLE has been explored in different pathologic conditions of the GI tract, the possibility of diagnosing premalignant and malignant lesions of the GI tract being particularly important considering the prognostic implications. Gastroenterologists have shown significant interest in this technique, looking for further potential applications in molecular imaging.

Cancers of the digestive tract nowadays represent a major cause of morbidity and mortality. Tumor growth and metastatic potential are strictly dependent on the development of a new and devoted capillary network, which will supply oxygen and nutrients to the newly formed tumor and will allow malignant cells to access the systemic circulation^[3]. Following intravenous administration of contrast agent, CLE allows *in vivo* real-time visualization of the tumor vasculature which is structurally and functionally altered by comparison with the pre-existing vessel network. Furthermore, pre-clinical trials have shown that quantitative characterization of microvessels *in vivo* is possible with confocal mini probes and the additional image processing software^[4]. Such analysis of the microvascular architecture is fundamental for early detection of neoplastic transformation and assessment of the tumor's metastatic potential. The complex, multistep process of neovascularization is the consequence of a dynamic balance between pro- and anti-angiogenic factors^[5]. Targeting markers of angiogenesis, such as vascular endothelial growth factor (VEGF) and epidermal growth factor receptor (EGFR), in association with endomicroscopic examination, as a future challenge, will add to the morphological aspect functional analysis of the neoplastic process. First steps towards such molecular endomicroscopic imaging have been made by recent studies on animal models.

PRINCIPLES AND TECHNIQUE

The newly developed endomicroscope integrates a miniature confocal microscope into the distal tip of a conventional endoscope enabling simultaneous standard video imaging and confocal microscopy of the mucosal layer. During CLE, an argon ion laser delivers an excitation beam of 488 nm wavelength at the surface of the tissue allowing targeted endomicroscopic images to be captured^[6]. By placing the distal tip of the endomicroscope in intimate contact with the mucosa, multiple grayscale optical sections are recorded at different depths within a range of 0-250 μm . The optical slices are parallel with

the mucosal surface with a 7 μm thickness and a lateral resolution of 0.7 μm , the field of view being $475\ \mu\text{m} \times 475\ \mu\text{m}$ ^[7,8].

Apart from this dedicated endomicroscope, CLE can be performed with a miniprobe. This stand-alone confocal probe can be passed through the working channel of most endoscopes for examination of both the upper and the lower digestive tract. The entire probe-based endomicroscopy system consists of a flexible catheter probe representing a bundle of optical fibers linked to a micro-objective, a laser scanning unit (excitation wavelength 488 nm) and control and acquisition software. A range of mini probes were designed with various optical parameters for different endoscopic procedures^[8,9]. The advanced image processing software allows real-time sequence display for an immediate morphologic diagnosis and also post-procedural analysis and editing. It enables vessel detection and quantitative microvascular measurements, features that make the system suitable for angiogenesis studies^[4].

Contrast agents

High-resolution confocal imaging is achieved by using an exogenous fluorescence technique. Of the potentially suitable contrast agents in humans, the most commonly used are intravenous fluorescein sodium (10%) and topically applied acriflavine (0.2%)^[10]. Acriflavine hydrochloride passes the cell membrane and strongly labels acidic constituents, providing clear visualization of the nuclei and cytoplasm, but only in the superficial layers of the mucosa (0-100 μm). Thus, it is particularly important in depicting intraepithelial neoplasia and cancer of the GI tract^[11]. Fluorescein is a slightly acidic, hydrophilic dye with nonspecific staining properties. Within seconds of intravenous administration it strongly binds to serum albumin and makes the vascular pattern easily detectable. The remaining unbound dye diffuses across the capillaries and, by entering the tissue, it highlights the extracellular matrix^[10,11].

With increasing interest by gastroenterologists in molecular imaging, novel fluorescent contrast agents have been developed targeting disease-specific biomarkers. These include labeled peptides which are easy to deliver to the target structure due to their low molecular weight, but they have variable affinity^[12]. A heptapeptide conjugated with fluorescein has been topically administered for specific *in vivo* imaging of human colorectal neoplasia^[13]. Fluorescently labeled antibodies, on the other hand, are highly selective, binding to their defined target, but may induce immune reactions. Already approved therapeutic antibodies could be labeled for imaging tumors, thus deciding the choice of targeted chemotherapy and potentially predicting the response to treatment^[12]. CLE was able to accurately classify human xenograft tumors in mice and human tissue specimens based on their EGFR expression using fluorescently labeled antibodies against EGFR^[14]. Anti-VEGF antibodies were also used as fluorescent contrast agents for *in vivo* molecular imaging in animal models^[15]. Extensive pharmacokinetic and safety studies are needed to define clinical applications for these molecular probes.

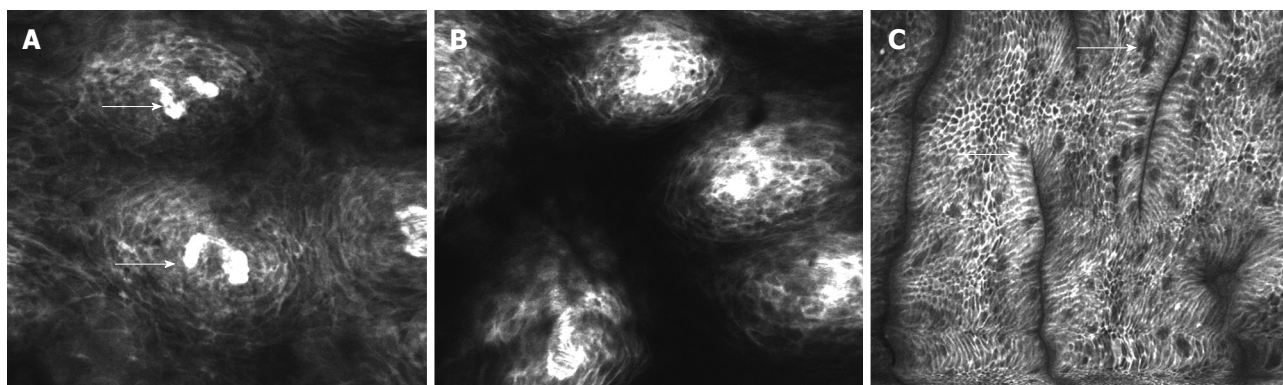


Figure 1 Esophageal surface epithelium visualized using intravenous fluorescein. A: Capillary loops (arrows) of the esophageal papillae; B: Dilatation of intercellular spaces and increased vasculature off the papillae in reflux esophagitis; C: Presence of cylindrical epithelial cells and goblet cells (arrows) in the distal esophagus suggesting Barrett's epithelium.

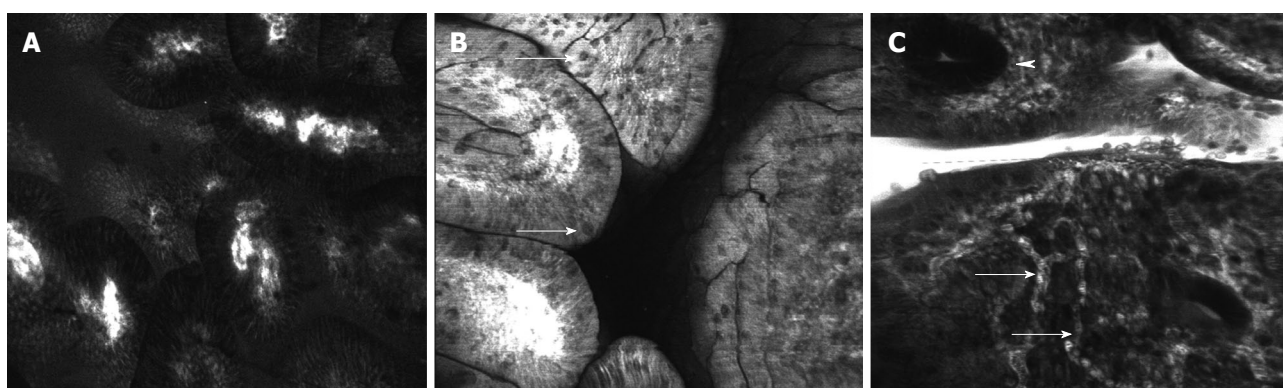


Figure 2 Confocal laser endomicroscopy of the stomach using intravenous fluorescein. A: Columnar epithelium of the antral gastric mucosa and regulated microvascular matrix; B: Atrophic gastritis with intestinal metaplasia and presence of goblet cells (arrows); C: Early gastric cancer with disorganized tissue architecture, few regular crypts (arrowhead) and very tortuous, dilated, irregular vessels (arrows).

CLINICAL APPLICATIONS IN GI CANCERS

The spectrum of potential indications for CLE is broad and includes pathology of both the upper and lower GI tract, most importantly screening and surveillance for cancer based on the cellular and vascular changes. Microscopic imaging of the mucosa is performed after previous detection by standard or optically enhanced endoscopy (autofluorescence imaging, narrow band imaging, i-scan, *etc.*) of “areas of interest”^[10].

Esophagus

The normal endomicroscopic view of the esophageal surface includes polygonal cells within the non-keratinized squamous epithelium and the regular capillary loops of the esophageal papillae directed towards the luminal surface (Figure 1A)^[7,11].

In patients with gastroesophageal reflux disease (Figure 1B), Barrett's epithelium is a well defined premalignant condition associated with adenocarcinoma of the lower esophagus. Although the main diagnostic feature of Barrett's esophagus is the presence of goblet cells, easily detectable with CLE, the vascular pattern, highlighted by fluorescein staining, can also be considered. The subepithelial capillaries are still regular in shape beneath a

specialized columnar epithelium (Figure 1C)^[7]. Significant alterations of the capillary loops are notable in neoplastic tissue with irregular, dilated vessels of increased permeability recognized in the lamina propria due to the brighter signal intensity. Thus CLE is able to detect early neoplastic transformation based on changes in the vascular architecture^[1,16]. In the progression of cancers associated with Barrett's esophagus, angiogenesis represents an essential step. Confocal endomicroscopy can detect this newly developed vascular network and also it enables quantitative measurements such as microvessel density (MVD). Becker *et al.*^[17] evaluated confocal microscopy images acquired from 20 patients, which showed that, in neoplastic Barrett's esophagus, MVD was significantly higher compared to benign conditions.

Stomach

In imaging the stomach, confocal diagnostic criteria have been established in clinical studies for normal gastric mucosa (Figure 2A) as well as for chronic gastritis with intestinal metaplasia (Figure 2B) and cancer by correlation with histopathological examination as the gold standard^[18-22]. While most of these studies classified lesions based mainly on the changes in cells and pit patterns, Liu *et al.*^[23] described endomicroscopic aspects of vascular architecture

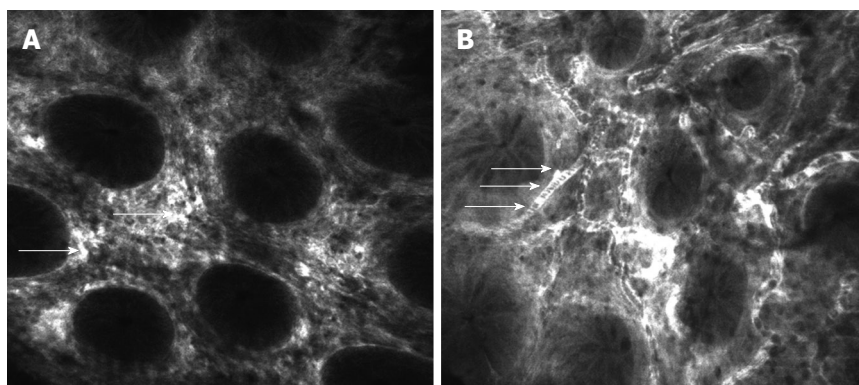


Figure 3 Confocal laser endomicroscopy of the normal colon using intravenous fluorescein. A: Normal aspect of colonic mucosa showing regular architecture of crypts and capillaries of lamina propria (arrows); B: Dark shadows in the lumen of the vessels representing the red blood cells (arrows).

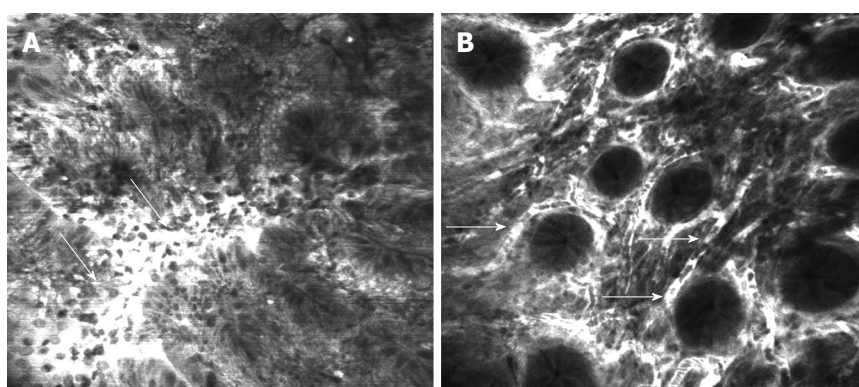


Figure 4 Confocal laser endomicroscopy of the colon using intravenous fluorescein. A: Colon carcinoma with total disorganization of cell architecture, invasion and destruction of the vessels with leakage of fluorescein (arrows); B: Severe inflammatory changes in ulcerative colitis with cellular infiltrate causing an increase in the distance between crypts and excessive vascularity (arrows).

in both normal and malignant mucosa of the upper GI tract. Contrast enhanced CLE (fluorescein sodium 10%, 5 mL) highlights the vascular network of the normal gastric mucosa revealing different aspects between parts of the stomach. The subepithelial capillaries of the gastric body show a honeycomb-like pattern surrounding the gastric pits while in the antrum they are typically coil-shaped. Differentiated early gastric cancer appears to be hypervascular with tortuous, dilated vessels, irregular in shape and size (Figure 2C). In contrast, a hypovascular aspect was described for undifferentiated cancer with isolated, short branch vessels that did not interconnect. In one case report, probe-based endomicroscopy made it possible to diagnose angiodysplasia as a cause of chronic anemia by real-time imaging of a dilated blood vessel with moving red blood cells^[24], adding proof to CLE's feasibility for vascular imaging.

Colon

Clinical trials have delineated potential applications for endomicroscopic examination of the colon. Following intravenous administration of fluorescein the capillaries of the normal colonic mucosa are clearly visualized in the deeper layers of the lamina propria as bright structures (Figure 3A) with moving dark shadows in the lumen representing

the red blood cells which are not labeled by fluorescein (Figure 3B). This network of capillaries circumscribing the regular round mucosal glands results in a typical honeycomb pattern in CLE sequences^[6,11]. In the proximal colon the vasculature appears more dense than in the distal colon, an aspect which correlates with the physiological profile of water absorption along the large intestine^[25].

Confocal patterns based on changes in vessel and crypt architecture have been defined to differentiate among neoplastic and non-neoplastic tissue^[26,27]. In contrast to the regular vascular pattern of the normal mucosa, in colonic cancer the vessels are dilated, distorted with little or no orientation to the adjacent tissue. Increased permeability of the new tumoral vessels is proved by fluorescein passing from the lumen into the interstice which appears intensely bright (Figure 4A)^[11,26]. Colon cancer, with 655 000 deaths worldwide per year, is the second leading cause of cancer-related death in the Western world^[28]. In order to improve the prognosis, colorectal cancer should be detected in the early stages or even precursor stages, when it is possible to cure the selected cases by immediate endoscopic resection. Flat lesions are difficult to detect using standard endoscopic methods and conventional colonoscopy has a significant false-negative rate for intraepithelial neoplasia. CLE is able to predict intraepithelial neoplasia with high

accuracy (99.1%) based on the morphological changes in vascularization mentioned above and the irregular cell architecture^[27].

Precursor neoplastic lesions are also detected by endomicroscopic examination, such as adenomatous polyps, the most important risk factor for colon cancer^[29]. They can be diagnosed microscopically *in situ* with high accuracy, taking into account the altered vascular pattern and also the lack of epithelial surface maturation, crypt budding, and loss of cell polarity^[30].

Patients with inflammatory bowel diseases (IBD), both ulcerative colitis (UC) and Crohn's disease (CD) have a higher risk of developing colorectal cancer as a result of persistent inflammation of the colon. In long-standing ulcerative colitis, CLE is a feasible solution for detecting neoplastic changes in suspect areas. When preceded by a wide-field examination technique, such as chromoendoscopy, CLE has been shown to increase the diagnostic yield of intraepithelial neoplasia while reducing the number of biopsy samples^[31,32]. Inflammatory changes are also depicted by endomicroscopic examination. Increased vasculature of the mucosa (Figure 4B) together with the chronic inflammatory infiltrate result in an enlarged distance between crypts, which show different shapes and sizes^[11].

A recent published study aimed to evaluate the role of CLE in the assessment of inflammatory activity in UC^[33]. On CLE images microvascular alterations and fluorescein leakage as well as crypt architecture were analyzed, and showed good correlation with the histological findings.

While the reported studies have considered mainly descriptive features of the vascular architecture for diagnosis purposes, quantitative measurements of the normal and tumoral vessels could be possible by translating results from preclinical research on small animal models to clinical trials. Laemmel *et al.*^[4] demonstrated in a murine model that is possible to make *in vivo* microvascular observation with a miniprobe confocal fluorescence microscope. They used fluorescein-isothiocyanate-labeled dextran (FITC-dextran) or FITC-albumin injected intra-arterially for clear visualization of the microvascular network. Confocal microscopy enabled observations and measurements usually provided by intravital microscopy: functional capillary density, capillary permeability, vasoconstriction and dilation effects in a minimally invasive procedure. Thus, confocal microscopy has shown potential in the field of microcirculation that should be explored for clinical translation.

IMMUNOENDOSCOPY

The association of endomicroscopic examination with tagged markers of inflammation and proliferation represents an evolutionary leap in GI endoscopy. Thus "immunoendoscopy" aims at the detection and characterization of lesions based on the molecular changes found in inflammation and neoplasia, with potential major impact on current diagnostic and therapeutic algorithms. The exogenous contrast agents for molecular imaging include

fluorescently labeled antibodies and peptides which directly bind to their targets, and "smart" probes with tumor-specific activation^[12].

Goetz *et al.*^[34] approached *in vivo* molecular imaging in a study of human inflammatory and neoplastic diseases in rodent models. They aimed to evaluate a newly developed, handheld confocal miniprobe for *in vivo* subsurface morphological, functional and molecular imaging. Octreotate was labeled with 5-carboxyfluorescein for targeted imaging of somatostatin receptors. After systemic application of developed tracer, neuroendocrine tumors and somatostatin-receptor-expressing pancreatic islet cells were visualized with excellent correlation with immunohistochemistry.

In a pilot *in vivo* human study, a phage library was screened to isolate a peptide that specifically bound colonic dysplasia. The identified heptapeptide sequence was then synthesized and conjugated with fluorescein for use in patients undergoing colonoscopy. After its topical administration, endomicroscopic examination visualized preferential binding of the labeled peptide to dysplastic colonocytes over normal mucosa with high sensitivity and specificity (81% and 82%, respectively), although the molecular target of the sequence was unknown^[13].

With constant interest in understanding angiogenesis and recent advances in antiangiogenic therapies for oncologic patients came the need for imaging this complex process *in vivo*. Targeting angiogenic regulators has been already performed on animal models with promising results for future clinical trials.

One trial evaluated the feasibility of CLE for real-time molecular imaging of EGFR expression, an already established therapeutic target for colorectal cancer^[14]. EGFR is overexpressed in many tumors, playing a central role in proliferation, angiogenesis, invasion, and metastasis^[35,36]. In this trial it was possible to visualize and differentiate EGFR expression patterns in human xenograft tumors in mice with a handheld CLE probe after injection of fluorescently labeled antibodies. Additionally, topical application of fluorescently labeled antibodies provided adequate contrast, enabling distinction of neoplastic from non-neoplastic human colorectal tissue samples based on their EGFR expression^[14]. The same team specifically targeted VEGF for imaging its expression in murine tumors, human xenografts and human tissue samples of colorectal cancer^[15]. VEGF has been intensely studied in basic and clinical research and is already a therapeutic target in metastatic colorectal cancer^[5]. CLE images showed a VEGF-specific signal which correlated well with immunohistochemistry. These studies provide evidence that "immunoendoscopy" is feasible, and results from basic research could be technically translated into clinical practice. *In vivo* molecular imaging could enable selection of patients who would benefit from targeted therapies and could monitor the response to treatment.

Chick embryo chorioallantoic membrane (CAM) is a very convenient experimental model for studying angiogenesis of grafted tumors^[37]. The feasibility of gastric and

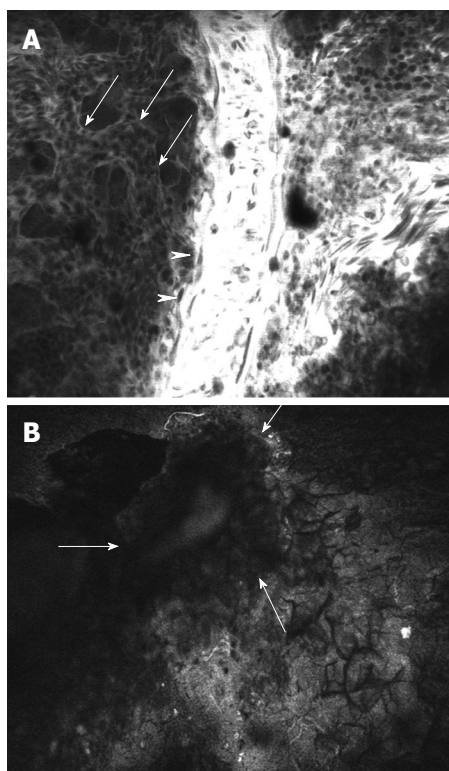


Figure 5 Confocal laser microscopy of the chick embryo chorioallantoic membrane. A: Chick normal chorioallantoic membrane with visualization of large vessels (arrowheads), medium vessels (arrows) and circulating nucleated erythrocytes; B: Fragment of viable human colon cancer tissue (arrows) implanted on chick embryo chorioallantoic membrane.

colonic biopsy implantation, both normal and neoplastic, on the chick CAM for the study of angiogenesis was recently demonstrated^[38]. Fragments of human gastric and colonic mucosa were obtained through endoscopic biopsy, immersed in saline and implanted within 60 min on the chick CAM. Next, the implanted tissue fragments were examined using the confocal laser microscope after previous intravascular administration of 10% fluorescein. Confocal microscopic examination managed to identify both the initial vascularization (Figure 5A) and the newly formed vessels of the grafted tissue (Figure 5B), including intravascular blood flow, representing a starting point for future immunoendoscopy studies in humans, with great therapeutic implications for angiogenic inhibitors.

In conclusion, CLE has led GI endoscopy into a new era. CLE is certainly no longer considered just another endoscopic technique, but a crucial and revolutionary imaging method for real-time assessment of changes in the vascularization pattern of GI structures. Furthermore, *in vivo* molecular imaging, combining CLE with targeted staining, will have a significant impact on both basic research and clinical practice.

REFERENCES

- 1 Deinert K, Kiesslich R, Vieth M, Neurath MF, Neuhaus H. In-vivo microvascular imaging of early squamous-cell cancer of the esophagus by confocal laser endomicroscopy. *Endoscopy* 2007; **39**: 366-368
- 2 Kiesslich R, Neurath MF. Endomicroscopy is born--do we still need the pathologist? *Gastrointest Endosc* 2007; **66**: 150-153
- 3 Folkman J. Fundamental concepts of the angiogenic process. *Curr Mol Med* 2003; **3**: 643-651
- 4 Laemmel E, Genet M, Le Goualher G, Perchant A, Le Gargasson JF, Vicaute E. Fibered confocal fluorescence microscopy (Cell-viZio) facilitates extended imaging in the field of microcirculation. A comparison with intravital microscopy. *J Vasc Res* 2004; **41**: 400-411
- 5 de Castro Junior G, Puglisi F, de Azambuja E, El Saghir NS, Awada A. Angiogenesis and cancer: A cross-talk between basic science and clinical trials (the "do ut des" paradigm). *Crit Rev Oncol Hematol* 2006; **59**: 40-50
- 6 Hoffman A, Goetz M, Vieth M, Galle PR, Neurath MF, Kiesslich R. Confocal laser endomicroscopy: technical status and current indications. *Endoscopy* 2006; **38**: 1275-1283
- 7 Kiesslich R, Goetz M, Neurath MF. Virtual histology. *Best Pract Res Clin Gastroenterol* 2008; **22**: 883-897
- 8 Meining A, Saur D, Bajbouj M, Becker V, Peltier E, Höfler H, von Weyhern CH, Schmid RM, Prinz C. In vivo histopathology for detection of gastrointestinal neoplasia with a portable, confocal miniprobe: an examiner blinded analysis. *Clin Gastroenterol Hepatol* 2007; **5**: 1261-1267
- 9 Wallace MB, Fockens P. Probe-based confocal laser endomicroscopy. *Gastroenterology* 2009; **136**: 1509-1513
- 10 De Palma GD. Confocal laser endomicroscopy in the "in vivo" histological diagnosis of the gastrointestinal tract. *World J Gastroenterol* 2009; **15**: 5770-5775
- 11 Kiesslich R, Galle PR, Neurath MF. Atlas of Endomicroscopy. Springer Medizin Verlag Heidelberg, 2007: 55-79
- 12 Goetz M, Wang TD. Molecular imaging in gastrointestinal endoscopy. *Gastroenterology* 2010; **138**: 828-833.e1
- 13 Hsiung PL, Hardy J, Friedland S, Soetikno R, Du CB, Wu AP, Sahbaie P, Crawford JM, Lowe AW, Contag CH, Wang TD. Detection of colonic dysplasia in vivo using a targeted heptapeptide and confocal microendoscopy. *Nat Med* 2008; **14**: 454-458
- 14 Goetz M, Ziebart A, Foersch S, Vieth M, Waldner MJ, Delaney P, Galle PR, Neurath MF, Kiesslich R. In vivo molecular imaging of colorectal cancer with confocal endomicroscopy by targeting epidermal growth factor receptor. *Gastroenterology* 2010; **138**: 435-446
- 15 Foersch S, Kiesslich R, Waldner MJ, Delaney P, Galle PR, Neurath MF, Goetz M. Molecular imaging of VEGF in gastrointestinal cancer in vivo using confocal laser endomicroscopy. *Gut* 2010; **59**: 1046-1055
- 16 Kiesslich R, Gossner L, Goetz M, Dahmann A, Vieth M, Stolte M, Hoffman A, Jung M, Nafe B, Galle PR, Neurath MF. In vivo histology of Barrett's esophagus and associated neoplasia by confocal laser endomicroscopy. *Clin Gastroenterol Hepatol* 2006; **4**: 979-987
- 17 Becker V, Vieth M, Bajbouj M, Schmid RM, Meining A. Confocal laser scanning fluorescence microscopy for in vivo determination of microvessel density in Barrett's esophagus. *Endoscopy* 2008; **40**: 888-891
- 18 Li WB, Zuo XL, Zuo F, Gu XM, Yu T, Zhao YA, Zhang TG, Zhang JP, Li YQ. Characterization and identification of gastric hyperplastic polyps and adenomas by confocal laser endomicroscopy. *Surg Endosc* 2010; **24**: 517-524
- 19 Guo YT, Li YQ, Yu T, Zhang TG, Zhang JN, Liu H, Liu FG, Xie XJ, Zhu Q, Zhao YA. Diagnosis of gastric intestinal metaplasia with confocal laser endomicroscopy in vivo: a prospective study. *Endoscopy* 2008; **40**: 547-553
- 20 Zhang JN, Li YQ, Zhao YA, Yu T, Zhang JP, Guo YT, Liu H. Classification of gastric pit patterns by confocal endomicroscopy. *Gastrointest Endosc* 2008; **67**: 843-853
- 21 Kitabatake S, Niwa Y, Miyahara R, Ohashi A, Matsuura T, Iguchi Y, Shimoyama Y, Nagasaka T, Maeda O, Ando T, Ohmiya N, Itoh A, Hirooka Y, Goto H. Confocal endomi-

- croscopy for the diagnosis of gastric cancer in vivo. *Endoscopy* 2006; **38**: 1110-1114
- 22 **Kakeji Y**, Yamaguchi S, Yoshida D, Tanoue K, Ueda M, Masunari A, Utsunomiya T, Imamura M, Honda H, Maehara Y, Hashizume M. Development and assessment of morphologic criteria for diagnosing gastric cancer using confocal endomicroscopy: an ex vivo and in vivo study. *Endoscopy* 2006; **38**: 886-890
 - 23 **Liu H**, Li YQ, Yu T, Zhao YA, Zhang JP, Zhang JN, Guo YT, Xie XJ, Zhang TG, Desmond PV. Confocal endomicroscopy for in vivo detection of microvascular architecture in normal and malignant lesions of upper gastrointestinal tract. *J Gastroenterol Hepatol* 2008; **23**: 56-61
 - 24 **Meining A**, Bajbouj M, Schmid RM. Confocal fluorescence microscopy for detection of gastric angiodysplasia. *Endoscopy* 2007; **39** Suppl 1: E145
 - 25 **Polglase AL**, McLaren WJ, Skinner SA, Kiesslich R, Neurath MF, Delaney PM. A fluorescence confocal endomicroscope for in vivo microscopy of the upper- and the lower-GI tract. *Gastrointest Endosc* 2005; **62**: 686-695
 - 26 **Kiesslich R**, Burg J, Vieth M, Gnaendiger J, Enders M, Delaney P, Polglase A, McLaren W, Janell D, Thomas S, Nafe B, Galle PR, Neurath MF. Confocal laser endoscopy for diagnosing intraepithelial neoplasias and colorectal cancer in vivo. *Gastroenterology* 2004; **127**: 706-713
 - 27 **Hurlstone DP**, Baraza W, Brown S, Thomson M, Tiffin N, Cross SS. In vivo real-time confocal laser scanning endomicroscopic colonoscopy for the detection and characterization of colorectal neoplasia. *Br J Surg* 2008; **95**: 636-645
 - 28 **Jemal A**, Siegel R, Ward E, Hao Y, Xu J, Murray T, Thun MJ. Cancer statistics, 2008. *CA Cancer J Clin* 2008; **58**: 71-96
 - 29 **Rickert RR**, Auerbach O, Garfinkel L, Hammond EC, Frasca JM. Adenomatous lesions of the large bowel: an autopsy survey. *Cancer* 1979; **43**: 1847-1857
 - 30 **Sanduleanu S**, Driessen A, Gomez-Garcia E, Hameeteman W, de Bruïne A, Masclee A. In vivo diagnosis and classification of colorectal neoplasia by chromoendoscopy-guided confocal laser endomicroscopy. *Clin Gastroenterol Hepatol* 2010; **8**: 371-378
 - 31 **Kiesslich R**, Goetz M, Lammersdorf K, Schneider C, Burg J, Stolte M, Vieth M, Nafe B, Galle PR, Neurath MF. Chromoscopy-guided endomicroscopy increases the diagnostic yield of intraepithelial neoplasia in ulcerative colitis. *Gastroenterology* 2007; **132**: 874-882
 - 32 **Hurlstone DP**, Kiesslich R, Thomson M, Atkinson R, Cross SS. Confocal chromoscopic endomicroscopy is superior to chromoscopy alone for the detection and characterisation of intraepithelial neoplasia in chronic ulcerative colitis. *Gut* 2008; **57**: 196-204
 - 33 **Li CQ**, Xie XJ, Yu T, Gu XM, Zuo XL, Zhou CJ, Huang WQ, Chen H, Li YQ. Classification of inflammation activity in ulcerative colitis by confocal laser endomicroscopy. *Am J Gastroenterol* 2010; **105**: 1391-1396
 - 34 **Goetz M**, Fottner C, Schirmacher E, Delaney P, Gregor S, Schneider C, Strand D, Kanzler S, Memadathil B, Weyand E, Holtmann M, Schirmacher R, Weber MM, Anlauf M, Klöppel G, Vieth M, Galle PR, Bartenstein P, Neurath MF, Kiesslich R. In-vivo confocal real-time mini-microscopy in animal models of human inflammatory and neoplastic diseases. *Endoscopy* 2007; **39**: 350-356
 - 35 **Grandis JR**, Sok JC. Signaling through the epidermal growth factor receptor during the development of malignancy. *Pharmacol Ther* 2004; **102**: 37-46
 - 36 **Dutta PR**, Maity A. Cellular responses to EGFR inhibitors and their relevance to cancer therapy. *Cancer Lett* 2007; **254**: 165-177
 - 37 **Deryugina EI**, Quigley JP. Chapter 2. Chick embryo chorioallantoic membrane models to quantify angiogenesis induced by inflammatory and tumor cells or purified effector molecules. *Methods Enzymol* 2008; **444**: 21-41
 - 38 **Gheonea DI**, Săftoiu A, Cârțână T, Mândrilă I, Iordache S, Filip M, Ciurea T. Imaging angiogenesis by confocal laser microscopy on digestive tumors grafted on the chick chorioallantoic membrane. *Gut* 2010; **59**: A241

S- Editor Sun H L- Editor Cant MR E- Editor Ma WH



Adrian Săftoiu, MD, PhD, Professor, and Peter Vilmann, MD, PhD, Professor, Series Editors

Contrast-enhanced and targeted ultrasound

Michiel Postema, Odd Helge Gilja

Michiel Postema, Emmy Noether Research Group, Institute of Medical Engineering, Department of Electrical Engineering and Information Sciences, Ruhr-Universität Bochum, 44780 Bochum, Germany

Michiel Postema, Department of Physics and Technology, University of Bergen, 5007 Bergen, Norway

Michiel Postema, Department of Engineering, The University of Hull, Kingston upon Hull HU6 7RX, United Kingdom

Michiel Postema, Centre de Biophysique Moléculaire, UPR 4301 CNRS affiliated to the University of Orléans, 45071 Orléans, France

Odd Helge Gilja, National Center for Ultrasound in Gastroenterology, Department of Medicine, Haukeland University Hospital, 5021 Bergen, Norway

Odd Helge Gilja, Institute of Medicine, University of Bergen, 5007 Bergen, Norway

Author contributions: Postema M and Gilja OH wrote the paper. Correspondence to: Dr. Michiel Postema, Professor, Department of Physics and Technology, University of Bergen, Allégaten 55, 5007 Bergen, Norway. michiel.postema@rub.de
Telephone: +47-555-82880 Fax: +47-555-89440

Received: July 2, 2010 Revised: September 3, 2010

Accepted: September 10, 2010

Published online: January 7, 2011

Abstract

Ultrasonic imaging is becoming the most popular medical imaging modality, owing to the low price per examination and its safety. However, blood is a poor scatterer of ultrasound waves at clinical diagnostic transmit frequencies. For perfusion imaging, markers have been designed to enhance the contrast in B-mode imaging. These so-called ultrasound contrast agents consist of microscopically small gas bubbles encapsulated in biodegradable shells. In this review, the physical principles of ultrasound contrast agent microbubble behavior and their adjustment for drug delivery including sonoporation are described. Furthermore, an outline of clinical imaging applications of contrast-enhanced ultrasound is given. It is a challenging task to quantify and predict which bubble phenomenon occurs under which acoustic condition, and how these phenomena may be utilized in

ultrasonic imaging. Aided by high-speed photography, our improved understanding of encapsulated microbubble behavior will lead to more sophisticated detection and delivery techniques. More sophisticated methods use quantitative approaches to measure the amount and the time course of bolus or reperfusion curves, and have shown great promise in revealing effective tumor responses to anti-angiogenic drugs in humans before tumor shrinkage occurs. These are beginning to be accepted into clinical practice. In the long term, targeted microbubbles for molecular imaging and eventually for directed anti-tumor therapy are expected to be tested.

© 2011 Baishideng. All rights reserved.

Key words: Ultrasound; Drug delivery systems; Drug targeting; Sonoporation; Contrast media; Liver; Pancreas; Gastrointestinal tract

Peer reviewer: Dr. Mirella Fraquelli, Postgraduate School of Gastroenterology, IRCCS Ospedale Maggiore, Milano, 20122, Italy

Postema M, Gilja OH. Contrast-enhanced and targeted ultrasound. *World J Gastroenterol* 2011; 17(1): 28-41 Available from: URL: <http://www.wjgnet.com/1007-9327/full/v17/i1/28.htm>
DOI: <http://dx.doi.org/10.3748/wjg.v17.i1.28>

INTRODUCTION

Advanced medical imaging has a strong impact on research and clinical decision-making in real-time assessment of angiogenesis in digestive cancers. Ultrasonic imaging is becoming the most popular medical imaging modality, owing to the low price per examination^[1] and its safety^[2]. A B-mode ultrasound scan shows contrasted regions from transitions in acoustic impedance, i.e. transitions in tissue type, in the form of brighter pixels. However, blood is a poor scatterer of ultrasound waves at clinical diagnostic transmit frequencies, which lie between 1 and 40 MHz. For perfusion imaging, markers have been designed to en-

hance the contrast in B-mode imaging. These so-called ultrasound contrast agents consist of microscopically small gas bubbles encapsulated in biodegradable shells.

Contrast-enhanced ultrasound (CEUS) represents a significant advancement in the evaluation of angiogenesis in digestive cancers. In particular, in the study of focal liver lesions, CEUS has been widely used for detection and characterization of malignancy. The unique feature of CEUS of non-invasive assessment in real-time liver perfusion throughout the vascular phases has led to a great improvement in diagnostic accuracy of ultrasound, but also in guidance and evaluation of responses to therapy. Currently, CEUS is part of the state-of-the-art diagnostic work-up of focal liver lesions, resulting in safe and cost-effective patient management.

In this review, the physical principles of ultrasound contrast agent microbubble behavior and adjustments for drug delivery, including sonoporation, are described. Furthermore, an outline of clinical imaging applications of CEUS is given.

Ultrasound

The sound that humans can perceive lies within the frequency range 20 Hz–20 kHz. Ultrasound is by definition all sound higher than 20 kHz. The ultrasound frequencies utilized in medical imaging are mainly in the range 1–40 MHz. Such high frequencies cannot be transmitted through air but can be transmitted satisfactorily through solid or fluid materials. An ultrasonic transducer serves a dual function as both transmitter and receiver of ultrasound. A signal generated by an ultrasonic transducer typically consists of a pulse of a few μ s with a certain center frequency. Part of this signal propagates through target tissue, part is reflected by macroscopic tissue structures, part is absorbed by tissue, and part is scattered by structures in the tissue smaller than the acoustic wavelength. Only a small portion of the transmitted acoustic energy is received by the transducer, but this portion is used to build an ultrasonic image. The received signal is the superposition of specular reflections at tissue boundaries and echoes from tissue backscattering^[3]. Current real-time 2-dimensional imaging capabilities are in excess of 30 frames per second^[4]. Contemporary imaging techniques have been summarized by Wells^[5].

The quality of a B-mode scan is expressed by the contrast-to-noise ratio, which is defined as the absolute difference of the signal-to-noise ratio in the target tissue and the signal-to-noise ratio in the surrounding tissue^[4].

On clinical ultrasound devices, the intensity of the ultrasonic field is generally adjusted with a switch for the mechanical index (MI) instead of the acoustic amplitude. The MI depends on the maximum value of peak negative pressure and the centre frequency of the ultrasound field^[6]. For $MI < 0.3$, the acoustic amplitude is considered low. For $0.3 < MI < 0.7$, there is a possibility of minor damage to neonatal lung or intestine^[6]. These are considered moderate acoustic amplitudes. For $MI > 0.7$, there is a risk of cavitation if an ultrasound contrast agent

containing gas microspheres is being used, and there is a theoretical risk of cavitation without the presence of ultrasound contrast agents^[6]. The risk increases with MI values above this threshold^[6]. These are considered high acoustic amplitudes^[7]. In commercial scanners, the MI has been limited to 1.9 for medical imaging^[8]. Figure 1 shows examples of B-mode scans recorded at different MI. At higher MI, the contrast-to-noise ratio increases.

Microbubble physics

The density and compressibility parameters of blood cells hardly differ from those of plasma. Therefore, blood cells are poor scatterers in the clinical diagnostic frequency range^[9]. Since imaging blood flow and measuring organ perfusion are desirable for diagnostic purposes, markers should be added to the blood to differentiate between blood and other tissue types. Such markers must have resonance frequencies in the medical ultrasonic range. Figure 2 shows the resonance frequencies of free and encapsulated gas microbubbles as a function of their equilibrium radius. The resonance frequencies of encapsulated microbubbles lie slightly higher than those of free gas bubbles^[10,11], but clearly well within the clinical diagnostic range, too. Based on their acoustic properties, microbubbles are well suited as an ultrasound contrast agent.

The pressure inside a bubble must be higher than the ambient pressure^[12]. This difference is generally referred to as the surface pressure. The smaller the bubble, the higher is the surface pressure. Since fluids are forced to flow from a location with a higher pressure to a location with a lower pressure, a bubble cannot exist in true equilibrium. For example, a free air bubble with a 6 μ m diameter dissolves within 100 ms^[13]. To prevent quick dissolution, ultrasound contrast agent microbubbles contain low-solubility gas, such as SF₆ or C₃F₈^[14]. The encapsulating shells are made of biodegradable materials, such as phospholipids or albumin^[15]. With mean diameters below 6 μ m, these microbubbles are small enough to pass through the lung capillaries. Detailed overviews of the compositions of the ultrasound contrast agents used most in imaging research have been given by Postema *et al.*^[3], Sboros^[16] and Tinkov *et al.*^[17]. In this section, we classify ultrasound contrast agents into only 4 categories, based on the presence of an encapsulating shell and its thickness, similar to Tinkov *et al.*^[17].

A bubble in a low-amplitude sound field can be considered a forced damped harmonic oscillator^[18,19] and its oscillating behavior can, as a result, be modeled as a mass-spring-dashpot system^[20]. The spherically symmetric oscillating behavior of ultrasound contrast agent microbubbles has been described with models based on the Rayleigh-Plesset equation^[21], modified for the presence of an encapsulating shell^[22–32]. Generally, the presence of blood has a relatively small effect on bubble dynamics^[33]. To give an indication of the vast amount of existing models: Qin *et al.*^[34] defined 16 separate dynamic bubble model classes. The reason for the high number of existing models is the fact that most physical properties of en-

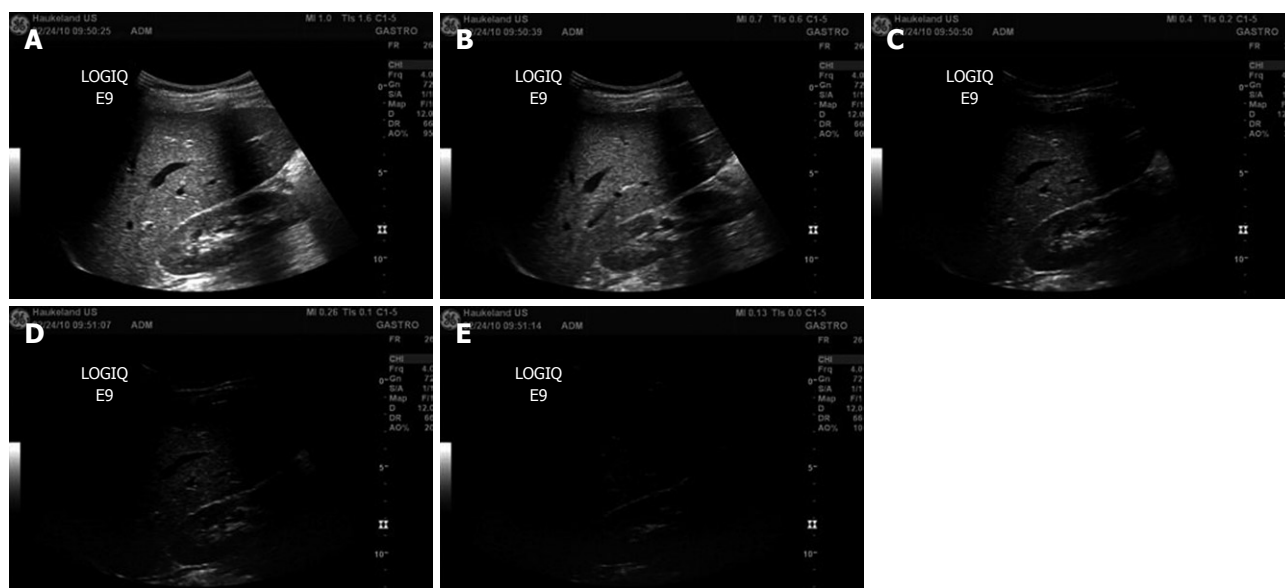


Figure 1 B-mode images of the liver recorded at decreasing mechanical index values (A-E). A: Mechanical index (MI) = 1.0; B: MI = 0.7; C: MI = 0.4; D: MI = 0.26; E: MI = 0.13.

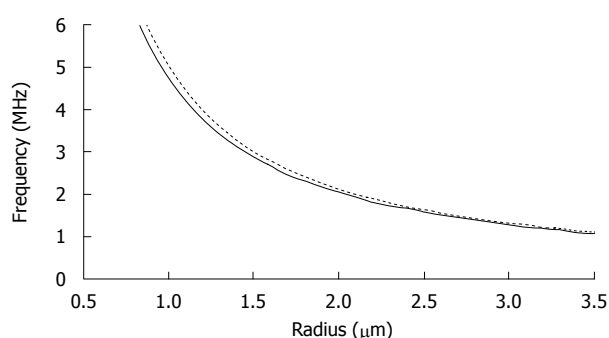


Figure 2 Resonance frequencies of free (unencapsulated) (solid line) and lipid-encapsulated (dotted line) microbubbles as a function of equilibrium radius.

capsulated microbubbles cannot actually be measured, so that pseudo-material properties have to be chosen when predicting ultrasound contrast agent microbubble behavior. Examples of such pseudo-material properties are shell elasticity parameters and shell friction parameters. At low-amplitude driving pressures, an ultrasound contrast agent microbubble oscillates linearly, i.e. the bubble excursion is proportional to the instantaneous pressure. However, at high-amplitude driving pressures, it oscillates nonlinearly. Figure 3 demonstrates the oscillation behavior of 2 contrast microbubbles subjected to continuous sine pressure waves with low, moderate, and high amplitudes. Both bubbles oscillate linearly at $MI = 0.01$. With increasing driving amplitude, asymmetries in radial excursion and expansion time rise, especially for the bigger bubble, which is closer to the resonance size. At $MI = 0.8$, both bubbles expand to a factor of the initial size, followed by a rapid collapse of the smaller bubble. The bigger bubble demonstrates collapse at $MI = 0.18$ and higher.

A dynamic bubble generates an acoustic signal that depends on the fluid displacement by the bubble as a func-

tion of time. Detection strategies have been developed to discriminate acoustic signal-generated by ultrasound contrast agent microbubbles from other acoustic signals such as specular reflections and tissue scattering. These strategies are the reason that CEUS is suitable for the detection of blood. The 10 most common detection strategies include coded excitation, harmonic power Doppler, phase inversion and power modulation^[34,35]. All single-pulse and multi-pulse imaging detection strategies make use of the nonlinear behavior of microbubbles^[34,35].

Other types of nonlinear behavior than asymmetric oscillations are discussed below.

If a bubble with a negligible shell collapses near a free or a solid boundary, the retardation of the liquid near the boundary may cause bubble asymmetry. This asymmetry causes differences in acceleration on the bubble surface. During further collapse, a funnel-shaped jet may protrude through the bubble, shooting liquid to the boundary^[36]. Such jets have been observed in high-speed observations of ultrasound contrast agent microbubbles^[37-40]. Empirical relations exist between the collapsing bubble radius, the jet length, and the pressure at the tip of jets^[41-43]. It has been speculated whether microbubble jetting can be applied for ultrasound-guided drug delivery^[38,39,42].

During the collapse phase, a bubble may fragment into a number of smaller bubbles^[44]. Fragmentation has been observed with contrast agents with thin elastic shells. The number of fragments into which a contrast microbubble breaks up has been associated with asymmetric oscillations^[40,45]. Fragmentation can be predicted from the moment when the kinetic energy of the bubble surpasses its surface energy^[27]. Bubble fragmentation costs energy, but the subsequent coalescence of bubble fragments generates enough acoustic energy to be detected^[27].

Thick-shelled microbubbles have demonstrated sonic cracking during a high-amplitude ultrasonic cycle^[46,47]. The

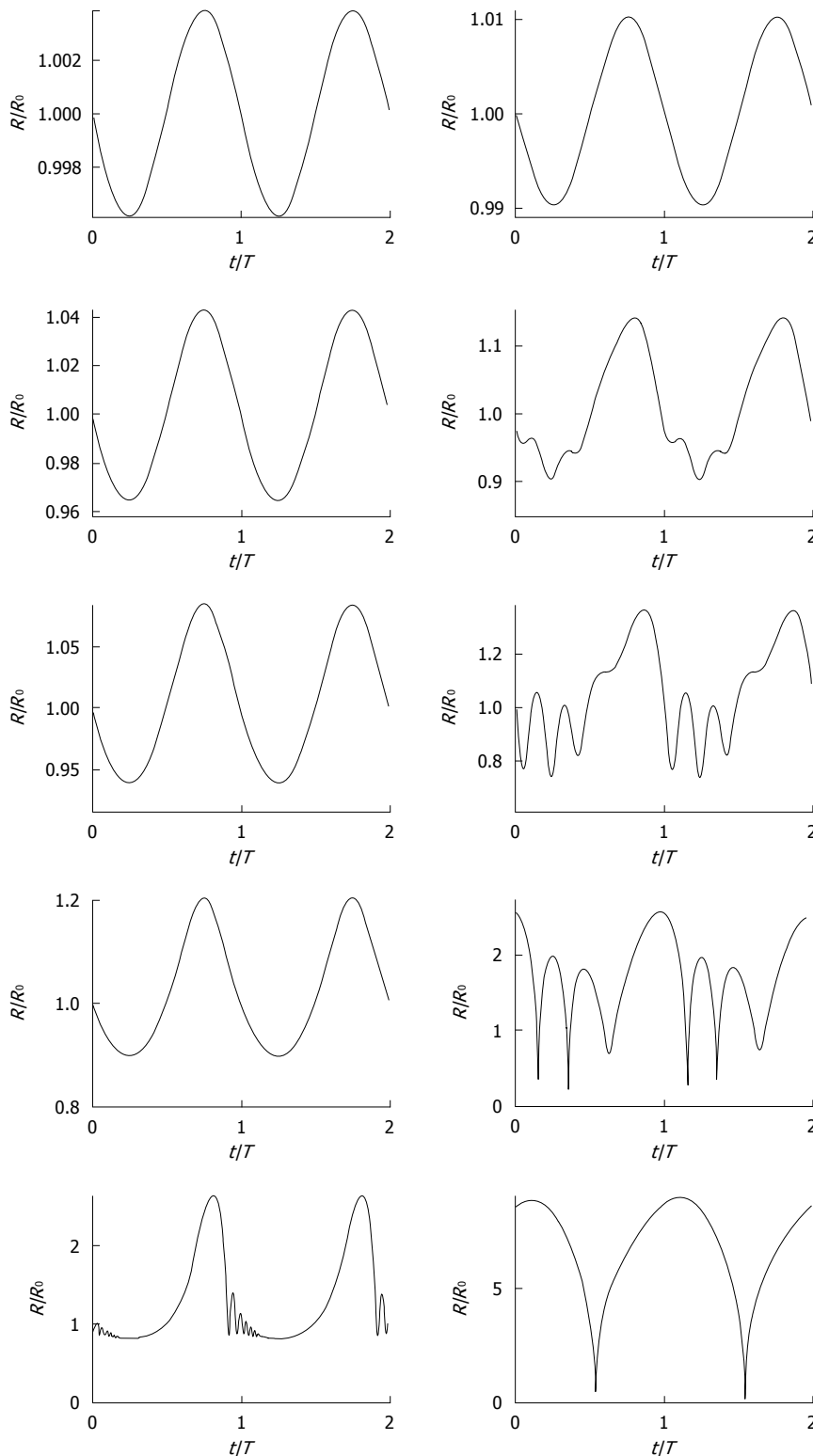


Figure 3 Simulated radius-time curves (radius R normalized with equilibrium radius R_0 , time t normalized with period T_0) of ultrasound contrast microbubbles with $0.55\ \mu\text{m}$ (left column) and $2.3\ \mu\text{m}$ (right column) equilibrium radii, respectively, modeled with a conservative Rayleigh-Plesset equation^[3], using a conservative shell stiffness parameter^[48]. The modeled ultrasound field was a continuous sine wave with a frequency of 0.5 MHz and acoustic amplitudes corresponding to (top-bottom) mechanical index = 0.01, 0.10, 0.18, 0.35, and 0.80, similar to the experiments by Karshafian *et al.*^[92].

increased pressure difference between inside and outside of the microbubble during the expansion phase of the wave^[48] causes the shell to be stretched until it surpasses a critical deformation^[49], resulting in its mechanical cracking. The

released bubble has an expansion amplitude much higher than an encapsulated bubble of identical size. Therefore, the acoustic signal from an ultrasound contrast agent after gas release differs from that of the same contrast agent be-







Phenomenon	Schematic representation	Microbubble classification	Acoustic regime
Translation		I ^[40] , II ^[34,40,149] , III ^[150] , IV ^[56]	L ^[34,56,149] , M, H ^[40]
Fragmentation		I ^[151] , II ^[40,152-155]	L ^[152] , M ^[151,152,154,155] , H ^[40,152,153]
Coalescence		I ^[151] , II ^[154,156]	L ^[154] , M ^[151] , H ^[156]
Jetting		I ^[38,39] , II ^[37,39]	H ^[38,39]
Clustering		II ^[61] , III ^[150]	L ^[61] , M ^[54] , H ^[61,150]
Cracking		II ^[157] , III ^[47,158,159] , IV ^[159]	L ^[158] , M ^[159] , H ^[47]

Figure 4 Nonlinear phenomena and the regimes for their occurrence. Microbubble shell classes: (I) free or released gas; (II) thin shells < 10 nm; (III) thick shells < 500 nm; (IV) very thick shells > 500 nm. Acoustic regimes: low (L) for mechanical index (MI) < 0.3; medium (M) for 0.3 < MI < 0.7; high (H) for MI > 0.7. The figure has been based on Postema^[12].

fore gas release, until the released gas has dissolved^[50].

After a disruptive ultrasonic burst, the disappearance of microbubble fragments or released gas can be traced with low-amplitude ultrasound, as well as the wash-in rate of fresh contrast agent^[51]. Hence, the efficiency of the disruptive burst can be measured.

Bubble translation in the direction of the sound field is caused by a primary radiation force resulting from a pressure gradient across the bubble surface^[52]. The translation is maximal in the contraction phase of the oscillating microbubble. Making use of this phenomenon, ultrasound contrast agent microbubbles can be forced to move farther away from the transducer, towards vessel walls^[53-61], increasing the success rate of targeting to a boundary.

In a standing sound wave field^[62], bubbles can aggregate to clusters ultimately a quarter of the acoustic wavelength apart^[61]. The formation of ultrasound contrast agent microbubble clusters and the ultrasonic pushing of these clusters towards a vessel wall have been recently observed using high-speed photography^[61].

The occurrence of the above-mentioned phenomena is influenced by (1) the ultrasonic parameters: transmit frequency, acoustic amplitude, pulse length, pulse repetition rate and transmit phase; (2) the ultrasound contrast agent composition: the composition of the shell, the bubble sizes, the size distribution and the gas; and (3) the physical properties of the medium: viscosity, surface tension, saturation.

Figure 4 gives an overview of the nonlinear phenomena that have been observed with ultrasound contrast agents, the type of ultrasound contrast agent in which they have occurred, and the minimum acoustic regime required.

Molecular imaging

Dayton *et al.*^[35] defined molecular imaging as the non-invasive application of an imaging modality to discern changes in physiology on a molecular level^[12]. Although ultrasound contrast agents were intended for perfusion imaging, they

have proven useful in molecular imaging as well, after modification of the microbubble shell. Dayton *et al.*^[35] discerned 2 targeting strategies: active targeting, in which a ligand specific for the molecular target, and passive targeting, in which the physiochemical properties of the agent are used to achieve retention at the target site^[12]. Molecular imaging and targeting have been reviewed elsewhere in depth^[35,63]. In summary, the main applications include the detection of angiogenesis, inflammation, plaques and thrombi^[8,12,17].

Drug delivery

It has been proven by numerous groups, that the cellular uptake of drugs and genes is increased, when the region of interest is under sonication, and even more so when a contrast agent is present^[12,64-91]. This increased uptake has been attributed to the formation of transient porosities in the cell membrane, which are big enough for the transport of drugs into the cell. The transient permeabilization and resealing of a cell membrane is called sonoporation^[64]. The sonoporation-induced cellular uptake of markers with molecular weights between 10 kDa and 3 MDa has been reported in several studies^[17,74,92]. Schlicher *et al.*^[93] showed that ultrasound-induced cavitation facilitated cellular uptake of macromolecules with diameters up to 56 nm. Even solid spheres with a 100 nm diameter have been successfully delivered with the aid of sonoporation^[82]. This implies that drug size is not a limiting factor for intracellular delivery^[92]. However, the pore opening times can be so short that, if the drug is to be effectively internalized, it should be released close to the cell membrane when poration occurs^[94].

There are 2 hypotheses for explaining the sonoporation phenomenon, the first being microbubble oscillations near a cell membrane, the second being microbubble jetting through the cell membrane. Based on modeling, high-speed photography, and recent cellular uptake measurements, we concluded that microbubble jetting behavior can be excluded as the dominant sonoporation

mechanism^[7]. The influence of microbubble disruption, i.e. fragmentation or sonic cracking, on sonoporation will have to be further investigated^[7]. Without the presence of an agent, it has been assumed that sonoporation is caused by bubbles, which have been generated in the transducer focus as a result of inertial cavitation^[95,96].

Instead of just facilitating the transient opening up of cell membranes, a microbubble might also act as the vehicle itself to carry a drug or gene load to a perfused region of interest, in which case the load has to be released with the assistance of ultrasound. Apart from mixing ultrasound contrast agent with a therapeutic agent, several schemes have been proposed to combine microbubbles with a therapeutic load^[97]. Tinkov *et al.*^[17] discriminated the following 7 microbubble structure classes for drug delivery: (1) attachment to the outer shell surface; (2) intercalation between monolayer phospholipids; (3) incorporation in a layer of oil; (4) formation of complexes with smaller particles (secondary carriers); (5) physical encapsulation in a polymer layer and coating with biocompatible material; (6) surface loading of protein-shelled microbubbles; and (7) entire volume loading of protein-shelled microbubbles. The drugs are to be released at the site of interest during insonication^[98], presumably by disrupting the microbubble shell. It has been demonstrated *in vitro*, that higher doses of DNA were delivered during ultrasound insonication when the DNA was loaded on albumin-encapsulated microbubbles than when unloaded microbubbles were mixed with plasmid DNA^[67]. Amounts of DNA loading on microbubbles have been between 0.002 (pg/ μm^3)^[99] and 2.4 (pg/ μm^3)^[17,67].

Instead of attaching a drug to the capsule, therapeutic compounds in the gas phase might be encapsulated with thick shells, to keep them from dissolving. At the region of interest, the shell should be cracked with ultrasound, releasing the gaseous content^[46,47,100,101]. However, only a few therapeutic compounds exist in the gaseous phase, e.g. nitric oxide^[48] and several gaseous anesthetics.

A therapeutic agent inside the microbubble shell may react with the shell and dampen the bubble oscillations. Therefore, it might be more suitable to have the therapeutic agent in the core of the microbubble, separated from the shell by a gaseous layer. Incorporating a liquid drop containing drugs or genes inside an ultrasound contrast agent microbubble, however, is technically challenging^[102]. As opposed to bubbles, antibubbles consist of a liquid core encapsulated by gas^[103]. Such a droplet inside a bubble may be generated with the jetting phenomenon: the collapse of a bubble near a free surface produces a liquid jet^[104], which may break up into one or several droplets^[105]. Another option would be to stabilize the liquid core by means of a biodegradable skeleton attached to the microbubble shell.

It has been noted, that, if microbubbles can create pores, it is also possible to create severe cell and tissue damage^[106]. There is an inverse correlation between cell permeability and cell viability^[92,107-109], i.e. not all cell membrane pores are temporary. This indicates that sonoporation is

just a transitory membrane damage in the surviving cell^[92]. Cell lysis results from irreversible mechanical cell membrane damage^[110], which allows the intracellular content to leak out^[64]. Only recently, ultrasound-induced apoptosis has been observed with cancer cells *in vitro*^[110,111], and also in the presence of an ultrasound contrast agent^[112]. Apart from situations where lysis is desired (sonolysis)^[113], ultrasonic settings should be chosen such that cell lysis is minimal. Side effects observed are capillary rupture, hemorrhage, and dye extravasation^[106]. These side effects, however, have been associated with relatively high microbubble concentrations, long ultrasonic pulse lengths, and high acoustic intensities^[106].

CLINICAL IMAGING APPLICATIONS

Liver

Ultrasonography is the most commonly used imaging modality worldwide for diseases of the liver. However, it has limited sensitivity in the detection of small tumor nodules. In addition, ultrasonographic findings are often nonspecific, as images of benign and malignant liver lesions overlap considerably. The introduction of microbubble contrast agents and the development of contrast-specific techniques have opened new prospects in liver ultrasonography. The advent of second-generation agents that enable continuous real-time contrast-enhanced imaging has been instrumental in improving the acceptance and reproducibility of the examination. With the publication of guidelines for the use of contrast agents in liver ultrasonography by the European Federation of Societies for Ultrasound in Medicine and Biology (EFSUMB)^[114,115], CEUS is now routinely used in clinical practice.

As opposed to contrast media used with computed tomography (CT) and magnetic resonance (MR) imaging, ultrasound contrast agents can visualize the capillary net of the examined tissue, because CEUS is considerably more sensitive to very small amounts of contrast agent, even to single bubbles. Furthermore, because sonography is a dynamic method that is performed in real time, additional information about tissue perfusion can be deduced from the influx and washout of the contrast media, thus facilitating the differential diagnosis of tumors. In addition, signals from the microbubbles enable the visualization of slow flow in microscopic vessels without Doppler-related artifacts. Various software packages have been developed to enable quantification of changes in contrast intensity and to provide additional objective information over the entire course of the contrast examination.

Microbubbles enable dynamic imaging of tumor angiogenesis. This approach is now routinely used for diagnosis, particularly for the detection and characterization of various liver tumors.

The most common malignancy of the liver is metastases. Hepatic metastasis is a sign of advanced tumor stage, and curative treatment is only possible in a very small number of patients. When the objective is cure, liver resection is the most effective therapy, but several ablation

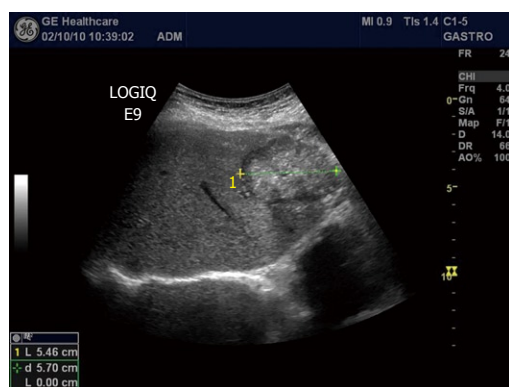


Figure 5 B-mode image of a metastasis from a colon cancer to the liver appearing hyperechoic with a dark halo.

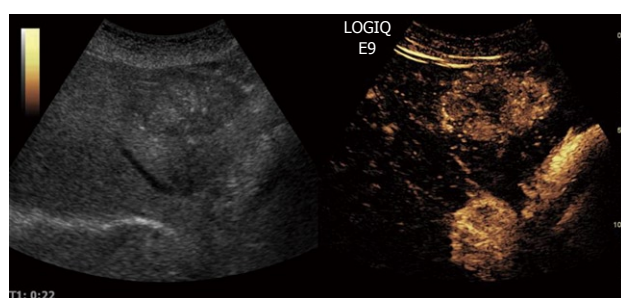


Figure 6 Contrast-enhanced ultrasound B-mode image of a colon cancer metastasis (same as in Figure 5) in the arterial phase showing marked hyperenhancement in the right panel. Note also the dark centre of the tumor, indicating a necrotic portion of the metastasis.

techniques have evolved. For directed tumor therapy, accurate imaging of the number and distribution of the metastases is required. On grey-scale ultrasound images, metastases may appear as hypo-, iso- or hyperechoic lesions, and some of them have a halo (Figure 5). Unenhanced ultrasonography achieves a sensitivity between 45% and 80% in detecting liver metastases^[116,117]. Not surprisingly, this compares unfavorably with the results of studies with contrast-enhanced CT and MR. However, the application of an intravascular ultrasound contrast agent during transcutaneous ultrasonography of the liver improves detection of metastases significantly^[118-120].

After injection, 3 phases of contrast enhancement can be differentiated: the arterial phase, in which the contrast agent reaches the liver first *via* the hepatic artery; the portal phase, where the contrast agent has passed circulation and spreads through the liver in the portal branches; and the late or parenchymal phase, in which the agent slowly distributes within the entire liver parenchyma. Metastases show characteristic features in all 3 phases after contrast agent injection. Differentiation of hypervascular from hypovascular metastases is achieved perfectly by real-time imaging during the arterial phase: hypervascular metastases, e.g. from malignant melanoma, thyroid carcinoma, or neuroendocrine carcinoma, appear as hyperenhancing, usually with a typical rim enhancement of varying size (Figure 6). In contrast, hypovascular metastases le-

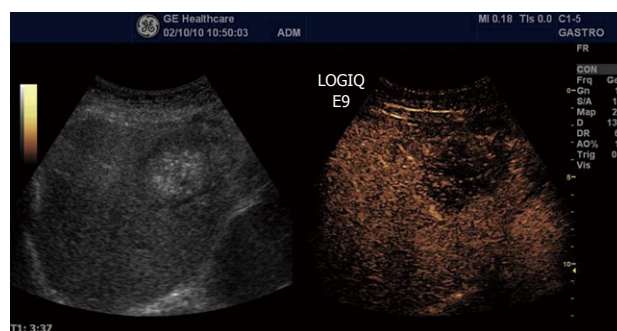


Figure 7 Contrast-enhanced ultrasound B-mode image of a colon cancer metastasis (same as in Figure 5) in the sinusoidal (late) phase, showing marked hypoenhancement in the right panel.

sions, e.g. from colorectal carcinoma (great variability) or bronchogenic carcinoma, may appear as hypoenhancing lesions in the arterial phase. Large metastases may have inhomogeneous enhancement because of necrosis, as shown in Figure 6. At the beginning of the portal phase, the enhancement fades and the entire lesion becomes increasingly hypoechoic. In the late phase, both hypovascular and hypervascular metastases invariably appear as dark defects, whereas the enhancement persists in the normal liver parenchyma (Figure 7). During this phase, the lesions are usually particularly well defined, often with sharp punched-out borders. Both portal venous and late-phase imaging markedly increase the contrast between the enhancing normal liver and the nonenhancing metastases and thus improve detection, particularly of small lesions, i.e. < 1 cm in diameter. The improved detection obtained by the use of ultrasound contrast agents allows for the implementation of CEUS for the follow-up of patients undergoing surgery and chemotherapy, to assess the efficacy of antineoplastic treatment^[121-124]. To determine the utility of CEUS as a prognostic tool for metastatic renal cell carcinoma patients receiving sunitinib, Lassau and co-workers studied 38 patients receiving 50 mg/d sunitinib^[125]. They found that time to peak intensity and slope of the wash-in curve were significantly associated with disease-free survival; time to peak intensity was also significantly associated with overall survival^[125]. Furthermore, they concluded that CEUS is a useful tool for predicting early efficacy of sunitinib in metastatic renal cell carcinoma patients^[125].

Hepatocellular carcinoma

Hepatocellular carcinoma (HCC) is the second common malignant liver tumor and the most common primary liver cancer, usually occurring as a complication of chronic liver disease and most often arising in a cirrhotic liver. The accurate and early diagnosis of HCC is essential for treatment of the affected patients. Surgical resection, liver transplantation, percutaneous alcohol ablation and radio-frequency ablation are potentially curative therapies. On grey-scale sonography, HCCs may be hypoechoic (26%), hyperechoic (13%) or have mixed (61%) echogenicity depending on the size of the tumor, the fat content, the degree of differentiation and the scarring of necrosis^[126].

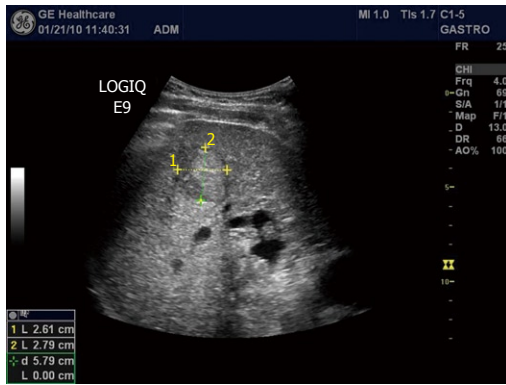


Figure 8 B-mode image of hepatocellular carcinoma with well-demarcated margins and a perilesional halo.

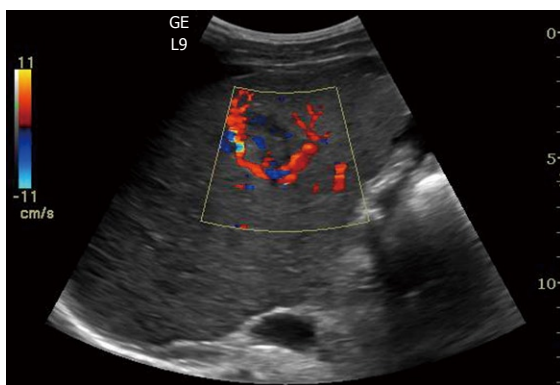


Figure 9 Color Doppler in hepatocellular carcinoma reveals a basket pattern around the tumor, illustrating the anatomy of the arterial tumor supply.

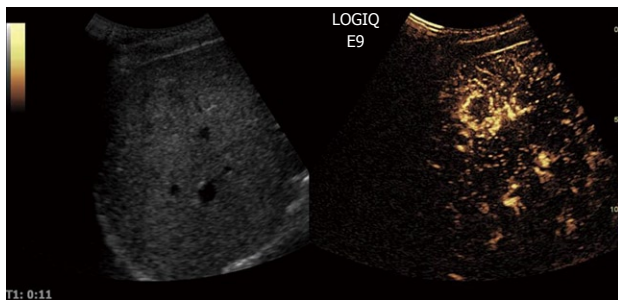


Figure 10 Contrast-enhanced ultrasound allows for visualization of the arteriogram of hepatocellular carcinoma in the early arterial phase. The feeding vessel is visible on the tumor right side. Typically there is initial peripheral enhancement before the centripetal influx to the center of the tumor.

HCCs with well-demarcated margins, perilesional halos or a hypoechoic pattern have a greater rate of detection by ultrasonography (Figure 8). Controversially, infiltrative or iso-hyperechoic HCCs without peripheral halos, as well as HCCs with internal septa or posterior echo enhancement, are harder to detect, with lower reported sensitivities. The use of Doppler in HCC can sometimes reveal a basket pattern around the tumor, depicting the anatomy of the arterial tumor supply (Figure 9).

When CEUS is applied, HCCs are typically characterized by hypervascularity in the arterial phase. Using real-

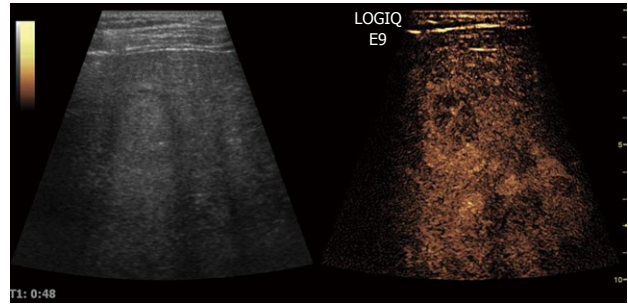


Figure 11 The portal phase of hepatocellular carcinoma. Because of high circulation velocity within hepatocellular carcinoma, there is relatively rapid washout, often starting in the portal phase.

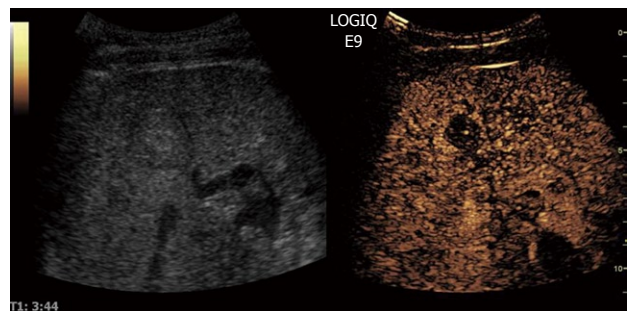


Figure 12 The sinusoidal (late) phase of hepatocellular carcinoma is shown. Typically, hepatocellular carcinoma is hypovascular (hypoechoic) during the late phase of perfusion confirming the malignant nature of the tumor.

time evaluation with low MI, early and usually intense arterial enhancement is identified and in most cases a feeding artery is clearly visible. Tumor vessels, often appearing with a basket-like pattern, tend to enhance in a centripetal fashion extending from the periphery to the centre of the tumor (Figure 10). Arterial enhancement may be inhomogeneous, because the tumor contains septa, regions of different tissue differentiation and shunting among the neo-formed vessels, and sometimes necrosis^[127]. Because of the high circulation velocity within HCC, there is relatively rapid nodular washout, often starting in the portal phase (Figure 11). Typically, HCC is hypovascular (hypoechoic) during the late phase of perfusion (Figure 12). At the same time, normal liver parenchyma increases the echogenicity and homogeneity because of portal venous enhancement.

Surveillance of patients at risk of developing HCC is based on ultrasound examinations performed at either 6 or 12 mo intervals. Early detection of HCC in patients with cirrhosis is a clinical challenge, since the different entities that are involved in the multi-step process of hepatocarcinogenesis, such as low-grade and high-grade dysplastic nodule, share common ultrasonic features. However, CEUS allows for reliable detection of arterial angiogenesis associated with a malignant transformation. When whole lesion enhancement or mosaic enhancement in the arterial phase with an enhancement defect in the portal phase was regarded as a positive finding of HCC, a sensitivity of 92% and a specificity of 87% were found^[128]. It has been shown that the ability of CEUS to diagnose HCC cur-

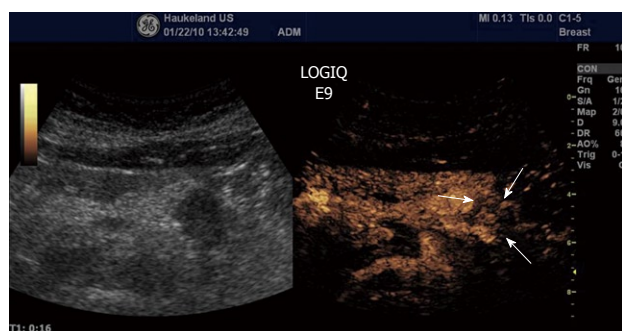


Figure 13 Ductal adenocarcinoma (between arrows) of the pancreas showing poor enhancement in the arterial phase. The same is true for the late venous phase.

rently approaches that of optimized multi-detector CT or dynamic MR imaging protocols^[129-136]. The use of CEUS to characterize nodular lesions in cirrhosis have been recommended by the clinical practice guidelines issued by the European Federation of Societies for Ultrasound in Medicine and Biology and the American Association for the Study of Liver Diseases^[115].

Pancreas

The pancreas, lying deep to the stomach and duodenum, is among the most inaccessible organs in the body for visualization with ultrasonography. Hence, confirmation of pancreatic disease has remained a great challenge in clinical imaging. However, transabdominal ultrasonography has developed to be a useful tool in the differential diagnosis of pancreatic tumors because the technique is inexpensive, easy to perform, and widely available. Nevertheless, only after the introduction of second-generation contrast media^[3], has transabdominal sonography yielded results comparable to those of other diagnostic modalities. CEUS can be used to improve detection of pancreatic lesions or to characterize pancreatic lesions already visible with ultrasonography. Furthermore, the staging of some pancreatic lesions can be improved by the use of contrast media. However, there is an important difference between a pancreatic CEUS study and the well-established liver CEUS study: the blood supply of the pancreas is entirely arterial and the enhancement of the gland begins almost together with the aortic enhancement. With CEUS the enhancement reaches its peak between 15 and 20 s after injection of the ultrasound contrast agent. Accordingly, pancreatic tissue enhancement is earlier and shorter than that of the liver because of the absence of a venous blood supply such as the portal vein in the liver. After a marked parenchymal enhancement in the early contrast-enhanced arterial phase, there is a progressive washout of contrast medium with gradual loss of echogenicity.

Ductal adenocarcinoma is the most frequent tumor of the pancreas, comprising between 80% and 90% of all tumors of the exocrine pancreas. Ultrasonographic findings typically are a hypoechoic lesion with ill-defined margins, often with spicules and tending to alter the gland contour^[137-139]. Characteristically, ductal adenocarcinoma

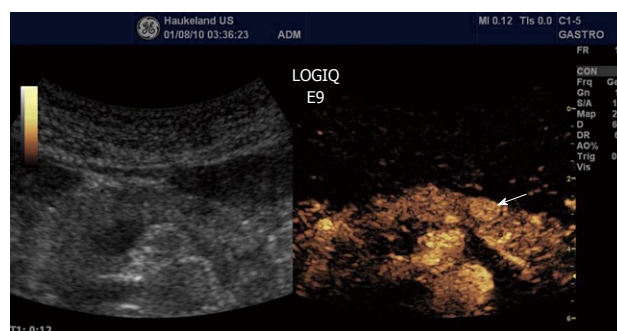


Figure 14 Neuroendocrine tumour (arrow) shows a rapid intense enhancement in the early arterial phase of contrast-enhanced ultrasound examination.

shows poor enhancement in all CEUS phases (Figure 13). On the contrary, neuroendocrine tumors (NETs) appear hypervascular in CEUS imaging. Imaging is important for the differentiation between NETs and ductal adenocarcinoma in selecting the correct therapeutic strategy and determining prognosis. With color- and power-Doppler ultrasonography a spotted pattern can sometimes be observed inside endocrine tumors^[140]. However, Doppler signals are not always detected because of the small size of the lesion or of the tumor vascular network. Typically, NETs show a rapid intense enhancement in the early contrast-enhanced phases (Figure 14), with the exception of possible necrotic intralesional areas.

Gastrointestinal tract

Colon cancer is one of the world's most common malignancies. The main therapy is surgical resection. To diagnose colon cancer, endoscopy is the preferred method, but in many places around the world, X-ray is still used. Using ultrasonography, the normal gastrointestinal (GI) wall is visualized as a layered structure consisting of 5 to 9 layers, depending on transmitted frequency^[141-143]. When digestive cancers develop, the wall layers become blurred, wall thickness is increased, and the ultrasound appearance of the GI wall resembles a kidney, i.e. pseudo-kidney sign or target lesion. However, CEUS does not yet have a place in the work-up of patients with suspected colonic cancer.

In oncology, early evaluation of targeted treatment response with functional imaging is of major importance. Dynamic CEUS is now recognized as a functional imaging technique able to evaluate new antiangiogenic drugs targeting cancers in the abdomen. This therapy evaluation is based on analysis of the curve of signal intensity over time after injection of ultrasound contrast agents (Figure 15). Novel quantification software allows for objective quantification of tumor perfusion parameters including maximum intensity of enhancement, mean transit time, time to peak, and wash-in slope coefficient. CEUS allows for early prediction of tumor response to treatment based on changes in vascularity, before morphological changes become apparent^[144]. Lassau and co-workers evaluated CEUS with perfusion software as a predictor of early tumor response to imatinib (Glivec) in c-kit-positive gas-

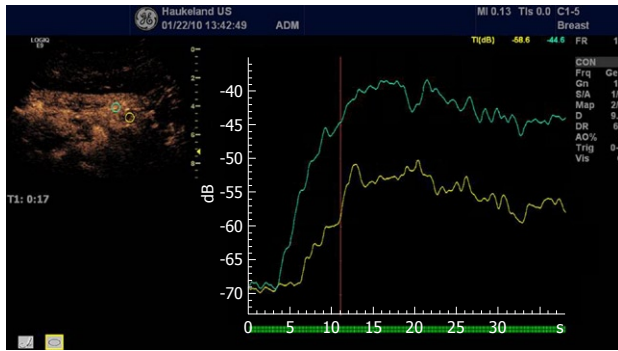


Figure 15 Analysis of time intensity curves after injection of contrast agents depicting a pancreatic carcinoma (same as Figure 13). The green curve depicts the normal pancreatic perfusion whereas the red curve illustrates the hypoenhancing malignancy.

trointestinal stromal tumors (GISTs)^[145]. They studied 59 tumors with metastases or a recurrence from a GIST prospectively and found that initial contrast uptake at day 1 was predictive of the future response^[145]. A strong correlation was found between the decline in tumor contrast uptake at days 7 and 14 and tumor response^[145]. They concluded that CEUS is a non-invasive imaging technique that allows the early prediction of tumor response in c-kit-positive GISTs treated with Glivec^[145].

Tumor growth is dependent on both endothelial and tumor cells. One question is whether changes in tumor vasculature are implicated in tumor tissue degeneration during antiangiogenic therapies. In a study using CEUS, it was shown that tumor cells abruptly became necrotic following antivascular therapy, whereas untreated tumors were protected from degeneration by a significant blood supply^[146]. Because antiangiogenic therapies inhibit the growth of new tumor-associated blood vessels, as well as prune newly formed vasculature, they would be expected to reduce the supply of oxygen and thus increase tumor hypoxia. Franco and co-workers used DC101, an anti-vascular endothelial growth factor receptor 2 antibody to study tumor hypoxia^[147]. Using ultrasonography, they observed consistent reductions in microvascular density, blood flow, and perfusion^[147]. The increase in tumor hypoxia was evident within 5 d and remained so throughout the entire course of treatment^[147]. These results suggest that sustained hypoxia and impairment of vascular function can be 2 consistent consequences of antiangiogenic drug treatment.

Concluding remarks

It is a challenging task to quantify and predict which bubble phenomenon occurs under which acoustic condition, and how these may be utilized in ultrasonic imaging. Aided by high-speed photography, our improved understanding of encapsulated microbubble behavior will lead to more sophisticated detection and delivery techniques.

More sophisticated methods use quantitative approaches to measure the amount and the time course of bolus or reperfusion curves and have shown great promise in revealing an effective tumor response to anti-angiogenic

drugs in humans before tumor shrinkage occurs. These are beginning to be accepted into clinical practice. In the long term, targeted microbubbles for molecular imaging and eventually for directed anti-tumor therapy are expected to be developed.

In principle, in any perfused region that can be reached by ultrasound, ultrasound-directed drug delivery could be performed. However, since the ultrasonic fields used with diagnostic ultrasound scanners differ greatly per organ targeted, some regions will be far from ideal. The ultrasonic frequencies transmitted in endoscopy are much higher than the resonance frequencies of conventional ultrasound contrast agents. Therefore, for such applications, smaller carriers will have to be developed for ultrasound-directed drug delivery.

In conclusion, combining ultrasound contrast agents with therapeutic substances may lead to simple and economic methods of treatment with fewer side effects, using conventional ultrasound scanners. Ultrasound-directed drug delivery has great potential in the treatment of malignancies in the digestive system.

REFERENCES

- 1 Postema M. Bubbles and ultrasound. *Appl Acoust* 2009; **70**: 1305
- 2 ter Haar G. Safety and bio-effects of ultrasound contrast agents. *Med Biol Eng Comput* 2009; **47**: 893-900
- 3 Postema M, Schmitz G. Bubble dynamics involved in ultrasonic imaging. *Expert Rev Mol Diagn* 2006; **6**: 493-502
- 4 Webb A. Introduction to Biomedical Imaging. Hoboken: John Wiley and Sons, 2003
- 5 Wells PNT. Ultrasonic imaging of the human body. *Rep Prog Phys* 1999; **62**: 671-722
- 6 British Medical Ultrasound Society. Guidelines for the safe use of diagnostic ultrasound equipment. *Ultrasound* 2010; **18**: 52-59
- 7 Postema M, Gilja OH. Ultrasound-directed drug delivery. *Curr Pharm Biotechnol* 2007; **8**: 355-361
- 8 Voigt JU. Ultrasound molecular imaging. *Methods* 2009; **48**: 92-97
- 9 Schmitz G. Ultrasound in medical diagnosis. In: Pike R, Sabatier P, editors. Scattering: scattering and inverse scattering in pure and applied science. London: Academic Press, 2002: 162-174
- 10 Macdonald CA, Sboros V, Gomatam J, Pye SD, Moran CM, Norman McDicken W. A numerical investigation of the resonance of gas-filled microbubbles: resonance dependence on acoustic pressure amplitude. *Ultrasonics* 2004; **43**: 113-122
- 11 Guan J, Matula TJ. Using light scattering to measure the response of individual ultrasound contrast microbubbles subjected to pulsed ultrasound in vitro. *J Acoust Soc Am* 2004; **116**: 2832-2842
- 12 Postema M. Fundamentals of medical ultrasonics. London: Spon Press, 2011
- 13 Postema M, Bouakaz A, de Jong N. Noninvasive microbubble-based pressure measurements: a simulation study. *Ultrasonics* 2004; **42**: 759-762
- 14 Schutt EG, Klein DH, Mattrey RM, Riess JG. Injectable microbubbles as contrast agents for diagnostic ultrasound imaging: the key role of perfluorochemicals. *Angew Chem Int Ed Engl* 2003; **42**: 3218-3235
- 15 Wrenn SP, Mleczko M, Schmitz G. Phospholipid-stabilized microbubbles: Influence of shell chemistry on cavitation threshold and binding to giant uni-lamellar vesicles. *Appl*

- Acoust 2009; **70**: 1313-1322
- 16 **Sboros V**. Response of contrast agents to ultrasound. *Adv Drug Deliv Rev* 2008; **60**: 1117-1136
- 17 **Tinkov S**, Bekeredian R, Winter G, Coester C. Microbubbles as ultrasound triggered drug carriers. *J Pharm Sci* 2009; **98**: 1935-1961
- 18 **Strasberg M**. Gas bubbles as sources of sound in liquids. *J Acoust Soc Am* 1956; **28**: 20-26
- 19 **Plesset MS**, Prosperetti A. Bubble dynamics and cavitation. *Annu Rev Fluid Mech* 1977; **9**: 145-185
- 20 **Attenborough K**, Postema M. A pocket-sized introduction to dynamics. Kingston upon Hull: The University of Hull, 2008
- 21 **Barlow E**, Mulholland AJ, Gachagan A, Nordon A, MacPherson K. Analysis of the Rayleigh-Plesset equation with chirp excitation. *IMA J Appl Math* 2009; **74**: 20-34
- 22 **Church CC**. The effects of an elastic solid surface layer on the radial pulsations of gas bubbles. *J Acoust Soc Am* 1995; **97**: 1510-1521
- 23 **Morgan KE**, Allen JS, Dayton PA, Chomas JE, Klubaov AL, Ferrara KW. Experimental and theoretical evaluation of microbubble behavior: effect of transmitted phase and bubble size. *IEEE Trans Ultrason Ferroelectr Freq Control* 2000; **47**: 1494-1509
- 24 **Hoff L**, Sontum PC, Hovem JM. Oscillations of polymeric microbubbles: effect of the encapsulating shell. *J Acoust Soc Am* 2000; **107**: 2272-2280
- 25 **Allen JS**, May DJ, Ferrara KW. Dynamics of therapeutic ultrasound contrast agents. *Ultrasound Med Biol* 2002; **28**: 805-816
- 26 **Stride E**, Saffari N. On the destruction of microbubble ultrasound contrast agents. *Ultrasound Med Biol* 2003; **29**: 563-573
- 27 **Postema M**, Schmitz G. Ultrasonic bubbles in medicine: influence of the shell. *Ultrason Sonochem* 2007; **14**: 438-444
- 28 **Doinikov AA**, Dayton PA. Spatio-temporal dynamics of an encapsulated gas bubble in an ultrasound field. *J Acoust Soc Am* 2006; **120**: 661-669
- 29 **Zheng H**, Mukdadi O, Shandas R. Theoretical predictions of harmonic generation from submicron ultrasound contrast agents for nonlinear biomedical ultrasound imaging. *Phys Med Biol* 2006; **51**: 557-573
- 30 **Sarkar K**, Shi WT, Chatterjee D, Forsberg F. Characterization of ultrasound contrast microbubbles using in vitro experiments and viscous and viscoelastic interface models for encapsulation. *J Acoust Soc Am* 2005; **118**: 539-550
- 31 **Stride E**, Tang MX, Eckersley RJ. Physical phenomena affecting quantitative imaging of ultrasound contrast agents. *Appl Acoust* 2009; **70**: 1352-1362
- 32 **Mleczko M**, Postema M, Schmitz G. Discussion of the application of finite Volterra series for the modeling of the oscillation behavior of ultrasound contrast agents. *Appl Acoust* 2009; **70**: 1363-1369
- 33 **Stride E**, Saffari N. Theoretical and experimental investigation of the behaviour of ultrasound contrast agent particles in whole blood. *Ultrasound Med Biol* 2004; **30**: 1495-1509
- 34 **Qin S**, Caskey CF, Ferrara KW. Ultrasound contrast microbubbles in imaging and therapy: physical principles and engineering. *Phys Med Biol* 2009; **54**: R27-R57
- 35 **Dayton PA**, Rychak JJ. Molecular ultrasound imaging using microbubble contrast agents. *Front Biosci* 2007; **12**: 5124-5142
- 36 **Philipp A**, Lauterborn W. Cavitation erosion by single laser-produced bubbles. *J Fluid Mech* 1998; **361**: 75-116
- 37 **Postema M**, Bouakaz A, de Jong N. March 2002. *IEEE Trans Ultrason Ferroelectr Freq Control* 2002; **49**: c1-c2
- 38 **Postema M**, van Wamel A, ten Cate FJ, de Jong N. High-speed photography during ultrasound illustrates potential therapeutic applications of microbubbles. *Med Phys* 2005; **32**: 3707-3711
- 39 **Prentice P**, Cuschieri A, Dholakia K, Prausnitz M, Campbell P. Membrane disruption by optically controlled microbubble cavitation. *Nat Phys* 2005; **1**: 107-110
- 40 **Postema M**, van Wamel A, Lancée CT, de Jong N. Ultrasound-induced encapsulated microbubble phenomena. *Ultrasound Med Biol* 2004; **30**: 827-840
- 41 **Kodama T**, Takayama K. Dynamic behavior of bubbles during extracorporeal shock-wave lithotripsy. *Ultrasound Med Biol* 1998; **24**: 723-738
- 42 **Ohl CD**, Ikink R. Shock-wave-induced jetting of micron-size bubbles. *Phys Rev Lett* 2003; **90**: 214502
- 43 **Ohl CD**, Ory E. Aspherical bubble collapse - comparison with simulations. In: Lauterborn W, Kurz T, editors. Non-linear acoustics at the turn of the millennium. New York: American Institute of Physics, 2000: 393-396
- 44 **Chomas JE**, Dayton P, May D, Ferrara K. Threshold of fragmentation for ultrasonic contrast agents. *J Biomed Opt* 2001; **6**: 141-150
- 45 **Brennen CE**. Fission of collapsing cavitation bubbles. *J Fluid Mech* 2002; **472**: 153-166
- 46 **Bloch SH**, Wan M, Dayton PA, Ferrara KW. Optical observation of lipid- and polymer-shelled ultrasound microbubble contrast agents. *Appl Phys Lett* 2004; **84**: 631-633
- 47 **Postema M**, Bouakaz A, Versluis M, de Jong N. Ultrasound-induced gas release from contrast agent microbubbles. *IEEE Trans Ultrason Ferroelectr Freq Control* 2005; **52**: 1035-1041
- 48 **Postema M**, Bouakaz A, ten Cate FJ, Schmitz G, de Jong N, van Wamel A. Nitric oxide delivery by ultrasonic cracking: some limitations. *Ultrasonics* 2006; **44** Suppl 1: e109-e113
- 49 **Fagan MJ**, Postema M. Introduction to stress and strain analysis. Kingston upon Hull: The University of Hull, 2007
- 50 **Bevan PD**, Karshafian R, Matsumura M, Tickner G, Burns PN. An acoustic study of disruption of polymer-shelled bubbles [microbubble contrast agents]. *Proc IEEE Ultrason Symp* 2004; **2**: 1391-1394
- 51 **Moran CM**, Anderson T, Pye SD, Sboros V, McDicken WN. Quantification of microbubble destruction of three fluorocarbon-filled ultrasonic contrast agents. *Ultrasound Med Biol* 2000; **26**: 629-639
- 52 **Leighton TG**. The acoustic bubble. London: Academic Press Ltd, 1994
- 53 **Dayton PA**, Allen JS, Ferrara KW. The magnitude of radiation force on ultrasound contrast agents. *J Acoust Soc Am* 2002; **112**: 2183-2192
- 54 **Dayton PA**, Morgan KE, Klivanov AL, Brandenburger G, Nightingale KR, Ferrara KW. A preliminary evaluation of the effects of primary and secondary radiation forces on acoustic contrast agents. *IEEE Trans Ultrason Ferroelectr Freq Control* 1997; **44**: 1264-1277
- 55 **Tortoli P**, Michelassi V, Corsi M, Righi D, Takeuchi Y. On the interaction between ultrasound and contrast agents during Doppler investigations. *Ultrasound Med Biol* 2001; **27**: 1265-1273
- 56 **Shortencarier MJ**, Dayton PA, Bloch SH, Schumann PA, Matsunaga TO, Ferrara KW. A method for radiation-force localized drug delivery using gas-filled lipospheres. *IEEE Trans Ultrason Ferroelectr Freq Control* 2004; **51**: 822-831
- 57 **Zhao S**, Borden M, Bloch SH, Kruse D, Ferrara KW, Dayton PA. Radiation-force assisted targeting facilitates ultrasonic molecular imaging. *Mol Imaging* 2004; **3**: 135-148
- 58 **Tortoli P**, Boni E, Corsi M, Arditi M, Frinking P. Different effects of microbubble destruction and translation in Doppler measurements. *IEEE Trans Ultrason Ferroelectr Freq Control* 2005; **52**: 1183-1188
- 59 **Rychak JJ**, Klivanov AL, Hossack JA. Acoustic radiation force enhances targeted delivery of ultrasound contrast microbubbles: in vitro verification. *IEEE Trans Ultrason Ferroelectr Freq Control* 2005; **52**: 421-433
- 60 **Lum AF**, Borden MA, Dayton PA, Kruse DE, Simon SI, Ferrara KW. Ultrasound radiation force enables targeted deposition of model drug carriers loaded on microbubbles. *J Control Release* 2006; **111**: 128-134
- 61 **Kotopoulos S**, Postema M. Microfoam formation in a capil-

- lary. *Ultrasonics* 2010; **50**: 260-268
- 62 **Mettin R**, Doinikov AA. Translational instability of a spherical bubble in a standing ultrasound wave. *Appl Acoust* 2009; **70**: 1330-1339
 - 63 **Kaul S**. Myocardial contrast echocardiography: a 25-year retrospective. *Circulation* 2008; **118**: 291-308
 - 64 **Bao S**, Thrall BD, Miller DL. Transfection of a reporter plasmid into cultured cells by sonoporation in vitro. *Ultrasound Med Biol* 1997; **23**: 953-959
 - 65 **Chen S**, Shohet RV, Bekeredian R, Frenkel P, Grayburn PA. Optimization of ultrasound parameters for cardiac gene delivery of adenoviral or plasmid deoxyribonucleic acid by ultrasound-targeted microbubble destruction. *J Am Coll Cardiol* 2003; **42**: 301-308
 - 66 **Delius M**, Hofschneider PH, Lauer U, Messmer K. Extracorporeal shock waves for gene therapy? *Lancet* 1995; **345**: 1377
 - 67 **Frenkel PA**, Chen S, Thai T, Shohet RV, Grayburn PA. DNA-loaded albumin microbubbles enhance ultrasound-mediated transfection in vitro. *Ultrasound Med Biol* 2002; **28**: 817-822
 - 68 **Greenleaf WJ**, Bolander ME, Sarkar G, Goldring MB, Greenleaf JF. Artificial cavitation nuclei significantly enhance acoustically induced cell transfection. *Ultrasound Med Biol* 1998; **24**: 587-595
 - 69 **Kondo I**, Ohmori K, Oshita A, Takeuchi H, Fuke S, ShiKondo I, Ohmori K, Oshita A, Takeuchi H, Fuke S, Shinomiya K, Noma T, Namba T, Kohno M. Treatment of acute myocardial infarction by hepatocyte growth factor gene transfer: the first demonstration of myocardial transfer of a "functional" gene using ultrasonic microbubble destruction. *J Am Coll Cardiol* 2004; **44**: 644-653
 - 70 **Lawrie A**, Briskin AF, Francis SE, Wyllie D, Kiss-Toth E, Qvarnstrom EE, Dower SK, Crossman DC, Newman CM. Ultrasound-enhanced transgene expression in vascular cells is not dependent upon cavitation-induced free radicals. *Ultrasound Med Biol* 2003; **29**: 1453-1461
 - 71 **Lindner JR**, Kaul S. Delivery of drugs with ultrasound. *Echocardiography* 2001; **18**: 329-337
 - 72 **Manome Y**, Nakayama N, Nakayama K, Furuhashi H. Insonation facilitates plasmid DNA transfection into the central nervous system and microbubbles enhance the effect. *Ultrasound Med Biol* 2005; **31**: 693-702
 - 73 **Miller DL**, Bao S, Gies RA, Thrall BD. Ultrasonic enhancement of gene transfection in murine melanoma tumors. *Ultrasound Med Biol* 1999; **25**: 1425-1430
 - 74 **Miller DL**, Bao S, Morris JE. Sonoporation of cultured cells in the rotating tube exposure system. *Ultrasound Med Biol* 1999; **25**: 143-149
 - 75 **Miller DL**, Dou C. Membrane damage thresholds for pulsed or continuous ultrasound in phagocytic cells loaded with contrast agent gas bodies. *Ultrasound Med Biol* 2004; **30**: 405-411
 - 76 **Miller DL**, Dou C. Membrane damage thresholds for 1- to 10-MHz pulsed ultrasound exposure of phagocytic cells loaded with contrast agent gas bodies in vitro. *Ultrasound Med Biol* 2004; **30**: 973-977
 - 77 **Mukherjee D**, Wong J, Griffin B, Ellis SG, Porter T, Sen S, Thomas JD. Ten-fold augmentation of endothelial uptake of vascular endothelial growth factor with ultrasound after systemic administration. *J Am Coll Cardiol* 2000; **35**: 1678-1686
 - 78 **Newman CM**, Lawrie A, Briskin AF, Cumberland DC. Ultrasound gene therapy: on the road from concept to reality. *Echocardiography* 2001; **18**: 339-347
 - 79 **Pislaru SV**, Pislaru C, Kinnick RR, Singh R, Gulati R, Greenleaf JF, Simari RD. Optimization of ultrasound-mediated gene transfer: comparison of contrast agents and ultrasound modalities. *Eur Heart J* 2003; **24**: 1690-1698
 - 80 **Porter TR**, Xie F. Targeted drug delivery using intravenous microbubbles. In: Goldberg BB, Raichlen JS, Forsberg F, editors. *Ultrasound Contrast Agents Basic principles and clinical applications*. 2nd ed. London: Martin Dunitz Ltd., 2001: 347-351
 - 81 **Porter TR**, Xie F. Therapeutic ultrasound for gene delivery. *Echocardiography* 2001; **18**: 349-353
 - 82 **Song J**, Chappell JC, Qi M, VanGieson EJ, Kaul S, Price RJ. Influence of injection site, microvascular pressure and ultrasound variables on microbubble-mediated delivery of microspheres to muscle. *J Am Coll Cardiol* 2002; **39**: 726-731
 - 83 **Tachibana K**, Tachibana S. The use of ultrasound for drug delivery. *Echocardiography* 2001; **18**: 323-328
 - 84 **Tachibana K**, Uchida T, Ogawa K, Yamashita N, Tamura K. Induction of cell-membrane porosity by ultrasound. *Lancet* 1999; **353**: 1409
 - 85 **Unger EC**, Hersh E, Vannan M, McCreery T. Gene delivery using ultrasound contrast agents. *Echocardiography* 2001; **18**: 355-361
 - 86 **Unger EC**, Matsunaga TO, McCreery T, Schumann P, Sweitzer R, Quigley R. Therapeutic applications of microbubbles. *Eur J Radiol* 2002; **42**: 160-168
 - 87 **Taniyama Y**, Tachibana K, Hiraoka K, Namba T, Yamasaki K, Hashiya N, Aoki M, Ogihara T, Yasufumi K, Morishita R. Local delivery of plasmid DNA into rat carotid artery using ultrasound. *Circulation* 2002; **105**: 1233-1239
 - 88 **van Wamel A**, Bouakaz A, Bernard B, ten Cate F, de Jong N. Radionuclide tumour therapy with ultrasound contrast microbubbles. *Ultrasonics* 2004; **42**: 903-906
 - 89 **Mehier-Humbert S**, Bettinger T, Yan F, Guy RH. Ultrasound-mediated gene delivery: kinetics of plasmid internalization and gene expression. *J Control Release* 2005; **104**: 203-211
 - 90 **Kudo N**, Okada K, Yamamoto K. Sonoporation by single-shot pulsed ultrasound with microbubbles adjacent to cells. *Biophys J* 2009; **96**: 4866-4876
 - 91 **Okada K**, Kudo N, Kondo T, Yamamoto K. Contributions of mechanical and sonochemical effects to cell membrane damage induced by single-shot pulsed ultrasound with adjacent microbubbles. *J Med Ultrasonics* 2008; **35**: 169-176
 - 92 **Karshafian R**, Bevan PD, Burns PN, Samac S, Banerjee M. Ultrasound-induced uptake of different size markers in mammalian cells. *Proc IEEE Ultrason Symp* 2005; **1**: 13-16
 - 93 **Schlicher RK**, Radhakrishna H, Tolentino TP, Apkarian RP, Zarnitsyn V, Prausnitz MR. Mechanism of intracellular delivery by acoustic cavitation. *Ultrasound Med Biol* 2006; **32**: 915-924
 - 94 **Mehier-Humbert S**, Bettinger T, Yan F, Guy RH. Plasma membrane poration induced by ultrasound exposure: implication for drug delivery. *J Control Release* 2005; **104**: 213-222
 - 95 **Miller DL**, Nyborg WL. Theoretical investigation of the response of gas-filled micropores and cavitation nuclei to ultrasound. *J Acoust Soc Am* 1983; **73**: 1537-1544
 - 96 **Miller DL**, Song J. Lithotripter shock waves with cavitation nucleation agents produce tumor growth reduction and gene transfer in vivo. *Ultrasound Med Biol* 2002; **28**: 1343-1348
 - 97 **Lentacker I**, De Smedt SC, Sanders NN. Drug loaded microbubble design for ultrasound triggered delivery. *Soft Matter* 2009; **5**: 2161-2170
 - 98 **Klibanov AL**. Targeted delivery of gas-filled microspheres, contrast agents for ultrasound imaging. *Adv Drug Deliv Rev* 1999; **37**: 139-157
 - 99 **Christiansen JP**, French BA, Klibanov AL, Kaul S, Lindner JR. Targeted tissue transfection with ultrasound destruction of plasmid-bearing cationic microbubbles. *Ultrasound Med Biol* 2003; **29**: 1759-1767
 - 100 **Dayton P**, Morgan K, Allietta M, Klibanov A, Brandenburg G, Ferrara K. Simultaneous optical and acoustical observations of contrast agents. *Proc IEEE Ultrason Symp* 1997; **2**: 1583-1591
 - 101 **Takeuchi Y**. July 1999. *IEEE Trans Ultrason Ferroelectr Freq Control* 1999; **46**: c1-c2
 - 102 **Postema M**, ten Cate FJ, Schmitz G, de Jong N, van Wamel A. Generation of a droplet inside a microbubble with the aid of

- an ultrasound contrast agent: first result. *Lett Drug Des Discov* 2007; **4**: 74-77
- 103 **Dorbolo S**, Caps H, Vandewalle N. Fluid instabilities in the birth and death of antibubbles. *New J Phys* 2003; **5**: 161
- 104 **Katz JL**. Jets from collapsing bubbles. *Proc R Soc Lond A* 1999; **455**: 323-328
- 105 **Duchemin L**, Popinet S, Josserand C, Zaleski S. Jet formation in bubbles bursting at a free surface. *Phys Fluids* 2002; **14**: 3000-3008
- 106 **Bekeredjian R**, Grayburn PA, Shohet RV. Use of ultrasound contrast agents for gene or drug delivery in cardiovascular medicine. *J Am Coll Cardiol* 2005; **45**: 329-335
- 107 **Miller DL**, Dou C, Song J. DNA transfer and cell killing in epidermoid cells by diagnostic ultrasound activation of contrast agent gas bodies in vitro. *Ultrasound Med Biol* 2003; **29**: 601-607
- 108 **van Wamel A**, Bouakaz A, ten Cate F, de Jong N. Effects of diagnostic ultrasound parameters on molecular uptake and cell viability. *Proc IEEE Ultrason Symp* 2002; **2**: 1419-1422
- 109 **Hallow DM**, Mahajan AD, McCutchen TE, Prausnitz MR. Measurement and correlation of acoustic cavitation with cellular bioeffects. *Ultrasound Med Biol* 2006; **32**: 1111-1122
- 110 **Feril LB Jr**, Kondo T, Takaya K, Riesz P. Enhanced ultrasound-induced apoptosis and cell lysis by a hypotonic medium. *Int J Radiat Biol* 2004; **80**: 165-175
- 111 **Watanabe A**, Kawai K, Sato T, Nishimura H, Kawashima N, Takeuchi S. Apoptosis induction in cancer cells by ultrasound exposure. *Jpn J Appl Phys* 2004; **43**: 3245-3248
- 112 **Abdollahi A**, Domhan S, Jenne JW, Hallaj M, Dell'Aqua G, Mueckenthaler M, Richter A, Martin H, Debus J, Ansoerge W, Hynynen K, Huber PE. Apoptosis signals in lymphoblasts induced by focused ultrasound. *FASEB J* 2004; **18**: 1413-1414
- 113 **Miller MW**, Miller DL, Brayman AA. A review of in vitro bioeffects of inertial ultrasonic cavitation from a mechanistic perspective. *Ultrasound Med Biol* 1996; **22**: 1131-1154
- 114 **Albrecht T**, Blomley M, Bolondi L, Claudon M, Correas JM, Cosgrove D, Greiner L, Jäger K, Jong ND, Leen E, Lencioni R, Lindsell D, Martegani A, Solbiati L, Thorelius L, Tranquart F, Weskott HP, Whittingham T. Guidelines for the use of contrast agents in ultrasound. January 2004. *Ultraschall Med* 2004; **25**: 249-256
- 115 **Claudon M**, Cosgrove D, Albrecht T, Bolondi L, Bosio M, Calliada F, Correas JM, Darge K, Dietrich C, D'Onofrio M, Evans DH, Filice C, Greiner L, Jäger K, Jong N, Leen E, Lencioni R, Lindsell D, Martegani A, Meairs S, Nolsøe C, Piscaglia F, Ricci P, Seidel G, Skjoldbye B, Solbiati L, Thorelius L, Tranquart F, Weskott HP, Whittingham T. Guidelines and good clinical practice recommendations for contrast enhanced ultrasound (CEUS) - update 2008. *Ultraschall Med* 2008; **29**: 28-44
- 116 **Bernatik T**, Becker D, Neureiter D, Hänsler J, Frieser M, Schaber S, Hahn EG, Strobel D. [Detection of liver metastases--comparison of contrast-enhanced ultrasound using first versus second generation contrast agents]. *Ultraschall Med* 2003; **24**: 175-179
- 117 **Strobel D**, Seitz K, Blank W, Schuler A, Dietrich C, von Herbay A, Friedrich-Rust M, Kunze G, Becker D, Will U, Kratzer W, Albert FW, Pachmann C, Dirks K, Strunk H, Greis C, Bernatik T. Contrast-enhanced ultrasound for the characterization of focal liver lesions--diagnostic accuracy in clinical practice (DEGUM multicenter trial). *Ultraschall Med* 2008; **29**: 499-505
- 118 **Albrecht T**, Hohmann J, Oldenburg A, Skrok J, Wolf KJ. Detection and characterisation of liver metastases. *Eur Radiol* 2004; **14** Suppl 8: P25-P33
- 119 **Dietrich CF**, Kratzer W, Strobe D, Danse E, Fessl R, Bunk A, Vossas U, Hauenstein K, Koch W, Blank W, Oudkerk M, Hahn D, Greis C. Assessment of metastatic liver disease in patients with primary extrahepatic tumors by contrast-enhanced sonography versus CT and MRI. *World J Gastroenterol* 2006; **12**: 1699-1705
- 120 **Konopke R**, Kersting S, Bergert H, Bloomenthal A, Gastmeier J, Saeger HD, Bunk A. Contrast-enhanced ultrasonography to detect liver metastases : a prospective trial to compare transcutaneous unenhanced and contrast-enhanced ultrasonography in patients undergoing laparotomy. *Int J Colorectal Dis* 2007; **22**: 201-207
- 121 **Torzilli G**. Contrast-enhanced intraoperative ultrasonography in surgery for liver tumors. *Eur J Radiol* 2004; **51** Suppl: S25-S29
- 122 **Torzilli G**, Botea F, Procopio F, Donadon M, Balzarini L, Lutman F, Calliada F, Montorsi M. Use of contrast-enhanced intraoperative ultrasonography during liver surgery for colorectal cancer liver metastases - Its impact on operative outcome. Analysis of a prospective cohort study. *Eur J Cancer Suppl* 2008; **6**: 16-23
- 123 **Lassau N**, Lamuraglia M, Koscielny S, Spatz A, Roche A, Leclerc J, Avril MF. Prognostic value of angiogenesis evaluated with high-frequency and colour Doppler sonography for preoperative assessment of primary cutaneous melanomas: correlation with recurrence after a 5 year follow-up period. *Cancer Imaging* 2006; **6**: 24-29
- 124 **Cosgrove D**, Lassau N. [Assessment of tumour angiogenesis using contrast-enhanced ultrasound]. *J Radiol* 2009; **90**: 156-164
- 125 **Lassau N**, Koscielny S, Albiges L, Chami L, Benatsou B, Chebil M, Roche A, Escudier BJ. Metastatic renal cell carcinoma treated with sunitinib: early evaluation of treatment response using dynamic contrast-enhanced ultrasonography. *Clin Cancer Res* 2010; **16**: 1216-1225
- 126 **Leen E**. The role of contrast-enhanced ultrasound in the characterisation of focal liver lesions. *Eur Radiol* 2001; **11** Suppl 3: E27-E34
- 127 **Nicolau C**, Catalá V, Vilana R, Gilabert R, Bianchi L, Solé M, Pagés M, Brú C. Evaluation of hepatocellular carcinoma using SonoVue, a second generation ultrasound contrast agent: correlation with cellular differentiation. *Eur Radiol* 2004; **14**: 1092-1099
- 128 **Ding H**, Wang WP, Huang BJ, Wei RX, He NA, Qi Q, Li CL. Imaging of focal liver lesions: low-mechanical-index real-time ultrasonography with SonoVue. *J Ultrasound Med* 2005; **24**: 285-297
- 129 **Camaggi V**, Piscaglia F, Bolondi L. Recent advances in the imaging of hepatocellular carcinoma. From ultrasound to positron emission tomography scan. *Saudi Med J* 2007; **28**: 1007-1014
- 130 **Dai Y**, Chen MH, Fan ZH, Yan K, Yin SS, Zhang XP. Diagnosis of small hepatic nodules detected by surveillance ultrasound in patients with cirrhosis: Comparison between contrast-enhanced ultrasound and contrast-enhanced helical computed tomography. *Hepatol Res* 2008; **38**: 281-290
- 131 **Forner A**, Vilana R, Ayuso C, Bianchi L, Solé M, Ayuso JR, Boix L, Sala M, Varela M, Llovet JM, Brú C, Bruix J. Diagnosis of hepatic nodules 20 mm or smaller in cirrhosis: Prospective validation of the noninvasive diagnostic criteria for hepatocellular carcinoma. *Hepatology* 2008; **47**: 97-104
- 132 **Giorgio A**, De Stefano G, Coppola C, Ferraioli G, Esposito V, Di Sarno A, Giorgio V, De Stefano M, Sangiovanni V, Liorre G, Del Viscovo L. Contrast-enhanced sonography in the characterization of small hepatocellular carcinomas in cirrhotic patients: comparison with contrast-enhanced ultrafast magnetic resonance imaging. *Anticancer Res* 2007; **27**: 4263-4269
- 133 **Koda M**, Matsunaga Y, Ueki M, Maeda Y, Mimura K, Okamoto K, Hosho K, Murawaki Y. Qualitative assessment of tumor vascularity in hepatocellular carcinoma by contrast-enhanced coded ultrasound: comparison with arterial phase of dynamic CT and conventional color/power Doppler ultrasound. *Eur Radiol* 2004; **14**: 1100-1108
- 134 **Lu MD**, Yu XL, Li AH, Jiang TA, Chen MH, Zhao BZ, Zhou

- XD, Wang JR. Comparison of contrast enhanced ultrasound and contrast enhanced CT or MRI in monitoring percutaneous thermal ablation procedure in patients with hepatocellular carcinoma: a multi-center study in China. *Ultrasound Med Biol* 2007; **33**: 1736-1749
- 135 **Suzuki S**, Iijima H, Moriyasu F, Sasaki S, Yanagisawa K, Miyahara T, Oguma K, Yoshida M, Horibe T, Ito N, Kakizaki D, Abe K, Tsuchiya K. Differential diagnosis of hepatic nodules using delayed parenchymal phase imaging of levovist contrast ultrasound: comparative study with SPIO-MRI. *Hepatol Res* 2004; **29**: 122-126
- 136 **Vallone P**, Gallipoli A, Izzo F, Fiore F, Delrio P. Local ablation procedures in primary liver tumors: Levovist US versus spiral CT to evaluate therapeutic results. *Anticancer Res* 2003; **23**: 5075-5079
- 137 **D'Onofrio M**, Zamboni G, Faccioli N, Capelli P, Pozzi Mucelli R. Ultrasonography of the pancreas. 4. Contrast-enhanced imaging. *Abdom Imaging* 2007; **32**: 171-181
- 138 **Faccioli N**, Crippa S, Bassi C, D'Onofrio M. Contrast-enhanced ultrasonography of the pancreas. *Pancreatology* 2009; **9**: 560-566
- 139 **Recalini C**, Carrafiello G, Bertolotti E, Angeretti MG, Fugazzola C. Contrast-enhanced ultrasonographic findings in pancreatic tumors. *Int J Med Sci* 2008; **5**: 203-208
- 140 **D'Onofrio M**, Mansueto G, Falconi M, Procacci C. Neuroendocrine pancreatic tumor: value of contrast enhanced ultrasonography. *Abdom Imaging* 2004; **29**: 246-258
- 141 **Gilja OH**, Heimdal A, Hausken T, Gregersen H, Matre K, Berstad A, Ødegaard S. Strain during gastric contractions can be measured using Doppler ultrasonography. *Ultrasound Med Biol* 2002; **28**: 1457-1465
- 142 **Ødegaard S**, Nesje LB, Hoff DA, Gilja OH, Gregersen H. Morphology and motor function of the gastrointestinal tract examined with endosonography. *World J Gastroenterol* 2006; **12**: 2858-2863
- 143 **Ødegaard S**, Nesje LB, Gilja OH. Atlas of endoscopic ultrasonography. Bergen: Fagbokforlaget, 2007
- 144 **Lassau N**, Brule A, Chami L, Benatsou B, Péronneau P, Roche A. [Evaluation of early response to antiangiogenic treatment with dynamic contrast enhanced ultrasound]. *J Radiol* 2008; **89**: 549-555
- 145 **Lassau N**, Lamuraglia M, Chami L, Leclère J, Bonvalot S, Terrier P, Roche A, Le Cesne A. Gastrointestinal stromal tumors treated with imatinib: monitoring response with contrast-enhanced sonography. *AJR Am J Roentgenol* 2006; **187**: 1267-1273
- 146 **Magnon C**, Galaup A, Rouffiac V, Opolon P, Connault E, Rosé M, Perricaudet M, Roche A, Germain S, Griscelli F, Lassau N. Dynamic assessment of antiangiogenic therapy by monitoring both tumoral vascularization and tissue degeneration. *Gene Ther* 2007; **14**: 108-117
- 147 **Franco M**, Man S, Chen L, Emmenegger U, Shaked Y, Cheung AM, Brown AS, Hicklin DJ, Foster FS, Kerbel RS. Targeted anti-vascular endothelial growth factor receptor-2 therapy leads to short-term and long-term impairment of vascular function and increase in tumor hypoxia. *Cancer Res* 2006; **66**: 3639-3648
- 148 **Krishna PD**, Shankar PM, Newhouse VL. Subharmonic generation from ultrasonic contrast agents. *Phys Med Biol* 1999; **44**: 681-694
- 149 **Guidi F**, Vos HJ, Nicchi F, Boni E, Tortoli P. Acoustical Imaging of Individual Microbubbles. In: André MP, editor. Acoustical imaging. Berlin: Springer, 2007: 257-265
- 150 **Postema M**, Mleczko M, Schmitz G. Mutual attraction of oscillation microbubbles. In: Buzug TM, Holz D, Weber S, Bongartz J, Kohl-Bareis M, Hartmann U, editors. Advances in medical engineering. Berlin: Springer, 2007: 75-80
- 151 **Postema M**, Marmottant P, Lancée CT, Versluis M, Hilgenfeldt S, de Jong N. Ultrasound-induced coalescence of free gas microbubbles. *Proc IEEE Ultrason Symp* 2004; **1**: 1-4
- 152 **Bevan PD**, Karshafian R, Burns PN. The influence of fragmentation on the acoustic response from shrinking bubbles. *Ultrasound Med Biol* 2008; **34**: 1152-1162
- 153 **Chomas JE**, Dayton PA, May D, Allen J, Klivanov A, Ferrara K. Optical observation of contrast agent destruction. *Appl Phys Lett* 2000; **77**: 1056-1058
- 154 **Borden MA**, Kruse DE, Caskey CF, Zhao S, Dayton PA, Ferrara KW. Influence of lipid shell physicochemical properties on ultrasound-induced microbubble destruction. *IEEE Trans Ultrason Ferroelectr Freq Control* 2005; **52**: 1992-2002
- 155 **Postema M**, de Jong N, Schmitz G. Shell rupture threshold, fragmentation threshold, Blake threshold. *Proc IEEE Ultrason Symp* 2005; **3**: 1708-1711
- 156 **Postema M**, Marmottant P, Lancée CT, Hilgenfeldt S, de Jong N. Ultrasound-induced microbubble coalescence. *Ultrasound Med Biol* 2004; **30**: 1337-1344
- 157 **Postema M**, de Jong N, Schmitz G. Nonlinear behavior of ultrasound-insonified encapsulated microbubbles. In: Atchley AA, Sparrow VW, Keolian RM, editors. Innovations in nonlinear acoustics. Melville: American Institute of Physics, 2006: 275-278
- 158 **Takeuchi Y**. Industrial use thermoplastic microballoon to mimic the contrast agents and its in-vitro behavior including released gas dynamics. *Proc Proc IEEE Ultrason Symp* 1997; **2**: 1579-1582
- 159 **Bevan PD**, Karshafian R, Tickner EG, Burns PN. Quantitative measurement of ultrasound disruption of polymer-shelled microbubbles. *Ultrasound Med Biol* 2007; **33**: 1777-1786

S- Editor Sun H L- Editor Cant MR E- Editor Zheng XM

Adrian Săftoiu, MD, PhD, Professor, and Peter Vilmann, MD, PhD, Professor, Series Editors

Contrast-enhanced endoscopic ultrasonography

Nischita K Reddy, Ana Maria Ionică, Adrian Săftoiu, Peter Vilmann, Manoop S Bhutani

Nischita K Reddy, Department of Medicine, University of Texas Medical Branch, Galveston, TX 77555-0144, United States
 Ana Maria Ionică, Adrian Săftoiu, Department of Gastroenterology and Hepatology, University of Medicine and Pharmacy Craiova, Craiova 200349, Romania

Peter Vilmann, Department of Surgical Gastroenterology, Gentofte and Herlev University Hospital, 2730 Herlev, Copenhagen, Denmark

Manoop S Bhutani, Department of Gastroenterology, Hepatology and Nutrition-Unit 1466, University of Texas, MD Anderson Cancer Center, Houston, TX 77030-4009, United States

Author contributions: All the authors contributed equally to this review.

Correspondence to: Manoop S Bhutani, MD, FASGE, FACP, AGAF, Professor of Medicine, Experimental Diagnostic Imaging and Biomedical Engineering, Director of Endoscopic Research and Development, Department of Gastroenterology, Hepatology and Nutrition-Unit 1466, UT MD Anderson Cancer Center, 1515 Holcombe Blvd., Houston, TX 77030-4009, United States. manoop.bhutani@mdanderson.org

Telephone: +1-713-7945073 Fax: +1-713-5634398

Received: July 2, 2010 Revised: October 27, 2010

Accepted: November 3, 2010

Published online: January 7, 2011

various pancreatic malignancies. The sensitivity of power Doppler sonography to depict tumor neovascularization can be increased by contrast agents. Contrast-enhanced harmonic imaging is a useful aid in identifying the tumor vasculature and studying pancreatic microperfusion. In the future, these techniques could potentially be used to quantify tumor perfusion, to assess and monitor the efficacy of antiangiogenic agents, to assist targeted drug delivery and allow molecular imaging.

© 2011 Baishideng. All rights reserved.

Key words: Contrast media; Endoscopic ultrasonography; Gastrointestinal neoplasms; Doppler ultrasonography; Pancreatic cancer

Peer reviewer: Richard Hu, MD, MSc, Division of Gastroenterology, Department of Medicine, Olive view-UCLA Medical Center, 14445 Olive View Drive, Los Angeles, CA 91342, United States

Reddy NK, Ionică AM, Săftoiu A, Vilmann P, Bhutani MS. Contrast-enhanced endoscopic ultrasonography. *World J Gastroenterol* 2011; 17(1): 42-48 Available from: URL: <http://www.wjgnet.com/1007-9327/full/v17/i1/42.htm> DOI: <http://dx.doi.org/10.3748/wjg.v17.i1.42>

Abstract

Contrast agents are increasingly being used to characterize the vasculature in an organ of interest, to better delineate benign from malignant pathology and to aid in staging and directing therapeutic procedures. We review the mechanisms of action of first, second and third generation contrast agents and their use in various endoscopic procedures in the gastrointestinal tract. Various applications of contrast-enhanced endoscopic ultrasonography include differentiating benign from malignant mediastinal lymphadenopathy, assessment of depth of invasion of esophageal, gastric and gall bladder cancers and visualization of the portal venous system and esophageal varices. In addition, contrast agents can be used to differentiate pancreatic lesions. The use of color Doppler further increases the ability to diagnose and differentiate

CONTRAST-ENHANCED ENDOSCOPIC ULTRASONOGRAPHY

The use of intravenous contrast agents in ultrasonography was first utilized in echocardiography to enhance imaging of cardiac chambers and great vessels^[1]. Since then, they have been used in transabdominal ultrasonography and more recently in endoscopic ultrasonography (EUS). Use of contrast agents in EUS has been shown to improve the characterization of the vasculature inside the organ of interest, to better delineate benign from malignant pathology^[2-8], to aid in staging and directing therapeutic procedures and thereby to determine prognosis.

CONTRAST AGENTS

Contrast agents are made of gas-filled microbubbles encapsulated by a phospholipid or albumin shell. They are categorized into first, second and third generation based on their capability for transpulmonary passage and their half-life in the human body. Commonly used first generation agents include Albunex, Levovist and Echovist. Second generation agents include SonoVue, Sonazoid, and Optison among others^[9,10]. The only third generation agent currently available is Echogen, capable of phase-shift from liquid to gas form once it attains body temperature^[11]. Contrast agents in use today are relatively safe and have demonstrated no severe, long-lasting adverse effects in humans (Table 1)^[12,13].

MECHANISMS OF ACTION

Contrast agents were specifically developed to image vascularity and vessel patterns, especially for small volume and slow velocity blood flow. This is highly important in tumors, where angiogenesis completely alters the vascular structure. The principle of ultrasound contrast agents is that they create multiple small interfaces with high echogenicity, a process best achieved by gaseous microbubbles, surrounded by a shell used to increase stability^[14]. Microbubbles are very good backscatters, effectively reflecting the ultrasound waves. However, the microbubbles respond and oscillate to sound pressure in a non-linear fashion, with an asymmetrical diameter induced by ultrasound pressure. The diameter is variable between 2 and 10 μm , about the size of red blood cells. Consequently, they do not leave the vascular system (blood pool contrast agents). The ultrasound contrast agents are administered through intravenous bolus injection, in a large arm vein. Second-generation contrast agents are those passing through the lungs, allowing contrast enhancement of the entire vascular system.

Contrast agents were used initially as Doppler signal enhancers, including in contrast-enhanced EUS examinations (CE-EUS). Both color Doppler and power Doppler can be used, especially for regions with very low flow volumes, where the unenhanced signal is too weak or the signal-noise ratio is too poor (Figures 1 and 2). Although the contrast agent selectively enhances the useful signal to the detriment of the noise, the main disadvantage of these techniques is the presence of artifacts. Both tissue motion (flash) artifacts and blooming artifacts appear and impede the examinations. Flash artifacts are specific to the Doppler mode, appearing as color signals caused by tissue motion, being most commonly seen in hypoechoic areas, induced by cardiac or respiratory motion^[15]. Blooming artifacts appear as a consequence of the high amplification of the backscattered signal, which saturates the receiver and causes smearing of the color signal. They appear immediately after the wash-in phase and disappear when the concentration of contrast is lower^[16]. The introduction of second generation contrast agents made it possible to

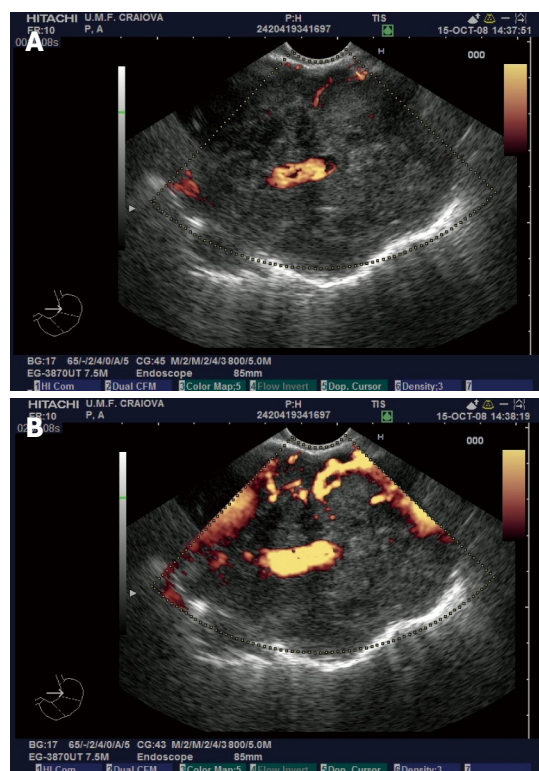


Figure 1 Contrast enhanced endoscopic ultrasonography exam of lung adenocarcinoma. A: Non-enhanced power Doppler image of a lung adenocarcinoma visualized in the aorto-pulmonary window from the mid-esophagus, with discrete Doppler signals in the periphery of the mass and embedding of a large branch of the left pulmonary artery; B: Same tumor visualized after contrast-enhancement with SonoVue, with a better depiction of the vascular peripheral signals and the possibility of quantification of the vascular index. The relationship to the aorta and pulmonary artery is clearly depicted.

enhance B-mode and contrast-harmonic imaging for improved visualization (Figure 3)^[17,18].

CLINICAL USES OF CE-EUS

Differentiating benign from malignant mediastinal lymphadenopathy

EUS-guided fine-needle aspiration (FNA) represents the current “gold-standard” for the diagnosis of malignant mediastinal lymphadenopathy^[19,20], and is further improved by localized cytopathologic assessment of the specimens^[21]. Nonetheless, EUS-FNA carries the risk of mediastinitis if inflammatory nodes are aspirated, contamination and tumor seeding. However, studies have not been consistent in their findings^[6,22]. CE-EUS may offer a non-invasive method to increase the specificity of diagnosis of benign lymph nodes, and aid in targeting aspiration of only high-yield lymph nodes.

Differentiating benign from malignant lymph nodes using appearance and type (arterial, venous) of vascularity may not be reliable since non-lymphomatous cancer cells invade lymph nodes heterogeneously^[23]. Currently, CE-EUS cannot replace EUS-guided FNA in confirming malignant mediastinal lymph nodes. The combination of CE-EUS and EUS-FNA will possibly improve diagnostic accuracy.

Table 1 Intravenous contrast agents, their composition and manufacturers^[10,13]

Contrast agent	Composition	Manufacturer
First generation		
Albunex	5% human albumin with stabilized microbubbles	Mallinckrodt
Echovist (SHU 454)	Standardized microbubbles with galactose shell	Schering
Levovist (SHU 508)	Stabilized, standardized microbubbles with galactose, 0.1% palmitic acid shell	Schering
Myomap	Albumin shell	Quadrant
Quantison	Albumin shell	Quadrant
Sonavist	Cyanoacrylate shell	Schering
Sonazoid	C ₄ F ₁₀ with lipid stabilizer shell	GE healthcare
Second generation		
Definity/luminy	C ₃ F ₈ with lipid stabilizer shell	Bristol-myers squibb medical imaging
Imagent-imavist	C ₆ H ₁₄ with lipid stabilizer shell	Alliance
Optison	C ₃ F ₈ with denatured human albumin shell	GE healthcare
Bisphere/cardiophere	Poly(lactide-coglycolide) shell with albumin overcoat	-
SonoVue (BR1, Bracco, Italy)	SF ₆ gas with lipid stabilizer shell	Bracco
AI700/imagify	C ₄ F ₁₀ gas core stabilized with polymer shell	Acusphere
Third generation		
Echogen	Dodecafluoropentane (DDEFP) liquid in phase shift colloid emulsion	Sonus pharmaceuticals

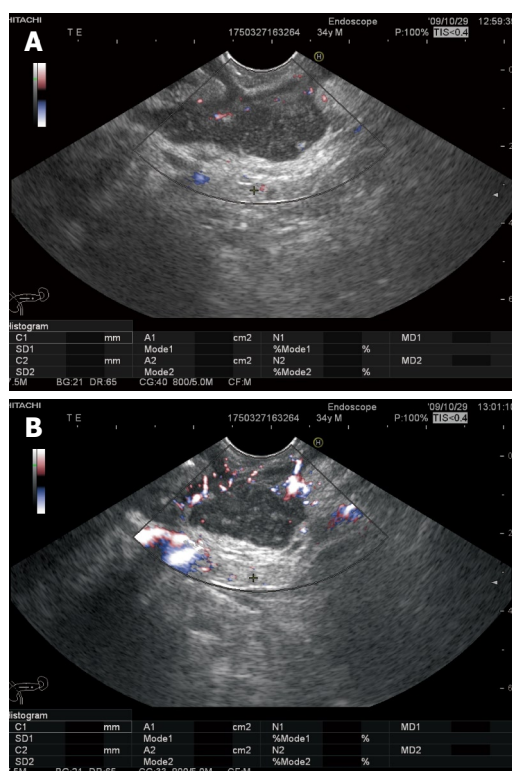


Figure 2 Contrast enhanced endoscopic ultrasonography of pancreatic cancer. A: Pancreatic head adenocarcinoma visualized in bidirectional non-enhanced power Doppler mode; B: Contrast-enhancement with SonoVue indicates a hypovascular mass with increased collateral circulation.

Esophageal and gastric cancer

EUS can provide cross-sectional imaging of the wall of the gastrointestinal tract, and determine the depth of invasion of cancers. The normal esophageal and gastric walls consist of five layers on EUS images with enhancement of the third and fifth layers (submucosa and subserosa, respectively). Esophageal cancers are not enhanced with CE-EUS because of their relative avascularity^[8]. In gastric cancer, assessment of the depth of invasion can be im-

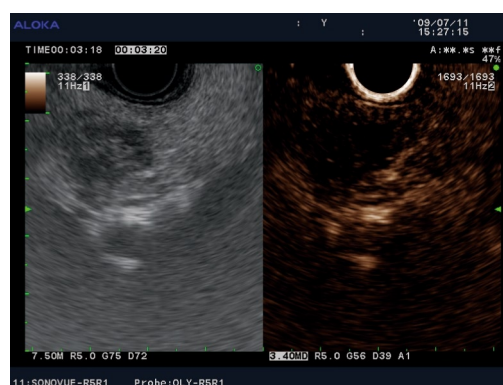


Figure 3 Contrast-enhanced (SonoVue) harmonic endoscopic ultrasound imaging showing a small (12 mm) hypovascular adenocarcinoma in the head of the pancreas. The tumor tissue did not enhance in the early arterial phase, nor in the late venous phase, as compared to the surrounding pancreatic parenchyma.

proved with CE-EUS, especially for depressed, endophytic cancers. Use of CE-EUS improves the overall accuracy of assessment of depth of invasion of gastric carcinoma from 70% to 90%. Active ulcers and scars in both malignant and non-malignant lesions are not enhanced post-contrast. This has been attributed to the nature of vascularity (linear convergence) and foci of fibrosis. Gastric myogenic tumors appear as hypoechoic masses linked to the fourth layer on EUS^[8]. Hirooka *et al*^[24] demonstrated that poorly differentiated gastric carcinomas were enhanced by infusion of Albunex whereas well differentiated ones were not. However, prediction of histologic type of gastric carcinoma by the nature of the enhancement has been inconsistent.

Gallbladder diseases

CE-EUS has the potential to differentiate gallbladder lesions and assess the depth of tumor infiltration in gallbladder carcinomas^[5]. It can differentiate chronic cholecystitis and cholesterol polyps from infiltrating and exophytic gallbladder cancer, respectively, since the three-layer structure

remains intact in the benign conditions. Majority of gallbladder adenocarcinomas enhance with EUS on administration of Alburnex^[5], unlike other gallbladder diseases including adenosquamous carcinoma cholesterol polyps and chronic cholecystitis^[5,24]. CE-EUS is also able to clearly differentiate the depth of invasion in the gallbladder wall from T1b from T1a, improving accuracy over standard EUS^[5].

Pancreatic diseases

First generation: CE-EUS has been used in pancreatic cancer to demarcate vascular landmarks, detect vascular obliteration by a thrombus or tumor, and examine microvascular blood flow to organs and lesions.

Alburnex was the earliest contrast agent used to enhance EUS images. Hirooka *et al.*^[24] demonstrated that peripheral injection of Alburnex can enhance B-mode images of pancreatic pathology during high-frequency EUS. Enhancement was marked in cases of pancreatic islet cell tumors. Pancreatic ductal cell carcinomas remained unenhanced compared to the surrounding normal parenchyma and fibrosis thereby making boundaries clearer^[24]. Administration of contrast also improved the capability for differential diagnosis of lesions identified by B-mode EUS^[25].

A study by the same authors in 1998 demonstrated similar findings with 100% image enhancement (at 12 Hz) using Alburnex in islet cell carcinomas and serous cystadenomas, 80% enhancement in mucin-producing tumors, and 75% in chronic pancreatitis. Also, no enhancement was noted with ductal cell carcinomas and pancreatic pseudocysts, consistent with hypovascularity. Differences in vascularity as demonstrated on angiography paralleled the enhancement patterns during CE-EUS, except in 20% and 25% of cases with mucin-producing tumors and chronic pancreatitis, respectively. In addition, they demonstrated that areas of normal parenchyma and fibrosis around a lesion can be enhanced, demarcating the boundaries. This could lead to accurate pre-operative staging and planning of surgical resection lines, in the case of mucinous tumors involving the main pancreatic duct^[4].

The authors propose that enhancement after Alburnex may be related, at least in part, to the nature of microcirculation and vascular permeability of the lesion, which determine the concentration of contrast agent within the lesion. This could account for the less predictive pattern of angiography with sonographic enhancement^[4]. Concentric bile duct wall thickening on intraductal ultrasonography with strong enhancement after administration of Levovist was seen in patients with autoimmune pancreatitis with a reduction in enhancement after steroid therapy likely indicating resolution of inflammation^[26].

Second generation: Using an experimental second generation microbubble contrast agent, Wong *et al.*^[27] demonstrated hypoechogenicity in normal pancreatic tissue after a bolus but not with continuous infusion. This could be related to a greater intravascular density of contrast material with bolus injection compared to a continuous infu-

sion. A decreased echo signal from the pancreatic parenchyma after contrast injection may be due to an increased signal from the pancreatic interface with adjacent structures^[27]. Whether this will have a clinically useful application remains to be determined. Certainly, lesions that are enhanced with contrast will be more easily distinguished from the surrounding normal pancreas.

CE-EUS reveals the characteristic vascularity and can diagnose and follow up intraductal papillary mucinous neoplasms (IPMN) of the pancreas. Enlargement or enhancement of a mural nodule accurately indicated the presence of atypical malignant epithelium and determined the need for surgical resection^[28]. Mural nodules were classified into four types based on morphology during EUS, before and after contrast: Type 1 (low papillary type), Type 2 (polypoid type), Type 3 (villous type) and Type 4 (invasive type with a blurred hypoechoic area between lesion and parenchyma). When IPMNs with Type 3/4 were diagnosed as malignant, accuracy was higher^[29].

The use of CE-EUS has also been used to differentiate between mass-forming chronic pancreatitis and pancreatic cancer. Focal lesions can be seen in alcohol and autoimmune pancreatitis, with presentation similar to that of pancreatic cancer. CE-EUS produces a “parenchymographic” enhancement (i.e. isovascular to pancreatic parenchyma) in inflammatory benign masses and shows an inverse correlation with the degree of fibrosis within the mass, the duration of the inflammatory process and the enhancement with contrast infusion. Ductal carcinomas exhibit complete absence or a low level of enhancement due to greater fibrosis within the tumor^[30,31].

Color Doppler

Combining B-mode EUS with CE-Doppler ultrasound improves the visualization of the vascularity of a pancreatic lesion, with malignant ductal adenocarcinoma demonstrating low flow and a relatively avascular pattern. Bhutani *et al.*^[32] described enhancement of color Doppler signals from the celiac artery, superior mesenteric artery, and portal vein during EUS in a swine model after administration of Levovist. This effect was easily appreciated without the need for complex quantitative measurements. No visually obvious enhancement was evident in vessels such as the aorta that already had a pronounced unenhanced color Doppler signal^[32]. Using Optison (FS069), Becker *et al.*^[33] demonstrated that the sensitivity and specificity of echo-enhanced color-Doppler EUS are comparable with the cytopathology results. Ueno *et al.*^[34] differentiated islet cell tumors and ductal cell cancer with color-Doppler EUS. Islet cell tumors had marked hypervascularization whereas patients with adenocarcinoma had vascularity only around the tumor. These results have been confirmed by several other investigators. Hypovascularity as a sign of malignancy in CE-EUS can provide 92% sensitivity and 100% specificity (89%-100%)^[2]. Using CE-Doppler EUS, hypovascularized malignant ductal adenocarcinoma and hypervascularized benign tumor entities, mostly neuroendocrine tumors, and serous microcystic adenomas of the pancreas

can be easily differentiated. This is of pivotal importance since serous microcystic adenomas can be observed due to low growth potential, and neuroendocrine tumors may be enucleated or otherwise and less radically resected compared to ductal adenocarcinoma.

Power Doppler

Unenhanced power Doppler ultrasonography is unable to provide tumor differentiation, as a previous study showed a very low specificity (77%) of unenhanced power Doppler EUS^[35]. Although other factors like the presence of peripancreatic collaterals, might improve the specificity, this was not confirmed in larger studies. It is possible to misdiagnose necrotic pancreatitis as ductal adenocarcinoma and also to find inflammation surrounding ductal adenocarcinomas. Indeed, the presence of power Doppler inside the inflammatory masses is variable as a function of inflammation and necrosis, thus complicating the differential diagnosis^[35].

The sensitivity of power Doppler sonography to depict tumor neovascularization can be increased by contrast agents. In an animal model of pancreatic vascular disruption using 50% ethanol plus purified carbon particle solution, standard EUS demonstrated hypoechogenicity in the ethanol treated area. With injection of Definity, power Doppler EUS revealed marked contrast enhancement of normal pancreatic parenchyma from the ethanol-treated area^[36]. Several studies using CE-EUS with power Doppler scanning also demonstrated an improvement in discrimination of pancreatic cancer from chronic pancreatitis^[33,37,38] and may also help to localize small benign tumors such as insulinomas^[7].

Hocke *et al.*^[38], using pulsed Doppler analysis with CE-Doppler EUS, demonstrated an improvement in the differentiation between chronic pancreatitis and malignancy. They used specific criteria to define malignancy: lack of vascularization before injection of SonoVue, irregular appearance of arterial vessels over a short distance post-injection, and absence of detection of venous vessels in the lesion^[38]. In contrast to the technique described by Becker *et al.*^[33], Hocke *et al.*^[38] combined the analysis of the detected vessels with pulsed wave Doppler analysis. They concluded that the use of second generation contrast agents with low mechanical index techniques will possibly allow real-time imaging with or without three-dimensional reconstructions in EUS imaging.

With CE power Doppler sonography, the signal intensity from flowing blood is lower compared to that of moving solid tissue structures. Harmonic imaging was specifically developed to overcome these obstacles, since tissue particles have fewer harmonic waves than intravascular microbubbles, thus avoiding flash and blooming artifacts^[35].

Harmonic imaging

CE harmonic imaging techniques are currently available for EUS, as a result of the improvement in transducer technology. Thus, the use of adequate broadband transducers that can detect harmonic signals was recently

been reported^[17,25]. A pilot study previously described an experimental technique with low mechanical index, which allowed differentiation between chronic pancreatitis and pancreatic cancer, based on tissue microperfusion characteristics^[17]. Another feasibility study demonstrated both parenchymal perfusion and microvasculature in the pancreas^[25]. Both intermittent homogeneous parenchymal perfusion images and real-time continuous images of finely branching vessels of the pancreas were obtained with a mechanical index of 0.4. Although the initial study included a small number of patients with pancreatic lesions, it seemed that tumor characterization was possible based on the vascular or perfusion pattern. Thus, pancreatic carcinomas had absent or heterogeneous perfusion images in the intermittent mode, while the vessels were visualized as irregular “network like” structures in real-time mode. Both neuroendocrine tumors and chronic pseudotumoral pancreatitis were homogenous and iso- or hyper-vascular. Several other research groups are testing the feasibility of CE-EUS^[39-41]. CE-EUS with low mechanical index (0.4) was tested in 25 patients, after peripheral injection of SonoVue^[39]. The method seemed feasible for differentiating adenocarcinoma from other focal mass lesions, being proposed as the method of choice to establish the management of patients when EUS-FNA is non-contributive. Harmonic imaging has also been used with CE-EUS after peripheral injection of Sonazoid in two settings, WPI (wide-band pulse inversion harmonic) and EXPHD (extended pure harmonic detection)^[40]. The change in echo-intensity was evaluated. Ductal carcinomas, IPMTs, chronic pancreatitis and endocrine tumors demonstrate varied echo-intensities after infusion of contrast agent. CE harmonic EUS can be a useful aid in identifying tumor vasculature, especially that of pancreatic masses^[41].

Esophageal varices and portal hypertension

B-mode EUS can detect grade II varices or larger. After administration of Levovist, flow signals can become evident beneath the third echogenic layer of the esophageal wall and help visualize perforating veins and periesophageal vessels^[42]. EUS-guided portal vein angiography by using CO₂ as a contrast agent, has been evaluated in a porcine model. This is less viscous, making it easier to inject through small-caliber needles, minimizing damage to the vascular wall compared with iodinated contrast (Table 2)^[43].

FUTURE PERSPECTIVES

Tumor blood flow was previously linked in several studies with both metastasis potential and poor prognosis. A clear correlation was also proven between microvessel density, different angiogenic factors [e.g. vascular endothelial growth factor (VEGF)] and the tumors with definite vascular signals demonstrated by CE ultrasound^[44]. Quantification of tumor perfusion has been proven feasible for the early assessment and monitoring of the efficacy of antiangiogenic agents in quantitative terms based on changes in vascularity, before morphological changes become apparent^[45].

Table 2 Indications for the use of contrast agents during endoscopic ultrasonography

Study	Indication	Agent used
Hocke <i>et al</i> ^[6]	Differentiating benign from malignant lymph nodes	SonoVue
Kanamori <i>et al</i> ^[22]		Levovist
Nomura <i>et al</i> ^[8]	Assessment of depth of invasion of esophageal cancer	Air-filled Albumin
Nomura <i>et al</i> ^[8]	Assessment of depth of invasion of gastric cancer	Air-filled Albumin
Itoh <i>et al</i> ^[28]	Differentiating benign from malignant intraductal papillary mucinous tumors of the pancreas	Levovist
Hirooka <i>et al</i> ^[5]	Gallbladder diseases	Albunex
Ueno <i>et al</i> ^[34]	Diagnosing Islet cell tumors	Levovist
Sakamoto <i>et al</i> ^[40]	Determining origin of solid pancreatic masses	Levovist with suspension of monosaccharide microparticles
Hirooka <i>et al</i> ^[24]		Albunex
Dietrich <i>et al</i> ^[2]		Levovist
Sofuni <i>et al</i> ^[41]		Levovist
Becker <i>et al</i> ^[33]	Discriminating between mass forming pancreatitis and pancreatic cancer	Optison
Hocke <i>et al</i> ^[6]		SonoVue
D'Onofrio <i>et al</i> ^[31]		SonoVue
Hyodo <i>et al</i> ^[26]	Diagnosing cause of chronic pancreatitis/mass forming pancreatitis (autoimmune pancreatitis)	Levovist
D'Onofrio <i>et al</i> ^[31]		SonoVue
Zhu <i>et al</i> ^[30]		SonoVue
Kasono <i>et al</i> ^[7]	Localizing small insulinomas	Levovist

The feasibility of new technologies using CE ultrasound with microbubbles targeted to VEGF receptor type 2 are currently being tested^[46-48]. Several applications of molecular imaging and targeted ultrasound therapy can also be envisioned in the near future, including determination of the detailed physical processes behind sonoporation (increased uptake of drugs inside the cell through transient porositities in the cell membrane in the presence of contrast agents).

In this context, the development of CE-EUS will be clearly beneficial for targeted ultrasound imaging and ultrasound-assisted drug-delivery applications in gastrointestinal tract tumors, as well as other tumors accessible by EUS (pancreatic and lung tumors, *etc.*).

REFERENCES

- Keller MW, Feinstein SB, Watson DD. Successful left ventricular opacification following peripheral venous injection of sonicated contrast agent: an experimental evaluation. *Am Heart J* 1987; **114**: 570-575
- Dietrich CF, Ignee A, Braden B, Barreiros AP, Ott M, Hocke M. Improved differentiation of pancreatic tumors using contrast-enhanced endoscopic ultrasound. *Clin Gastroenterol Hepatol* 2008; **6**: 590-597.e1
- Goldberg BB, Hilpert PL, Burns PN, Liu JB, Newman LM, Merton DA, Witlin LA. Hepatic tumors: signal enhancement at Doppler US after intravenous injection of a contrast agent. *Radiology* 1990; **177**: 713-717
- Hirooka Y, Goto H, Ito A, Hayakawa S, Watanabe Y, Ishiguro Y, Kojima S, Hayakawa T, Naitoh Y. Contrast-enhanced endoscopic ultrasonography in pancreatic diseases: a preliminary study. *Am J Gastroenterol* 1998; **93**: 632-635
- Hirooka Y, Naitoh Y, Goto H, Ito A, Hayakawa S, Watanabe Y, Ishiguro Y, Kojima S, Hashimoto S, Hayakawa T. Contrast-enhanced endoscopic ultrasonography in gallbladder diseases. *Gastrointest Endosc* 1998; **48**: 406-410
- Hocke M, Menges M, Topalidis T, Dietrich CF, Stallmach A. Contrast-enhanced endoscopic ultrasound in discrimination between benign and malignant mediastinal and abdominal lymph nodes. *J Cancer Res Clin Oncol* 2008; **134**: 473-480
- Kasono K, Hyodo T, Suminaga Y, Sugiura Y, Namai K, Ikoma A, Tamemoto H, Imawari M, Kawakami M, Ishikawa SE. Contrast-enhanced endoscopic ultrasonography improves the preoperative localization of insulinomas. *Endocr J* 2002; **49**: 517-522
- Nomura N, Goto H, Niwa Y, Arisawa T, Hirooka Y, Hayakawa T. Usefulness of contrast-enhanced EUS in the diagnosis of upper GI tract diseases. *Gastrointest Endosc* 1999; **50**: 555-560
- Straub JA, Chickering DE, Church CC, Shah B, Hanlon T, Bernstein H. Porous PLGA microparticles: AI-700, an intravenously administered ultrasound contrast agent for use in echocardiography. *J Control Release* 2005; **108**: 21-32
- Klibanov AL. Ultrasound molecular imaging with targeted microbubble contrast agents. *J Nucl Cardiol* 2007; **14**: 876-884
- Maresca G, Summaria V, Colagrande C, Manfredi R, Calliada F. New prospects for ultrasound contrast agents. *Eur J Radiol* 1998; **27** Suppl 2: S171-S178
- Karl-Jurgen Wolf FF. Color Duplex Sonography Principles and Clinical Applications. New York: Thieme Publishing Group, 1995
- Quaia E. Microbubble ultrasound contrast agents: an update. *Eur Radiol* 2007; **17**: 1995-2008
- Greis C, Dietrich C. Ultrasound contrast agents and contrast-enhanced ultrasonography. In: Dietrich CF, editor. *Endoscopic Ultrasound. An introductory manual and atlas*. New York: Thieme Publishing Group, 2006: 44-57
- Campbell SC, Cullinan JA, Rubens DJ. Slow flow or no flow? Color and power Doppler US pitfalls in the abdomen and pelvis. *Radiographics* 2004; **24**: 497-506
- Forsberg F, Liu JB, Burns PN, Merton DA, Goldberg BB. Artifacts in ultrasonic contrast agent studies. *J Ultrasound Med* 1994; **13**: 357-365
- Dietrich CF, Ignee A, Frey H. Contrast-enhanced endoscopic ultrasound with low mechanical index: a new technique. *Z Gastroenterol* 2005; **43**: 1219-1223
- Sanchez MV, Varadarajulu S, Napoleon B. EUS contrast agents: what is available, how do they work, and are they effective? *Gastrointest Endosc* 2009; **69**: S71-S77
- Micames CG, McCrory DC, Pavey DA, Jowell PS, Gress FG. Endoscopic ultrasound-guided fine-needle aspiration for non-small cell lung cancer staging: A systematic review and metaanalysis. *Chest* 2007; **131**: 539-548
- Yasuda I, Tsurumi H, Omar S, Iwashita T, Kojima Y, Yamada T, Sawada M, Takami T, Moriwaki H, Soehendra N. Endoscopic ultrasound-guided fine-needle aspiration biopsy for lymphadenopathy of unknown origin. *Endoscopy* 2006; **38**: 919-924

- 21 **Tournoy KG**, Praet MM, Van Maele G, Van Meerbeeck JP. Esophageal endoscopic ultrasound with fine-needle aspiration with an on-site cytopathologist: high accuracy for the diagnosis of mediastinal lymphadenopathy. *Chest* 2005; **128**: 3004-3009
- 22 **Kanamori A**, Hirooka Y, Itoh A, Hashimoto S, Kawashima H, Hara K, Uchida H, Goto J, Ohmiya N, Niwa Y, Goto H. Usefulness of contrast-enhanced endoscopic ultrasonography in the differentiation between malignant and benign lymphadenopathy. *Am J Gastroenterol* 2006; **101**: 45-51
- 23 **Nakase K**, Yamamoto K, Hiasa A, Tawara I, Yamaguchi M, Shiku H. Contrast-enhanced ultrasound examination of lymph nodes in different types of lymphoma. *Cancer Detect Prev* 2006; **30**: 188-191
- 24 **Hirooka Y**, Naitoh Y, Goto H, Ito A, Taki T, Hayakawa T. Usefulness of contrast-enhanced endoscopic ultrasonography with intravenous injection of sonicated serum albumin. *Gastrointest Endosc* 1997; **46**: 166-169
- 25 **Kitano M**, Takagi T, Sakamoto H, Das K, Komaki T, Noda K, Yamao K, Kudo M. Dynamic imaging of pancreatic tumors by contrast-enhanced harmonic EUS with long-lasting contrast. *Gastrointestinal Endoscopy* 2009; **69**: S228
- 26 **Hyodo N**, Hyodo T. Ultrasonographic evaluation in patients with autoimmune-related pancreatitis. *J Gastroenterol* 2003; **38**: 1155-1161
- 27 **Wong RF**, Tarcin O, Reddy N, Ahmed I, Brining D, Matsunaga TO, Bhutani MS. Contrast-enhanced EUS (CE-EUS) using a new microbubble contrast agent (MRX-815) - a feasibility study in a porcine model. *Gastrointestinal Endoscopy* 2006; **63**: AB274
- 28 **Itoh T**, Hirooka Y, Itoh A, Hashimoto S, Kawashima H, Hara K, Kanamori A, Ohmiya N, Niwa Y, Goto H. Usefulness of contrast-enhanced transabdominal ultrasonography in the diagnosis of intraductal papillary mucinous tumors of the pancreas. *Am J Gastroenterol* 2005; **100**: 144-152
- 29 **Ohno E**, Hirooka Y, Itoh A, Kawashima H, Hara K, Nonogaki K, Kasugai T, Ishikawa T, Ohmiya N, Niwa Y, Goto H. Usefulness of contrast-enhanced endoscopic ultrasonography (CE-EUS) in the diagnosis of mural nodule of intraductal papillary mucinous neoplasms of the pancreas. the comparison of the ce-eus findings with the pathological findings. *Gastrointestinal Endoscopy* 2008; **67**: AB209
- 30 **Zhu Q**. Study on contrast enhanced EUS in differential diagnosis of pancreatic tumor. *Gastrointestinal Endoscopy* 2009; **69**: S265
- 31 **D'Onofrio M**, Zamboni G, Tognolini A, Malago R, Faccioli N, Frulloni L, Pozzi Mucelli R. Mass-forming pancreatitis: value of contrast-enhanced ultrasonography. *World J Gastroenterol* 2006; **12**: 4181-4184
- 32 **Bhutani MS**, Hoffman BJ, van Velse A, Hawes RH. Contrast-enhanced endoscopic ultrasonography with galactose microparticles: SHU508 A (Levovist). *Endoscopy* 1997; **29**: 635-639
- 33 **Becker D**, Strobel D, Bernatik T, Hahn EG. Echo-enhanced color- and power-Doppler EUS for the discrimination between focal pancreatitis and pancreatic carcinoma. *Gastrointest Endosc* 2001; **53**: 784-789
- 34 **Ueno N**, Tomiyama T, Tano S, Wada S, Aizawa T, Kimura K. Utility of endoscopic ultrasonography with color Doppler function for the diagnosis of islet cell tumor. *Am J Gastroenterol* 1996; **91**: 772-776
- 35 **Rickes S**, Unkrodt K, Neye H, Ocran KW, Wermke W. Differentiation of pancreatic tumours by conventional ultrasound, unenhanced and echo-enhanced power Doppler sonography. *Scand J Gastroenterol* 2002; **37**: 1313-1320
- 36 **Giday SA**, Canto MI, Magno P, Buscaglia J, Clarke J, Ko CW, Wroblewski L, Kalloo AN, Kantsevov SV, Jagannath S. Contrast-enhanced endoscopic ultrasonography (CE-EUS) improves visualization of pancreatic vasculature. *Gastrointestinal Endoscopy* 2006; **63**: AB266
- 37 **Okamoto Y**, Kawamoto H, Takaki A, Ishida E, Ogawa T, Kuwaki K, Kobayashi Y, Sakaguchi K, Shiratori Y. Contrast-enhanced ultrasonography depicts small tumor vessels for the evaluation of pancreatic tumors. *Eur J Radiol* 2007; **61**: 163-169
- 38 **Hocke M**, Schulze E, Gottschalk P, Topalidis T, Dietrich CF. Contrast-enhanced endoscopic ultrasound in discrimination between focal pancreatitis and pancreatic cancer. *World J Gastroenterol* 2006; **12**: 246-250
- 39 **Hirooka Y**, Itoh A, Kawashima H, Hara K, Nonogaki K, Kasugai T, Ohno E, Ishikawa T, Ohmiya N, Niwa Y, Goto H. Utility of contrast-enhanced endoscopic ultrasonography (CE-EUS) in the diagnosis of pancreatic diseases using perflubutane microbubbles. *Gastrointestinal Endoscopy* 2008; **67**: AB214
- 40 **Sakamoto H**, Kitano M, Suetomi Y, Maekawa K, Takeyama Y, Kudo M. Utility of contrast-enhanced endoscopic ultrasonography for diagnosis of small pancreatic carcinomas. *Ultrasound Med Biol* 2008; **34**: 525-532
- 41 **Sofuni A**, Iijima H, Moriyasu F, Nakayama D, Shimizu M, Nakamura K, Itokawa F, Itoi T. Differential diagnosis of pancreatic tumors using ultrasound contrast imaging. *J Gastroenterol* 2005; **40**: 518-525
- 42 **Ernst H**, Nusko G, Hahn EG, Heyder N. Color Doppler endosonography of esophageal varices: signal enhancement after intravenous injection of the ultrasound contrast agent Levovist. *Endoscopy* 1997; **29**: S42-S43
- 43 **Giday SA**, Ko CW, Clarke JO, Shin EJ, Magno P, Jagannath SB, Buscaglia JM, Kantsevov SV. EUS-guided portal vein carbon dioxide angiography: a pilot study in a porcine model. *Gastrointest Endosc* 2007; **66**: 814-819
- 44 **Ohshima T**, Yamaguchi T, Ishihara T, Yoshikawa M, Kobayashi A, Sakaue N, Baba T, Yamada S, Saisho H. Evaluation of blood flow in pancreatic ductal carcinoma using contrast-enhanced, wide-band Doppler ultrasonography: correlation with tumor characteristics and vascular endothelial growth factor. *Pancreas* 2004; **28**: 335-343
- 45 **Lassau N**, Brule A, Chami L, Benatsou B, Péronneau P, Roche A. [Evaluation of early response to antiangiogenic treatment with dynamic contrast enhanced ultrasound]. *J Radiol* 2008; **89**: 549-555
- 46 **Lyshchik A**, Fleischer AC, Huamani J, Hallahan DE, Brissova M, Gore JC. Molecular imaging of vascular endothelial growth factor receptor 2 expression using targeted contrast-enhanced high-frequency ultrasonography. *J Ultrasound Med* 2007; **26**: 1575-1586
- 47 **Palmowski M**, Huppert J, Ladewig G, Hauff P, Reinhardt M, Mueller MM, Woenne EC, Jenne JW, Maurer M, Kauffmann GW, Semmler W, Kiessling F. Molecular profiling of angiogenesis with targeted ultrasound imaging: early assessment of antiangiogenic therapy effects. *Mol Cancer Ther* 2008; **7**: 101-109
- 48 **Willmann JK**, Lutz AM, Paulmurugan R, Patel MR, Chu P, Rosenberg J, Gambhir SS. Dual-targeted contrast agent for US assessment of tumor angiogenesis in vivo. *Radiology* 2008; **248**: 936-944

S- Editor Sun H L- Editor Cant MR E- Editor Ma WH



Adrian Săftoiu, MD, PhD, Professor, and Peter Vilmann, MD, PhD, Professor, Series Editors

Hybrid ultrasound imaging techniques (fusion imaging)

Daniela Larisa Sandulescu, Daniela Dumitrescu, Ion Rogoveanu, Adrian Saftoiu

Daniela Larisa Sandulescu, Daniela Dumitrescu, Ion Rogoveanu, Adrian Saftoiu, Research Center of Gastroenterology and Hepatology, University of Medicine and Pharmacy Craiova, Craiova 200638, Romania

Author contributions: Sandulescu DL drafted the manuscript; Rogoveanu I and Dumitrescu D gathered the data; Saftoiu A reviewed and edited the manuscript.

Supported by Research Grant No. 570/2008, Entitled "Integrative Prediction Model of Malignant Transformation of Regeneration Lesions in Cirrhotic Liver Using Noninvasive Imaging Techniques, Immunohistochemical and Molecular Genetic Methods" Financed by the Romanian Ministry of Education and Research-National Authority for Scientific Research (PN2-ID-PCE)

Correspondence to: Daniela Larisa Sandulescu, MD, Research Center of Gastroenterology and Hepatology, University of Medicine and Pharmacy Craiova, Petru Rares Street, No. 2, Craiova 200638, Dolj, Romania. larisasandulescu@yahoo.com
Telephone: +40-251-522458 Fax: +40-251-593077

Received: July 2, 2010 Revised: September 29, 2010

Accepted: October 6, 2010

Published online: January 7, 2011

Key words: Hybrid imaging; Real time virtual sonography; Angiogenesis; Focal liver lesions

Peer reviewers: Giedrius Barauskas, Professor, Department of Surgery, Kaunas University of Medicine, Eiveniu str. 2, Kaunas, LT-50009, Lithuania; Naoaki Sakata, MD, PhD, Division of Hepato-Biliary Pancreatic Surgery, Tohoku University Graduate School of Medicine, 1-1 Seiryomachi, Aoba-ku, Sendai, Miyagi 980-8574, Japan

Sandulescu DL, Dumitrescu D, Rogoveanu I, Saftoiu A. Hybrid ultrasound imaging techniques (fusion imaging). *World J Gastroenterol* 2011; 17(1): 49-52 Available from: URL: <http://www.wjgnet.com/1007-9327/full/v17/i1/49.htm> DOI: <http://dx.doi.org/10.3748/wjg.v17.i1.49>

INTRODUCTION

Conventional cross-sectional imaging techniques [ultrasound, computed tomography (CT), magnetic resonance (MR), etc.] have important roles in noninvasive diagnosis, and in tumor treatment strategies. The techniques employed have different working principles, consequently complementing each other with respect to the information obtained. The combination (fusion) of two imaging techniques was developed in recent years, defining the so-called "hybrid techniques" or "fusion imaging". Combinations of anatomical imaging techniques (ultrasound with CT or MR imaging), as well as associations between anatomical (CT or MR imaging) and molecular (SPECT or PET) imaging modalities are currently used in clinical practice.

TECHNICAL ISSUES

One example of fusion imaging is real-time virtual sonography (RVS), a technique that enables the display of an ultrasound B mode image and CT or MR images in real-time^[1]. The system includes a magnetic positioning sensor fixed on the convex-shaped probe of the ultrasound scanner, for the creation of images with identical cross-

Abstract

Visualization of tumor angiogenesis can facilitate non-invasive evaluation of tumor vascular characteristics to supplement the conventional diagnostic imaging goals of depicting tumor location, size, and morphology. Hybrid imaging techniques combine anatomic [ultrasound, computed tomography (CT), and/or magnetic resonance imaging (MRI)] and molecular (single photon emission CT and positron emission tomography) imaging modalities. One example is real-time virtual sonography, which combines ultrasound (grayscale, colour Doppler, or dynamic contrast harmonic imaging) with contrast-enhanced CT/MRI. The benefits of fusion imaging include an increased diagnostic confidence, direct comparison of the lesions using different imaging modalities, more precise monitoring of interventional procedures, and reduced radiation exposure.

© 2011 Baishideng. All rights reserved.

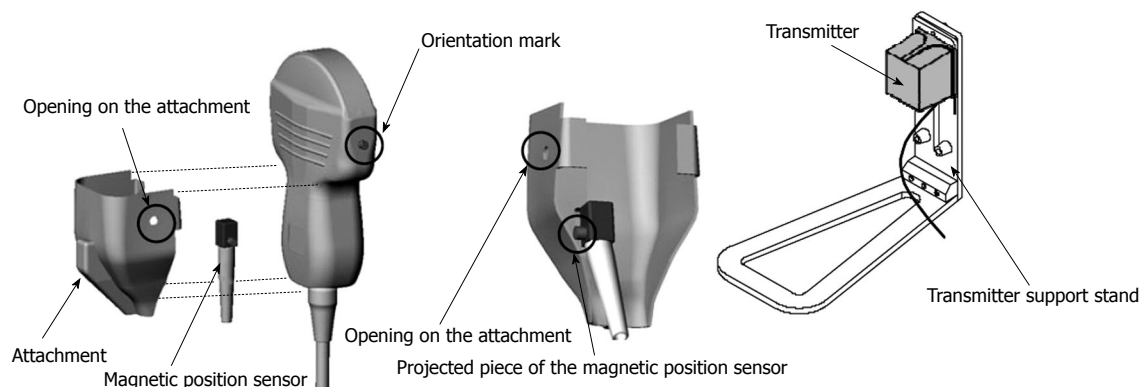


Figure 1 The probe and the magnetic sensor are assembled with careful attention to the positions of the orientation marks.

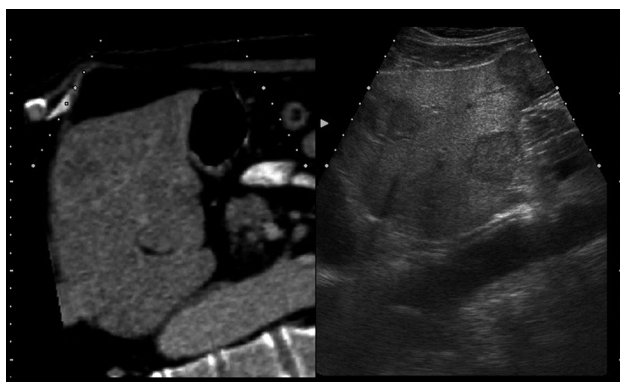


Figure 2 The left liver lobe ultrasound and computed tomography images are visualized at the same time in real-time virtual sonography.

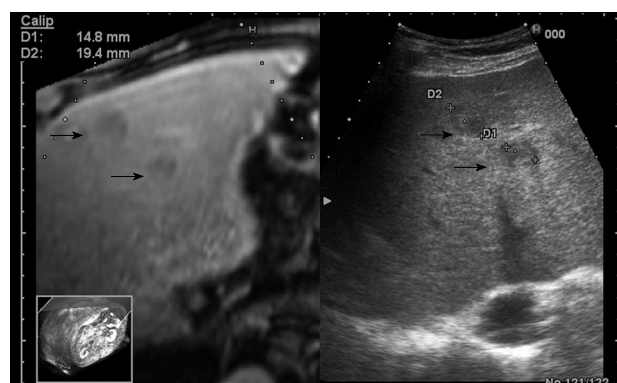


Figure 3 A 65-year-old male patient with liver metastases. The workstation monitor displays the ultrasound and computed tomography images in real-time.

sections in real-time. This is done according to the position and the angle of the probe in relation to previously acquired CT and MR volume data. To be compatible with the RVS module, CT examination must meet certain requirements: (1) the volume data must be archived in the DICOM format; (2) the slice thickness should be 3 mm or less and image reconstruction the same; and (3) the CT scan area must include the xiphoid process.

To display virtual images, it is necessary to transfer the CT or MR data to the ultrasound machine^[2]. The magnetic positioning sensor unit is carefully assembled, based on the position of orientation marks. It uses a distal attachment, which helps install the magnetic positioning sensor on the probe, as shown in Figure 1. The magnetic sensor detects the changes in location, direction, and rotation of the probe during normal ultrasound scanning of the patient. The transmitter (the instrument that produces the magnetic waves) for the magnetic positioning sensor unit is installed on the left flank of the patient. Using a probe equipped with the magnetic sensor, a sagittal section of the left hepatic lobe is then captured (Figure 2). The xiphoid process is usually chosen as a reference anatomical point. In case of a mismatch between the ultrasound and the virtual image (CT or MR), it is possible to readjust and correct the mismatch during the exam. The adjustment is made possible by freezing the CT/MR images on a section with clearly visible anatomical landmarks, for

example the portal vein bifurcation or the right kidney in a longitudinal view, followed by identification of a similar ultrasound image and continuation of examination^[3]. The workstation monitor displays two images: the ultrasound real-time image and the virtual reconstructed CT/MR image (Figure 3).

CLILINICAL APPLICATIONS

The founding principles of combining the ultrasound image and the CT/MR images were based on several observations. In recent years, frequent imaging investigations led to the discovery of small focal liver lesions, which can be treated locally by ultrasound-guided radiofrequency ablation (RFA) or other ablation techniques. However, ultrasound exams are cannot always identify isoechoic tumors, tumors recurring locally in areas treated with lipiodol following transarterial chemoembolization (TACE), or tumors recurring in areas treated previously by RFA or percutaneous ethanol injection (PEI) procedures^[4]. In addition, in ultrasound examinations, there are a few dead angles and it is difficult to examine the whole liver, especially in obese patients. Nodules that are poorly identified on ultrasound are clearly visible on CT/MR. However, interventional treatment is easier to perform under ultrasound-guidance, while the exposure to increased doses of radiation is also avoided. Thus, real-time virtual sonogra-

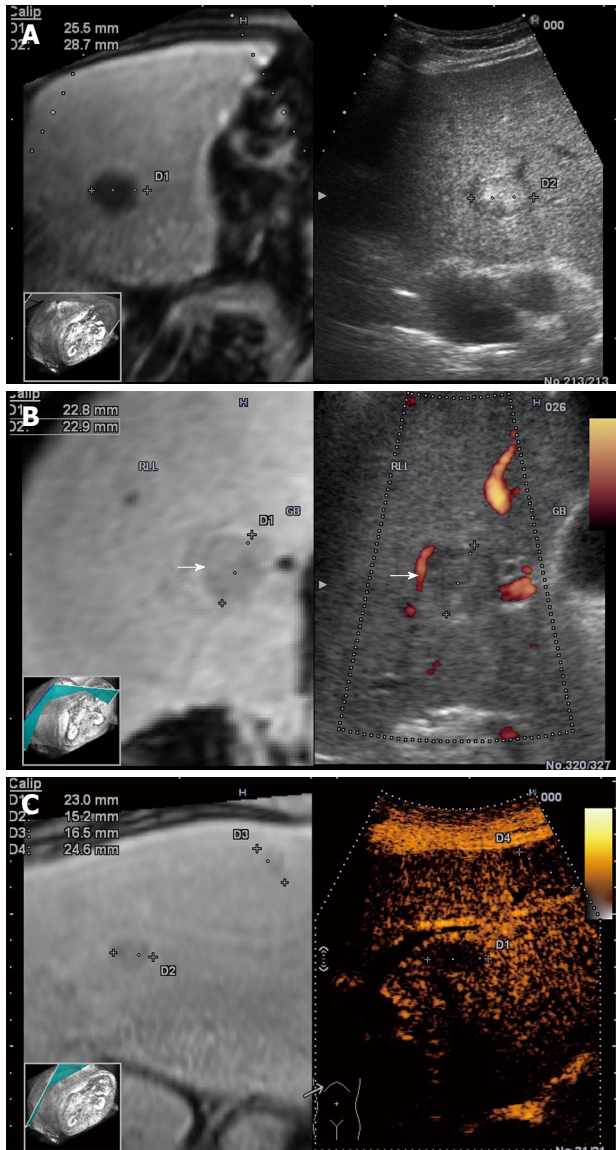


Figure 4 Real-time virtual sonography of liver nodules with simultaneous display of the contrast-enhanced magnetic resonance section and ultrasound images. 2D (A), Power Doppler (B), and contrast enhanced ultrasound (C) vs the reconstructed corresponding image.

phy combines the imaging advantages of both techniques. Several studies have already proved the feasibility of the RVS module, especially for percutaneous RFA of poorly visible or unidentifiable focal liver lesions during B-mode sonography^[5-7].

The RVS module is compatible with B-mode (Figure 4A), color Doppler imaging (CDI) mode (Figure 4B), and dynamic contrast harmonic imaging (D-CHI) mode (Figure 4C)^[8]. Therefore, RVS might have important clinical applications in the assessment of tumor angiogenesis. Hepatocellular carcinoma, a hypervascular tumor mainly supplied by hepatic arteries, shows a typical pattern in contrast-enhanced ultrasound: arterial hypervascularization (Figure 5A) with washout in the portal venous during the late phase (Figure 5B)^[9]. Real-time virtual ultrasound can reveal the contrast-enhanced ultrasound image in a similar way to contrast-enhanced CT/MR, although the

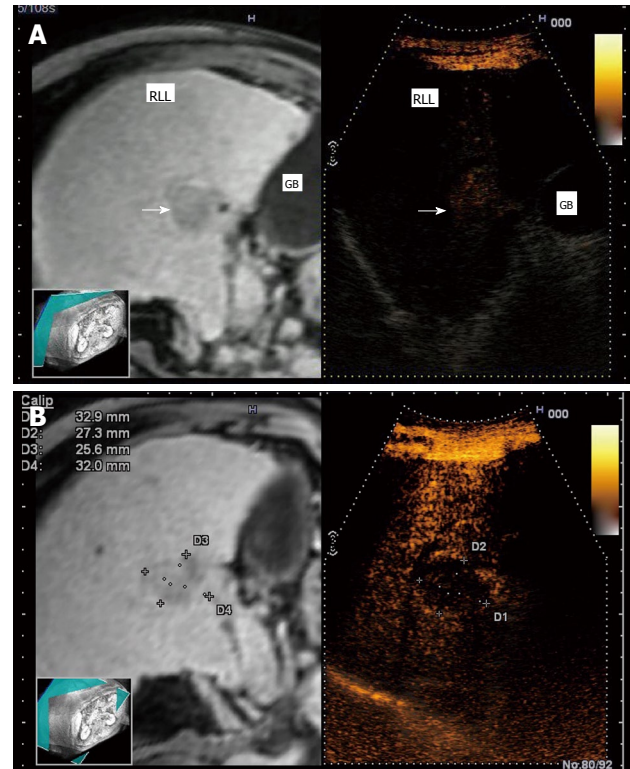


Figure 5 Single hepatocellular carcinoma (3 cm) nodule in a cirrhotic patient. In real-time virtual ultrasonography, after contrast agent injection, a progressive and intense enhancement is observed in the arterial phase (A), followed by wash-out in the tardive phase (B), on contrast-enhanced ultrasound, versus corresponding contrast-enhanced magnetic resonance images.



Figure 6 Real-time virtual sonography showing multiple metastases, better depicted on contrast-enhanced computed tomography as compared with ultrasound. A nodule in nodule aspect is visualized with excellent correlation on both contrast-enhanced magnetic resonance and real-time ultrasound.

mechanism of action is clearly different^[8]. Likewise, liver metastases that are poorly visible in 2D ultrasound can also be discovered in real-time virtual ultrasound, especially if contrast-enhancement is used (Figure 6). Although, the combined use of contrast-enhanced images has not yet been described in terms of accuracy for the positive and differential diagnosis of small focal liver lesions, RVS might combine the advantages of both methods (ultrasound and CT/MR).

For oncological patients, the tumor response to che-

motherapy is conventionally assessed by RECIST and WHO size criteria, obtained during CT/MR follow-up^[10]. Anti-angiogenic treatments induce lesion necrosis with no change in volume of the initial tumor; therefore, the use of size criteria appear inappropriate. Several studies have shown that the use of microbubble contrast agents can detect changes in vascularization, by calculation of maximal perfusion parameters, such as peak intensity, time to peak intensity, area under the curve, and slope coefficient of wash-in^[11-14]. Thus, the simultaneous use of real-time virtual sonography with dynamic contrast-enhanced ultrasound can be also employed. The method might allow the quantification of tumor perfusion for early assessment and quantitative monitoring of the efficacy of antiangiogenic agents, based on changes in vascularity, even before morphological changes become apparent^[10].

LIMITS

RVS cannot be used in patients if CT/MR is contraindicated (patients with known contrast medium allergies, renal failure, or metallic implants). Another limitation of RVS is that the technique does not always show the best synchronization between ultrasound and CT/MR images, although the discrepancy can be adjusted with careful visualization of neighboring portal and hepatic veins in most cases^[8]. The use of the RVS module does prolong the examination time; therefore, the clinical impact, in terms of improved decision making, should be further assessed. The technique adds the costs of CT/MR to the costs of the contrast-enhanced ultrasound exam; thus the cost-effectiveness of this approach must be evaluated in future studies^[15].

CONCLUSION

In conclusion, hybrid ultrasound imaging techniques now play a pivotal role in diagnosis, staging, and follow-up during treatment. During local ablation of focal liver lesions hybrid ultrasound imaging allows better control of the procedure and less radiation exposure.

REFERENCES

- 1 <http://www.hitachi-medical-systems.es/index.php?id=768&0>; cited on 18th February 2010
- 2 **Real-time Virtual Sonography Unit.** Instruction Manual. Hitachi Medical Corporation. 2004-2006
- 3 **Sandulescu L, Saftoiu A, Dumitrescu D, Ciurea T.** The role of real-time contrast-enhanced and real-time virtual sonography in the assessment of malignant liver lesions. *J Gastrointestin Liver Dis* 2009; **18**: 103-108
- 4 **Kawasoe H, Eguchi Y, Mizuta T, Yasutake T, Ozaki I, Shimonishi T, Miyazaki K, Tamai T, Kato A, Kudo S, Fujimoto K.** Radiofrequency ablation with the real-time virtual sonography system for treating hepatocellular carcinoma difficult to detect by ultrasonography. *J Clin Biochem Nutr* 2007; **40**: 66-72
- 5 **Minami Y, Kudo M, Chung H, Inoue T, Takahashi S, Hatanaka K, Ueda T, Hagiwara H, Kitai S, Ueshima K, Fukunaga T, Shiozaki H.** Percutaneous radiofrequency ablation of sonographically unidentifiable liver tumors. Feasibility and usefulness of a novel guiding technique with an integrated system of computed tomography and sonographic images. *Oncology* 2007; **72** Suppl 1: 111-116
- 6 **Minami Y, Chung H, Kudo M, Kitai S, Takahashi S, Inoue T, Ueshima K, Shiozaki H.** Radiofrequency ablation of hepatocellular carcinoma: value of virtual CT sonography with magnetic navigation. *AJR Am J Roentgenol* 2008; **190**: W335-W341
- 7 **Kitada T, Murakami T, Kuzushita N, Minamitani K, Nakajo K, Osuga K, Miyoshi E, Nakamura H, Kishino B, Tamura S, Hayashi N.** Effectiveness of real-time virtual sonography-guided radiofrequency ablation treatment for patients with hepatocellular carcinomas. *Hepatol Res* 2008; **38**: 565-571
- 8 **Sandulescu L, Saftoiu A, Dumitrescu D, Ciurea T.** Real-time contrast-enhanced and real-time virtual sonography in the assessment of benign liver lesions. *J Gastrointestin Liver Dis* 2008; **17**: 475-478
- 9 **Bruix J, Sherman M.** Management of hepatocellular carcinoma. *Hepatology* 2005; **42**: 1208-1236
- 10 **Claudon M, Cosgrove D, Albrecht T, Bolondi L, Bosio M, Calliada F, Correas JM, Darge K, Dietrich C, D'Onofrio M, Evans DH, Filice C, Greiner L, Jäger K, Jong N, Leen E, Lencioni R, Lindsell D, Martegani A, Meairs S, Nolsøe C, Piscaglia F, Ricci P, Seidel G, Skjoldbye B, Solbiati L, Thorelius L, Tranquart F, Weskott HP, Whittingham T.** Guidelines and good clinical practice recommendations for contrast enhanced ultrasound (CEUS) - update 2008. *Ultraschall Med* 2008; **29**: 28-44
- 11 **De Giorgi U, Aliberti C, Benea G, Conti M, Marangolo M.** Effect of angiosonography to monitor response during imatinib treatment in patients with metastatic gastrointestinal stromal tumors. *Clin Cancer Res* 2005; **11**: 6171-6176
- 12 **Lassau N, Lamuraglia M, Chami L, Leclère J, Bonvalot S, Terrier P, Roche A, Le Cesne A.** Gastrointestinal stromal tumors treated with imatinib: monitoring response with contrast-enhanced sonography. *AJR Am J Roentgenol* 2006; **187**: 1267-1273
- 13 **Lassau N, Chami L, Benatsou B, Peronneau P, Roche A.** Dynamic contrast-enhanced ultrasonography (DCE-US) with quantification of tumor perfusion: a new diagnostic tool to evaluate the early effects of antiangiogenic treatment. *Eur Radiol* 2007; **17** Suppl 6: F89-F98
- 14 **Lassau N, Brule A, Chami L, Benatsou B, Péronneau P, Roche A.** [Evaluation of early response to antiangiogenic treatment with dynamic contrast enhanced ultrasound] *J Radiol* 2008; **89**: 549-555
- 15 **Giesel FL, Delorme S, Sibbel R, Kauczor HU, Krix M.** [Contrast-enhanced ultrasound for the characterization of incidental liver lesions - an economical evaluation in comparison with multi-phase computed tomography] *Ultraschall Med* 2009; **30**: 259-268

S- Editor Sun H L- Editor Stewart GJ E- Editor Ma WH

Adrian Săftoiu, MD, PhD, Professor, and Peter Vilmann, MD, PhD, Professor, Series Editors

Optical molecular imaging for detection of Barrett's-associated neoplasia

Nadhi Thekkek, Sharmila Anandasabapathy, Rebecca Richards-Kortum

Nadhi Thekkek, Rebecca Richards-Kortum, Department of Bioengineering, Rice University, Houston, TX 77005, United States
 Sharmila Anandasabapathy, Division of Gastroenterology, Mount Sinai Medical Center, New York, NY 10029, United States
 Author contributions: Thekkek N performed the research; Thekkek N, Anandasabapathy S and Richards-Kortum R reviewed the data; Thekkek N and Richards-Kortum R wrote the paper.

Supported by The National Institute of Health Grants BRP CA103830 and RO1 EB007594

Correspondence to: Rebecca Richards-Kortum, PhD, Professor, Department of Bioengineering, Rice University, 6100 Main St, MS 142, Houston, TX 77005, United States. rkortum@rice.edu

Telephone: +1-713-3483823 Fax: +1-713-3485877

Received: July 2, 2010 Revised: November 17, 2010

Accepted: November 24, 2010

Published online: January 7, 2011

Key words: Barrett's esophagus; Barrett's metaplasia; Dysplasia; Esophageal adenocarcinoma; Endoscopy; Imaging

Peer reviewers: Ralph Graeser, PhD, Group Leader, Molecular and Cellular Biology, ProQinase GmbH, Breisacher Str. 117, Freiburg, 79106, Germany; Alexander S Rosemurgy, MD, FACS, Professor, Department of Surgery, Department of Medicine, University of South Florida, Tampa General Hospital, PO Box 1289, Room F145, Tampa, Florida, FL 33601, United States

Thekkek N, Anandasabapathy S, Richards-Kortum R. Optical molecular imaging for detection of Barrett's-associated neoplasia. *World J Gastroenterol* 2011; 17(1): 53-62 Available from: URL: <http://www.wjgnet.com/1007-9327/full/v17/i1/53.htm> DOI: <http://dx.doi.org/10.3748/wjg.v17.i1.53>

Abstract

Recent advancements in the endoscopic imaging of Barrett's esophagus can be used to probe a wide range of optical properties that are altered with neoplastic progression. This review summarizes relevant changes in optical properties as well as imaging approaches that measures those changes. Wide-field imaging approaches include narrow-band imaging that measures changes in light scattering and absorption, and autofluorescence imaging that measure changes in endogenous fluorophores. High-resolution imaging approaches include optical coherence tomography, endocytoscopy, confocal microendoscopy, and high-resolution microendoscopy. These technologies, some coupled with an appropriate contrast agent, can measure differences in glandular morphology, nuclear morphology, or vascular alterations associated with neoplasia. Advances in targeted contrast agents are further discussed. Studies that have explored these technologies are highlighted; as are the advantages and limitations of each.

© 2011 Baishideng. All rights reserved.

BACKGROUND

The incidence of esophageal adenocarcinoma (EAC) is rapidly increasing; over the last 40 years, the incidence rate of EAC has risen by over 300% in the United States^[1]. This is of particular concern because the overall 5-year survival rate for patients diagnosed with EAC is only 12%^[2]. Although detecting and treating esophageal neoplasia at an early stage has been reported to increase 5-year survival to rates as high as 81%^[3], current methods of early detection have significant limitations. As a result, more than 60% of patients with EAC are diagnosed at a late stage, after local, regional, or distant metastases have occurred^[4].

EAC arises primarily in patients with Barrett's esophagus (BE)^[5,6], which is a highly prevalent condition in which the squamous epithelium of the esophagus is replaced by intestinal metaplasia (IM) near the gastroesophageal (GE) junction^[7-9]. Because of this increased risk, patients with BE undergo regular surveillance endoscopy at designated intervals in an attempt to identify neoplastic lesions at an early stage^[10,11]. Surveillance involves endoscopic examination with random four-quadrant biopsies

taken every 1-2 cm along the BE segment^[10].

Despite surveillance efforts, routine biopsy protocols have been shown to miss up to 57% of neoplastic lesions in patients with BE^[12]. This is largely due to the fact that dysplasia or neoplasia may be focal, flat and endoscopically indistinguishable from non-neoplastic epithelium on routine white-light endoscopy (WLE). The ability to delineate better superficial mucosal changes associated with early neoplasia at a macroscopic level, and subsequently, identify the subcellular changes associated with neoplastic progression would greatly enhance the yield and efficacy of current surveillance practices.

CHANGES IN OPTICAL PROPERTIES

In a standard WLE examination, the endoscopist views white light reflected from the surface of the esophagus; although visual examination of reflected white light can identify some changes in tissue morphology associated with neoplasia, it does not exploit the full range of changes in tissue optical properties that are associated with dysplasia and cancer. Neoplasia alters the light absorption and scattering properties of esophageal tissue^[13,14]; in addition, neoplasia is associated with changes in the autofluorescence properties of esophageal tissue^[13,15-17].

A number of new endoscopic approaches have been developed to more effectively probe neoplasia-related changes in optical properties to improve visualization of early neoplastic lesions. For example, the color of illumination light can be optimized to probe better changes in tissue absorption and/or scattering. Autofluorescence endoscopy can be used to image changes in tissue fluorescence that are associated with neoplasia. Moreover, improving spatial resolution of endoscopic imaging can help reveal changes in cellular architecture and morphology associated with neoplasia. Finally, optically active contrast agents can be used to improve further image contrast and probe specific molecular and morphologic features of neoplastic tissue that may not be associated with changes in native optical properties.

Here, we first review changes in the optical properties of esophageal tissue associated with neoplasia, and then outline new endoscopic imaging approaches to use these changes to improve early detection of esophageal neoplasia. Finally, we discuss the use of targeted contrast agents to expand the range of molecular changes that can be imaged *in vivo*.

Neoplasia-associated changes in tissue light scattering and absorption

Light attenuation in esophageal tissue is governed by a combination of absorption and scattering. In the visible region of the spectrum, the primary source of light absorption in esophageal tissue is hemoglobin. Esophageal neoplasia is associated with increased angiogenesis^[18], and endoscopic imaging approaches to enhance vascular contrast may improve early detection^[19,20]. Oxyhemoglobin has absorption peaks at 420, 542, and 577 nm^[13]; examining the tissue at these illumination wavelengths can enhance

vascular contrast, with vasculature appearing visibly darker than the surrounding tissue due to the increase in light absorption^[21]. Neovascularization is an important quantifiable tool for distinguishing neoplasia from non-neoplastic Barrett's epithelium. Irregular angiogenesis occurs within the lamina propria at various levels of the mucosal layer in high-grade dysplasia (HGD) and cancer. These features have been verified by analysis of microvessels and overexpression of relevant markers such as vascular endothelial growth factor and CD34, which results in a statistically significant difference between the microvessel density in BE versus HGD and cancer^[19,20].

Light scattering in tissue is a result of spatial fluctuations in the refractive index. In general, the scattering of stroma is significantly greater than that of the epithelium and is the dominant source of reflected white light from intact tissue. Neoplasia is associated with a small decrease in stromal scattering that is attributed to degradation in collagen fibers, possibly due to proteases secreted by pre-neoplastic epithelial cells^[18,22,23]. The attenuation of light in tissue is wavelength dependent, with longer red wavelengths able to penetrate more deeply than shorter blue wavelengths. Thus, tuning the illumination wavelength provides some ability to control penetration depth, and highlight vascular contrast.

Neoplasia-associated changes in tissue autofluorescence

Some endogenous constituents of esophageal tissue can reemit absorbed light in the form of fluorescence. Endogenous fluorophores are found in both the epithelium and the stroma of esophageal tissue, and fluorescence imaging provides a way to monitor changes in the concentration and composition of these fluorophores. When esophageal tissue undergoes malignant transformation, endogenous fluorophores undergo alterations^[24-26], which can be probed *via* autofluorescence imaging (AFI), to detect abnormalities that may not be visible during standard WLE. Tuning the excitation wavelength provides a way to selectively probe various fluorophores that can then be quantified by measuring light intensity at specific emission wavelengths^[26].

The primary fluorophores within the epithelium include mitochondrial NADH and FAD found in epithelial cells. Epithelial cells show cytoplasmic autofluorescence attributed to NADH using UV excitation wavelengths (330-370 nm) and FAD using green excitation wavelengths (510-550 nm)^[27,28]. Levels of mitochondrial NADH^[15] and mitochondrial FAD increase due to dysplastic changes in the epithelium^[29,30].

Stromal fluorescence of esophageal tissue is predominantly associated with covalent collagen crosslinks, which are characterized by relatively high autofluorescence intensity across a broad range of UV, blue, and green excitation wavelengths^[16]. Esophageal neoplasia is associated with a loss of stromal autofluorescence, which has been attributed to a decrease in collagen crosslinking^[18,22,23]. Finally, invasive esophageal cancers are often associated with porphyrin fluorescence, with maximal excitation near 400 nm and emission in the red spectral region^[13,31,32].

Table 1 Advantages and disadvantages of optical technologies for identification of neoplasia in Barrett's esophagus

Technology	Advantages	Disadvantages	Stage of clinical translation
Standard WLE	Capable of scanning wide area, widely available outside of tertiary care centers, no exogenous contrast	Limited sensitivity and specificity	Commercially available
High-definition WLE	Capable of scanning wide area, increased image contrast, no exogenous contrast	Performance evaluated in moderate-sized studies	Commercially available
AFI	Capable of scanning wide area, consistently high sensitivity, no exogenous contrast	High rate of false positives, performance evaluated only in small pilot studies	Commercially available
NBI	Capable of scanning wide area, consistently high sensitivity, no exogenous contrast	Performance evaluated in small pilot studies	Commercially available
OCT	Resolves subsurface structure, no exogenous contrast	Technology still under development	Clinical studies
Endocytoscopy	Histology-like imaging, high specificity	Low sensitivity, limited field of view, requires exogenous contrast	Commercially available
CME	Nuclear morphology can be viewed, high sensitivity and specificity	Limited field of view, high cost, uses IV exogenous contrast	Commercially available
High-resolution microendoscopy	Some nuclear morphology can be viewed, lower cost, adaptable to any endoscope	Limited field of view, requires exogenous contrast, technology still in development	Clinical studies

AFI: Autofluorescence imaging; OCT: Optical coherence tomography; CME: Confocal microendoscopy; WLE: White-light endoscopy; NBI: Narrow-band imaging.

High-resolution imaging

The spatial resolution of optical imaging is governed by diffraction, and with visible wavelengths of light, subcellular resolution imaging is possible. Typically, standard endoscopic imaging approaches do not achieve diffraction-limited resolution, however, recent advances in high-resolution imaging techniques such as optical coherence tomography (OCT), endocytoscopy, and endomicroscopy afford the ability to image with subcellular resolution. Such approaches are often termed "optical biopsy", because they allow visualization of glandular and cellular alterations associated with neoplasia. Optical contrast in high-resolution imaging is governed by the same alterations in tissue absorption, scattering and fluorescence described above. In addition, optically active contrast agents are often used to increase contrast for high-resolution imaging.

IN VIVO ASSESSMENT OF IMAGING TECHNOLOGIES

In the past decade, advances in imaging technologies have enabled gastroenterologists to optically image Barrett's-associated neoplasia with better contrast *in vivo*. The development of wide-field imaging technologies affords clinicians a macroscopic view of the tissue, serving as a "red-flag technique" for relevant abnormalities. High-resolution technologies assess microscopic features of the tissue and, if coupled with an ideal source of contrast, may measure biochemical, molecular, and vascular changes. Table 1 summarizes a number of different optical technologies currently under investigation, describes the advantages and disadvantages of each, and describes which stage they have reached in terms of clinical translation. Table 2 summarizes the accuracy of the technologies that have been translated to clinical use and have been used in large clinical trials.

Narrow-band imaging

Narrow-band imaging (NBI) is a wide-field imaging technology that takes advantage of changes in light scat-

Table 2 Summary of performance of emerging optical technologies

Type of detection	Study size	Sensitivity, specificity
AFI	60 patients, 116 images	91%, 43% ^[36]
NBI	63 patients, 175 images	94%, 76% ^[33]
	51 patients, 204 images	100%, 98% ^[34]
	21 patients, 75 images	89%, 95% ^[38]
High-resolution imaging (1-15 μ m resolution)		
OCT	33 patients, 314 images	68%, 82% ^[43]
	55 patients, 177 images	83%, 75% ^[58]
Endocytoscopy	16 patients, 166 images	56%, 68% (425 \times)
		42%, 83% (1125 \times) ^[47]
Confocal imaging	63 patients, 433 images	93%, 98% ^[48]
	38 patients, 296 images	75%, 90% ^[50]

AFI: Autofluorescence imaging; OCT: Optical coherence tomography; NBI: Narrow-band imaging.

tering and absorption in neoplastic tissue. Systems that implement NBI illuminate tissue with one or more narrow-band wavelength ranges corresponding to hemoglobin absorption peaks. Reflected light in these bandwidths is recombined to create a digital image with enhanced vascular contrast. This approach can also enhance visualization of villous mucosal patterns due to lining of vessels in mucosal folds^[21]. An example is shown in Figure 1.

For example, one NBI system combines information from three wavelength ranges: 400-430 nm (blue), 530-550 nm (green), and 600-620 nm (red). Higher relative intensity from the blue region is used to enhance surface level vasculature associated with neoplasia, due to its shallow penetration depth. In a 63 patient study using this approach, researchers in Amsterdam used features such as mucosal morphology and vascular contrast to determine grade of disease. The presence and regularity of these patterns were found to be essential for image evaluation. Out of the 175 areas, 52 were used as training material for endoscopists and the remaining 123 were used as a validation set. In the validation set, 94% of HGD images were



Figure 1 Endoscopic images from an area positive for esophageal adenocarcinoma. Abnormal areas (arrow) can be seen in the high-resolution white light image (A), and the narrow-band image (B) [Copyright (2008), with permission from Elsevier]^[36]; in the narrow-band image, the irregular mucosal morphology is visible (arrow); an abnormal area (arrow) can be seen in the autofluorescence image (C) where areas with loss of fluorescence are indicated as purple regions in the pseudo-colored overlay [Copyright (2005), with permission from Elsevier]^[36].

noted to show irregular or disrupted villous/gyrus mucosal pattern, and 85% were noted to show irregular vascular patterns. Using these features and others, they developed a multi-step hierarchical classification system based on mucosal morphology, including features such as type and regularity of mucosal patterns, regularity of vasculature patterns, and presence and type of abnormal blood vessels. Using this multistep evaluation, they determined the overall sensitivity and specificity to be 94% and 76%, respectively^[33]. Similarly promising performance was also obtained using the same NBI system in a 51 patient study by Sharma and colleagues; sensitivity and specificity for detection of HGD were 100% and 99%, respectively^[34].

Of continued debate, however, is the question of how NBI compares to high-definition white-light endoscopy (HD-WLE) using the current generation of endoscopes. This new generation of endoscopes offers markedly higher pixel densities and high-definition images that result in increased contrast in villous mucosal patterns, and a marked improvement in resolution^[35,36] over standard WLE^[37]. In a study with 65 patients, Wolfson and colleagues, using a narrow-band system in which only two of the shorter wavelength ranges associated with hemoglobin were used, observed that the combination of HD-WLE and NBI did find higher grades of dysplasia in 18% of the study patients, using fewer biopsies than for standard endoscopy. They also observed that out of five of the cases in which HGD or EAC was detected, three were detected by HD-WLE as well. Although results favored NBI, the study was not designed to determine the efficacy of one modality over the other^[38]. Another study by Curvers and colleagues has observed that, while expert endoscopists preferred the image contrast provided by NBI, this did not improve overall interobserver agreement or accuracy when compared to HD-WLE^[39,40]. Larger studies are needed to determine which is the more accurate technique.

AFI

AFI can also increase contrast between non-neoplastic and neoplastic sites, as a result of the loss of autofluorescence associated with esophageal neoplasia. Typically, tissue auto-

fluorescence is excited in the blue region (395–475 nm) and fluorescence emission is collected at longer wavelengths (> 490 nm) to detect changes in fluorophores associated with malignant transformation. Because the intensity of autofluorescence can be low, this technique requires the use of highly sensitive CCDs to collect the autofluorescence signal. In recent systems, reflected light is also collected through a second CCD. Co-registered images can be used to compensate for changes in fluorescence intensity associated with variations in illumination and distance from the tip of the endoscope to the tissue, thereby further enhancing autofluorescence contrast. The resulting effect is pseudo-colored purple to highlight neoplastic lesions^[36,37]. An example is shown in Figure 1.

In a recent 60 patient study using a standard endoscope with an added AFI component, Kara was able to detect HGD in 22 patients, 14 of which were detected with AFI and WLE, and six of which were detected using AFI alone; thereby increasing the detection rate from 23% to 33% using AFI. Only one of the patients was diagnosed using four-quadrant biopsies alone^[36]. Results suggest that AFI may aid in the detection of additional HGD sites; however, it may not exclude the need for the standard four-quadrant biopsies. Sensitivity and specificity based on the 116 samples used for this study were 91% and 43%, respectively. Although no patient was diagnosed without AFI and four-quadrant biopsies, they cite a high rate of false positives using AFI alone, due in part to the loss of autofluorescence associated with acute inflammation^[36].

Although individually these enhanced endoscopic technologies have shown success, the high rate of false positives is a major drawback. To address this limitation, a combination of modalities is being explored to utilize the benefits of each; potentially increasing the accuracy of detection at the point of surveillance. Kara and colleagues have conducted a 20 patient pilot study in which HD-WLE and AFI were used initially to locate suspicious lesions. Once the lesions were identified, an NBI scope was introduced for detailed inspection of vascular and mucosal patterns. They found that 40% of the HGD lesions were discovered with AFI alone. However, the false-positive rate of

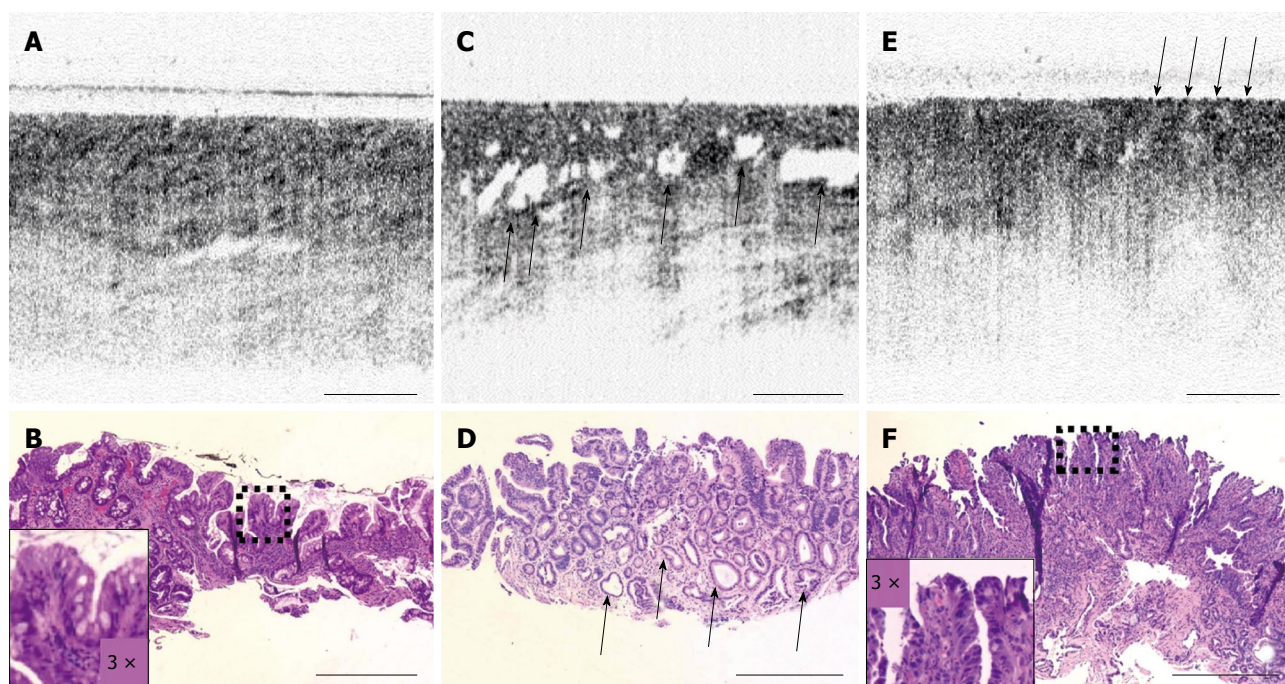


Figure 2 Optical coherence tomography images of intestinal metaplasia (A), and of neoplasia (C, E) are shown with corresponding histological images shown below [Copyright (2006), with permission from Elsevier]^[43], dilated glands (C) and increased surface reflectivity (E) can be seen in the optical coherence tomography images of neoplastic tissue, corresponding histopathology is shown (B, D, F). Scale bars, 500 μm .

the modality was 40% and the positive predictive value was 60%. Following NBI inspection, the false-positive rate was reduced to 10%, which achieved a positive predictive value of 85%^[41]. A more recent study with one scope containing both modalities achieved similar results. In that study, AFI was able to detect more lesions than high-resolution WLE alone, however, the false-positive rate remained a high 81%; following detailed inspection with NBI the rate was reduced to 26%^[42]. In both cases however, random four-quadrant biopsies detected additional lesions that the optical modalities did not identify, which indicates the need for further development of these and other technologies.

High-resolution imaging

Wide-field imaging techniques, such as AFI and NBI, were developed to measure large surface areas of gastrointestinal tissue. More recently, high-resolution systems have been developed to achieve near diffraction-limited imaging from small fields of view. Four primary approaches have been pursued to increase spatial resolution. OCT can image esophageal tissue with 10–15 μm resolution and a penetration depth of 1–2 mm. Endocytoscopy can image surface level esophageal tissue with up to 1–2 μm resolution using the highest magnification setting. Confocal microscopy can image esophageal tissue with 1–2 μm spatial resolution with a penetration depth of 300–400 μm . High-resolution microendoscopy can image surface level esophageal tissue with 4–5 μm spatial resolution. Recent clinical studies with these modalities highlight the benefits and limitations of high-resolution imaging.

OCT uses variations in the time it takes light to be reflected from structures beneath the tissue surface to image

sub-surface tissue structures as seen in Figure 2, in a manner analogous to ultrasound imaging. In a 55 patient study, researchers have determined that OCT could differentiate HGD and EAC from BE with a sensitivity of 83% and a specificity of 75%^[43]. An advantage of OCT is that it relies on endogenous differences in light scattering to generate image contrast. OCT may be a particularly useful tool in the detection and surveillance of sub-squamous BE because of its relatively greater depth of penetration^[44]. However, the technology is still under development^[45] and further clinical studies are needed to assess performance in a wide variety of clinical settings.

Endocytoscopy uses a probe that is passed through the instrumentation channel of an endoscope to image with subcellular resolution. Essentially, high-resolution epi-reflectance microscopy is used with methylene blue contrast to highlight relevant nuclear features (Figure 3A and B). Although models vary, there are generally two types each with different magnifications settings; one at 450 \times where the field of view can be as wide as 300 μm \times 300 μm , and a higher magnification setting of 1125 \times where a field of view as small as 120 μm \times 120 μm is made visible^[46]. A large study evaluating 166 sites in 16 patients with endocytoscopy by Pohl and colleagues reported a sensitivity and specificity of 42% and 83%, respectively^[47]. Although high specificity was encouraging, they did emphasize the need for an initial wide-field surveillance technique to identify suspicious areas. This technology is certainly promising; however, larger studies need to be performed.

Confocal microendoscopy (CME) images subsurface tissue structure with high resolution by using a spatial filter to reduce the background signal produced by scat-

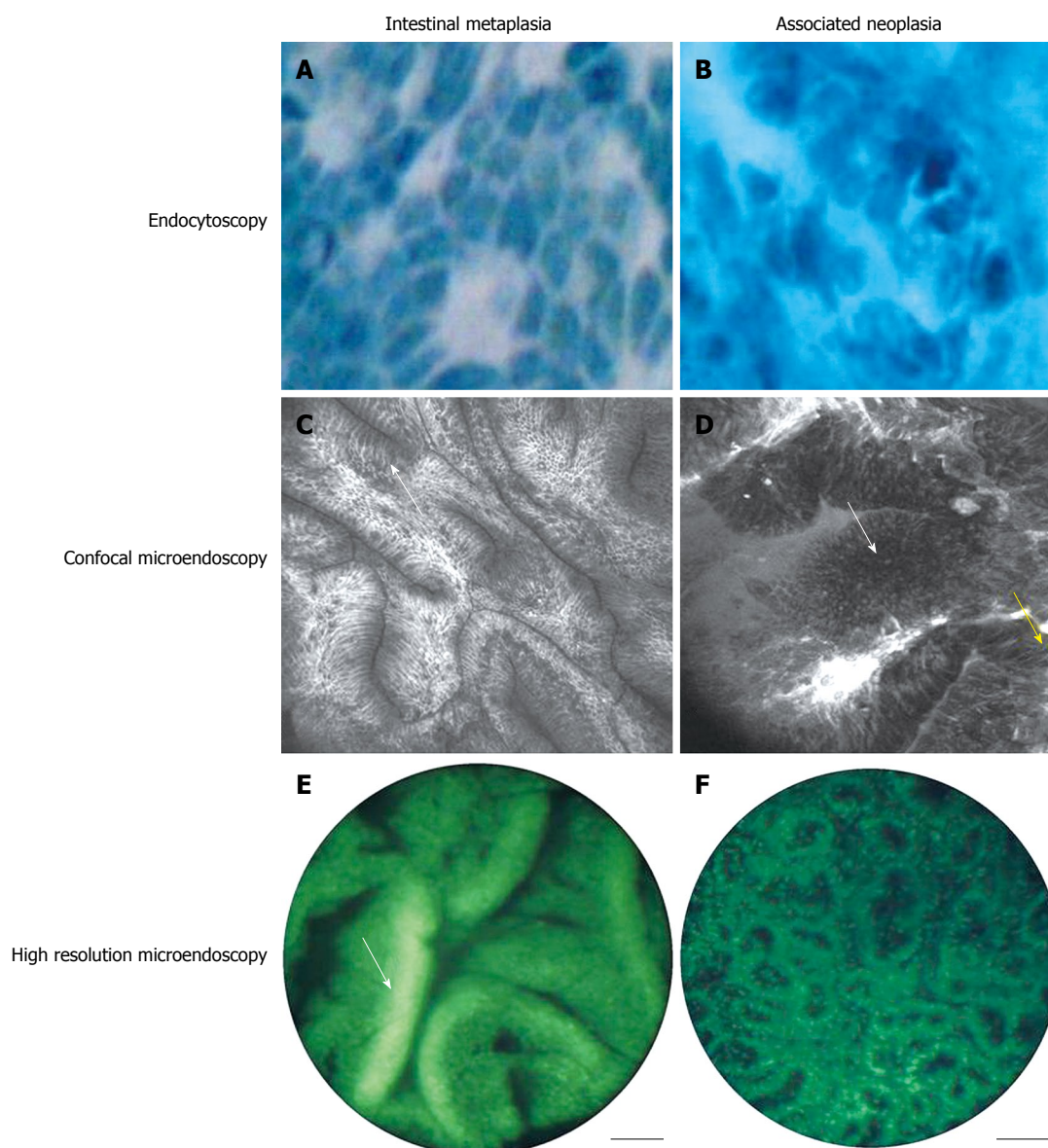


Figure 3 Images representing intestinal metaplasia and neoplasia collected using endocytoscopy (A, B) [Copyright (2007), with permission from Thieme]^[47], confocal microendoscopy (C, D) [Copyright (2006), with permission from Elsevier]^[48], and high-resolution microendoscopy (E, F) [Copyright (2008), with permission from Elsevier]^[51]. Typically applied methylene blue is used in endocytoscopy to highlight nuclear changes (A, B); In metaplasia (A), nuclei appear organized and regular; this is in stark contrast to neoplasia (B) where nuclei appear pleomorphic. Both images were taken using 1125 × magnification. Confocal images were taken using intravenous fluorescein to enhance contrast of subepithelial capillaries (C, D); for intestinal metaplasia (C), confocal microendoscopy allows visualization of mucin-containing goblet cells (white arrow); For Barrett's-associated neoplasia (B), cells are irregularly oriented (white arrow) and malignant invasion of the lamina propria can be seen (yellow arrow). Confocal images are 500 μm × 500 μm . High-resolution microendoscopy uses proflavine for contrast enhancement, highlighting changes in glandular and nuclear patterns (E, F). High-resolution images are 750 μm in diameter.

tered out-of-focus light, which produces images with 1-2 μm spatial resolution. Although CME images can be generated either in reflectance or fluorescence mode, in the context of esophageal imaging, fluorescence CME has been primarily used. Since tissue autofluorescence is weak, typically fluorescent contrast agents are used to generate image contrast in CME. Kiesslich and researchers conducted a 63 patient study in Germany using an endoscope that incorporated standard WLE and confocal microscopy; fluorescein (10% w/v) was administered intravenously to generate vascular contrast. Subepithelial capillaries located in the upper and deeper layers of the lamina propria were identified due to fluorescein con-

trast. Leakage of fluorescein due to irregular capillary formation indicated neoplastic areas (Figure 3C and D). Indeed, due to these irregularities, neoplasia could be detected with a sensitivity and specificity of 94% and 98% respectively^[48]. In a prospective, randomized, double-blind, controlled, crossover study with 39 patients using the same system, CME with targeted biopsy was shown to not only be accurate, but to nearly double the diagnostic yield of collected biopsies. In examining the biopsies identified by standard four-quadrant biopsies and the biopsies identified by CME, there was no statistically significant difference in detection of neoplasia between the two techniques^[49]. However, although accuracy and

diagnostic yield is impressive, the high cost may limit this technology to tertiary care centers.

A fiber-bundle, probe-based confocal system that can be passed through the instrument channel of any standard endoscope was used in a 38 patient study by Pohl and other researchers. A major benefit of this technology is its adaptability to existing endoscopes. This system also requires exogenous contrast; fluorescein was administered intravenously. The sensitivity and specificity of the two study endoscopists were 75% and 89% and 75% and 91%, respectively. They concluded that the confocal fiber probe showed a high negative predictive value for detecting unapparent neoplasia in BE; however, sensitivity was not ideal^[50].

An alternative approach to high-resolution fluorescence imaging uses a coherent fiber bundle placed in direct contact with the surface of tissue labeled with fluorescent dyes to yield high resolution images that reveal subcellular structure (Figure 3E and F)^[51]. This low-cost alternative to confocal imaging may be suited for community-wide surveillance outside of tertiary care centers. In a small pilot study of nine patients, with topical proflavine for contrast enhancement of cell nuclei, researchers achieved a sensitivity and specificity of 87% and 85% using fluorescence microendoscopy^[52].

Contrast enhancement

As optical imaging technology continues to advance, the concurrent development of appropriate contrast agents that target biomarkers of neoplasia is crucial. Two general classes of optical contrast agents have been explored to improve image contrast: vital dyes and targeted contrast agents. Absorbing or fluorescent dyes that have an affinity for specific tissue constituents have often been used to improve the ability to visualize specific features associated with neoplasia. Often referred to as vital dyes, these stains can help delineate features such as angiogenesis, leaky vasculature, and cell morphology. In contrast, targeted contrast agents use a high affinity probe molecule to target a specific molecular biomarker associated with neoplasia^[53]. The probe molecule must be coupled to an optically active component, such as a fluorescent dye or scattering nanoparticle. Here, we briefly review the utility of both types of contrast agents for improved detection of esophageal neoplasia.

Vital dyes can be utilized to delineate better morphological changes associated with epithelial neoplasia. For example, the absorptive dye methylene blue localizes primarily in nuclei and can enhance visualization of nuclei when coupled with appropriate high-resolution instrumentation. Using an endocytoscope, nuclear characteristics associated with neoplasia such as homogeneity, nuclear-to-cytoplasmic ratio, and organization can be resolved. However, since methylene blue dye is known to induce oxidative damage of DNA when exposed to white light illumination^[54], the risks of the contrast agent need to be weighed against the benefits to determine potential use.

Fluorescent vital dyes may be advantageous due to the lack of interference with standard endoscopy. Fluorescein

is a dye that is administered intravenously, thus enhancing the view of vasculature in epithelial tissue. When coupled with confocal imaging, subsurface vasculature can be seen. The illumination and collection wavelengths of commercially available confocal systems correspond to fluorescein excitation (about 490 nm) and emission (about 520 nm)^[48,50]. Acriflavine is another vital fluorescent dye that can be seen using similar excitation (about 450 nm) and emission (about 510 nm) wavelengths. Acriflavine stains cell nuclei, highlighting nuclear characteristics such as size, shape, and spacing, and has been used previously *in vivo* for gastrointestinal imaging^[55].

Targeted contrast agents serve as beacons that signal specific molecular events associated with pre-cancer formation. The benefit of targeted agents is the potential to achieve a high signal to background ratio by virtue of selective binding to a molecular target. Lu and researchers used a phage display library with about 2.8×10^9 unique sequences to select a cancer-specific peptide. The library was biopanned against three cultured human esophageal cell types: adenocarcinoma, metaplasia, and normal, to identify a peptide with specificity for the adenocarcinoma cell line. They used the selected peptide labeled with FITC to image Barrett's-associated neoplasia *in vivo*. The agent was topically applied and imaged with a concurrently developed prototype fluorescence endoscope. Initial results showed a significant increase in binding to Barrett's-associated neoplasia over Barrett's alone when imaged with wide-field fluorescence imaging (Figure 4)^[56]. In a different study, Hsiung and colleagues fluorescently labeled a high-affinity heptapeptide sequence selected with similar phage display techniques for the colon, and were able to differentiate dysplastic from non-dysplastic colonic crypts using confocal imaging^[57]. In both of these cases, the topically applied contrast agent was incubated *in vivo* for a short period of time before the unbound agent was washed off to reduce non-specific signals. Although the excitation and emission wavelengths of these agents correspond well with commercially available confocal endoscopes, another important advantage demonstrated by these studies is the ability to image these agents with both wide-field fluorescence and CME.

DISCUSSION

Recent advances in imaging technologies afford visualization of endogenous optical alterations associated with gastrointestinal neoplasia. NBI shows contrast associated with light absorption due to hemoglobin. High sensitivity and specificity is cited in studies using this technology, however some indicate that there is no significant difference between contrast associated with NBI imaging and HD-WLE, which is becoming increasingly available. AFI measures the signal decrease associated with loss of stromal collagen fluorescence and increased fluorescence associated with porphyrin. Various studies evaluating AFI have cited high sensitivity, but a high rate of false positives. The combination of NBI and AFI may afford better sensitivity and specificity rates; NBI has shown to reduce

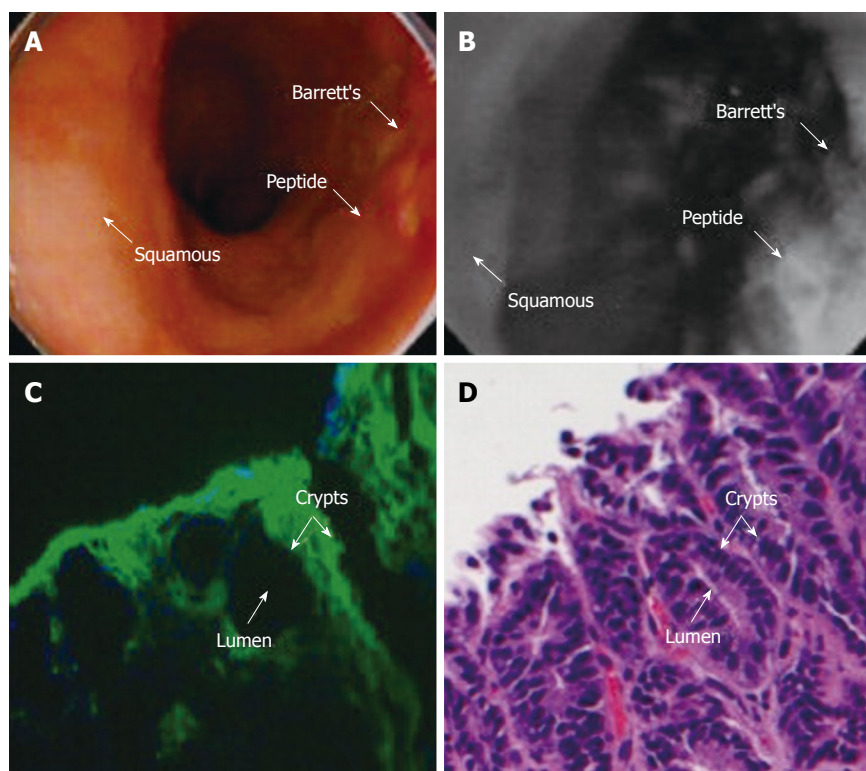


Figure 4 *In vivo* localization of contrast agent localized to a neoplasia region visualized using wide-field fluorescence endoscopy. White light endoscopic image (A) shows no evidence of lesion; topical administration of peptide-targeted fluorescent dye reveals neoplastic area (B) [Copyright (2008), with permission from IOS Press]^[56]; targeted neoplastic crypts seen with fluorescence microscopy (C), and corresponding histology (D) [Copyright (2010), with permission from Elsevier]^[59].

the number of false positives identified by AFI from 81% to 26%^[42].

High-resolution imaging will also play a major role in improving detection, affording clinicians an “optical biopsy” of epithelial tissue. Confocal imaging allows for optical sectioning of up to 250 μm deep, and coupled with vital dyes such as fluorescein, allows evaluation of vascular regularity. High sensitivity and specificity have been cited; however, high cost and the limited field of view remain concerns. Endocytoscopy allows for histology-like reflectance imaging where nuclei appear dark blue due to methylene blue contrast. The technology achieves high specificity; however, the dye has been shown to interfere with white light imaging and image quality has been an issue. When combined with wide-field imaging techniques, high-resolution technologies may reduce false-positive rates if coupled with the appropriate contrast agent.

Unfortunately, despite all the advances in optical imaging methods, there are still lesions that are only detected by standard four-quadrant biopsies. Improvements in contrast agents are also needed to facilitate early detection. A number of contrast agents are commercially available; primarily vital dyes such as fluorescein and methylene blue. However, recent *in vivo* testing of optically labeled high-affinity peptide and heptapeptide sequences has paved the way for molecule-specific contrast agents for gastrointestinal neoplasia^[56,57]. Although advances have translated the use of vital dyes and contrast agents *in vivo*, there are still many unanswered questions regarding their ultimate clinical role. What will be the ideal mechanism of delivery?

How will the development of *in vivo* imaging technologies accommodate the use of new contrast agents? Finally, will the addition of contrast agents create a multifaceted platform that can improve overall accuracy of surveillance?

Although these new imaging technologies may be appropriate for tertiary care centers, additional considerations are necessary as these technologies are disseminated more widely. A potential solution may be a lower cost technology such as the high-resolution microscope, or an adaptable technology such as the confocal miniprobe with topically applied contrast agents; both of which have been cited to achieve reasonably high sensitivity and specificity. Objective, quantitative algorithms will also be important because clinicians outside of tertiary care clinics may not be as familiar with optical characteristics of abnormal lesions detected with new technologies. Various groups have begun work in this area; however, larger trials need to be conducted to determine effectiveness^[52,58].

At this point, larger studies are needed to test the combination of multi-scale, multi-modal technologies against the current surveillance standard, and to test whether the use of contrast agent is advantageous. This multifaceted optical approach has the potential to improve surveillance in BE; once validated, it has the potential to be utilized for surveillance of neoplasia along the gastrointestinal tract and can be further developed for screening.

DISCLOSURE STATEMENT

Thekkek N and Anandasabapathy S have no financial

conflicts to disclose. One of the co-authors (Richards-Kortum R) has a small ownership interest in Remicalm, Inc which has licensed related technology from the University of Texas at Austin and Rice University.

REFERENCES

- 1 Devesa SS, Blot WJ, Fraumeni JF Jr. Changing patterns in the incidence of esophageal and gastric carcinoma in the United States. *Cancer* 1998; **83**: 2049-2053
- 2 Sihvo EI, Luostarinen ME, Salo JA. Fate of patients with adenocarcinoma of the esophagus and the esophagogastric junction: a population-based analysis. *Am J Gastroenterol* 2004; **99**: 419-424
- 3 Portale G, Hagen JA, Peters JH, Chan LS, DeMeester SR, Gandamihardja TA, DeMeester TR. Modern 5-year survival of resectable esophageal adenocarcinoma: single institution experience with 263 patients. *J Am Coll Surg* 2006; **202**: 588-596; discussion 596-598
- 4 Farrow DC, Vaughan TL. Determinants of survival following the diagnosis of esophageal adenocarcinoma (United States). *Cancer Causes Control* 1996; **7**: 322-327
- 5 Blot WJ, Devesa SS, Kneller RW, Fraumeni JF Jr. Rising incidence of adenocarcinoma of the esophagus and gastric cardia. *JAMA* 1991; **265**: 1287-1289
- 6 Cameron AJ. Epidemiology of columnar-lined esophagus and adenocarcinoma. *Gastroenterol Clin North Am* 1997; **26**: 487-494
- 7 Mueller J, Werner M, Stolte M. Barrett's esophagus: histopathologic definitions and diagnostic criteria. *World J Surg* 2004; **28**: 148-154
- 8 Morales TG, Sampliner RE, Bhattacharyya A. Intestinal metaplasia of the gastric cardia. *Am J Gastroenterol* 1997; **92**: 414-418
- 9 Spechler SJ. Columnar-lined esophagus. Definitions. *Chest Surg Clin N Am* 2002; **12**: 1-13, vii
- 10 Sampliner RE. Updated guidelines for the diagnosis, surveillance, and therapy of Barrett's esophagus. *Am J Gastroenterol* 2002; **97**: 1888-1895
- 11 Katz D, Rothstein R, Schned A, Dunn J, Seaver K, Antonioli D. The development of dysplasia and adenocarcinoma during endoscopic surveillance of Barrett's esophagus. *Am J Gastroenterol* 1998; **93**: 536-541
- 12 Vieth M, Ell C, Gossner L, May A, Stolte M. Histological analysis of endoscopic resection specimens from 326 patients with Barrett's esophagus and early neoplasia. *Endoscopy* 2004; **36**: 776-781
- 13 Georgakoudi I, Jacobson BC, Van Dam J, Backman V, Wallace MB, Müller MG, Zhang Q, Badizadegan K, Sun D, Thomas GA, Perelman LT, Feld MS. Fluorescence, reflectance, and light-scattering spectroscopy for evaluating dysplasia in patients with Barrett's esophagus. *Gastroenterology* 2001; **120**: 1620-1629
- 14 Wallace MB, Perelman LT, Backman V, Crawford JM, Fitzmaurice M, Seiler M, Badizadegan K, Shields SJ, Itzkan I, Dasari RR, Van Dam J, Feld MS. Endoscopic detection of dysplasia in patients with Barrett's esophagus using light-scattering spectroscopy. *Gastroenterology* 2000; **119**: 677-682
- 15 Georgakoudi I, Jacobson BC, Müller MG, Sheets EE, Badizadegan K, Carr-Locke DL, Crum CP, Boone CW, Dasari RR, Van Dam J, Feld MS. NAD(P)H and collagen as in vivo quantitative fluorescent biomarkers of epithelial precancerous changes. *Cancer Res* 2002; **62**: 682-687
- 16 Kara MA, DaCosta RS, Streutker CJ, Marcon NE, Bergman JJ, Wilson BC. Characterization of tissue autofluorescence in Barrett's esophagus by confocal fluorescence microscopy. *Dis Esophagus* 2007; **20**: 141-150
- 17 DaCosta RS, Wilson BC, Marcon NE. Photodiagnostic techniques for the endoscopic detection of premalignant gastrointestinal lesions. *Digest Endosc* 2003; **15**: 153-173
- 18 Auvinen MI, Sihvo EI, Ruohutula T, Salminen JT, Koivistoinen A, Siivola P, Rönholm R, Rämö JO, Bergman M, Salo JA. Incipient angiogenesis in Barrett's epithelium and lymphangiogenesis in Barrett's adenocarcinoma. *J Clin Oncol* 2002; **20**: 2971-2979
- 19 Couvelard A, Paraf F, Gratio V, Scoazec JY, Hénin D, Degott C, Fléjou JF. Angiogenesis in the neoplastic sequence of Barrett's oesophagus. Correlation with VEGF expression. *J Pathol* 2000; **192**: 14-18
- 20 Möbius C, Stein HJ, Becker I, Feith M, Theisen J, Gais P, Jütting U, Siewert JR. The 'angiogenic switch' in the progression from Barrett's metaplasia to esophageal adenocarcinoma. *Eur J Surg Oncol* 2003; **29**: 890-894
- 21 Gono K, Obi T, Yamaguchi M, Ohyama N, Machida H, Sano Y, Yoshida S, Hamamoto Y, Endo T. Appearance of enhanced tissue features in narrow-band endoscopic imaging. *J Biomed Opt* 2004; **9**: 568-577
- 22 Herszenyi L, Hritz I, Pregun I, Sipos F, Juhasz M, Molnar B, Tulassay Z. Alterations of glutathione S-transferase and matrix metalloproteinase-9 expressions are early events in esophageal carcinogenesis. *World J Gastroenterol* 2007; **13**: 676-682
- 23 Salmela MT, Karjalainen-Lindsberg ML, Puolakkainen P, Saarialho-Kere U. Upregulation and differential expression of matrilysin (MMP-7) and metalloelastase (MMP-12) and their inhibitors TIMP-1 and TIMP-3 in Barrett's oesophageal adenocarcinoma. *Br J Cancer* 2001; **85**: 383-392
- 24 DaCosta RS, Wilson BC, Marcon NE. Spectroscopy and fluorescence in esophageal diseases. *Best Pract Res Clin Gastroenterol* 2006; **20**: 41-57
- 25 Georgakoudi I, Van Dam J. Characterization of dysplastic tissue morphology and biochemistry in Barrett's esophagus using diffuse reflectance and light scattering spectroscopy. *Gastrointest Endosc Clin N Am* 2003; **13**: 297-308
- 26 DaCosta RS, Andersson H, Wilson BC. Molecular fluorescence excitation-emission matrices relevant to tissue spectroscopy. *Photochem Photobiol* 2003; **78**: 384-392
- 27 Drezek R, Brookner C, Pavlova I, Boiko I, Malpica A, Lotan R, Follen M, Richards-Kortum R. Autofluorescence microscopy of fresh cervical-tissue sections reveals alterations in tissue biochemistry with dysplasia. *Photochem Photobiol* 2001; **73**: 636-641
- 28 Pavlova I, Sokolov K, Drezek R, Malpica A, Follen M, Richards-Kortum R. Microanatomical and biochemical origins of normal and precancerous cervical autofluorescence using laser-scanning fluorescence confocal microscopy. *Photochem Photobiol* 2003; **77**: 550-555
- 29 Gullledge CJ, Dewhirst MW. Tumor oxygenation: a matter of supply and demand. *Anticancer Res* 1996; **16**: 741-749
- 30 Mayevsky A, Chance B. Intracellular oxidation-reduction state measured in situ by a multichannel fiber-optic surface fluorometer. *Science* 1982; **217**: 537-540
- 31 Harris DM, Werkhaven J. Endogenous porphyrin fluorescence in tumors. *Lasers Surg Med* 1987; **7**: 467-472
- 32 Panjehpour M, Overholt BF, Vo-Dinh T, Haggitt RC, Edwards DH, Buckley FP 3rd. Endoscopic fluorescence detection of high-grade dysplasia in Barrett's esophagus. *Gastroenterology* 1996; **111**: 93-101
- 33 Kara MA, Ennahachi M, Fockens P, ten Kate FJ, Bergman JJ. Detection and classification of the mucosal and vascular patterns (mucosal morphology) in Barrett's esophagus by using narrow band imaging. *Gastrointest Endosc* 2006; **64**: 155-166
- 34 Sharma P, Bansal A, Mathur S, Wani S, Cherian R, McGregor D, Higbee A, Hall S, Weston A. The utility of a novel narrow band imaging endoscopy system in patients with Barrett's esophagus. *Gastrointest Endosc* 2006; **64**: 167-175
- 35 Endo T, Awakawa T, Takahashi H, Arimura Y, Itoh F, Yamashita K, Sasaki S, Yamamoto H, Tang X, Imai K. Classification of Barrett's epithelium by magnifying endoscopy. *Gastrointest Endosc* 2002; **55**: 641-647

- 36 **Kara MA**, Peters FP, Ten Kate FJ, Van Deventer SJ, Fockens P, Bergman JJ. Endoscopic video autofluorescence imaging may improve the detection of early neoplasia in patients with Barrett's esophagus. *Gastrointest Endosc* 2005; **61**: 679-685
- 37 **Kara MA**, Smits ME, Rosmolen WD, Bultje AC, Ten Kate FJ, Fockens P, Tytgat GN, Bergman JJ. A randomized crossover study comparing light-induced fluorescence endoscopy with standard videoendoscopy for the detection of early neoplasia in Barrett's esophagus. *Gastrointest Endosc* 2005; **61**: 671-678
- 38 **Wolfsen HC**, Crook JE, Krishna M, Achem SR, Devault KR, Bouras EP, Loeb DS, Stark ME, Woodward TA, Hemminger LL, Cayer FK, Wallace MB. Prospective, controlled tandem endoscopy study of narrow band imaging for dysplasia detection in Barrett's Esophagus. *Gastroenterology* 2008; **135**: 24-31
- 39 **Curvers W**, Baak L, Kiesslich R, Van Oijen A, Rabenstein T, Ragunath K, Rey JF, Scholten P, Seitz U, Ten Kate F, Fockens P, Bergman J. Chromoendoscopy and narrow-band imaging compared with high-resolution magnification endoscopy in Barrett's esophagus. *Gastroenterology* 2008; **134**: 670-679
- 40 **Curvers WL**, Bohmer CJ, Mallant-Hent RC, Naber AH, Pon-sioen CI, Ragunath K, Singh R, Wallace MB, Wolfsen HC, Song LM, Lindeboom R, Fockens P, Bergman JJ. Mucosal morphology in Barrett's esophagus: interobserver agreement and role of narrow band imaging. *Endoscopy* 2008; **40**: 799-805
- 41 **Kara MA**, Peters FP, Fockens P, ten Kate FJ, Bergman JJ. Endoscopic video-autofluorescence imaging followed by narrow band imaging for detecting early neoplasia in Barrett's esophagus. *Gastrointest Endosc* 2006; **64**: 176-185
- 42 **Curvers WL**, Singh R, Song LM, Wolfsen HC, Ragunath K, Wang K, Wallace MB, Fockens P, Bergman JJ. Endoscopic trimodal imaging for detection of early neoplasia in Barrett's oesophagus: a multi-centre feasibility study using high-resolution endoscopy, autofluorescence imaging and narrow band imaging incorporated in one endoscopy system. *Gut* 2008; **57**: 167-172
- 43 **Evans JA**, Poneros JM, Bouma BE, Bressner J, Halpern EF, Shishkov M, Lauwers GY, Mino-Kenudson M, Nishioka NS, Tearney GJ. Optical coherence tomography to identify intra-mucosal carcinoma and high-grade dysplasia in Barrett's esophagus. *Clin Gastroenterol Hepatol* 2006; **4**: 38-43
- 44 **Cobb MJ**, Hwang JH, Upton MP, Chen Y, Oelschlager BK, Wood DE, Kimmey MB, Li X. Imaging of subsquamous Barrett's epithelium with ultrahigh-resolution optical coherence tomography: a histologic correlation study. *Gastrointest Endosc* 2010; **71**: 223-230
- 45 **Suter MJ**, Vakoc BJ, Yachinski PS, Shishkov M, Lauwers GY, Mino-Kenudson M, Bouma BE, Nishioka NS, Tearney GJ. Comprehensive microscopy of the esophagus in human patients with optical frequency domain imaging. *Gastrointest Endosc* 2008; **68**: 745-753
- 46 **Tomizawa Y**, Abdulla HM, Prasad GA, Wong Kee Song LM, Lutzke LS, Borkenhagen LS, Wang KK. Endocytoscopy in esophageal cancer. *Gastrointest Endosc Clin N Am* 2009; **19**: 273-281
- 47 **Pohl H**, Koch M, Khalifa A, Papanikolaou IS, Scheiner K, Wiedenmann B, Rösch T. Evaluation of endocytoscopy in the surveillance of patients with Barrett's esophagus. *Endoscopy* 2007; **39**: 492-496
- 48 **Kiesslich R**, Gossner L, Goetz M, Dahlmann A, Vieth M, Stolte M, Hoffman A, Jung M, Nafe B, Galle PR, Neurath MF. In vivo histology of Barrett's esophagus and associated neoplasia by confocal laser endomicroscopy. *Clin Gastroenterol Hepatol* 2006; **4**: 979-987
- 49 **Dunbar KB**, Okolo P 3rd, Montgomery E, Canto MI. Confocal laser endomicroscopy in Barrett's esophagus and endoscopically inapparent Barrett's neoplasia: a prospective, randomized, double-blind, controlled, crossover trial. *Gastrointest Endosc* 2009; **70**: 645-654
- 50 **Pohl H**, Rösch T, Vieth M, Koch M, Becker V, Anders M, Khalifa AC, Meining A. Miniprobe confocal laser microscopy for the detection of invisible neoplasia in patients with Barrett's oesophagus. *Gut* 2008; **57**: 1648-1653
- 51 **Muldoon TJ**, Anandasabapathy S, Maru D, Richards-Kortum R. High-resolution imaging in Barrett's esophagus: a novel, low-cost endoscopic microscope. *Gastrointest Endosc* 2008; **68**: 737-744
- 52 **Muldoon TJ**, Thekkek NT, Roblyer D, Maru D, Harpaz N, Potack J, Anandasabapathy S, Richards-Kortum R. Evaluation of quantitative image analysis criteria for the high-resolution micro-endoscopic detection of neoplasia in Barrett's esophagus. *J Biomed Opt* 2010; **15**: 026027
- 53 **Pierce MC**, Javier DJ, Richards-Kortum R. Optical contrast agents and imaging systems for detection and diagnosis of cancer. *Int J Cancer* 2008; **123**: 1979-1990
- 54 **Olliver JR**, Wild CP, Sahay P, Dexter S, Hardie LJ. Chromoendoscopy with methylene blue and associated DNA damage in Barrett's oesophagus. *Lancet* 2003; **362**: 373-374
- 55 **Polglase AL**, McLaren WJ, Skinner SA, Kiesslich R, Neurath MF, Delaney PM. A fluorescence confocal endomicroscope for in vivo microscopy of the upper- and the lower-GI tract. *Gastrointest Endosc* 2005; **62**: 686-695
- 56 **Lu S**, Wang TD. In vivo cancer biomarkers of esophageal neoplasia. *Cancer Biomark* 2008; **4**: 341-350
- 57 **Hsiung PL**, Hardy J, Friedland S, Soetikno R, Du CB, Wu AP, Sahbaie P, Crawford JM, Lowe AW, Contag CH, Wang TD. Detection of colonic dysplasia in vivo using a targeted heptapeptide and confocal microendoscopy. *Nat Med* 2008; **14**: 454-458
- 58 **Qi X**, Sivak MV, Isenberg G, Willis JE, Rollins AM. Computer-aided diagnosis of dysplasia in Barrett's esophagus using endoscopic optical coherence tomography. *J Biomed Opt* 2006; **11**: 044010
- 59 **Goetz M**, Wang TD. Molecular imaging in gastrointestinal endoscopy. *Gastroenterology* 2010; **138**: 828-833.e1

S- Editor Sun H L- Editor Kerr C E- Editor Ma WH

New endoscopic approaches in IBD

Helmut Neumann, Markus F Neurath, Jonas Mudter

Helmut Neumann, Markus F Neurath, Jonas Mudter, Department of Medicine I, University of Erlangen-Nuremberg, 91054 Erlangen, Germany

Author contributions: Neumann H contributed to the study idea, study design, literature search, manuscript writing and final revision of the article; Neurath MF contributed to the manuscript writing and the final revision of the article; Mudter J contributed to study design, manuscript writing and the final revision of the article.

Correspondence to: Helmut Neumann, MD, Department of Medicine I, University of Erlangen-Nuremberg, Ulmenweg 18, 91054 Erlangen, Germany. helmut.neumann@uk-erlangen.de

Telephone: +49-9131-8535000 Fax: +49-9131-8535209

Received: August 14, 2010 Revised: December 1, 2010

Accepted: December 8, 2010

Published online: January 7, 2011

Abstract

Recent advances in endoscopic imaging techniques have revolutionized the diagnostic approach of patients with inflammatory bowel disease (IBD). New, emerging endoscopic imaging techniques visualized a plethora of new mucosal details even at the cellular and subcellular level. This review offers an overview about new endoscopic techniques, including chromoendoscopy, magnification endoscopy, spectroscopy, confocal laser endomicroscopy and endocytoscopy in the face of IBD.

© 2011 Baishideng. All rights reserved.

Key words: Endoscopy; Inflammatory bowel disease; Endomicroscopy; Endocytoscopy; Narrow band imaging; Fujinon intelligent color enhancement; i-Scan; Spectroscopy; Chromoendoscopy; Ulcerative colitis; Crohn's disease; Fluorescence endoscopy

Peer reviewers: Zvi Fireman, Department of Gastroenterology, Hillel- yaffe Med. Ctr., PO Box 169, Hadera 38100, Israel; Atsushi Nakajima, Professor, Division of Gastroenterology, Yokohama City University Graduate School of Medicine, 3-9 Fuku-ura, Kanazawa-ku, Yokohama 236-0004, Japan

Neumann H, Neurath MF, Mudter J. New endoscopic approaches

in IBD. *World J Gastroenterol* 2011; 17(1): 63-68 Available from: URL: <http://www.wjgnet.com/1007-9327/full/v17/i1/63.htm> DOI: <http://dx.doi.org/10.3748/wjg.v17.i1.63>

INTRODUCTION

Patients with long standing ulcerative colitis and Crohn's disease are at an increased risk for the development of intraepithelial neoplasia (formerly known as dysplasia) and colorectal neoplasia. Therefore, surveillance endoscopy is mandatory in these patients. Nevertheless, standard white light endoscopy with multiple random biopsies may miss a quantum of lesions^[1].

During the last ten years, a variety of new endoscopic techniques were introduced to improve diagnosis and patient outcome in inflammatory bowel disease (IBD). Traditionally, standard white light endoscopy only allows the investigation of the mucosal surface and surrounding blood vessels at low magnification (Figure 1). To overcome these limitations, new endoscopic imaging techniques were developed providing a more detailed view of the mucosa. Emerging endoscopic imaging techniques include chromoendoscopy and magnification endoscopy. Additionally, new endoscopic devices now allow real time *in vivo* histology during ongoing endoscopy.

This review describes the concept of advanced endoscopic imaging techniques in IBD.

CHROMOENDOSCOPY

Chromoendoscopy uses different staining techniques to enhance the mucosal detail and submucosal vascular pattern, thereby improving the detection of pathological lesions and enabling a more precise diagnosis. Currently, chromoendoscopy is distinguished in dye-based and dyeless imaging techniques.

The basic principle of dye-based chromoendoscopy (DBC) is the use of biocompatible dye agents (Figure 2). Dyes include absorptive (methylene blue 0.1%-0.5%, cresyl violet 0.2%) and contrast agents (indigo carmine

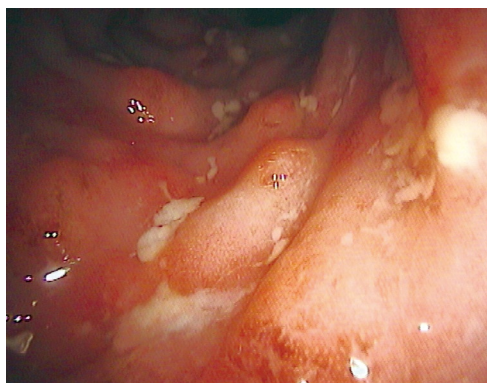


Figure 1 High-resolution standard white light endoscopic image of active Crohn's disease. Endoscopy shows ulcerations, mucosal edema and erythema.

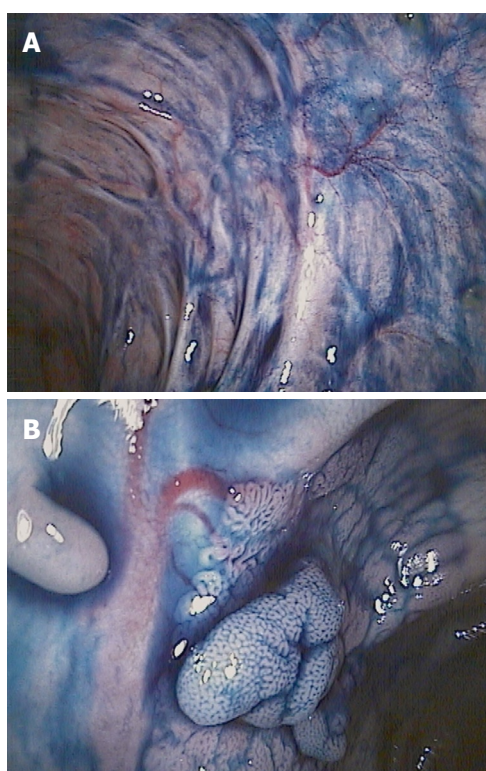


Figure 2 Chromoendoscopy with indigo carmine. A better distinction of mucosal changes in long standing ulcerative colitis (A) and pit pattern analysis of suspicious lesions (B).

0.2%-0.4%). DBC yields an additional diagnostic value with a 3-4 higher detection rate of intraepithelial neoplasia^[2,3]. However, dye-based chromoendoscopy has some potential limitations. There are additional costs for the equipment needed for dye spraying, it is a time consuming procedure, the dye does not always coat the surface evenly and it does not allow for a detailed analysis of the subepithelial capillary network, which is an important feature in the early diagnosis of gastrointestinal neoplasia.

Therefore, dye-less chromoendoscopy (DLC; also called virtual chromoendoscopy) has been developed (Figure 3). DLC includes narrow band imaging (NBI; Olympus, Tokyo, Japan), Fujinon intelligent color enhancement (FICE; Fujinon, Tokyo, Japan) and i-Scan (Pentax, Tokyo, Japan).

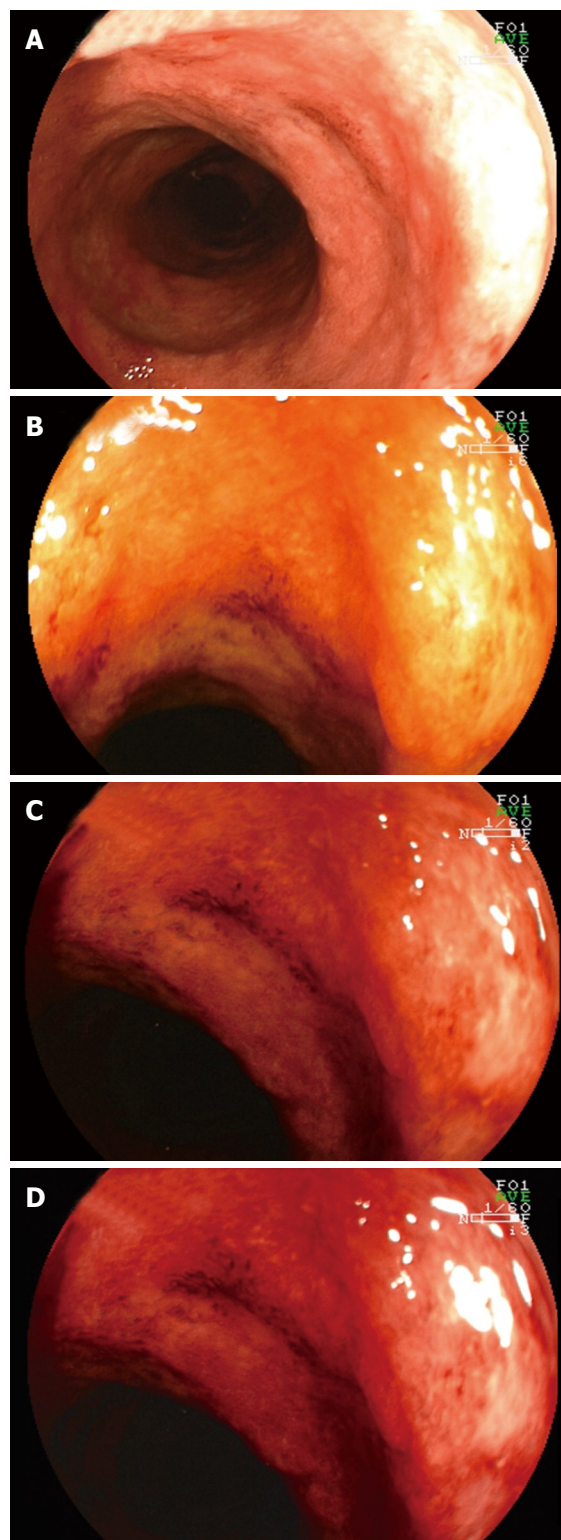


Figure 3 Virtual chromoendoscopy using the fujinon intelligent color enhancement-system. A: Shows standard white light endoscopic image; B-D: Illustrate different fujinon intelligent color enhancement settings to improve mucosal detail.

NBI is based on optical filters within the light source of the endoscope which narrow the bandwidth of spectral transmittance such that the blood vessels are enhanced and thus seen more easily.

FICE and i-Scan are based on the same physical prin-

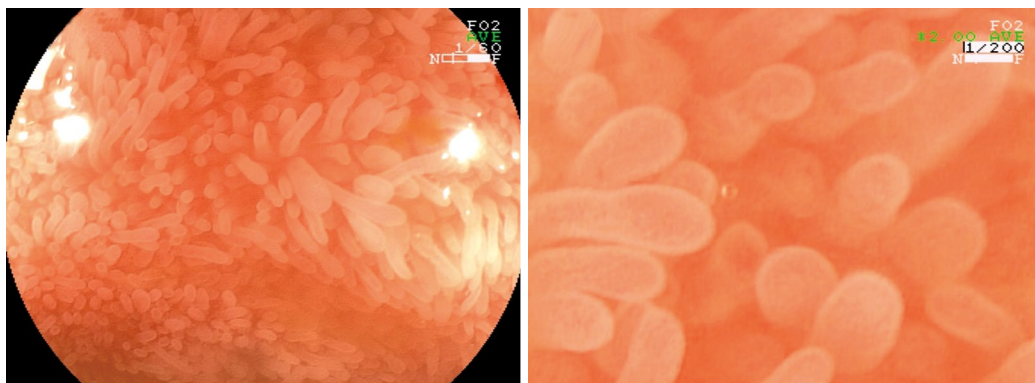


Figure 4 High-magnification endoscopy of ileum mucosa in patient with Crohn's disease without activity. Villi are clearly visualized.

circle as NBI, but due to a computed spectral estimation technology, they are not dependent on the presence of optical filters inside of the video endoscope. In contrast to NBI, FICE and i-Scan use an endoscopic image from the video processor and reconstruct virtual images in real time by increasing the intensity of narrowed blue light to a maximum and by decreasing narrowed red light and green light to a minimum resulting in an improved contrast of the capillary patterns and enhancement of the mucosal surface.

One recent study evaluated magnifying colonoscopy with NBI for the diagnosis of intraepithelial neoplasia in ulcerative colitis. It was found that the tortuous pattern determined by NBI colonoscopy may be a clue for the identification of dysplasia during surveillance for ulcerative colitis^[4]. Another study included 50 patients with longstanding ulcerative colitis and reported on a moderate accuracy (sensitivity 75%, specificity 81%) for the NBI diagnosis of intraepithelial neoplasia^[5]. Additionally, NBI colonoscopy may be of value for determining the grade of inflammation in patients with quiescent ulcerative colitis^[6].

Very recently, it was shown that FICE could not improve the detection or delineation of ulcers and erosions due to Crohn's disease^[7]. Nevertheless, these preliminary data have to be proven in larger prospective trials.

One recent published study tested the efficacy of high definition endoscopy alone compared to i-Scan or chromoendoscopy with methylene blue (0.1%) in screening for colorectal cancer^[8]. It was found that both i-Scan and chromoendoscopy identified more lesions compared to high definition endoscopy alone. Additionally, i-Scan was able to predict neoplasia as precisely as chromoendoscopy.

MAGNIFICATION ENDOSCOPY

Magnification endoscopy (also called zoom endoscopy) utilizes a movable lens to vary the degree of magnification up to 150-fold (Figure 4). By staining the entire colon with methylene blue, it has been shown that chromoendoscopy combined with magnification endoscopy has the potential to improve targeting biopsy examination in patients with long-standing colitis and facilitate early detection of intraepithelial neoplasia and colorectal cancer^[2]. In the chro-

moendoscopy arm a significantly better correlation was found between the endoscopic assessment of degree ($P = 0.0002$) and extent ($P < 0.0001$) of colonic inflammation and the histopathologic findings compared with the conventional colonoscopy group. Additionally, more targeted biopsies were possible, and significantly more intraepithelial neoplasia were detected in the chromoendoscopy group ($P = 0.003$).

These data were confirmed by Hurlstone and colleagues^[3]. In a prospective study, 162 patients with longstanding ulcerative colitis underwent total colonoscopy. After detection of subtle mucosal changes intravital staining with indigo carmine was used. Subsequently, the macroscopic type and the staining pattern were defined. Chromoendoscopy with magnification and targeted biopsies significantly increased diagnostic yield for intraepithelial neoplasia and the number of flat neoplastic changes as opposed to conventional colonoscopy.

The largest prospective study to date comparing conventional endoscopy with magnification endoscopy enrolled 300 patients with ulcerative colitis^[9]. Magnification imaging was significantly better than conventional colonoscopy for predicting disease extent *in vivo* ($P < 0.0001$). The authors concluded that high-magnification imaging provides a sensitive and specific *in vivo* "virtual biopsy" in ulcerative colitis. High-accuracy optical biopsy could limit the number of biopsies required, with significant cost savings for pathology services.

SPECTROSCOPY

Spectroscopy includes several optical techniques, including fluorescence-, reflectance-, light scattering spectroscopy and optical coherence tomography. Spectroscopy depends on the wavelength of the light source and on tissue characteristics. Based on differences between the spectra of light that is backscattered between cells, different spectra can be identified that are specific for various diseases such as ischemia, inflammation, and malignancy^[10].

One study assessed fluorescence endoscopy for the detection of intraepithelial neoplasia in ulcerative colitis by taking optical guided biopsies. By using 5-aminolevulinic acid as an exogenous fluorophore agent, sensitivity

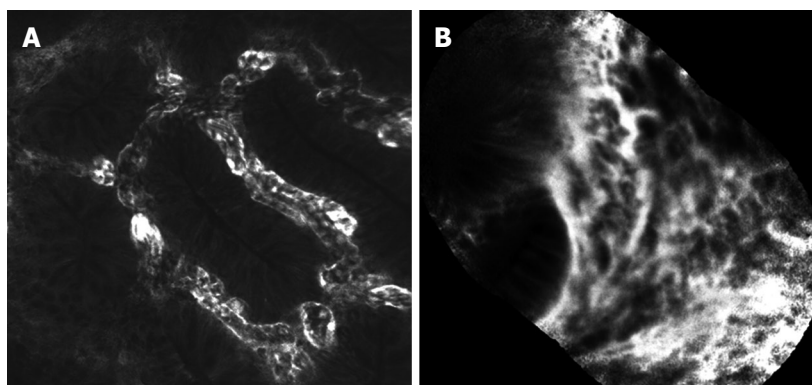


Figure 5 Confocal laser endomicroscopy using either the integrated system (iCLE, A) or the probe-based system (pCLE, B) visualizes dilated microvessels, leakage and disturbed crypt architecture in active ulcerative colitis.

and specificity for dysplastic lesions was 100% and 62%, respectively^[11]. Very recently, the detection of invisible flat intraepithelial neoplasia with protoporphyrin IX fluorescence was compared to standard 4-quadrant biopsies^[12]. Flat intraepithelial neoplasia was detected in 7% of patients by standard white light 4-quadrant biopsies and in 24% of patients using fluorescence-guided endoscopy ($P = 0.02$). Sensitivity and specificity for differentiating patients with and without dysplasia were 100% and 81%, respectively. Additionally, dysplastic and non-dysplastic mucosa could be discriminated with a sensitivity and specificity of 73% and 81%, respectively.

CONFOCAL LASER ENDOMICROSCOPY

In 2004, confocal laser endomicroscopy was introduced, allowing real time *in vivo* histology of 1000-fold magnification during ongoing endoscopy^[13]. Currently, two FDA approved devices are available (Figure 5). One is integrated into the distal tip of a high resolution endoscope (iCLE; Pentax, Tokyo, Japan), one represents a stand-alone probe which is capable of passage through the working channel of most standard endoscopes (pCLE; Cellvizio, Mauna Kea Technologies, Paris, France). A blue laser light source delivers an excitation wavelength of 488 nm and returning light is detected at > 505 nm. Endomicroscopy requires the application of fluorescence agents, either systemically (fluorescein) or topically (e.g. acriflavine, cresyl violet)^[14].

While endomicroscopy only covers a limited field of view within the mucosa, pan-endomicroscopy of the whole gastrointestinal tract is not feasible. Therefore, macroscopic visualization of suspected areas is necessary before performing targeted endomicroscopy.

To date, different studies have addressed the utility of endomicroscopy for the *in vivo* diagnosis of IBD associated mucosal changes.

To compare endomicroscopic imaging of inflamed and non-inflamed rectal mucosa in patients with ulcerative colitis, Watanabe *et al.*^[15] enrolled 17 patients with ulcerative colitis and 14 controls. Confocal images were compared to standard histopathology. Endomicroscopy was able to visualize crypt architecture, capillaries and inflammatory cells, providing equivalent information to histopathology.

Recently, a new classification of inflammation activity in ulcerative colitis using endomicroscopy was proposed^[16], including crypt architecture and microvascular alterations. In this study, endomicroscopy was reliable for real-time assessment of inflammation activity in ulcerative colitis showing good correlations with histological results (Spearman's rho, both $P < 0.001$).

Our group addressed the utility of endomicroscopy for the *in vivo* evaluation of Crohn's disease associated changes. Using the pCLE system, endomicroscopy was able to diagnose Crohn's disease associated changes with high accuracy. Furthermore, pCLE could detect residual macroscopic non-visible mucosal inflammation as precisely as histology (κ values 0.8, unpublished data).

Current guidelines recommend a large number of biopsy specimens during surveillance colonoscopy in ulcerative colitis. Nevertheless, flat lesions still may be missed. In a trial of longstanding ulcerative colitis, chromoendoscopy was used to unmask lesions for endomicroscopy and compared with standard white light endoscopy with random biopsies^[17]. Chromoendoscopy in combination with endomicroscopy detected 4.75-fold more neoplasia compared to conventional colonoscopy ($P = 0.005$). Additionally, 50% fewer biopsy specimens were required ($P = 0.008$). The presence of neoplastic changes could be predicted with high sensitivity, specificity and accuracy (94.7%, 98.3%, 97.8%, respectively).

One recent study prospectively evaluated the clinical applicability and predictive power of endomicroscopy for the *in vivo* differentiation of dysplasia-associated lesion mass (DALM) or adenoma-like mass (ALM)^[18]. Accuracy of endomicroscopy was 97% and an excellent agreement between endomicroscopy and histopathological diagnosis was found ($\kappa = 0.91$).

ENDOCYTOSCOPY

Endocytoscopy (Olympus, Tokyo, Japan) is a new imaging technique, enabling microscopic imaging of the mucosal layer of the gut at a magnification up to 1400-fold (Figure 6). Endocytoscopy is based on a contact light microscope which enables real-time visualization of cellular structures of the superficial epithelial layer in a plane parallel to the

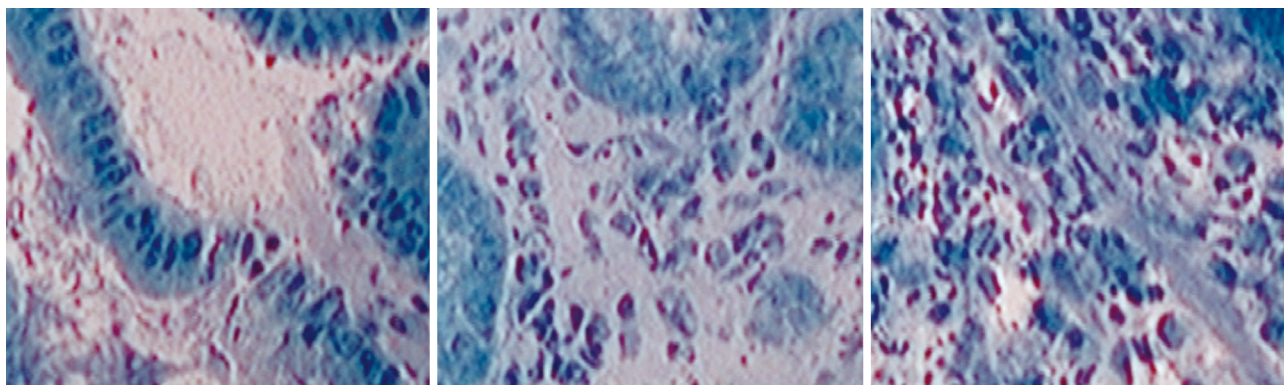


Figure 6 Endocytoscopy enables visualization of different cytological and architectural features, including size, arrangement, and density of cells.

mucosal surface. Currently, systems integrated into the distal tip of an endoscope (iEC) and probe-based (pEC) systems are available. Probe-based systems consist of handheld miniproboscopes, which are capable of being inserted through the accessory channel of a standard endoscope. The device provides ultra high magnification imaging at $\times 570$ (pEC), $\times 580$ (iEC) or $\times 1400$ (pEC) on a 19-inch monitor from an optical sampling site of about 0.5 mm in diameter. Endocytoscopy requires preparation of the mucosal layer with absorptive contrast agents like methylene blue or toluidine blue^[19].

Recently, endocytoscopy has been established as a useful tool to examine mucosal surfaces^[20-23]. Different studies suggest the potential of endocytoscopy for the *in vivo* evaluation of duodenal mucosa in celiac disease^[21]. Furthermore, endocytoscopy was able to detect tissue abnormalities in normal mucosa surrounding colorectal cancer and to identify neoplasia in aberrant crypt foci^[22]. Additionally, endocytoscopy was shown to distinguish neoplastic from non-neoplastic lesions, and also to differentiate invasive colon cancer from adenoma^[23,24].

Currently, data on endocytoscopy for *in vivo* diagnosis of IBD are still lacking. Nevertheless, this new imaging technique is a promising development allowing surface magnification at cellular and subcellular resolution.

CAPSULE ENDOSCOPY

In order to evaluate the small intestine capsule endoscopy (CE) was introduced. Currently two CE systems are available. One is distributed by Given Imaging (Norcross, Ga), and one by Olympus (Tokyo, Japan). The capsule is passively propelled through the intestine by peristalsis while transmitting color images of the intestine^[25].

CE is useful for the evaluation of the small intestine in patients in whom the diagnosis of Crohn's disease is elusive^[26]. Due to the danger of capsule retention in patients with established Crohn's disease, a patency capsule is available which is self-dissolved approximately 30 h after ingestion. In addition, balloon-guided endoscopy could be used to remove impacted capsules^[27]. Dubcenco and coworkers studied CE findings in patients with established and suspected small-intestine Crohn's disease and correlated the findings with radiologic, endoscopic and histologic

findings. Final diagnosis of active small-intestine Crohn's disease was made in 74% of patients. In addition, CE yielded a sensitivity and specificity of 89.6% and 100%, respectively, and a positive predictive value and a negative predictive value of 100% and 76.9%, respectively^[28]. Furthermore, CE was shown to be superior compared to push enteroscopy and enteroclysis^[29].

CONCLUSION

Modern endoscopy has revolutionized the diagnosis and management of patients with IBD. The newly developed endoscopic devices offer features that allow more and more mucosal and submucosal details to be seen. According to high magnification and respective reduced field of view, prior assessment of suspicious lesions is mandatory. Chromoendoscopy, using either vital or virtual staining techniques unmasks circumscribed lesions and confocal laser endomicroscopy or endocytoscopy can then be used to predict intraepithelial neoplasia with high accuracy. Nevertheless, the assessment of these new endoscopic imaging modalities in clinical practice still warrants further investigation. In addition, currently there is no reimbursement for advanced endoscopic imaging methods including endomicroscopy, endocytoscopy and spectroscopy. Therefore, endoscopy with multiple random biopsies remains the gold standard for surveillance in patients with IBD.

REFERENCES

- 1 **Connell WR**, Lennard-Jones JE, Williams CB, Talbot IC, Price AB, Wilkinson KH. Factors affecting the outcome of endoscopic surveillance for cancer in ulcerative colitis. *Gastroenterology* 1994; **107**: 934-944
- 2 **Kiesslich R**, Fritsch J, Holtmann M, Koehler HH, Stolte M, Kanzler S, Nafe B, Jung M, Galle PR, Neurath MF. Methylene blue-aided chromoendoscopy for the detection of intraepithelial neoplasia and colon cancer in ulcerative colitis. *Gastroenterology* 2003; **124**: 880-888
- 3 **Hurlstone DP**, McAlindon ME, Sanders DS, Koegh R, Lobo AJ, Cross SS. Further validation of high-magnification chromoscopic-colonoscopy for the detection of intraepithelial neoplasia and colon cancer in ulcerative colitis. *Gastroenterology* 2004; **126**: 376-378
- 4 **Matsumoto T**, Kudo T, Jo Y, Esaki M, Yao T, Iida M. Magnifying colonoscopy with narrow band imaging system for

- the diagnosis of dysplasia in ulcerative colitis: a pilot study. *Gastrointest Endosc* 2007; **66**: 957-965
- 5 **van den Broek FJ**, Fockens P, van Eeden S, Reitsma JB, Hardwick JC, Stokkers PC, Dekker E. Endoscopic tri-modal imaging for surveillance in ulcerative colitis: randomised comparison of high-resolution endoscopy and autofluorescence imaging for neoplasia detection; and evaluation of narrow-band imaging for classification of lesions. *Gut* 2008; **57**: 1083-1089
 - 6 **Kudo T**, Matsumoto T, Esaki M, Yao T, Iida M. Mucosal vascular pattern in ulcerative colitis: observations using narrow band imaging colonoscopy with special reference to histologic inflammation. *Int J Colorectal Dis* 2009; **24**: 495-501
 - 7 **Neumann H**, Fry LC, Bellutti M, Malfertheiner P, Mönkemüller K. Double-balloon enteroscopy-assisted virtual chromoendoscopy for small-bowel disorders: a case series. *Endoscopy* 2009; **41**: 468-471
 - 8 **Hoffman A**, Kagel C, Goetz M, Tresch A, Mudter J, Bisterfeld S, Galle PR, Neurath MF, Kiesslich R. Recognition and characterization of small colonic neoplasia with high-definition colonoscopy using i-Scan is as precise as chromoendoscopy. *Dig Liver Dis* 2010; **42**: 45-50
 - 9 **Hurlstone DP**, Sanders DS, McAlindon ME, Thomson M, Cross SS. High-magnification chromoscopic colonoscopy in ulcerative colitis: a valid tool for in vivo optical biopsy and assessment of disease extent. *Endoscopy* 2006; **38**: 1213-1217
 - 10 **Hommers DW**, van Deventer SJ. Endoscopy in inflammatory bowel diseases. *Gastroenterology* 2004; **126**: 1561-1573
 - 11 **Messmann H**, Endlicher E, Freunek G, Rümmele P, Schölmmerich J, Knüchel R. Fluorescence endoscopy for the detection of low and high grade dysplasia in ulcerative colitis using systemic or local 5-aminolaevulinic acid sensitisation. *Gut* 2003; **52**: 1003-1007
 - 12 **Ortner MA**, Fusco V, Ebert B, Sukowski U, Weber-Eibel J, Fleige B, Stolte M, Oberhuber G, Rinneberg H, Lochs H. Time-gated fluorescence spectroscopy improves endoscopic detection of low-grade dysplasia in ulcerative colitis. *Gastrointest Endosc* 2010; **71**: 312-318
 - 13 **Kiesslich R**, Burg J, Vieth M, Gnaendiger J, Enders M, Delaney P, Polglase A, McLaren W, Janell D, Thomas S, Nafe B, Galle PR, Neurath MF. Confocal laser endoscopy for diagnosing intraepithelial neoplasias and colorectal cancer in vivo. *Gastroenterology* 2004; **127**: 706-713
 - 14 **Neumann H**, Kiesslich R, Wallace MB, Neurath MF. Confocal laser endomicroscopy: technical advances and clinical applications. *Gastroenterology* 2010; **139**: 388-392, 392.e1-e2
 - 15 **Watanabe O**, Ando T, Maeda O, Hasegawa M, Ishikawa D, Ishiguro K, Ohmiya N, Niwa Y, Goto H. Confocal endomicroscopy in patients with ulcerative colitis. *J Gastroenterol Hepatol* 2008; **23** Suppl 2: S286-S290
 - 16 **Li CQ**, Xie XJ, Yu T, Gu XM, Zuo XL, Zhou CJ, Huang WQ, Chen H, Li YQ. Classification of inflammation activity in ulcerative colitis by confocal laser endomicroscopy. *Am J Gastroenterol* 2010; **105**: 1391-1396
 - 17 **Kiesslich R**, Goetz M, Lammersdorf K, Schneider C, Burg J, Stolte M, Vieth M, Nafe B, Galle PR, Neurath MF. Chromoscopy-guided endomicroscopy increases the diagnostic yield of intraepithelial neoplasia in ulcerative colitis. *Gastroenterology* 2007; **132**: 874-882
 - 18 **Hurlstone DP**, Thomson M, Brown S, Tiffin N, Cross SS, Hunter MD. Confocal endomicroscopy in ulcerative colitis: differentiating dysplasia-associated lesional mass and adenoma-like mass. *Clin Gastroenterol Hepatol* 2007; **5**: 1235-1241
 - 19 **Kwon RS**, Wong Kee Song LM, Adler DG, Conway JD, Diehl DL, Farraye FA, Kantsevoy SV, Kaul V, Kethu SR, Mamula P, Pedrosa MC, Rodriguez SA, Tierney WM. Endocytoscopy. *Gastrointest Endosc* 2009; **70**: 610-613
 - 20 **Neumann H**, Vieth M, Neurath MF, Fuchs FS. In Vivo Diagnosis of Small-Cell Lung Cancer by Endocytoscopy. *J Clin Oncol* 2010; Epub ahead of print
 - 21 **Pohl H**, Rösch T, Tanczos BT, Rudolph B, Schlüns K, Baumgart DC. Endocytoscopy for the detection of microstructural features in adult patients with celiac sprue: a prospective, blinded endocytoscopy-conventional histology correlation study. *Gastrointest Endosc* 2009; **70**: 933-941
 - 22 **Cipolletta L**, Bianco MA, Rotondano G, Piscopo R, Meucci C, Prisco A, Cipolletta F, de Gregorio A, Salvati A. Endocytoscopy can identify dysplasia in aberrant crypt foci of the colorectum: a prospective in vivo study. *Endoscopy* 2009; **41**: 129-132
 - 23 **Neumann H**, Vieth M, Neurath MF. Endocytoscopy-Based Detection of Focal High-Grade Intraepithelial Neoplasia in Colonic Polyps. *Clin Gastroenterol Hepatol* 2010; Epub ahead of print
 - 24 **Sasajima K**, Kudo SE, Inoue H, Takeuchi T, Kashida H, Hidaka E, Kawachi H, Sakashita M, Tanaka J, Shiokawa A. Real-time in vivo virtual histology of colorectal lesions when using the endocytoscopy system. *Gastrointest Endosc* 2006; **63**: 1010-1017
 - 25 **Mishkin DS**, Chuttani R, Croffie J, Disario J, Liu J, Shah R, Somogyi L, Tierney W, Song LM, Petersen BT. ASGE Technology Status Evaluation Report: wireless capsule endoscopy. *Gastrointest Endosc* 2006; **63**: 539-545
 - 26 **Papadakis KA**, Lo SK, Fireman Z, Hollerbach S. Wireless capsule endoscopy in the evaluation of patients with suspected or known Crohn's disease. *Endoscopy* 2005; **37**: 1018-1022
 - 27 **Mönkemüller K**, Bellutti M, Fry LC, Malfertheiner P. Enteroscopy. *Best Pract Res Clin Gastroenterol* 2008; **22**: 789-811
 - 28 **Dubcenco E**, Jeejeebhoy KN, Petroniene R, Tang SJ, Zalev AH, Gardiner GW, Baker JP. Capsule endoscopy findings in patients with established and suspected small-bowel Crohn's disease: correlation with radiologic, endoscopic, and histologic findings. *Gastrointest Endosc* 2005; **62**: 538-544
 - 29 **Chong AK**, Taylor A, Miller A, Hennessy O, Connell W, Desmond P. Capsule endoscopy vs. push enteroscopy and enteroclysis in suspected small-bowel Crohn's disease. *Gastrointest Endosc* 2005; **61**: 255-261

S- Editor Sun H L- Editor O'Neill M E- Editor Ma WH

S100A4 over-expression underlies lymph node metastasis and poor prognosis in colorectal cancer

Li-Yong Huang, Ye Xu, Guo-Xiang Cai, Zu-Qing Guan, Wei-Qi Sheng, Hong-Fen Lu, Li-Qi Xie, Hao-Jie Lu, San-Jun Cai

Li-Yong Huang, Ye Xu, Guo-Xiang Cai, Zu-Qing Guan, San-Jun Cai, Department of Colorectal Surgery, Fudan University Shanghai Cancer Center, Shanghai 200032, China

Li-Yong Huang, Ye Xu, Guo-Xiang Cai, Zu-Qing Guan, Wei-Qi Sheng, Hong-Fen Lu, San-Jun Cai, Department of Oncology, Shanghai Medical College, Fudan University, Shanghai 200032, China

Wei-Qi Sheng, Hong-Fen Lu, Department of Pathology, Fudan University Shanghai Cancer Center, Shanghai 200032, China

Li-Qi Xie, Hao-Jie Lu, Department of Chemistry, Fudan University, Shanghai 200032, China

Li-Qi Xie, Hao-Jie Lu, Institute of Biomedical Sciences, Fudan University, Shanghai 200032, China

Author contributions: Huang LY, Xu Y, Cai GX, Guan ZQ, Lu HJ and Cai SJ designed the research; Huang LY and Xie LQ performed the research; Huang LY, Cai GX, Sheng WQ and Lu HF analyzed the data; Huang LY and Cai SJ wrote the paper.

Supported by Shanghai Momentous Program, Grant No. 07dz19505; and Shanghai Rising-star Program from the Science and Technology Commission of Shanghai Municipality, No. 10QA1401400, China

Correspondence to: San-Jun Cai, MD, Professor of Medicine, Chief, Department of Colorectal Surgery, Fudan University Shanghai Cancer Center, 270 Dong'an Road, Shanghai 200032, China. caisanjun@csco.org.cn

Telephone: +86-21-64175590 Fax: +86-21-64035387

Received: April 20, 2010 Revised: August 10, 2010

Accepted: August 17, 2010

Published online: January 7, 2011

Abstract

AIM: To develop lymph node metastasis (LNM)-associated biomarkers for colorectal cancer (CRC) using quantitative proteome analysis.

METHODS: Differences in protein expression between primary CRC with LNM (LNM CRC) and without LNM (non-LNM CRC) were assessed using methyl esterification stable isotope labeling coupled with 2D liquid chromatography followed by tandem mass spectrometry (2D-LC-MS/MS). The relationship to clinicopatholog-

ical parameters and prognosis of candidate biomarkers was examined using an independent sample set.

RESULTS: Forty-three proteins were found to be differentially expressed by at least 2.5-fold in two types of CRC. S100A4 was significantly upregulated in LNM CRC compared with non-LNM CRC, which was confirmed by Western blotting, immunohistochemistry and real-time quantitative polymerase chain reaction. Further immunohistochemistry on another 112 CRC cases showed that overexpression of S100A4 frequently existed in LNM CRC compared with non-LNM CRC ($P < 0.001$). Overexpression of S100A4 was significantly associated with LNM ($P < 0.001$), advanced TNM stage ($P < 0.001$), increased 5-year recurrence rate ($P < 0.001$) and decreased 5-year overall survival rate ($P < 0.001$). Univariate and multivariate analyses indicated that S100A4 expression was an independent prognostic factor for recurrence and survival of CRC patients ($P < 0.05$).

CONCLUSION: S100A4 might serve as a powerful biomarker for LNM and a prognostic factor in CRC.

© 2011 Baishideng. All rights reserved.

Key words: Colorectal cancer; Lymph node metastasis; Prognosis; Proteome analysis; S100A4

Peer reviewers: Mark De Ridder, MD, PhD, Professor, Dienst Radiotherapie, UZ Brussel, Vrije Universiteit Brussel, Laarbeeklaan 101, B-1090 Brussel, Belgium; Shashi Bala, PhD, Post Doctoral Associate, Department of Medicine, LRB 270L, 364 Plantation street, UMass Medical School, Worcester, MA 01605, United States

Huang LY, Xu Y, Cai GX, Guan ZQ, Sheng WQ, Lu HF, Xie LQ, Lu HJ, Cai SJ. S100A4 over-expression underlies lymph node metastasis and poor prognosis in colorectal cancer. *World J Gastroenterol* 2011; 17(1): 69-78 Available from: URL: <http://www.wjgnet.com/1007-9327/full/v17/i1/69.htm> DOI: <http://dx.doi.org/10.3748/wjg.v17.i1.69>

INTRODUCTION

Colorectal cancer (CRC) is the third most prevalent human cancer worldwide, with 1 million estimated new cases annually, of which, about 50% die^[1]. CRC frequently migrates through the lymphatic route, depositing tumor cells into local lymph nodes, namely lymph node metastasis (LNM). The status of the local lymph nodes delivers crucial information concerning cancer staging, prognosis, and clinical decision making, on the understanding that the existence of LNM notably reduces the chance of CRC survival^[2]. Unfortunately, the mechanisms related to LNM remain poorly understood at present because LNM is a complicated process that involves cancer cell detachment from the primary tumor, migration, invasion, adhesion and implantation in the new environment. A variety of dysregulated molecules play a significant role in this highly sophisticated process^[3,4]. Therefore, LNM-related investigations have attracted much attention.

Clinicopathological features such as poorly differentiated cancer, depth of wall penetration, lymphovascular invasion, and tumor size are considered to be associated with CRC with LNM (LNM CRC)^[5,6]; however, these characteristics are still insufficient to predict the existence of LNM. In order to improve the diagnosis and prognosis of CRC, there is an urgent need to identify specific tumor molecular markers to recognize patients with LNM, which can define a subset of CRC patients who could benefit from rational management.

It is presently in progress to develop new strategies for the identification of cancer-related molecular markers. Proteomics, the emerging technology that examines the overall characteristics of the expressed proteins, has identified many differential proteins associated with tumor development and progression in various diseases^[7-10]. The recent development of proteomic technology, which presents better sensitivity than conventional gel-based strategies - coupling stable isotope labeling with liquid chromatography followed by tandem mass spectrometry (LC-MS/MS) - introduces a powerful approach to accurate qualitative and quantitative proteomic analysis of clinical samples, as successfully applied to research on difference cancers^[11-14]. This procedure can provide new opportunities to develop biomarkers associated with LNM for CRC.

In the present study, we employed the combination of methyl esterification stable isotope labeling and 2D-LC-MS/MS to perform an accurate quantitative analysis. A total of 43 proteins were identified that were differently expressed by at least 2.5-fold, including S100A4, which was significantly upregulated in LNM CRC compared with non-LNM CRC. S100A4 was recently reported in association with LNM in several studies that attracted our interest^[15-17]. Meanwhile, there have been a limited number of similar studies on the association of S100A4 with CRC. As a result, we focused our attention on S100A4. After confirmation by Western blotting, immunohistochemistry and real-time quantitative polymerase chain reaction (PCR), we further investigated the relationship between S100A4 expression and the lymph node metastatic phe-

notype of CRC, and determined its prognostic value on another independent set of 112 CRC cases.

MATERIALS AND METHODS

Patients and samples

A total of 144 colorectal carcinoma samples were collected after obtaining informed consent in our hospital (Fudan University Shanghai Cancer Center, Shanghai, China). None of the patients received chemotherapy or radiotherapy before surgery. Resected specimens were reviewed by two senior pathologists according to the criteria described in the American Joint Committee on Cancer Cancer Staging Manual (6th edition, 2002)^[18]. For the screening and confirmation study, 32 primary CRC tissue samples that were obtained from patients who underwent curative resection in 2009 were collected and divided into two groups of LNM CRC and non-LNM CRC, with 16 cases in each group. The number of lymph nodes retrieved was not less than 12 in the non-LNM CRC. None of them had distant metastasis. The fresh colorectal tumor tissues were obtained immediately after surgery, washed twice with chilled phosphate buffered saline (PBS), immediately stored in liquid nitrogen and at -80°C in our tissue bank until further use. The detailed clinical data of these patients is provided in Table 1. For the S100A4 expression study, paraffin-embedded tissues in another independent set of 112 primary CRC samples between January and August 2004 were used for immunohistochemistry assessment. Ethical approval was obtained from the Cancer Center Research Ethics Committee.

Sample preparation, methyl esterification stable isotope labeling and 2D-LC-MS/MS

Frozen samples were crushed to powder in liquid nitrogen, and dissolved in lysis buffer [7 mol/L urea, 2 mol/L thiourea, 100 mmol/L DTT and 1 × protease inhibitor cocktail (Roche, Penzberg, Germany)] by continuous vortex at 4°C for 1 h. After centrifugation at 15000 r/min for 45 min at 4°C, equal amounts of each sample from LNM CRC and non-LNM CRC groups were pooled together. One hundred micrograms of proteins from each sample pool were reduced with 10 mmol/L dithiothreitol (60 min, 56°C) and alkylated with 12 mmol/L iodoacetamide in darkness (45 min, 37°C), followed by digestion with 1:20 (w/w) ratio of trypsin (Promega, Madison, WI, USA) overnight at 37°C. The lyophilized peptides from LNM CRC sample were tagged with d0-methanolic HCl, whereas those from non-LNM CRC samples were labeled with d3-methanolic HCl (Sigma-Aldrich, St. Louis, MO, USA) as previously described^[13,19]. Briefly, 100 µL of d0-methanolic HCl or d3-methanolic HCl (created by dropwise addition of 160 µL acetyl chloride with stirring to 1 mL d0-methanol or d3-methanol) was added to the corresponding sample. The reaction was allowed to proceed for 2 h at room temperature. After lyophilization and re-dissolving in 100 µL 5% acetonitrile in 0.1% formic acid, the two peptides were mixed, followed by desalination using Sep-Pak Vac C18 (Waters, Milford, MA, USA).

Table 1 Clinicopathological characteristics of colorectal cancer patients included in screening and confirmation study

Patient No.	TNM	Sex	Age (yr)	Location
Non-LNM CRC				
1	T2N0M0	Male	73	Colon
2	T4N0M0	Male	44	Rectum
3	T2N0M0	Male	49	Colon
4	T3N0M0	Female	53	Colon
5	T3N0M0	Male	54	Colon
6	T4N0M0	Female	52	Colon
7	T3N0M0	Male	69	Rectum
8	T3N0M0	Female	59	Colon
9	T4N0M0	Male	66	Colon
10	T2N0M0	Male	73	Colon
11	T2N0M0	Female	72	Rectum
12	T3N0M0	Male	68	Rectum
13	T2N0M0	Male	71	Colon
14	T4N0M0	Male	68	Colon
15	T3N0M0	Male	59	Rectum
16	T2N0M0	Female	43	Rectum
LNM CRC				
1	T4N2M0	Male	41	Colon
2	T3N1M0	Male	60	Rectum
3	T2N1M0	Male	63	Rectum
4	T2N2M0	Female	37	Rectum
5	T4N1M0	Female	40	Colon
6	T4N2M0	Male	80	Colon
7	T4N1M0	Male	32	Colon
8	T4N2M0	Female	65	Colon
9	T3N1M0	Female	49	Colon
10	T2N1M0	Female	47	Rectum
11	T2N2M0	Female	55	Rectum
12	T4N1M0	Male	86	Colon
13	T3N1M0	Female	71	Colon
14	T3N2M0	Male	79	Colon
15	T3N1M0	Male	70	Colon
16	T4N1M0	Male	56	Colon

LNM: Lymph node metastasis; CRC: Colorectal cancer.

They were lyophilized again and re-dissolved in 40 μ L of the above-mentioned solution. Subsequently, the resultant sample was separated by a 2D microcapillary HPLC system, followed by MS/MS analysis using an LTQ Orbitrap (Thermo Fisher, San Jose, CA, USA). LC solvent gradients were controlled by the chameleon 6.5 (Dionex, Amsterdam, The Netherlands). The MS scan was operated in the data-dependent mode to switch automatically between MS and MS/MS acquisition. Fragment ion selection was based on ion intensity (above 10 counts) and charge state (+2, +3).

Data analysis

Bioworks 3.3.1 was used to generate the peaklists of all acquired MS/MS spectra, which were then automatically searched against the International Protein Index human protein sequence database, version 3.43 using SEQUEST (University of Washington, licensed to Thermo Fisher), with a 95% confidence level. Except for 57 Da reductive alkylation modification on Cys, static modifications were set on Asp, Glu, C-terminal (+14 Da and +17 Da for light and heavy isotope labeling, respectively). The mass tolerance of the peptides and fragment ions was 10 ppm and 1.0 Da, respectively. The identified peptides were further ana-

lyzed with two computer software programs, PeptideProphet and ProteinProphet. PeptideProphet with a probability score of 0.9 and ProteinProphet with a probability score of 0.95 were used to ensure an overall false-positive rate below 0.005. Quantification of the ratio of each protein was achieved using the Xpress program. Proteins with expression fold change > 2.5, $P < 0.05$ were defined as differentially expressed proteins.

Western blotting

The same protein samples for screening were used for Western blotting. Briefly, 30- μ g protein samples from each case were separated by 10% SDS-PAGE and subsequently transferred to PVDF membranes. The membranes were incubated with rabbit polyclonal antibody against S100A4 (1:1000 dilution; Abcam, Cambridge, UK) and then incubated with a horseradish-peroxidase-conjugated secondary antibody (1:100 dilution; Proteintech, Chicago, IL, USA). β -actin was detected simultaneously as a loading control (anti- β -actin, 1:1000 dilution; Kangchen, Beijing, China). All blots were visualized using an ECL detection system (Amersham, Arlington Heights, IL, USA) and quantitated by densitometry using an LAS-3000 imager.

Immunohistochemistry

S100A4 expression was examined immunohistochemically using paraffin-embedded tissues. In brief, 4- μ m-thick tissue sections were heated in 6.5 mmol/L citrate buffer (pH 6.0) at 100°C for 28 min, and incubated with antibody against S100A4 (1:200 dilution). Immunostaining was performed employing the DAKO En-Vision System (Dako Diagnostics, Zug, Switzerland). In the negative control group, PBS was used instead of primary antibody. S100A4 expression was scored by two independent experienced pathologists. Each sample was graded according to the intensity and extent of staining as described previously^[11]. The intensity of staining was scored as 0 (no staining), 1 (weak staining), and 2 (strong staining). The extent of staining was based on the percentage of positive tumor cells: 0 (no staining), 1 (1%-25%), 2 (26%-50%), 3 (51%-75%), and 4 (76%-100%). The final score was assessed by summarizing the results of intensity and extent of staining. The case was considered negative if the final score was 0 or 1 (-) or 2 or 3 (\pm), and positive if the score was 4 or 5 (+) or 6 or 7 (++). In most cases, the two reviewers provided consistent results. Any inconsistencies were resolved by discussion to achieve a consensus score.

Real-time quantitative PCR

Total tissue RNA was extracted using the Rneasy Mini Kit (Qiagen, Valencia, CA, USA). Real-time quantitative PCR analysis was performed according to the manufacturer's instructions (the Quant SYBR Green PCR Kit, TIAN-GEN BIOTECH, Beijing, China). β -actin was applied as an internal control. The primers for β -actin (205 bp) were 5'-TGACGTGGACATCCGCAAAG-3' (sense) and 5'-CTGGAAGGTGGACAGCGAGG-3' (antisense). The primers for S100A4 (185 bp) were 5'-GCCCTGGATGT-

Table 2 Protein expression upregulated and downregulated at least 2.5-fold in lymph node metastasis colorectal cancer compared with non-lymph node metastasis colorectal cancer

Accession No.	Protein name	Protein ratio ¹	SD	Peptide	Coverage rate (%)
Upregulated					
IPI00171494	Isoform 2 of cytoplasmic dynein 2 heavy chain 1	21.8	0	1	2.4
IPI00103253	Isoform 5 of pyrin and hin domain-containing protein 1	8.68	2.85	19	4.9
IPI00298520	Putative uncharacterized protein dkfzp686m09245	7.39	0	1	2.5
IPI00027194	Syntaxin-18	6.30	0	1	3.9
IPI00410639	Isoform 2 of fch and double sh3 domains protein 2	5.25	1.03	5	2.1
IPI00300631	Scaffold attachment factor B1	4.69	0	1	1.51
IPI00009236	Isoform α of caveolin-1	4.42	3.75	2	3.0
IPI00216654	Isoform β of nucleolar phosphoprotein P130	4.35	0	1	1.6
IPI00004273	RNA binding motif protein 25	3.87	0	1	1.5
IPI00239077	Histidine triad nucleotide-binding protein 1	3.73	0.38	5	7.91
IPI00010320	Chromobox protein homolog 1	3.56	1.90	4	1.8
IPI00010274	Isoform 1 of tryptase α -1 precursor	3.52	0.09	2	9.0
IPI00010414	Pdz and lim domain protein 1	3.41	0	1	4.0
IPI00014852	Isoform 1 of phosphoglucomutase-like protein 5	3.24	1.07	4	11.1
IPI00000156	Ligase III, DNA, ATP-dependent isoform β precursor	3.10	0.60	2	2.1
IPI00102821	Isoform 1 of proapoptotic caspase adapter protein precursor	3.09	0.40	2	36.1
IPI00032313	Protein S100-A4	3.04	0.69	2	7.9
IPI00008750	Metallothionein-1H	2.95	0.11	2	27.9
IPI00216153	40S Ribosomal protein S15	2.94	0.57	4	9.0
IPI00654777	Eukaryotic translation initiation factor 3 subunit 5	2.90	0.24	2	5.1
IPI00024933	60S Ribosomal protein L12	2.86	1.02	11	14.4
IPI00025366	Citrate synthase, mitochondrial precursor	2.85	0.47	4	5.9
IPI00007928	Pre-mRNA-processing-splicing factor 8	2.81	0	1	1.3
IPI00024976	Mitochondrial import receptor subunit tom22 homolog	2.78	0	1	8.5
IPI00577039	Annexin A2	2.77	0.32	2	3.6
IPI00062151	Similar to 60s ribosomal protein L15	2.70	0.37	6	6.5
IPI00219757	Glutathione S-transferase P1	2.55	0.37	2	9.1
IPI00396437	Isoform 2 of drebrin-like protein	2.51	0.45	5	2.8
Downregulated					
IPI00023673	Galectin-3-binding protein precursor	0.09	0	1	2.2
IPI00011062	Isoform 1 of carbamoyl-phosphatesynthase, mitochondrial precursor	0.10	0	1	1.0
IPI00030279	Isoform 1 of zinc finger ran-binding domain-containing protein 3	0.11	0	1	7.6
IPI00219682	Erythrocyte band 7 integral membrane protein	0.20	0	1	9.8
IPI00433499	Rhomboid, veinlet-like 6 isoform 1	0.20	0	1	2.1
IPI00000230	Tropomyosin 1 α chain isoform 2	0.26	0.06	32	51.8
IPI00029631	Enhancer of rudimentary homolog	0.27	0	1	7.7
IPI00009950	Vesicular integral-membrane protein vip36 precursor	0.30	0	1	3.4
IPI00384603	Isoform 2 of ribonuclease p protein subunit P21	0.30	0.11	13	10.7
IPI00177543	Peptidylglycine α -amidating monooxygenase isoform A	0.31	0.08	2	8.1
IPI00000330	Isoform 1 of uncharacterized protein c9orf80	0.35	0	1	17.6
IPI00298949	Cyclin G-associated kinase	0.35	0	1	1.3
IPI00008964	RAS-related protein rab-1B	0.37	0	1	7.5
IPI00013860	3-Hydroxyisobutyrate dehydrogenase, mitochondrial precursor	0.37	0	1	5.4
IPI00296053	Isoform mitochondrial of fumarate hydratase, mitochondrial precursor	0.39	0.18	1	2.4

¹Protein ratio represents the abundance ratio between lymph node metastasis group and non-lymph node metastasis group. LNM: Lymph node metastasis; CRC: Colorectal cancer.

GATGGTGT-3' (sense) and 5'-TCGTTGTCCCTGTT-GCTGTC-3' (antisense). Each assay was done in triplicate, and the average was calculated. For relative quantification, $2^{-\Delta\Delta C_t}$ was calculated and used as an indication of the relative expression levels.

Statistical analysis

The Student *t* test was used to evaluate the differences in S100A4 expression between LNM CRC and non-LNM CRC. The χ^2 test was used to assess the relationships between S100A4 expression and clinicopathological factors. The cumulative recurrence and survival probability were

estimated using the Kaplan-Meier method, and differences were calculated by log-rank test. Prognostic factors were determined using Cox regression analysis. The recurrence-free and overall survival times were calculated from the first resection of the primary tumor to first evidence of recurrence or to death from any cause, respectively. The diagnosis of recurrence was based on the typical features presented on computed tomography/magnetic resonance imaging and elevated serum carcinoembryonic antigen. All *P* values were two-sided, and *P* < 0.05 was considered to be significant. Statistical analyses were performed using SPSS 13.0 software.

RESULTS

Quantitative proteome analysis with methyl esterification stable isotope labeling combined with 2D-LC-MS/MS

To perform accurate quantitative analysis, we compared the protein expression profiles between LNM CRC and non-LNM CRC using methyl esterification stable isotope labeling combined with 2D-LC-MS/MS. The quantitative differential expression of 644 proteins was identified, after calibration with β -casein. Significantly, 43 of these (6.7%) proteins were displayed differentially (at least 2.5-fold) in LNM CRC compared with non-LNM CRC. Among these 43 proteins, 28 were found to be upregulated in LNM CRC (Table 2), and 15 were downregulated (Table 2). The identification of S100A4 significantly upregulated in LNM CRC is shown in Figure 1 as an example. These differentially expressed proteins formed the possible protein profiles associated with LNM in CRC.

Confirmation of S100A4 expression by Western blotting, immunohistochemistry and real-time quantitative PCR

We extended the experiments to confirm the differential expression of S100A4 in the same samples described above.

Thirty micrograms of total proteins from LNM CRC and non-LNM CRC were analyzed *via* Western blotting. The expression of S100A4 was dramatically higher in LNM CRC compared with non-LNM CRC ($P < 0.001$). A representative Western blotting result is presented in Figure 2A.

To confirm upregulation of S100A4 at the protein level, we used immunohistochemistry to evaluate S100A4 expression *in situ*. In normal mucosa, there was no immunoreactivity in cells. In non-LNM CRC, there was weak staining in cancer cells. In LNM CRC, there was notable brown staining in both primary and matched metastatic lymph node cancer cells. Positive staining was present mainly in the cytoplasm and/or nucleus of cancer cells (Figure 2B).

Real-time quantitative PCR revealed that S100A4 mRNA level was higher in LNM CRC than in non-LNM CRC ($P < 0.001$, Figure 2C), which is consistent with the trend at the protein level.

Association of S100A4 expression with clinicopathological features and postoperative prognosis of CRC patients

To detect the relationship between S100A4 expression and clinicopathological features and whether S100A4 could be a prognostic factor in predicting clinical outcomes of CRC patients, we evaluated S100A4 expression in an additional archived 112 CRC samples. In the group of 53 LNM CRC samples, 83% were positive for S100A4 expression, whereas 16.9% of the 59 non-LNM CRC samples had positive expression.

After division of these patients into S100A4-positive and S100A4-negative groups, statistical analysis revealed that positive expression of S100A4 was significantly associated with LNM, and advanced TNM stage ($P < 0.001$).

Table 3 Relationships of S100A4 expression with clinicopathological factors in colorectal cancer

Clinicopathological factors	n	S100A4 expression		P value ¹
		Negative	Positive	
Sex				
Male	59	32	27	0.252
Female	53	23	30	
Age (yr)				
≤ 60	76	39	37	0.497
> 60	36	16	20	
Tumor size (cm)				
≤ 5	74	32	42	0.083
> 5	38	23	15	
Tumor location				
Colon	47	23	24	0.975
Rectum	65	32	33	
Tumor differentiation ²				
I - II	82	43	39	0.244
III-IV	30	12	18	
Tumor status ²				
T1-2	34	18	16	0.592
T3-4	78	37	41	
Lymph node metastasis ²				
N0	59	49	10	< 0.001
N1-2	53	9	44	
TNM stage ²				
I - II	57	46	11	< 0.001
III-IV	55	9	46	

¹Statistical analysis was estimated with χ^2 test, and $P < 0.05$ was considered statistically significant; ²Grading of differentiation status and TNM classification for colorectal cancer were based on the American Joint Committee on Cancer Cancer Staging Manual (6th edition, 2002). The tumors were classified into two groups: well differentiated (grades I and II) and poorly differentiated (grades III and IV).

However, no significant correlations were observed between S100A4 expression and other clinicopathological parameters of sex, age, tumor size, tumor differentiation and tumor location (Table 3).

Furthermore, we found that patients with S100A4-positive CRC had significantly poorer prognosis than those with S100A4-negative CRC. The 5-year cumulative recurrence rate was significantly higher in patients with S100A4-positive CRC than in the S100A4-negative group ($P < 0.001$, Figure 3A). The 5-year cumulative survival rate in patients with S100A4-positive CRC was much lower than in those with S100A4-negative CRC ($P < 0.001$, Figure 3B). Univariate analyses revealed that LNM, TNM stage and S100A4 expression were associated with recurrence and overall survival. In multivariate analysis, LNM, TNM stage and S100A4 expression were also independent prognostic factors of recurrence and overall survival ($P < 0.05$, Table 4).

DISCUSSION

Metastasis remains one of the major challenges in management of CRC patients. LNM is the most common form of metastasis in CRC. To develop LNM-associated biomarkers for CRC, we employed the quantitative proteomic strategy of methyl esterification stable isotope

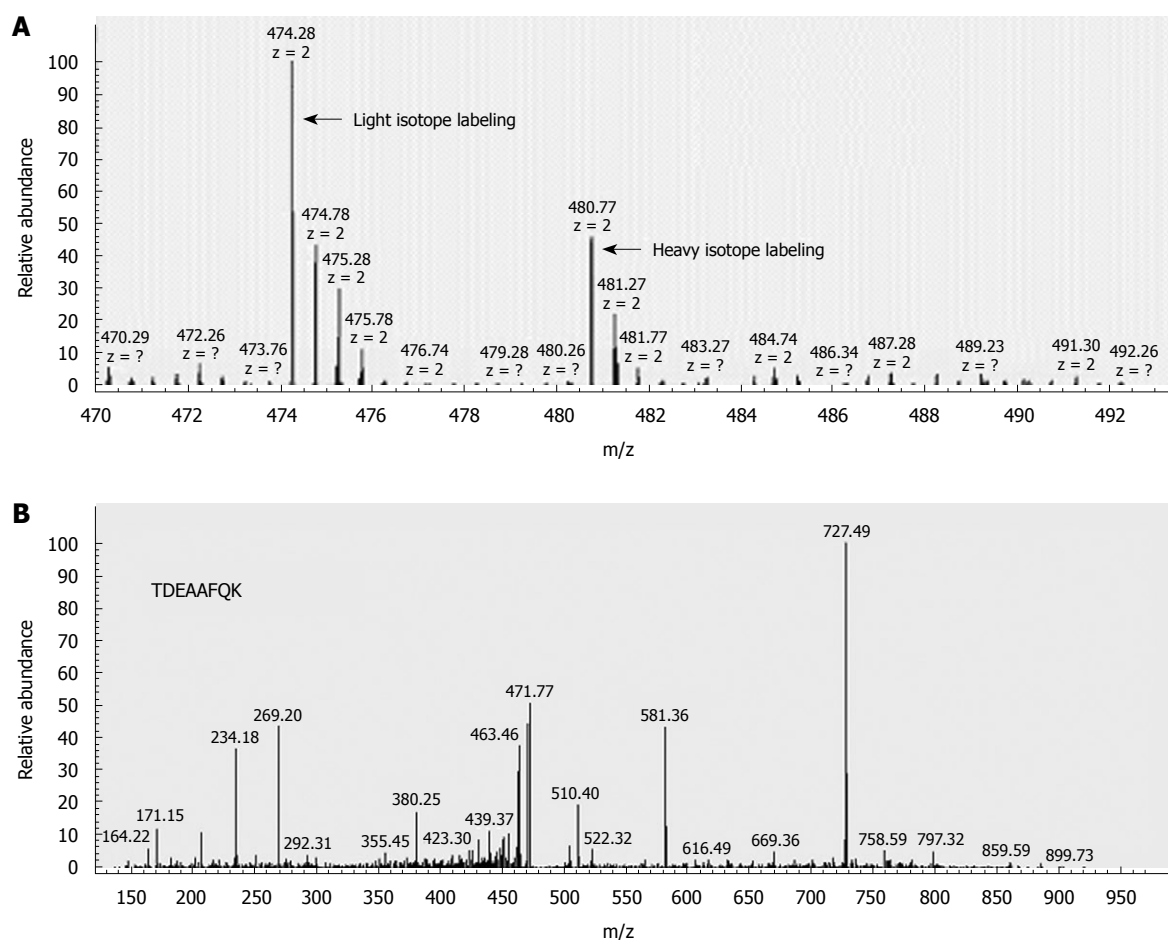


Figure 1 Identification of quantitatively dysregulated expression of S100A4. A: Quantification of S100A4 through the isotopically labeled fragment ion signals of the peptide "TDEAAFQK". The areas under the monoisotopic peaks represent the relative abundance of peptides, light [lymph node metastasis (LNM)]/heavy (non-LNM) = 3.04:1; B: Identification of the peptide "TDEAAFQK" from S100A4 by MS/MS.

labeling coupled with 2D-LC-MS/MS. A total of 644 proteins were identified, including 43 that were differentially expressed by at least 2.5-fold between LNM CRC and non-LNM CRC. We found many of the 43 proteins that possibly participate in the biological processes associated with tumor metastasis, such as cell motility and adhesion, migration, and signal transduction.

Among the upregulated proteins, annexin A2, one of the calcium- and phospholipid-binding proteins, has been widely reported in various cancers with the regulation of cell growth, motility, invasion and signaling pathways^[20]. The increase in caveolin-1 performs the functions of signal transduction, cell transformation and anti-apoptotic activity^[21]. Moreover, caveolin-1 has been found to be overexpressed in several multidrug-resistant cancer cell lines^[22,23]. In addition, some downregulated proteins identified in our study have also been observed to possess similar biological effects, including galectin-3-binding protein^[24] and cyclin-G-associated kinase^[25].

Previously, Pei *et al.*^[26] have carried out a proteomic study on 10 CRC samples using conventional 2D electrophoresis coupled with MALDI-TOF-MS, and have reported a pattern of four differentially expressed proteins potentially associated with LNM. In contrast, our results revealed up to 43 proteins that were differentially

expressed by at least 2.5-fold. Annexin A2 and glutathione S-transferase P1 both correlated with LNM in our study and that of Pei *et al.* Heat shock protein-27 and liver fatty acid binding protein (L-FABP) were found to correlate with LNM by Pei *et al.*, but not in our study, whereas 41 proteins identified in our study were not listed by Pei *et al.* This discordance is probably due to the different clinical background of the samples included in the studies, and the different proteomic strategies used. It is required to analyze systemically and integrate all the complementary data from various institutions into a common databank to elucidate exactly the molecular background of CRC. In addition, Pang *et al.*^[27] have identified and confirmed six differentially expressed proteins (e- fatty acid binding protein 5, methylcrotonoyl Coenzyme A carboxylase 2, pyrophosphatase 2, synaptotagmin-like protein 2, Ezrin, and smooth muscle protein) that are associated with LNM in prostate cancer by DIGE-based proteome analysis. However, there was no concordance between the results in that study and our study, which is probably mainly due to the different cancers and proteomic approaches included.

Recently, several studies have shown that S100A4 is an important factor relevant to progression and prognosis in various human cancers, such as thyroid^[28], breast^[29], pancreatic^[30], bladder^[31], gastric^[17] and colorectal^[32] cancer.

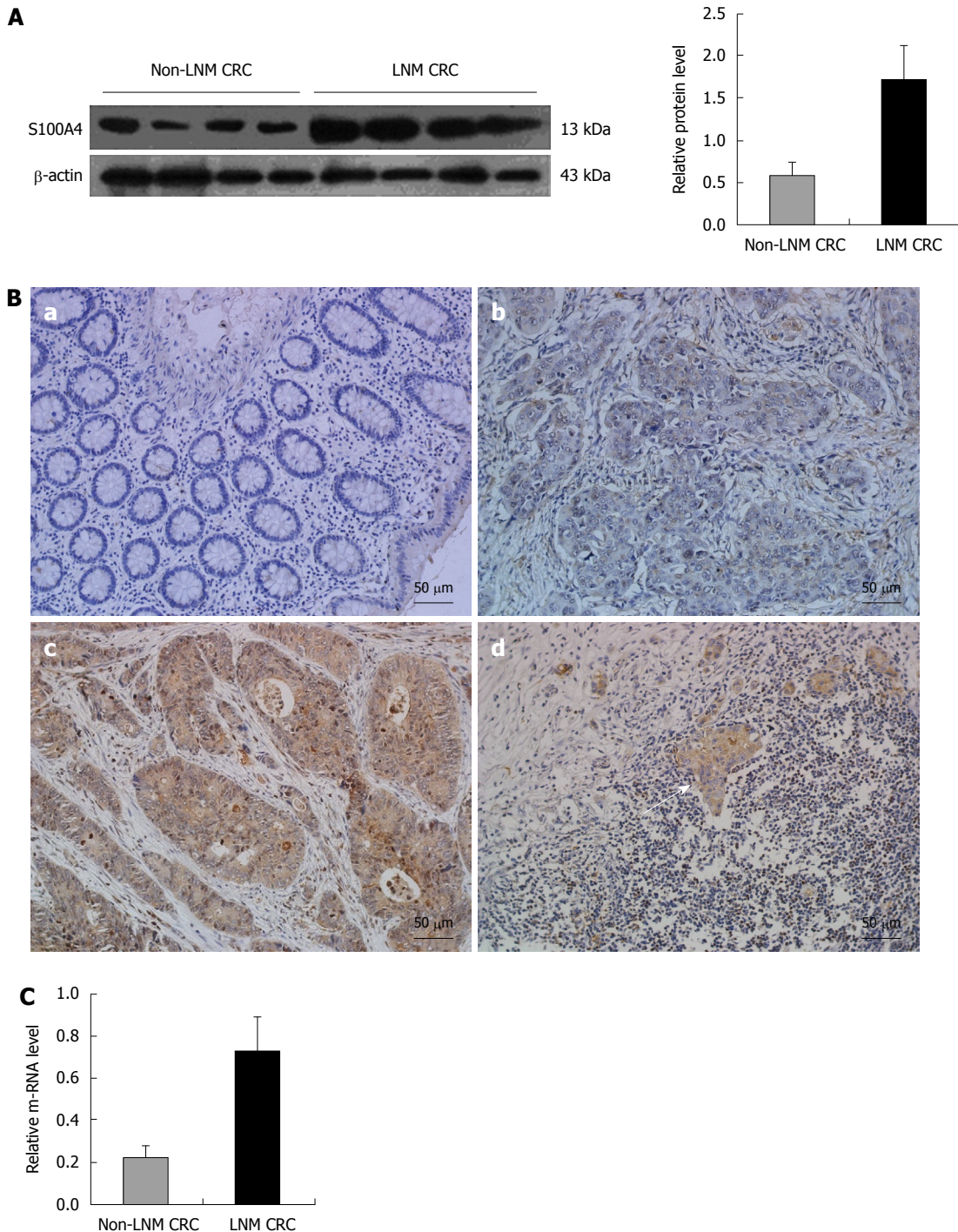


Figure 2 Confirmation of the overexpression of S100A4 in colorectal cancer. A: Western blotting analysis for S100A4 expression in colorectal cancer (CRC) specimens. β -actin was used as the internal loading control. The histogram shows the relative expression levels of S100A4 in non-LNM (16 cases) and lymph node metastasis (LNM) (16 cases) groups. Data represent the mean \pm SE ($P < 0.001$, Student *t* test); B: Immunohistochemical study of S100A4 distribution and expression in CRC specimens at 20×10 magnification. a: There was no immunoreactivity in the normal mucosa; b: Weak staining in cancer cells in the non-LNM group; c: Strong staining in cancer cells in the LNM group; d: Marked metastatic lymph nodes (arrow); C: mRNA level of S100A4 via real-time quantitative polymerase chain reaction. S100A4 was consistently increased in the LNM group (16 cases) compared with non-LNM group (16 cases). The mRNA level was normalized to that of β -actin. Data represent the mean \pm SE ($P < 0.001$, Student *t* test).

In particular, several studies have revealed that overexpression of S100A4 strongly indicates the presence of LNM^[15-17], which agrees with our original study aim. However, similar investigations have been limited between S100A4 expression and LNM in CRC. In view of the above reasons, S100A4, one of the significantly upregulated proteins identified in LNM CRC compared with non-

LNM CRC, which has been confirmed at the protein and mRNA levels, attracted our attention and interest.

S100A4, also known as 18A2/mts1, CAPL, PEL-98, 42A, p9Ka, and metastasin, belongs to the S100 superfamily of calcium-binding proteins^[33]. S100A4-mediated calcium signaling plays a major role in crucial biological functions that influence various aspects of cell physiology,

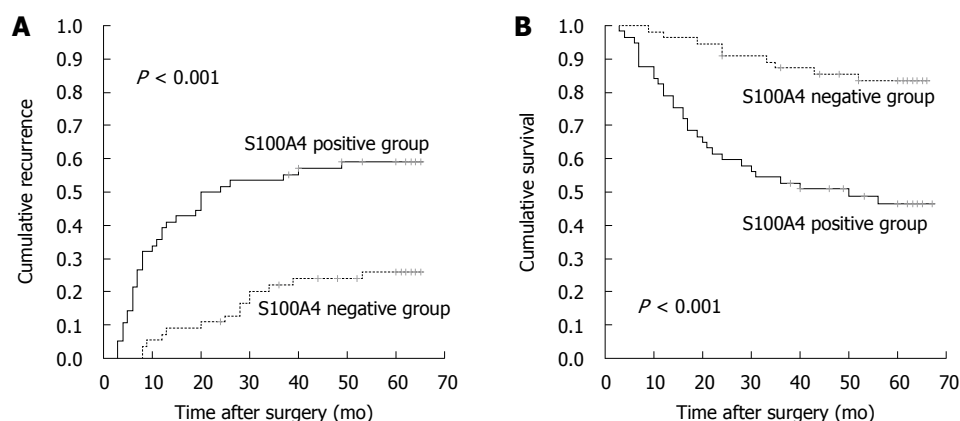


Figure 3 Overexpression of S100A4 correlated with poor prognosis in 112 colorectal cancer patients. A: Cumulative recurrence between the S100A4-positive and S100A4-negative groups ($P < 0.001$, log-rank test); B: Cumulative survival between the S100A4-positive and S100A4-negative groups ($P < 0.001$, log-rank test).

Table 4 Univariate and multivariate analyses of recurrence and survival (Cox regression)

Variables	Recurrence		Survival	
	HR (95% CI)	P value	HR (95% CI)	P value
Univariate analysis				
Sex				
Male/female	0.872 (0.490-1.549)	0.640	0.857 (0.452-1.624)	0.636
Age (yr)				
≤ 60/> 60	1.517 (0.842-2.732)	0.165	1.842 (0.967-3.508)	0.063
Tumor size (cm)				
≤ 5/> 5	0.881 (0.165-0.685)	0.687	0.880 (0.444-1.745)	0.715
Tumor location				
Colon/rectum	0.823 (0.463-1.464)	0.508	0.920 (0.483-1.752)	0.799
Tumor differentiation				
I - II / III-IV	1.234 (0.660-2.305)	0.511	1.171 (0.581-2.361)	0.659
Tumor status				
T1-2/T3-4	0.886 (0.484-1.620)	0.693	1.026 (0.517-2.033)	0.942
Lymph node metastasis				
N0/N1-2	2.727 (1.510-4.923)	0.001	2.852 (1.463-5.559)	0.002
TNM stage				
I - II / III-IV	3.560 (1.940-6.534)	< 0.001	3.393 (1.680-6.850)	< 0.001
S100A4 expression				
Negative/positive	3.666 (1.929-6.964)	< 0.001	4.154 (1.963-8.792)	< 0.001
Multivariate analysis				
LNM				
N0/N1-2	0.205 (0.055-0.769)	0.019	0.193 (0.044-0.857)	0.031
TNM stage				
I - II / III-IV	8.915 (2.081-38.189)	0.003	9.057 (1.705-48.108)	0.010
S100A4 expression				
Negative/positive	2.454 (1.056-5.705)	0.037	2.888 (1.131-7.379)	0.027

HR: Hazard ratio; CI: Confidence interval.

including proliferation and apoptosis, and differentiation and morphogenesis. It is also significantly involved in cell adhesion and motility, and cancer invasion and metastasis^[34,35]. A large body of evidence suggests that S100A4 is involved in cell metastatic phenotype by modulating the cytoskeletal dynamics, cadherin/catenin complex cytoskeletal linkage, CD44/cytoskeletal linkage, and extracellular-matrix-associated proteolytic enzyme. Furthermore, S100A4 can participate in the activation of the matrix metalloproteinase/tissue inhibitor of metalloproteinase system and angiogenic factor vascular endothelial growth factor, which in turn can lead to tumor neovascularization^[36,37].

To study further the relationship between S100A4 expression and the LNM phenotype of CRC, and determine whether S100A4 could be a prognostic factor in predicting clinical outcomes of CRC patients, we examined an additional 112 archived CRC samples for S100A4 expression. We found that the elevation in S100A4 expression level was significantly correlated with LNM and advanced TNM stage, which suggests that S100A4 plays an important part in the progression of CRC from a localized to lymph node metastatic disease. In addition, patients with S100A4-positive CRC had an increasing risk of recurrence and significantly reduced overall survival. Univariate and

multivariate analyses indicated that S100A4 expression is a powerful independent prognostic factor for recurrence and overall survival in CRC, which indicates the considerable prognostic value of S100A4 expression.

In conclusion, our current study employed a quantitative proteome analysis to profile the differently expressed proteins associated with LNM in CRC. S100A4 was identified and confirmed to be significantly overexpressed in LNM CRC. Further evaluation in an independent sample set has suggested that S100A4 acts as a powerful biomarker for LNM and prognosis in CRC. However, many questions remain to be answered with respect to the cellular function of S100A4 and how it exerts its influence on metastatic progression, with further investigations on our part in progress. We also identified a number of proteins besides S100A4 that might provide a more profound insight into the mechanism of LNM in CRC and merit further research.

COMMENTS

Background

Colorectal cancer (CRC) is one of the most prevalent cancers worldwide, and it is estimated that half of the patients die from cancer annually. Lymph node metastasis (LNM) is the most common form of metastasis although the mechanism is largely unknown. Studies on metastasis of CRC were performed in order to improve the diagnosis and prognosis.

Research frontiers

LNM is a complicated process that involves a variety of dysregulated molecules playing a significant role. Increasingly, it has become a hot research topic to employ proteome analysis to identify proteins associated with tumor development and progression in various diseases.

Innovations and breakthroughs

To date, there has been a limited number of studies regarding specific tumor molecular markers associated with LNM in CRC. In this study, the authors employed more sensitive proteome analysis than conventional strategies to identify a set of differently expressed proteins associated with LNM. Furthermore, the authors confirmed the significant correlation between overexpression of S100A4 and LNM, advanced TNM stage, increased recurrence rate and decreased overall survival rate.

Applications

By identifying the protein S100A4 as being associated with LNM, the authors evaluated the biological features and prognosis in CRC, which could improve our understanding of CRC, and provide a scientific basis for the application of S100A4 inhibitors in the treatment of CRC.

Terminology

Proteome: all proteins that derive from the genome of cells, a tissue or an organism. It is a dynamic collection that reflects both the intrinsic genetic information of the cell and the impact of its immediate environment. Compared with gene analysis, proteome analysis can provide a more accurate view of the biological status and be expected to be more useful for evaluating, for example, disease development, progression and response to treatment.

Peer review

The authors performed also an extensive proteomics analysis, and identified 43 proteins that were differentially regulated in metastatic cancer, including 16 proteins that were upregulated even more than S100A4. The results indicate that overexpression of S100A4 could be used as biomarker for LNM in CRC. However, none of the latter candidate biomarkers were further examined in terms of prognostic value.

REFERENCES

- 1 Parkin DM, Bray F, Ferlay J, Pisani P. Global cancer statistics, 2002. *CA Cancer J Clin* 2005; **55**: 74-108
- 2 O'Connell JB, Maggard MA, Ko CY. Colon cancer survival

- rates with the new American Joint Committee on Cancer sixth edition staging. *J Natl Cancer Inst* 2004; **96**: 1420-1425
- 3 Royston D, Jackson DG. Mechanisms of lymphatic metastasis in human colorectal adenocarcinoma. *J Pathol* 2009; **217**: 608-619
- 4 Sundar SS, Ganesan TS. Role of lymphangiogenesis in cancer. *J Clin Oncol* 2007; **25**: 4298-4307
- 5 Ricciardi R, Madoff RD, Rothenberger DA, Baxter NN. Population-based analyses of lymph node metastases in colorectal cancer. *Clin Gastroenterol Hepatol* 2006; **4**: 1522-1527
- 6 Fang W, Fan B, Xiong B. Analysis of pathological risk factors for lymph node metastasis in colorectal cancer. *Hepatogastroenterology* 2009; **56**: 663-666
- 7 Alfonso P, Núñez A, Madoz-Gurpide J, Lombardia L, Sánchez L, Casal JI. Proteomic expression analysis of colorectal cancer by two-dimensional differential gel electrophoresis. *Proteomics* 2005; **5**: 2602-2611
- 8 Suehara Y, Kondo T, Seki K, Shibata T, Fujii K, Gotoh M, Hasegawa T, Shimada Y, Sasako M, Shimoda T, Kurosawa H, Beppu Y, Kawai A, Hirohashi S. Pftin as a prognostic biomarker of gastrointestinal stromal tumors revealed by proteomics. *Clin Cancer Res* 2008; **14**: 1707-1717
- 9 Farina A, Dumonceau JM, Frossard JL, Hadengue A, Hochstrasser DF, Lescuyer P. Proteomic analysis of human bile from malignant biliary stenosis induced by pancreatic cancer. *J Proteome Res* 2009; **8**: 159-169
- 10 Liu YF, Xiao ZQ, Li MX, Li MY, Zhang PF, Li C, Li F, Chen YH, Yi H, Yao HX, Chen ZC. Quantitative proteome analysis reveals annexin A3 as a novel biomarker in lung adenocarcinoma. *J Pathol* 2009; **217**: 54-64
- 11 Bai DS, Dai Z, Zhou J, Liu YK, Qiu SJ, Tan CJ, Shi YH, Huang C, Wang Z, He YF, Fan J. Capn4 overexpression underlies tumor invasion and metastasis after liver transplantation for hepatocellular carcinoma. *Hepatology* 2009; **49**: 460-470
- 12 Niu D, Sui J, Zhang J, Feng H, Chen WN. iTRAQ-coupled 2-D LC-MS/MS analysis of protein profile associated with HBV-modulated DNA methylation. *Proteomics* 2009; **9**: 3856-3868
- 13 Ficarro SB, McClelland ML, Stukenberg PT, Burke DJ, Ross MM, Shabanowitz J, Hunt DF, White FM. Phosphoproteome analysis by mass spectrometry and its application to *Saccharomyces cerevisiae*. *Nat Biotechnol* 2002; **20**: 301-305
- 14 Ibarrola N, Kalume DE, Gronborg M, Iwahori A, Pandey A. A proteomic approach for quantitation of phosphorylation using stable isotope labeling in cell culture. *Anal Chem* 2003; **75**: 6043-6049
- 15 Min HS, Choe G, Kim SW, Park YJ, Park do J, Youn YK, Park SH, Cho BY, Park SY. S100A4 expression is associated with lymph node metastasis in papillary microcarcinoma of the thyroid. *Mod Pathol* 2008; **21**: 748-755
- 16 Lee OJ, Hong SM, Razvi MH, Peng D, Powell SM, Smoklin M, Moskaluk CA, El-Rifai W. Expression of calcium-binding proteins S100A2 and S100A4 in Barrett's adenocarcinomas. *Neoplasia* 2006; **8**: 843-850
- 17 Wang YY, Ye ZY, Zhao ZS, Tao HQ, Chu YQ. High-level expression of S100A4 correlates with lymph node metastasis and poor prognosis in patients with gastric cancer. *Ann Surg Oncol* 2010; **17**: 89-97
- 18 Greene FL, Page DL, Fleming ID, Fritz AG, Balch CM, Haller DG, Morrow M. *AJCC Cancer Staging Manual*. 6th ed. New York: Springer-Verlag, 2002: 113-124
- 19 Hunt DF, Yates JR 3rd, Shabanowitz J, Winston S, Hauer CR. Protein sequencing by tandem mass spectrometry. *Proc Natl Acad Sci USA* 1986; **83**: 6233-6237
- 20 Rescher U, Gerke V. Annexins--unique membrane binding proteins with diverse functions. *J Cell Sci* 2004; **117**: 2631-2639
- 21 Williams TM, Lisanti MP. The Caveolin genes: from cell biology to medicine. *Ann Med* 2004; **36**: 584-595
- 22 Lavie Y, Fiucci G, Liscovitch M. Up-regulation of caveolae and caveolar constituents in multidrug-resistant cancer cells. *J Biol Chem* 1998; **273**: 32380-32383
- 23 Yang CP, Galbiati F, Volonte D, Horwitz SB, Lisanti MP.

- Upregulation of caveolin-1 and caveolae organelles in Taxol-resistant A549 cells. *FEBS Lett* 1998; **439**: 368-372
- 24 **Hancq S**, Salmon I, Brotchi J, Gabius HJ, Heizmann CW, Kiss R, Decaestecker C. Detection of S100B, S100A6 and galectin-3 ligands in meningiomas as markers of aggressiveness. *Int J Oncol* 2004; **25**: 1233-1240
 - 25 **Zhang L**, Gjoerup O, Roberts TM. The serine/threonine kinase cyclin G-associated kinase regulates epidermal growth factor receptor signaling. *Proc Natl Acad Sci USA* 2004; **101**: 10296-10301
 - 26 **Pei H**, Zhu H, Zeng S, Li Y, Yang H, Shen L, Chen J, Zeng L, Fan J, Li X, Gong Y, Shen H. Proteome analysis and tissue microarray for profiling protein markers associated with lymph node metastasis in colorectal cancer. *J Proteome Res* 2007; **6**: 2495-2501
 - 27 **Pang J**, Liu WP, Liu XP, Li LY, Fang YQ, Sun QP, Liu SJ, Li MT, Su ZL, Gao X. Profiling protein markers associated with lymph node metastasis in prostate cancer by DIGE-based proteomics analysis. *J Proteome Res* 2010; **9**: 216-226
 - 28 **Zou M**, Al-Baradie RS, Al-Hindi H, Farid NR, Shi Y. S100A4 (Mts1) gene overexpression is associated with invasion and metastasis of papillary thyroid carcinoma. *Br J Cancer* 2005; **93**: 1277-1284
 - 29 **Rudland PS**, Platt-Higgins A, Renshaw C, West CR, Winstanley JH, Robertson L, Barraclough R. Prognostic significance of the metastasis-inducing protein S100A4 (p9Ka) in human breast cancer. *Cancer Res* 2000; **60**: 1595-1603
 - 30 **Ai KX**, Lu LY, Huang XY, Chen W, Zhang HZ. Prognostic significance of S100A4 and vascular endothelial growth factor expression in pancreatic cancer. *World J Gastroenterol* 2008; **14**: 1931-1935
 - 31 **Matsumoto K**, Irie A, Satoh T, Ishii J, Iwabuchi K, Iwamura M, Egawa S, Baba S. Expression of S100A2 and S100A4 predicts for disease progression and patient survival in bladder cancer. *Urology* 2007; **70**: 602-607
 - 32 **Gongoll S**, Peters G, Mengel M, Piso P, Klempnauer J, Kreipe H, von Wasielewski R. Prognostic significance of calcium-binding protein S100A4 in colorectal cancer. *Gastroenterology* 2002; **123**: 1478-1484
 - 33 **Marenholz I**, Volz A, Ziegler A, Davies A, Ragoussis I, Korge BP, Mischke D. Genetic analysis of the epidermal differentiation complex (EDC) on human chromosome 1q21: chromosomal orientation, new markers, and a 6-Mb YAC contig. *Genomics* 1996; **37**: 295-302
 - 34 **Parker C**, Whittaker PA, Usmani BA, Lakshmi MS, Sherbet GV. Induction of 18A2/mts1 gene expression and its effects on metastasis and cell cycle control. *DNA Cell Biol* 1994; **13**: 1021-1028
 - 35 **Garrett SC**, Varney KM, Weber DJ, Bresnick AR. S100A4, a mediator of metastasis. *J Biol Chem* 2006; **281**: 677-680
 - 36 **Sherbet GV**. Metastasis promoter S100A4 is a potentially valuable molecular target for cancer therapy. *Cancer Lett* 2009; **280**: 15-30
 - 37 **Helfman DM**, Kim EJ, Lukanidin E, Grigorian M. The metastasis associated protein S100A4: role in tumour progression and metastasis. *Br J Cancer* 2005; **92**: 1955-1958

S- Editor Shi ZF L- Editor Kerr C E- Editor Lin YP

MiRNA profile in esophageal squamous cell carcinoma: Downregulation of miR-143 and miR-145

Bing-Li Wu, Li-Yan Xu, Ze-Peng Du, Lian-Di Liao, Hai-Feng Zhang, Qiao Huang, Guo-Qiang Fang, En-Min Li

Bing-Li Wu, Hai-Feng Zhang, Qiao Huang, Guo-Qiang Fang, En-Min Li, Department of Biochemistry and Molecular Biology, Medical College of Shantou University, Shantou 515041, Guangdong Province, China

Li-Yan Xu, Ze-Peng Du, Lian-Di Liao, Institute of Oncologic Pathology, Medical College of Shantou University, Shantou 515041, Guangdong Province, China

Author contributions: Li EM and Xu LY designed the research; Wu BL, Du ZP, Liao LD, Zhang HF, Huang Q and Fang GQ performed the research and analyzed the data; Wu BL wrote the paper.

Supported by Grants from the NSFC-Guangdong Joint Fund, No. U0932001 and the National Natural Science Foundation of China, No. 30900560

Correspondence to: En-Min Li, Professor, Department of Biochemistry and Molecular Biology, Medical College of Shantou University, Shantou 515041, Guangdong Province, China. nmli@stu.edu.cn

Telephone: +86-754-88900413 Fax: +86-754-88900847

Received: June 10, 2010 Revised: July 29, 2010

Accepted: August 5, 2010

Published online: January 7, 2011

Abstract

AIM: To investigate the expression profile of miRNA in esophageal squamous cell carcinoma (ESCC).

METHODS: The expression profile of miRNA in ESCC tissues was analyzed by miRNA microarray. The expression levels of miR-143 and miR-145 in 86 ESCC patients were determined by real-time polymerase chain reaction (PCR) using TaqMan assay. The mobility effect was estimated by wound-healing using esophageal carcinoma cells transfected with miRNA expression plasmids.

RESULTS: A set of miRNAs was found to be deregulated in the ESCC tissues, and the expression levels of miR-143 and -145 were significantly decreased in most of the ESCC tissues examined. Both miR-143 and miR-145 expression correlated with tumor inva-

sion depth. The transfection of human esophageal carcinoma cells with miR-143 and miR-145 expression plasmids resulted in a greater inhibition of cell mobility, however, the protein level of the previously reported target of miR-145, *FSCN1*, did not show any significant downregulation.

CONCLUSION: These findings suggest that the deregulation of miRNAs plays an important role in the progression of ESCC. Both miR-143 and miR-145 might act as anti-oncomirs common to ESCC.

© 2011 Baishideng. All rights reserved.

Key words: Esophageal squamous cell carcinoma; MicroRNA; miR-143; miR-145; Tumor invasion depth

Peer reviewer: Leonidas G Koniaris, Professor, Alan Livingstone Chair in Surgical Oncology, 3550 Sylvester Comprehensive Cancer Center (310T), 1475 NW 12th Ave., Miami, FL 33136, United States

Wu BL, Xu LY, Du ZP, Liao LD, Zhang HF, Huang Q, Fang GQ, Li EM. MiRNA profile in esophageal squamous cell carcinoma: Downregulation of miR-143 and miR-145. *World J Gastroenterol* 2011; 17(1): 79-88 Available from: URL: <http://www.wjgnet.com/1007-9327/full/v17/i1/79.htm> DOI: <http://dx.doi.org/10.3748/wjg.v17.i1.79>

INTRODUCTION

MicroRNAs (miRNAs) are an endogenous conserved class of non-coding 20-22 nt small RNAs that regulate gene expression at post-transcriptional level by mainly binding to 3'-UTR of target mRNAs, leading to mRNA degradation or translation inhibition^[1]. Many miRNAs show sequence and function conservation between distantly related organisms, suggesting that this class of small RNAs is an integral part of essential cellular processes^[2]. It was predicted that about 30% of human genes are

regulated by miRNAs^[3]. miRNAs regulate a variety of biological processes, including developmental timing, signal transduction, cell growth, and cell death^[4]. The importance of microRNA in cancer is highlighted by the observation that about 50% of miRNAs are located in cancer-associated genomic regions or fragile sites, which are frequently amplified or deleted in tumorigenesis^[5]. Moreover, accumulated evidence shows that miRNAs are aberrantly expressed in various cancers, suggesting that they play a vital role as a novel class of oncogenes or tumor suppressor genes, depending on the targets they regulate^[6]. Recent reports demonstrate a role for miRNA expression in disease progression and outcome^[7].

Esophageal carcinoma is one of the most lethal malignancies in China and other Asian areas, with a significant low 5-year survival rate after curative surgery^[8,9]. There are two major histologic types of esophageal cancer: esophageal squamous cell carcinoma (ESCC) and esophageal adenocarcinoma. To date, many studies focusing on miRNA expression profiles in Barrett's esophagus and esophageal adenocarcinoma have been reported^[10]. Yang *et al.*^[11] identified 11 miRNAs showing statistically significant differences between the different progression stages of esophageal adenocarcinoma. Nevertheless, there is still little information available on specific miRNA expression patterns and their roles in ESCC. Feber *et al.*^[12] identified a set of differentially expressed miRNAs that could distinguish different esophageal tissue types and also discriminate malignant from normal esophageal tissue, including adenocarcinoma, squamous cell carcinoma, Barrett's esophagus and high-grade dysplasia. These data suggest that miRNA expression profiling is now a promising method to identify key miRNAs which play important roles in esophageal carcinogenesis.

Chaoshan Area in China is the main coastal area and has a high ESCC morbidity rate^[13]. The specific geographical environment and dietary habits of the population may characterize some of the specific features of ESCC in this area, which might also be reflected in the miRNA expression profile in ESCC tissues. To develop novel diagnostic and therapeutic targets for esophageal squamous cell cancer, we first investigated the expression profile of miRNA in three pairs of clinical ESCC samples and confirmed the differences in expression of relevant miRNAs using real-time quantitative reverse transcription-polymerase chain reaction (qRT-PCR) in 86 pairs of ESCC samples. The associations between miRNA expression and clinicopathological features were analyzed. Furthermore, we tried to identify the targets of these differentially expressed miRNAs.

MATERIALS AND METHODS

Cell lines

Human ESCC cell lines EC8712, KYSE150, EC109, EC18, SHEEC, KYSE180, KYSE70, and KYSE140 were cultured in 199 or DMEM medium (Invitrogen, Carlsbad, CA, USA) plus 10% newly born calf serum.

Table 1 Clinical characteristics of esophageal squamous cell carcinoma used for quantitative reverse transcription-polymerase chain reaction analysis

Clinical parameter	n
Gender	
Male	62
Female	24
Age (yr)	
< 55	35
≥ 55	51
Diameter	
< 5 cm	57
≥ 5 cm	29
LN	
N0	53
N1	33
Invasion	
T1	4
T2	18
T3	64
Histological type	
Ulcerative	49
Medullary	24
Fungating	10
Others	3
Differentiation	
I	23
II	51
III	12
TNM stage	
I	3
II a	49
II b	4
III	30

Specimen collection

ESCC tissues and matched normal tissues were obtained from surgical specimens immediately after resection from patients undergoing primary surgical treatment of esophageal carcinoma from Oct 2007 to Dec 2008 in the Department of Tumor Surgery of Shantou Central Hospital, China. No patient had received preoperative irradiation or chemotherapy. The samples were flash frozen in liquid nitrogen and stored at -80°C until RNA extraction. Among these samples, three were used for microRNA microarray analysis and 86 were using for qRT-PCR analysis. Tumor specimens underwent histological examination by a pathologist to confirm the diagnosis, verify the presence of tumor, select those samples with at least 75% tumor tissue, and establish the pathological stage. Clinical and pathological information was extracted from the patients' medical charts and pathology reports. The clinical data used for qRT-PCR analysis are shown in Table 1. Written consent for tissue donation (for research purposes) was obtained from the patients before tissue collection and the protocol was approved by the Institutional Review Board of Shantou Central Hospital.

miRNA microarray

RNA labeling and hybridization were completed by KangChen Bio-tech Inc. (Shanghai, China) according to

the manufacturer's instructions. Briefly, total RNA from three pairs of esophageal carcinoma and matched normal tissues were isolated using Trizol (Invitrogen, USA) and purified using the RNeasy mini kit (QIAGEN, Germany). The concentration and quality of total RNA were measured by NanoDrop ND-1000 at 260 and 280 nm (A260/280) and confirmed by gel electrophoresis. Each RNA sample from three pairs of ESCC was separately labeled using the miRCURY Hy3/Hy5 labeling kit and hybridized on the six miRCURYTM locked nucleic acid (LNA) array version 11.0 (Exiqon, Denmark), which contains probes for 1700 mature miRNAs. Scans were quantified using GenePix software (Molecular Devices). The data were exported to Microsoft Excel worksheets, log₂ transformed, normalized using global Lowess (Locally Weighted Scatter plot Smoothing) regression algorithm (MIDAS, TIGR Microarray Data Analysis System), which we previously found to produce the best within-slide normalization to minimize the intensity-dependent differences between the dyes. Replicated spots on the same slide were averaged by obtaining a median ratio of replicated spots. Between slides normalization was performed by scale normalization to reduce between-slide variability. Only those with a greater than 2-fold increase or 2-fold decrease in expression in two samples were considered significantly changed. Samples were clustered according to their miRNA profile using Cluster 3.0 and shown using Treeview.

miRNA real-time RT-PCR quantification

qRT-PCR analysis of miRNA expression was carried out using TaqMan MicroRNA Assay kits according to the manufacturer's protocol (Applied Biosystems, USA). Briefly, total RNA was extracted using TRIzol Reagent (Invitrogen, USA) from clinical samples and ESCC cell lines. cDNAs were synthesized from total RNA using gene-specific primers. Reverse transcriptase reactions contained 10 ng RNA samples, 50 nmol/L stem-loop RT primer, 1 × RT buffer, 0.25 mmol/L each of the dNTPs, 3.33 U/μL MultiScribe reverse transcriptase and 0.25 U/μL RNase inhibitor. The 15 μL reactions were incubated for 30 min at 16°C, 30 min at 42°C, 5 min at 85°C, and then held at 4°C. The 20 μL PCR reaction included 1.33 μL RT product, 1 × TaqMan Universal PCR master mix and 1 μL primers and probe mix of the TaqMan MicroRNA Assay kit. Reactions were incubated in a 96-well optical plate at 95°C for 10 min, followed by 40 cycles at 95°C for 15 s and 60°C for 1 min. PCR reactions were run on a 7500 Real Time PCR machine (Applied Biosystems) and analyzed using 7500 System SDS software.

U6 small nuclear RNA was used as an internal control to normalize RNA input. The Ct value is defined as the fractional cycle number at which the fluorescence passes the fixed threshold. The fold change was calculated using the 2^{-ΔΔCt} method, presented as the fold-expression change in tumors relative to their corresponding normal tissues after normalization to the endogenous control. All experiments were carried out in triplicate.

Plasmid construction

Human genomic fragments of miR-145 and miR-143 pre-

cursors with flanking about 200 bp were amplified by PCR using human genomic DNA as a template. PCR primers were designed as follows: miR143 forward: 5'-AAGCT-TAAGGTCAAGGTTTGGTCCT-3'; miR143 reverse: 5'-CTCGAGTGCTAAGATGGACACACTGG-3'; miR145 forward: 5'-AAGCTTCAGAGGGTTTCCGGTACTT-3'; miR-145 reverse: 5'-CTCGAGAGCCTCACAGGGAT-GTTATG-3'. The PCR products were cloned into the pDNA3.0 vector and named pcDNA-miR145 and pcDNA-miR143, respectively.

Transfection

Approximately 2 × 10⁵ of KYSE150 and KYSE180 cells were seeded and cultured in 6-well plates, respectively. For each well, 2.0 μg of plasmids were added to 100 μL Opti-MEM medium and 10 μL of Superfect (QIAGEN, Germany). The mixture was added to the cells and incubated for 2 h before replacing the medium. Stable clones were generated by selection in complete culture medium containing 400 mg/L of G418.

In vitro wound-healing assay

KYSE150 and KYSE180 cells were seeded in a 6-well dish, and incubated overnight yielding a confluent monolayer for wounding. Wound healing was performed using a tip with a flat point. An image was taken at different time points in each visual field at 50 ×.

miRNA target prediction

TargetScan (release 5.1, <http://www.targetscan.org/>) was used to analyze potential target genes for the deregulated microRNAs.

Western blotting

Total cell lysates were prepared in RIPA buffer [50 mmol/L TrisHCl, pH 8.0, 150 mmol/L NaCl, 1% (vol/vol) Nonidet P-40, 0.5% (wt/vol) sodium desoxycholate, 0.1% (wt/vol) SDS] containing the complete protease inhibitor cocktail. Western blotting analysis was performed as described with the following primary antibodies: monoclonal mouse anti-fascin (DAKO, Denmark) and mouse anti-β-actin (Sigma, MO, USA). Experiments were repeated in triplicate.

Statistical analysis

Statistical differences between tumor and normal tissue were evaluated using the paired *t*-test. Statistical differences between clinicopathologic parameters and miRNA fold change were evaluated using ANOVA. The correlation coefficients of miR-143 and miR-145 were calculated using the Spearman correlation. *P* values less than 0.05 were considered statistically significant. All calculations were performed using Statistical Program for Social Sciences (SPSS) software 13.0 (SPSS Inc., Chicago, IL, USA).

RESULTS

Patient characteristics

The group specimen used for qRT-PCR was obtained

from 62 males and 24 females and their details are shown in Table 1. The average age of these patients was 54 years and ranged from 40 to 75 years. Fifty-seven patients (66.3%) had tumors smaller than 5 cm, and 29 (33.7%) had tumors greater than 5 cm. Lymph node metastases were observed in 38.4% of the patients ($n = 33$), while the remaining patients had no lymph node metastases. Of these patients, 4 (4.7%) of 86 were diagnosed at invasion T1, 18 (20.9%) at invasion T2 and 64 (74.4%) at invasion T3. Histological type was ulcerative in 49 cases, medullary in 24 cases, fungating in 10 cases and 3 cases were unidentified. Seventy-four cases were well differentiated (I + II) and 12 cases were poorly differentiated. Taken together, the numbers diagnosed in the four clinical stages were 3, 49, 4 and 30, respectively. After two years of follow-up, the overall survival rate of the 86 ESCC patients was as high as 84.9% with only 13 deaths reported. The impact of the expression of miRNAs on patient survival will be analyzed in a future study.

Differential expression of miRNAs found in ESCC

Using miRNA microarray, we then identified the miRNAs that were differentially expressed in tumor and non-tumor samples. Only miRNAs that were altered by at least 2-fold in at least two of the samples were considered significant candidates. Using these strict criteria, we identified 33 upregulated miRNAs and 40 downregulated miRNAs between normal and cancer tissues. Heat maps depict the relative expression level of mature miRNAs indicated by microarray analyses of the samples from three patients (Figure 1). This showed that the changes from two chips in each clinical case were consistent.

In accordance with previous reports^[12,14], miR-21 was observed to be the most upregulated miRNA with an average 24.4-fold change. miR-203 was the most downregulated with an average 4.3-fold change. miR-203, miR-99a and miR-100 were also found to be downregulated in this study. With the exception of these, several miRNAs such as miR-143 and miR-145 were found to be changed in esophageal squamous cell carcinoma (Figure 1). On average miR-143 was downregulated 4.3-fold, while miR-145 was downregulated 3.2-fold. miR-25 was only detected in one chip and was upregulated 2.3-fold. However, a previous report of significant differential expression of miRNAs in ESCC^[12,14-16], including miR-106b, -103, -107, -34b, -139 and -129, did not show significant changes in our study. All raw and normalized miRNA expression data are available from GEO publicly accessible server (<http://www.ncbi.nlm.nih.gov/geo/>) with the accession number: GSE23142.

Downregulation of miR-143 and miR-145 in ESCC

To confirm our microarray data and to determine the clinical significance of deregulated expression of miRNAs in esophageal carcinoma, we evaluated the expression of two cancer-associated miRNAs, miR-143 and miR-145, in 86 clinical samples of esophageal carcinoma and their matched normal tissues using qRT-PCR. These microR-

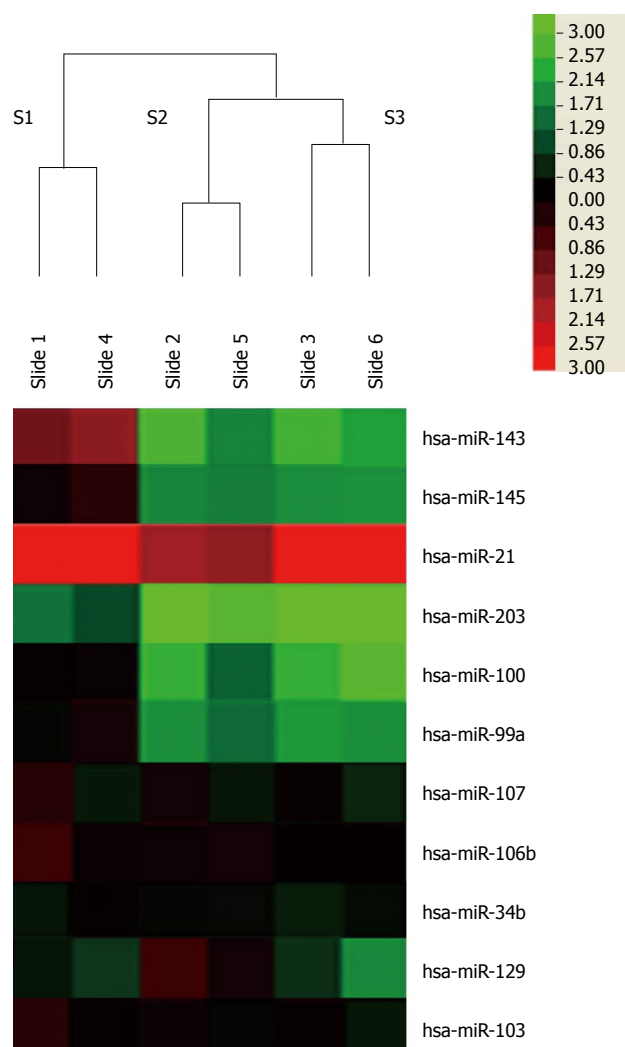


Figure 1 miRNAs are deregulated in esophageal squamous cell carcinoma as detected by microRNA microarray. Three pairs of esophageal carcinoma and normal tissue matches were analyzed by miRCURY LNA™ microRNA Arrays v.11.0. Each RNA sample was dye-swap labeled. Unsupervised hierarchical cluster analysis of miRNA expression in three esophageal carcinoma patients. Rows: miRNAs; columns: cases. The analysis showed that two chips in each case were consistent. For each miRNA, red represents higher expression and blue represents lower expression than the average expression. S1, sample 1; S2, sample 2; S3, sample 3.

NAs were chosen as they had previously been shown to be differentially expressed in various tumors. U6 RNA expression did not differ significantly between tumor and non-tumor tissue in our study population (data not shown). As shown in Figure 2, the expression level of miR-145 was significantly downregulated in ESCC compared to matched normal tissues ($P = 0.001$), and no statistically significant difference in miR-143 expression between the two groups was observed ($P = 0.436$).

Using the $2^{-\Delta\Delta Ct}$ method and a 2-fold change criterion, the qRT-PCR results showed that the expression of miR-143 was downregulated in 47.7% (41/86) and miR-145 was downregulated in 61.6% (53/86) of the clinical samples of esophageal carcinoma (Figure 3). The qRT-PCR results showed good consistency with the microRNA microarray results. In order to investigate the

Table 2 Associations between expression levels of miR-143 and miR-145 and clinicopathological features

	miR-143		miR-145	
	median \pm SD	P value	median \pm SD	P value
Gender				
Male	1.43 \pm 2.99	0.805	0.82 \pm 1.61	0.718
Female	1.27 \pm 1.72		0.95 \pm 1.32	
Age (yr)				
< 55	1.67 \pm 3.54	0.418	1.15 \pm 1.99	0.138
\geq 55	1.19 \pm 1.92		0.65 \pm 1.08	
Diameter (cm)				
< 5	1.47 \pm 2.02	0.701	0.93 \pm 1.31	0.497
\geq 5	1.23 \pm 3.71		0.69 \pm 1.89	
LNM				
N0	1.47 \pm 3.17	0.717	0.88 \pm 1.71	0.815
N1	1.25 \pm 1.70		0.80 \pm 1.16	
Tumor stage				
T1	6.31 \pm 9.33	0.000 ^b	3.33 \pm 4.70	0.001 ^b
T2	0.80 \pm 1.32		0.34 \pm 0.30	
T3	1.25 \pm 1.87		0.84 \pm 1.26	
Histological type				
Ulcerative	1.45 \pm 3.28	0.996	0.79 \pm 1.76	0.955
Medullary	1.29 \pm 1.72		0.90 \pm 1.23	
Fungating	1.32 \pm 1.70		0.90 \pm 1.13	
Others	1.48 \pm 1.18		1.27 \pm 0.98	
Differentiation				
I	1.60 \pm 2.11	0.907	0.87 \pm 1.31	0.925
II	1.30 \pm 3.12		0.81 \pm 1.70	
III	1.38 \pm 1.60		1.00 \pm 1.15	
TNM stage				
I	0.76 \pm 1.00	0.971	0.94 \pm 1.39	0.998
II a	1.41 \pm 2.18		0.83 \pm 1.31	
II b	1.06 \pm 1.47		0.95 \pm 1.48	
III	1.46 \pm 3.60		0.87 \pm 1.90	

^b $P < 0.01$.

clinical values of miR-143 and miR-145, we analyzed the relationships between the expression levels of these two miRNAs in cancer tissues and clinicopathological factors of patients with esophageal carcinoma. The mean fold changes of miRNAs in esophageal carcinoma samples and their possible connections with cancer are presented in Table 2. Significant correlations between miR-143 and miR-145 levels in the primary tumors and tumor invasion were observed ($P = 0.000$ and $P = 0.001$, respectively, Figure 4). Furthermore, the co-expression of miR-143 and miR-145 was analyzed with the Spearman correction and showed a value of 0.967 ($P = 0.000$).

miR-143 and miR-145 inhibit cell mobility

The expression levels of miR-143 and miR-145 were significantly downregulated in ESCC cell lines (Figure 5A). Following transfection with pcDNA-miR143 and pcDNA-miR145, the expression levels of these two microRNAs were significantly increased (Figure 5B). In the wound-healing assays, the distance KYSE150 and KYSE180 stably transfected cells moved in a wounded cell monolayer on plastic was determined, together with pcDNA transfected cells which were used as controls. The results showed that the cells transfected with

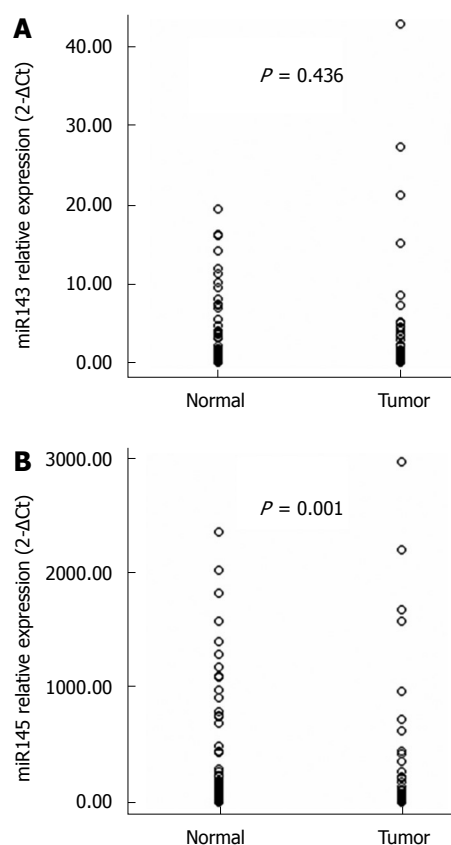


Figure 2 Differential expression of miR-143 (A) and miR-145 (B) in esophageal squamous cell carcinoma compared to normal tissue. Each value represents the relative expression using the 2- Δ Ct method with U6 RNA as an endogenous control. miR-145 is significantly deregulated in esophageal carcinoma patients ($P = 0.001$).

miR-145 and miR-143 migrated very small distances and were unable to achieve wound closure (Figure 5C and D, respectively). For stably transfected KYSE150 cells, 89% of the wounds containing the control cells (16/18 visual fields) were closed or were healing, while only 58% of the miR-143 transfectant (7/12 visual fields) and 18% of the miR-145 transfectant (3/17 visual fields) were healing. For stably transfected KYSE180 cells, the percentage of healing in the control, miR-143 transfectant and miR-145 transfectant was 50% (6/12), 42% (5/12) and 0% (0/6), respectively.

miRNA target prediction and identification

Since miR-143 and miR-145 can inhibit the mobility of esophageal carcinoma cells, we tried to identify their targets that related to cell mobility. Recently, *FSCN1* has been proved to be a target of miR-145 both in the esophageal squamous cell lines TE2 and TE13 and in bladder cancer^[17,18]. However, our results showed that the protein level of *FSCN1* did not significantly change in the miR-143 and miR-145 stable expressing KYSE150 and KYSE180 cells, respectively (Figure 6A and B). Using TargetScan, we found that the 3'-UTR of *FSCN1* contained hundreds of miRNA binding sites, especially four conserved binding sites for miR-145 and two non-conserved

Table 3 miR-143 and miR-145 predicted targets related to cell mobility

Predicted targets	Functions
miR-143	
LASP1 (LIM and SH3 protein 1)	Functions as an actin-binding protein and possibly in cytoskeletal organization
RICTOR (RPTOR independent companion of MTOR, complex 2)	Functions upstream of Rho GTPases to regulate the actin cytoskeleton
ARHGAP26 (Rho GTPase activating protein 26)	Regulates the organization of the actin-cytoskeleton
EPB41 [erythrocyte membrane protein band 4.1 (elliptocytosis 1, RH-linked)]	Together with spectrin and actin, constitute the red cell membrane cytoskeletal network.
MYO3A (myosin III A)	Belongs to the myosin superfamily, an actin-dependent motor protein
MARCKS (myristoylated alanine-rich protein kinase C substrate)	An actin filament crosslinking protein involved in cell motility
SVIL (supervillin)	Tightly associated with both actin filaments and plasma membranes
miR-145	
ARF6 (ADP-ribosylation factor 6)	Regulates vesicular trafficking, remodeling of membrane lipids, and signaling pathways that lead to actin remodeling.
ABLIM2 (actin binding LIM protein family, member 2)	Bound strongly to F-actin, localized to actin stress fibers
ADD3 [adducin 3 (γ)]	Involved in assembly of the spectrin-actin network in erythrocytes and at sites of cell-cell contact in epithelial tissues
CAPZB (c apping protein (actin filament) muscle Z-line, β)	Regulates growth of the actin filament by capping the barbed end of growing actin filaments.
ELMO1 (engulfment and cell motility 1)	Mediates cytoskeletal rearrangements during phagocytosis of apoptotic cells and cell motility
PHACTR2 (phosphatase and actin regulator 2)	Coprecipitated with both PP1 and actin
TMOD1 (tropomodulin 1)	Inhibits depolymerization and elongation of the pointed end of actin filaments

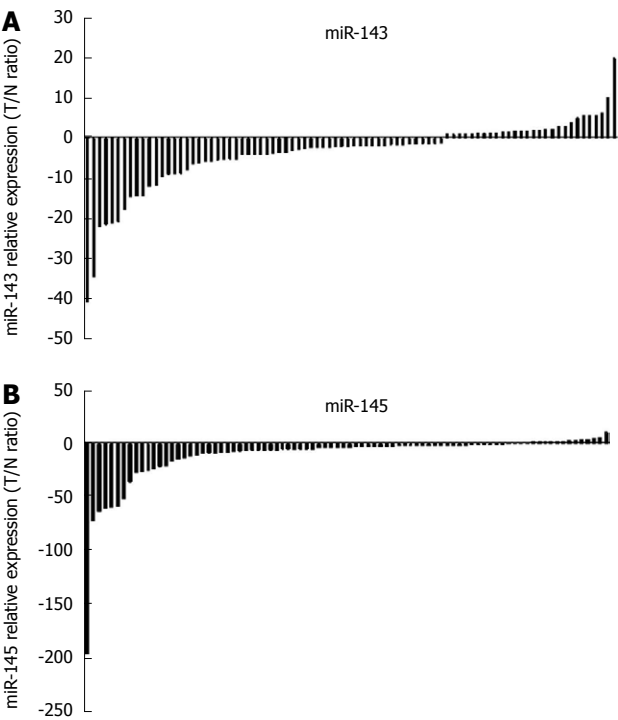


Figure 3 Downregulation of miR-143 and miR-145 in esophageal squamous cell carcinoma. Using the $2^{-\Delta\Delta Ct}$ method, those with a greater than 2-fold change were considered significant. The expression of miR-143 was downregulated in 48.9% (46/94) and miR-145 was downregulated in 60.6% (57/94) clinical samples of esophageal carcinoma.

binding sites for miR-143 (Figure 7). Moreover, we also found other predicted targets of miR-143 and miR-145 that related to cell mobility using TargetScan (Table 3).

DISCUSSION

Accumulated studies have indicated that microRNAs,

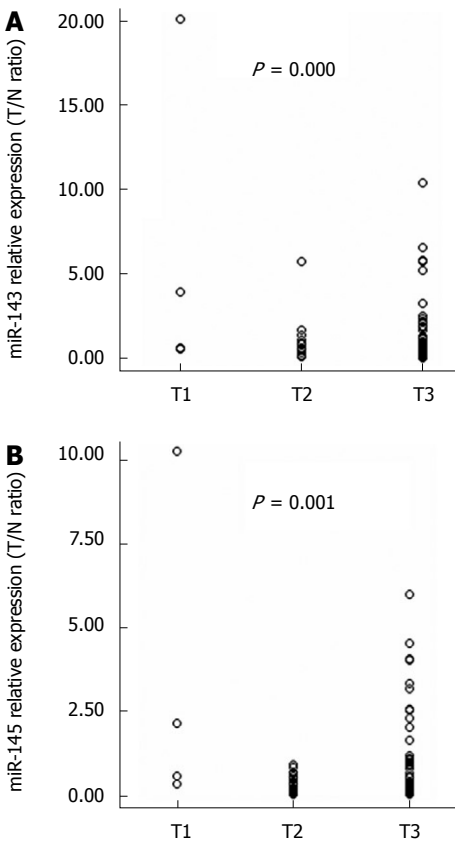


Figure 4 Associations between the expression of miR-143 and miR-145 and clinicopathologic features. The expression of both miR-143 and miR-145 were significantly associated with esophageal squamous cell carcinoma tumor invasion ($P = 0.000$ and $P = 0.001$, respectively).

posttranscriptional modulators of gene expression, are involved in the initiation and progression of various malignancies. Many studies have demonstrated that some human miRNAs are consistently deregulated in human

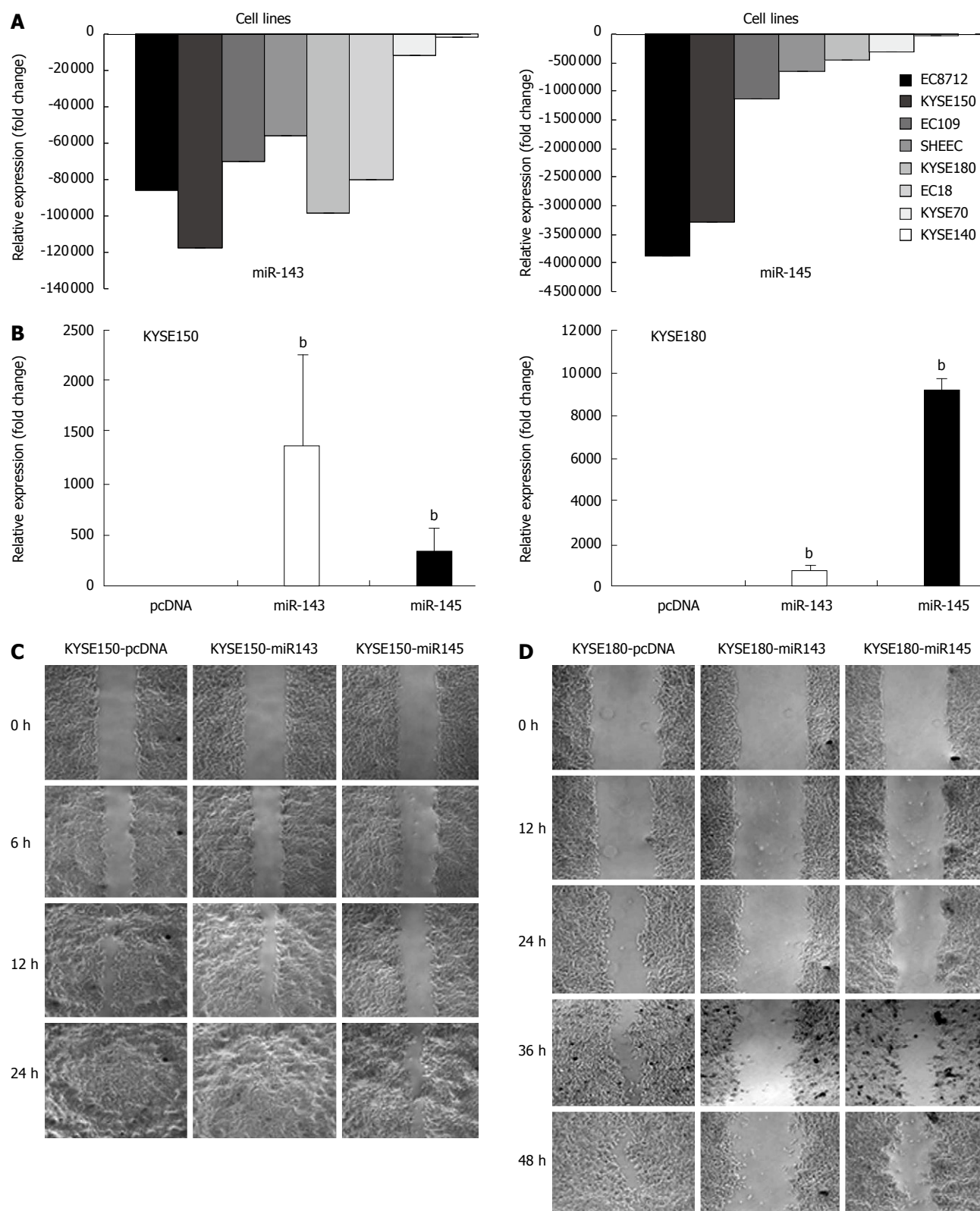


Figure 5 miR-143 and miR-145 inhibited esophageal squamous cell carcinoma cell mobility. A: The expression levels of miR-143 and miR-145 in esophageal squamous cell carcinoma (ESCC) cell lines. Using normal tissue as the control, both miRNAs were significantly downregulated in ESCC cell lines; B: The increased expression of miR-143 and miR-145 following stable transfection. Quantitative reverse transcription-polymerase chain reaction demonstrated a significant increase in the expression levels of miR-143 and miR-145 in KYSE150 and KYSE180 cells transfected with the respective expression plasmids compared with the levels in control cells ($P < 0.01$); C, D: The increased expression of miR-143 and miR-145 inhibited the mobility of both KYSE150 and KYSE180 cells. The miRNA stably transfected cells were seeded in a 6-well plate, streaks were made using a tip when the cells were grown to almost confluence 24 h later. Streaks were photographed at different intervals at 50 \times . This showed that upregulation of miR-143 and miR-145 can prevent ESCC cell wound healing. These findings are shown in (C) and (D).

cancer, suggesting a role for these genes in tumorigene-

sis^[19]. A comparison between human cancers and adjacent

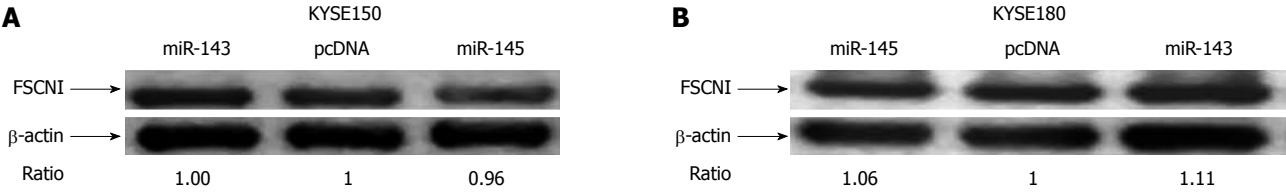


Figure 6 Identification of miR-143 and miR-145 targets. A, B: The protein level of the reported miR-145 target, *FSCN1*, did not change significantly in KYSE150 and KYSE180 cells when the expression of both miRNAs was upregulated by transfection with their corresponding expression plasmids.

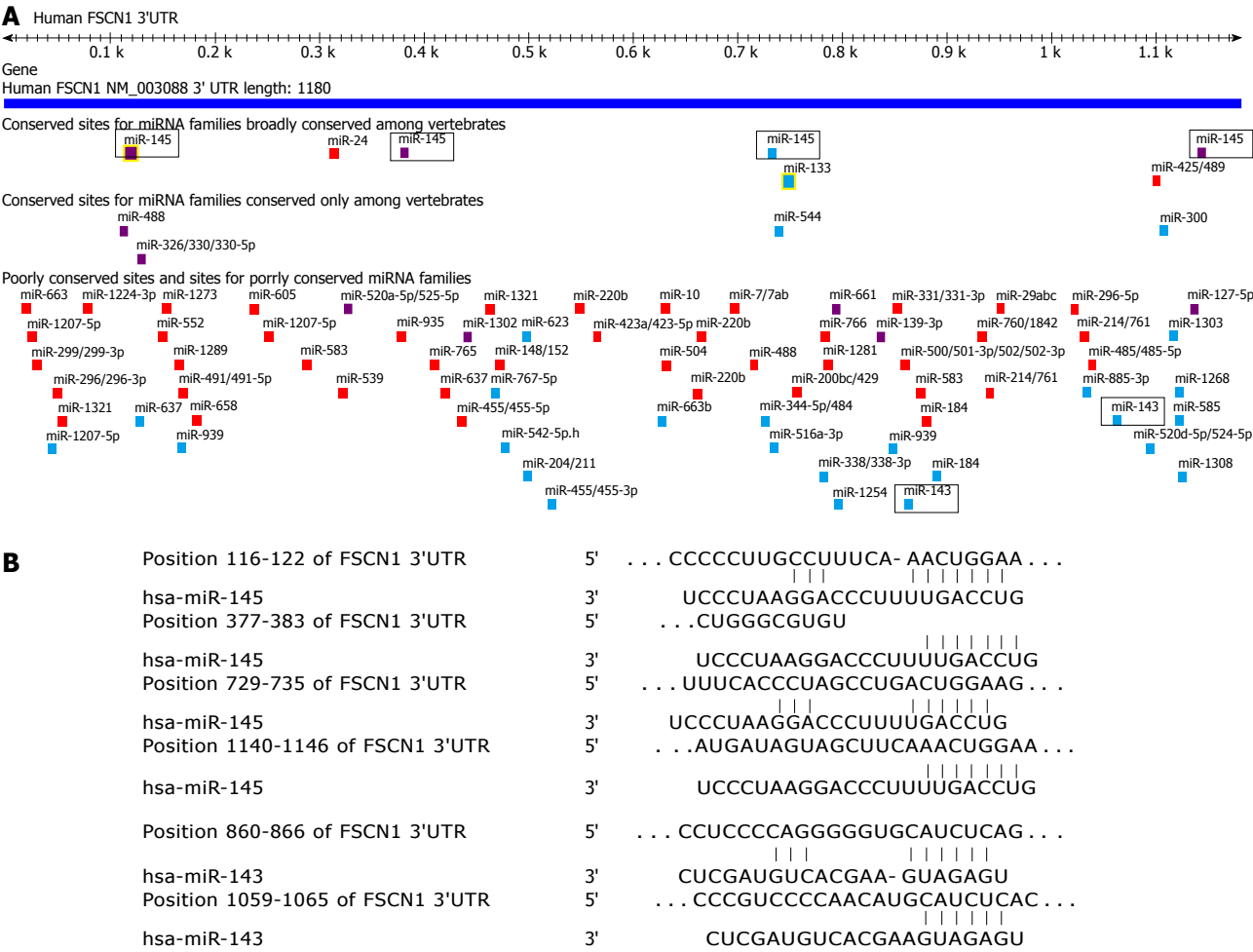


Figure 7 Human *FSCN1* 3'-UTR and its possible miRNA target sites predicted by the TargetScan program. A: The four conserved binding sites for miR-145 and two non-conserved binding sites for miR-143 are indicated by black boxes; B: The detailed seed sequence positions and sequence pairing for miR-143 and miR-145 with *FSCN1*.

normal tissues have revealed distinct miRNA expression profiles. To develop novel diagnostic and therapeutic targets for ESCC, we investigated the expression profile of miRNA in ESCC.

In this study, our miRNA microarray results partially agree with Feber's and Guo's findings, including miR-21 and miR-203, miR-99a and miR-100, respectively, which further support the robustness of our results. With the exception of deregulated miRNAs identified in Feber's and Guo's reports, we also found common differentially expressed miRNAs as reported recently by Ogawa *et al*^[16], including the upregulation of miR-21 and the downregulation of miR-133b and miR-145. Nevertheless, this is the

first time that the downregulation of both miR-143 and miR-145 in esophageal squamous cell carcinoma has been reported. All these results indicate that the miRNA expression profile in ESCC from the Chaoshan Area in China was significantly altered and showed apparent regional features. These results have provided new ways of understanding the mechanism of ESCC in Chaoshan Area.

A number of reports have shown that miR-143 and miR-145 are downregulated in various cancer cells, including colorectal cancer, nasopharyngeal carcinoma, lung cancer and B-cell malignancies^[20-23]. To our knowledge, we have performed the largest study to date which assesses the potential diagnostic and prognostic utility of

miRNAs in esophageal squamous cell cancer. Consistent with the aforementioned previous reports, our miRNA microarray and qRT-PCR results revealed that miR-143 and miR-145 were under-expressed in most esophageal carcinoma specimens, compared with matched normal tissue samples. These results imply that these two miRNAs might serve as novel diagnostic and therapeutic targets for esophageal squamous cell cancer.

However, the pathobiological significance of aberrant miRNA expression in human esophageal squamous cell carcinoma has not been well documented. In this study, we found that both miR-143 and miR-145 correlated with tumor invasion. This suggested that both of these miRNAs might be associated with esophageal carcinoma progression. To date, little information is available on the correlations between miR-143 and miR-145 and the clinicopathologic features of other tumors. It was reported that there was no relationship between miR-143 and miR-145 expression and other clinicopathological features, except that miR-145 expression was related to cancer site following the analysis of 98 primary colorectal cancer specimens^[20]. Slaby *et al.*^[24] also found that colorectal cancer tumors larger than 50 mm in maximum diameter were characterized by low expression of miR-143 and miR-145. Clapé *et al.*^[25] showed that miR-143 expression levels were inversely correlated with advanced stages of prostate cancer. Therefore, the roles of miR-143 and miR-145 in esophageal squamous cell carcinoma progression remain to be revealed.

Xin *et al.*^[26] showed that miR-143 and miR-145 selectively target genes that regulate the actin cytoskeleton in smooth muscle cells, which is intimately coupled to cell migration. Migration of esophageal squamous carcinoma cells was consistently reduced by over-expression of miR-143 and miR-145 in our wound-healing experiments. It has been reported that *FSCN1* is a target of miR-145 both in bladder cancer and esophageal carcinoma^[17,18]. However, no significant downregulation of *FSCN1* protein was found in ESCC KYSE150 and KYSE180 cells, while the expression of miR-143 and miR-145 was rescued. This controversial result may be due to the specificity of these cell lines. Using TargetScan, we also found other predicted targets of miR-143 and miR-145 related to cell mobility, such as *LASP1* and *ARF6*. These results implied that *FSCN1* could be regulated by other miRNAs in ESCC cell lines except the TE series^[16]. The targets of miR-143 and miR-145 in KYSE150 and KYSE180 cells remain to be identified.

Interestingly, the chromosome loci of both miR-143 and miR-145 are very close to each other within approximately 2 kb on 5q32, which led us to speculate that both precursors originate from the same primary transcript. In our study, we found that these two miRNAs were highly co-expressed in 86 esophageal tumors, with Spearman correlation coefficients of 0.967 ($P = 0.000$). This indicated that miR-143 and miR-145 might be regulated by the same factor(s) and generated from the same primary transcript (pri-miRNAs). However, various results have suggested that there may be different mechanisms for the transcriptional regulation of this locus. miR-143 and

miR-145 could be transcribed individually and co-transcribed. Zhang *et al.*^[27] demonstrated that miR-143 is transcribed by nuclear factor κ B, and the expression levels of miR-143 were dramatically increased in metastatic HBV-HCC and HCC patients. Xu *et al.*^[28] found that the 1.5 kb sequence upstream of miR-145 has an intrinsic promoter activity, and such activity is repressed by OCT4, which is one of the targets of miR-145. Cordes *et al.*^[29] also found that miR-143 and miR-145 were direct transcriptional targets of the serum response factors, myocardin and Nkx2-5, in multipotent murine cardiac progenitors. The transcription regulation of miR-143/-145 seems to be tissue-specific.

In summary, we report that miRNAs were deregulated and miR-143 and miR-145 were downregulated in ESCC. Furthermore, rescued expression of miR-143 and miR-145 can inhibit cell mobility. This study provides the first evidence for the anti-oncogenic activity of miR-143 and miR-145 in the development of esophageal squamous cell cancer. Targets of these two miRNAs remain to be defined. These results indicate that miRNAs may eventually constitute useful biomarkers as well as therapeutic targets.

COMMENTS

Background

MicroRNAs (miRNAs) regulate gene expression by mainly binding to the 3'-UTR of target mRNAs, leading to mRNA degradation or translation inhibition. miRNAs are aberrantly expressed in various cancers, suggesting that they play a vital role as a novel class of oncogenes or tumor suppressor genes, depending on the targets they regulate.

Research frontiers

Esophageal squamous cell carcinoma is one of the most lethal malignancies in China. Many studies have reported the miRNA expression profiles in Barrett's esophagus and esophageal adenocarcinoma. In this study, the authors report the expression profile of miRNA in esophageal squamous cell carcinoma (ESCC) and investigate the expression and functions of miR-143 and miR-145 in ESCC.

Innovations and breakthroughs

Some human miRNAs are consistently deregulated in human cancer, suggesting a role for these genes in tumorigenesis. A set of miRNAs was found to be deregulated in ESCC and the expression levels of miR-143 and miR-145 were significantly decreased in most of the ESCC tissues examined. The authors performed the largest study to date which assessed the potential diagnostic and prognostic utility of miRNAs in ESCC. It is the first study to show that both miR-143 and miR-145 were correlated with tumor invasion depth. The anti-oncogenic role of miR-143 and miR-145 was demonstrated as significant cell mobility inhibition.

Applications

This study provides the first evidence of the anti-oncogenic activity of miR-143 and miR-145 in the development of ESCC. These results indicated that miRNAs may eventually constitute useful biomarkers as well as therapeutic targets.

Peer review

Many miRNAs are found deregulated in ESCC tissue and miR-143 and -145 are significantly decreased in ESCC. Both miR-143 and miR-145 correlated with tumor invasion depth. This study provides the evidence for an anti-oncogenic activity of miR-143 and miR-145 in the development of ESCC and may develop to be useful biomarkers or therapeutic targets in ESCC. It's an excellent study.

REFERENCES

- 1 Roush SF, Slack FJ. Micromanagement: a role for microRNAs in mRNA stability. *ACS Chem Biol* 2006; 1: 132-134
- 2 Pasquinelli AE, Reinhart BJ, Slack F, Martindale MQ, Ku-

- roda MI, Maller B, Hayward DC, Ball EE, Degnan B, Müller P, Spring J, Srinivasan A, Fishman M, Finnerty J, Corbo J, Levine M, Leahy P, Davidson E, Ruvkun G. Conservation of the sequence and temporal expression of let-7 heterochronic regulatory RNA. *Nature* 2000; **408**: 86-89
- 3 **Rajewsky N.** microRNA target predictions in animals. *Nat Genet* 2006; **38** Suppl: S8-S13
 - 4 **Hwang HW, Mendell JT.** MicroRNAs in cell proliferation, cell death, and tumorigenesis. *Br J Cancer* 2006; **94**: 776-780
 - 5 **Calin GA, Sevignani C, Dumitru CD, Hyslop T, Noch E, Yendamuri S, Shimizu M, Rattan S, Bullrich F, Negrini M, Croce CM.** Human microRNA genes are frequently located at fragile sites and genomic regions involved in cancers. *Proc Natl Acad Sci USA* 2004; **101**: 2999-3004
 - 6 **Croce CM.** Causes and consequences of microRNA dysregulation in cancer. *Nat Rev Genet* 2009; **10**: 704-714
 - 7 **Tricoli JV, Jacobson JW.** MicroRNA: Potential for Cancer Detection, Diagnosis, and Prognosis. *Cancer Res* 2007; **67**: 4553-4555
 - 8 **Pisani P, Parkin DM, Bray F, Ferlay J.** Estimates of the worldwide mortality from 25 cancers in 1990. *Int J Cancer* 1999; **83**: 18-29
 - 9 **Enzinger PC, Mayer RJ.** Esophageal cancer. *N Engl J Med* 2003; **349**: 2241-2252
 - 10 **Kan T, Meltzer SJ.** MicroRNAs in Barrett's esophagus and esophageal adenocarcinoma. *Curr Opin Pharmacol* 2009; **9**: 727-732
 - 11 **Yang H, Gu J, Wang KK, Zhang W, Xing J, Chen Z, Ajani JA, Wu X.** MicroRNA expression signatures in Barrett's esophagus and esophageal adenocarcinoma. *Clin Cancer Res* 2009; **15**: 5744-5752
 - 12 **Feber A, Xi L, Luketich JD, Pennathur A, Landreneau RJ, Wu M, Swanson SJ, Godfrey TE, Litle VR.** MicroRNA expression profiles of esophageal cancer. *J Thorac Cardiovasc Surg* 2008; **135**: 255-260; discussion 260
 - 13 **Su M, Liu M, Tian DP, Li XY, Zhang GH, Yang HL, Fan X, Huang HH, Gao YX.** Temporal trends of esophageal cancer during 1995-2004 in Nanao Island, an extremely high-risk area in China. *Eur J Epidemiol* 2007; **22**: 43-48
 - 14 **Guo Y, Chen Z, Zhang L, Zhou F, Shi S, Feng X, Li B, Meng X, Ma X, Luo M, Shao K, Li N, Qiu B, Mitchelson K, Cheng J, He J.** Distinctive microRNA profiles relating to patient survival in esophageal squamous cell carcinoma. *Cancer Res* 2008; **68**: 26-33
 - 15 **Lee KH, Goan YG, Hsiao M, Lee CH, Jian SH, Lin JT, Chen YL, Lu PJ.** MicroRNA-373 (miR-373) post-transcriptionally regulates large tumor suppressor, homolog 2 (LATS2) and stimulates proliferation in human esophageal cancer. *Exp Cell Res* 2009; **315**: 2529-2538
 - 16 **Ogawa R, Ishiguro H, Kuwabara Y, Kimura M, Mitsui A, Katada T, Harata K, Tanaka T, Fujii Y.** Expression profiling of micro-RNAs in human esophageal squamous cell carcinoma using RT-PCR. *Med Mol Morphol* 2009; **42**: 102-109
 - 17 **Kano M, Seki N, Kikkawa N, Fujimura L, Hoshino I, Akutsu Y, Chiyomaru T, Enokida H, Nakagawa M, Matsubara H.** miR-145, miR-133a and miR-133b: Tumor suppressive miRNAs target FSCN1 in esophageal squamous cell carcinoma. *Int J Cancer* 2010; Epub ahead of print
 - 18 **Chiyomaru T, Enokida H, Tatarano S, Kawahara K, Uchida Y, Nishiyama K, Fujimura L, Kikkawa N, Seki N, Nakagawa M.** miR-145 and miR-133a function as tumour suppressors and directly regulate FSCN1 expression in bladder cancer. *Br J Cancer* 2010; **102**: 883-891
 - 19 **Zhang B, Pan X, Cobb GP, Anderson TA.** microRNAs as oncogenes and tumor suppressors. *Dev Biol* 2007; **302**: 1-12
 - 20 **Wang CJ, Zhou ZG, Wang L, Yang L, Zhou B, Gu J, Chen HY, Sun XF.** Clinicopathological significance of microRNA-31, -143 and -145 expression in colorectal cancer. *Dis Markers* 2009; **26**: 27-34
 - 21 **Chen HC, Chen GH, Chen YH, Liao WL, Liu CY, Chang KP, Chang YS, Chen SJ.** MicroRNA deregulation and pathway alterations in nasopharyngeal carcinoma. *Br J Cancer* 2009; **100**: 1002-1011
 - 22 **Liu X, Sempere LF, Galimberti F, Freemantle SJ, Black C, Dragnev KH, Ma Y, Fiering S, Memoli V, Li H, DiRenzo J, Korc M, Cole CN, Bak M, Kauppinen S, Dmitrovsky E.** Uncovering growth-suppressive MicroRNAs in lung cancer. *Clin Cancer Res* 2009; **15**: 1177-1183
 - 23 **Akao Y, Nakagawa Y, Kitade Y, Kinoshita T, Naoe T.** Down-regulation of microRNAs-143 and -145 in B-cell malignancies. *Cancer Sci* 2007; **98**: 1914-1920
 - 24 **Slaby O, Svoboda M, Fabian P, Smerdova T, Knoflickova D, Bednarikova M, Nenutil R, Vyzula R.** Altered expression of miR-21, miR-31, miR-143 and miR-145 is related to clinicopathologic features of colorectal cancer. *Oncology* 2007; **72**: 397-402
 - 25 **Clapé C, Fritz V, Henriquet C, Apparailly F, Fernandez PL, Iborra F, Avancès C, Villalba M, Culine S, Fajas L.** miR-143 interferes with ERK5 signaling, and abrogates prostate cancer progression in mice. *PLoS One* 2009; **4**: e7542
 - 26 **Xin M, Small EM, Sutherland LB, Qi X, McAnally J, Plato CF, Richardson JA, Bassel-Duby R, Olson EN.** MicroRNAs miR-143 and miR-145 modulate cytoskeletal dynamics and responsiveness of smooth muscle cells to injury. *Genes Dev* 2009; **23**: 2166-2178
 - 27 **Zhang X, Liu S, Hu T, Liu S, He Y, Sun S.** Up-regulated microRNA-143 transcribed by nuclear factor kappa B enhances hepatocarcinoma metastasis by repressing fibronectin expression. *Hepatology* 2009; **50**: 490-499
 - 28 **Xu N, Papagiannakopoulos T, Pan G, Thomson JA, Kosik KS.** MicroRNA-145 regulates OCT4, SOX2, and KLF4 and represses pluripotency in human embryonic stem cells. *Cell* 2009; **137**: 647-658
 - 29 **Cordes KR, Sheehy NT, White MP, Berry EC, Morton SU, Muth AN, Lee TH, Miano JM, Ivey KN, Srivastava D.** miR-145 and miR-143 regulate smooth muscle cell fate and plasticity. *Nature* 2009; **460**: 705-710

S- Editor Wang JL L- Editor Webster JR E- Editor Ma WH

Impact of diet on long-term decline in gastric cancer incidence in Poland

Mirosław Jarosz, Włodzimierz Sekuła, Ewa Rychlik, Katarzyna Figurska

Mirosław Jarosz, Ewa Rychlik, Department of Dietetics and Nutrition in Hospitals with Clinic of Metabolic Diseases and Gastroenterology, National Food and Nutrition Institute, 02-903 Warsaw, Poland

Włodzimierz Sekuła, Katarzyna Figurska, Independent Laboratory of the Economics of Food and Nutrition, National Food and Nutrition Institute, 02-903 Warsaw, Poland

Author contributions: Jarosz M designed the research; Sekuła W and Figurska K performed the research; Sekuła W, Rychlik E and Figurska K analyzed the data; Jarosz M, Sekuła W and Rychlik E wrote the paper.

Supported by Statutory action of the National Food and Nutrition Institute

Correspondence to: Mirosław Jarosz, Professor, Department of Dietetics and Nutrition in Hospitals with Clinic of Metabolic Diseases and Gastroenterology, National Food and Nutrition Institute, Powsińska St. 61/63, 02-903 Warsaw, Poland. jarosz@izz.waw.pl

Telephone: +48-22-5509677 Fax: +48-22-8421103

Received: July 6, 2010 Revised: September 7, 2010

Accepted: September 14, 2010

Published online: January 7, 2011

of refrigerators in the household (-0.77 and -0.80; $P < 0.0001$). A decline in these rates could also be linked to reduction in salt intake.

CONCLUSION: The decline of gastric cancer incidence probably resulted from increased consumption of vegetables, fruit and vitamin C and a decrease in salt consumption.

© 2011 Baishideng. All rights reserved.

Key words: Vegetables; Fruit; Vitamin C; Salt; Gastric cancer

Peer reviewer: Maria Gabriella Caruso, MD, Piazza Giuseppe Garibaldi 49, 70122 Bari, Italy

Jarosz M, Sekuła W, Rychlik E, Figurska K. Impact of diet on long-term decline in gastric cancer incidence in Poland. *World J Gastroenterol* 2011; 17(1): 89-97 Available from: URL: <http://www.wjgnet.com/1007-9327/full/v17/i1/89.htm> DOI: <http://dx.doi.org/10.3748/wjg.v17.i1.89>

Abstract

AIM: To examine the relationship between the trends in food consumption and gastric cancer morbidity in Poland.

METHODS: The study was based on gastric cancer incidence rates and consumption of vegetables, fruit, vitamin C and salt in Poland between 1960 and 2006. Food consumption data were derived from the national food balance sheets or household budget surveys. Spearman correlation coefficients were used to estimate the relationship between the variables.

RESULTS: A negative correlation was found between vegetables (-0.70 both for men and women; $P < 0.0001$), fruit (-0.65 and -0.66; $P < 0.0001$) and vitamin C (-0.75 and -0.74; $P < 0.0001$) consumption and stomach cancer incidence rates. The same applied to the availability

INTRODUCTION

Gastric cancer ranks fourth in morbidity and second in mortality for malignant cancers worldwide^[1]. However, in numerous countries, in particular in economically developed ones, gastric cancer morbidity within the past few decades has reduced significantly. Several epidemiological studies have shown that this phenomenon is most probably related to favorable changes in dietary pattern in the developed countries, that is, mostly to increased consumption of fresh fruit and vegetables, and decreased consumption of salt-preserved food^[2] and greater availability of refrigerators^[3]. It is assumed that lower gastric cancer morbidity rates are also related to lower prevalence of *Helicobacter pylori* (*H. pylori*) infection, which is considered as an essential factor for the development of a majority of gastric cancers^[4,5]. In these countries, prevalence of

H. pylori infections affects 20%-40% of the population.

Against this background, Poland seems to be a particular case. Despite the fact that, according to national epidemiological studies, the percentage of people infected with *H. pylori* is unusually high and amounts to 73% of the total population and 85%-95% of those aged > 25 years^[6], in 2006, gastric cancer morbidity rate was twofold lower compared to that in 1960^[7,8].

What was the reason for such a significant decrease in morbidity rate, taking such widespread dissemination of *H. pylori* as a major carcinogen into consideration? This intriguing phenomenon might be most probably assigned to specific changes in dietary pattern, as in the case of western countries.

Data that reflect average food consumption per capita in Poland in 1950-2006 show that this period was highly diversified with regard to dietary trends^[9-11]. In relation to the above, the two following periods can be distinguished: 1950-1989 and 1990-2006. Within the first period, consumption of products of animal origin (meat and meat products, animal fat, milk and dairy products, butter, fish and eggs) as well as sugar and sugar products showed a growing trend. At the same time, consumption of cereals and potatoes had decreased. Growth of vegetable consumption had come to an end in the 1950s and 1960s. Fruit consumption was low, particularly compared to other countries, due to frequent fluctuations in crops and limited fruit import, which was insufficient to mitigate the effect of such fluctuations.

Within the second period, a reversal in these trends was noticeable, particularly in relation to consumption of butter and other animal fats, red meat as well as milk and dairy products. This period was also characterized by a significant increase in fruit consumption and, despite no increasing trend, also in relatively high vegetable consumption^[9-11].

The above-mentioned favorable phenomena are considered to have brought about a significant improvement in the health situation in Poland. It can be assumed that positive changes in diet have influenced the decline in overall mortality seen since 1992, and stabilization of total malignant cancer mortality as well as a significant decrease in morbidity.

MATERIALS AND METHODS

Data on gastric cancer incidence rates were derived from the National Cancer Registry administered by the Maria Skłodowska-Curie Memorial Cancer Center and Institute of Oncology in Warsaw^[7,8]. They showed standardized gastric cancer incidence rates for men and women covering individual years between 1960 and 2006, excepting 1984, 1986, 1997 and 1998, for which no such data were available; in the case of the missing data for 1997-1998, the physicians' strike was the main contributing reason.

The source of information on the dietary pattern in the same time period was the database that was established and maintained for several decades by the National Food and Nutrition Institute^[9-11]. This database covers both

published and unpublished data derived from the national food balance sheets and shows major food quantities available for consumption per capita/year. They are converted into energy and nutrients with the use of a set of nutrient conversion factors developed at the institute and based on the national food composition tables^[12]. The resultant estimates show energy and nutrient amounts derived from food and available for consumption per capita/d.

In Poland, no data on average consumption of table salt per capita over the long term are available. Such data are available only for the period before World War II^[13]. After the war, this practice has not been continued. Data on salt consumption re-appeared, however, in 1998. They show average monthly consumption of salt per capita in households, which participated in budget surveys, carried out on annual basis using a sampling method that allowed for generalization of the results to all households in the country^[14]; these data were used for the analyses in the present study.

The features of the data on food quantities available for consumption and the derived estimates of the amounts of energy and nutrients made them particularly useful in the analysis of the trends over time, and to compare them with the trends in the health situation. In such a way, they were utilized in the present study. The study was focused on identification and measurement of the relationship between gastric cancer incidence rates and variables related to dietary pattern represented by the consumption of fruit, vegetables, vitamin C and kitchen salt. A trend in the equipment of Polish households with refrigerators was taken into consideration also as an important factor that affected perishable food quality and protected against nutrient loss.

Spearman's rank correlation coefficients (r_s) were estimated as a measure of the relationship between stomach cancer incidence rates and selected parameters.

RESULTS

Gastric cancer has a much higher incidence among men than women. In a base year of our analysis, i.e. 1960, the standardized rate for men amounted to 25.1/100 000, which exceeded twice the incidence rate for women (10.4/100 000)^[7]. For men, this rate reached a maximum level in 1970 and was 38% higher compared to 1960. In the same year, the maximum morbidity level was observed among women also; the rate was 39% higher than in 1960. The following years brought a decline in morbidity, and in 2006, the rates for men and women were approximately two times lower compared to the base year^[8].

Due to the fact that gastric cancer is one of two major types of cancer for which the risk is commonly agreed to be modified mainly by food and nutrition^[15], correlations between morbidity rates and consumption of certain food products and nutrients, which had both a positive and negative impact on this type of cancer, were analyzed. Due to reliable evidence that diets rich in fruit and vegetables protect against gastric cancer, these groups of products were analyzed first.

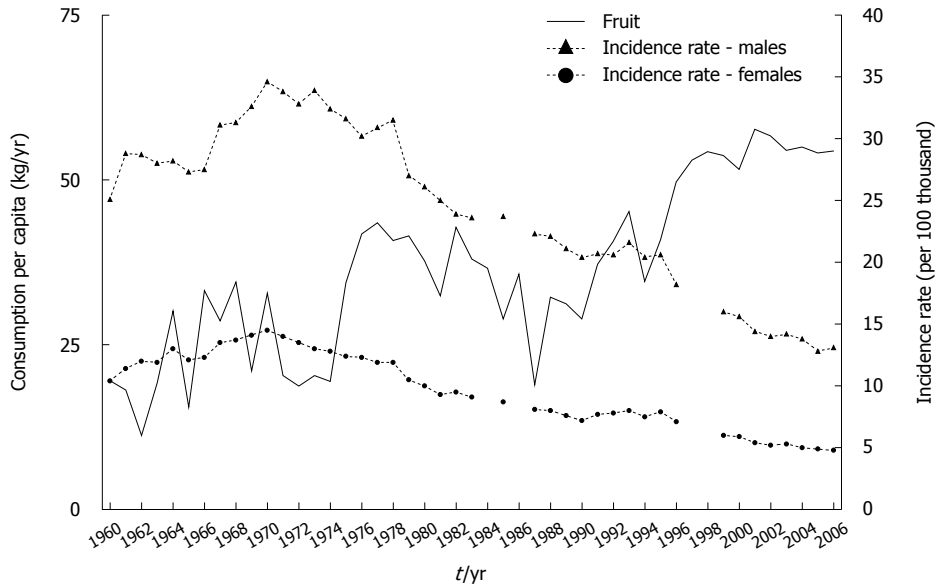


Figure 1 Fruit consumption and gastric cancer morbidity in 1960-2006.

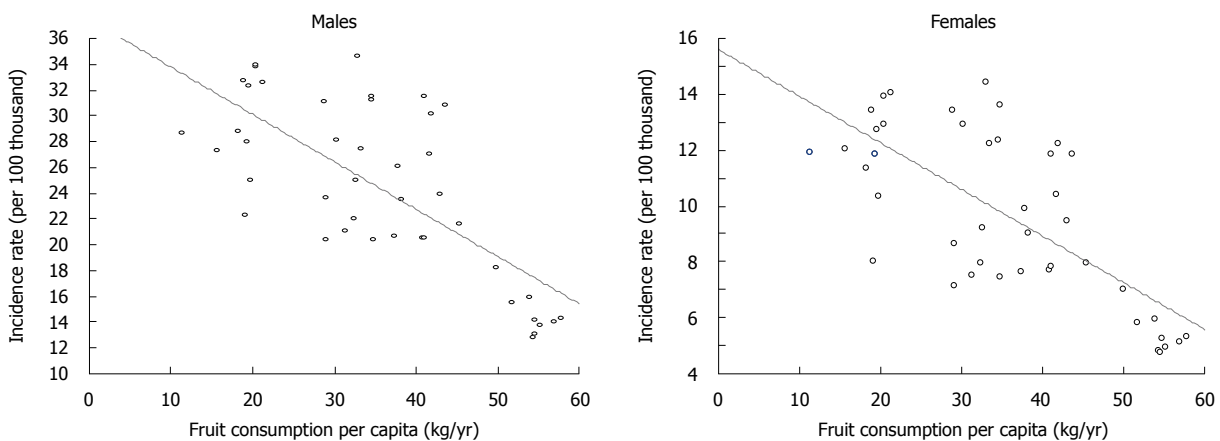


Figure 2 Correlation between fruit consumption and gastric cancer morbidity. Spearman's rank correlation coefficient (r_s) for men: $r_s = -0.65$ ($P < 0.001$), and for women: $r_s = -0.66$ ($P < 0.001$).

At the beginning of the 1960s, fruit was of minor importance in the average dietary pattern in our country, which resulted from low domestic production levels and no imports (Figure 1)^[10]. In the following years, the role of fruit has been gradually increased due to its greater availability. A particular improvement has been observed within the past 12 years, i.e. after initiation of political, economic and social transformation, accompanied by an increase in domestic fruit production and import^[9,11]. Also, changes in retail price relations between fruit and other food products have stimulated consumer demand for fruit and this has had a great impact.

Spearman's rank correlation coefficient, which covered fruit consumption in 1960-2006 and gastric cancer morbidity in the same period, showed a high correlation between the increase in fruit consumption and decrease in morbidity rate (Figure 2).

Vegetables traditionally have been more prominent than fruit in the dietary pattern in Poland, which has resulted from their greater availability and, in consequence,

lower prices. Consumption of this group of products, similarly to fruit, has been subject to a growing trend, and in 2006 was almost 30% higher compared to 1960 (Figure 3)^[9-11].

Estimate of the Spearman's rank correlation coefficient showed a very high correlation between the trend in vegetable consumption and gastric cancer morbidity (Figure 4).

Increased consumption of both food groups resulted in the growth of vitamin C content in the diet, despite a reduction in potato consumption: total vitamin C content grew from approximate 100 mg/d in 1960 to 124 mg in 2006, and a rise in the proportion contributed by fruit and vegetables was noted (Figure 5)^[9-11]. Calculations made for the purposes of this study showed a very high correlation between increased vitamin C intake and decreased gastric cancer morbidity (Figure 6).

Reliable evidence that confirmed that storing food in refrigerators protects against gastric cancer^[15-17] has focused attention on the trend in their availability in Polish

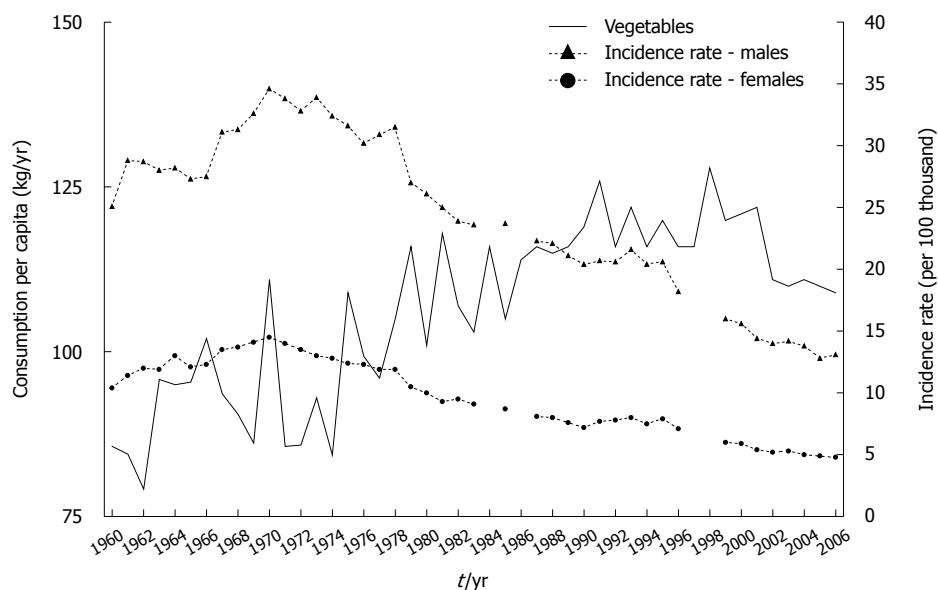


Figure 3 Vegetables consumption and gastric cancer morbidity in 1960-2006.

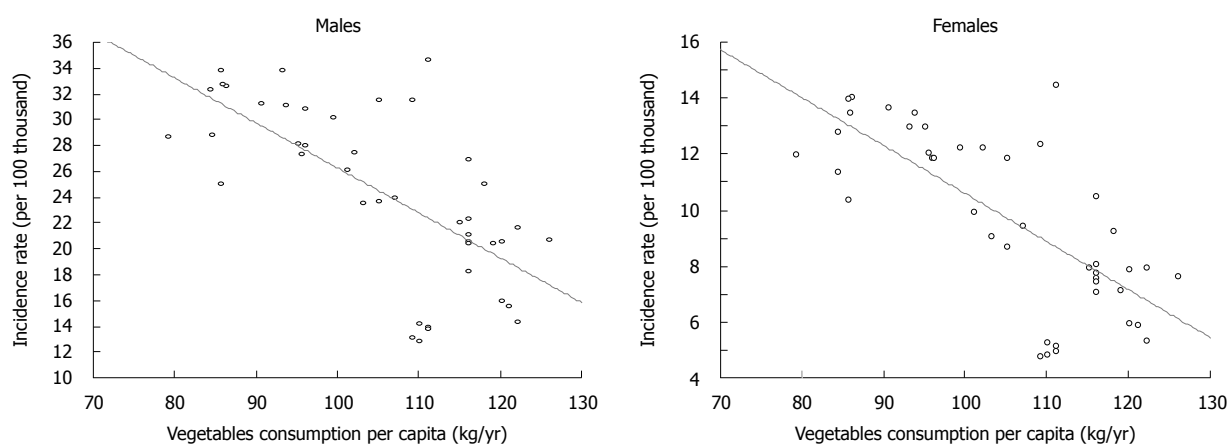


Figure 4 Correlation between vegetable consumption and gastric cancer morbidity. Spearman's rank correlation coefficient (r_s) for men: $r_s = -0.70$ ($P < 0.001$), and for women: $r_s = -0.70$ ($P < 0.001$).

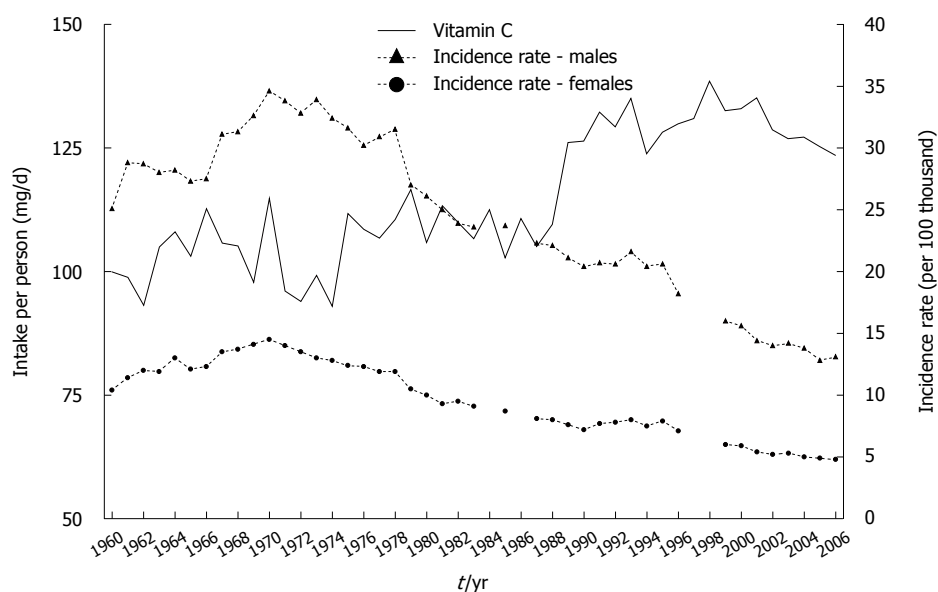


Figure 5 Vitamin C intake and gastric cancer morbidity in 1960-2006.

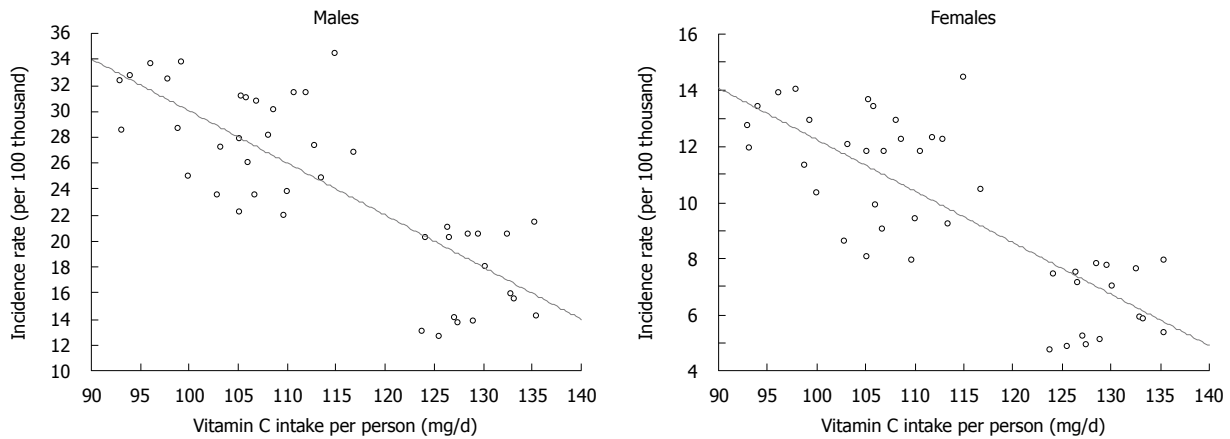


Figure 6 Correlation between vitamin C intake and gastric cancer morbidity. Spearman's rank correlation coefficient (r_s) for men: $r_s = -0.75$ ($P < 0.001$), and for women $r_s = -0.74$ ($P < 0.001$).

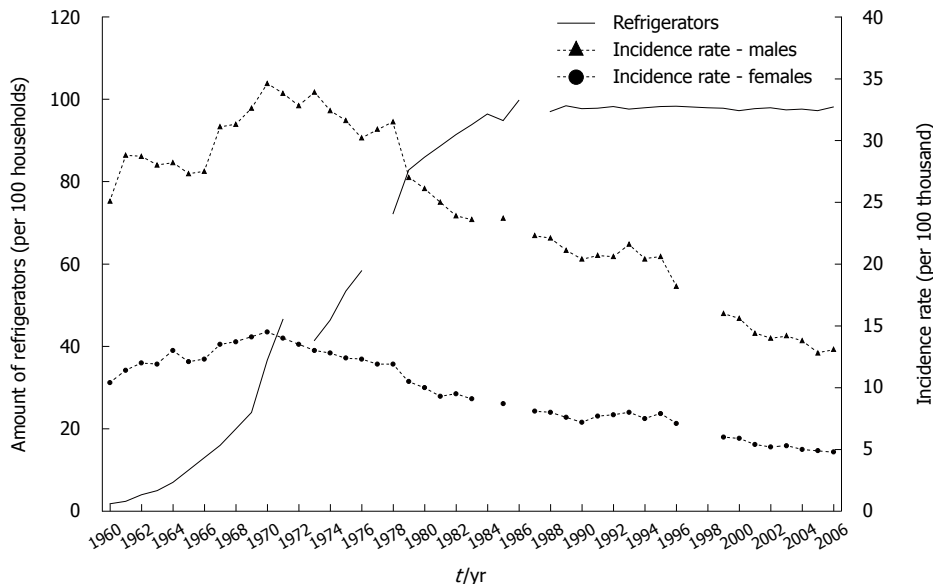


Figure 7 Equipment of households with refrigerators and gastric cancer morbidity in 1960-2006.

households. This equipment has become popular relatively late in our country. In 1960, there were only an average of 1.8 refrigerators per 100 households, which contrasts with western countries (Figure 7). The above situation has also related to the availability of refrigerators in the retail and catering trades.

Up to 1970, the number of refrigerators increased to approximate 37 per 100 households, although still only about one-third of the total number of households. Only at the beginning of the 1980s were > 90% of households equipped with refrigerators.

Estimates made for the purposes of this study demonstrated a very high correlation between the equipment of households with refrigerators and gastric cancer morbidity (Figure 8).

It has been proven that diets with high salt content have an unfavorable effect on gastric cancer. Consumption of table salt in 1929 amounted to 9.9 kg per capita (27 g/d), and decreased to 8.4 kg in 1938 (23 g/d). Despite the decrease,

this amount was still very high, which resulted mainly from its common usage as a preserving agent, which in turn, was determined by insufficient development of commercial food processing. Slow progress in this area in the early years after World War II allows us to assume that salt consumption was maintained at the same very high level observed in the pre-war period, and then decreased. According to the results of household budget surveys, table salt consumption in 2006 amounted to 0.25 kg/mo per person, that is, 3 kg/year (8.2 g/d)^[14]. This is almost threefold lower compared to consumption in 1938, but the fact that data from food balance sheets and budget surveys are not fully comparable should be mentioned. Despite this reservation, the decrease in salt consumption is unquestionable.

Data on total sodium chloride consumption, including both table salt and salt contained in food products (calculated on the basis of sodium content) showed that between 1999 and 2006, this consumption decreased significantly (Figure 9). At the same time, similar to previous

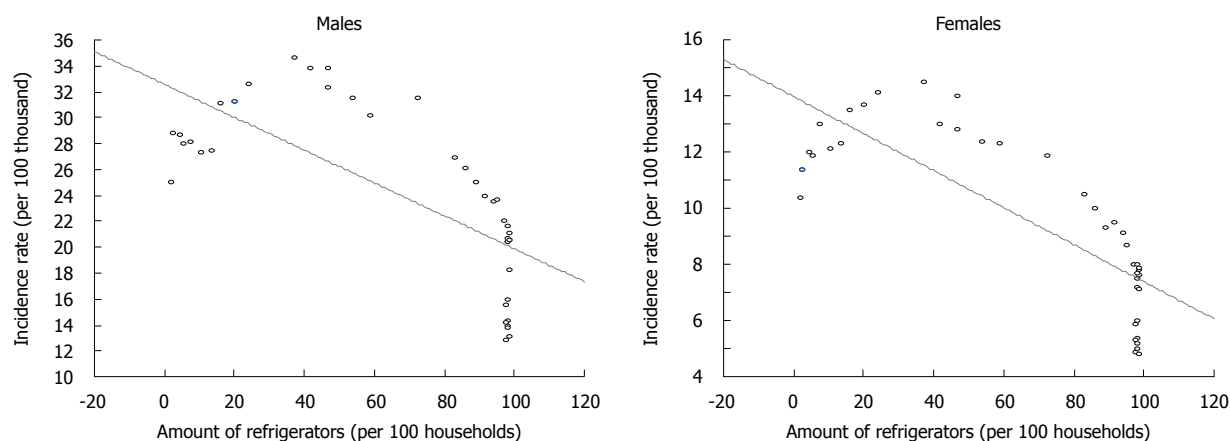


Figure 8 Correlation between equipment of households with refrigerators and gastric cancer morbidity. Spearman's rank correlation coefficient (r_s) for men: $r_s = -0.77$ ($P < 0.001$), and for women: $r_s = -0.80$ ($P < 0.001$).

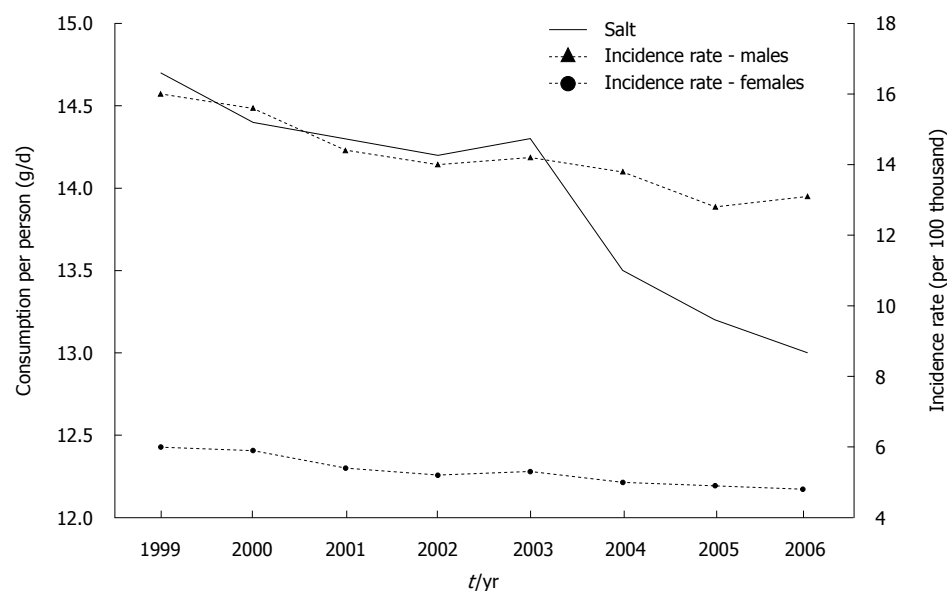


Figure 9 Total salt consumption and gastric cancer morbidity in 1999-2006. Kitchen salt and salt calculated from sodium content in food products.

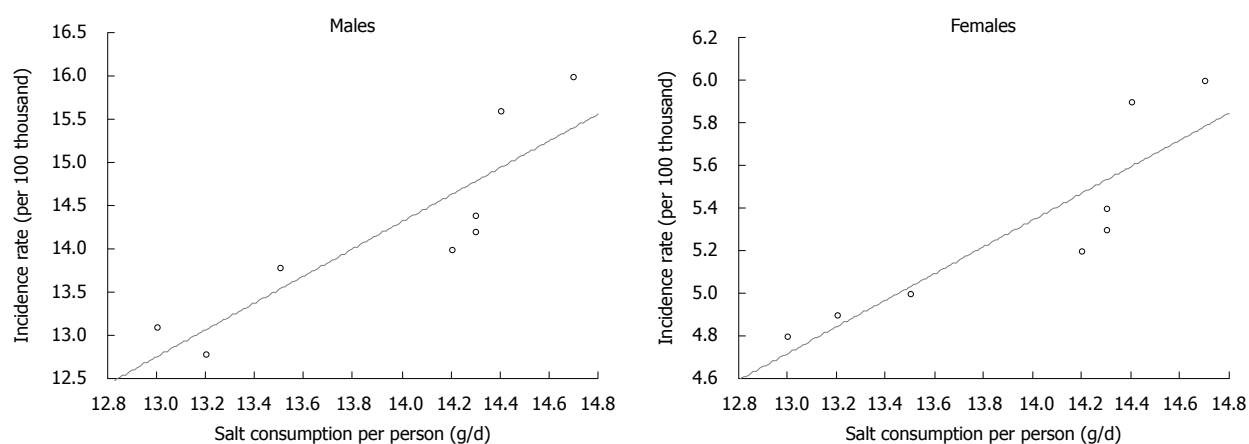


Figure 10 Correlation between total salt consumption and gastric cancer morbidity. Spearman's rank correlation coefficient (r_s) for men: $r_s = 0.97$ ($P < 0.001$), and for women: $r_s = 0.99$ ($P < 0.001$). Kitchen salt and salt calculated from sodium content in food products.

years, a regular decrease in gastric cancer morbidity has been recorded, both for men and women. Calculations

made for the purposes of this study demonstrated almost full correlation between the analyzed factors (Figure 10).

DISCUSSION

Our results enabled us to conclude that dietary factors have had a significant impact on gastric cancer risk in Poland. Their importance was underlined by the very high decrease in gastric cancer morbidity rate within the past few decades, despite a significant prevalence of *H. pylori* infection (73% of total population and 85-95% of adults aged > 25 years)^[6] and smoking, which are important, commonly accepted factors that increase gastric cancer risk.

Infection with *H. pylori* (first-class carcinogen) is considered to be an essential factor for initiation of a series of inflammatory lesions in gastric mucous membrane, from chronic superficial inflammation to pre-cancer lesions (atrophic inflammation, metaplasia, dysplasia), from which gastric cancer may develop^[18,19]. Gastric cancer grows as a result of complex interactions between genetic factors, virulence of *H. pylori* and environmental factors (dietary pattern, smoking). Our study shows that nutritional factors probably constitute one of the most important elements in these complex interactions.

For many years vitamin C has been considered as a significant factor for decreasing the risk of gastric cancer morbidity. As some studies have demonstrated, high concentrations of this vitamin in gastric juice and gastric mucous membrane can establish unfavorable conditions for development of *H. pylori* in the stomach, and its administration in high doses can even lead to eradication of this bacterium^[20]. It has been proven that vitamin C reduces growth of bacteria in culture, and the activity of urease produced by these bacteria^[21]. This enzyme enables *H. pylori* to survive in the acid environment of gastric juice, because it alkalizes the microenvironment by decomposition of urea to ammonium and carbon dioxide. However, it should be emphasized that the most important mechanism by which vitamin C can reduce the carcinogenic effect of *H. pylori* infection is destruction of free oxygen radicals that are produced in great amounts during infection^[22]. They damage the genetic material of gastric epithelial cells, which leads to mutations.

It can be assumed that increased vitamin C intake reduces the deficiency in vitamin C in smokers. Smoking, similar to *H. pylori* infection, results in lower concentration of vitamin C in gastric juice. This decrease is greater in smokers infected with *H. pylori* compared with non-smokers^[21]. An increase in consumption of fruit, vegetables and fruit juices could reduce the risk of gastric cancer development in smokers.

The impact of vitamin C on the decreased concentration of N-nitro compounds in the stomach in patients with chronic atrophic gastritis might also be significant^[23,24]. A previous study has proven that vitamin C has the ability to slow down the nitrosation process, which results in the presence of nitrosamines in the stomach; compounds that have a mutagenic effect and are considered as carcinogens^[25]. *In vitro* and *in vivo* tests have shown that ascorbic acid is the strongest inhibitor of this process^[26]. It reacts with nitrites to produce nitrogen oxides. It oxidizes itself to dehydroascorbic acid, which reduces the nitrosation reaction; details of which remain unknown. In addition,

ascorbic acid reduces transformation of nitrates to nitrites, which are direct substrates for nitrosamine production. The above is of significant importance in *H. pylori* infection, because, in the course of such infection, there is a significant increase in the concentration of nitrous compounds that are the source for nitrosamine production.

We found a very high correlation between decrease in gastric cancer morbidity and increase in dietary vitamin C content, which was related to growing consumption of fruit and vegetables. The purpose of many studies has been to examine the association between fruit and vegetable consumption and the incidence of gastric cancer. In a prospective study of Swedish women and men, consumption of vegetables was inversely associated with risk of gastric cancer after controlling for potential confounders^[27]. However, no significant association was observed between fruit consumption and gastric cancer risk. In a Canadian study that evaluated associations between dietary patterns and incident gastric cancer risk, dietary patterns characterized by increased consumption of fruit and vegetables were associated with lower risk^[28]. The association between vegetables and fruit consumption and gastric cancer risk was investigated in the Japan Public Health Center-based Prospective Study^[29]. That study suggested that vegetable and fruit intake, even in low amounts, was associated with a lower risk of stomach cancer. In contrast, a different Japanese study (Japan Collaborative Cohort Study) found no association between stomach cancer mortality and consumption of fruit and vegetables^[30]. The Netherlands Cohort Study found evidence for an inverse association between stomach cancer and the consumption of vegetables and fruit, however, it became weaker and non-significant in multivariate analysis^[31].

The nested case-control EPIC study is one of the largest prospective analyses of the association of nutrition with cancer. That study found no association between total vegetable intake or specific groups of vegetables and gastric cancer risk, except for the intestinal type, for which a negative association was found for total vegetable intake. There was no evidence of any association between fresh fruit intake and gastric cancer risk^[32]. Within the EPIC cohort, dietary vitamin C also showed no significant association with gastric cancer risk at any level of intake^[33].

In Poland, decreased salt consumption within the past few decades has probably also contributed to the decrease in gastric cancer morbidity. High concentrations of sodium chloride in the stomach facilitate damage and inflammation of mucous membranes, which leads to development of atrophic lesions, which are pre-cancerous lesions^[34]. A high-salt diet is considered to alter the viscosity of the protective mucous barrier and facilitate exposure to carcinogenic factors such as nitrates. Some information suggests that high salt intake in some way facilitates colonization with *H. pylori*^[35,36]. However, other studies have suggested that high salt intake *per se* does not promote *H. pylori* infection^[37].

According to the WCRF/AICR report, any effect of salt on stomach cancer is principally the result of regular consumption of salted or salt-preserved food, rather than salt as such^[15]. Some studies have investigated only salt added in cooking or at the table, but this is usually a small

proportion of total salt consumption. The results from such studies are liable to produce different conclusions. For example in the Netherlands Cohort Study, an inverse association was found between stomach cancer and salt added to hot meals^[38].

However many studies have confirmed the association between salt and/or salty food intake and the risk of stomach cancer. In a case-control study in Lithuania, a higher risk of gastric cancer was found in subjects who added salt to prepared meals or those who liked salty food^[39]. In a cohort study conducted in a rural area of Japan, the frequent intake of highly salted food remained as a significant risk factor for gastric cancer mortality^[40].

It is not entirely clear whether high salt intake and *H. pylori* infection are independent or interdependent risk factors. In a prospective study of a Japanese population, the effect of high salt intake on gastric carcinogenesis was strong in subjects who had atrophic gastritis and *H. pylori* infection^[37]. A study of 67 Chinese rural counties has suggested an interaction between high salt consumption and *H. pylori* infection^[41]. The significant correlation between *H. pylori* prevalence and stomach cancer mortality was only observed in counties with high levels of urinary sodium, and the significant correlation between urinary sodium and stomach cancer mortality only existed in counties with high *H. pylori* prevalence. In a case-control study in Korea, subjects with positive *H. pylori* infection and a high salt preference had a 10-fold higher risk of early gastric cancer than those without *H. pylori* infection and a low salt preference^[42].

In light of the above-mentioned results, the observed decrease in gastric cancer morbidity in Poland could be explained by the fact that, in the years when salt consumption was very high, the impact of *H. pylori* infection on carcinogenesis was significantly higher compared to the time in which dietary salt content was lower. Another factor that could have influenced the decrease in gastric cancer morbidity in Poland could be improvement in food storage, which has resulted from better equipment of households with refrigerators. This method of food storage protects fruit and vegetables against loss of vitamin C. It also prevents growth of microorganisms that can reduce nitrates contained in food products to nitrites.

The WCRF/AICR report has concluded that there is convincing evidence that use of refrigeration indirectly protects against gastric cancer^[15]. Some surveys have shown a significant association between the use of refrigeration and reduced risk of gastric cancer. According to a case-control study conducted in Northern Italy, 5% of all gastric cancer cases were attributable to less than 30 years use of an electric refrigerator^[16]. In a case-control study in Germany, the use of a refrigerator at home for ≥ 30 years compared to ≤ 24 years showed an inverse relationship with stomach cancer risk^[17]. However, in the Netherlands Cohort Study, no association was observed for duration of refrigerator use^[38]. Similarly, in a Polish case-control study, no association was found between stomach cancer risk and long-term refrigerator use^[43].

To summarize, our study shows that the effect of certain nutritional factors (increase in fruit and vegetable

consumption and related increase in dietary vitamin C and decrease in salt consumption) within the past few decades could have had a positive preventive impact on gastric cancer. The preventive effect probably depends on recognized and well-documented mechanisms reducing the risk of carcinogenesis, and perhaps on still unknown mechanisms. The prevention might also occur in populations that are exposed to other, strong, unfavorable environmental factors (carcinogens), such as *H. pylori* or smoking. Our results constitute a crucial argument for aiming to improve diet in the population through nutritional education, food production and mass catering.

COMMENTS

Background

In many countries, gastric cancer morbidity within the past few decades has reduced significantly. This phenomenon is most probably related to favorable changes in the dietary pattern in developed countries; mostly to increased consumption of fresh fruit and vegetables and decreased consumption of salt-preserved food. Lower gastric cancer morbidity is also related to lower prevalence of *Helicobacter pylori* (*H. pylori*) infection, which is considered to be essential for development of the majority of gastric cancer cases. However, Poland seems to be a particular case. Despite the fact that the percentage of people infected with *H. pylori* is unusually high, in 2006, gastric cancer morbidity rate was twofold lower compared to that in 1960.

Research frontiers

Gastric cancer ranks fourth in morbidity and second in mortality among malignant cancers worldwide. Despite the decline in incidence of this cancer, it is important to investigate the factors that could decrease or increase the risk of the disease. In this study, the relationship between diet and gastric cancer morbidity during the past few decades in Poland was evaluated.

Innovations and breakthroughs

The relationship between diet and cancer morbidity is mainly based on the results of case-control studies or prospective cohort studies. The present study was conducted using national data on diet that were derived from food balance sheets or household budget surveys.

Applications

The results suggest a positive influence of increased fruit and vegetable consumption, and related increase in dietary vitamin C content and reduced salt consumption, on the decline in gastric cancer morbidity. These results could be useful in preparation of dietary guidelines for cancer prevention.

Terminology

Metaplasia is the reversible replacement of one differentiated cell type with another mature differentiated cell type. Dysplasia is an expansion of immature cells, with a decrease in the number and location of mature cells. Urease is an enzyme that catalyzes the hydrolysis of urea into carbon dioxide and ammonia. Nitrosation is a process of converting organic compounds into nitroso derivatives.

Peer review

The manuscript is well written and underlines in an exhaustive manner the cause of the decline in gastric cancer incidence in Poland.

REFERENCES

- 1 Boyle P, Levin B. World Cancer Report 2008. World Health Organization. Lyon: IARC Press, 2008: 344-349
- 2 Coggon D, Barker DJ, Cole RB, Nelson M. Stomach cancer and food storage. *J Natl Cancer Inst* 1989; **81**: 1178-1182
- 3 La Vecchia C, Negri E, D'Avanzo B, Franceschi S. Electric refrigerator use and gastric cancer risk. *Br J Cancer* 1990; **62**: 136-137
- 4 Bruce MG, Maaroos HI. Epidemiology of *Helicobacter pylori* infection. *Helicobacter* 2008; **13** Suppl 1: 1-6
- 5 Mbulaiteye SM, Hisada M, El-Omar EM. *Helicobacter Pylori* associated global gastric cancer burden. *Front Biosci* 2009; **14**: 1490-1504
- 6 Matysiak-Budnik T, Mégraud F. Epidemiology of *Helico-*

- bacter pylori infection with special reference to professional risk. *J Physiol Pharmacol* 1997; **48** Suppl 4: 3-17
- 7 **Koszarowski T**, Gadomska H, Wronkowski Z, Romejko M. Malignant carcinoma in Poland in years 1952-1982. Warsaw: Maria Skłodowska-Curie Memorial Cancer Center and Institute of Oncology, 1987
 - 8 **Maria Skłodowska-Curie Memorial Cancer Center and Institute of Oncology**. Reports based on data of National Cancer Registry. Available from: URL: <http://85.128.14.124/krm/english/index.asp>
 - 9 **Sekuła W**, Figurska K, Jutrowska I, Barysz A. Changes in the food consumption pattern during the political and economic transition in Poland and their nutritional and health implications. *Polish Popul Rev* 2005; **27**: 141-158
 - 10 **Sekuła W**, Niedziałek Z, Figurska K, Morawska M, Boruc T. Food Consumption in Poland Converted into Energy and Nutrients, 1950-1995. Warsaw: National Food and Nutrition Institute, 1996
 - 11 **Sekuła W**. Political and economic determinants of dietary changes-focus on Poland. *Żywn Człow Metab* 2001; **28**: 146-159
 - 12 **Kunachowicz H**, Nadolna I, Przygoda B, Iwanow K. Tables of content and nutritional value of food. Warsaw: Wydawnictwo Lekarskie PZWL, 2005
 - 13 **Central Statistical Office**. Concise Statistical Yearbook 1939. Warsaw: Central Statistical Office, 1939
 - 14 **Sekuła W**, Oltarzewski M, Barysz A. An estimate of the sodium chloride consumption in Poland based on the results of the households budget surveys. *Żywn Człow Metab* 2008; **35**: 265-282
 - 15 **World Cancer Research Fund, American Institute for Cancer Research**. Food, Nutrition and the Prevention of Cancer: A Global Perspective. Washington, DC: WCRF/AICR, 2007
 - 16 **La Vecchia C**, D'Avanzo B, Negri E, Decarli A, Benichou J. Attributable risks for stomach cancer in northern Italy. *Int J Cancer* 1995; **60**: 748-752
 - 17 **Boeing H**, Frentzel-Beyme R, Berger M, Berndt V, Göres W, Körner M, Lohmeier R, Menarcher A, Männl HF, Meinhardt M. Case-control study on stomach cancer in Germany. *Int J Cancer* 1991; **47**: 858-864
 - 18 **Correa P**. Human gastric carcinogenesis: a multistep and multifactorial process--First American Cancer Society Award Lecture on Cancer Epidemiology and Prevention. *Cancer Res* 1992; **52**: 6735-6740
 - 19 **Lauwers GY**. Defining the pathologic diagnosis of metaplasia, atrophy, dysplasia, and gastric adenocarcinoma. *J Clin Gastroenterol* 2003; **36**: S37-S43; discussion S61-S62
 - 20 **Jarosz M**, Dzieniszewski J, Dabrowska-Ufniaz E, Wartanowicz M, Ziemiński S, Reed PI. Effects of high dose vitamin C treatment on *Helicobacter pylori* infection and total vitamin C concentration in gastric juice. *Eur J Cancer Prev* 1998; **7**: 449-454
 - 21 **Jarosz M**, Dzieniszewski J, Dabrowska-Ufniaz E, Wartanowicz M, Ziemiński S. Tobacco smoking and vitamin C concentration in gastric juice in healthy subjects and patients with *Helicobacter pylori* infection. *Eur J Cancer Prev* 2000; **9**: 423-428
 - 22 **Davies GR**, Simmonds NJ, Stevens TR, Sheaff MT, Banatvala N, Laurenson IF, Blake DR, Rampton DS. *Helicobacter pylori* stimulates antral mucosal reactive oxygen metabolite production in vivo. *Gut* 1994; **35**: 179-185
 - 23 **Kyrtopoulos SA**. Ascorbic acid and the formation of N-nitroso compounds: possible role of ascorbic acid in cancer prevention. *Am J Clin Nutr* 1987; **45**: 1344-1350
 - 24 **Mirvish SS**. Effects of vitamins C and E on N-nitroso compound formation, carcinogenesis, and cancer. *Cancer* 1986; **58**: 1842-1850
 - 25 **Mirvish SS**. Inhibition by vitamins C and E of in vivo nitrosation and vitamin C occurrence in the stomach. *Eur J Cancer Prev* 1996; **5** Suppl 1: 131-136
 - 26 **Mirvish SS**. Blocking the formation of N-nitroso compounds with ascorbic acid in vitro and in vivo. *Ann N Y Acad Sci* 1975; **258**: 175-180
 - 27 **Larsson SC**, Bergkvist L, Wolk A. Fruit and vegetable consumption and incidence of gastric cancer: a prospective study. *Cancer Epidemiol Biomarkers Prev* 2006; **15**: 1998-2001
 - 28 **Campbell PT**, Sloan M, Kreiger N. Dietary patterns and risk of incident gastric adenocarcinoma. *Am J Epidemiol* 2008; **167**: 295-304
 - 29 **Kobayashi M**, Tsubono Y, Sasazuki S, Sasaki S, Tsugane S. Vegetables, fruit and risk of gastric cancer in Japan: a 10-year follow-up of the JPHC Study Cohort I. *Int J Cancer* 2002; **102**: 39-44
 - 30 **Tokui N**, Yoshimura T, Fujino Y, Mizoue T, Hoshiyama Y, Yatsuya H, Sakata K, Kondo T, Kikuchi S, Toyoshima H, Hayakawa N, Kubo T, Tamakoshi A. Dietary habits and stomach cancer risk in the JACC Study. *J Epidemiol* 2005; **15** Suppl 2: S98-S108
 - 31 **Botterweck AA**, van den Brandt PA, Goldbohm RA. A prospective cohort study on vegetable and fruit consumption and stomach cancer risk in The Netherlands. *Am J Epidemiol* 1998; **148**: 842-853
 - 32 **González CA**, Pera G, Agudo A, Bueno-de-Mesquita HB, Ceroti M, Boeing H, Schulz M, Del Giudice G, Plebani M, Carneiro F, Berrino F, Sacerdote C, Tumino R, Panico S, Berglund G, Simán H, Hallmans G, Stenling R, Martinez C, Dorronsoro M, Barricarte A, Navarro C, Quiros JR, Allen N, Key TJ, Bingham S, Day NE, Linseisen J, Nagel G, Overvad K, Jensen MK, Olsen A, Tjønneland A, Büchner FL, Peeters PH, Numans ME, Clavel-Chapelon F, Boutron-Ruault MC, Roukos D, Trichopoulou A, Psaltopoulou T, Lund E, Casagrande C, Slimani N, Jenab M, Riboli E. Fruit and vegetable intake and the risk of stomach and oesophagus adenocarcinoma in the European Prospective Investigation into Cancer and Nutrition (EPIC-EURGAST). *Int J Cancer* 2006; **118**: 2559-2566
 - 33 **Jenab M**, Riboli E, Ferrari P, Sabate J, Slimani N, Norat T, Friesen M, Tjønneland A, Olsen A, Overvad K, Boutron-Ruault MC, Clavel-Chapelon F, Touvier M, Boeing H, Schulz M, Linseisen J, Nagel G, Trichopoulou A, Naska A, Oikonomou E, Krogh V, Panico S, Masala G, Sacerdote C, Tumino R, Peeters PH, Numans ME, Bueno-de-Mesquita HB, Büchner FL, Lund E, Pera G, Sanchez CN, Sánchez MJ, Arriola L, Barricarte A, Quirós JR, Hallmans G, Stenling R, Berglund G, Bingham S, Khaw KT, Key T, Allen N, Carneiro F, Mahlkne U, Del Giudice G, Palli D, Kaaks R, Gonzalez CA. Plasma and dietary vitamin C levels and risk of gastric cancer in the European Prospective Investigation into Cancer and Nutrition (EPIC-EURGAST). *Carcinogenesis* 2006; **27**: 2250-2257
 - 34 **Kono S**, Hirohata T. Nutrition and stomach cancer. *Cancer Causes Control* 1996; **7**: 41-55
 - 35 **Fox JG**, Dangler CA, Taylor NS, King A, Koh TJ, Wang TC. High-salt diet induces gastric epithelial hyperplasia and parietal cell loss, and enhances *Helicobacter pylori* colonization in C57BL/6 mice. *Cancer Res* 1999; **59**: 4823-4828
 - 36 **Beavers DG**, Lip GY, Blann AD. Salt intake and *Helicobacter pylori* infection. *J Hypertens* 2004; **22**: 1475-1477
 - 37 **Shikata K**, Kiyohara Y, Kubo M, Yonemoto K, Ninomiya T, Shirota T, Tanizaki Y, Doi Y, Tanaka K, Oishi Y, Matsumoto T, Iida M. A prospective study of dietary salt intake and gastric cancer incidence in a defined Japanese population: the Hisayama study. *Int J Cancer* 2006; **119**: 196-201
 - 38 **van den Brandt PA**, Botterweck AA, Goldbohm RA. Salt intake, cured meat consumption, refrigerator use and stomach cancer incidence: a prospective cohort study (Netherlands). *Cancer Causes Control* 2003; **14**: 427-438
 - 39 **Strumylaitė L**, Zickute J, Dudzevicius J, Dregval L. Salt-preserved foods and risk of gastric cancer. *Medicina (Kaunas)* 2006; **42**: 164-170
 - 40 **Kurosawa M**, Kikuchi S, Xu J, Inaba Y. Highly salted food and mountain herbs elevate the risk for stomach cancer death in a rural area of Japan. *J Gastroenterol Hepatol* 2006; **21**: 1681-1686
 - 41 **Wang X**, Terry P, Yan H. Stomach cancer in 67 Chinese counties: evidence of interaction between salt consumption and *Helicobacter pylori* infection. *Asia Pac J Clin Nutr* 2008; **17**: 644-650
 - 42 **Lee SA**, Kang D, Shim KN, Choe JW, Hong WS, Choi H. Effect of diet and *Helicobacter pylori* infection to the risk of early gastric cancer. *J Epidemiol* 2003; **13**: 162-168
 - 43 **Jedrychowski W**, Boeing H, Popiela T, Wahrendorf J, Tobiasz-Adamczyk B, Kulig J. Dietary practices in households as risk factors for stomach cancer: a familial study in Poland. *Eur J Cancer Prev* 1992; **1**: 297-304

Endoscopic management of occluded biliary uncovered metal stents: A multicenter experience

Panagiotis Katsinelos, Athanasios Beltsis, Grigoris Chatzimavroudis, Dimitris Paikos, George Paroutoglou, Dimitris Kapetanios, Sotiris Terzoudis, Georgia Lazaraki, Ioannis Pilpilidis, Kostas Fasoulas, Stefanos Atmatzidis, Christos Zavos, Jannis Kountouras

Panagiotis Katsinelos, Athanasios Beltsis, Grigoris Chatzimavroudis, Sotiris Terzoudis, Kostas Fasoulas, Stefanos Atmatzidis, Department of Endoscopy and Motility Unit, "G. Gennimatas" General Hospital, 55132, Thessaloniki, Greece
Dimitris Paikos, Georgia Lazaraki, Ioannis Pilpilidis, Department of Gastroenterology, Theagenion Anticancer Hospital, 54642, Thessaloniki, Greece

George Paroutoglou, Department of Gastroenterology, University Hospital of Thessaly, 41222, Larissa, Greece

Dimitris Kapetanios, Department of Gastroenterology, "G. Papanikolaou" General Hospital, 55236, Thessaloniki, Greece

Christos Zavos, Jannis Kountouras, 2nd Department of Internal Medicine, Medical School, Aristotle University of Thessaloniki, Ippokraton Hospital, 54642, Thessaloniki, Greece

Author contributions: Katsinelos P, Paikos D, Paroutoglou G, Kapetanios D, Lazaraki G and Pilpilidis I performed the endoscopies; Beltsis A, Chatzimavroudis G, Terzoudis S, Fasoulas K and Atmatzidis S analyzed and interpreted the patient data and reviewed the relative literature; Chatzimavroudis G performed the statistical analysis of data; Katsinelos P designed the study and wrote the manuscript; Zavos C and Kountouras J were major contributors in revising the manuscript critically for important intellectual content.

Correspondence to: Dr. Panagiotis Katsinelos, Assistant Professor, Head, Department of Endoscopy and Motility Unit, "G. Gennimatas" General Hospital, 55132, Thessaloniki, Greece. gchatzim@med.auth.gr

Telephone: +30-2310-211221 Fax: +30-2310-210401

Received: May 6, 2010 Revised: July 13, 2010

Accepted: July 20, 2010

Published online: January 7, 2011

Abstract

AIM: To compare diverse endoscopic interventions in the management of occluded uncovered self-expanding metal stents (SEMSs) that had been placed for palliative treatment of unresectable malignant biliary obstruction.

METHODS: A retrospective review was undertaken

in 4 tertiary endoscopic centers to determine optimal management of different types of occluded SEMSs. The technical success of performed treatment in occluded SEMSs, the patency of the stent, the need for re-intervention and the financial costs of each treatment were analyzed.

RESULTS: Fifty four patients were included in the analysis; 21 received Hanaro, 19 Wallstent and 14 Flexus. For the relief of obstruction, a plastic stent was inserted in 24 patients, a second SEMS in 25 and mechanical cleaning was performed in 5 patients. The overall median second patency rates between second SEMSs and plastic stents did not differ (133 d for SEMSs vs 106 d for plastic stents; $P = 0.856$). Similarly, no difference was found between the overall survival of SEMS and plastic stent groups, and no procedure-related complications occurred. Incremental cost analysis showed that successive plastic stenting was a cost-saving strategy at least in Greece.

CONCLUSION: Insertion of uncovered SEMSs or plastic stents is a safe and effective treatment for occluded uncovered SEMSs; insertion of plastic stents appears to be the most cost-effective strategy.

© 2011 Baishideng. All rights reserved.

Key words: Biliary obstruction; Gastrointestinal neoplasms; Stents; Cost effectiveness

Peer reviewers: Ibrahim A Al Mofleh, Professor, Department of Medicine, College of Medicine, King Saud University, PO Box 2925, Riyadh 11461, Saudi Arabia; Yuk-Tong Lee, MD, Department of Medicine and Therapeutics, Prince of Wales Hospital, Shatin, New Territories, Hong Kong, China

Katsinelos P, Beltsis A, Chatzimavroudis G, Paikos D, Paroutoglou G, Kapetanios D, Terzoudis S, Lazaraki G, Pilpilidis I, Fasoulas K, Atmatzidis S, Zavos C, Kountouras J. Endoscopic

management of occluded biliary uncovered metal stents: A multicenter experience. *World J Gastroenterol* 2011; 17(1): 98-104 Available from: URL: <http://www.wjgnet.com/1007-9327/full/v17/i1/98.htm> DOI: <http://dx.doi.org/10.3748/wjg.v17.i1.98>

INTRODUCTION

The treatment of choice for patients with unresectable malignant biliary obstructions with survival time beyond 6 mo, is the insertion of self-expanding metal stents (SEMSs), either endoscopically or percutaneously^[1-4]. The main advantages of SEMSs over plastic stents in the palliation of malignant biliary strictures are their longer patency, greater complication-free survival, and cost-effectiveness, despite the initial cost; stent patency is critical because it significantly affects patient survival^[5-7]. However, despite their large lumen, SEMSs are prone to occlusion by tissue ingrowth or overgrowth and biliary sludge/debris^[8,9], resulting in recurrent jaundice or cholangitis; unlike plastic stents, the major disadvantage of SEMSs is the difficulty with repositioning or extraction once deployed^[10]. In contrast, plastic stents are less expensive and easier to remove or to change, although they have a shorter duration of patency and a higher risk of clogging and dislocation^[11]. There are currently limited data comparing the efficacy of different treatment options and reporting on the follow-up of SEMS occlusion; only 3 studies^[12-14] described the management of occluded Wallstents and one with different types of SEMSs^[15]. As SEMSs with different characteristics are more frequently used worldwide, we anticipate that occluded SEMSs of different types will be more commonly encountered in current clinical practice. Since experience and consensus regarding the optimal management of occlusion of different types of SEMSs is lacking, such data would be useful in clinical decisions. In this respect, in countries (e.g. Greece) where endoscopic retrograde cholangiopancreatography (ERCP) costs are very low compared to those with SEMSs, initial endoscopic retrograde biliary drainage by a plastic stent appears to be less expensive.

We conducted this study to compare diverse endoscopic interventions, but with significant cost difference, in the management of different types of occluded SEMSs by 4 tertiary level centers over a 10-year period.

MATERIALS AND METHODS

A retrospective study was performed between September 1999 and December 2008 in 4 tertiary endoscopic centers in Northern ($n = 3$) and Central ($n = 1$) Greece, in patients undergoing therapeutic ERCP for unresectable malignant distal biliary obstruction. Medical records were reviewed to determine the management and clinical course until death of patients with occluded SEMSs or the end of the study period (cut-off date, January 31, 2009). Additional information was also obtained by phone contact with the patients' referring physicians or relatives. The study was approved by the institutional re-

view boards of all participating hospitals.

We identified patients through the endoscopy database. Age, sex, indication for first SEMS placement, information from outpatient visits, diagnostic tests, interventions and treatments that patients underwent at the 4 centers were reviewed. Three types of uncovered SEMS had been used. The Wallstent (Boston Scientific, USA) original SEMS is considered the industry standard. It consists of a braided stainless steel mesh with soft barbed ends, is available in 40, 60 and 80 mm lengths, and 8 or 10 mm diameter, and costs 2200 Euros. The Flexus (formerly Mometherm and Luminex) (ConMed, USA) is a highly flexible nitinol stent with flared ends. The stent is made from a laser-cut single piece of nitinol, a nickel-titanium alloy that provides a high degree of flexibility, and the interstices of the lattice work are large enough to permit cannulation and, after dilatation, placement of another stent in "Y" configuration for palliation of hilar strictures and costs 1950 Euros. The Hanaro (MI Tech, Korea) is also made of nitinol and costs 1650 Euros. The interstices of the lattice are larger compared to those of a Wallstent and similar to those of the Flexus stent.

Stent occlusion was diagnosed when a patient developed symptoms and/or signs of cholangitis (fever, right upper quadrant tenderness, and/or a ≥ 2 -fold increase in bilirubin concentration above baseline at the post endoscopic retrograde biliary drainage period) or when bilirubin concentration increased ≥ 2 -fold above baseline after endoscopic retrograde biliary drainage, even without cholangitis symptoms and/or signs or an imaging study confirming biliary obstruction recurrence. The reason for stent occlusion was classified as predominantly tumor ingrowth, tumor proximal or distal overgrowth or obstruction from sludge/debris. Tumor ingrowth and proximal overgrowth were identified when cholangiography showed a stricture within the stent (Figure 1A) or a new stricture proximal to the stent, respectively. Distal overgrowth was diagnosed by direct endoscopic visualization (Figure 1B). Occlusion from debris or sludge was diagnosed when cholangiography showed filling defects within the lumen of the stent and cleaning of the stent produced passage of debris/sludge confirmed endoscopically. Management of occluded SEMSs included insertion of either an additional uncovered SEMS (Figure 1C and D) or a 10 Fr plastic stent (length 7, 9 or 10 cm) (Figure 1E) within the first or mechanical cleaning of the occluded SEMS. Mechanical cleaning was accomplished by flushing the obstructed SEMS with normal saline solution and repetitive passage of an inflated stone extraction balloon through the SEMS. Successful endoscopic management of stent occlusion was defined as a significant decrease in bilirubin level after the procedure and/or resolution of cholangitis or imaging improvement. First stent patency was defined as the time (in days) elapsed from the initial stent placement to the first occlusion that required one of the aforementioned interventions (placement of a second SEMS, plastic stent or mechanical cleaning). Second stent patency was defined as the time (in days) elapsed from the intervention to resolve the first occlusion to the first subsequent intervention or patient death with a

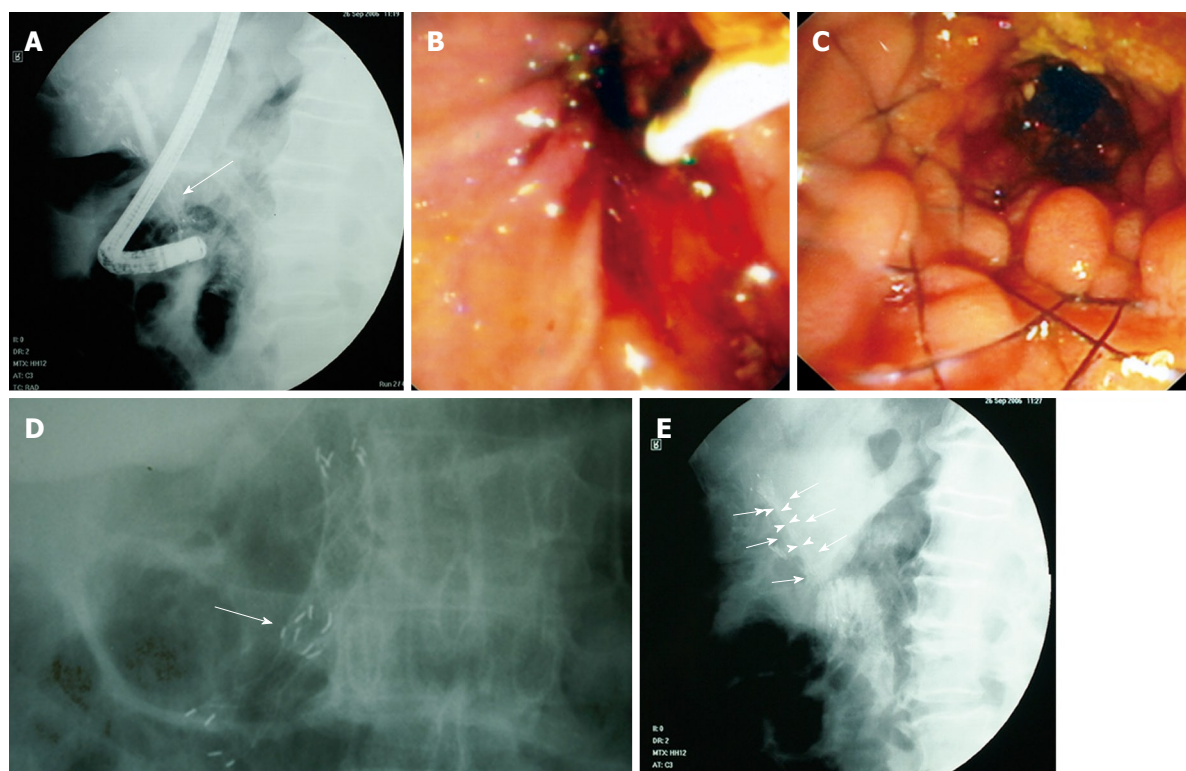


Figure 1 The reasons for stent occlusion (A, B) and the management of occluded self-expanding metal stents (C-E). A: Cholangiogram showing self-expanding metal stent (SEMS) occlusion by tumor ingrowth (arrow); B: Endoscopic view showing the distal end of a SEMS completely occluded by tumor overgrowth; C: Insertion of a new SEMS within the distally occluded stent; D: The second SEMS (arrows) was placed to resolve the occlusion by tumor overgrowth; E: Plastic biliary stent (arrowheads) passed through the occluded SEMS (arrows) that had been placed for palliation of pancreatic carcinoma.

patent stent. Overall second stent patency was defined as the time until a second SEMS became obstructed or the patient died with a patent SEMS, or, in the case of plastic stents, the time until no further stent exchanges could be performed or the patient died with a patent stent. For each treatment strategy to resolve the first SEMS obstruction (new SEMS, plastic stent or mechanical cleaning) we retrospectively counted the total amount of stents of either type used until the patient's death and calculated the cost per patient.

The incremental cost per patient (excluding the cost of the initial SEMS) was calculated by multiplying the number of stents of each type used by their price adding the cost of a balloon catheter (160 Euros) for each mechanical cleaning procedure, 70 Euros for daily hospital charges and cost of hospitalization because of cholangitis until the endpoint, and 150 Euros for each ERCP, according to the financial policy of the Greek National Health System.

Statistical analysis

The analysis was performed using the statistical program Statistical Package for Social Sciences (SPSS, version 13.0, Chicago, IL, USA). The estimation of patient survival and stent patency in the various groups of the study was performed using the Kaplan-Meier method, supplemented by the log-rank test used for comparisons of groups in relation to their survival and the duration of patency of the stents.

For the purpose of statistical data analysis the χ^2 test,

Fisher's exact test, the Mann-Whitney *U* test and the Kruskal-Wallis test were used. For comparisons between groups the Bonferroni adjusted *P*-value was used. Significance was set at $P < 0.025$.

RESULTS

Between September 1999 and December 2008, 219 patients with distal unresectable biliary obstruction received uncovered SEMSs of 3 different types, at 4 tertiary endoscopy centers. Hanaro stents were used in 74, Wallstents in 81 and Flexus stents in 64 patients. Sixty-three (28.8%) patients who underwent an ERCP because of SEMS (Hanaro 26, Wallstent 20 and Flexus 17) occlusion as determined by an increasing serum bilirubin level and/or an imaging study confirming recurrence of biliary obstruction were identified. Nine patients were excluded from the study because data were incomplete for analysis. There were 54 patients, 31 male, 23 female; median age 71 (range, 54-86 years) who were followed up until death and were included in the analysis. Of the 54 uncovered SEMSs that were occluded, 21 were Hanaro, 19 Wallstent and 14 Flexus stents (Table 1). Indications for SEMSs insertion were: pancreatic carcinoma in 28, cholangiocarcinoma in 10, papillary cancer in 8, metastatic lymphadenopathy in 7 and hepatocellular carcinoma in 1 case (Table 1). Hepatic metastases were present in 6 patients with metastatic lymphadenopathy (Table 1). The cause of first SEMS occlusion was ingrowth in 35 patients (64.8%), overgrowth

Table 1 Patient characteristics

	Flexus	Hanaro	Wallstent	All stents
No. of patients	14	21	19	54
Sex (M/F)	5/9	9/12	9/10	23/31
Median age (range)	75 (59-86)	69 (54-83)	73 (60-83)	71 (54-86)
Indication				
Pancreatic cancer	7	12	9	28
Biliary cancer	3	3	4	10
Hilar metastatic lymphadenopathy	1	4	2	7
Papillary tumor	3	2	3	8
Hepatocellular carcinoma			1	1
Hepatic metastases	1	3	2	6
Prior plastic stent	5	2	2	9
Presentation of first occlusion				
Painless jaundice	3	12	8	23
Cholangitis	11	9	11	31
Cause of obstruction				
Ingrowth	7	16	12	35
Overgrowth	4	5	5	14
Sludge and/or debris	3		2	5
Median time to first occlusion (range) (d)	228.5 (178-398)	248 (74-582)	176 (98-754)	242.5 (7-754)
Type of intervention for first occlusion				
Self-expanding metal stent	5	15	5	25
Plastic stent	6	6	12	24
Mechanical cleaning	3		2	5

Table 2 Outcomes of interventions and financial cost in the course of treatment of first self-expanding metal stent occlusion, median (range) (d)

	Plastic stent	Second SEMS	Mechanical cleaning	All types	P
Intervention for first occlusion					
No. of patients	24	25	5	54	
No further interventions required					
No. of patients	13 (54.2%)	17 (68%)	1 (20%)	31 (57.4%)	
Survival after first occlusion without further interventions	84 (40-179)	116 (62-227)	39	97 (39-227)	
Further intervention(s) required					
No. of patients	11 (45.8%)	8 (32%)	4 (80%)	23 (42.6%)	
Types of intervention	11 plastic stents insertion	5 plastic stents insertion 3 mechanical cleaning	3 plastic stents insertion 1 insertion of SEMS	19 plastic stents insertion 1 insertion of SEMS 3 mechanical cleaning	
Time to second occlusion (d)	91 (60-74)	144 (26-331)	112 (21-180)	96 (21-331)	
Overall second stent patency	106 (39-645)	133 (26-331)			0.856
Second stent patency	88 (40-179)	133 (26-331)			< 0.001
Survival after first occlusion	106 (40-645)	177 (60-870)	210 (39-390)	142 (39-870)	0.180
Number of interventions per patient	1 (1-5)	1 (1-4)	2 (1-3)	1 (1-5)	0.199
Cost per patient in euros	590 (380-2550)	2170 (1870-3620)	1020 (380-2550)	1685 (380-3620)	< 0.001

SEMS: Self-expanding metal stent.

in 14 patients (25.9%) and sludge/debris in 5 patients (9.3%) (Table 1). There was no difference in the etiology of occlusion between the 3 types of SEMS ($P = 0.773$) (Table 1). The first occlusion presented as cholangitis in 31 (57.4%) and painless jaundice in 23 (42.6%) patients, without any significant difference between the 3 types of SEMS ($P = 0.116$) (Table 1). A plastic stent had been placed before SEMS insertion in 9 patients (Table 1). The overall median (range) duration of the first SEMS patency was 242.5 (74-754) d. More specifically, for Hanaro stents the patency period was 248 (74-582) d, for Wallstents 176 (98-754) d, and for Flexus stents 228.5 (178-398) d, with

no significant difference between them ($P = 0.936$) (Table 1 and Figure 2A).

The outcomes and financial costs of interventions in the course of treatment of first SEMS occlusion are summarized in Table 2. From the 25 patients managed by a second SEMS insertion, 17 (68%) died after a median 116 (62-227) d without requiring further intervention, but 8 (32%) patients presented with re-occluded stents after a median 144 (26-331) d (Table 2). Those with re-occluded stents were treated with either plastic stent insertion (5 patients) or mechanical cleaning (3 patients) and 9 plastic stents were required in total (Table 2). From the 24

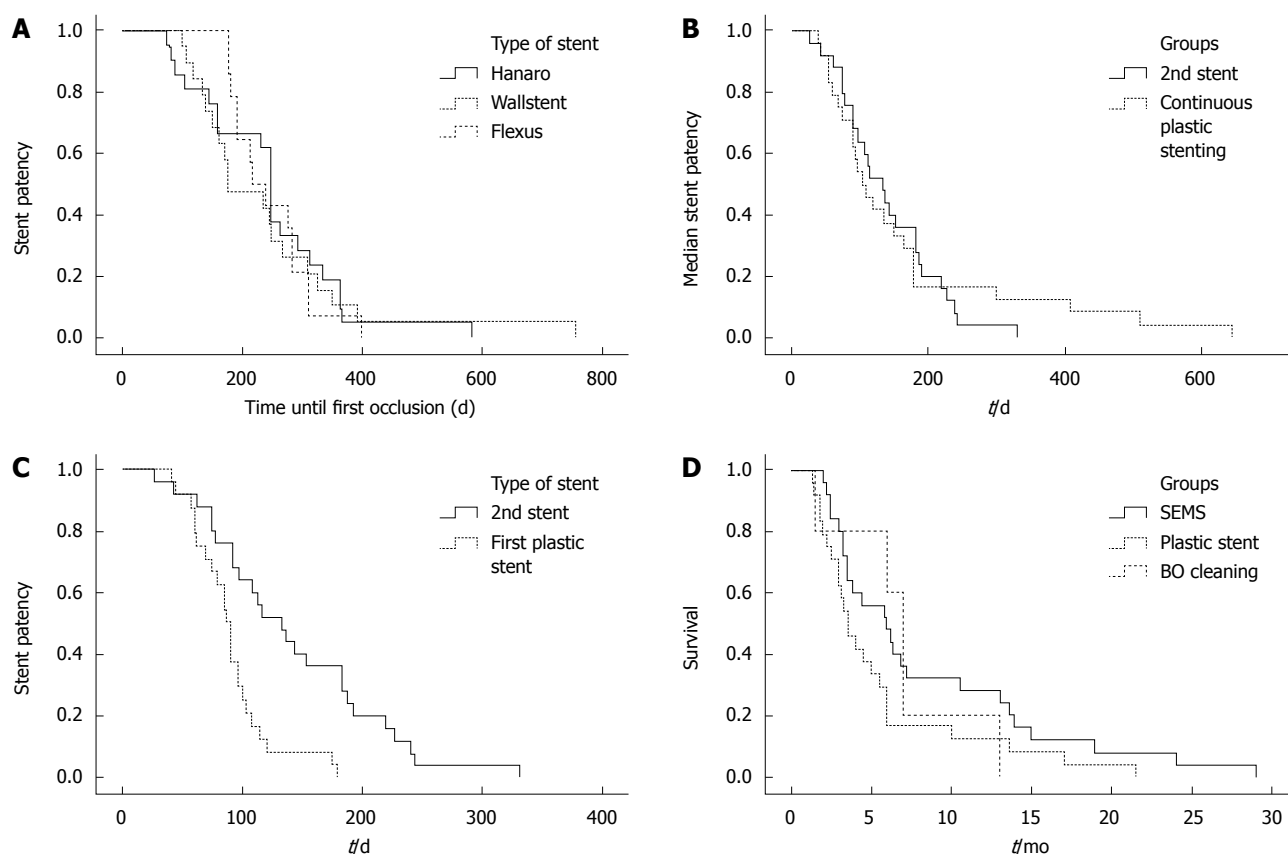


Figure 2 Patency of different stent (A-C) and survival after first self-expanding metal stent occlusion (D). A: Patency of 3 self-expanding metal stent (SEMS) until first occlusion; B: Patency of second SEMS vs overall plastic stent patency; C: Patency of second SEMS vs first plastic stent; D: Survival after first SEMS occlusion.

patients managed by plastic stent insertion, 13 patients (54.2%) died after a median 84 (40-179) d without requiring further intervention but 11 (45.8%) patients presented with re-occluded stents after a median 91 (60-74) d and were treated with plastic stent exchanges as many times as required, resulting in the insertion of 20 additional plastic stents (Table 2). In 2 patients, both with papillary tumors, stent exchange was unsuccessful on the third and fourth ERCP due to duodenal invasion by the tumor. They refused further intervention and died. Of the 5 patients who were treated by mechanical cleaning alone, only one (20%) required no further interventions and died 39 d later, while the other 4 (80%) presented with a second obstruction after a median 112 (21-180) d, treated by plastic stent insertion in 3 patients and SEMS insertion in one (Table 2). Two patients required an additional plastic stent. Overall, 31 patients (57.4%) required no further interventions until their death after a median 97 (39-227) d and 23 patients (42.6%) presented with a second obstruction after a median 96 (21-331) d (Table 2).

Apart from cholangitis, other complications including post-endoscopic retrograde biliary drainage bleeding, cholecystitis, pancreatitis or stent migration were not observed and there was no complication-related mortality.

Median overall patency of the second SEMS was 133 (range, 26-331) d and for successive plastic stenting 106 (range, 39-645) d ($P = 0.856$) (Figure 2B). However, when compared with the patency of the first plastic stent, which

was 88 (range, 40-179) d, the patency of the second SEMS was significantly longer ($P < 0.001$) (Figure 2C). Survival after the first occlusion was 142 (range, 39-870) d: 106 (range, 40-645) d for plastic stent placement, 177 (range, 60-870) d for a second SEMS, and 210 (range, 39-870) d for mechanical cleaning ($P = 0.180$) (Figure 2D).

Overall, the average cost was 1685 (380-3620) Euros per patient: 2170 (1870-3620) Euros per patient for insertion of a second SEMS at initial obstruction, 590 (380-2550) Euros per patient for insertion of a plastic stent at the same setting and 1020 (380-2550) Euros per patient treated by mechanical cleaning ($P < 0.001$) (Table 2).

DISCUSSION

Although endoscopic biliary stenting is accepted as the treatment of choice in patients with inoperable malignant biliary obstruction, and has been associated with reduced morbidity and short hospital stay, the major problem faced after endoscopic stent insertion is stent occlusion. Relative data on the optimal management of occluded SEMSs, are very limited to case reports and small retrospective studies^[12-15]. Our retrospective multicenter series includes the largest number of patients with occluded SEMSs managed endoscopically and is the second study to include different types of occluded SEMSs, thereby better depicting the daily practice worldwide. The initial occlusion rate of SEMSs in our series was 28.8%, consistent with that

of previous studies^[12,13]. Moreover, the occlusion rate was similar between the 3 types of SEMS (Hanaro 35.1%, Wallstent 24.7%, Flexus 26.6%), irrespective of the different design and material. The major cause of SEMSs occlusion was tumor ingrowth (64.8%), confirming the previous observations^[12-15]. This is thought to have been secondary to the growth of tumors within the interstices of the uncovered SEMSs. It is interesting that the rate of ingrowth was similar among the 3 types of SEMS (Hanaro 76.2%, Wallstent 63.2%, Flexus 50%) despite the larger interstices of mesh in Hanaro and Flexus stents.

Our finding that mechanical cleaning of sludge/debris is an ineffective treatment for occluded SEMSs, presenting with high re-occlusion rates in a short time (median: 94 d, range: 21-180) is compatible with other series^[12-14]. Notably, sludge is accrued because the stent surface allows for the adherence of proteins, glycoproteins, or bacteria and the bile flow is insufficient to clean the surface; stent clogging may be caused by microbiological adhesion and biliary stasis. In this regard, treatment with antibiotics and/or ursodeoxycholic acid to prevent clogging of biliary stents in patients with malignant stricture of the biliary tract, however, cannot be recommended routinely on the basis of the existing randomized clinical trials^[16].

Placement of either a second SEMS, independent of its type, or a plastic stent inside the occluded SEMS, was equally effective in resolving the jaundice or the symptoms of cholangitis, in accordance with other series^[12-15,17]. We found that the overall stent patency between second SEMSs and plastic stents for resolution of the first obstruction was not statistically different (133 d *vs* 106 d, $P = 0.856$) (Figure 2B). However, the patency of the second SEMS was significantly longer than that of the first plastic stent [133 (26-331) d *vs* 88 (40-179) d, $P < 0.001$] (Figure 2C), confirming the previous series. There was no difference on second SEMS patency between the 3 types of SEMS [Hanaro 144 (range, 42-331) d, Wallstent 97 (range, 26-243) days, Flexus 133 (range, 92-184) d] ($P = 0.943$). SEMS patency before the first occlusion was not predictive of the duration of the patency of the SEMS placed within the initial stent. This is in contrast to the observation of Katsinelos *et al*^[11] of a positive correlation between the patency of the first Wallstent and the period of patency of the second Wallstent, but in accordance with Bueno *et al*^[3] and Rogart *et al*^[13] studies.

Kaplan-Meier analysis in our study revealed that survival of patients with a second SEMSs was similar to that with plastic stents (Figure 2D). Interestingly, patients who underwent a second SEMS placement had fewer subsequent interventions compared with patients who had plastic stents inserted, but the difference was not statistically significant ($P = 0.33$).

Several studies^[3-10,12-15] have attempted to address the cost-effective management of occluded SEMS for malignant biliary obstruction. In our series, incremental cost analysis showed that the most cost-effective method appeared to be plastic stent insertion ($P < 0.001$) unlike the previous studies^[3,12,13], but similar to the study by Abraham *et al*^[11]. However, based on the special characteristics of

our health system, our financial analysis is disproportionately influenced by the direct cost of stents, either SEMS or plastic, over the cost of ERCPs and the indirect cost of hospitalizations related to stent occlusion. Therefore, the cost-effectiveness data from our study may not apply directly to countries with different health systems.

Our study has limitations similar to those of prior studies, with retrospective analysis and a relatively small number of patients having a variety of causes for SEMS placement and expected survival. Because the subjects were not randomly allocated, firm conclusions cannot be drawn until a prospective randomized and stratified study in larger numbers confirms our findings. However, data from such a study are unlikely to be available in the near future.

In conclusion, our findings support the use of plastic stents as the main intervention in patients with occluded SEMSs despite the increased number of subsequent ERCPs, because it is cost-effective, especially in health systems where the cost of expendables markedly exceeds that of the medical services.

COMMENTS

Background

Self-expandable metal stents (SEMSs) remain the treatment of choice for patients with unresectable malignant biliary stricture and survival time beyond 6 mo. However, despite their large lumen, they are prone to occlusion. The reported experience on the management of occluded SEMSs of different types is limited.

Research frontiers

Experience and consensus on the optimal management of occlusion of different types of SEMSs, which are used more frequently worldwide is lacking. However, such data are useful in clinical decisions about the treatment of occluded biliary uncovered SEMSs.

Innovations and breakthroughs

The present retrospective multicenter study investigated the diverse endoscopic interventions in the management of different types of occluded SEMSs. The findings support the use of a cost-effective plastic stent as the main intervention in patients with occluded uncovered SEMSs.

Applications

These findings are of potential financial importance especially in healthy systems where the cost of SEMSs markedly exceeds the medical service costs.

Terminology

Uncovered SEMSs are occluded by tissue ingrowth or overgrowth and biliary sludge/debris, resulting in recurrent jaundice or cholangitis.

Peer review

In this good retrospective study, the authors found that a cheap plastic biliary stent was as good as an expensive SEMS for the treatment of occluded SEMSs.

REFERENCES

- 1 Abraham NS, Barkun JS, Barkun AN. Palliation of malignant biliary obstruction: a prospective trial examining impact on quality of life. *Gastrointest Endosc* 2002; **56**: 835-841
- 2 Arguedas MR, Heudebert GH, Stinnett AA, Wilcox CM. Biliary stents in malignant obstructive jaundice due to pancreatic carcinoma: a cost-effectiveness analysis. *Am J Gastroenterol* 2002; **97**: 898-904
- 3 Bueno JT, Gerdes H, Kurtz RC. Endoscopic management of occluded biliary Wallstents: a cancer center experience. *Gastrointest Endosc* 2003; **58**: 879-884
- 4 Katsinelos P, Kountouras J, Paroutoglou G, Paikos D, Mos-

- chos J, Chatzimavroudis G, Zavos C, Makrigrannis E. Uncovered Hanaro Versus Luminex metal stents for palliation of malignant biliary strictures. *J Clin Gastroenterol* 2008; **42**: 539-545
- 5 **Dauids PH**, Groen AK, Rauws EA, Tytgat GN, Huibregtse K. Randomised trial of self-expanding metal stents versus polyethylene stents for distal malignant biliary obstruction. *Lancet* 1992; **340**: 1488-1492
- 6 **Hawes RH**. Diagnostic and therapeutic uses of ERCP in pancreatic and biliary tract malignancies. *Gastrointest Endosc* 2002; **56**: S201-S205
- 7 **Kaassis M**, Boyer J, Dumas R, Ponchon T, Coumaros D, Delcenserie R, Canard JM, Fritsch J, Rey JF, Burtin P. Plastic or metal stents for malignant stricture of the common bile duct? Results of a randomized prospective study. *Gastrointest Endosc* 2003; **57**: 178-182
- 8 **Kim HS**, Lee DK, Kim HG, Park JJ, Park SH, Kim JH, Yoo BM, Roe IH, Moon YS, Myung SJ. Features of malignant biliary obstruction affecting the patency of metallic stents: a multicenter study. *Gastrointest Endosc* 2002; **55**: 359-365
- 9 **Maire F**, Hammel P, Ponsot P, Aubert A, O'Toole D, Hentic O, Levy P, Ruszniewski P. Long-term outcome of biliary and duodenal stents in palliative treatment of patients with unresectable adenocarcinoma of the head of pancreas. *Am J Gastroenterol* 2006; **101**: 735-742
- 10 **Katsinelos P**, Paikos D, Kountouras J, Chatzimavroudis G, Paroutoglou G, Moschos I, Gatopoulou A, Beltsis A, Zavos C, Papaziogas B. Tannenbaum and metal stents in the palliative treatment of malignant distal bile duct obstruction: a comparative study of patency and cost effectiveness. *Surg Endosc* 2006; **20**: 1587-1593
- 11 **Katsinelos P**, Kountouras J, Paroutoglou G, Chatzimavroudis G, Paikos D, Zavos C, Karakousis K, Gelas G, Tzilves D. Migration of plastic biliary stents and endoscopic retrieval: an experience of three referral centers. *Surg Laparosc Endosc Percutan Tech* 2009; **19**: 217-221
- 12 **Menon K**, Barkun A. Management of occluded biliary Wallstents. *Gastrointest Endosc* 1999; **49**: 403-405
- 13 **Rogart JN**, Boghos A, Rossi F, Al-Hashem H, Siddiqui UD, Jamidar P, Aslanian H. Analysis of endoscopic management of occluded metal biliary stents at a single tertiary care center. *Gastrointest Endosc* 2008; **68**: 676-682
- 14 **Tham TC**, Carr-Locke DL, Vandervoort J, Wong RC, Lichtenstein DR, Van Dam J, Ruymann F, Chow S, Bosco JJ, Qaseem T, Howell D, Pleskow D, Vannerman W, Libby ED. Management of occluded biliary Wallstents. *Gut* 1998; **42**: 703-707
- 15 **Togawa O**, Kawabe T, Isayama H, Nakai Y, Sasaki T, Arizumi T, Matsubara S, Ito Y, Yamamoto N, Sasahira N, Hirano K, Tsujino T, Toda N, Tada M, Yoshida H, Omata M. Management of occluded uncovered metallic stents in patients with malignant distal biliary obstructions using covered metallic stents. *J Clin Gastroenterol* 2008; **42**: 546-549
- 16 **Galandi D**, Schwarzer G, Bassler D, Allgaier HP. Ursodeoxycholic acid and/or antibiotics for prevention of biliary stent occlusion. *Cochrane Database Syst Rev* 2002; CD003043
- 17 **Moss AC**, Morris E, Mac Mathuna P. Palliative biliary stents for obstructing pancreatic carcinoma. *Cochrane Database Syst Rev* 2006; CD004200

S- Editor Tian L L- Editor Cant MR E- Editor Ma WH

Effect of ginger on gastric motility and symptoms of functional dyspepsia

Ming-Luen Hu, Christophan K Rayner, Keng-Liang Wu, Seng-Kee Chuah, Wei-Chen Tai, Yeh-Pin Chou, Yi-Chun Chiu, King-Wah Chiu, Tsung-Hui Hu

Ming-Luen Hu, Keng-Liang Wu, Seng-Kee Chuah, Wei-Chen Tai, Yeh-Pin Chou, Yi-Chun Chiu, King-Wah Chiu, Tsung-Hui Hu, Division of Hepatogastroenterology, Department of Internal Medicine, Chang Gung Memorial Hospital-Kaohsiung Medical Center, Chang Gung University College of Medicine, Kaohsiung 83301, Taiwan

Christophan K Rayner, Discipline of Medicine, University of Adelaide, Royal Adelaide Hospital, Adelaide SA 5000, Australia

Author contributions: Wu KL, Rayner CK and Hu TH designed the research; Hu ML, Wu KL, Tai WC, Chou YP and Chuah SK performed the research; Wu KL, Chiu YC and Chuah SK collected and analyzed the data; Hu ML and Chiu KW wrote the paper; Rayner CK and Wu KL revised the paper.

Supported by Grant from National Research Program from National Science Council (NMRP870071)

Correspondence to: Dr. Keng-Liang Wu, Division of Hepatogastroenterology, Department of Internal Medicine, Chang Gung Memorial Hospital-Kaohsiung Medical Center, Chang Gung University College of Medicine, Kaohsiung 83301, Taiwan. kengliang_wu@yahoo.com.tw

Telephone: +886-7-7317123 Fax: +886-7-7322402

Received: July 21, 2010 Revised: August 16, 2010

Accepted: August 23, 2010

Published online: January 7, 2011

Abstract

AIM: To evaluate the effects of ginger on gastric motility and emptying, abdominal symptoms, and hormones that influence motility in dyspepsia.

METHODS: Eleven patients with functional dyspepsia were studied twice in a randomized double-blind manner. After an 8-h fast, the patients ingested three capsules that contained ginger (total 1.2 g) or placebo, followed after 1 h by 500 mL low-nutrient soup. Antral area, fundus area and diameter, and the frequency of antral contractions were measured using ultrasound at frequent intervals, and the gastric half-emptying time was calculated from the change in antral area. Gastrointestinal sensations and appetite were scored using

visual analog questionnaires, and blood was taken for measurement of plasma glucagon-like peptide-1 (GLP-1), motilin and ghrelin concentrations, at intervals throughout the study.

RESULTS: Gastric emptying was more rapid after ginger than placebo [median (range) half-emptying time 12.3 (8.5-17.0) min after ginger, 16.1 (8.3-22.6) min after placebo, $P \leq 0.05$]. There was a trend for more antral contractions ($P = 0.06$), but fundus dimensions and gastrointestinal symptoms did not differ, nor did serum concentrations of GLP-1, motilin and ghrelin.

CONCLUSION: Ginger stimulated gastric emptying and antral contractions in patients with functional dyspepsia, but had no impact on gastrointestinal symptoms or gut peptides.

© 2011 Baishideng. All rights reserved.

Key words: Ginger (*Zinger officinale*); Functional dyspepsia; Gastric emptying; Antral contraction; Abdominal ultrasound; Ghrelin; Glucagon-like peptide-1; Motilin

Peer reviewer: Ted Dinan, Professor, Department of Psychiatry, Cork University Hospital, Wilton, Cork, C1, Ireland

Hu ML, Rayner CK, Wu KL, Chuah SK, Tai WC, Chou YP, Chiu YC, Chiu KW, Hu TH. Effect of ginger on gastric motility and symptoms of functional dyspepsia. *World J Gastroenterol* 2011; 17(1): 105-110 Available from: URL: <http://www.wjgnet.com/1007-9327/full/v17/i1/105.htm> DOI: <http://dx.doi.org/10.3748/wjg.v17.i1.105>

INTRODUCTION

Functional dyspepsia is a clinical syndrome that is characterized by chronic or recurrent upper abdominal pain or discomfort in the absence of underlying organic disease

that can explain the symptoms^[1]. Pharmacological therapy for patients with functional dyspepsia remains unsatisfactory^[2]. The results of controlled trials have generally been disappointing, and only small benefits relative to placebo have been found with histamine H₂-receptor antagonists^[3], proton-pump inhibitors^[4], and *Helicobacter pylori* eradication^[5]. In addition to poor efficacy, pharmacological agents (e.g. cisapride) are associated with a risk of adverse effects.

Herbal medicine might be an attractive alternative based on the perception of its natural approach and low risk of adverse effects. However, the lack of standardization of herbal ingredients has limited the number of rigorous clinical studies available.

Ginger (*Zingiber officinale*) has been used to treat a number of medical conditions, including those affecting the digestive tract^[6,7], such as dyspepsia, flatulence, nausea and abdominal pain. However, the mechanisms responsible for its beneficial effects are not well understood. Yamahara *et al.*^[8] and Micklefield *et al.*^[9] have reported that gastrointestinal motility is enhanced by ginger and its active constituents, but they did not measure gastric emptying. We previously have shown that ginger increases the frequency of antral contractions and accelerates gastric emptying of a low-nutrient liquid in healthy volunteers^[10].

There have been few studies on the effects of ginger in patients with functional dyspepsia. We hypothesized that acceleration of gastric emptying in patients with functional dyspepsia might be accompanied by a reduction in upper gastrointestinal symptoms, and that its action on gastric motility could be mediated *via* increased secretion of ghrelin^[11] or motilin^[12], or by suppression of glucagon-like peptide-1 (GLP-1)^[13].

MATERIALS AND METHODS

Patients

Eleven patients diagnosed with functional dyspepsia on the basis of Rome III criteria were invited to take part. Patients had persistent or recurrent upper abdominal pain or discomfort, which was characterized by the presence of one or more of early satiety, postprandial fullness, bloating, and nausea. Symptoms had been present for at least 6 wk within the preceding 6 mo, without an identifiable structural or biochemical abnormality to which they could be attributed^[1]. Symptoms of retrosternal pain, burning, and regurgitation were considered features of gastroesophageal reflux disease, rather than of functional dyspepsia. Therefore, patients who had predominantly reflux-related symptoms were excluded. Patients were screened by physical examination, laboratory tests (blood picture, fasting glucose, and liver-function tests), abdominal ultrasonography, and upper gastrointestinal endoscopy to exclude other causes of dyspepsia, and none was taking any medication known to affect gastric motility.

Each subject was studied on two afternoons, separated by at least 7 d, in double-blind randomized order. Following a fast of 8 h for solids and liquids, the patients ingested three capsules that contained a total of 1.2 g ginger root powder (Ginger Root; Nature's Way Products

Inc., Springville, UT, USA), or three identical placebo capsules that contained starch, together with 50 mL water. One hour later, they consumed 500 mL chicken and corn soup (United Kanboo, Taipei, Taiwan), which contained 118.6 kcal (2.6 g protein, 2.6 g fat, 21.2 g carbohydrate). The soup was boiled and subsequently cooled to 37°, and was consumed over 5 min ($t = -5$ to 0 min). All patients underwent trans-abdominal ultrasound to measure antral area, fundic area and diameter^[14], and antral contractions at intervals using an Aloka SSD-2000 CL Ultrasound Machine (Aloka, Tokyo, Japan) with a 3.5-MHz annular array probe. Antral contractions were defined as > 50% change in antral area compared to the relaxed area ($\Delta A/A$)^[15], and their frequency as the number of contractions during 5-min periods beginning at 5, 30, 60 and 120 min after soup ingestion. A questionnaire with visual analogue scales (VASs)^[16] for symptoms pain, nausea, abdominal discomfort, bloating and abdominal fullness, was administered at 10-min intervals between $t = -10$ and 90 min. Grading was made on a 100-mm unmarked line between "no symptoms" at one end and "excruciating symptoms" at the other. Venous blood was sampled at $t = -10$, 30, 60 and 90 min for measurement of blood glucose and plasma peptides. Blood glucose concentrations were determined immediately using a portable blood glucose meter (MediSense Companion 2 meter; MediSense Inc., Waltham, MA, USA). The accuracy of this method has been confirmed using the hexokinase technique^[17]. The remainder of the samples was collected into ice-chilled EDTA-treated tubes that contained 400 KIU/mL aprotinin. Plasma was separated and samples stored at -70°C for subsequent analysis of GLP-1, ghrelin and motilin concentrations, using ELISA. Ghrelin was measured by a commercial ELISA kit (Phoenix Pharmaceuticals Inc., Burlingame, CA, USA); intra- and interassay coefficients of variation (CV) were < 5% and < 9%, respectively; motilin and GLP-1 were also measured by a commercial ELISA kit from Phoenix Pharmaceuticals.

Statistical analysis

Gastric half-emptying time (T₅₀) was defined as the time for antral area to decrease to half the maximum increase above baseline, and was calculated by linear interpolation between time points^[10]. The values on the two study days were compared using the Wilcoxon signed rank test. Antral area, fundic area and diameter, frequency of antral contractions and gastrointestinal sensation scores were compared using repeated measures ANOVA. Results are shown as median and range for T₅₀, and mean \pm SD for other variables. $P < 0.05$ was considered significant.

RESULTS

All subjects tolerated the study well.

Antral area and gastric emptying

Gastric emptying was more rapid after ginger than placebo [T₅₀: 12.3 (8.5-17.0) min *vs* 16.1 (8.3-22.6) min, P

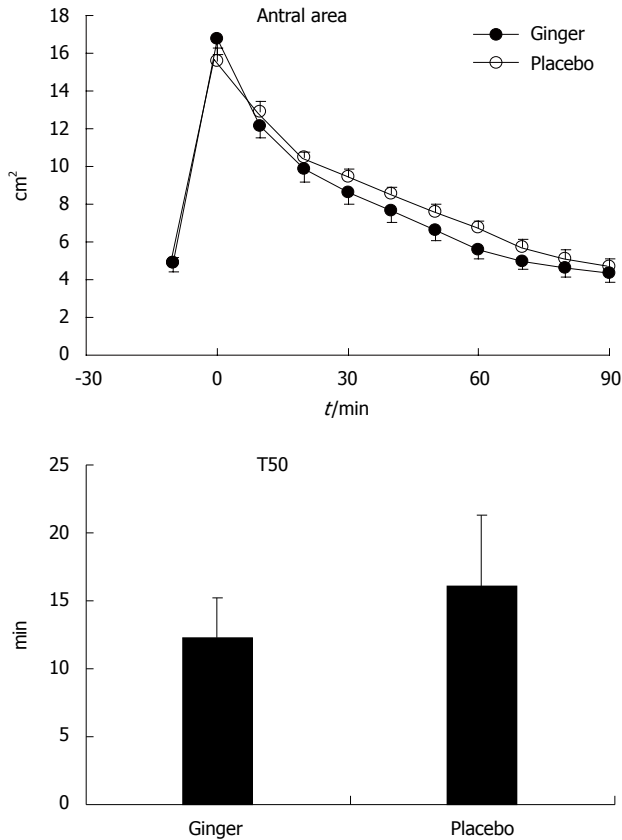


Figure 1 Antral area after ginger and placebo in patients with functional dyspepsia who consumed 500 mL low-nutrient soup between -5 and 0 min. Gastric emptying was more rapid after ginger than with placebo [T50: 12.3 (8.5-17.0) min vs 16.1 (8.3-22.6) min, $P \leq 0.05$]. There was a trend for smaller antral area after ginger ($P = 0.13$); data are means \pm SE, $n = 11$.

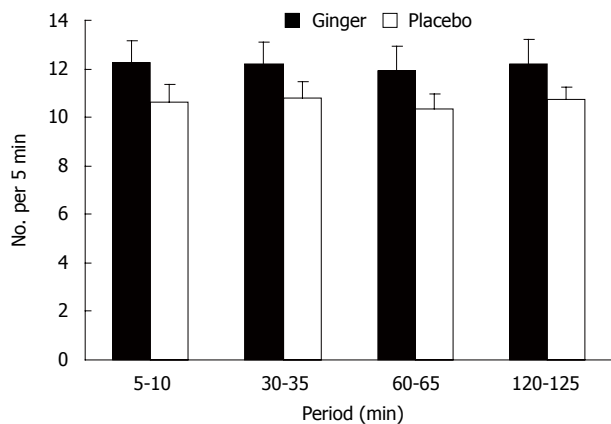


Figure 2 Frequency of antral contractions after ginger and placebo in patients with functional dyspepsia. There was a trend for a higher frequency of antral contractions after ginger ($P = 0.06$). Data are means \pm SE, $n = 11$.

≤ 0.05]. There was a trend for smaller antral area after ginger, although this did not reach statistical significance ($P = 0.13$) (Figure 1).

Antral contractions

There was a trend for more antral contractions after ginger compared to placebo ($P = 0.06$) (Figure 2).

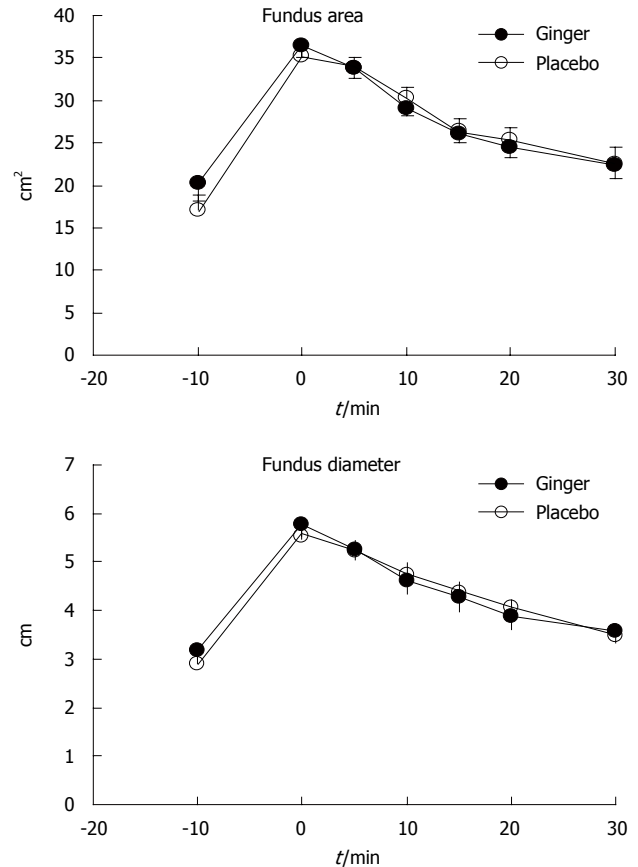


Figure 3 Fundus area and diameter in patients with functional dyspepsia. There was no difference in either measure between ginger and placebo. Data are means \pm SE, $n = 11$.

Fundic area and diameter

Fundus dimensions did not differ between the two study days (Figure 3).

Gastrointestinal sensations

Soup ingestion was associated with increased fullness and bloating, and decreased hunger and appetite scores, but without any difference between ginger and placebo. There were no significant changes in nausea or abdominal discomfort from baseline, or any differences in these sensations between study days (Figure 4).

Gastrointestinal peptide concentrations

There were no differences in plasma concentrations of motilin, ghrelin, or GLP-1 between the two study days (Figure 5).

DISCUSSION

In this study, we demonstrated that ginger increased the rate of gastric emptying in patients with functional dyspepsia when compared to placebo, and that this was associated with a trend for an increased frequency of gastric antral contractions, but no change in dimensions of the fundus. This was consistent with our previous study in healthy volunteers^[10]. Despite more rapid emptying, ginger

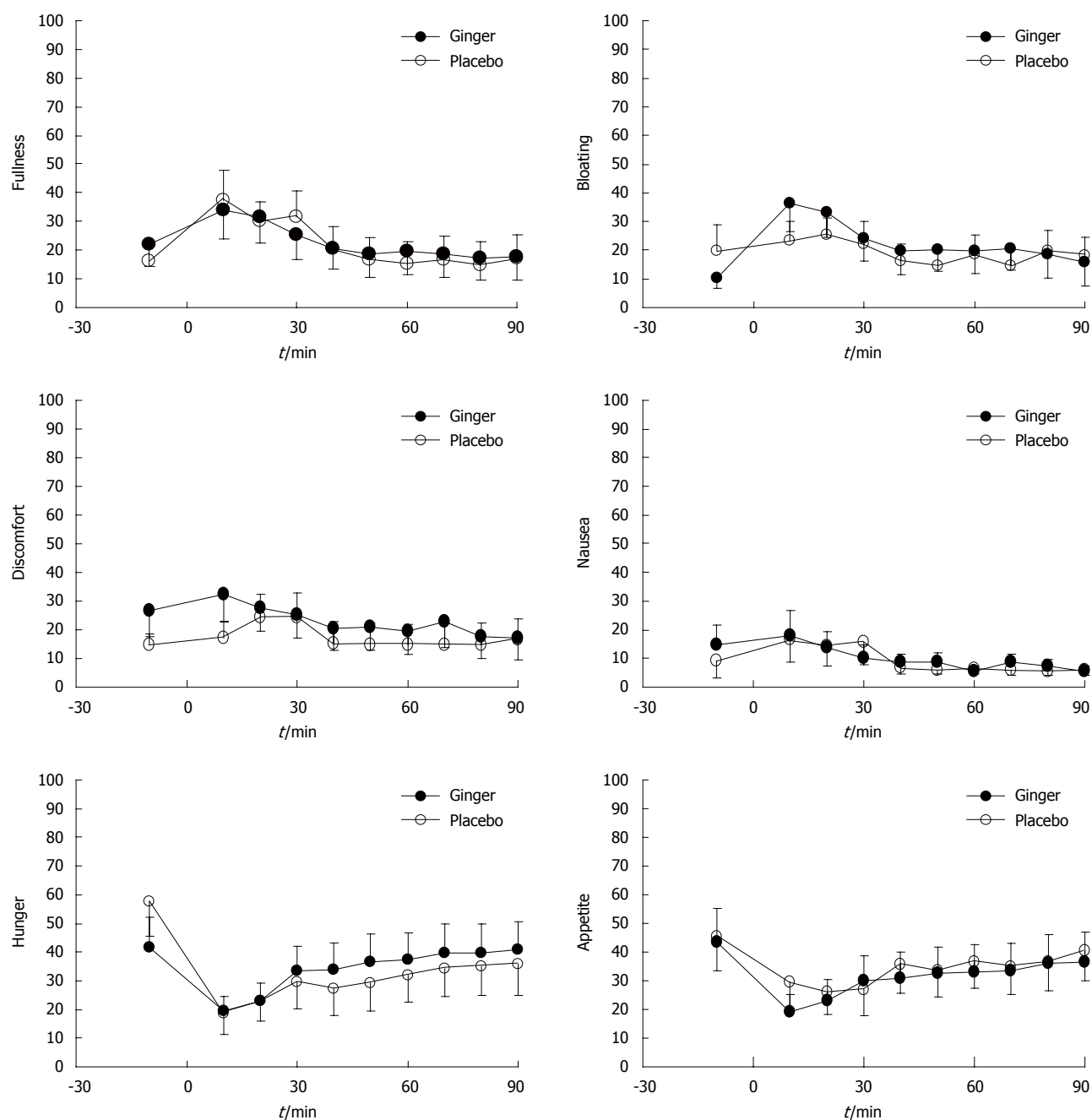


Figure 4 Visual analogue scale scores for gastrointestinal symptoms after ginger and placebo in patients with functional dyspepsia who consumed 500 mL low-nutrient soup between -5 and 0 min. There was no difference in any sensation between the two study days. Data are means \pm SE, $n = 11$.

had no effect on gastrointestinal symptom scores in our patients.

About 40% of patients with functional dyspepsia have abnormally delayed gastric emptying^[18], and prokinetic medications have often been used in the treatment of this condition^[19]. We did not select our dyspeptic patients on the basis of delayed gastric emptying, and as a group, their rate of gastric emptying was comparable to the healthy volunteers that we had studied previously using the same technique^[10]. It is possible that ginger could have improved symptoms in a more selected group of patients who had delayed emptying, and in particular, those with an abnormally wide antrum, a feature that has been associated particularly with bloating^[20].

It is also possible that the lack of symptomatic improvement with ginger was related to the low-nutrient nature of the soup meal. Although this meal was associated with increases in fullness and bloating, the changes were modest. A meal with a higher caloric load, particularly one that contained more lipid^[21], might have provoked more symptoms, from which it would be possible to demonstrate an improvement with ginger. Similarly, although we used the same dose of ginger as Lien *et al.*^[22], who reported a reduction in nausea induced by circularvection, our subjects reported low ratings for nausea throughout the study, thus, it would be difficult to demonstrate an effect of ginger if one existed. Stadelmann *et al.*^[23] have reported that a combination of peppermint oil and ginger extract

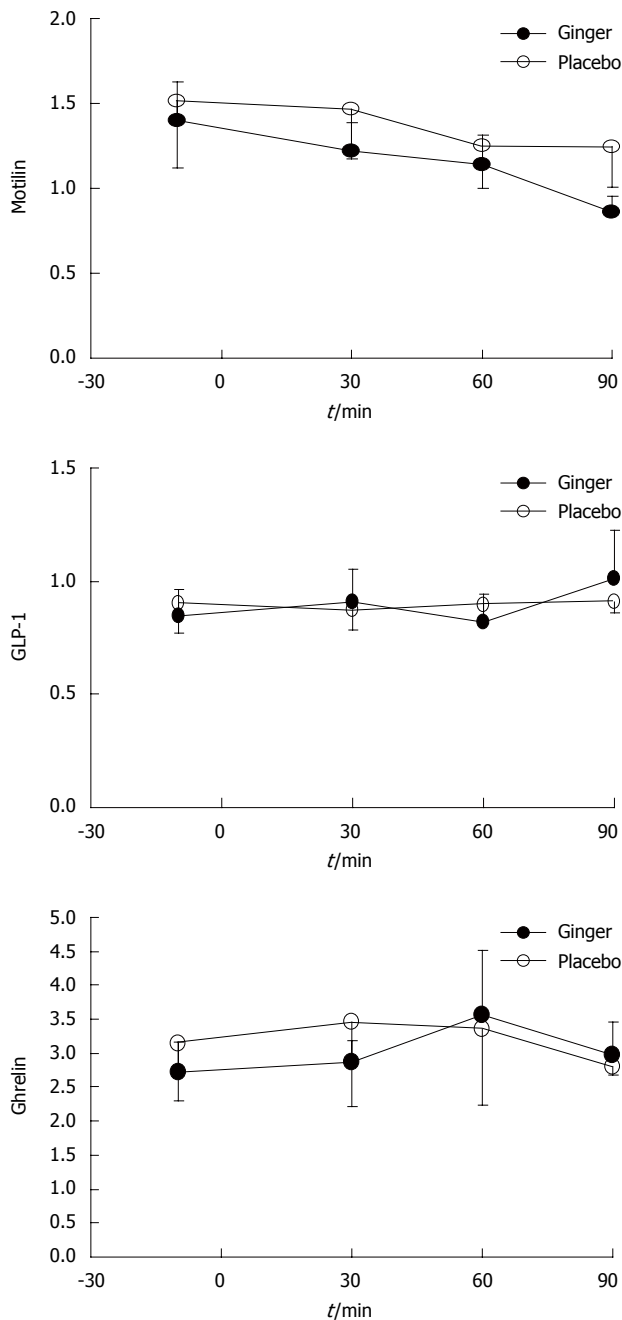


Figure 5 Plasma concentrations of glucagon-like peptide-1, motilin and ghrelin in patients with functional dyspepsia. There was no difference in the concentrations of any hormone between the ginger and placebo groups. Data are means \pm SE, $n = 11$. GLP-1: Glucagon-like peptide-1.

for 4 wk improved gastrointestinal symptom scores when compared to placebo, but the relative contribution of each active agent is unclear.

The mechanism by which ginger could enhance antral contractions and gastric emptying is not clear. We could not demonstrate any modulation of gut-derived hormones that are known to affect gastric motility, including motilin, ghrelin or GLP-1. It would be of interest to examine whether ginger affects the plasma concentrations or the actions of cholecystokinin, because this hormone is reported to be elevated in patients with functional dyspepsia.

sia^[21]. Abdel-Aziz *et al*^[24] have reported the potential for ginger to act on the 5-HT₃ receptor ion-channel complex, by binding the serotonin binding site, and Shibata *et al*^[25] have reported that a component of Dai-Kenchu-Tou (which contains ginger) stimulated gastric motility through cholinergic and 5-HT₃ receptors in dogs. The limitation of this study is that our observation was limited to 90 min of gastric emptying, and a single dose of ginger would not have been adequate for treatment of dyspepsia symptoms in patients with functional dyspepsia, especially as this disease is chronic and recurrent. Therefore, it is difficult to draw any clear conclusion. Further proper clinical trials of several weeks' treatment with ginger capsules seem to be necessary before starting trials in subgroups of patients with functional dyspepsia.

In summary, we confirmed that the acceleration of gastric emptying by ginger that we initially demonstrated in healthy volunteers extended to patients with functional dyspepsia. Further studies could be indicated in specific subgroups of patients (e.g. those with predominant bloating or nausea, or those with known delayed gastric emptying), to determine whether this can be a useful therapeutic approach.

ACKNOWLEDGMENTS

The authors thank Miss Ya-Hui Huang, Division of Hepatogastroenterology, Department of Internal Medicine, Chang Gung Memorial Hospital-Kaohsiung Medical Center for her assistance for blood sample collection and ELISA study.

COMMENTS

Background

Pharmacological therapy for patients with functional dyspepsia remains unsatisfactory. There have been few studies on the effects of ginger in patients with functional dyspepsia.

Research frontiers

Ginger (*Zingiber officinale*) has been used to treat a number of medical conditions, including those that affect the digestive tract. In this study, the authors demonstrated that the effect of ginger could be a potential mechanism for mediating gastric motility.

Innovations and breakthroughs

The authors had previously shown that ginger increases the frequency of antral contractions and accelerates gastric emptying of a low-nutrient liquid in healthy volunteers. However, the actual effect of ginger on patients with functional dyspepsia is still unknown, and this is believed to be the first study to explore this issue. Furthermore, current *in vivo* studies suggest that ginger is an effective therapy for patients with functional dyspepsia.

Applications

By understanding how ginger works on gastric motility, this study might represent a future strategy for therapeutic intervention in patients with delayed gastric emptying.

Terminology

The acceleration of gastric emptying by ginger that we initially demonstrated in healthy volunteers extends to patients with functional dyspepsia.

Peer review

Overall, this preliminary study of 11 patients with functional dyspepsia seems well designed. The data were appropriately analyzed and indicate that ginger has an impact on symptoms and gastric emptying. A large study needs to be undertaken to demonstrate its efficacy convincingly.

REFERENCES

- 1 **Clouse RE**, Mayer EA, Aziz Q, Drossman DA, Dumitrascu DL, Mönnikes H, Naliboff BD. Functional abdominal pain syndrome. *Gastroenterology* 2006; **130**: 1492-1497
- 2 **Holtmann G**, Talley NJ. Functional dyspepsia. Current treatment recommendations. *Drugs* 1993; **45**: 918-930
- 3 **Talley NJ**, McNeil D, Hayden A, Piper DW. Randomized, double-blind, placebo-controlled crossover trial of cimetidine and pirenzepine in nonulcer dyspepsia. *Gastroenterology* 1986; **91**: 149-156
- 4 **Moayyedi P**, Delaney BC, Vakil N, Forman D, Talley NJ. The efficacy of proton pump inhibitors in nonulcer dyspepsia: a systematic review and economic analysis. *Gastroenterology* 2004; **127**: 1329-1337
- 5 **Laine L**, Schoenfeld P, Fennerty MB. Therapy for *Helicobacter pylori* in patients with nonulcer dyspepsia. A meta-analysis of randomized, controlled trials. *Ann Intern Med* 2001; **134**: 361-369
- 6 **Johns Cupp M**. Toxicology and clinical pharmacology of herbal products. Totowa, New Jersey (USA): Humana Press, 2000: 123-129
- 7 **Capasso F**, Gaginella TS, Grandolini G, Izzo AA. Phytotherapy. A quick reference to herbal medicine SpringerVerlag, Heidelberg (Germany), 2003
- 8 **Yamahara J**, Huang QR, Li YH, Xu L, Fujimura H. Gastrointestinal motility enhancing effect of ginger and its active constituents. *Chem Pharm Bull (Tokyo)* 1990; **38**: 430-431
- 9 **Micklefield GH**, Redeker Y, Meister V, Jung O, Greving I, May B. Effects of ginger on gastroduodenal motility. *Int J Clin Pharmacol Ther* 1999; **37**: 341-346
- 10 **Wu KL**, Rayner CK, Chuah SK, Changchien CS, Lu SN, Chiu YC, Chiu KW, Lee CM. Effects of ginger on gastric emptying and motility in healthy humans. *Eur J Gastroenterol Hepatol* 2008; **20**: 436-440
- 11 **Tack J**, Depoortere I, Bisschops R, Delparte C, Coulie B, Meulemans A, Janssens J, Peeters T. Influence of ghrelin on interdigestive gastrointestinal motility in humans. *Gut* 2006; **55**: 327-333
- 12 **Luiking YC**, Akkermans LM, van der Reijden AC, Peeters TL, van Berge-Henegouwen GP. Differential effects of motilin on interdigestive motility of the human gastric antrum, pylorus, small intestine and gallbladder. *Neurogastroenterol Motil* 2003; **15**: 103-111
- 13 **Wishart JM**, Horowitz M, Morris HA, Jones KL, Nauck MA. Relation between gastric emptying of glucose and plasma concentrations of glucagon-like peptide-1. *Peptides* 1998; **19**: 1049-1053
- 14 **Gilja OH**, Lunding J, Hausken T, Gregersen H. Gastric accommodation assessed by ultrasonography. *World J Gastroenterol* 2006; **12**: 2825-2829
- 15 **Hausken T**, Odegaard S, Berstad A. Antroduodenal motility studied by real-time ultrasonography. Effect of enprostil. *Gastroenterology* 1991; **100**: 59-63
- 16 **Sepple CP**, Read NW. Gastrointestinal correlates of the development of hunger in man. *Appetite* 1989; **13**: 183-191
- 17 **Horowitz M**, Edelbroek MA, Wishart JM, Straathof JW. Relationship between oral glucose tolerance and gastric emptying in normal healthy subjects. *Diabetologia* 1993; **36**: 857-862
- 18 **Talley NJ**, Locke GR 3rd, Lahr BD, Zinsmeister AR, Tougas G, Ligozio G, Rojavin MA, Tack J. Functional dyspepsia, delayed gastric emptying, and impaired quality of life. *Gut* 2006; **55**: 933-939
- 19 **Chen SL**, Ji JR, Xu P, Cao ZJ, Mo JZ, Fang JY, Xiao SD. Effect of domperidone therapy on nocturnal dyspeptic symptoms of functional dyspepsia patients. *World J Gastroenterol* 2010; **16**: 613-617
- 20 **Hausken T**, Berstad A. Wide gastric antrum in patients with non-ulcer dyspepsia. Effect of cisapride. *Scand J Gastroenterol* 1992; **27**: 427-432
- 21 **Pilichiewicz AN**, Feltrin KL, Horowitz M, Holtmann G, Wishart JM, Jones KL, Talley NJ, Feinle-Bisset C. Functional dyspepsia is associated with a greater symptomatic response to fat but not carbohydrate, increased fasting and postprandial CCK, and diminished PYY. *Am J Gastroenterol* 2008; **103**: 2613-2623
- 22 **Lien HC**, Sun WM, Chen YH, Kim H, Hasler W, Owyang C. Effects of ginger on motion sickness and gastric slow-wave dysrhythmias induced by circularvection. *Am J Physiol Gastrointest Liver Physiol* 2003; **284**: G481-G489
- 23 **Stadelmann O**, Kohler S, Kieser M, Stolte M. Pfefferminzol/Ingwerextrakt bei funktioneller Dyspepsie. Randomisierte plazebokontrollierte Wirksamkeits und Vertraglichkeitsstudie mit Kombinationspräparat. *Leber Magen Darm* 1999; **29**: 1-8
- 24 **Abdel-Aziz H**, Windeck T, Ploch M, Verspohl EJ. Mode of action of gingerols and shogaols on 5-HT₃ receptors: binding studies, cation uptake by the receptor channel and contraction of isolated guinea-pig ileum. *Eur J Pharmacol* 2006; **530**: 136-143
- 25 **Shibata C**, Sasaki I, Naito H, Ueno T, Matsuno S. The herbal medicine Dai-Kencho-Tou stimulates upper gut motility through cholinergic and 5-hydroxytryptamine 3 receptors in conscious dogs. *Surgery* 1999; **126**: 918-924

S- Editor Sun H L- Editor Kerr C E- Editor Ma WH

Protection of the liver against CCl₄-induced injury by intramuscular electrotransfer of a kallistatin-encoding plasmid

Yong Diao, Xiao-Feng Zhao, Jun-Sheng Lin, Qi-Zhao Wang, Rui-An Xu

Yong Diao, Xiao-Feng Zhao, Qi-Zhao Wang, Rui-An Xu, Institute of Molecular Medicine, Huaqiao University, Quanzhou 362021, Fujian Province, China

Jun-Sheng Lin, Centre for Reproduction and Genomics, AgResearch, Invermay, Mosgiel 9053, New Zealand

Author contributions: Diao Y, Zhao XF and Wang QZ performed the majority of experiments; Lin JS provided analytical tools and was also involved in editing the manuscript; Diao Y and Xu RA designed the study and wrote the manuscript.

Supported by The State High Technology Research and Development Program of China (863 Program), No. 2008AA02Z135; the Important National Science and Technology Specific Projects, No. 2009ZX09103-643; and the Natural Science Foundation of China, No. 30973591

Correspondence to: Yong Diao, Professor, Institute of Molecular Medicine, Huaqiao University, Quanzhou 362021, Fujian Province, China. diaoyong@hqu.edu.cn

Telephone: +86-595-22692516 Fax: +86-595-22690516

Received: July 9, 2010 Revised: October 16, 2010

Accepted: October 23, 2010

Published online: January 7, 2011

ferred mice, protection against CCl₄-induced liver injury was reflected by significantly decreased serum ALT, AST, MDA and TNF- α levels compared to those in control mice ($P < 0.01$ to 0.05 in a dose-dependent manner). Histological observations also revealed that hepatocyte necrosis, hemorrhage, vacuolar change and hydropic degeneration were apparent in mice after CCl₄ administration. In contrast, the damage was markedly attenuated in the Kal gene-transferred mice. The expression of hepatic fibrogenesis marker transforming growth factor- β 1 was also reduced in the pKal transferred mice.

CONCLUSION: Intramuscular electrotransfer of plasmid pKal which was formulated with PLG significantly alleviated the CCl₄-induced oxidative stress and inflammatory response, and reduced the liver damage in a mouse model.

© 2011 Baishideng. All rights reserved.

Key words: Kallistatin; Gene delivery systems; Electroporation; Drug formulation; Liver injury

Peer reviewers: Dr. Juan Carlos Laguna Egea, Professor of Pharmacology, Unitat de Farmacologia, Facultat de Farmàcia, Universitat de Barcelona, Avenida Diagonal 643, Barcelona 08028, Spain; Valentina Medici, MD, Assistant Professor, Division of Gastroenterology and Hepatology, Department of Internal Medicine, University of California Davis, 4150 V Street, Suite 3500, Sacramento, CA 95817, United States

Abstract

AIM: To investigate the effect of transgenic expression of kallistatin (Kal) on carbon tetrachloride (CCl₄)-induced liver injury by intramuscular (im) electrotransfer of a Kal-encoding plasmid formulated with poly-L-glutamate (PLG).

METHODS: The pKal plasmid encoding Kal gene was formulated with PLG and electrotransferred into mice skeletal muscle before the administration of CCl₄. The expression level of Kal was measured. The serum biomarker levels of alanine aminotransferase (ALT), aspartate aminotransferase (AST), malonyldialdehyde (MDA), and tumor necrosis factor (TNF)- α were monitored. The extent of CCl₄-induced liver injury was analyzed histopathologically.

RESULTS: The transgene of Kal was sufficiently expressed after an im injection of plasmid formulated with PLG followed by electroporation. In the Kal gene-trans-

Diao Y, Zhao XF, Lin JS, Wang QZ, Xu RA. Protection of the liver against CCl₄-induced injury by intramuscular electrotransfer of a kallistatin-encoding plasmid. *World J Gastroenterol* 2011; 17(1): 111-117 Available from: URL: <http://www.wjgnet.com/1007-9327/full/v17/i1/111.htm> DOI: <http://dx.doi.org/10.3748/wjg.v17.i1.111>

INTRODUCTION

Gene therapy refers to a therapeutic approach by introduction and expression of genetic material in particular cells

or tissues. Over the past two decades, great efforts and abundant resources have been invested into the development of an effective, safe and relatively long-lasting gene therapy strategy. Great success has been made recently so that gene therapy was elected as one of the breakthroughs of 2009 by Science^[1]. In order to achieve the goal of therapy, a carrier, or “vector”, is the key required to deliver the genetic material into the target cells. Whilst exciting progress in the development of gene therapy have been made, a safe and efficient method of gene delivery has been elusive thus far. Initially, a number of viral vectors were chosen, owing to their high efficiency in gene transfer. Unfortunately, they also bring added risks to the patients, even though their virulence was genetically disabled. Non-viral vectors avoid the risks. However, lower transferring efficiency has limited their clinical use thus far. To boost efficacy of non-viral gene therapies several delivery methods have been under investigation. Electro-gene therapy is one of the most efficient non-viral approaches for gene therapy^[2-4]. It has already been considered a safe method because naked DNA is not immunogenic and plasmid DNA does not have the risk of insertional mutagenesis^[5]. Moreover, DNA electrotransfer can be accomplished using devices that have already been used on human cancer patients to deliver cytotoxic molecules such as bleomycin and cisplatin to solid tumors by electrochemotherapy^[6,7]. Thus all elements are available for safe and widespread use of this efficient technology and for implementing the use of genes for medical purposes^[8]. To further improve the transfer efficiency, plasmids were formulated in poly-L-glutamate (PLG) prior to intramuscular (im) injection and electroporation. Such a combined approach significantly elevated transgene expression in myofibers^[9].

Kallistatin (Kal) that belongs to the serine protease inhibitor family is widely expressed in organs such as the liver, kidneys, and blood vessels. Previous studies have demonstrated kallistatin to be a potent anti-inflammatory agent. Kallistatin administration by gene delivery attenuates oxidative stress, apoptosis, inflammation, and organ damage in animal models^[10-13]. These findings indicate that kallistatin may play an important role as an antioxidant in maintaining oxidative balance and preventing oxidative endothelial and tissue injury.

Oxidative stress is a state of redox imbalance caused by increased reactive oxygen species (ROS) generation and decreased antioxidant capacity. Administration of carbon tetrachloride (CCl₄) is an established experimental model of severe toxic liver injury involving generation of oxidative stress and is frequently used for the screening of anti-hepatotoxic and/or hepatoprotective activities of drugs^[14]. Antioxidants and anti-inflammatory agents can play a role in liver protection by scavenging active oxygen and free radicals and neutralizing lipid peroxides.

In the present study, we first investigated the feasibility of improving the expression of the transgene after introducing the PLG formulated plasmid into mouse skeletal muscle by electroporation, then investigated the therapeutic efficacy of Kal expression in the circulation on CCl₄-induced liver injury. After CCl₄ had been injected into mice to induce liver injury, evaluations of liver marker

enzymes, the extent of oxidative stress and liver histology were performed, revealing that elevated levels of human Kal were effective in alleviating oxidative stress and protecting liver against CCl₄-induced liver damage.

MATERIALS AND METHODS

Materials

Sodium salt of PLG (15-50 kDa) was purchased from Stsien Co (Nanjing, China); EndoFree plasmid Giga kit was purchased from Qiagen GmbH (Hilden, Germany); DNA Delivery Device was purchased from TERESA Healthcare Sci-Tech Company (Shanghai, China); reporter lysis buffer and β -galactosidase enzyme assay system was purchased from Promega (Madison, USA); BCA Protein Assay Kit was purchased from Pierce (Rockford, USA); Quantikine kit was purchased from R&D Systems Inc (Minneapolis, USA).

Experimental animals

Balb/c mice (6- to 8-wk-old females, Slaccas Company, Shanghai) were used throughout this study. The animals were maintained on a 12/12 h day/night cycle at room temperature 18-24°C. Food and water were provided *ad libitum*. The Animal Studies Ethics Committee of Huaqiao University approved all the experiments reported here.

Plasmid DNA

The expression plasmid pLac encoding β -galactosidase under the control of the cytomegalovirus immediate-early promoter, and the pKal under the control of the same promoter and driving a coding sequence for the human Kal, were constructed as reported previously^[15] and kept in our laboratory. The integrity of the sequence was determined by DNA sequencing. Plasmids were transformed and expanded into *E. coli* strain JM-109 and purified with the EndoFree plasmid Giga kit in accordance with the supplier's protocol. DNA was dissolved in Endofree TE buffer and kept frozen in aliquots at a concentration of 2 mg/mL.

Formulation of plasmid DNA

Formulation was made by mixing the plasmid DNA with the sodium salt of PLG before adjusting the NaCl concentration to 0.15 mol/L with a 5 mol/L stock solution. The plasmid and polymers were allowed to incubate at room temperature for 15 min prior to adding NaCl for tonicity adjustment. The pH of the formulation was adjusted using dilute hydrochloric acid or sodium hydroxide to 7.0. Sterility of the formulation was achieved by sterile filtration through sterile 0.22 μ m pore size filters, and was injected immediately after preparation.

Im injection

Mice were anesthetized by intraperitoneal (ip) injection of pentobarbital sodium at a dose of 30 mg/kg body weight. The plasmid was injected directly into the tibialis anterior (TA) muscles of the mice using a 500 μ L syringe. The injected volumes were 50 μ L for each side of the TA muscles.

In vivo electroporation

Two minutes after the im injection of plasmid DNA, an electrical field was applied to the area around the injection. Two silver needle electrodes were inserted 3 mm apart into the TA muscles and 6 electric pulses were applied using the TERESA DNA delivery device. The electric pulses were 50 ms in duration at a voltage of 60 V.

β-galactosidase assay

The TA muscles treated with plasmid pLac were excised at different time points post delivery, and were analyzed for β-galactosidase expression. The samples were collected immediately after euthanizing the animals. The samples were frozen by keeping in liquid nitrogen and then stored at -70°C until further use. These samples were weighed, minced into small pieces and homogenized with reporter lysis buffer using a homogenizer. The tissue homogenate was then centrifuged at 15000 g and 4°C for 15 min and the clear supernatant was separated for further analysis. The β-galactosidase activity was measured using the β-galactosidase enzyme assay system. The total protein content of the samples was measured with the BCA protein assay kit. Finally, the enzyme activity in the samples was expressed as milliunits/mg of protein.

CCl₄ treatment

The mice were divided into the following groups: (1) control; (2) CCl₄; (3) pLac (50 μg) + CCl₄; (4) pKal (100 μg) + CCl₄; (5) pKal (50 μg) + CCl₄; and (6) pKal (25 μg) + CCl₄. Each group was composed of 8 mice. CCl₄ was dissolved in corn oil vehicle (1:1, v/v). The mice received a single ip injection with the CCl₄ preparation at a dose of 0.8 mL/kg body weight to induce liver injury 6 d after plasmid administration. Control mice received an ip injection of an equal volume of corn oil alone. The mice were sacrificed and the blood samples were collected *via* the inferior vena cava 24 h after CCl₄ treatment. The livers were sampled immediately afterwards.

Measurement of serum biomarker levels

The serum concentration of kallistatin and tumor necrosis factor (TNF)-α were measured with the Quantikine Immunoassay kit following the manufacturer's instructions. Serum alanine aminotransferase (ALT) and aspartate aminotransferase (AST) activities were measured using a Hitachi 7020 biochemical analyzer. Lipid peroxidation was detected by measuring the serum level of malonyldialdehyde (MDA) spectrophotometrically, the end product derived from the breakdown of polyunsaturated fatty acids and related esters, with the classical thiobarbituric acid method^[16].

Histological analysis

The excised liver was fixed in buffered formalin, embedded in paraffin, cut into 5 μm-thick sections, and examined with hematoxylin eosin (HE) staining. Pathology was scored in a blinded manner by a trained pathologist by counting the number of necrotic or inflammatory foci per microscopic field^[17]. Five fields were checked at 200 × magnification as follows: 0 (absent), 1 (< 2foci), 2

(2-4 foci), and 3 (> 4 foci). The inflammatory response and muscle damage arising from plasmid injection and electroporation was evaluated by analysis of HE-stained slides of TA muscles.

Immunohistochemical analysis

After deparaffinization in xylene and rehydration in graded ethanols, endogenous peroxidase activity of the paraffin-embedded slides was blocked by incubation with 3% hydrogen peroxide (H₂O₂) at 37°C for 10 min. The slides were then treated twice in a microwave oven for 5 min in citrate buffer (pH 6.0) at high power to retrieve antigens. After blocking with goat serum at 37°C for 30 min, the specimens were incubated with the rabbit polyclonal antibodies (primary antibody) against transforming growth factor (TGF)-β1 overnight at 4°C, followed by incubation with biotinylated anti-rabbit antibody at 37°C for 30 min and then horseradish peroxidase conjugated streptavidin at 37°C for 10 min. The slides were stained using 3,3'-diaminobenzidine-H₂O₂, counterstained with hematoxylin, and examined under a light microscope.

Statistical analysis

Data are given as means ± SD. Analysis of variance was performed to test the significance; *P*-values were considered significant when less than 0.05.

RESULTS

Transgene expression

The transgene expression in the TA muscle was enhanced by the PLG formulation (Figure 1). The expression of β-galactosidase in the animals that received plasmid formulated in 6 mg/mL PLG reached its peak level at 5 d post-delivery and was 5-fold higher than that in the mice who received naked plasmid. Thus PLG could enhance the expression of an electroporated plasmid injected im in muscles.

The electroporation of an increasing dose of plasmid pKal (25-100 μg) into TA muscle led to a dose-dependent increase in human Kal plasma concentration, detected on the 7th day after plasmid injection (Figure 2). The level of serum Kal in the 50 μg group was almost 2-fold higher than that in the 25 μg group, but was only slightly lower than in the 100 μg group, suggesting there was a saturation of expression such that the relationship of plasmid dose and transgene expression level was not linear.

Protective effects on CCl₄-induced liver damage

The mice induced with a single dose of CCl₄ developed hepatic damage as compared with the normal control group (*P* < 0.01), as shown by marked changes in ALT and AST activities in the serum (Table 1). Injection of pKal resulted in a significant reduction in ALT and AST activities with each of the 3 doses compared with the CCl₄ alone group (*P* < 0.01-0.05).

Effects on serum TNF-α level

TNF-α is one of the pro-inflammatory cytokines which

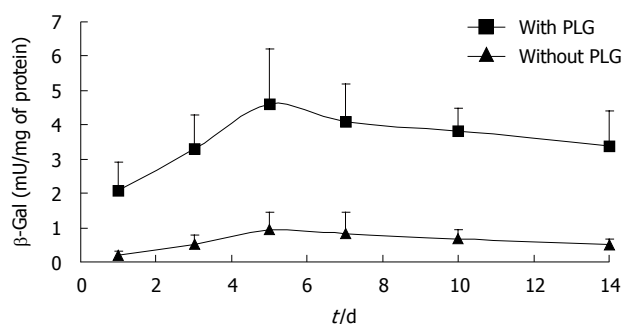


Figure 1 Time-course study of the effect of the poly-L-glutamate formulation on transgene expression of pLac in the tibialis anterior muscle after electroporation transfer. The plasmids were transferred with (square) and without (triangle) poly-L-glutamate (PLG) formulation. The values shown are mean \pm SD, $n = 8$.

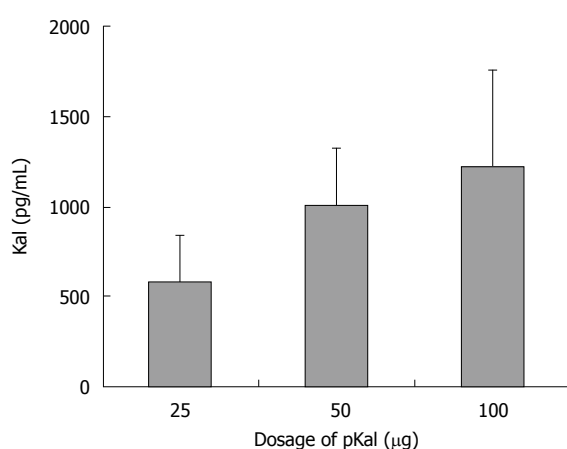


Figure 2 Dose-dependent kallistatin concentrations in the serum responded to intramuscular electrotransfer of a plasmid pKal in poly-L-glutamate formulation. The values shown are mean \pm SD, $n = 8$. Kal: Kallistatin.

are early mediators of tissue damage and repair. Mouse serum TNF- α concentration was measured to evaluate the influence of Kal on CCl₄-induced inflammatory responses (Table 1). CCl₄ exposure markedly stimulated TNF- α releasing in comparison with the control group ($P < 0.01$). The serum TNF- α levels in the 3 pKal + CCl₄ groups were significantly lower than that in the CCl₄ group ($P < 0.01-0.05$) in a dose-dependent manner. These results clearly suggested that the CCl₄-induced inflammatory response could be suppressed by pretreatment with pKal.

Effects on hepatic oxidative stress

The generation of ROS and increase of hepatic lipid peroxidation are important features of chronic liver diseases. To examine the effects of Kal on hepatic oxidative stress, liver tissue was homogenized to determine the hepatic MDA level 24 h after CCl₄ administration (Table 1). MDA is the end product of lipid peroxidation; its level indirectly reflects the degree of oxidative stress. The hepatic MDA concentration in the group treated with CCl₄ was only significantly higher than in the control group ($P < 0.01$). The 3 pKal pretreatment groups significantly attenuated the elevated MDA compared with CCl₄ and pLac + CCl₄ groups ($P < 0.01-0.05$).

Table 1 Serum biomarker levels affected by transgene of kallistatin on carbon tetrachloride-induced liver injury ($n = 8$, mean \pm SD)

Group	ALT (U/L)	AST (U/L)	MDA (nmol/mg protein)	TNF- α (pg/mL)
Control	37 \pm 7	48 \pm 7	0.46 \pm 0.10	2.9 \pm 2.1
CCl ₄	134 \pm 26 ^b	183 \pm 20 ^b	1.15 \pm 0.29 ^b	28.1 \pm 11.8 ^b
pLac + CCl ₄	123 \pm 18 ^b	181 \pm 28 ^b	1.07 \pm 0.33 ^b	28.8 \pm 9.4 ^b
pKal (100 μ g) + CCl ₄	95 \pm 24 ^d	121 \pm 35 ^d	0.48 \pm 0.27 ^d	12.4 \pm 4.0 ^d
pKal (50 μ g) + CCl ₄	98 \pm 28 ^c	143 \pm 37 ^c	0.65 \pm 0.25 ^d	14.5 \pm 3.5 ^d
pKal (25 μ g) + CCl ₄	101 \pm 32 ^c	151 \pm 37 ^c	0.82 \pm 0.21 ^c	17.3 \pm 4.8 ^c

^b $P < 0.01$ vs control group; ^c $P < 0.05$, ^d $P < 0.01$ vs CCl₄ group. ALT: Alanine aminotransferase; AST: Aspartate aminotransferase; MDA: Malonyldialdehyde; TNF: Tumor necrosis factor; CCl₄: Carbon tetrachloride.

Histological analysis

To analyze the extent of liver injury, liver sections were stained with hematoxylin and eosin (Figure 3). No apparent damage was found in the liver sections from the control mice (Figure 3A). In contrast, extensive damage was detected in the sections from CCl₄ and pLac + CCl₄ groups (Figure 3B and C). Hepatocyte necrosis was the predominant histopathologic lesion, and the affected livers displayed hemorrhage, vacuolar change, hydropic degeneration of hepatocytes and infiltration of inflammatory cells. All these lesions in the pKal + CCl₄ groups were significantly attenuated (Figure 3D-G).

Immunohistochemical detection of TGF- β 1

In liver tissue from the control group, the expression of TGF- β 1 was negative in liver cells and weakly positive in stromal cells of the portal area (Figure 4A). In the CCl₄ and pLac + CCl₄ groups, the expression of TGF- β 1 was strongly positive in the cytoplasm of both hepatic parenchymal cells and stromal cells (Figure 4B and C). Compared with the CCl₄ group, the expression of TGF- β 1 was significantly reduced in the pKal treatment groups (Figure 4D-F).

Treatment-associated muscle damage

The safety of plasmid injection and electroporation was evaluated by im injection of 50 μ g pLac followed by electroporation. Fifty μ L saline injections were used as a control. The injected TA muscles were harvested on day 7, fixed, dehydrated, and analyzed by HE staining. The representative images of the muscle samples in various groups are shown in Figure 5. The treatment induced low inflammatory responses at the injection site. No necrosis was observed for any of the groups.

DISCUSSION

The transfer ability of the recombinant plasmid can be improved by the combination of proper formulation, im injection, and electroporation. To improve the efficacy and reproducibility of plasmid delivery, protective, interactive, non-condensing polymers and non-ionic block co-polymers, consisting of ethylene oxide and propylene

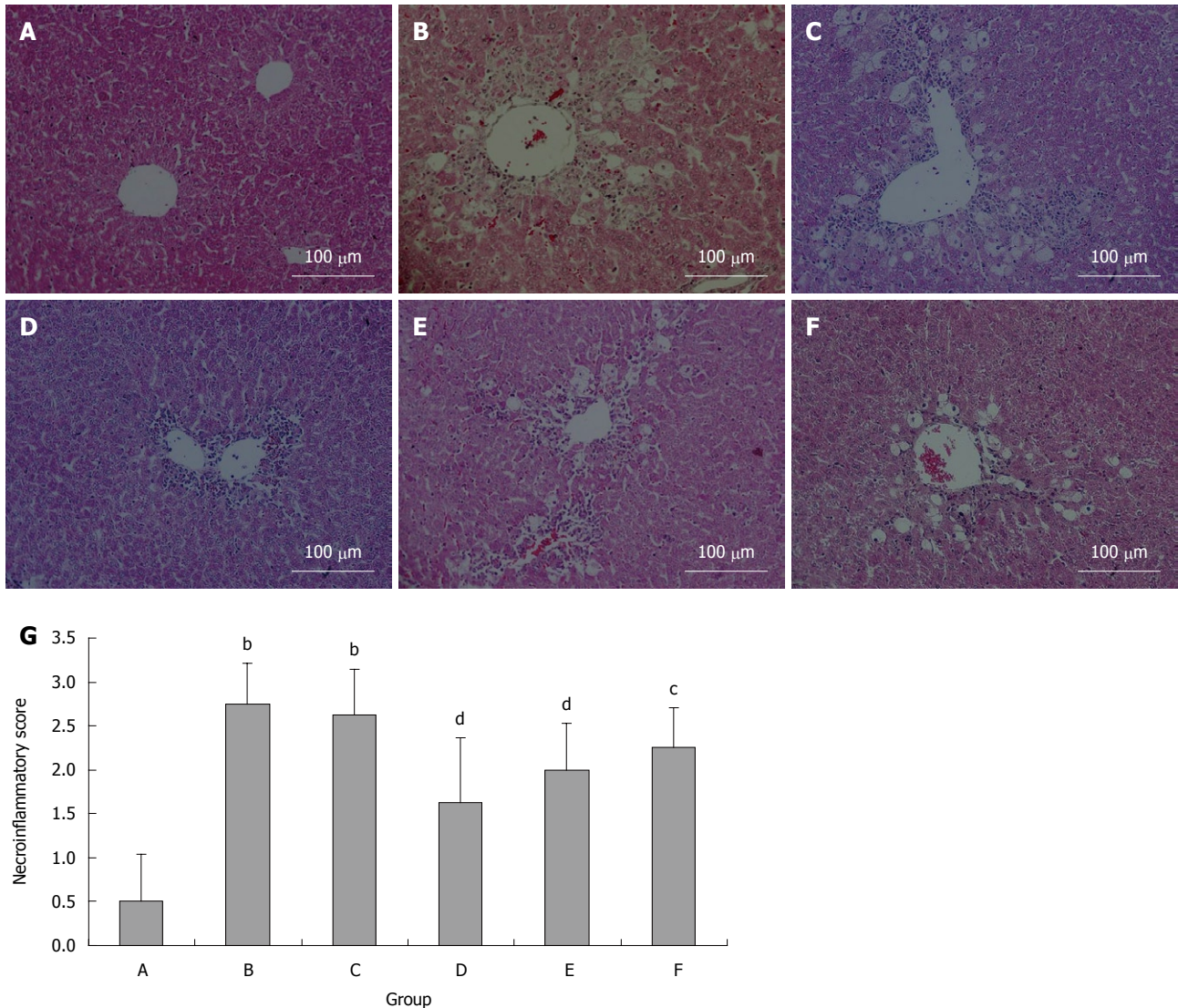


Figure 3 Protective effects of kallistatin expression against carbon tetrachloride-induced liver injury in mice. HE staining was performed on paraffin embedded sections of the liver tissues. Representative sections are shown for each group. A: Control; B: Carbon tetrachloride (CCl₄); C: pLac + CCl₄; D: pKal (100 μg) + CCl₄; E: pKal (50 μg) + CCl₄; F: pKal (25 μg) + CCl₄; G: Necroinflammatory scores. ^b*P* < 0.01 vs control group; ^c*P* < 0.05, ^d*P* < 0.01 vs CCl₄ group.

oxide monomers, have been developed^[18,19]. Both systems have increased distribution of DNA within the muscle tissue and augmented transgene expression compared with DNA in saline. Negatively charged polymers, such as PLG, could also improve the expression of genes delivered by im injection and electroporation, and elevated levels of secreted gene products in multiple *in vivo* models have been reported^[18,20]. Although the mechanism by which PLG enhances transgene expression is unknown, based on our data we concur with other authors' findings that the formulation of PLG can (1) disperse plasmids throughout the electrical field at the time of electroporation; (2) protect plasmids from nuclease degradation; and (3) facilitate intracellular uptake and trafficking of transcriptional active plasmid in muscle cells^[9].

The technique of electroporation has been used for nearly 30 years as a means of introducing DNA into cells *in vitro*, and is now widely used for transfection of plasmids into different tissues *in vivo*. More recently, electroporation has been used for the treatment of cutaneous and

subcutaneous tumors in humans and its safety was proved clinically^[21]. Our results also showed that electroporation treatment-associated muscle damage was minimal. These experiences have paved the way for the clinical use of gene electroporation in humans. The DNA electroporation is reaching the clinical stage as several clinical trials to transfer genes in tumors and in muscle are ongoing^[22,23].

Using an intramuscular electrotransfer method, we demonstrated that the PLG formulation of pKal provided a satisfactory expression level of Kal. The expressed Kal possesses antioxidant properties and the secreted Kal could contribute to protection of liver against CCl₄-induced damage in a mouse model, as indicated by both histological observation and biochemical evaluation. The Kal gene-transferred mice demonstrated a significant reduction in the level of serum peroxidation marker MDA, with a concomitant improvement in the activities of the hepatic antioxidative defense system. This suggests that Kal is able to protect against hepatic cellular membrane oxidative damage *via* a free radical scavenging property.

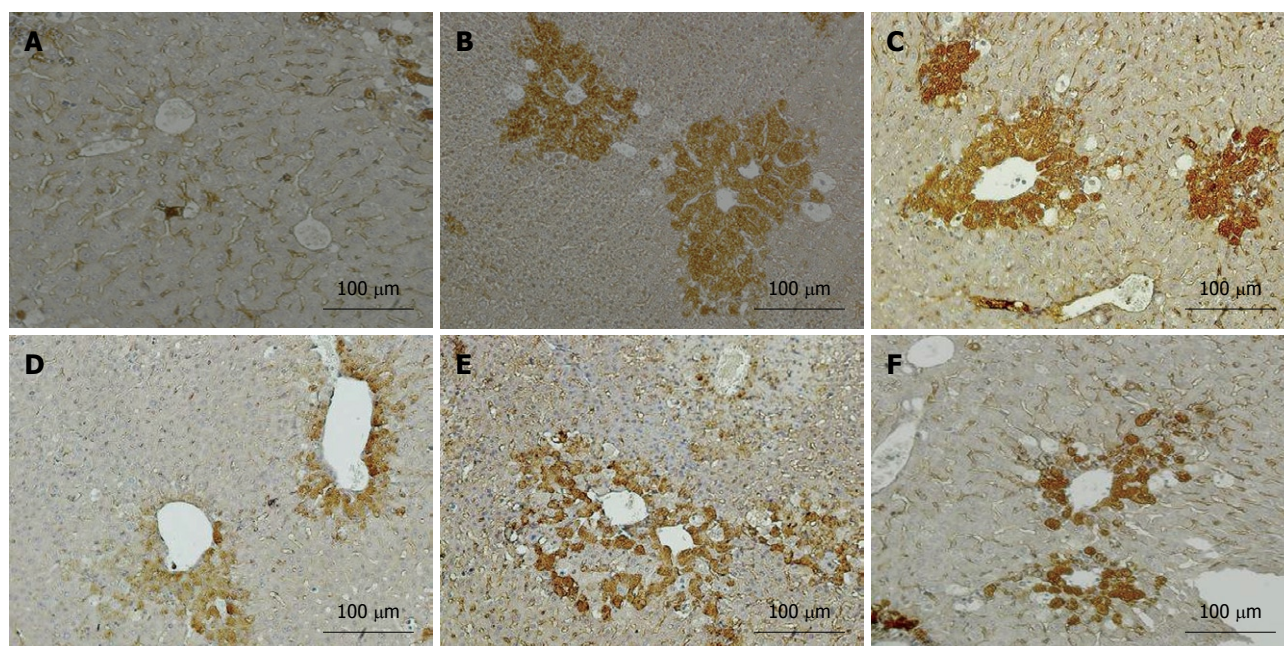


Figure 4 Immunohistological analysis of transforming growth factor- β 1 (brown) in the mice livers treated with carbon tetrachloride. A: Control; B: Carbon tetrachloride (CCl₄); C: pLac + CCl₄; D: pKal (100 μ g) + CCl₄; E: pKal (50 μ g) + CCl₄; F: pKal (25 μ g) + CCl₄.

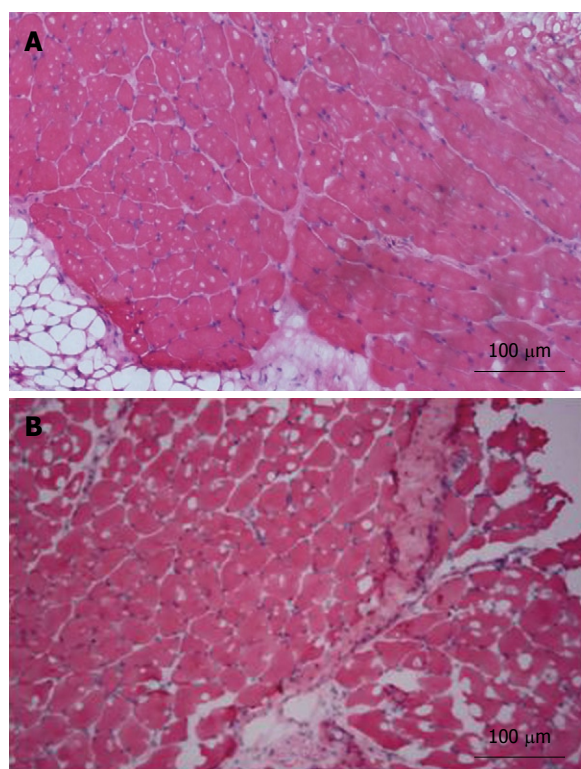


Figure 5 Inflammatory response and muscle damage arising from plasmid injection and electroporation. A: Saline; B: pLac.

Our results also exhibited the anti-inflammatory activity of Kal. TNF- α is a proinflammatory cytokine produced predominantly by macrophages and plays a key role in the host defense response to injury and infection. The expression of Kal in the circulation inhibited the increase in TNF- α production from Kupffer cells following CCl₄ injection, due to its anti-inflammatory activity.

The efficiency of most protein drugs, whose half-life *in vivo* is generally shorter than chemical drugs, markedly depends on their plasma kinetics. Taking the advantages of gene transfer, a steady-state therapeutic level of the recombinant protein in the circulation could be maintained for a long time. This is especially important in the treatment of chronic disease or the prevention of disease. Our results showed that the constant expression level of Kal in the pKal group with the lowest dosage was already sufficient to prevent CCl₄-induced liver damage. These data provided compelling and mechanistic evidences for the importance of Kal in regulation of liver injury.

TGF- β 1 in the liver is secreted by hepatocytes, Kupffer cells, stellate cells (HSC), endothelial cells and infiltrating mononuclear cells, and plays a pivotal role in hepatic fibrogenesis. Among many inflammatory cytokines involved in liver fibrosis, TGF- β 1 appears to be the most important, because (1) there is higher TGF- β 1 expression in activated HSC; (2) TGF- β 1 has potency in upregulating extracellular matrix expression; (3) there is higher expression of TGF- β receptors on HSC; and (4) TGF- β 1 increases the expression of tissue inhibitor of metalloproteinases-1. Therefore, many antifibrosis strategies focus on reducing the secretion of TGF- β 1 and blocking the TGF- β signal transduction pathway to reduce TGF- β 1-induced HSC proliferation. Our results clearly demonstrated the inhibitory effect of Kal expression on the hepatic TGF- β 1 level in an experimental animal model of liver damage induced by CCl₄.

In conclusion, the data of this study provided the evidence that the combination of PLG formulation, im injection and electroporation of plasmid encoding the Kal gene is an effective gene therapeutic method in a CCl₄-induced liver damage model. The beneficial effects of this technique to reduce the expression of TGF- β 1 also make

it a promising strategy for the treatment of hepatic fibrosis in the future.

COMMENTS

Background

Acute and chronic hepatic injuries cause high morbidity and mortality worldwide. Although the pathogenesis is not fully understood, it is clear that reactive oxygen species play a key function in the pathological changes in the liver. Kallistatin is a member of the serine proteinase inhibitor superfamily and was shown to have pleiotropic effects, including anti-oxidative stress, anti-inflammation and angiogenesis. Studies show it can attenuate oxidative stress, apoptosis, inflammation, and organ damage. However, the short half-life of kallistatin protein *in vivo* limits its efficiency. In contrast, long-term transgene expression can be achieved by gene therapy.

Research frontiers

Gene therapy has already proven to be a novel and promise modality in reducing liver injury, but is still in its infancy, and ideal gene delivery systems for gene transfer with high and prolonged gene expression, as well as less cytotoxicity or immunogenicity remain to be developed. Viral vectors are so far the most efficient tools for delivery of genes into mammalian cells. Drawbacks such as cost, immunogenicity, and difficulties in manufacture have shifted the interest towards nonviral vectors. However, the low efficiency of gene transfer hampers the development of nonviral vectors severely.

Innovations and breakthroughs

In order to boost the efficacy of non-viral gene therapy delivery, DNA electrotransfer technology was applied and the plasmid formulation was also optimized. The kallistatin expression *in vivo* was increased greatly; the animal model showed that the gene therapy strategy was effective in alleviating oxidative stress and protecting the liver against carbon tetrachloride (CCl₄)-induced liver damage.

Applications

Although additional studies are necessary to translate this technology into clinical trials in humans, the results provide a rationale to develop new pharmacological strategies in the clinical management of patients with acute and chronic liver injury.

Terminology

Electro-gene therapy: a method involving injection of a naked plasmid encoding a marker gene or a therapeutic gene, followed by *in vivo* electroporation, where short electrical pulses are applied to the injected tissue. The gene expression of the injected plasmid was reported to increase more than 100-fold.

Peer review

The paper described the improvement of the intramuscular electrotransfer of a kallistatin-encoding plasmid by using poly-L-glutamate in plasmid formulation. The ensuing increased presence of kallistatin in plasma protected those transfected mice from the hepatotoxic effects of a single dosage of CCl₄. In general, results are sound and their interpretation is correct.

REFERENCES

- 1 **Alberts B.** The breakthroughs of 2009. *Science* 2009; **326**: 1589
- 2 **Mir LM, Bureau MF, Gehl J, Rangara R, Rouy D, Caillaud JM, Delaere P, Branellec D, Schwartz B, Scherman D.** High-efficiency gene transfer into skeletal muscle mediated by electric pulses. *Proc Natl Acad Sci USA* 1999; **96**: 4262-4267
- 3 **Bloquel C, Fabre E, Bureau MF, Scherman D.** Plasmid DNA electrotransfer for intracellular and secreted proteins expression: new methodological developments and applications. *J Gene Med* 2004; **6** Suppl 1: S11-S23
- 4 **André FM, Gehl J, Sersa G, Prémat V, Hojman P, Eriksen J, Golzio M, Cemazar M, Pavselj N, Rols MP, Miklavcic D, Neumann E, Teissié J, Mir LM.** Efficiency of high- and low-voltage pulse combinations for gene electrotransfer in muscle, liver, tumor, and skin. *Hum Gene Ther* 2008; **19**: 1261-1271
- 5 **Cukjati D, Batuskaite D, André F, Miklavcic D, Mir LM.** Real time electroporation control for accurate and safe *in vivo* non-viral gene therapy. *Bioelectrochemistry* 2007; **70**: 501-507
- 6 **Miklavcic D, Snoj M, Zupanec A, Kos B, Cemazar M, Kropivnik M, Bracko M, Pecnik T, Gadzijev E, Sersa G.** Towards treatment planning and treatment of deep-seated solid tumors by electrochemotherapy. *Biomed Eng Online* 2010; **9**: 10
- 7 **Hui SW.** Overview of drug delivery and alternative methods to electroporation. *Methods Mol Biol* 2008; **423**: 91-107
- 8 **Ferber D.** Gene therapy. Safer and virus-free? *Science* 2001; **294**: 1638-1642
- 9 **Nicol F, Wong M, MacLaughlin FC, Perrard J, Wilson E, Nordstrom JL, Smith LC.** Poly-L-glutamate, an anionic polymer, enhances transgene expression for plasmids delivered by intramuscular injection with *in vivo* electroporation. *Gene Ther* 2002; **9**: 1351-1358
- 10 **Chao J, Yin H, Yao YY, Shen B, Smith RS Jr, Chao L.** Novel role of kallistatin in protection against myocardial ischemia-reperfusion injury by preventing apoptosis and inflammation. *Hum Gene Ther* 2006; **17**: 1201-1213
- 11 **Gao L, Yin H, S Smith R Jr, Chao L, Chao J.** Role of kallistatin in prevention of cardiac remodeling after chronic myocardial infarction. *Lab Invest* 2008; **88**: 1157-1166
- 12 **Shen B, Hagiwara M, Yao YY, Chao L, Chao J.** Salutary effect of kallistatin in salt-induced renal injury, inflammation, and fibrosis via antioxidative stress. *Hypertension* 2008; **51**: 1358-1365
- 13 **Wang CR, Chen SY, Wu CL, Liu MF, Jin YT, Chao L, Chao J.** Prophylactic adenovirus-mediated human kallistatin gene therapy suppresses rat arthritis by inhibiting angiogenesis and inflammation. *Arthritis Rheum* 2005; **52**: 1319-1324
- 14 **Tuñón MJ, Alvarez M, Culebras JM, González-Gallego J.** An overview of animal models for investigating the pathogenesis and therapeutic strategies in acute hepatic failure. *World J Gastroenterol* 2009; **15**: 3086-3098
- 15 **Diao Y, Ma J, Xiao WD, Luo J, Li XY, Chu KW, Fung PW, Habib N, Farzaneh F, Xu RA.** Inhibition of angiogenesis and HCT-116 xenograft tumor growth in mice by kallistatin. *World J Gastroenterol* 2007; **13**: 4615-4619
- 16 **Xu R, Harrison PM, Chen M, Li L, Tsui TY, Fung PC, Cheung PT, Wang G, Li H, Diao Y, Krissansen GW, Xu S, Farzaneh F.** Cytoglobin overexpression protects against damage-induced fibrosis. *Mol Ther* 2006; **13**: 1093-1100
- 17 **de Meijer VE, Sverdlow DY, Popov Y, Le HD, Meisel JA, Nosé V, Schuppan D, Puder M.** Broad-spectrum matrix metalloproteinase inhibition curbs inflammation and liver injury but aggravates experimental liver fibrosis in mice. *PLoS One* 2010; **5**: e11256
- 18 **Fewell JG, MacLaughlin F, Mehta V, Gondo M, Nicol F, Wilson E, Smith LC.** Gene therapy for the treatment of hemophilia B using PINC-formulated plasmid delivered to muscle with electroporation. *Mol Ther* 2001; **3**: 574-583
- 19 **Gaymalov ZZ, Yang Z, Pisarev VM, Alakhov VY, Kabanov AV.** The effect of the nonionic block copolymer pluronic P85 on gene expression in mouse muscle and antigen-presenting cells. *Biomaterials* 2009; **30**: 1232-1245
- 20 **Sersa G, Miklavcic D, Cemazar M, Rudolf Z, Pucihar G, Snoj M.** Electrochemotherapy in treatment of tumours. *Eur J Surg Oncol* 2008; **34**: 232-240
- 21 **Testori A, Tosti G, Martinoli C, Spadola G, Cataldo F, Verrecchia F, Baldini F, Mosconi M, Soteldo J, Tedeschi I, Pasoni C, Pari C, Di Pietro A, Ferrucci PF.** Electrochemotherapy for cutaneous and subcutaneous tumor lesions: a novel therapeutic approach. *Dermatol Ther* 2010; **23**: 651-661
- 22 **Villemejeane J, Mir LM.** Physical methods of nucleic acid transfer: general concepts and applications. *Br J Pharmacol* 2009; **157**: 207-219
- 23 **Daud AI, DeConti RC, Andrews S, Urbas P, Riker AI, Sondak VK, Munster PN, Sullivan DM, Ugen KE, Messina JL, Heller R.** Phase I trial of interleukin-12 plasmid electroporation in patients with metastatic melanoma. *J Clin Oncol* 2008; **26**: 5896-5903

S- Editor Sun H L- Editor Cant MR E- Editor Lin YP

Risk factors and gene polymorphisms of inflammatory bowel disease in population of Zhejiang, China

Zi-Wei Wang, Feng Ji, Wei-Jun Teng, Xiao-Gang Yuan, Xiao-Ming Ye

Zi-Wei Wang, Feng Ji, Wei-Jun Teng, Xiao-Gang Yuan, Xiao-Ming Ye, Department of Digestive Diseases, First Affiliated Hospital, College of Medicine, Zhejiang University, Hangzhou 310003, Zhejiang Province, China

Author contributions: Wang ZW and Ji F designed the research and wrote the paper; Teng WJ, Yuan XG and Ye XM performed the research and analyzed the data.

Correspondence to: Feng Ji, Professor, Department of Digestive Diseases, First Affiliated Hospital, College of Medicine, Zhejiang University, Hangzhou 310003, Zhejiang Province, China. jifeng1126@sina.com

Telephone: +86-571-87236532 Fax: +86-571-87236611

Received: July 12, 2010

Revised: September 20, 2010

Accepted: September 27, 2010

Published online: January 7, 2011

tients with IBD and healthy controls had heterozygous or homozygous SNPs variants.

CONCLUSION: Milk, fried food and stress are associated with increased risk of IBD. The common variants in *NOD2/CARD15* gene are not associated with IBD in China's Zhejiang population.

© 2011 Baishideng. All rights reserved.

Key words: Inflammatory bowel disease; Risk factors; Epidemiology; Gene polymorphism; *NOD2/CARD15* gene

Peer reviewer: Dr. John B Schofield, MB, BS, MRCP, FRCP, Department of Cellular Pathology, Preston Hall, Maidstone, Kent, ME20 7NH, United Kingdom

Abstract

AIM: To identify the risk factors and three single nucleotide polymorphisms (SNPs) of *NOD2/CARD15* gene in inflammatory bowel disease (IBD) of the population in Zhejiang, China.

METHODS: A case-control study was conducted using recall questionnaire to collect data on demographic, socioeconomic, lifestyle characteristics and dietary behaviors from 136 determined IBD patients and 136 paired healthy controls. COX regression method was used to screen the statistically significant risk factors for IBD. The polymorphisms of *NOD2/CARD15* gene *Arg702Trp*, *Gly908Arg* and *Leu1007fsinsC* were genotyped and further compared between 60 patients with IBD and 60 healthy controls by polymerase chain reaction and restriction fragment length polymorphism.

RESULTS: IBD occurred primarily in young and middle-aged people. The mean age for IBD patients was 42.6 years. The ratio of males to females was 1.23:1. COX regression indicated a higher statistical significance in milk, fried food and stress compared with the other postulated risk factors for IBD. None of the pa-

Wang ZW, Ji F, Teng WJ, Yuan XG, Ye XM. Risk factors and gene polymorphisms of inflammatory bowel disease in population of Zhejiang, China. *World J Gastroenterol* 2011; 17(1): 118-122 Available from: URL: <http://www.wjgnet.com/1007-9327/full/v17/i1/118.htm> DOI: <http://dx.doi.org/10.3748/wjg.v17.i1.118>

INTRODUCTION

Crohn's disease (CD) and ulcerative colitis (UC) are the two main types of idiopathic inflammatory bowel disease (IBD) whose etiology is multifactorial and still vague. Currently, the development of IBD is considered to have a close relationship with immunology, genetics, environment and infection. The incidence of IBD in Western populations increased during the past few decades with an estimated incidence of 0.35%-1.00% for CD and 0.10%-1.00% for UC^[1]. *NOD2/CARD15* is the first verified predisposing gene of CD where three *NOD2* variants *Arg702Trp*, *Gly908Arg* and *Leu1007fsinsC* were found to be associated with CD in the Caucasian populations^[2,3]. Nevertheless, these single nucleotide polymorphisms

(SNPs) were not found to predispose to CD in Japanese and Hong Kong populations^[4,5], leaving controversies on their exact role in CD. The number of patients with IBD has been increasing in China, but only a few studies have investigated the risk factors in IBD. Moreover, association between *NOD2* gene and the development of IBD has seldom been evaluated in the Chinese population^[6]. Therefore, the purpose of this study was to identify the risk factors by case-control studies and determine whether the *NOD2* variants are associated with IBD in the population of Zhejiang, China.

MATERIALS AND METHODS

Subjects

One hundred and thirty six patients with IBD and 136 age and sex-matched healthy controls were recruited from the First Affiliated Hospital of Zhejiang University, Jinhua Central Hospital, Ningbo Medical Treatment Center, Lihuili Hospital and Taizhou Hospital of Zhejiang Province between January 2005 and December 2008. The age of IBD patients (84 UC and 52 CD) ranged from 18 to 85 years. Written informed consent was obtained from all the cases and controls. Blood samples were collected from 60 patients (32 UC and 28 CD) and 60 healthy controls randomly. IBD was diagnosed based on the clinical, radiographic, endoscopic and histologic criteria.

Questionnaire

Each subject received a questionnaire to obtain demographic data. The questionnaire also contained items specifically related to IBD: education background, heredity, occupation condition (occupation classification and stress), habitat condition during the past 5 years (drinking water and toilet), infection, appendectomy, measles, oral contraceptive use, estrogen replacement, dietary habits (vegetarian diet or carnivorous diet), smoking history, tea drinking, and alcohol, milk, fried food and spicy food intake. All questionnaires were checked for completeness, and doubtful responses from both patients and healthy controls were confirmed upon return of the questionnaire.

Genotyping

DNA was isolated from peripheral blood using the Genomic DNA Isolation Kit (Sangon, Shanghai, China). All polymerase chain reaction (PCR) assays were performed in a 25 µL volume reaction. Three single nucleotide polymorphisms (SNPs) of *NOD2/CARD15* gene were amplified by specific primers (Table 1)^[7] under the following conditions: an initial denaturation at 95°C for 5 min, followed by 35 cycles of denaturing at 94°C for 20 s, annealing at 60°C (*Arg702Trp*), 55°C (*Gly908Arg*) or 58°C (*Leu1007fsinsC*) for 30 s and extension at 72°C for 1 min, and final incubation at 72°C for 7 min. PCR products were electrophoresed in a 2% agarose gel and visualized by ethidium bromide staining.

Genotyping for *Arg702Trp*, *Gly908Arg* and *Leu1007fsinsC* was performed using polymerase chain reaction and restriction fragment length polymorphism (PCR-RFLP):

Table 1 The primers for *NOD2/CARD15* gene

SNPs	Primers	Length of products (bp)
<i>Arg702Trp</i>	Forward 5'-CTTCCTG-GCAGGGCTGTGTC3' Reverse 5'-CATGCAC-GCTCTTGGCCTCAC3'	176
<i>Gly908Arg</i>	Forward 5'-AAGTCTGTAAT-GTAAAGCCAC3' Reverse 5'-CCCAGCTCCTCCCTCTTC3'	380
<i>Leu1007fsinsC</i>	Forward 5'-CCTG-CAGTCTCTTTAACTGG3' Reverse 5'-CTTAC-CAGACTTCCAGGATG3'	168

SNPs: Single nucleotide polymorphisms.

a 10 µL aliquot of the product was digested with an appropriate restriction enzyme. The tubes were incubated at 37°C for 4 h, and then transferred to 65°C for 20 min. After digestion, fragment sizes for carriers of the polymorphic alleles decreased, resulting in the presence of different fragments (Table 2). Products were electrophoresed in a 15% polyacrylamide gel and visualized by silver nitrate staining.

Statistical analysis

Semi-quantitative data were analyzed using COX regression to calculate relative risk (RR) and their 95% confidence interval. Frequencies and susceptibilities of mutations among CD, UC and controls were compared based on χ^2 or Fisher exact test. All data were analyzed in SPSS (version 13.0), where *P* value of 0.05 or less was considered statistically significant in all cases.

RESULTS

A total of 272 subjects were enrolled in the study who all completed the questionnaires. The mean age for IBD patients was 42.6 years and the ratio of males to females was 1.23:1. The result showed that milk, fried food intake and stress were risk factors for IBD in both univariate and multivariate logistic regression analysis (Tables 3 and 4). The number of cases of infection, appendectomy, oral contraceptive use, and estrogen replacement was too small for statistical analysis, so the data of these variables were not shown in the tables.

Electropherogram of the amplified DNA fragments is shown in Figure 1. PCR-PFLP analyses showed that *Arg702Trp*, *Gly908Arg* and *Leu1007fsinsC* alleles of 60 IBD patients and 60 healthy controls were all wild type. None of the patients with IBD and healthy controls had heterozygous or homozygous SNPs variants.

DISCUSSION

The etiology and pathogenesis of IBD have been and continue to be intensely investigated. Accumulating evi-

Table 2 The single nucleotide polymorphisms, restriction enzymes and products of *NOD2* gene

SNPs	Polymorphic alleles	Restriction enzymes	Wild-type alleles (bp)	Mutant alleles (bp)
Arg702Trp	C2104T	<i>Msp</i> I	76 + 54 + 24 + 22	130 + 24 + 22
Gly908Arg	G2722C	<i>Hha</i> I	380	242 + 138
Leu1007fsinsC	3020insC	<i>Nla</i> IV	168	128 + 40

SNPs: Single nucleotide polymorphisms.

Table 3 Univariate logistic regression analysis of risk factors for inflammatory bowel disease

Variables	χ^2	<i>P</i>	RR	95% CI	
				Lower bound	Upper bound
Habitat condition during the past 5 yr	1.192	0.274	0.653	0.303	1.404
Educational background	1.250	0.265	0.724	0.284	1.528
Occupation classification	0.894	0.293	0.615	0.314	1.412
Alcoholic drinking	0.987	0.361	0.712	0.194	1.512
Cigarette smoking	1.215	0.194	0.843	0.247	1.384
Tea drinking	1.523	0.165	0.631	0.315	1.423
Stress	18.452	< 0.001	1.295	1.151	1.457
Milk intake	25.425	< 0.001	1.279	1.162	1.407
Fried food intake	24.378	< 0.002	1.286	1.154	1.417

RR: Risk ratio; CI: Confidence interval.

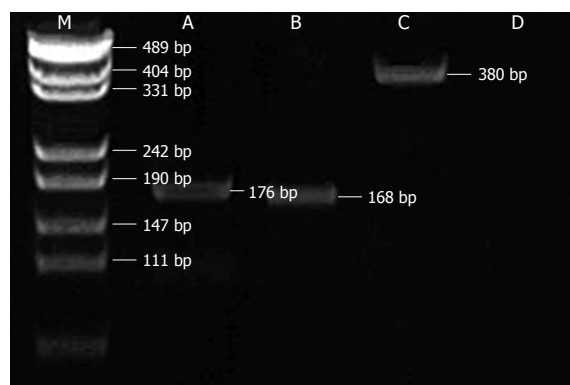
Table 4 Multivariate logistic regression analysis of risk factors for inflammatory bowel disease

Variables	χ^2	<i>P</i>	RR	95% CI	
				Lower bound	Upper bound
Milk intake	10.713	0.0011	1.243	1.091	1.415
Fried food intake	14.267	0.0002	1.238	1.108	1.383
Stress	13.377	0.0003	1.241	1.102	1.394

RR: Risk ratio; CI: Confidence interval.

dences strongly suggest that it is mediated immunologically and that the inflammatory process is influenced by environmental and host factors. In this study, we found a higher prevalence of IBD in young and middle-aged people which may be associated with the strong gastrointestinal immune function and intense immune response. The prevalence of CD was higher in males (36 cases) than in females (16 cases), but the prevalence of UC was similar among males (39 cases) and females (45 cases), which is consistent with other studies.

Many environmental factors may be involved in the pathogenesis of IBD, including: dietary habits, cigarette smoking, appendectomy, oral contraceptive use, infection and so on. However, the epidemiologic evidence for an etiologic role of these potential risk factors in IBD is inconsistent. In this study, there was a strong evidence for an increased risk of developing IBD associated with stress, milk intake and fried food. Stress increases gut muscle tone and intestinal transit time. Several studies reported that people with functional gastrointestinal disorders had significantly more behavioral and emotional symptoms than

**Figure 1** Amplified fragments of *NOD2/CARD15* gene. M: DNA marker; A: Amplified fragment of Arg702Trp; B: Amplified fragment of Leu1007fsinsC; C: Amplified fragment of Gly908Arg; D: Negative control.

healthy people^[8]. UC patients are most likely to experience the problems like mood and anxiety^[9]. Some hormones released during stress (e.g. corticotrophin-releasing factor) can promote intestinal inflammation and alter visceral sensitivity when released locally in the gut^[10]. Epidemiological studies showed that the prevalence of IBD varies among populations. The immigrants had a different incidence of IBD within a generation. It has been suggested that different food antigens play a significant role. The present study confirms an increased risk of developing IBD associated with milk intake. IgE-mediated allergy to cow's milk proteins is common in the children and adults who experience repeated gastrointestinal symptoms, and often is the first manifestation of food allergy. Cow's milk protein allergy may induce the abnormal immune response of digestive tract that increases the relative risk of IBD. In epidemio-

logic studies, high-temperature cooking methods have been associated with the formation of carcinogenic substances such as heterocyclic amines, acrylamide and polycyclic aromatic hydrocarbons^[11]. These products have been associated with endothelial dysfunction and inappropriate immune responses, which results in the development of IBD and intestinal cancer.

Cigarette smoking that has been reported as a risk factor for IBD in many studies might even have beneficial effects on the course of UC, but exacerbates the course of CD. The potential mechanisms involved in this dual relationship may include the effects of nicotine administration on inflammatory cytokine, changes in blood flow and gut permeability^[12]. In this study, cigarette smoking was not significantly associated with the development of IBD. Studies showed that IBD patients were more likely to be white collar and urban residents with high educational background. Infection and oral contraceptive use were considered to increase the risk of developing IBD, whereas vegetarian diet, tea drinking, spicy food intake and appendectomy decreased the risk. In this study, no significant association was found between these factors and IBD.

Monozygotic twin concordance, familial predisposition, and segregation analyses have shown that genetic factors confer susceptibility to IBD. *NOD2/CARD15* gene locates on chromosome 16q12, encoding a member of the Apat-1/Ced-4 superfamily of apoptosis regulator that is expressed in monocytes. *NOD2/CARD15* gene is involved in the recognition of lipopolysaccharide and subsequent activation of necrosis factor- κ B, and disturbs the activation of the innate immune system by bacterial antigens. *NOD2/CARD15* gene mutation or deletion induces the abnormal innate immune response, which is important for immunological protection against intestinal microbes and may contribute to the development of IBD. Increased *CARD15* was detected in mononuclear and epithelial cells of colon in CD patients^[13,14]. Hugot *et al.*^[2] showed that a frame shift variant and two missense variants were associated with CD. This result is in accordance with the studies in different populations^[3,7]. In our study, common *NOD2* variants associated with increased susceptibility to CD in Caucasian populations were not verified in the Zhejiang population. It is conceivable that the *NOD2* variants present in Caucasian patients are rare or nonexistent in the Zhejiang population and not detected in our limited population sample. Our results are in agreement with those studies in Asian patients^[4,5]. This diversity of linkage analyses may arise from the heterogeneity of the disease and differences in genetic background of the population studied.

Human epidemiologic studies combine both parts of the typical risk assessment process into a single study by assessing the degree of exposure and the association with the risk of disease in a single study. The present study supports that intestinal environmental and genetic factors are vital for the pathogenesis of IBD. However, the heterogeneity among the small number of studies limited the ability to draw conclusions. Further studies using a larger cohort of patients with IBD are warranted to identify the risk factors and gene susceptibility to IBD.

COMMENTS

Background

Crohn's disease (CD) and ulcerative colitis (UC) are the two main types of idiopathic inflammatory bowel disease (IBD) whose etiology is multifactorial and still vague. The development of IBD is considered to be closely related to immunology, genetics, environment and infection. *NOD2/CARD15* is the first verified predisposing gene of CD in the Caucasian populations.

Research frontiers

The etiology and pathogenesis of IBD have been and continue to be intensely investigated. Three *NOD2* variants *Arg702Trp*, *Gly908Arg* and *Leu1007fsinsC* were found to be associated with CD in the Caucasian populations, but not in Japanese and Hong Kong populations. In this study, the authors identified the risk factors by case-control study and determined whether the *NOD2* variants are associated with IBD in China's Zhejiang population.

Innovations and breakthroughs

Only a few studies have investigated the risk factors of IBD in China. Moreover, the association between *NOD2* gene and the development of IBD has seldom been evaluated in the Chinese population. This study demonstrated that milk, fried food and stress are associated with increased risk of IBD, and the common variants in *NOD2/CARD15* gene are not associated with IBD in the Zhejiang population.

Applications

NOD2 variants present in Caucasian patients may be rare or nonexistent in the Zhejiang population. Milk, fried food and stress are the potential risk factors for IBD.

Terminology

NOD2/CARD15 gene locates on chromosome 16q12, encoding a member of the Apat-1/Ced-4 superfamily of apoptosis regulator that is expressed in monocytes. *NOD2/CARD15* gene is involved in the recognition of lipopolysaccharide and subsequent activation of necrosis factor- κ B, and disturbs the activation of the innate immune system by bacterial antigens. *NOD2/CARD15* gene mutation or deletion can induce the abnormal innate immune response.

Peer review

This is an interesting paper looking at 136 IBD patients and paired healthy controls from the Zhejiang population comparing risk factors, and SNP analysis of *NOD2/CARD15* in 60 patients and paired controls. No patients had variants in the *NOD2/CARD15* gene by the methods used. Milk, fried food and stress were cited as potential risk factors. This work adds to the existing literature on *NOD2*, and supports the finding of lack of association with IBD in oriental populations.

REFERENCES

- 1 Chinese Medical Association Digestion Branch. Guidelines for diagnosis and management of inflammatory bowel disease. *Zhonghua Xiaohua Zazhi* 2001; **21**: 236-239
- 2 Hugot JP, Chamaillard M, Zouali H, Lesage S, Cézard JP, Belaiche J, Almer S, Tysk C, O'Morain CA, Gassull M, Binder V, Finkel Y, Cortot A, Modigliani R, Laurent-Puig P, Gower-Rousseau C, Macry J, Colombel JF, Sahbatou M, Thomas G. Association of *NOD2* leucine-rich repeat variants with susceptibility to Crohn's disease. *Nature* 2001; **411**: 599-603
- 3 Hampe J, Cuthbert A, Croucher PJ, Mirza MM, Mascheretti S, Fisher S, Frenzel H, King K, Hasselmeier A, MacPherson AJ, Bridger S, van Deventer S, Forbes A, Nikolaus S, Lennard-Jones JE, Foelsch UR, Krawczak M, Lewis C, Schreiber S, Mathew CG. Association between insertion mutation in *NOD2* gene and Crohn's disease in German and British populations. *Lancet* 2001; **357**: 1925-1928
- 4 Inoue N, Tamura K, Kinouchi Y, Fukuda Y, Takahashi S, Ogura Y, Inohara N, Núñez G, Kishi Y, Koike Y, Shimosegawa T, Shimoyama T, Hibi T. Lack of common *NOD2* variants in Japanese patients with Crohn's disease. *Gastroenterology* 2002; **123**: 86-91
- 5 Leong RW, Armuzzi A, Ahmad T, Wong ML, Tse P, Jewell DP, Sung JJ. *NOD2/CARD15* gene polymorphisms and Crohn's disease in the Chinese population. *Aliment Pharmacol Ther* 2003; **17**: 1465-1470
- 6 Ouyang Q. Research strategies of inflammatory bowel dis-

- ease. *Zhonghua Xiaohua Zazhi* 2005; **25**: 385-386
- 7 **Tukel T**, Shalata A, Present D, Rachmilewitz D, Mayer L, Grant D, Risch N, Desnick RJ. Crohn disease: frequency and nature of CARD15 mutations in Ashkenazi and Sephardi/Oriental Jewish families. *Am J Hum Genet* 2004; **74**: 623-636
- 8 **Wang L**, Xia XZ, Jiang SD. Psychological analysis of functional gastrointestinal diseases. *Tiedao Yixue* 2002; **30**: 31-32
- 9 **Liu FQ**, Chu GW, Li ZH, Li P, Zhang RQ. Psychological factors and ulcerative colitis. *Zhongguo Jianshang Xinlixue Zazhi* 2001; **9**: 307-308
- 10 **Larauche M**, Kiank C, Tache Y. Corticotropin releasing factor signaling in colon and ileum: regulation by stress and pathophysiological implications. *J Physiol Pharmacol* 2009; **60** Suppl 7: 33-46
- 11 **Terry PD**, Lagergren J, Wolk A, Steineck G, Nyrén O. Dietary intake of heterocyclic amines and cancers of the esophagus and gastric cardia. *Cancer Epidemiol Biomarkers Prev* 2003; **12**: 940-944
- 12 **Karban A**, Eliakim R. Effect of smoking on inflammatory bowel disease: Is it disease or organ specific? *World J Gastroenterol* 2007; **13**: 2150-2152
- 13 **Berrebi D**, Maudinas R, Hugot JP, Chamaillard M, Chareyre F, De Lagausie P, Yang C, Desreumaux P, Giovannini M, Cézard JP, Zouali H, Emilie D, Peuchmaur M. Card15 gene overexpression in mononuclear and epithelial cells of the inflamed Crohn's disease colon. *Gut* 2003; **52**: 840-846
- 14 **Lala S**, Ogura Y, Osborne C, Hor SY, Bromfield A, Davies S, Ogunbiyi O, Nuñez G, Keshav S. Crohn's disease and the NOD2 gene: a role for paneth cells. *Gastroenterology* 2003; **125**: 47-57

S- Editor Sun H L- Editor Ma JY E- Editor Ma WH

Surgical vs percutaneous radiofrequency ablation for hepatocellular carcinoma in dangerous locations

Ji-Wei Huang, Roberto Hernandez-Alejandro, Kristopher P Croome, Lu-Nan Yan, Hong Wu, Zhe-Yu Chen, Pankaj Prason, Yong Zeng

Ji-Wei Huang, Lu-Nan Yan, Hong Wu, Zhe-Yu Chen, Pankaj Prason, Yong Zeng, Department of Hepato-Biliary-Pancreatic Surgery, Division of Liver Transplantation, West China Hospital, Sichuan University, Chengdu 610041, Sichuan Province, China

Roberto Hernandez-Alejandro, Kristopher P Croome, Department of Surgery, University of Western Ontario, Hepato-biliary and Liver Transplant Surgery, London Health Sciences Centre, London Ontario, N6A 4S2, Canada

Author contributions: Hernandez-Alejandro R and Croome KP designed the study; Huang JW, Yan LN, Wu H, Chen ZY, Prason P and Zeng Y performed the research; Huang JW, Zeng Y, Hernandez-Alejandro R and Croome KP made the analyses and wrote the article.

Correspondence to: Yong Zeng, MD, Department of Hepato-Biliary-Pancreatic Surgery, Division of Liver Transplantation, West China Hospital, Sichuan University, Chengdu 610041, Sichuan Province, China. zengyongmd@gmail.com

Telephone: +86-28-85422475 Fax: +86-28-85422475

Received: August 2, 2010 Revised: October 11, 2010

Accepted: October 18, 2010

Published online: January 7, 2011

Abstract

AIM: To compare the long-term outcome of percutaneous vs surgical radiofrequency ablation (RFA) for hepatocellular carcinoma (HCC) in dangerous locations.

METHODS: One hundred and sixty-two patients with HCC in dangerous locations treated with percutaneous or surgical RFA were enrolled in this study. The patients were divided into percutaneous RFA group and surgical RFA group. After the patients were regularly followed up for a long time, their curative rate, hospital stay time, postoperative complications and 5-year local tumor progression were compared and analyzed.

RESULTS: No significant difference was observed in curative rate between the two groups (91.3% vs 96.8%, $P = 0.841$). The hospital stay time was longer

and more analgesics were required while the incidence of bile duct injury and RFA-related hemorrhage was lower in surgical RFA group than in percutaneous RFA group ($P < 0.05$). The local progression rate of HCC in dangerous locations was significantly lower in surgical RFA group than in percutaneous RFA group ($P = 0.05$). The relative risk of local tumor progression was 14.315 in percutaneous RFA group.

CONCLUSION: The incidence of severe postoperative complications and local tumor progression is lower after surgical RFA than after percutaneous RFA.

© 2011 Baishideng. All rights reserved.

Key words: Hepatocellular carcinoma; Radiofrequency ablation; Liver cirrhosis; Recurrence; Local therapy

Peer reviewer: Emanuel K Manesis, MD, Professor of Medicine, Athens University School of Medicine, Liver Unit, Euro-clinic, 19 Mavromateon Street, Athens 10 34, Greece

Huang JW, Hernandez-Alejandro R, Croome KP, Yan LN, Wu H, Chen ZY, Prason P, Zeng Y. Surgical vs percutaneous radiofrequency ablation for hepatocellular carcinoma in dangerous locations. *World J Gastroenterol* 2011; 17(1): 123-129 Available from: URL: <http://www.wjgnet.com/1007-9327/full/v17/i1/123.htm> DOI: <http://dx.doi.org/10.3748/wjg.v17.i1.123>

INTRODUCTION

Hepatocellular carcinoma (HCC) is currently the fifth most common malignant neoplasm in the world^[1], causing more than 500 000 deaths every year^[2]. HCC is prevalent in Asia and Africa and its incidence has steadily increased in European and American populations^[3,4]. Theoretically, the best treatment of HCC is orthotopic liver transplantation (OLT) which provides the opportunity for its cure^[5], but the scarcity of donors limits this treatment.

In the last two decades, local ablative therapy has become a safe and effective procedure for small HCC, of which radiofrequency ablation (RFA) is considered the most promising one^[6]. It was reported that RFA for small HCC provides a comparable survival time and local tumor control after surgical resection^[7,8], and may also be used as a bridge therapy for liver transplantation^[9-11]. RFA is minimally invasive with a lower complication rate and a shorter hospital stay time than hepatectomy^[12,13].

Although the indication of RFA is much wider than that of surgical resection for HCC, tumors in some circumstances are reported^[14-18] not quite suitable for RFA, such as a central nodule near the porta hepatis due to the risk of injuring major bile ducts, a nodule near large vessels due to a heat sink effect-induced incomplete ablation, a peripheral nodule near extrahepatic organs due to the risk of alimentary tract perforation or pleural effusion caused by heat injury.

In our institute, tumor location is not simply regarded as a contraindication of RFA. This retrospective study was designed to compare the long-term outcome of percutaneous and surgical RFA for HCC in these so-called dangerous locations. To the best of our knowledge, it is the first study comparing the efficacy of surgical and percutaneous RFA for HCC in dangerous locations of the liver.

MATERIALS AND METHODS

Diagnostic criteria

Diagnosis of HCC was made according to the diagnostic criteria for HCC recommended by the European Association for the Study of the Liver^[19], which was based on ultrasound-guided biopsy, or the concordant classical dynamic radiological features of HCC in two radiologic techniques, or one radiologic technique showing typical features of HCC together with an elevated α fetoprotein (AFP) level over 400 ng/mL.

Definition

Tumor in dangerous locations^[18] was defined as a lesion (\leq 0.5 cm in diameter) near large vessels such as a primary or secondary branch of the portal vein, the base of hepatic veins, or the inferior vena cava (IVC), or as a lesion (less than 0.5 cm in diameter) near extrahepatic organs measured on radiological images.

A curative treatment^[19] was defined as no residual viable tumor tissue within the treatment zone confirmed by a 4-wk-afterward-performed spiral triphasic enhanced CT after a complete ablation of the lesion assessed by intraoperative ultrasonography (IOUS).

Local tumor progression^[20] was defined as the appearance of viable tumor tissue that was contiguous with the area completely ablated during follow-up.

Inclusion criteria and enrollment

In our institute, a curative RFA is usually expected for patients conforming to the Milan criteria for liver transplantation. The inclusion criteria in this study included patients with a confirmed diagnosis of HCC or a solitary HCC (\leq

5 cm in diameter) or up to 3 nodules ($<$ 3 cm in diameter), liver function of Child-Pugh class A or B, a prothrombin time of less than 5 s, a HBV-DNA-PCR quantitation of less than 10^5 copies/mL, but without extrahepatic metastasis or obvious vascular invasion, previous or simultaneous malignancies or evident bleeding tendency (a platelet count $> 50 \times 10^9$ /L or correctable by transfusion, no previous treatment of HCC, and those suitable and willing to be treated with RFA).

The study was performed according to the guidelines of the Helsinki Declaration. A written informed consent was obtained from each patient before intervention. Between February 2003 and February 2007, RFA was performed for 794 consecutive HCC patients in West China Hospital. Of these patients, 513 were diagnosed as primary HCC, 484 of them met the inclusion criteria. Of these 484 patients, 162 had at least one nodule in dangerous locations.

Follow-up

Patients were followed up at a three month interval after treatment. Abdominal ultrasonography and helical computer tomography (CT), serum AFP measurement and liver function tests were performed during each visit. When intrahepatic recurrence was suspected, spiral CT or magnetic resonance imaging (MRI) was performed. When extrahepatic metastases were suspected, thoracic CT and bone scintigraphy were performed. Local tumor progression was specifically noticed as the endpoint in this study.

Statistical analysis

Differences in the surgical and percutaneous RFA groups were analyzed by the unpaired *t* test for continuous variables and by the χ^2 test or continuity correction method for categorical variables. Local tumor progression curves were plotted with the Kaplan-Meier method and compared by the log-rank test. Relative prognostic significance of the variables in predicting local tumor progression was assessed with univariate and multivariate Cox proportional hazards regression models. All variables with their *P* $<$ 0.05 by univariate comparison were subjected to multivariate analysis. Results of multivariate analysis were presented as relative risk (RR) with corresponding 95% confidence intervals (CI). Statistical analysis was performed using the SPSS 13.0 statistical software (SPSS Company, Chicago, Illinois, USA). All statistical tests were two-sided and differences were considered when *P* $<$ 0.05.

RFA procedure

Equipments: All RFA procedures were performed on an inpatient basis by surgeons from the Department of Hepato-biliary-pancreatic Surgery using a commercially available system (Radionics, Cool-Tip System, Burlington, MA, USA), single/clustered needle electrode(s) with a 2 cm or 3 cm exposed tip and ultrasound guidance (Vivid4, GE, USA; iU22, Philips, USA). Clustered electrodes were used systematically for lesions ($>$ 3 cm in diameter).

Percutaneous RFA: General anesthesia was employed, 2-4 grounding pads were attached to the thighs of pa-

tients and the electrode was inserted into the lesion according to a route assessment via ultrasound. The needle tip was inserted to the bottom of the tumor (i.e. the most distal border from the skin puncture site) in the first session to avoid gas formation between non-ablated lesion and ultrasound transducer. At the time of subsequent RFA sessions, the electrode position was determined via IOUS scrutiny. The ablation subsequence was always from “bottom” to “top” to provide a clear, real-time ultrasound image. The electrode was inserted at different sites and overlapping ablations were performed until the entire lesion was ablated as determined by IOUS.

Assessment of ablation: After measurement of the baseline impedance, generator output power was gradually increased from 80 W to 200 W, with a peristaltic pump infusing cold saline into the electrode lumen to maintain the tip temperature below 20°C. The timer was usually set to 12 min for each session. Impedance was synchronously monitored with the system. Session in the same site was repeated until the impedance increased at least 10 Ohms over baseline and became stable. The electrode was heated to 90-100°C before it was drawn back in order to eliminate seeding cancer cells and prevent bleeding. Treatment was continued until complete ablation features were achieved in IOUS.

RFA in dangerous locations

Percutaneous RFA: The route of electrode insertion should be carefully considered on ultrasound scrutiny. When the tumor was in segment VII, close to the diaphragm, the electrode was inserted through the right pleural cavity of patients. Saline was infused into the right pleural cavity to compress the right lobe of the lung, then the electrode reached the target under the ultrasound-guidance and percutaneous RFA was achieved through an artificial serothorax. A thoracic close drainage was needed for 2 d after therapy.

Surgical RFA: A right subcostal incision with a midline extension was chosen. Extensive dissociation of the liver was usually performed from the ligaments and adhesions to other organs, such stomach, colon or kidneys and large vessels. The route of surgical RFA was assessed by IOUS on the liver surface. The distance between the tumor and other vulnerable organs or vessels could be enlarged when the operator rotated the liver.

Ablation timing: The time of RFA was usually irregular in the dangerous locations, RFA was stopped as soon as the ultrasound detected microbubbles generated by RFA reaching the distal border of the assumed area. An experienced operator managed most injuries to adjacent organs and structures as well as the heat sink effect from large vessels with RFA.

Assessment of response

Response was assessed according to the modified European Association for the Study of the Liver criteria^[19].

Table 1 Demographic parameters of patients undergoing percutaneous and surgical radiofrequency ablation

Parameters	Patients undergoing percutaneous RFA (n = 63)	Patients undergoing surgical RFA (n = 93)	P value
Age (yr)	57.8 ± 16.1	52.4 ± 11.7	0.531
Gender (M/F)	55/14	81/12	0.205
HBV infected	58	91	0.006
HCV infected	1	0	
None-HBV&HCV	10	2	
Liver cirrhosis	46	71	0.174
AST (IU/L)	47.3 ± 36.2	44.6 ± 33.8	0.311
ALT (IU/L)	42.3 ± 31.4	44.1 ± 19.6	0.354
TB (μmol/L)	15.4 ± 3.4	14.2 ± 5.6	0.601
ALB (g/L)	39.1 ± 9.8	41.7 ± 5.4	0.852
Child A/B	61/8	93/0	0.001
PLT (< 10 ¹¹)	13	9	0.092
PT (> 15')	6	14	0.224
Tumor number, 1/2/3	51/16/2	79/13/1	0.095
Tumor size (cm), > 3/≤ 3	11/78	23/85	0.099
Solitary HCC (cm), ≤ 3	39	62	0.188
Tumor in dangerous locations	73	95	0.242
AFP (ng/mL), ≤ 400/> 400/> 1210	13/41/15	17/60/16	0.000

Non-hepatitis B virus (HBV) & hepatitis C virus (HCV): Patients who were negative for HBV and HCV antibody but not for anti-HBs. RFA: Radiofrequency ablation; ALT: Alanine aminotransferase; AST: Aspartate aminotransferase; AFP: α fetoprotein; TB: Total bilirubin; PLT: Platelet; PT: Prothrombin time; ALB: Albumin.

Spiral triphasic enhanced CT was performed one month after RFA. Residual viable tumor was diagnosed if an enhanced area was noted within the treatment zone. If RFA was repeated, another CT was performed four weeks later to assess the response to RFA. If residual viable tissue of the tumor still existed, RFA was considered a failure and the patient was treated with transcatheter hepatic arterial chemoembolization (TACE).

Potential conflict of interest

This study did not receive any support from industry or private corporations.

RESULTS

Of the 482 patients, 162 had at least one nodule in the dangerous locations (156 had a lesion and 6 had 2 lesions in the dangerous locations) and 320 had HCC in the ordinary location. Of the 162 patients with HCC in dangerous locations, 34 had their diagnosis made by biopsy and 128 were diagnosed non-invasively, 69 received percutaneous RFA and 93 underwent surgical RFA. The demographic parameters of patients who underwent percutaneous and surgical RFA are listed in Table 1. A significant difference was found in HBV/HCV-infection and serum AFP level ($P < 0.05$). The tumor locations and adjacent vessels and organs in patients who underwent percutaneous and surgical RFA are shown in Table 2. The mean follow-up time of patients who underwent percutaneous and surgical RFA was 28.4 ± 14.7 mo (range 3-81 mo) and 31.6 ± 24.1 mo

Table 2 Locations of lesions in patients undergoing percutaneous and surgical radiofrequency ablation

	RFA	
	Percutaneous (<i>n</i> = 89)	Surgical (<i>n</i> = 108)
Segment location		
I	0	0
II	7	12
III	13	17
IV	9	12
V	10	14
VI	6	11
VII	12	20
VIII	12	7
Adjacent vessels or organs		
PH	8	12
RHV	17	15
MHV	8	12
LHV	11	16
IVC	6	8
Heart	3	5
Stomach	9	17
Lung	15	2
R.Kidney	4	7
Colon	5	12
GB	3	2

$P = 0.640$ by Pearson χ^2 test for segment location and $P = 0.054$ by Pearson χ^2 test for adjacent vessels or organs. Lesion between segments was registered at the major location. *n*: Lesion number; RFA: Radiofrequency ablation; PH: Porta hepatis; RHV: Right hepatic vein; MHV: Middle hepatic vein; LHV: Left hepatic vein; IVC: Inferior vena cava; GB: Gall bladder.

(range 6–78 mo), respectively ($P > 0.05$). Censored patients included 17 out of the 69 patients who underwent percutaneous RFA and 22 out of the 93 patients who underwent surgical RFA ($P = 0.885$).

Patients who underwent percutaneous RFA

Eighty-nine lesions were found in 69 patients who underwent percutaneous RFA (Table 1). The mean treatment session was 2.0 ± 1.2 /lesion for the 78 nodules (≤ 3 cm in diameter) and 3.4 ± 0.8 /lesion for the 7 nodules (larger than 3 cm but smaller than 5 cm in diameter). Of the 89 lesions, 73 nodules were found in the dangerous locations, the mean tumor size was 1.7 ± 1.1 cm, and the mean treatment session was 3.7 ± 2.1 /lesion. The complete RFA rate was 98.6% (68/69) assessed intraoperatively, and the curative rate was 91.3% (63/69) assessed by CT 4 wk thereafter. The RFA failure rate was 4.3% (3/69). Two patients failed to achieve a curative outcome after 2 times of percutaneous RFA. The last patient had one nodule (1 cm in diameter) in 2 tumors very close to the pericardium. RFA was aborted due to the concern of malpositioning the electrode byIOUS. These three patients were later treated with TACE.

Patients who underwent surgical RFA

One hundred and eight lesions were found in 93 patients who underwent surgical RFA (Table 1). The mean treatment session was 1.2 ± 0.5 /lesion for the 85 nodules (≤ 3 cm in diameter) and 2.8 ± 0.9 /lesion for the 23 nodules

Table 3 Major complications of radiofrequency ablation

Classification of complications	Percutaneous RFA (<i>n</i> = 69)	Surgical RFA (<i>n</i> = 93)	<i>P</i> value
Grade I			
Analgesics requirement	17	58	0.000
Fever above 38.5°C	23	45	0.055
Grade II			
Ascites	4	11	0.190
Persistent jaundice	2	0	0.315
Gastric hemorrhage	0	3	0.132
Grade III			
Hydrothorax requiring drainage	5	9	0.586
Skin burn	1	0	0.244
Encapsulated effusion needing drainage	3	1	0.184
Grade IV			
Partial hepatic infarction	1	3	0.471
Gastric perforation	1	0	0.244
Bile duct injury	5	1	0.040
Procedure-related hemorrhage	6	1	0.018
Malignant seeding	2	0	0.315

RFA: Radiofrequency ablation.

(larger than 3 cm but smaller than 5 cm in diameter). The mean tumor size and mean treatment session were 1.8 ± 1.0 cm and 2.9 ± 2.0 /lesion, respectively, for the 95 nodules in the dangerous locations. The complete RFA rate was 100% (93/93) assessed intraoperatively, and the curative rate was 96.8% (90/93) assessed by CT 4 wk afterward. The RFA failure rate was 1.1% (1/93). A nodule (4 cm in diameter) in a patient who failed to RFA compressed the right hepatic duct. To avoid the bile duct injury, a stent was inserted into the compressed bile duct, and ethanol was injected into the adjacent tumor border to the bile duct before RFA. Unfortunately, bile fistula still occurred on day 25 after operation, and CT showed an incomplete ablation of the tumor. A T-tube drainage was placed *via* laparotomy later. Tumor encroaching on the right hepatic duct wall was highly suspected, and treated with palliative therapy due to poor liver function.

Hospital stay time and mortality of patients, and complications of RFA

The hospital stay time of HCC patients was significantly longer after surgical RFA than after percutaneous RFA (6.1 ± 3.1 d *vs* 3.5 ± 2.9 d, $P < 0.001$).

No patient died within 30 d after surgical and percutaneous RFA with a mortality of 0%.

According to the accorcion severity grading system of surgical complications^[21], the complications of percutaneous and surgical RFA are shown in Table 3. The number of patients requiring analgesics was significantly greater after surgical RFA than after percutaneous RFA ($P < 0.001$). However, the incidence of bile duct injury and RFA-related hemorrhage was higher in patients after percutaneous RFA than after surgical RFA ($P = 0.05$).

Local tumor progression

During the 5-year study period after treatment, the local

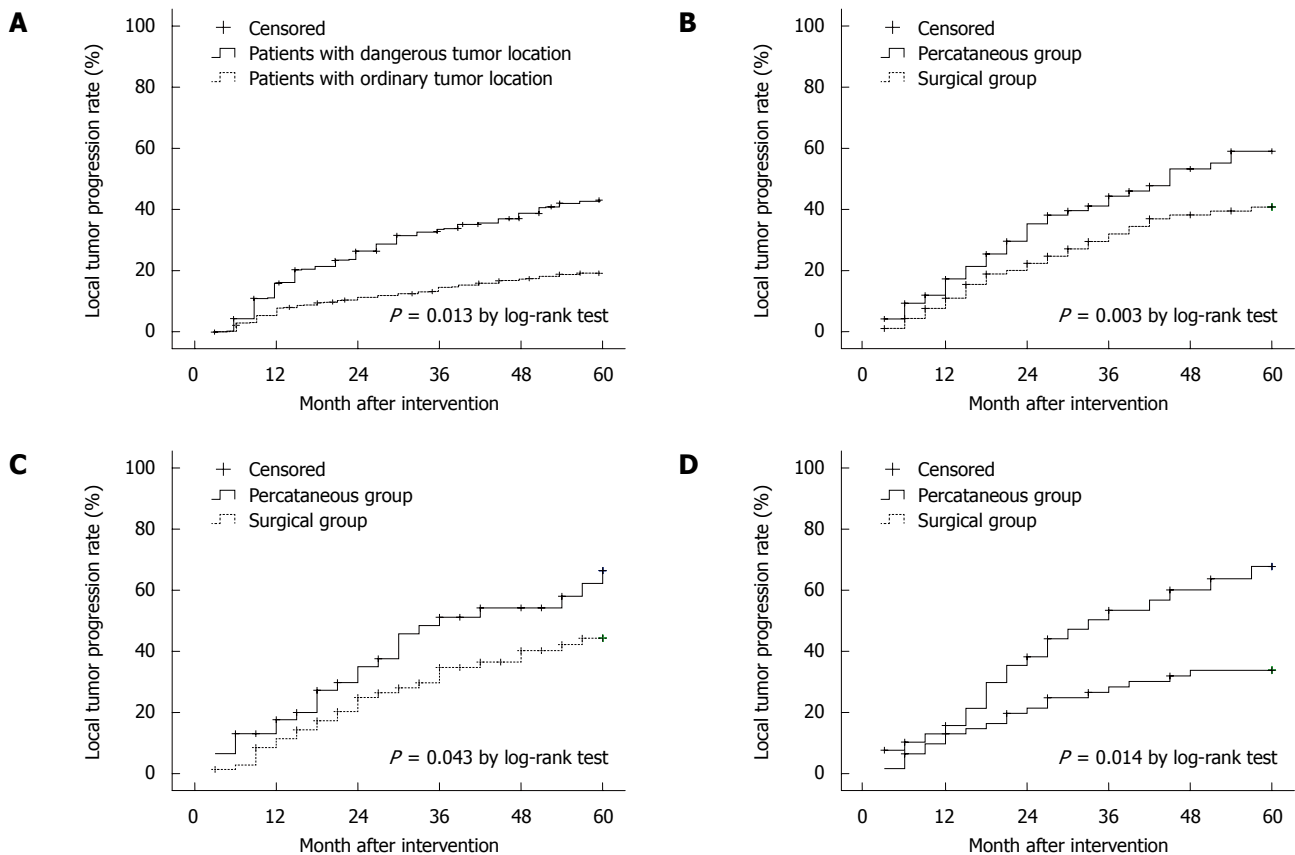


Figure 1 Local tumor progression in patients with hepatocellular carcinoma at common and dangerous locations (A), and hepatocellular carcinoma (B), cirrhosis (C), solitary hepatocellular carcinoma with its diameter ≥ 3 cm (D) after percutaneous and surgical radiofrequency ablation.

tumor progression was observed in 75 (46.3%) out of the 162 patients with HCC in the dangerous locations and in 71 (22.2%) out of the 320 patients with HCC in the general locations. The local tumor progression was more severe in patients with HCC in the dangerous locations than in those with HCC in the general locations ($P < 0.015$, Figure 1A).

Of the 162 patients with HCC in the dangerous locations, 69 and 93 were treated with percutaneous RFA and surgical RFA, respectively. Local tumor progression was observed in 40 out of the 69 patients with HCC after percutaneous RFA and in 35 out of the 93 patients after surgical RFA. The 1-, 2-, 3-, 4-, 5-year local tumor progression rate was 17.4%, 36.2%, 46.4%, 53.6%, 57.6%, respectively, for patients after percutaneous RFA, and 9.9%, 21.5%, 30.1%, 35.5%, 37.6%, respectively, for those after surgical RFA. The local tumor progression was more severe in patients after percutaneous RFA than after surgical RFA ($P < 0.003$, Figure 1B).

Forty-six out of the 63 cirrhotic patients underwent percutaneous RFA and 71 out of the 93 cirrhotic patients underwent surgical RFA (Table 1). The local tumor progression was more severe in patients after percutaneous RFA than after surgical RFA ($P < 0.05$, Figure 1C).

Thirty-nine out of the 69 patients with solitary HCC (≤ 3 cm in diameter) underwent percutaneous RFA and 62 out of the 93 patients with HCC underwent surgical RFA (Table 1). The local tumor progression was more

severe in patients after percutaneous RFA than after surgical RFA ($P < 0.05$, Figure 1D).

Univariate analysis revealed that 5 out of the 10 variables (RFA approach, Child-Pugh class, total bilirubin level, serum AFP level and tumor size) were related to local tumor progression. Multivariate Cox proportional hazards regression analysis showed that percutaneous RFA, total bilirubin level > 10 ng/L and tumor size > 3 cm were the related risk factors for HCC. The corresponding relative risks were 14.315 (95% CI: 4.857-25.412), 8.124 (95% CI: 2.325-101.587), and 11.741 (95% CI: 3.754-21.665), respectively (Table 4).

DISCUSSION

One important advantage of RFA for liver tumors is micro-invasive when compared with partial hepatectomy^[12,13,22-25]. Some institutes have reported RFA on an out-patients basis^[26]. However, even though the morbidity of malignant seeding in the needle tract is low, it is hard to avoid^[27,28]. Moreover, hemorrhage after the electrode is drawn out appears undetectable in a short time by ultrasonography.

In this study, the hospital stay time of patients with HCC was significantly longer with more analgesics required after surgical RFA than after percutaneous RFA. Surgical RFA seemed more invasive than percutaneous RFA. However, the incidence of more severe complica-

Table 4 Univariate and multivariate analysis of relative risks for local tumor progression

Variable	Univariate analysis	Multivariate analysis	
	<i>P</i> value	Relative risk (95% CI)	<i>P</i> value
Percutaneous vs surgical RFA	0.000	14.315 (4.857-25.412)	0.000
Age (yr) (> 60 vs ≤ 60)	0.402		
HBV- infected (Y vs N)	0.455		
Child-Pugh (B vs A)	0.038		
Albumin (IU/L), ≤ 35 vs > 35	0.233		
Total bilirubin (mg/L), > 10 vs ≤ 10	0.010	8.124 (2.325-101.587)	0.012
Serum AFP (ng/mL), ≥ 400 vs < 400	0.019		
Prothrombin time, ≤ 15' vs > 15'	0.512		
Tumor size (cm), > 3 vs ≤ 3	0.003	11.741 (3.754-21.665)	0.005
Tumor number, multiple vs single	0.111		

RFA: Radiofrequency ablation; HBV: Hepatitis B virus; AFP: α fetoprotein.

tions, such as bile duct injury and procedure-related hemorrhage, was lower in patients after surgical RFA than after percutaneous RFA.

It was reported that a lesion in dangerous locations of the liver is treated with artificial hydrothorax and ascites to achieve percutaneous RFA^[18]. A curative RFA was achieved with artificial hydrothorax in 3 patients in this study. However, artificial ascites was not applied when HCC near extrahepatic organs was treated, because the local ascites was not always capable of dividing a safety zone, the fluidity of liquid made the ascites lack of tension to support a safety zone, membrane adhesions unusually existed between organs and liver, the lesion was often located very close to the surface of the liver when the artificial ascites was needed, and ascites decreased the temperature at the outer part of the lesion when RFA was performed. Thus viable tumor cells could survive.

Compared with surgical RFA, IIOUS of percutaneous RFA is indirect (through abdominal wall), and the choice of route to the lesion is restricted. Injury of important structures, such as bile ducts or extrahepatic organs, should be avoided and RFA should eliminate the viable tumor cells in the assumed area as complete as possible. RFA should be stopped as soon as the ultrasonography shows microbubbles generated by RFA reaching the assumed distal border. In this study, the mean session for each lesion in the dangerous locations was 3.7 ± 2.1 /lesion in percutaneous RFA group and 2.9 ± 2.0 /lesion in surgical RFA group. The patients undergoing percutaneous RFA needed significantly more sessions than those undergoing surgical RFA to ablate a lesion ($P < 0.05$). The effect of percutaneous RFA mainly depends on the experience of operators. On the contrary, surgical RFA may provide a direct ultrasonography monitoring the liver surface, even a visual contact during the procedure. A mobilized liver could offer more choices of route for the electrode and a reliable safety zone in extrahepatic organs or IVC. Thus more attention should be paid to tumor elimination, even the routine impedance-dependent assessment technique can be applied in some surgical RFA procedures and in evaluation by IIOUS, which may be more accurate than that used in percutaneous RFA procedures

and can at least in part explain why more severe local tumor progression was found in patients after percutaneous RFA than after surgical RFA.

This study has the following limitations. First, it was a retrospective study and therefore had inherent defects due to the nature of the method. Second, the rate of censor patients was relatively high in patients undergoing percutaneous and surgical RFA. Third, physicians with diverse experiences might achieve different outcomes of percutaneous RFA. Finally, there was a significant difference in proportion of HBV/HCV-infection and serum AFP level between the patients who underwent surgical or percutaneous RFA.

In conclusion, surgical RFA seems more invasive than percutaneous RFA and the incidence of severe postoperative complications and local tumor progression is lower after surgical RFA than after percutaneous RFA for HCC in dangerous locations.

COMMENTS

Background

The efficacy of radiofrequency ablation (RFA) on hepatocellular carcinoma (HCC) has been debated for a long time. Whether RFA is effective against HCC both in dangerous location and in common location remains controversial.

Research frontiers

The corona of micro-invasion makes lots of colleagues concentrate on percutaneous RFA. Although laparoscopic RFA has been applied recently in some major institutes, laparoscopic ultrasonography needs a long time to be evaluated. Surgical RFA seems more suitable to be employed in most hospitals when difficult circumstances are encountered.

Innovations and breakthroughs

This study was a retrospective study assessing the value of surgical and percutaneous RFA for local or regional HCC in difficult anatomical positions with a large number of patients and a long follow-up time.

Applications

This study may help clinicians to choose RFA when encountering HCC in difficult anatomical positions.

Terminology

Tumor in the dangerous location is defined as a lesion (≤ 0.5 cm in diameter) near large vessels, such as a primary or secondary branch of the portal vein, the base of hepatic veins, or the inferior vena cava (IVC), or a lesion near extrahepatic organs (less than 0.5 cm in diameter) measured on radiological images.

Peer review

This article is a multinational collaborative study, assessing the value of percu-

taneous vs surgical RFA for local or regional HCC in difficult anatomical positions. It is a very interesting and clinically useful study with a large number of patients who were followed up for a long time, thus permitting evaluation of the final outcome of respective treatment modalities.

REFERENCES

- 1 **El-Serag HB.** Hepatocellular carcinoma: an epidemiologic view. *J Clin Gastroenterol* 2002; **35**: S72-S78
- 2 **Padma S, Martinie JB, Iannitti DA.** Liver tumor ablation: percutaneous and open approaches. *J Surg Oncol* 2009; **100**: 619-634
- 3 **Taylor-Robinson SD, Foster GR, Arora S, Hargreaves S, Thomas HC.** Increase in primary liver cancer in the UK, 1979-94. *Lancet* 1997; **350**: 1142-1143
- 4 **El-Serag HB, Mason AC.** Rising incidence of hepatocellular carcinoma in the United States. *N Engl J Med* 1999; **340**: 745-750
- 5 **Gane EJ, Portmann BC, Naoumov NV, Smith HM, Underhill JA, Donaldson PT, Maertens G, Williams R.** Long-term outcome of hepatitis C infection after liver transplantation. *N Engl J Med* 1996; **334**: 815-820
- 6 **Duffy JP, Hiatt JR, Busuttill RW.** Surgical resection of hepatocellular carcinoma. *Cancer J* 2008; **14**: 100-110
- 7 **Curley SA, Izzo F, Ellis LM, Nicolas Vauthey J, Vallone P.** Radiofrequency ablation of hepatocellular cancer in 110 patients with cirrhosis. *Ann Surg* 2000; **232**: 381-391
- 8 **Livraghi T, Goldberg SN, Lazzaroni S, Meloni F, Solbiati L, Gazelle GS.** Small hepatocellular carcinoma: treatment with radio-frequency ablation versus ethanol injection. *Radiology* 1999; **210**: 655-661
- 9 **Fontana RJ, Hamidullah H, Nghiem H, Greenson JK, Hussain H, Marrero J, Rudich S, McClure LA, Arenas J.** Percutaneous radiofrequency thermal ablation of hepatocellular carcinoma: a safe and effective bridge to liver transplantation. *Liver Transpl* 2002; **8**: 1165-1174
- 10 **Yamashiki N, Tateishi R, Yoshida H, Shiina S, Teratani T, Sato S, Mine N, Kondo Y, Kawabe T, Omata M.** Ablation therapy in containing extension of hepatocellular carcinoma: a simulative analysis of dropout from the waiting list for liver transplantation. *Liver Transpl* 2005; **11**: 508-514
- 11 **Llovet JM, Bruix J.** Novel advancements in the management of hepatocellular carcinoma in 2008. *J Hepatol* 2008; **48** Suppl 1: S20-S37
- 12 **Lau WY, Leung TW, Yu SC, Ho SK.** Percutaneous local ablative therapy for hepatocellular carcinoma: a review and look into the future. *Ann Surg* 2003; **237**: 171-179
- 13 **Chen MS, Li JQ, Zheng Y, Guo RP, Liang HH, Zhang YQ, Lin XJ, Lau WY.** A prospective randomized trial comparing percutaneous local ablative therapy and partial hepatectomy for small hepatocellular carcinoma. *Ann Surg* 2006; **243**: 321-328
- 14 **N'Kontchou G, Mahamoudi A, Aout M, Ganne-Carrié N, Grando V, Coderc E, Vicaute E, Trinchet JC, Sellier N, Beaugrand M, Seror O.** Radiofrequency ablation of hepatocellular carcinoma: long-term results and prognostic factors in 235 Western patients with cirrhosis. *Hepatology* 2009; **50**: 1475-1483
- 15 **McGhana JP, Dodd GD 3rd.** Radiofrequency ablation of the liver: current status. *AJR Am J Roentgenol* 2001; **176**: 3-16
- 16 **Livraghi T, Solbiati L, Meloni MF, Gazelle GS, Halpern EF, Goldberg SN.** Treatment of focal liver tumors with percutaneous radio-frequency ablation: complications encountered in a multicenter study. *Radiology* 2003; **226**: 441-451
- 17 **Meloni MF, Goldberg SN, Moser V, Piazza G, Livraghi T.** Colonic perforation and abscess following radiofrequency ablation treatment of hepatoma. *Eur J Ultrasound* 2002; **15**: 73-76
- 18 **Teratani T, Yoshida H, Shiina S, Obi S, Sato S, Tateishi R, Mine N, Kondo Y, Kawabe T, Omata M.** Radiofrequency ablation for hepatocellular carcinoma in so-called high-risk locations. *Hepatology* 2006; **43**: 1101-1108
- 19 **Bruix J, Sherman M, Llovet JM, Beaugrand M, Lencioni R, Burroughs AK, Christensen E, Pagliaro L, Colombo M, Rodés J.** Clinical management of hepatocellular carcinoma. Conclusions of the Barcelona-2000 EASL conference. European Association for the Study of the Liver. *J Hepatol* 2001; **35**: 421-430
- 20 **Goldberg SN, Charboneau JW, Dodd GD 3rd, Dupuy DE, Gervais DA, Gillams AR, Kane RA, Lee FT Jr, Livraghi T, McGahan JP, Rhim H, Silverman SG, Solbiati L, Vogl TJ, Wood BJ.** Image-guided tumor ablation: proposal for standardization of terms and reporting criteria. *Radiology* 2003; **228**: 335-345
- 21 **Strasberg SM, Linehan DC, Hawkins WG.** The accordion severity grading system of surgical complications. *Ann Surg* 2009; **250**: 177-186
- 22 **Jiang HC, Liu LX, Piao DX, Xu J, Zheng M, Zhu AL, Qi SY, Zhang WH, Wu LF.** Clinical short-term results of radiofrequency ablation in liver cancers. *World J Gastroenterol* 2002; **8**: 624-630
- 23 **Guglielmi A, Ruzzenente A, Battocchia A, Tonon A, Fracastoro G, Cordiano C.** Radiofrequency ablation of hepatocellular carcinoma in cirrhotic patients. *Hepatogastroenterology* 2003; **50**: 480-484
- 24 **Tateishi R, Shiina S, Teratani T, Obi S, Sato S, Koike Y, Fujishima T, Yoshida H, Kawabe T, Omata M.** Percutaneous radiofrequency ablation for hepatocellular carcinoma. An analysis of 1000 cases. *Cancer* 2005; **103**: 1201-1209
- 25 **Liang HH, Chen MS, Peng ZW, Zhang YJ, Zhang YQ, Li JQ, Lau WY.** Percutaneous radiofrequency ablation versus repeat hepatectomy for recurrent hepatocellular carcinoma: a retrospective study. *Ann Surg Oncol* 2008; **15**: 3484-3493
- 26 **Nazir B, Chaturvedi AK, Rao A.** Image-guided radiofrequency ablation of tumors: Current status. *Indian J Radiol Imaging* 2003; **13**: 315-322
- 27 **Stigliano R, Marelli L, Yu D, Davies N, Patch D, Burroughs AK.** Seeding following percutaneous diagnostic and therapeutic approaches for hepatocellular carcinoma. What is the risk and the outcome? Seeding risk for percutaneous approach of HCC. *Cancer Treat Rev* 2007; **33**: 437-447
- 28 **Al-Leswas D, O'Reilly DA, Poston GJ.** Biopsy of solid liver tumors: adverse consequences. *Hepatobiliary Pancreat Dis Int* 2008; **7**: 325-327

S- Editor Sun H L- Editor Wang XL E- Editor Ma WH

Foregut duplication cysts: A report of two cases with emphasis on embryogenesis

Thaer Khoury, Louis Rivera

Thaer Khoury, Department of Pathology, Roswell Park Cancer Institute, Buffalo, NY 14263, United States

Louis Rivera, Surgical Oncology, Roswell Park Cancer Institute, Buffalo, NY 14263, United States

Author contributions: Khoury T and Rivera L contributed equally to this work; Khoury T designed the research and provided discussion of the pathology; Rivera L provided the discussion of the clinical features; both authors contributed equally to the writing of the manuscript.

Correspondence to: Thaer Khoury, MD, Department of Pathology, Roswell Park Cancer Institute, Elm and Carlton Streets, Buffalo, NY 14263, United States. thaer.khoury@roswellpark.org
Telephone: +1-716-8454178 Fax: +1-716-8452370

Received: April 15, 2010 Revised: May 24, 2010

Accepted: May 31, 2010

Published online: January 7, 2011

Abstract

Duplication cyst of the stomach with a pseudostratified columnar ciliated epithelium is extremely rare. We describe two cases of these cysts, with emphasis on their immunophenotype and embryogenesis. The first patient was a 29-year-old man who presented with cramping abdominal pain in his left lower quadrant. The second patient was a 26-year-old woman who had a history, over several years, of chronic epigastric abdominal pain radiating to her back. Both lesions were surgically removed. They showed the same histomorphology. The cysts were lined by a pseudostratified respiratory epithelium with ciliated cells. The first cyst was connected to the stomach, while the second cyst was not connected. Both cysts expressed thyroid transcription factor-1 (TTF-1) and surfactant. In this report, we explore the possible embryogenesis of these lesions in the light of TTF-1 and surfactant expression.

© 2011 Baishideng. All rights reserved.

Key words: Duplication cyst; Stomach; Thyroid transcription factor-1; Surfactant; Embryogenesis

Peer reviewer: Alexander Becker, MD, Department of Surgery, Haemek Medical Center, Afula 18000, Israel

Khoury T, Rivera L. Foregut duplication cysts: A report of two cases with emphasis on embryogenesis. *World J Gastroenterol* 2011; 17(1): 130-134 Available from: URL: <http://www.wjg-net.com/1007-9327/full/v17/i1/130.htm> DOI: <http://dx.doi.org/10.3748/wjg.v17.i1.130>

INTRODUCTION

A gastrointestinal duplication is defined as a spherical hollow structure with a smooth muscle coat, lined by a mucous membrane, and attached to any part of the gastrointestinal tract, from the base of the tongue to the anus. However, foregut duplication cyst of the stomach is rare^[1,2]. Foregut duplications may or may not communicate with the gastrointestinal tract, and are usually diagnosed at a young age^[2]. There have been relatively few case reports describing this entity^[3-12]. Adenocarcinoma has been reported in four cases of gastric duplication cyst, but not in cysts that have a ciliated epithelium^[13-16]. Controversy exists concerning the embryological origin of these anomalies^[11,17,18]. Here, we present two cases of gastric ciliated duplication cyst with emphasis on immunophenotype and embryogenesis.

CASE REPORT

Case 1

Case history: The patient was a 29-year-old Caucasian man who presented to his local emergency department for evaluation of acute abdominal pain. The pain started in the lower abdomen and then localized to the left lower quadrant. He had mild nausea, but no vomiting. He had a history of gastroesophageal reflux disease. Physical examination was notable only for left lower quadrant tenderness to palpation. A computed tomography scan (CT-scan) of the abdomen and pelvis was performed and revealed a



Figure 1 A computed tomography scan of the abdomen and pelvis was performed utilizing intravenous and oral contrast. A 4 cm × 5 cm cystic mass (arrow) appears along the greater curvature of the stomach adjacent to the spleen.

mass at the greater curvature of the stomach (Figure 1). An esophagogastroduodenoscopy was performed, revealing a submucosal mass in the fundus of the stomach, approximately 2 cm from the gastroesophageal junction (Figure 2), which was soft on compression. Endoscopic ultrasound revealed a cystic mass in the submucosa of the fundus of the stomach. The imaging and endoscopic findings were most consistent with a gastric duplication cyst. To secure the diagnosis and prevent possible malignant degeneration, the patient was advised to undergo a partial gastrectomy.

Pathological findings: Macroscopically, a sack-like lesion (8.5 cm × 5.5 cm × 4.8 cm) was found with a smooth capsulated wall. The inner wall was also smooth. Microscopically, the cyst was lined by an antrum-type gastric mucosa and a respiratory epithelium with ciliated cells (Figure 3A and B). No intestinal-type epithelium was present. The outside layer consisted of a circular and a longitudinal muscle wall, with a myenteric plexus. The gastric epithelium immunophenotype was cytokeratin 20+, MUC5a/c+, cytokeratin 7+, MUC1-, MUC2-, CDX-2-, TTF-1-, and surfactant-, while the ciliated epithelium had the following immunophenotype: cytokeratin 20-, MUC5a/c-, cytokeratin 7+, MUC1-, MUC2-, CDX-2-, TTF-1+, and surfactant+ (Figure 3C-F).

Case 2

Case history: The patient was a 26-year-old woman with history of chronic epigastric pain for eight years following her first childbirth. The pain was intermittent, and colicky, without identifiable aggravating factors. More recently, the pain had become severe in intensity and required narcotics for relief. The pain was not associated with nausea, vomiting, abdominal distention, fevers, or chills. She admitted to a normal appetite, but had had an unintentional 50-pound weight loss over the last year. She underwent an esophagogastroduodenoscopy, which revealed a normal esophagus, a small hiatal hernia, and diffuse moderate inflammation of the stomach. A CT-scan of the abdomen revealed a cystic mass near the gastroesophageal junction along the lesser curvature of the stomach, which extended to the

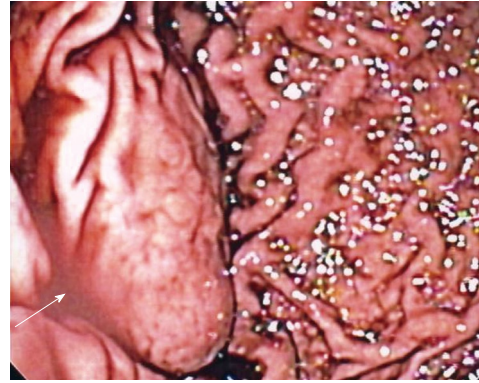


Figure 2 Retroflexed endoscopic view of a gastric mass arising in the fundus (arrow). Overlying rugae are effaced, suggestive of a submucosal process.

superior margin of the pancreas and abutted the liver and inferior vena cava (Figure 4). The mass was nonenhancing and cystic in appearance. The primary suspicion was that this represented a congenital gastrointestinal duplication cyst. A partial gastrectomy was performed for further evaluation and treatment.

Pathological findings: Macroscopically, the cyst was an ovoid-shaped structure (5 cm × 2.2 cm × 2 cm). The external surface was covered with tan, shiny serosa. The cystic cavity was filled with a tan-white mucoid material. The cyst inner surface was unremarkable, tan, and smooth. Microscopically, the cyst was lined by a respiratory epithelium with ciliated cells (Figure 5A and B). No intestinal-type epithelium was present. The outside layer consisted of a circular and a longitudinal muscle wall, with a myenteric plexus. The epithelium had the following immunophenotype: cytokeratin 20-, MUC5a/c-, cytokeratin 7+, MUC1-, MUC2-, CDX-2, TTF-1+, and surfactant+ (Figure 5C and D).

DISCUSSION

Gastrointestinal duplication can occur in any region of the gastrointestinal tract; however, a foregut duplication cyst of the stomach is rare. The stomach is the site of only 24% of all alimentary tract duplication cysts, which is the least common site after the ileum, esophagus, and colon. Of reported gastric duplication cysts, most occur in females, with 80% presenting in patients younger than 12 years of age. They are characteristically located on the distal greater curvature, and the majority are cystic and non-communicating. Histologically, they are usually lined with a typical gastric mucosa^[15]. As in the present two cases, a ciliated pseudostratified epithelium has been reported^[3-12].

We present two foregut duplication cysts of the stomach, one connected and one separated, in a 29-year old woman and a 26-year old man, respectively. These two cases showed distinct morphological and immunoprofile findings. Both cysts were lined with pseudostratified ciliated epithelia, and expressed TTF-1 and surfactant.

The pathogenesis of alimentary tract duplications is

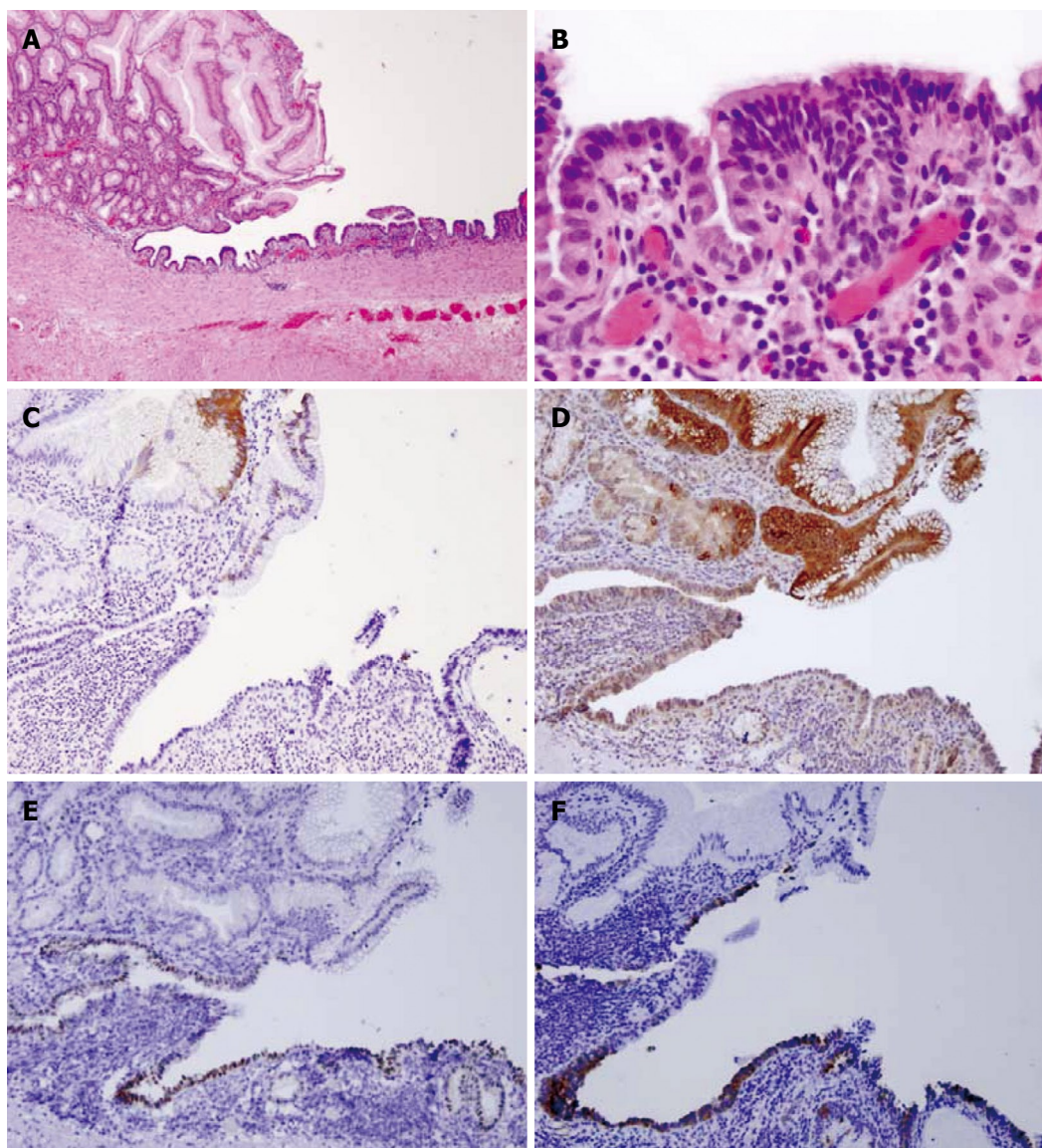


Figure 3 Case 1. A: Hematoxylin and eosin stain of gastric/ciliated epithelium (4 ×); B: High power view of the ciliated epithelium (40 ×); C: CK20 showing staining in the surface gastric epithelium, but not in the ciliated epithelium (10 ×); D: MUC5a/c staining showing positive expression in the gastric epithelium but not in the ciliated epithelium (10 ×); E: Thyroid transcription factor-1 nuclear staining in the ciliated epithelium only (10 ×); F: Surfactant staining in the ciliated epithelium only (10 ×).



Figure 4 Case 2. Computed tomography-scan of the abdomen and pelvis with intravenous and oral contrast showing a non-enhancing cystic structure (arrow) abutting the lesser curvature of the stomach and liver along the ligamentum venosum.

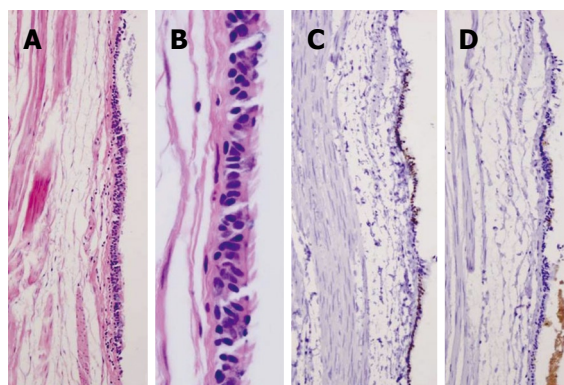


Figure 5 Case 2. A, B: Hematoxylin and eosin staining of pseudostratified ciliated epithelium (A: 4 ×, B: 40 ×); C: Thyroid transcription factor-1 nuclear staining in the ciliated epithelium (10 ×); D: Surfactant staining in the ciliated epithelium (10 ×).

controversial. There has been no suggestion of an explanation based on embryological development^[17]. However, others have suggested theory of embryological origin from supernumerary foregut buds^[11]. Others have proposed that abnormal recanalization after the solid epithelial stage of embryonic bowel development is the underlying cause of these lesions^[18].

We found that these cysts are lined with a ciliated pseudostratified epithelium and express TTF-1 and surfactant. These two factors are involved in lung embryogenesis. These findings might partially explain the embryogenesis of these lesions. When the embryo is approximately four weeks old, the respiratory diverticulum appears along the ventral wall of the pharyngeal gut. The esophagotracheal septum gradually partitions this diverticulum from the dorsal part of the foregut. In this manner, the foregut divides into the ventral portion, the respiratory primordium, and a dorsal portion, which becomes the esophagus and stomach^[19]. The middle branch of the tracheal trifurcation is grossly and histologically identical to the other two branches of the trifurcation, including expression of TTF1, which become the lungs^[20]. Early in the development of the esophagus, it is lined by a pseudostratified columnar epithelium. This is a characteristic of the respiratory epithelium, but the mucosa of the esophagus apparently undergoes subsequent metaplasia and squamous differentiation^[1,8]. Based on the presence of the ciliated epithelium, we propose that a branch coming off the trifurcation gives rise to the duplication cyst. Later, the cyst either remains connected to the esophagus/stomach or becomes separated.

TTF-1 is a homeobox transcription factor whose expression in the developing foregut is specifically limited to the respiratory tract^[21-23]. It is particularly important for normal lung development^[24-28]. TTF-1 enhances branching morphogenesis of embryonic lung explants *in vitro*^[29]. A *TTF-1* knockout mouse developed no distal lung parenchyma^[30]. Furthermore, TTF-1 is thought to be important for terminal respiratory epithelial cytodifferentiation. It has the capacity to regulate expression of surfactant proteins, A, B, and C, as well as the Clara cell secretory protein, all markers of respiratory cell specific differentiation^[25,26,28,31-33]. Thus, the presence of TTF-1 and surfactant expression is a function of lung differentiation. The presence of these two factors in the described cysts might explain why these cysts maintain their phenotype of a respiratory epithelium with no squamous metaplasia. As with tracheo-esophageal fistulae^[20], TTF-1 might have lost its normal patterning role in the developing lung, preventing induction of branching morphogenesis in the duplication cyst. The nonbranching pattern of growth of the duplication cyst might be attributable to local mesenchymal-epithelial interactions that override TTF-1 patterning activity.

In conclusion, gastric duplication cysts are rare, and their origin remains uncertain. The two cases presented here, and the resulting histological findings, suggest a novel origin. In both cases, the cysts are lined with a pseudostratified respiratory epithelium with ciliated cells, which express TTF-1 and surfactant. This suggests an origin from

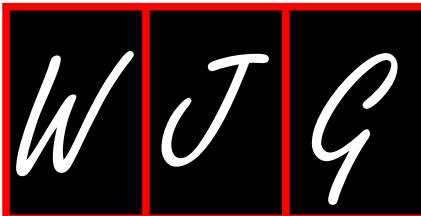
the respiratory diverticulum, which arises from the ventral foregut and could also explain why these cysts do or do not maintain their connection to the gastrointestinal tract.

REFERENCES

- 1 Glaser C, Kuzinkovas V, Maurer C, Glättli A, Mouton WG, Baer HU. A large duplication cyst of the stomach in an adult presenting as pancreatic pseudocyst. *Dig Surg* 1998; **15**: 703-706
- 2 Perek A, Perek S, Kapan M, Göksoy E. Gastric duplication cyst. *Dig Surg* 2000; **17**: 634-636
- 3 Laraja RD, Rothenberg RE, Chapman J, Imran-ul-Haq, Sabatini MT. Foregut duplication cyst: a report of a case. *Am Surg* 1995; **61**: 840-841
- 4 Takahara T, Torigoe T, Haga H, Yoshida H, Takeshima S, Sano S, Ishii Y, Furuya T, Nakamura E, Ishikawa M. Gastric duplication cyst: evaluation by endoscopic ultrasonography and magnetic resonance imaging. *J Gastroenterol* 1996; **31**: 420-424
- 5 Kim DH, Kim JS, Nam ES, Shin HS. Foregut duplication cyst of the stomach. *Pathol Int* 2000; **50**: 142-145
- 6 Ikehata A, Sakuma T. Gastric duplication cyst with markedly elevated concentration of carbohydrate antigen 19-9. *Am J Gastroenterol* 2000; **95**: 842-843
- 7 Gensler S, Seidenberg B, Rifkin H, Rubinstein BM. Ciliated lined intramural cyst of the stomach: case report and suggested embryogenesis. *Ann Surg* 1966; **163**: 954-956
- 8 Shireman PK. Intramural cyst of the stomach. *Hum Pathol* 1987; **18**: 857-858
- 9 Melo N, Pitman MB, Rattner DW. Bronchogenic cyst of the gastric fundus presenting as a gastrointestinal stromal tumor. *J Laparoendosc Adv Surg Tech A* 2005; **15**: 163-165
- 10 Cunningham SC, Hansel DE, Fishman EK, Cameron JL. Foregut duplication cyst of the stomach. *J Gastrointest Surg* 2006; **10**: 620-621
- 11 Theodosopoulos T, Marinis A, Karapanos K, Vassilikostas G, Dafnios N, Samanides L, Carvounis E. Foregut duplication cysts of the stomach with respiratory epithelium. *World J Gastroenterol* 2007; **13**: 1279-1281
- 12 Murakami S, Isozaki H, Shou T, Sakai K, Toyota H. Foregut duplication cyst of the stomach with pseudostratified columnar ciliated epithelium. *Pathol Int* 2008; **58**: 187-190
- 13 Mayo HW Jr, McKee EE, Anderson RM. Carcinoma arising in reduplication of the stomach (gastrogenous cyst): a case report. *Ann Surg* 1955; **141**: 550-555
- 14 Treiger M, Rubens J, Chindler J, Lobão M, Keiserman I, Martins JD, San Juan F. [Stomach duplication. Report of a 2d case in literature complicated by a peptic ulcer and malignant neoplasms]. *Hospital (Rio J)* 1969; **75**: 1-10
- 15 Coit DG, Mies C. Adenocarcinoma arising within a gastric duplication cyst. *J Surg Oncol* 1992; **50**: 274-277
- 16 Lee MY, Jensen E, Kwak S, Larson RA. Metastatic adenocarcinoma arising in a congenital foregut cyst of the esophagus: a case report with review of the literature. *Am J Clin Oncol* 1998; **21**: 64-66
- 17 De Roeck A, Vervloessem D, Mattelaer C, Schwagten K. Isolated enteric duplication cyst with respiratory epithelium: case report and review of the literature. *Eur J Pediatr Surg* 2008; **18**: 337-339
- 18 Gross RE, Holcomb GW Jr, Farber S. Duplications of the alimentary tract. *Pediatrics* 1952; **9**: 448-468
- 19 Sadler TW. Langman medical embryology. 8th ed. Lippincott Philadelphia 2000. Part II: special embryology. Digestive system, 2000: 273-177
- 20 Crisera CA, Connelly PR, Marmureanu AR, Colen KL, Rose MI, Li M, Longaker MT, Gittes GK. Esophageal atresia with tracheoesophageal fistula: suggested mechanism in faulty organogenesis. *J Pediatr Surg* 1999; **34**: 204-208

- 21 **Dahns B**. The gastrointestinal tract. In: Stocker J, Dehner L, editors. *Pediatric Pathology*. Philadelphia: Lippincott, 1992: 653-702
- 22 **Berry C**, Keeling J. Gastrointestinal system. In: Berry C, editor. *Paediatric Pathology*. London: Springer-Verlag, 1996: 207-274
- 23 **Lazzaro D**, Price M, de Felice M, Di Lauro R. The transcription factor TTF-1 is expressed at the onset of thyroid and lung morphogenesis and in restricted regions of the foetal brain. *Development* 1991; **113**: 1093-1104
- 24 **Cardoso WV**. Transcription factors and pattern formation in the developing lung. *Am J Physiol* 1995; **269**: L429-L442
- 25 **Bohinski RJ**, Di Lauro R, Whitsett JA. The lung-specific surfactant protein B gene promoter is a target for thyroid transcription factor 1 and hepatocyte nuclear factor 3, indicating common factors for organ-specific gene expression along the foregut axis. *Mol Cell Biol* 1994; **14**: 5671-5681
- 26 **Hackett BP**, Bingle CD, Gitlin JD. Mechanisms of gene expression and cell fate determination in the developing pulmonary epithelium. *Annu Rev Physiol* 1996; **58**: 51-71
- 27 **Stahlman MT**, Gray ME, Whitsett JA. Expression of thyroid transcription factor-1(TTF-1) in fetal and neonatal human lung. *J Histochem Cytochem* 1996; **44**: 673-678
- 28 **Zhou L**, Lim L, Costa RH, Whitsett JA. Thyroid transcription factor-1, hepatocyte nuclear factor-3beta, surfactant protein B, C, and Clara cell secretory protein in developing mouse lung. *J Histochem Cytochem* 1996; **44**: 1183-1193
- 29 **Minoo P**, Li C, Liu HB, Hamdan H, deLemos R. TTF-1 is an epithelial morphoregulatory transcriptional factor. *Chest* 1997; **111**: 135S-137S
- 30 **Oguchi H**, Kimura S. Transcription factors and thyroid disease. *Mol Med* 1995; **32**: 518
- 31 **Kelly SE**, Bachurski CJ, Burhans MS, Glasser SW. Transcription of the lung-specific surfactant protein C gene is mediated by thyroid transcription factor 1. *J Biol Chem* 1996; **271**: 6881-6888
- 32 **Bruno MD**, Bohinski RJ, Huelsman KM, Whitsett JA, Korfhaugen TR. Lung cell-specific expression of the murine surfactant protein A (SP-A) gene is mediated by interactions between the SP-A promoter and thyroid transcription factor-1. *J Biol Chem* 1995; **270**: 6531-6536
- 33 **Yan C**, Whitsett JA. Protein kinase A activation of the surfactant protein B gene is mediated by phosphorylation of thyroid transcription factor 1. *J Biol Chem* 1997; **272**: 17327-17332

S- Editor Wang JL L- Editor Stewart GJ E- Editor Ma WH



Duplicated appendix complicated by appendiceal cancer

Hugh J Freeman

Hugh J Freeman, Department of Medicine (Gastroenterology), University of British Columbia Hospital, Vancouver, BC, V6T 1W5, Canada

Author contributions: Freeman HJ contributed to all of this work.

Correspondence to: Hugh J Freeman, MD, Professor, Department of Medicine (Gastroenterology), University of British Columbia Hospital, 2211 Wesbrook Mall, Vancouver, BC, V6T 1W5, Canada. hugfree@shaw.ca

Telephone: +1-604-8227216 Fax: +1-604-8227236

Received: October 15, 2010 Revised: December 1, 2010

Accepted: December 8, 2010

Published online: January 7, 2011

Abstract

A 37-year old male presented with an acute abdomen suggestive of an appendiceal perforation. Urgent laparotomy showed a duplicated appendix with one of the lumens involved with appendicitis and a focal peri-appendicular abscess while the other lumen had a localized appendiceal cancer. Recognition of congenital intestinal duplications in adults is important to avoid serious clinical consequences.

© 2011 Baishideng. All rights reserved.

Key words: Duplicated appendix; Bifid appendix; Appendiceal cancer; Congenital duplication.

Peer reviewer: Dr. Benjamin Perakath, Professor, Department of Surgery Unit 5, Christian Medical College, Vellore 632004, Tamil Nadu, India

Freeman HJ. Duplicated appendix complicated by appendiceal cancer. *World J Gastroenterol* 2011; 17(1): 135-136 Available from: URL: <http://www.wjgnet.com/1007-9327/full/v17/i1/135.htm> DOI: <http://dx.doi.org/10.3748/wjg.v17.i1.135>

TO THE EDITOR

An article recently published in the *World Journal of Gas-*

troenterology concerned a duplicated vermiform appendix in an adult^[1]. The authors emphasized the need for surgical intervention to avoid any future complication, in particular, the disconcerting possibility of malignant degeneration within the duplication^[2,3]. Duplication of the appendix, fortunately, is distinctly rare, reportedly occurring in only 1/25 000 patients (0.04%) operated on for acute appendicitis^[4]. Clinical features may depend on the type of appendiceal duplication as a number of variants have been described, specifically, type A with incomplete duplication and a common base (so-called bifid appendix), and types B or C, both forms having complete duplication with independent bases^[5,6].

We had a similar, but unusual experience in a 37-year old adult male in August 1996. He presented with an acute abdomen thought to be a perforated appendix. An urgent laparotomy showed a type A duplicated or bifid appendix with an acute appendicitis involving only one lumen associated with a focal periappendiceal abscess and localized peritonitis. The other lumen showed a well-differentiated carcinoma extending into, but not through the muscularis propria. No vascular or lymphatic invasion was identified. Imaging studies and carcinoembryonic antigen testing were negative. Two weeks later, a further ileocecal resection was done. The resected intestine and 17 mesenteric lymph nodes showed no malignancy. Family history revealed that his father had synchronous mucinous colon cancers at the age of 45 years and his brother was diagnosed with colon cancer at the age of 26 years. A paternal uncle died of colon cancer at the age of 35 years. No other congenital abnormalities were recognized and there was no known contact with a toxic or noxious agent *in utero*. Colonoscopy screening at the ages of 20, 24 and 30 years was completed in other centers because of his family history of colon cancer and no abnormalities were detected. A colonoscopy in November 1996 in our hospital revealed no other abnormalities, similar to colonoscopies in 2000, 2005 and 2010. Because of his family history, genetic evaluation to exclude a HNPCC was negative including gene testing for MLH1 and MSH2.

Carcinoma in the intestinal tract developing with co-existent duplication has been rarely reported and appears

limited to only a small number of cases^[3,7]. Appendiceal cancer has been associated with a duplication thought to represent a Meckel's diverticulum^[8] as well as in a single prior report of a duplicated appendix^[9]. While this presentation may also mimic colon cancer^[10], missing a second duplicated appendix in this setting could lead to serious clinical consequences. In the present case, appendiceal duplication was fortunately recognized and an early stage carcinoma was successfully resected.

REFERENCES

- 1 **Kabay S**, Yucel M, Yaylak F, Hacıoglu A, Algin MC, Olgun EG, Sahin L, Aydin T. Combined duplication of the colon and vermiform appendix in an adult patient. *World J Gastroenterol* 2008; **14**: 641-643
- 2 **Orr MM**, Edwards AJ. Neoplastic change in duplications of the alimentary tract. *Br J Surg* 1975; **62**: 269-274
- 3 **Holcomb GW 3rd**, Gheissari A, O'Neill JA Jr, Shorter NA, Bishop HC. Surgical management of alimentary tract duplications. *Ann Surg* 1989; **209**: 167-174
- 4 **Sobhian B**, Mostegel M, Kunc C, Karner J. [Appendix vermiformis duplex--a rare surprise]. *Wien Klin Wochenschr* 2005; **117**: 492-494
- 5 **Cave AJ**. Appendix Vermiformis Duplex. *J Anat* 1936; **70**: 283-292
- 6 **Wallbridge PH**. Double appendix. *Br J Surg* 1962; **50**: 346-347
- 7 **Chen CC**, Yeh DC, Wu CC, Li MC, Kwan PC. Huge cystic duplication of the ascending colon in adult. *Zhonghua Yixue Zazhi (Taipei)* 2001; **64**: 174-178
- 8 **Lochman P**, Cáp R, Kohout A. Adenocarcinoma of the appendix and a Meckel's diverticulum in a case of acute appendicitis. *Onkologie* 2007; **30**: 457-458
- 9 **Sington JD**, Warren BF, Manek S. Reduplication cyst of appendix with mucinous carcinoma and Müllerian metaplasia: a case report. *J Clin Pathol* 2002; **55**: 551-553
- 10 **Bluett MK**, Halter SA, Salhany KE, O'Leary JP. Duplication of the appendix mimicking adenocarcinoma of the colon. *Arch Surg* 1987; **122**: 817-820

S- Editor Tian L L- Editor Wang XL E- Editor Ma WH



ACKNOWLEDGMENTS

Acknowledgments to reviewers of World Journal of Gastroenterology

Many reviewers have contributed their expertise and time to the peer review, a critical process to ensure the quality of *World Journal of Gastroenterology*. The editors and authors of the articles submitted to the journal are grateful to the following reviewers for evaluating the articles (including those published in this issue and those rejected for this issue) during the last editing time period.

Philip Abraham, Dr., Professor, Consultant Gastroenterologist and Hepatologist, P. D. Hinduja National Hospital and Medical Research Centre, Veer Savarkar Marg, Mahim, Mumbai 400 016, India

Antonio Basoli, Professor, General Surgery "Paride Stefanini", Università di Roma - Sapienza, Viale del Policlinico 155, Roma 00161, Italy

John Beynon, BSc, MB BS, MS, FRCS (ENG.), Consultant Colorectal Surgeon, Singleton Hospital, Sketty Lane, Swansea, SA2 8QA, United Kingdom

Erwin Biecker, MD, PhD, Department of Gastroenterology and Hepatology, Helios Klinikum Siegburg, Siegburg 53343, Germany

Mauro Bortolotti, MD, Professor, Department of Internal Medicine and Gastroenterology, University of Bologna, Via Massarenti 48 Bologna, 40138, Italy

Lisardo Boscá, Dr., Professor, Instituto de Investigaciones Biomédicas Alberto Sols (CSIC-UAM), Arturo Duperier 4, 28029 Madrid, Spain

Luis Bujanda, PhD, Professor, Departament of Gastroenterology, CIBEREHD, University of Country Basque, Donostia Hospital, Paseo Dr. Beguiristain s/n, 20014 San Sebastián, Spain

Giuseppe Currò, MD, University of Messina, Via Panoramica, 30/A, 98168 Messina, Italy

Uday C Ghoshal, Dr., MD, DNB, DM, FACC, Additional Professor, Department of Gastroenterology, Sanjay Gandhi Postgraduate

Institute of Medical Science, Lucknow 226014, India

Maria Concepción Gutiérrez-Ruiz, PhD, Department of Health Sciences, Universidad Autónoma Metropolitana-Iztapalapa, DCBS, Av San Rafael Atlixco 186, Colonia Vicentina, México, DF 09340, México

Serdar Karakose, Dr., Professor, Department of Radiology, Meram Medical Faculty, Selcuk University, Konya 42080, Turkey

Sang Geon Kim, Dr., PhD, MS, BS, Professor, Chairman, College of Pharmacy, Seoul National University, Sillim-dong, Kwanak-gu, Seoul 151-742, South Korea

Marshall John Marshall, MD, Professor of Medicine, Division of Gastroenterology, University of Missouri School of Medicine, Columbia, MO 65201, United States

Seung Woon Paik, MD, PhD, Professor, Division of Gastroenterology, Samsung Medical Center, Sungkyunkwan University School of Medicine, 50 Irwon-dong, Gangnam-gu, Seoul 135-710, South Korea

Mihaela Petrova, Dr., MD, PhD, Clinic of Gastroenterology, Medical Institute, Ministry of Interior, Sofia 1606, Bulgaria

Jorgen Rask-Madsen, MD, FRCP, Professor of Gastroenterology, Department of Gastroenterology, Herlev Hospital, Skodsborg Strandvej 280A, 2942, Herlev, DK-2730, Denmark

Ekihiro Seki, MD, PhD, Department of Medicine, University of California San Diego, Leichag Biomedical Research Building Rm 349H, 9500 Gilman Drive MC#0702, La Jolla, CA 92093-0702, United States

Hiroyuki Uehara, MD, PhD, Chief, Division of Pancreatology, Department of Gastroenterology, Osaka Medical Center for Cancer and Cardiovascular Diseases, 1-3-3 Nakamichi, Higashinari, Osaka 537-8511, Japan

Julian RF Walters, Dr., PhD, MD, BSc, MBBS, Department of Gastroenterology, Imperial College London, Hammersmith Hospital, Du Cane Road, London, W12 0HS, United Kingdom



Meetings

Events Calendar 2011

January 14-15, 2011
AGA Clinical Congress of
Gastroenterology and Hepatology:
Best Practices in 2011 Miami, FL
33101, United States

January 20-22, 2011
Gastrointestinal Cancers Symposium
2011, San Francisco, CA 94143,
United States

January 27-28, 2011
Falk Workshop, Liver and
Immunology, Medical University,
Franz-Josef-Strauss-Allee 11, 93053
Regensburg, Germany

January 28-29, 2011
9. Gastro Forum München, Munich,
Germany

February 04-05, 2011
13th Duesseldorf International
Endoscopy Symposium,
Duesseldorf, Germany

February 13-27, 2011
Gastroenterology: New Zealand
CME Cruise Conference, Sydney,
NSW, Australia

February 17-20, 2011
APASL 2011-The 21st Conference of
the Asian Pacific Association for the
Study of the Liver
Bangkok, Thailand

February 22, 2011-March 04, 2011
Canadian Digestive Diseases Week
2011, Vancouver, BC, Canada

February 24-26, 2011
Inflammatory Bowel Diseases
2011-6th Congress of the European
Crohn's and Colitis Organisation,
Dublin, Ireland

February 24-26, 2011
2nd International Congress on
Abdominal Obesity, Buenos Aires,
Brazil

February 24-26, 2011
International Colorectal Disease
Symposium 2011, Hong Kong, China

February 26-March 1, 2011
Canadian Digestive Diseases Week,

Westin Bayshore, Vancouver, British
Columbia, Canada

February 28-March 01, 2011
Childhood & Adolescent Obesity:
A whole-system strategic approach,
Abu Dhabi, United Arab Emirates

March 03-05, 2011
42nd Annual Topics in Internal
Medicine, Gainesville, FL 32614,
United States

March 07-11, 2011
Infectious Diseases: Adult Issues
in the Outpatient and Inpatient
Settings, Sarasota, FL 34234,
United States

March 14-17, 2011
British Society of Gastroenterology
Annual Meeting 2011, Birmingham,
England, United Kingdom

March 17-19, 2011
41. Kongress der Deutschen
Gesellschaft für Endoskopie und
Bildgebende Verfahren e.V., Munich,
Germany

March 17-20, 2011
Mayo Clinic Gastroenterology &
Hepatology 2011, Jacksonville, FL
34234, United States

March 18, 2011
UC Davis Health Informatics:
Change Management and Health
Informatics, The Keys to Health
Reform, Sacramento, CA 94143,
United States

March 25-27, 2011
MedicReS IC 2011 Good Medical
Research, Istanbul, Turkey

March 26-27, 2011
26th Annual New Treatments in
Chronic Liver Disease, San Diego,
CA 94143, United States

April 06-07, 2011
IBS-A Global Perspective, Pfister
Hotel, 424 East Wisconsin Avenue,
Milwaukee, WI 53202, United States

April 07-09, 2011
International and Interdisciplinary
Conference Excellence in Female
Surgery, Florence, Italy

April 15-16, 2011
Falk Symposium 177, Endoscopy
Live Berlin 2011 Intestinal Disease
Meeting, Stauffenbergstr. 26, 10785
Berlin, Germany

April 18-22, 2011
Pediatric Emergency Medicine:
Detection, Diagnosis and Developing
Treatment Plans, Sarasota, FL 34234,
United States

April 20-23, 2011
9th International Gastric Cancer
Congress, COEX, World Trade
Center, Samseong-dong, Gangnam-
gu, Seoul 135-731, South Korea

April 25-27, 2011
The Second International Conference
of the Saudi Society of Pediatric
Gastroenterology, Hepatology &
Nutrition, Riyadh, Saudi Arabia

April 25-29, 2011
Neurology Updates for Primary
Care, Sarasota, FL 34230-6947,
United States

April 28-30, 2011
4th Central European Congress of
Surgery, Budapest, Hungary

May 07-10, 2011
Digestive Disease Week, Chicago, IL
60446, United States

May 12-13, 2011
2nd National Conference Clinical
Advances in Cystic Fibrosis, London,
England, United Kingdom

May 19-22, 2011
1st World Congress on Controversies
in the Management of Viral Hepatitis
(C-Hep), Palau de Congressos de
Catalunya, Av. Diagonal, 661-671
Barcelona 08028, Spain

May 21-24, 2011
22nd European Society of
Gastrointestinal and Abdominal
Radiology Annual Meeting and
Postgraduate Course, Venice, Italy

May 25-28, 2011
4th Congress of the Gastroenterology
Association of Bosnia and
Herzegovina with international
participation, Hotel Holiday Inn,
Sarajevo, Bosnia and Herzegovina

June 11-12, 2011
The International Digestive Disease
Forum 2011, Hong Kong, China

June 13-16, 2011
Surgery and Disillusion XXIV
SPIGC, II ESYS, Napoli, Italy

June 14-16, 2011
International Scientific Conference

on Probiotics and Prebiotics-
IPC2011, Kosice, Slovakia

June 22-25, 2011
ESMO Conference: 13th World
Congress on Gastrointestinal Cancer,
Barcelona, Spain

June 29-02, 2011
XI Congreso Interamericano
de Pediatría "Monterrey 2011",
Monterrey, Mexico

September 2-3, 2011 Falk Symposium
178, Diverticular Disease, A Fresh
Approach to a Neglected Disease,
Gürzenich Cologne, Martinstr. 29-37,
50667 Cologne, Germany

September 10-11, 2011
New Advances in Inflammatory
Bowel Disease, La Jolla, CA 92093,
United States

September 10-14, 2011
ICE 2011-International Congress of
Endoscopy, Los Angeles Convention
Center, 1201 South Figueroa Street
Los Angeles, CA 90015,
United States

September 30-October 1, 2011
Falk Symposium 179, Revisiting
IBD Management: Dogmas to be
Challenged, Sheraton Brussels
Hotel, Place Rogier 3, 1210 Brussels,
Belgium

October 19-29, 2011
Cardiology & Gastroenterology |
Tahiti 10 night CME Cruise, Papeete,
French Polynesia

October 22-26, 2011
19th United European
Gastroenterology Week, Stockholm,
Sweden

October 28-November 02, 2011
ACG Annual Scientific Meeting &
Postgraduate Course, Washington,
DC 20001, United States

November 11-12, 2011
Falk Symposium 180, IBD 2011:
Progress and Future for Lifelong
Management, ANA Interconti Hotel,
1-12-33 Akasaka, Minato-ku, Tokyo
107-0052, Japan

December 01-04, 2011
2011 Advances in Inflammatory
Bowel Diseases/Crohn's & Colitis
Foundation's Clinical & Research
Conference, Hollywood, FL 34234,
United States



Instructions to authors

GENERAL INFORMATION

World Journal of Gastroenterology (*World J Gastroenterol*, *WJG*, print ISSN 1007-9327, online ISSN 2219-2840, DOI: 10.3748) is a weekly, open-access (OA), peer-reviewed journal supported by an editorial board of 1144 experts in gastroenterology and hepatology from 60 countries.

The biggest advantage of the OA model is that it provides free, full-text articles in PDF and other formats for experts and the public without registration, which eliminates the obstacle that traditional journals possess and usually delays the speed of the propagation and communication of scientific research results. The open access model has been proven to be a true approach that may achieve the ultimate goal of the journals, i.e. the maximization of the value to the readers, authors and society.

Maximization of personal benefits

The role of academic journals is to exhibit the scientific levels of a country, a university, a center, a department, and even a scientist, and build an important bridge for communication between scientists and the public. As we all know, the significance of the publication of scientific articles lies not only in disseminating and communicating innovative scientific achievements and academic views, as well as promoting the application of scientific achievements, but also in formally recognizing the "priority" and "copyright" of innovative achievements published, as well as evaluating research performance and academic levels. So, to realize these desired attributes of *WJG* and create a well-recognized journal, the following four types of personal benefits should be maximized. The maximization of personal benefits refers to the pursuit of the maximum personal benefits in a well-considered optimal manner without violation of the laws, ethical rules and the benefits of others. (1) Maximization of the benefits of editorial board members: The primary task of editorial board members is to give a peer review of an unpublished scientific article via online office system to evaluate its innovativeness, scientific and practical values and determine whether it should be published or not. During peer review, editorial board members can also obtain cutting-edge information in that field at first hand. As leaders in their field, they have priority to be invited to write articles and publish commentary articles. We will put peer reviewers' names and affiliations along with the article they reviewed in the journal to acknowledge their contribution; (2) Maximization of the benefits of authors: Since *WJG* is an open-access journal, readers around the world can immediately download and read, free of charge, high-quality, peer-reviewed articles from *WJG* official website, thereby realizing the goals and significance of the communication between authors and peers as well as public reading; (3) Maximization of the benefits of readers: Readers can read or use, free of charge, high-quality peer-reviewed articles without any limits, and cite the arguments, viewpoints, concepts, theories, methods, results, conclusion or facts and data of pertinent literature so as to validate the innovativeness, scientific and practical values of their own research achievements, thus ensuring that their articles have novel arguments or viewpoints, solid evidence and correct conclu-

sion; and (4) Maximization of the benefits of employees: It is an iron law that a first-class journal is unable to exist without first-class editors, and only first-class editors can create a first-class academic journal. We insist on strengthening our team cultivation and construction so that every employee, in an open, fair and transparent environment, could contribute their wisdom to edit and publish high-quality articles, thereby realizing the maximization of the personal benefits of editorial board members, authors and readers, and yielding the greatest social and economic benefits.

Aims and scope

The major task of *WJG* is to report rapidly the most recent results in basic and clinical research on esophageal, gastrointestinal, liver, pancreas and biliary tract diseases, *Helicobacter pylori*, endoscopy and gastrointestinal surgery, including: gastroesophageal reflux disease, gastrointestinal bleeding, infection and tumors; gastric and duodenal disorders; intestinal inflammation, microflora and immunity; celiac disease, dyspepsia and nutrition; viral hepatitis, portal hypertension, liver fibrosis, liver cirrhosis, liver transplantation, and metabolic liver disease; molecular and cell biology; geriatric and pediatric gastroenterology; diagnosis and screening, imaging and advanced technology.

Columns

The columns in the issues of *WJG* will include: (1) Editorial: To introduce and comment on major advances and developments in the field; (2) Frontier: To review representative achievements, comment on the state of current research, and propose directions for future research; (3) Topic Highlight: This column consists of three formats, including (A) 10 invited review articles on a hot topic, (B) a commentary on common issues of this hot topic, and (C) a commentary on the 10 individual articles; (4) Observation: To update the development of old and new questions, highlight unsolved problems, and provide strategies on how to solve the questions; (5) Guidelines for Basic Research: To provide guidelines for basic research; (6) Guidelines for Clinical Practice: To provide guidelines for clinical diagnosis and treatment; (7) Review: To review systematically progress and unresolved problems in the field, comment on the state of current research, and make suggestions for future work; (8) Original Article: To report innovative and original findings in gastroenterology; (9) Brief Article: To briefly report the novel and innovative findings in gastroenterology and hepatology; (10) Case Report: To report a rare or typical case; (11) Letters to the Editor: To discuss and make reply to the contributions published in *WJG*, or to introduce and comment on a controversial issue of general interest; (12) Book Reviews: To introduce and comment on quality monographs of gastroenterology and hepatology; and (13) Guidelines: To introduce consensus and guidelines reached by international and national academic authorities worldwide on basic research and clinical practice gastroenterology and hepatology.

Name of journal

World Journal of Gastroenterology

CSSN

ISSN 1007-9327 (print)
ISSN 2219-2840 (online)

Indexed and Abstracted in

Current Contents®/Clinical Medicine, Science Citation Index Expanded (also known as SciSearch®), Journal Citation Reports®, Index Medicus, MEDLINE, PubMed, PubMed Central, and Digital Object Identifier. ISI, Thomson Reuters, 2009 Impact Factor: 2.092 (33/65 Gastroenterology and Hepatology).

Published by

Baishideng Publishing Group Co., Limited

SPECIAL STATEMENT

All articles published in this journal represent the viewpoints of the authors except where indicated otherwise.

Biostatistical editing

Statistical review is performed after peer review. We invite an expert in Biomedical Statistics from to evaluate the statistical method used in the paper, including *t*-test (group or paired comparisons), chi-squared test, Ridit, probit, logit, regression (linear, curvilinear, or stepwise), correlation, analysis of variance, analysis of covariance, *etc.* The reviewing points include: (1) Statistical methods should be described when they are used to verify the results; (2) Whether the statistical techniques are suitable or correct; (3) Only homogeneous data can be averaged. Standard deviations are preferred to standard errors. Give the number of observations and subjects (*n*). Losses in observations, such as drop-outs from the study should be reported; (4) Values such as ED50, LD50, IC50 should have their 95% confidence limits calculated and compared by weighted probit analysis (Bliss and Finney); and (5) The word 'significantly' should be replaced by its synonyms (if it indicates extent) or the *P* value (if it indicates statistical significance).

Conflict-of-interest statement

In the interests of transparency and to help reviewers assess any potential bias, *WJG* requires authors of all papers to declare any competing commercial, personal, political, intellectual, or religious interests in relation to the submitted work. Referees are also asked to indicate any potential conflict they might have reviewing a particular paper. Before submitting, authors are suggested to read "Uniform Requirements for Manuscripts Submitted to Biomedical Journals: Ethical Considerations in the Conduct and Reporting of Research: Conflicts of Interest" from International Committee of Medical Journal Editors (ICMJE), which is available at: http://www.icmje.org/ethical_4conflicts.html.

Sample wording: [Name of individual] has received fees for serving as a speaker, a consultant and an advisory board member for [names of organizations], and has received research funding from [names of organizations]. [Name of individual] is an employee of [name of organization]. [Name of individual] owns stocks and shares in [name of organization]. [Name of individual] owns patent [patent identification and brief description].

Statement of informed consent

Manuscripts should contain a statement to the effect that all human studies have been reviewed by the appropriate ethics committee or it should be stated clearly in the text that all persons gave their informed consent prior to their inclusion in the study. Details that might disclose the identity of the subjects under study should be omitted. Authors should also draw attention to the Code of Ethics of the World Medical Association (Declaration of Helsinki, 1964, as revised in 2004).

Statement of human and animal rights

When reporting the results from experiments, authors should follow the highest standards and the trial should conform to Good Clinical Practice (for example, US Food and Drug Administration Good Clinical Practice in FDA-Regulated Clinical Trials; UK Medicines Research Council Guidelines for Good Clinical Practice in Clinical Trials) and/or the World Medical Association Declaration of Helsinki. Generally, we suggest authors follow the lead investigator's national standard. If doubt exists whether the research was conducted in accordance with the above standards, the authors must explain the rationale for their approach and demonstrate that the institutional review body explicitly approved the doubtful aspects of the study.

Before submitting, authors should make their study approved by the relevant research ethics committee or institutional review board. If human participants were involved, manuscripts must be accompanied by a statement that the experiments were undertaken with the understanding and appropriate informed consent of each. Any personal item or information will not be published without explicit consents from the involved patients. If experimental animals were used, the materials and methods (experimental procedures) section must clearly indicate that appropriate measures were taken to minimize pain or discomfort, and details of animal care should be provided.

SUBMISSION OF MANUSCRIPTS

Manuscripts should be typed in 1.5 line spacing and 12 pt. Book Antiqua with ample margins. Number all pages consecutively, and start each of the following sections on a new page: Title Page, Abstract, Introduction, Materials and Methods, Results, Discussion, Acknowledgements, References, Tables, Figures, and Figure Legends. Neither the editors nor the publisher are responsible for the opinions expressed by contributors. Manuscripts formally accepted for publication become the permanent property of Baishideng Publishing Group Co., Limited, and may not be reproduced by any means, in whole or in part, without the written permission of both the authors and the publisher. We reserve the right to copy-edit and put onto our website accepted manuscripts. Authors should follow the relevant guidelines for the care and use of laboratory animals of their institution or national animal welfare committee. For the sake of transparency in regard to the performance and reporting of clinical trials, we endorse the policy of the ICMJE to refuse to publish papers on clinical trial results if the trial was not recorded in a publicly-accessible registry at its outset. The only register now available, to our knowledge, is <http://www.clinicaltrials.gov> sponsored by the United States National Library of Medicine and we encourage all potential contributors to register with it. However, in the case that other registers become available you will be duly notified. A letter of recommendation from each author's organization should be provided with the contributed article to ensure the privacy and secrecy of research is protected.

Authors should retain one copy of the text, tables, photographs and illustrations because rejected manuscripts will not be returned to the author(s) and the editors will not be responsible for loss or damage to photographs and illustrations sustained during mailing.

Online submissions

Manuscripts should be submitted through the Online Submission System at: <http://www.wjgnet.com/1007-9327/office>. Authors are highly recommended to consult the ONLINE INSTRUCTIONS TO AUTHORS (http://www.wjgnet.com/1007-9327/g_info_20100315215714.htm) before attempting to submit on-

line. For assistance, authors encountering problems with the Online Submission System may send an email describing the problem to wjg@wjgnet.com, or by telephone: +86-10-5908-0039. If you submit your manuscript online, do not make a postal contribution. Repeated online submission for the same manuscript is strictly prohibited.

MANUSCRIPT PREPARATION

All contributions should be written in English. All articles must be submitted using word-processing software. All submissions must be typed in 1.5 line spacing and 12 pt. Book Antiqua with ample margins. Style should conform to our house format. Required information for each of the manuscript sections is as follows:

Title page

Title: Title should be less than 12 words.

Running title: A short running title of less than 6 words should be provided.

Authorship: Authorship credit should be in accordance with the standard proposed by ICMJE, based on (1) substantial contributions to conception and design, acquisition of data, or analysis and interpretation of data; (2) drafting the article or revising it critically for important intellectual content; and (3) final approval of the version to be published. Authors should meet conditions 1, 2, and 3.

Institution: Author names should be given first, then the complete name of institution, city, province and postcode. For example, Xu-Chen Zhang, Li-Xin Mei, Department of Pathology, Chengde Medical College, Chengde 067000, Hebei Province, China. One author may be represented from two institutions, for example, George Sgourakis, Department of General, Visceral, and Transplantation Surgery, Essen 45122, Germany; George Sgourakis, 2nd Surgical Department, Korgialenio-Benakio Red Cross Hospital, Athens 15451, Greece.

Author contributions: The format of this section should be: Author contributions: Wang CL and Liang L contributed equally to this work; Wang CL, Liang L, Fu JF, Zou CC, Hong F and Wu XM designed the research; Wang CL, Zou CC, Hong F and Wu XM performed the research; Xue JZ and Lu JR contributed new reagents/analytic tools; Wang CL, Liang L and Fu JF analyzed the data; and Wang CL, Liang L and Fu JF wrote the paper.

Supportive foundations: The complete name and number of supportive foundations should be provided, e.g. Supported by National Natural Science Foundation of China, No. 30224801

Correspondence to: Only one corresponding address should be provided. Author names should be given first, then author title, affiliation, the complete name of institution, city, postcode, province, country, and email. All the letters in the email should be in lower case. A space interval should be inserted between country name and email address. For example, Montgomery Bissell, MD, Professor of Medicine, Chief, Liver Center, Gastroenterology Division, University of California, Box 0538, San Francisco, CA 94143, United States. montgomery.bissell@ucsf.edu

Telephone and fax: Telephone and fax should consist of +, country number, district number and telephone or fax number, e.g. Telephone: +86-10-59080039 Fax: +86-10-85381893

Peer reviewers: All articles received are subject to peer review.

Normally, three experts are invited for each article. Decision for acceptance is made only when at least two experts recommend an article for publication. Reviewers for accepted manuscripts are acknowledged in each manuscript, and reviewers of articles which were not accepted will be acknowledged at the end of each issue. To ensure the quality of the articles published in *WJG*, reviewers of accepted manuscripts will be announced by publishing the name, title/position and institution of the reviewer in the footnote accompanying the printed article. For example, reviewers: Professor Jing-Yuan Fang, Shanghai Institute of Digestive Disease, Shanghai, Affiliated Renji Hospital, Medical Faculty, Shanghai Jiaotong University, Shanghai, China; Professor Xin-Wei Han, Department of Radiology, The First Affiliated Hospital, Zhengzhou University, Zhengzhou, Henan Province, China; and Professor Anren Kuang, Department of Nuclear Medicine, Huaxi Hospital, Sichuan University, Chengdu, Sichuan Province, China.

Abstract

There are unstructured abstracts (no more than 256 words) and structured abstracts (no more than 480). The specific requirements for structured abstracts are as follows:

An informative, structured abstracts of no more than 480 words should accompany each manuscript. Abstracts for original contributions should be structured into the following sections. AIM (no more than 20 words): Only the purpose should be included. Please write the aim as the form of "To investigate/study/..."; MATERIALS AND METHODS (no more than 140 words); RESULTS (no more than 294 words): You should present *P* values where appropriate and must provide relevant data to illustrate how they were obtained, e.g. 6.92 ± 3.86 vs 3.61 ± 1.67 , $P < 0.001$; CONCLUSION (no more than 26 words).

Key words

Please list 5-10 key words, selected mainly from *Index Medicus*, which reflect the content of the study.

Text

For articles of these sections, original articles and brief articles, the main text should be structured into the following sections: INTRODUCTION, MATERIALS AND METHODS, RESULTS and DISCUSSION, and should include appropriate Figures and Tables. Data should be presented in the main text or in Figures and Tables, but not in both. The main text format of these sections, editorial, topic highlight, case report, letters to the editors, can be found at: http://www.wjgnet.com/1007-9327/g_info_20100315215714.htm.

Illustrations

Figures should be numbered as 1, 2, 3, etc., and mentioned clearly in the main text. Provide a brief title for each figure on a separate page. Detailed legends should not be provided under the figures. This part should be added into the text where the figures are applicable. Figures should be either Photoshop or Illustrator files (in tiff, eps, jpeg formats) at high-resolution. Examples can be found at: <http://www.wjgnet.com/1007-9327/13/4520.pdf>; <http://www.wjgnet.com/1007-9327/13/4554.pdf>; <http://www.wjgnet.com/1007-9327/13/4891.pdf>; <http://www.wjgnet.com/1007-9327/13/4986.pdf>; <http://www.wjgnet.com/1007-9327/13/4498.pdf>. Keeping all elements compiled is necessary in line-art image. Scale bars should be used rather than magnification factors, with the length of the bar defined in the legend rather than on the bar itself. File names should identify the figure and panel. Avoid layering type directly over shaded or textured areas. Please use

Instructions to authors

uniform legends for the same subjects. For example: Figure 1 Pathological changes in atrophic gastritis after treatment. A:..., B:..., C:..., D:..., E:..., F:..., G: ...*etc.* It is our principle to publish high resolution-figures for the printed and E-versions.

Tables

Three-line tables should be numbered 1, 2, 3, *etc.*, and mentioned clearly in the main text. Provide a brief title for each table. Detailed legends should not be included under tables, but rather added into the text where applicable. The information should complement, but not duplicate the text. Use one horizontal line under the title, a second under column heads, and a third below the Table, above any footnotes. Vertical and italic lines should be omitted.

Notes in tables and illustrations

Data that are not statistically significant should not be noted. ^a $P < 0.05$, ^b $P < 0.01$ should be noted ($P > 0.05$ should not be noted). If there are other series of P values, ^c $P < 0.05$ and ^d $P < 0.01$ are used. A third series of P values can be expressed as ^e $P < 0.05$ and ^f $P < 0.01$. Other notes in tables or under illustrations should be expressed as ¹F, ²F, ³F; or sometimes as other symbols with a superscript (Arabic numerals) in the upper left corner. In a multi-curve illustration, each curve should be labeled with ●, ○, ■, ▲, △, *etc.*, in a certain sequence.

Acknowledgments

Brief acknowledgments of persons who have made genuine contributions to the manuscript and who endorse the data and conclusions should be included. Authors are responsible for obtaining written permission to use any copyrighted text and/or illustrations.

REFERENCES

Coding system

The author should number the references in Arabic numerals according to the citation order in the text. Put reference numbers in square brackets in superscript at the end of citation content or after the cited author's name. For citation content which is part of the narration, the coding number and square brackets should be typeset normally. For example, "Crohn's disease (CD) is associated with increased intestinal permeability^[1,2]". If references are cited directly in the text, they should be put together within the text, for example, "From references^[19,22-24], we know that...".

When the authors write the references, please ensure that the order in text is the same as in the references section, and also ensure the spelling accuracy of the first author's name. Do not list the same citation twice.

PMID and DOI

Please provide PubMed citation numbers to the reference list, e.g. PMID and DOI, which can be found at <http://www.ncbi.nlm.nih.gov/sites/entrez?db=pubmed> and <http://www.crossref.org/SimpleTextQuery/>, respectively. The numbers will be used in E-version of this journal.

Style for journal references

Authors: the name of the first author should be typed in bold-faced letters. The family name of all authors should be typed with the initial letter capitalized, followed by their abbreviated first and middle initials. (For example, Lian-Sheng Ma is abbreviated as Ma LS, Bo-Rong Pan as Pan BR). The title of the cited article and italicized journal title (journal title should be in its abbreviated form as shown in PubMed), publication date,

volume number (in black), start page, and end page [PMID: 11819634 DOI: 10.3748/wjg.13.5396].

Style for book references

Authors: the name of the first author should be typed in bold-faced letters. The surname of all authors should be typed with the initial letter capitalized, followed by their abbreviated middle and first initials. (For example, Lian-Sheng Ma is abbreviated as Ma LS, Bo-Rong Pan as Pan BR) Book title. Publication number. Publication place: Publication press, Year: start page and end page.

Format

Journals

English journal article (list all authors and include the PMID where applicable)

- 1 **Jung EM**, Clevert DA, Schreyer AG, Schmitt S, Rennert J, Kubale R, Feuerbach S, Jung F. Evaluation of quantitative contrast harmonic imaging to assess malignancy of liver tumors: A prospective controlled two-center study. *World J Gastroenterol* 2007; **13**: 6356-6364 [PMID: 18081224 DOI: 10.3748/wjg.13.6356]

Chinese journal article (list all authors and include the PMID where applicable)

- 2 **Lin GZ**, Wang XZ, Wang P, Lin J, Yang FD. Immunologic effect of Jianpi Yishen decoction in treatment of Pixu-diarrhoea. *Shijie Huaren Xiaohua Zazhi* 1999; **7**: 285-287

In press

- 3 **Tian D**, Araki H, Stahl E, Bergelson J, Kreitman M. Signature of balancing selection in Arabidopsis. *Proc Natl Acad Sci USA* 2006; In press

Organization as author

- 4 **Diabetes Prevention Program Research Group**. Hypertension, insulin, and proinsulin in participants with impaired glucose tolerance. *Hypertension* 2002; **40**: 679-686 [PMID: 12411462 PMID:2516377 DOI:10.1161/01.HYP.00000035706.28494.09]

Both personal authors and an organization as author

- 5 **Vallancien G**, Emberton M, Harving N, van Moorseelaar RJ, Alf-One Study Group. Sexual dysfunction in 1, 274 European men suffering from lower urinary tract symptoms. *J Urol* 2003; **169**: 2257-2261 [PMID: 12771764 DOI:10.1097/01.ju.0000067940.76090.73]

No author given

- 6 21st century heart solution may have a sting in the tail. *BMJ* 2002; **325**: 184 [PMID: 12142303 DOI:10.1136/bmj.325.7357.184]

Volume with supplement

- 7 **Geraud G**, Spierings EL, Keywood C. Tolerability and safety of frovatriptan with short- and long-term use for treatment of migraine and in comparison with sumatriptan. *Headache* 2002; **42** Suppl 2: S93-99 [PMID: 12028325 DOI:10.1046/j.1526-4610.42.s2.7.x]

Issue with no volume

- 8 **Banit DM**, Kaufer H, Hartford JM. Intraoperative frozen section analysis in revision total joint arthroplasty. *Clin Orthop Relat Res* 2002; **(401)**: 230-238 [PMID: 12151900 DOI:10.1097/00003086-200208000-00026]

No volume or issue

- 9 Outreach: Bringing HIV-positive individuals into care. *HRSA Careaction* 2002; 1-6 [PMID: 12154804]

Books

Personal author(s)

- 10 **Sherlock S**, Dooley J. Diseases of the liver and biliary system. 9th ed. Oxford: Blackwell Sci Pub, 1993: 258-296

Chapter in a book (list all authors)

- 11 **Lam SK.** Academic investigator's perspectives of medical treatment for peptic ulcer. In: Swabb EA, Azabo S. Ulcer disease: investigation and basis for therapy. New York: Marcel Dekker, 1991: 431-450

Author(s) and editor(s)

- 12 **Breedlove GK,** Schorfheide AM. Adolescent pregnancy. 2nd ed. Wiczorek RR, editor. White Plains (NY): March of Dimes Education Services, 2001: 20-34

Conference proceedings

- 13 **Harnden P,** Joffe JK, Jones WG, editors. Germ cell tumours V. Proceedings of the 5th Germ cell tumours Conference; 2001 Sep 13-15; Leeds, UK. New York: Springer, 2002: 30-56

Conference paper

- 14 **Christensen S,** Oppacher F. An analysis of Koza's computational effort statistic for genetic programming. In: Foster JA, Lutton E, Miller J, Ryan C, Tettamanzi AG, editors. Genetic programming. EuroGP 2002: Proceedings of the 5th European Conference on Genetic Programming; 2002 Apr 3-5; Kinsdale, Ireland. Berlin: Springer, 2002: 182-191

Electronic journal (list all authors)

- 15 Morse SS. Factors in the emergence of infectious diseases. Emerg Infect Dis serial online, 1995-01-03, cited 1996-06-05; 1(1): 24 screens. Available from: URL: <http://www.cdc.gov/ncidod/eid/index.htm>

Patent (list all authors)

- 16 **Pagedas AC,** inventor; Ancel Surgical R&D Inc., assignee. Flexible endoscopic grasping and cutting device and positioning tool assembly. United States patent US 20020103498. 2002 Aug 1

Statistical data

Write as mean \pm SD or mean \pm SE.

Statistical expression

Express *t* test as *t* (in italics), *F* test as *F* (in italics), chi square test as χ^2 (in Greek), related coefficient as *r* (in italics), degree of freedom as ν (in Greek), sample number as *n* (in italics), and probability as *P* (in italics).

Units

Use SI units. For example: body mass, *m* (B) = 78 kg; blood pressure, *p* (B) = 16.2/12.3 kPa; incubation time, *t* (incubation) = 96 h; blood glucose concentration, *c* (glucose) 6.4 ± 2.1 mmol/L; blood CEA mass concentration, *p* (CEA) = 8.6 $24.5 \mu\text{g/L}$; CO₂ volume fraction, 50 mL/L CO₂, not 5% CO₂; likewise for 40 g/L formaldehyde, not 10% formalin; and mass fraction, 8 ng/g, etc. Arabic numerals such as 23, 243, 641 should be read 23 243 641.

The format for how to accurately write common units and quantum numbers can be found at: http://www.wjgnet.com/1007-9327/g_info_20100315223018.htm.

Abbreviations

Standard abbreviations should be defined in the abstract and on first mention in the text. In general, terms should not be abbreviated unless they are used repeatedly and the abbreviation is helpful to the reader. Permissible abbreviations are listed in Units, Symbols and Abbreviations: A Guide for Biological and Medical Editors and Authors (Ed. Baron DN, 1988) published by The Royal Society of Medicine, London. Certain commonly used abbreviations, such as DNA, RNA, HIV, LD50, PCR, HBV, ECG, WBC, RBC, CT, ESR, CSF, IgG, ELISA, PBS, ATP, EDTA, mAb, can be used directly without further explanation.

Italics

Quantities: *t* time or temperature, *c* concentration, *A* area, *l* length, *m* mass, *V* volume.

Genotypes: *gyrA*, *arg 1*, *c myc*, *c fos*, etc.

Restriction enzymes: *EcoRI*, *HindIII*, *BamHI*, *Kho I*, *Kpn I*, etc.

Biology: *H. pylori*, *E. coli*, etc.

Examples for paper writing

Editorial: http://www.wjgnet.com/1007-9327/g_info_20100315220036.htm

Frontier: http://www.wjgnet.com/1007-9327/g_info_20100315220305.htm

Topic highlight: http://www.wjgnet.com/1007-9327/g_info_20100315220601.htm

Observation: http://www.wjgnet.com/1007-9327/g_info_20100312232427.htm

Guidelines for basic research: http://www.wjgnet.com/1007-9327/g_info_20100315220730.htm

Guidelines for clinical practice: http://www.wjgnet.com/1007-9327/g_info_20100315221301.htm

Review: http://www.wjgnet.com/1007-9327/g_info_20100315221554.htm

Original articles: http://www.wjgnet.com/1007-9327/g_info_20100315221814.htm

Brief articles: http://www.wjgnet.com/1007-9327/g_info_20100312231400.htm

Case report: http://www.wjgnet.com/1007-9327/g_info_20100315221946.htm

Letters to the editor: http://www.wjgnet.com/1007-9327/g_info_20100315222254.htm

Book reviews: http://www.wjgnet.com/1007-9327/g_info_20100312231947.htm

Guidelines: http://www.wjgnet.com/1007-9327/g_info_20100312232134.htm

RESUBMISSION OF THE REVISED MANUSCRIPTS

Please revise your article according to the revision policies of *WJG*. The revised version includes manuscript and high-resolution image figures. The author should re-submit the revised manuscript online, along with printed high-resolution color or black and white photos; Copyright transfer letter, and responses to the reviewers, and science news are sent to us *via* email.

Editorial Office**World Journal of Gastroenterology**

Editorial Department: Room 903, Building D,
Ocean International Center,
No. 62 Dongsihuan Zhonglu,
Chaoyang District, Beijing 100025, China
E-mail: wjg@wjgnet.com
<http://www.wjgnet.com>
Telephone: +86-10-5908-0039
Fax: +86-10-85381893

Instructions to authors

Language evaluation

The language of a manuscript will be graded before it is sent for revision. (1) Grade A: priority publishing; (2) Grade B: minor language polishing; (3) Grade C: a great deal of language polishing needed; and (4) Grade D: rejected. Revised articles should reach Grade A or B.

Copyright assignment form

Please download a Copyright assignment form from http://www.wjgnet.com/1007-9327/g_info_20100315222818.htm.

Responses to reviewers

Please revise your article according to the comments/suggestions provided by the reviewers. The format for responses to the reviewers' comments can be found at: http://www.wjgnet.com/1007-9327/g_info_20100315222607.htm.

Proof of financial support

For paper supported by a foundation, authors should provide a copy of the document and serial number of the foundation.

Links to documents related to the manuscript

WJG will be initiating a platform to promote dynamic interac-

tions between the editors, peer reviewers, readers and authors. After a manuscript is published online, links to the PDF version of the submitted manuscript, the peer-reviewers' report and the revised manuscript will be put on-line. Readers can make comments on the peer reviewer's report, authors' responses to peer reviewers, and the revised manuscript. We hope that authors will benefit from this feedback and be able to revise the manuscript accordingly in a timely manner.

Science news releases

Authors of accepted manuscripts are suggested to write a science news item to promote their articles. The news will be released rapidly at EurekAlert/AAAS (<http://www.eurekalert.org>). The title for news items should be less than 90 characters; the summary should be less than 75 words; and main body less than 500 words. Science news items should be lawful, ethical, and strictly based on your original content with an attractive title and interesting pictures.

Publication fee

Authors of accepted articles must pay a publication fee. EDITORIAL, TOPIC HIGHLIGHTS, BOOK REVIEWS and LETTERS TO THE EDITOR are published free of charge.